ISSN 2071-4726
2071-0305

Инженерно-строительный журнал

НАУЧНОЕ ИЗДАНИЕ

№8(76) 2017

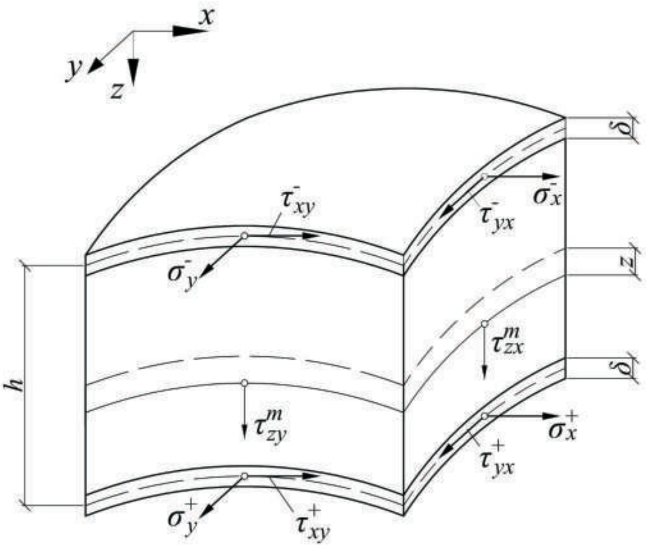

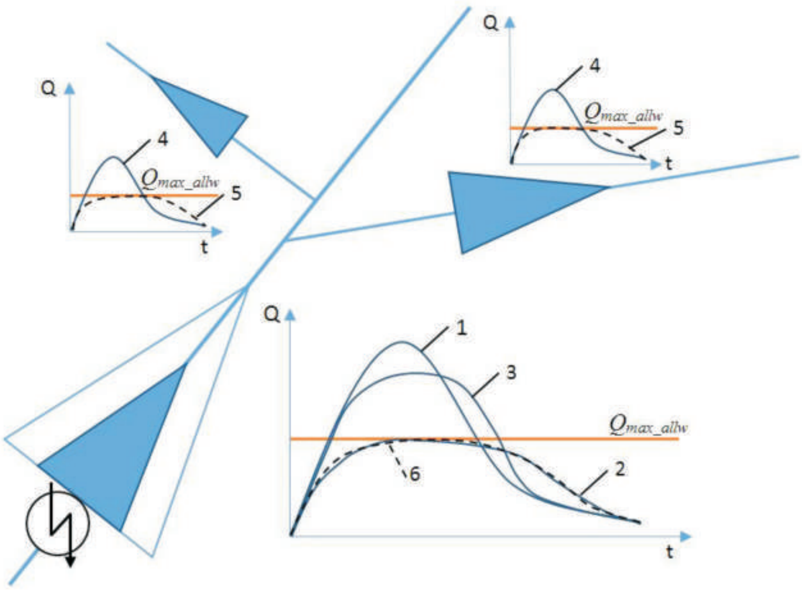

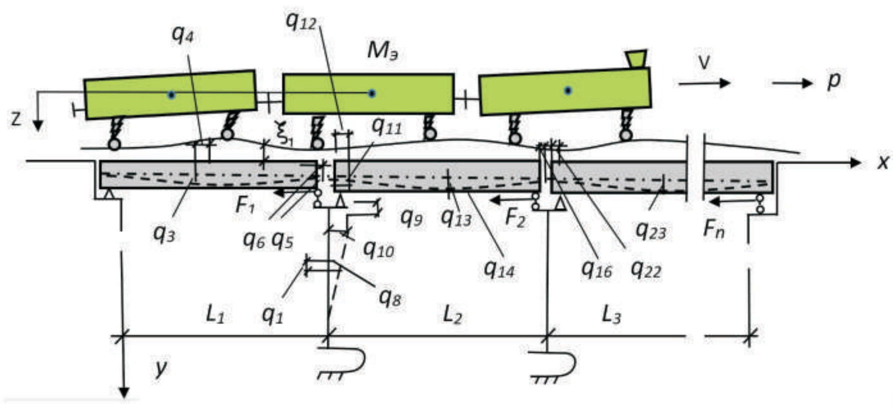

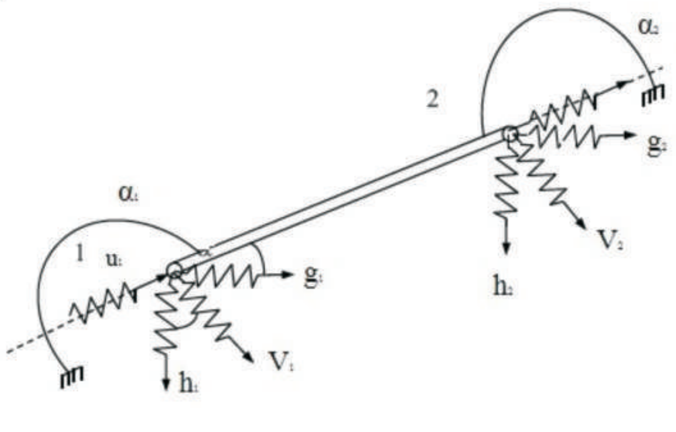

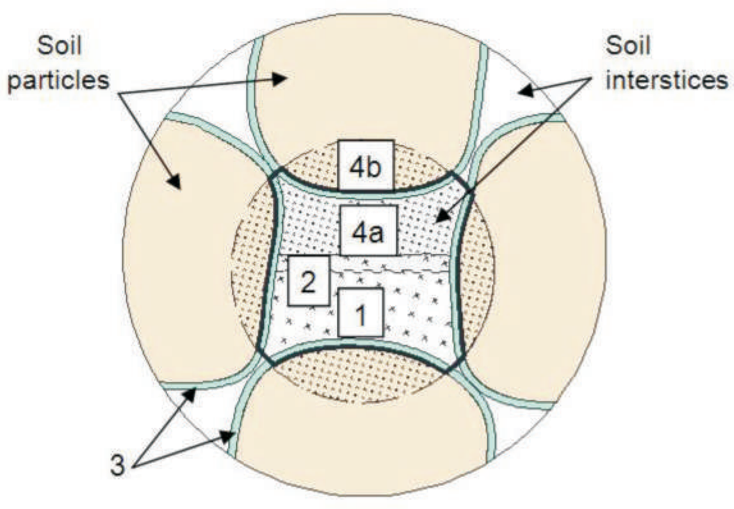

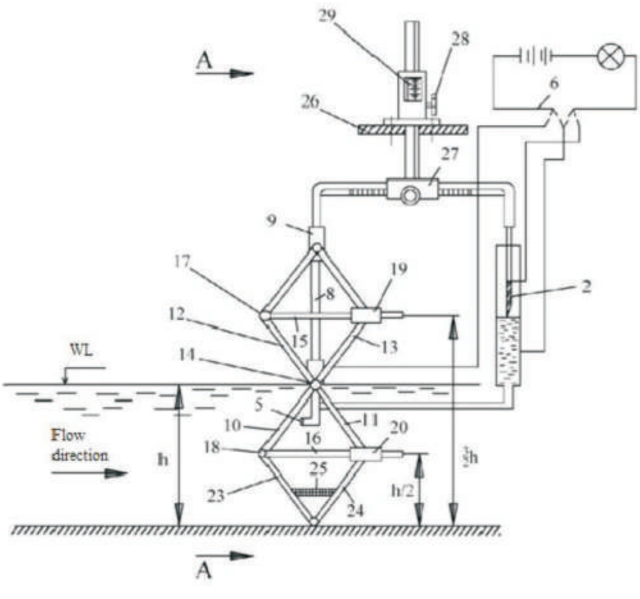

**Федеральное государственное автономное образовательное учреждение
высшего образования
Санкт-Петербургский политехнический университет Петра Великого**

ПОЛИТЕХ
Санкт-Петербургский
политехнический университет
Петра Великого

**Инженерно-строительный институт
Центр дополнительных профессиональных программ**

***195251, г. Санкт-Петербург, Политехническая ул., 29,
тел/факс: 552-94-60, www.stroikursi.spbstu.ru,
stroikursi@mail.ru***

**Приглашает специалистов организаций, вступающих в СРО,
на курсы повышения квалификации (72 часа)**

Код	Наименование программы	Виды работ*
	Курсы по строительству	
БС-01-04	«Безопасность и качество выполнения общестроительных работ»	**п.1,2, 3, 5, 6, 7, 9, 10, 11, 12, 13, 14**
БС-01	«Безопасность и качество выполнения геодезических, подготовительных и земляных работ, устройства оснований и фундаментов»	**1,2,3,5**
БС-02	«Безопасность и качество возведения бетонных и железобетонных конструкций»	**6,7**
БС-03	«Безопасность и качество возведения металлических, каменных и деревянных конструкций»	**9,10,11**
БС-04	«Безопасность и качество выполнения фасадных работ, устройства кровель, защиты строительных конструкций, трубопроводов и оборудования»	**12,13,14**
БС-05	«Безопасность и качество устройства инженерных сетей и систем»	**15,16,17,18,19**
БС-06	«Безопасность и качество устройства электрических сетей и линий связи»	**20,21**
БС-08	«Безопасность и качество выполнения монтажных и пусконаладочных работ»	**23,24**
БС-12	«Безопасность и качество устройства мостов, эстакад и путепроводов»	**29**
БС-13	«Безопасность и качество выполнения гидротехнических, водолазных работ»	**30**
БС-14	«Безопасность и качество устройства промышленных печей и дымовых труб»	**31**
БС-15	«Осуществление строительного контроля»	**32**
БС-16	«Организация строительства, реконструкции и капитального ремонта. Выполнение функций технического заказчика и генерального подрядчика»	**33**
	Курсы по проектированию	
БП-01	«Разработка схемы планировочной организации земельного участка, архитектурных решений, мероприятий по обеспечению доступа маломобильных групп населения»	**1,2,11**
БП-02	«Разработка конструктивных и объемно-планировочных решений зданий и сооружений»	**3**
БП-03	«Проектирование внутренних сетей инженерно-технического обеспечения»	**4**
БП-04	«Проектирование наружных сетей инженерно-технического обеспечения»	**5**
БП-05	«Разработка технологических решений при проектировании зданий и сооружений»	**6**
БП-06	«Разработка специальных разделов проектной документации»	**7**
БП-07	«Разработка проектов организации строительства»	**8**
БП-08	«Проектные решения по охране окружающей среды»	**9**
БП-09	«Проектные решения по обеспечению пожарной безопасности»	**10**
БП-10	«Обследование строительных конструкций и грунтов основания зданий и сооружений»	**12**
БП-11	«Организация проектных работ. Выполнение функций генерального проектировщика»	**13**
Э-01	«Проведение энергетических обследований с целью повышения энергетической эффективности и энергосбережения»	
	Курсы по инженерным изысканиям	
И-01	«Инженерно-геодезические изыскания в строительстве»	**1**
И-02	«Инженерно-геологические изыскания в строительстве»	**2,5**
И-03	«Инженерно-гидрометеорологические изыскания в строительстве»	**3**
И-04	«Инженерно-экологические изыскания в строительстве»	**4**
И-05	«Организация работ по инженерным изысканиям»	**7**

***(согласно приказам Минрегионразвития РФ N 624 от 30 декабря 2009 г.)**

По окончании курса слушателю выдается удостоверение о краткосрочном повышении квалификации установленного образца (72 ак. часа)

Для регистрации на курс необходимо выслать заявку на участие, и копию диплома об образовании по телефону/факсу: 8(812) 552-94-60, 535-79-92, , e-mail: stroikursi@mail.ru.

http://www.engstroy.spbstu.ru – полнотекстовая версия журнала в сети Интернет.
Бесплатный доступ, обновление с каждым новым выпуском

Инженерно-строительный журнал

ISSN 2071-4726, 2071-0305

Свидетельство о государственной регистрации: ПИ №ФС77-38070, выдано Роскомнадзором

Специализированный научный журнал. Выходит с 09.2008.

Включен в Перечень ведущих периодических изданий ВАК РФ

Периодичность: 8 раз в год

Учредитель и издатель:

Санкт-Петербургский политехнический университет Петра Великого

Адрес редакции:

195251, СПб, ул. Политехническая, д. 29, Гидрокорпус-2, ауд. 227А

Дата выхода: 05.03.2018

Содержание

На обложке: иллюстрации авторов к статьям номера

Контакты:
Тел. +7(812)535-52-47 E-mail: mce@spbstu.ru
Web: http://www.engstroy.spbstu.ru

http://www.engstroy.spbstu.ru – full-text open-access version in Internet. It is updated immediately with each new issue.

Magazine of Civil Engineering
SCHOLAR JOURNAL

ISSN 2071-4726

Peer-reviewed scientific journal

Start date: 2008/09

8 issues per year

Publisher:

Peter the Great St. Petersburg Polytechnic University

Indexing:

Scopus, Russian Science Citation Index (WoS), Compendex, DOAJ, EBSCO, Google Academia, Index Copernicus, ProQuest, Ulrich's Serials Analysis System

Corresponding address:

227a Hydro Building, 29 Polytechnicheskaya st., Saint-Petersburg, 195251, Russia

Contents

On the cover: authors' illustrations

+7(812) 535-52-47

E-mail: mce@spbstu.ru

Web: http://www.engstroy.spbstu.ru/eng/index.html

doi: 10.18720/MCE.76.1

Dynamic programming in optimization of comprehensive housing stock modernization

Динамическое программирование в оптимизации комплексной модернизации жилищного фонда

S.H. Bayramukov,
Z.N. Dolaeva,
North-Caucasian State Humanitarian-Technological Academy, Cherkessk, Russia

Д-р техн. наук, заведующий кафедрой, профессор С.Х. Байрамуков,
старший преподаватель З.Н. Долаева,
Северо-Кавказская государственная гуманитарно-технологическая академия, г. Черкесск, Россия

Key words: housing stock; comprehensive modernization; economic efficiency; payback period; energy saving technologies; optimization; dynamic programming

Ключевые слова: жилищный фонд; комплексная модернизация; экономическая эффективность; срок окупаемости; энергосберегающие технологии; оптимизация; динамическое программирование

Abstract. Research in the area of dynamic programming in optimization of comprehensive housing stock modernization has shown that there are a number of important issues that require effective and rapid solutions. The purpose of research is the organization of repair and construction works by modeling the organizational and technological solutions to the use of energy-saving technologies for the comprehensive modernization of the housing stock. The proposed method of an integrated approach to the modernization of the housing stock and, accordingly, the implementation of energy saving measures will reduce the cost of homeowners to pay for housing and communal services by improving the thermal performance of buildings. Formulated and discussed the theoretical aspects of dynamic programming for solving problems of optimal allocation of allocated funds having minimal losses, which allows calculating the conditions for the implementation of energy-modernization. The mathematical model of optimization of process of energy-modernization. Is executed economic assessment of energy saving decisions in the course of complex energy-modernization, are given results of calculations of distribution of the allocated funds and payback periods on of holding actions for increase in indicators of energy saving.

Аннотация. Исследования в области динамического программирования в оптимизации комплексной модернизации жилищного фонда показали, что имеется ряд важных проблем, требующих эффективного и быстрого решения. Целью исследования является организация ремонтно-строительных работ путем моделирования организационно-технологических решений с использованием энергосберегающих технологий при комплексной модернизации жилищного фонда. Предложенная методика комплексного подхода к модернизации жилищного фонда и, соответственно, реализации энергосберегающих мероприятий позволит снизить расходы собственников жилья на оплату жилищно-коммунальных услуг за счет улучшения теплотехнических характеристик зданий. Сформулированы и рассмотрены теоретические аспекты динамического программирования для решения задач оптимального распределения выделяемых денежных средств, имеющего минимальные потери, которая позволяет рассчитать условия реализации энергетической модернизации. Построена математическая модель оптимизации процесса энергетической модернизации. Выполнена экономическая оценка энергосберегающих решений в процессе комплексной энергетической модернизации, приведены результаты расчетов распределения выделенных средств и сроков окупаемости проведения мероприятий по повышению показателей энергосбережения.

Introduction

One of the most important tasks of the state level and the level of regional public authorities is the development and implementation of effective programs to upgrade the housing stock in order to solve major social problems connected with availability and comfort of housing [1]. The housing sector should

Байрамуков С.Х., Долаева З.Н. Динамическое программирование в оптимизации комплексной модернизации жилищного фонда // Инженерно-строительный журнал. 2017. № 8(76). С. 3–19.

be regarded as a complex system, the development of which depends on the final number of factors. Identification of the most significant factors affecting the dynamics of the housing stock is of fundamental importance. A clear definition of the relationship within the system in question leads to a correct or adequate accounting and forecasting the state of the housing stock.

At the present stage, it is possible to allocate the following main problems of the housing sphere in general:

- Shortage of housing;
- A high percentage of the moral and physical deterioration of buildings;
- Low quality of housing and communal services and maintenance of residential buildings;
- Rising prices for housing and communal services;
- Low and very low class's energy-efficiency housing [1, 2].

It should be noted the need to develop a comprehensive approach for the organization of an integrated mechanism for the modernization of the housing stock, taking into account energy- and resource-saving in the first place, using a variety of innovative technologies that improve the level of development of the city and the territory [1]. For the organization of the control method it is appropriate to use elements of computer mathematical modeling, numerical methods, which allows a certain accuracy to optimize the process of modernization. This process cannot be comprehended within static representations, as its sense is always connected with the future, with forecasting [3]. Therefore, task of complex modernization can be considered as a problem of dynamic optimization, the analysis tool that is a dynamic programming [3].

The need to systematization and maximize the cost-effectiveness of energy retrofit as part of a comprehensive modernization of housing stock led to the choice of the theme of scientific work.

Research problems in the housing and communal services, energy issues and resource conservation, the development of methods to solve them were engaged in domestic and foreign scientists: V.Ya. Mishchenko, V.S. Bogolyubov, S.G. Sheina, P.G. Hornbeam, L.B. Zelencov, O.N. Popova, T. L. Simankina, N.G. Selyutina, E.B. Smirnov, A.K. Schreiber, V.V. Klimenko, A.N. Dmitriev, V.G. Gagarin, A.S. Bolotin, I.A. Bashmakova, L.N. Chernyshov, G. Arman, A. Thumann, C.M. Carol, T. Goven, J.M. Clapp, G. Payne, A.D. Russell, A. Shtub, S. Selinger, J.F. Bard, B. Cheong-Hoon, J.M. Clapp, S. Globerson, K. Davar, M. Kataoka, H. Kim et al. [1, 4-9, 24].

Methodological issues of dynamic optimization of multistage processes, which include the possibility of different processes and a fundamental principle of optimality system control, have been proposed and investigated further by R. Bellman, R. Kalaba, I. Glicksberg, O.A. Gross, S.E. Dreyfus, R. Aris, G.L. Nemhauser, D. Wilde [10–13].

Foreign and domestic scientists S.V. Chukanov, O.A. Shcherbina, M.V. Lewis, D. Coen, K.D. Kuhn, A. Flint, C. Mei, D. Murray, Z.C. Lin, Y. Zhao, W.T. Ziemba, J. Doucette and others analyzed the possibility of using the dynamic programming method to solve the economic problems and modeling of economic systems [14–19].

The cycle of articles is earlier published by us was devoted to development of techniques of the description of a problem of complex updating of housing stock with application of methods of linear and dynamic programming [1, 14, 20, 21]. On the basis of these researches, and also the idea of the integrated application of methods of mathematical and information modeling in management of processes of the organization of construction, repair construction works and in general housing stock we offer the scheme of optimization of processes of complex modernization of housing stock.

Methods

Updating of conceptual structure of the theory of reproduction of the real estate.

Housing sector includes a number of methods of reproduction, depending on the degree of comfort under consideration specific property [2]. For the most complete review and study, the issue of housing modernization is necessary to update the conceptual structure theory. Any abstract theory is considered on some set of elements. A set is called set of elements, distinguishable among themselves and imaginable as a unit. In the theory of reproduction is explored the set of buildings, constructions and accompanying them the engineering infrastructure. We will call a set of residential buildings the city or country the housing stock.

On a set of residential objects, we will set various functional representation, which transform the given object in object with the minimum level physical and obsolescence. For any object of a given set is determined the number of parameters that can be divided into certain groups according to the degree of similarity. Let us allocate the main functional displays:

- new construction;
- reconstruction;
- modernization;
- Overhaul;
- current repair;
- sanitation;
- restoration;
- Renovation.

Analysis of the above types reproduction of objects of housing facilities was given in the works of V.Ya. Mishchenko, E.P. Gorbaneva, A.P. Prokopshina, V.V. Buzyrev, V.I. Tavina, E.B. Smirnov, A.I. Deeva and other scientists. In the studies of E.P. Gorbaneva an overview of these concepts and their definitions was given. Based on the results of the studies and an attempt to further formalize these terms, we proposed their understanding of both functional mappings; the concept of complex modernization of the housing stock has also been introduced.

New construction - function, domain of definition of which is housing stock, through which happens the compensation of physical and moral deterioration of old and obsolete assets, and increases the main index fund - the total area. This display is an old dilapidated facility assigns a new building with a completely new qualitative and quantitative indicators, it remains only invariant construction site with a number of fixed parameters.

Reconstruction - the display object with the old qualitative and quantitative indicators in themselves, but updated. Here, the update is meant reorganization, a change in the basic technical and economic indices of the building: the total area, the number of apartments, the area of apartments, capacity, bandwidth, construction volume (outbuilding, superstructure, remodeling), the provisions of a functional purpose in whole or in part (in this case, this area will not be included in the set under consideration). As the differences between the new building reconstruction of a partial refund of wear and tear can be distinguished [2, 22].

By upgrading is meant a functional image of the subject in itself, in which there is a qualitative improvement in the housing using the latest technologies and innovative materials, improving its comfort, partial or total compensation of moral and physical wear and tear. From the reconstruction is characterized in that the total value of the volume and area of a building, the appointment object remain unchanged.

Overhaul – a display object, the functional value of which is to reduce the percentage of physical deterioration by replacing or restoring the structures of the building or its parts, engineering equipment. The level of comfort of the building, however, the overhaul does not provide a change of its volume, the total area of rooms and spaces. [7]

As many authors have studied the literature, include the process of overhaul and redesign of the building, which leads to a decrease in the degree of identification of the concepts of modernization and overhaul. This is a significant disadvantage in the design of computer mathematical process model [2, 11–12].

Object Maintenance work is a map in which there is a restoration of working capacity of structural elements and systems engineering equipment facility. Maintenance work includes a partial reduction for deterioration by keeping the operational performance of the building. Allocate by type of construction work scheduled (planned on the implementation of the time, volume and value) and unscheduled maintenance overhaul (identified in the operation and made a matter of urgency, is random) [18].

Remediation – a functional image of the subject, providing for the rehabilitation of the technical condition of the building, improvement of hygiene and living conditions, improvement of intra territories. Decompression development and improvement of intra-area can be carried out by demolition of inefficient buildings for different purposes and using them to build underground, surface parking lots, recreation areas and a variety of modern sports and cultural complexes. That is, in the application of the reporting function display must be considered multi-criteria indicator of the quality of intra territories.

Restoration – is a functional image of the subject in itself, and its functional significance – it recreated the ancient appearance of the building. When the restoration is carried out a complex range of repair and construction works aimed at restoring the cultural heritage. It consists of the following operations:

- Reconstruction of the object by removing later distorting its parts;
- Recovery of lost items;
- Elimination of physical deterioration.

Renovation of housing – functional display, including a general, a sequence of transformations: new construction, capital repairs, modernization, restoration, reconstruction, demolition of buildings, sanitation. Thus, a housing renovation is understood one of the above functional maps for a particular object of the housing stock.

We introduce the concept of a comprehensive modernization of housing. Comprehensive modernization of housing – a functional domain that serves a variety of functions (reconstruction, modernization, repair, maintenance, restoration, rehabilitation, renovation), thus reverses the physical and moral property of wear, that is, improvement of qualitative and quantitative indicators. Here it is obligatory to carry out energy modernization of housing stock and taking into account the funds allocated for this purpose. Under the modernization of energy, we mean an element of a comprehensive modernization of the housing stock, which is carried out in the course of repair and construction work using energy-saving technologies, leading to an increase in comfort and property owners a significant reduction of costs for housing and communal services [1].

Effective management of the modernization process in the public financial support would solve the problem of ensuring the proper use, maintenance and repair, reconstruction of the facility; preservation in the required state of the technical and operational characteristics of the property; creation of comfortable living conditions for the citizens; resource; a phased increase in energy systems engineering; reduce the size of obligatory payments.

The economic situation in the country is usually characterized by local instability. Examining the growth and development of the housing stock in general, we concluded that it was necessary to develop methods for strategic planning of all spheres with a view to more effective management. There have sharp differences in growth, while at the same time, there are no clear long-term development prospects. If we introduce the assumption that the more distant future will be stable, that is stationary or quasi-stationary, it can be divided into a model for the current period and the period of "steady-state" of the future. For the model of "steady-state" of the future ask Bellman function, which has developed in non-stationary model of the current phase [3]. This will allow responding to emerging changes in the housing sector. The method will be to address the dynamic functional Bellman equation [10]. Next, we consider an element of a comprehensive modernization of housing – the modernization of energy, in which the following
energy-saving technologies have been introduced:

- Installation of curtains from PVC film into space windows (ET 1);
- Automation of lighting in the common areas (ET 2);
- Organization of the automated thermal points (ET 3);
- The use of automatic door closers on the doors (ET 4);
- The use of automatic sensor faucets (ET 5);
- Improving the thermal insulation properties of the building envelope (walls) (ET 6);
- Improving the thermal insulation properties of the roof (ET 7);
- Insulation of external doors (ET 8);
- The use of motion sensors (ET 9);
- Installation of heat-reflective designs for radiators (ET 10) [7,20].

Application of methods of dynamic programming in solving this problem is conditioned by the fact that it allows controlling both energy-saving efficiency and implemented energy-saving technologies. This methodology has a complex character and allows us to investigate the economic effect of the implementation of ET in the renovation of the housing stock as a whole, rather than individual objects.

The composition and structure of the so-called energy modernization can be changed depending on the types of buildings and their technical properties.

When carrying out repair and construction works that have a complex nature, the main criterion for their implementation or non-performance is the restriction in financial resources. Proceeding from this, in our article it is offered in parallel with carrying out of various repair-building works to realize energy-saving measures with the optimum distribution of means leading accordingly to the maximum economic effect.

Statement of research problem

Let the volume investments (*C*) it is allocated for carrying out for energy action the modernization of housing stock. As the input data is set the volume of funds allocated for holding *n* energy-saving measures.

Consider the generalized scheduling problem for an energy modernization using two types of energy saving measures I and II for a period of *m* years.

The quantity of means *x*, enclosed in an action of *I* yields revenue in one year

$$f(x) = A \cdot x \tag{1}$$

and at the expense of it decreases to

$$\varphi(x) = A' \cdot x. \tag{2}$$

The quantity of means *y*, enclosed in an action of *II* yields revenue in one year

$$g(y) = B \cdot y \tag{3}$$

and decreases to

$$\psi(y) = B' \cdot y. \tag{4}$$

It is required distribution is of resources Z_0 between the carrying out of action I and II for each year of the planned period. Income is understood here as an economic effect from the introduction of energy-saving technologies in the process of modernization of housing stock.

Decision. Conditional optimal control x_m^* in the last step (quantity of the funds allocated in action of I) is defined as value x_m at which the income reaches maximum on the last step:

$$W_m^*(Z_{m-1}) = \max_{0 \le x_m \le Z_{m-1}} \{w_m(Z_{m-1}, x_m)\},$$

where

$$w_m(Z_{m-1}, x_m) = A \cdot x_m + B \cdot (Z_{m-1} - x_m) = (A - B) \cdot x_m + B \cdot Z_{m-1}, \quad A \ne B \text{ [15].} \tag{5}$$

The graph of the function $w_m = w_m(Z_{m-1}, x_m)$, depending on the argument x_m for a given Z_{m-1}, will be a straight line. The maximum value can be reached only at the boundaries of the gap $(0, Z_{m-1})$. To define on what border, let's substitute in formula (5) $x_m = 0$ and $x_m = Z_{m-1}$. Proceeding from the submitted schedules, obvious that in case of the decreasing function the maximum value $w_m = B \cdot Z_{m-1}$ at $x_m = 0$. In the second case at $x_m = Z_{m-1}$, is reached the maximum value of function w_m, equal to the value $A \cdot Z_{m-1}$ [23].

Consequently, the maximum income for the last step is independent of Z_{m-1} and its value depends on the values *A* and *B*, and it means that at the beginning of the final year, all available investment must be invested in action of I, if *B*<*A* or in II, if *B*>*A*. It is natural as the income from the chosen action is more, and expenses of means does not interest us any more (last stage).

At this optimum control of final year will bring us income $w_m = B \cdot Z_{m-1}$ or $w_m = A \cdot Z_{m-1}$.

Let us pass to distribution of funds for (*m*-1)-th year. Let we approached it with a stock of means Z_{m-2}. Let us define the conditional maximum income in the last two years:

$$W_{m-1,m}^*(Z_{m-2}) = \max_{0 \le x_{m-1} \le Z_{m-2}} \{A \cdot x_{m-1} + B \cdot (Z_{m-2} - x_{m-1}) + W_m^*(Z_{m-1})\}$$

But $Z_{m-1} = A' \cdot x_{m-1} + B' \cdot (Z_{m-2} - x_{m-1})$, consequently,

$$W_m^*(Z_{m-1}) = B \cdot (A' \cdot x_{m-1} + B' \cdot (Z_{m-2} - x_{m-1}))$$ or
$$W_m^*(Z_{m-1}) = A \cdot (A' \cdot x_{m-1} + B' \cdot (Z_{m-2} - x_{m-1})).$$

From here we will receive

$$W_{m-1,m}^*(Z_{m-2}) = \max_{0 \le x_{m-1} \le Z_{m-2}} \{A \cdot x_{m-1} + B \cdot (Z_{m-2} - x_{m-1}) + A \cdot (A' \cdot x_{m-1} + B' \cdot (Z_{m-2} - x_{m-1}))\}$$

or

$$W_{m-1,m}^*(Z_{m-2}) = \max_{0 \le x_{m-1} \le Z_{m-2}} \{A \cdot x_{m-1} + B \cdot (Z_{m-2} - x_{m-1}) + B \cdot (A' \cdot x_{m-1} + B' \cdot (Z_{m-2} - x_{m-1}))\}$$

[23–25].

Expression in braces represents a polynom of the first degree relatively x_{m-1}, and its schedule – a straight line, function, proceeding from the received parameters can be increasing or decreasing: $x_{m-1} = 0$ and $x_{m-1} = Z_{m-2}$.

In the first case (at $x_{m-1} = 0$) we receive $W_{m-1,m}^*(Z_{m-2}) = (B + A \cdot B') \cdot Z_{m-2}$ or $W_{m-1,m}^*(Z_{m-2}) = (1 + B') \cdot B \cdot Z_{m-2}$; in the second case (at $x_{m-1} = Z_{m-2}$) $W_{m-1,m}^*(Z_{m-2}) = (1 + A') \cdot A \cdot Z_{m-2}$ or $W_{m-1,m}^*(Z_{m-2}) = (A + A' \cdot B) \cdot Z_{m-2}$.

From the given expressions clearly that the maximum of the income depends on values: *A, B, A', B'.*

We turn to the (m - 2)-th step. Here it is necessary to maximize value of $W_{m-2,m-1,m}^*(Z_{m-3})$ on a similar principle [23].

Thus, the optimal control is found. Let us notice, that this solution will be obtained regardless of any number of steps, and any of the initial stock of assets Z_o.

Results and Discussion

The results calculations of economic efficiency (the economic efficiency from introduction of the energy saving technologies (ET) within one year), of considered energy saving actions are presented graphically in the form circulars charts in the figure 1. Values of the coefficients used in calculations were chosen from normative documents, statistical data on the Karachay-Cherkess Republic and other reliable data [26–31].

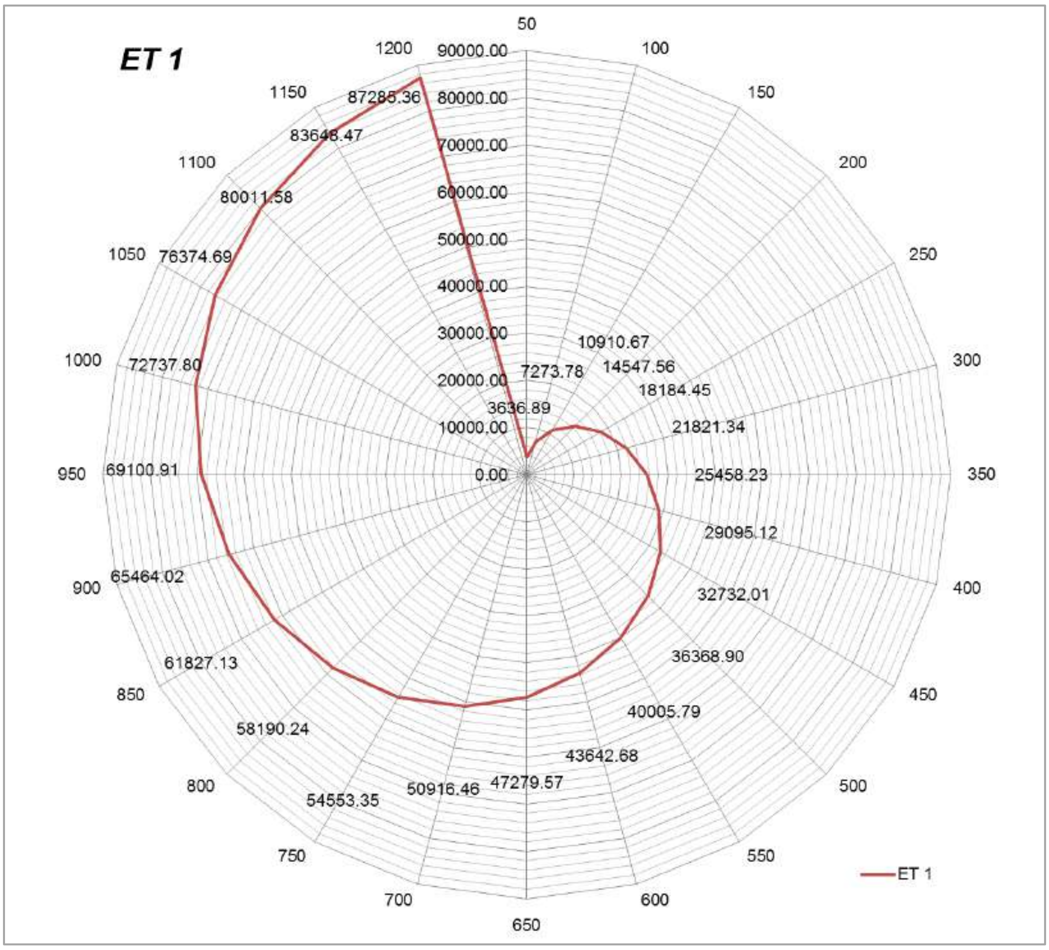
ET 1
50
100
150
200
250
300
350
400
450
500
550
600
650
700
750
800
850
900
950
1000
1050
1100
1150
1200
90000.00
80000.00
70000.00
60000.00
50000.00
40000.00
30000.00
20000.00
10000.00
0.00
3636.89
7273.78
10910.67
14547.56
18184.45
21821.34
25458.23
29095.12
32732.01
36368.90
40005.79
43642.68
47279.57
50916.46
54553.35
58190.24
61827.13
65464.02
69100.91
72737.80
76374.69
80011.58
83648.47
87285.36
ET 1

a).

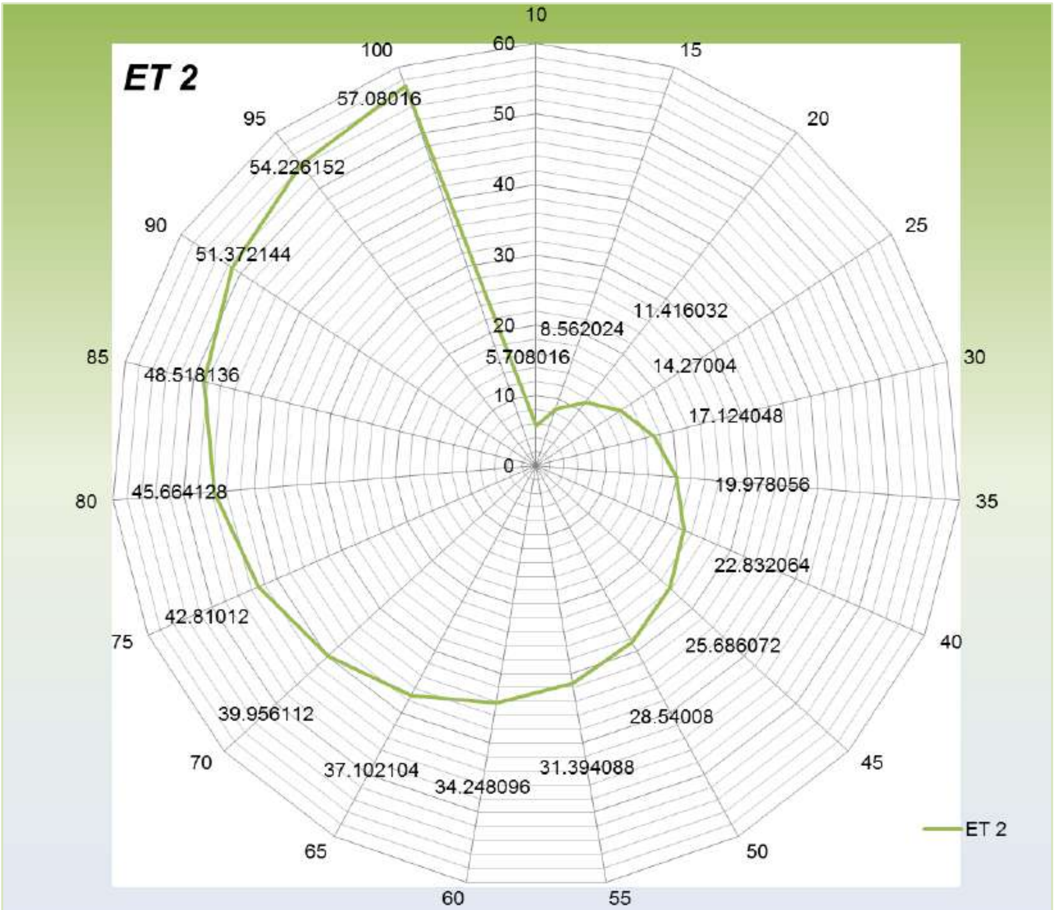
ET 2
10
15
20
25
30
35
40
45
50
55
60
65
70
75
80
85
90
95
100
60
50
40
30
20
10
0
5.708016
8.562024
11.416032
14.27004
17.124048
19.978056
22.832064
25.686072
28.54008
31.394088
34.248096
37.102104
39.956112
42.81012
45.664128
48.518136
51.372144
54.226152
57.08016
ET 2

b).

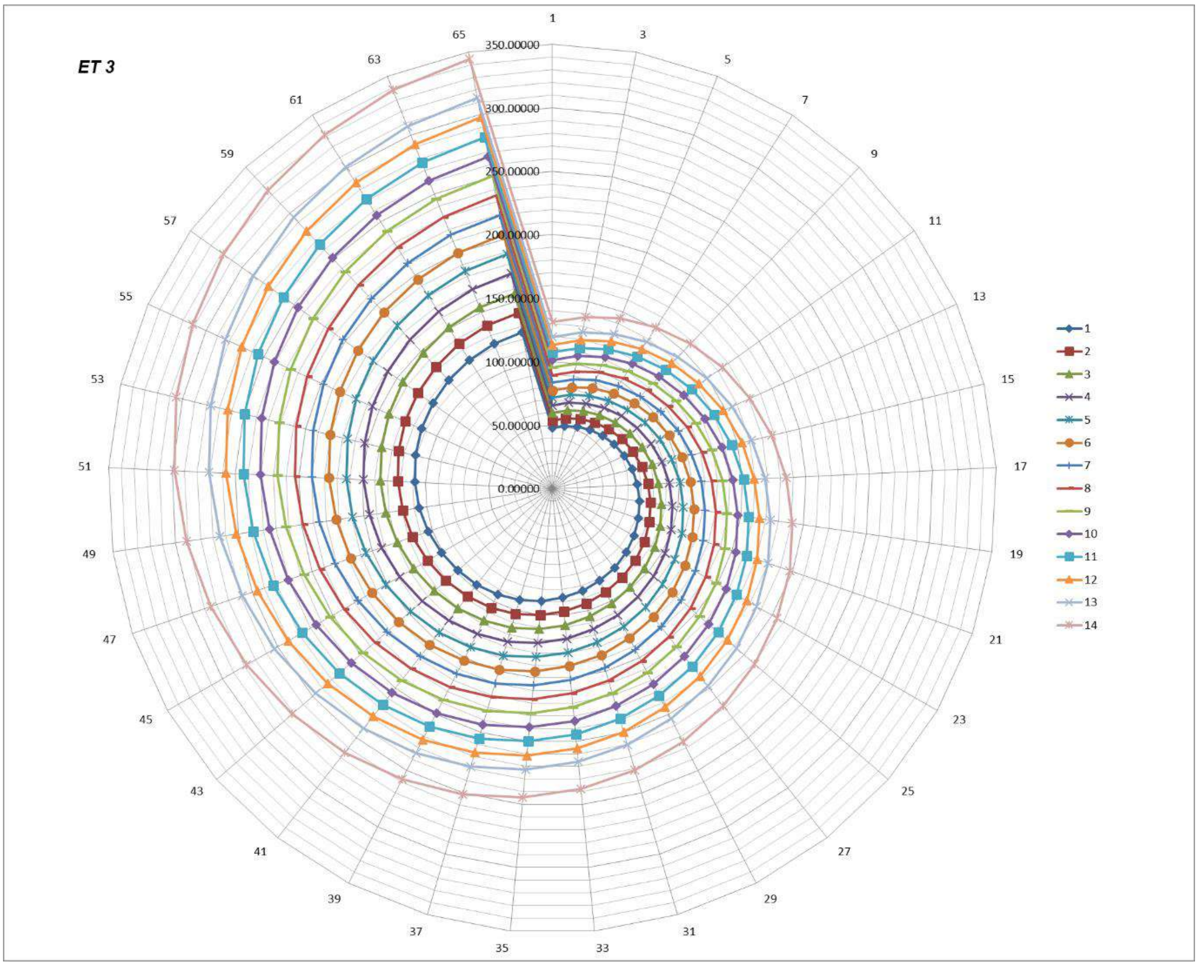
ET 3
1
3
5
7
9
11
13
15
17
19
21
23
25
27
29
31
33
35
37
39
41
43
45
47
49
51
53
55
57
59
61
63
65
0.00000
50.00000
100.00000
150.00000
200.00000
250.00000
300.00000
350.00000
1
2
3
4
5
6
7
8
9
10
11
12
13
14

c).

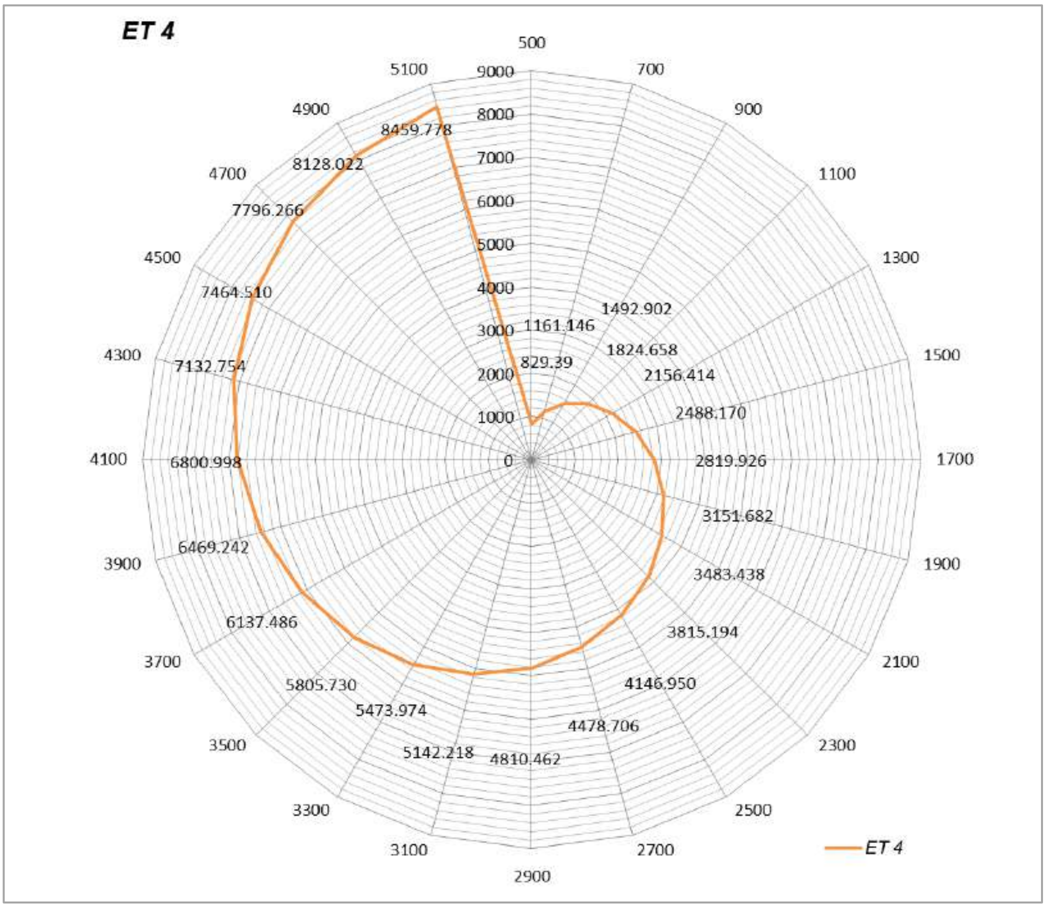
ET 4
500
700
900
1100
1300
1500
1700
1900
2100
2300
2500
2700
2900
3100
3300
3500
3700
3900
4100
4300
4500
4700
4900
5100
0
1000
2000
3000
4000
5000
6000
7000
8000
9000
829.39
1161.146
1492.902
1824.658
2156.414
2488.170
2819.926
3151.682
3483.438
3815.194
4146.950
4478.706
4810.462
5142.218
5473.974
5805.730
6137.486
6469.242
6800.998
7132.754
7464.510
7796.266
8128.022
8459.778
ET 4

d).

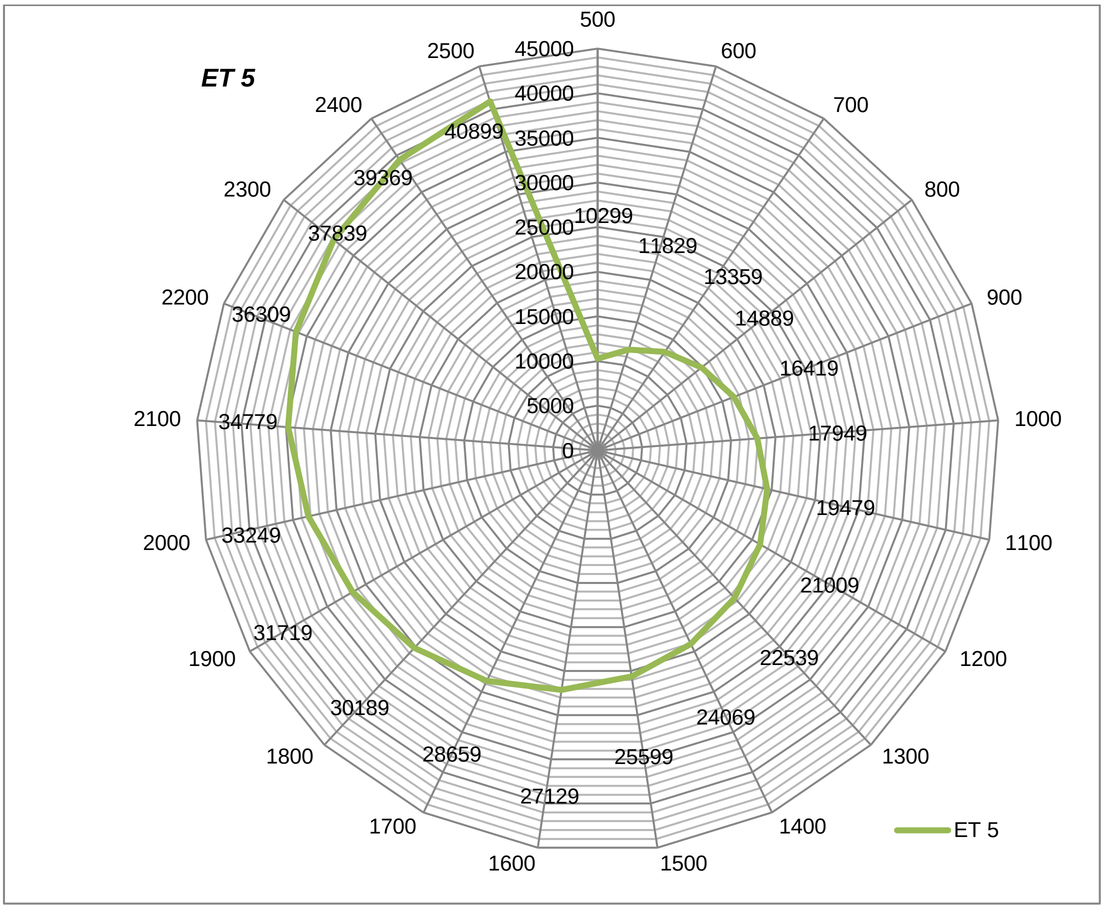

ET 5
500
600
700
800
900
1000
1100
1200
1300
1400
1500
1600
1700
1800
1900
2000
2100
2200
2300
2400
2500
45000
40000
35000
30000
25000
20000
15000
10000
5000
0
10299
11829
13359
14889
16419
17949
19479
21009
22539
24069
25599
27129
28659
30189
31719
33249
34779
36309
37839
39369
40899
ET 5

e).

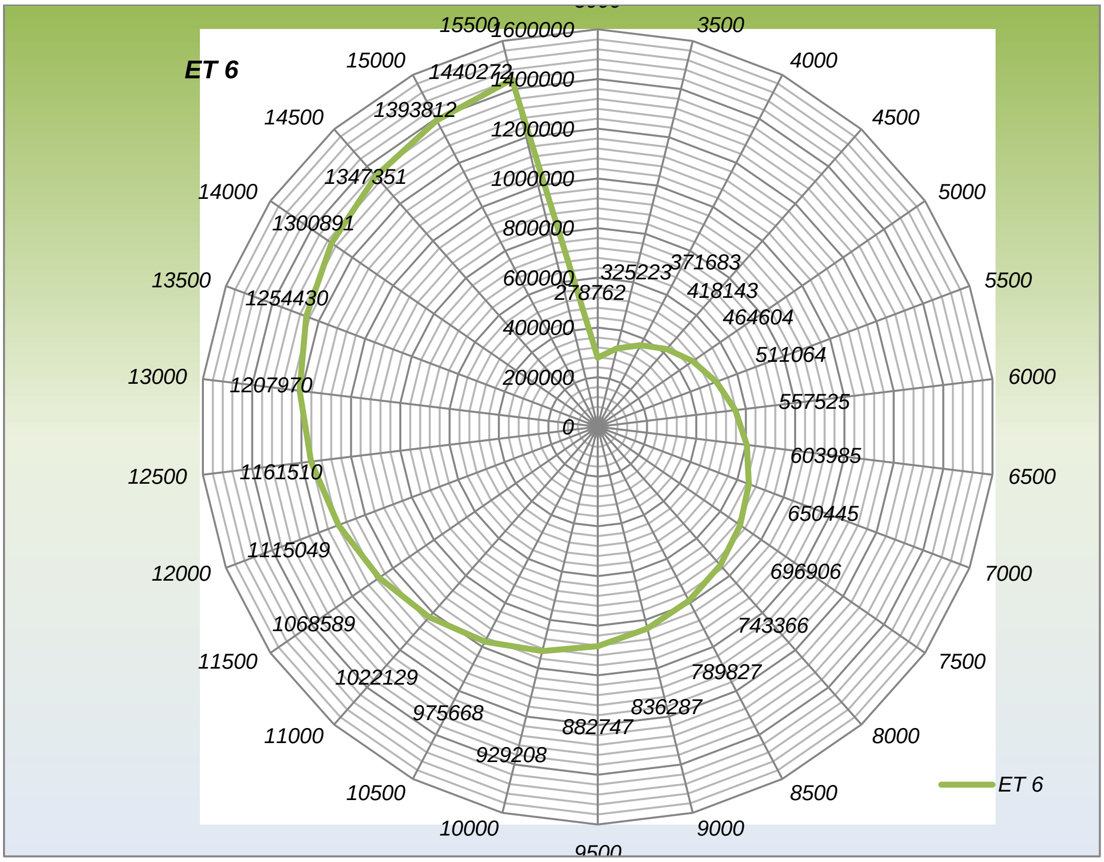

ET 6
3500
4000
4500
5000
5500
6000
6500
7000
7500
8000
8500
9000
9500
10000
10500
11000
11500
12000
12500
13000
13500
14000
14500
15000
15500
1600000
1400000
1200000
1000000
800000
600000
400000
200000
0
278762
325223
371683
418143
464604
511064
557525
603985
650445
696906
743366
789827
836287
882747
929208
975668
1022129
1068589
1115049
1161510
1207970
1254430
1300891
1347351
1393812
1440272
ET 6

f).

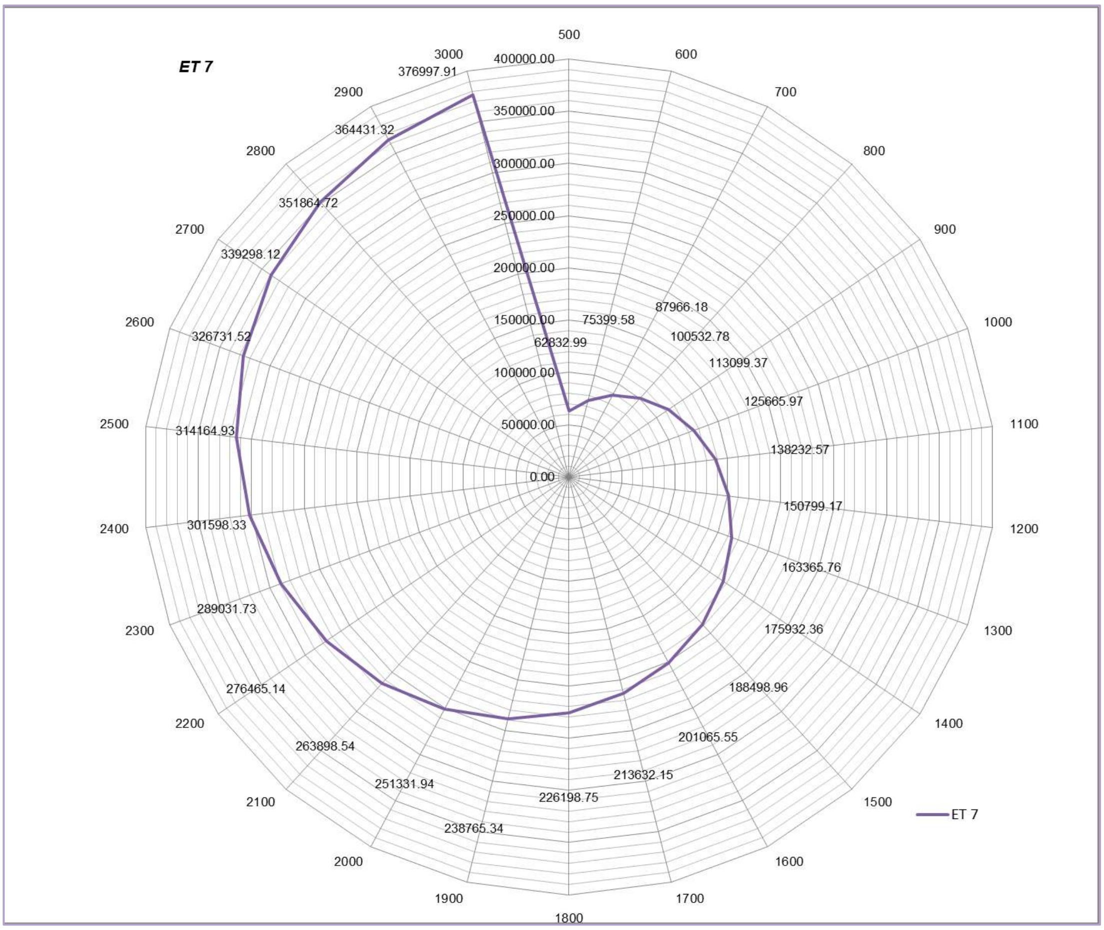

g).

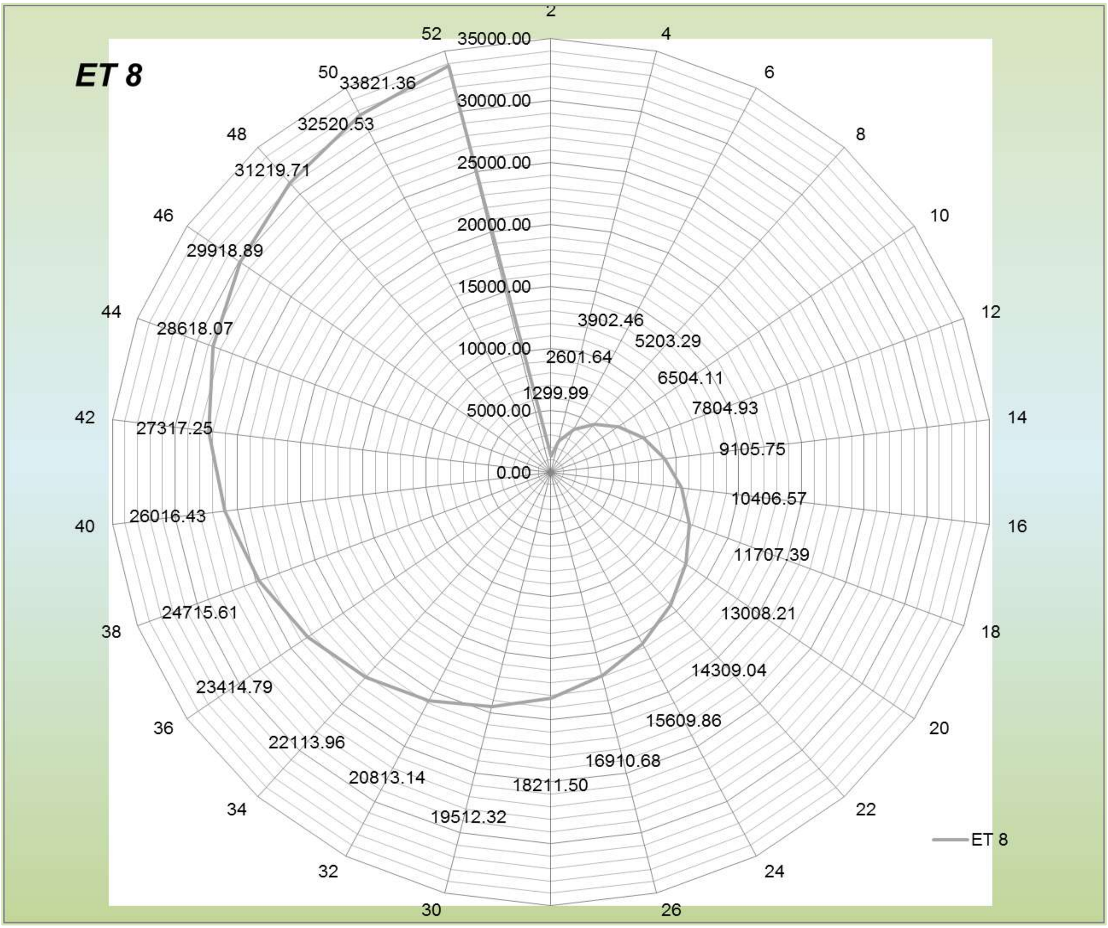

h).

Bayramukov S.H., Dolaeva Z.N. Dynamic programming in optimization of comprehensive housing stock modernization. *Magazine of Civil Engineering*. 2017. No. 8. Pp. 3–19. doi: 10.18720/MCE.76.1.

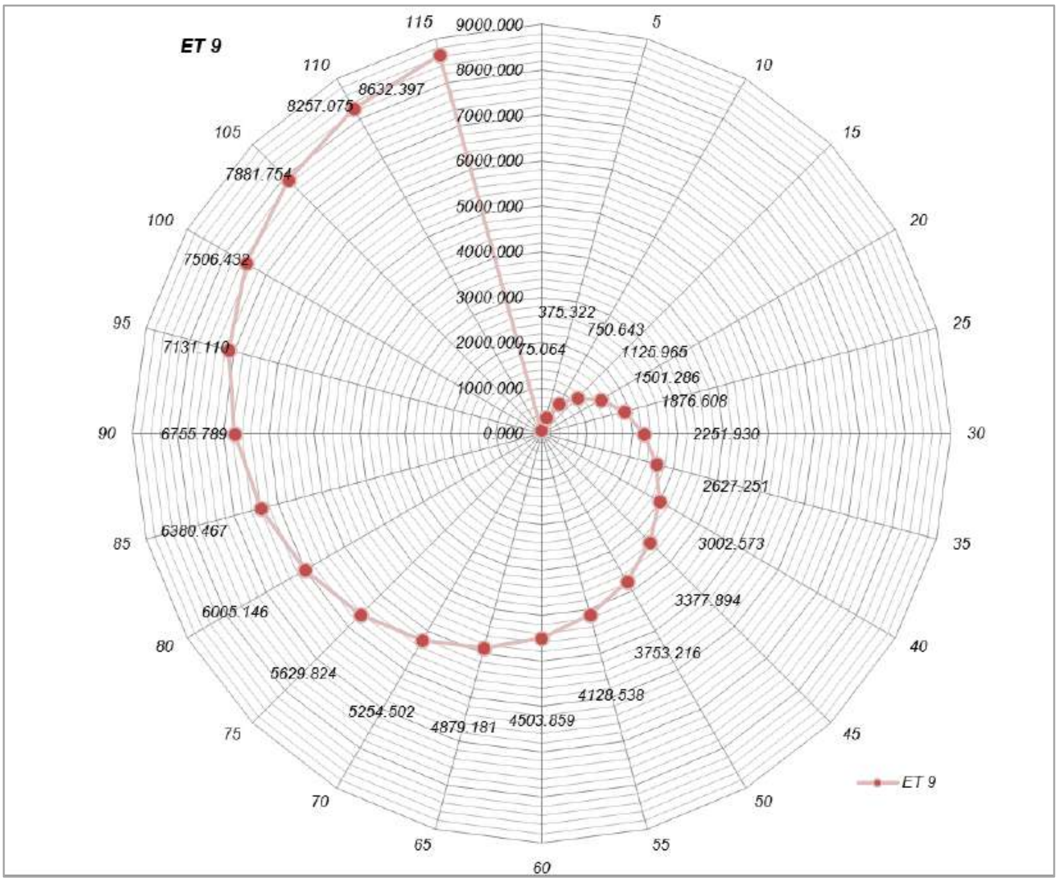

i).

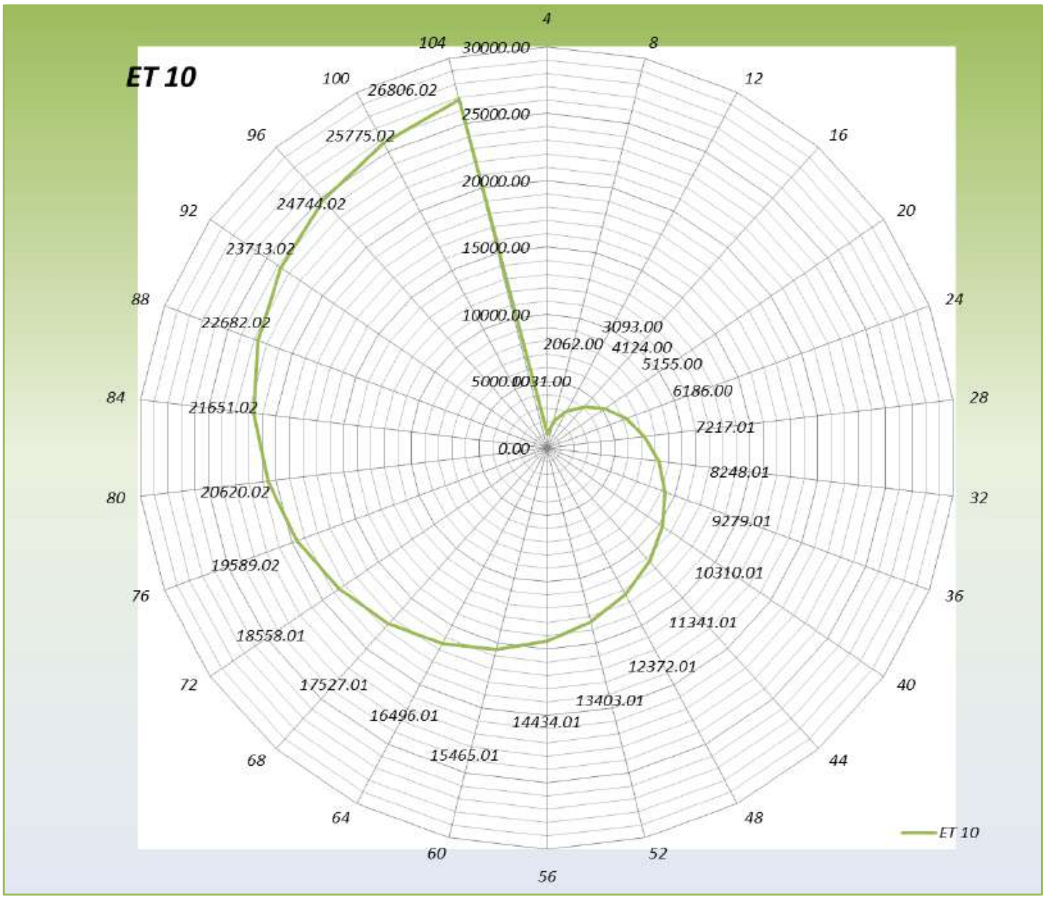

j).

Figure 1. The cost-effectiveness of the introduction of ET

Байрамуков С.Х., Долаева З.Н. Динамическое программирование в оптимизации комплексной модернизации жилищного фонда // Инженерно-строительный журнал. 2017. № 8(76). С. 3–19.

a. ET 1 (depending on an indicator of the area of a glazing), rub.

b. ET 2 (depending on the number of glow lamps in places with temporary stay of people), thousand rubles.

c. ET 3 (depending on the number of completely heated days in the heating period and an indicator of annual consumption of thermal energy on heating of the building), thousand rubles.

d. ET 4 (depending on the volume of the thermal energy consumed during the heating period in the base year), rub.

e. ET 5 (depending on volumes of consumption of hot and cold water), rub.

f. ET 6 (depending on the surface area of walls), rub.

g. ET 7 (depending on the area of a roof), rub.

h. ET 8 (depending on the total area of surfaces of external doors), rub.

i. ET 9 (depending on the electric power of lamps), rub.

j. ET 10 (depending on the total area of projections of heating devices on of wall), rub.

On basis of the received results, it is visible that energy-saving actions not only increase technical comfort of a residential facility, but also make it possible to optimize parameters of internal temperature background. So ET 3 assumes to maintain the required temperature schedule in the heating system installation of regulators for heating with sensors for external and internal air. Under the appropriate program, the regulator can reduce the temperature of the air in the rooms. Automated control of the heating load allows you to save in the autumn-spring period. Figure 1, c) shows the graphs of financial savings, depending on the number of heated days in the heating season, with different annual heat loads for the heating system of the building.

Introduction of energy saving technologies of economy increases of thermal and electric energy. So at change of heat-shielding properties of a roof the percent of economy of thermal energy increases by 8–12%, 6–15% – due to increase in a heat-shielding of windows and external doors; 15–20% – at the expense of the device of the automated knot of management of system of heating and installation of thermostats on the heating devices; 10–25% (electric energy) – due to application of energy saving lamps and motion sensors. The received values will be applied for realization of a problem of optimum distribution of investments in processes of complex modernization housing stock.

The given pie charts are the input material for modeling the system based on the methods of dynamic programming. The task is to carry out repair work in such a way to the results of their performance lead to a significant increase in the savings that have been spent on them taking into account the introduction of energy-saving technologies.

The task to distribute the specified amount of money between n actions so that in general the maximum effect of economy of money was gained is set. The solution of this problem must be divided into several stages. Generally we considered a problem of scheduling of carrying out energy-modernization with use of two types of energy saving actions for m of years, it can be generalized also prior to a final set of actions. But since the state programs for renovation (for example, the program "Capital repairs of common property in apartment buildings in the territory of Karachay-Cherkess Republic for 2014-2044 years") is carried out over a certain object at a time, we consider m = 1 year, And the criterion for splitting into stages is not a time factor, and the solution of the problem of allocation of funds at the 1st stage – between 2 measures, in the second stage it is necessary to optimally distribute between activities 1 + 2 and 3, etc.

If modernization works are planned in a residential building, they can be profitably combined with energy-saving measures. Additional costs for energy-saving investments are often a smaller amount. So, when updating the facade, the framework of the woods has to be established anyway. Then the surcharge for thermal insulation becomes comparatively less. In the future, this same event can cost much more expensive only because you will again need to install the framework of the woods. Saving energy pays off: additional investment will pay off due to lower energy costs.

A number of measures of the program "Capital repairs of common property in apartment buildings in the territory of the Karachay-Cherkess Republic for 2014–2044 years" can be combined with appropriate energy-saving actions, so repair of in-house engineering systems of electricity, heat, gas, water supply, water disposal – with ET2 , ET3, ET4, ET5, ET9, ЭТ10; repair of the roof, including the conversion of an unventilated roof to a ventilated roof, the device of exits to the roof – with ET7; repair of the facade with ET1, ET6, ET8. Financing of complex modernization is made by the saved-up funds of implementation of the state and regional programs of updating of housing stock of updating of housing stock of the housing stock and additional funds for energy modernization, collected own means of tenants, or taken on credit.

Using the results of the energy survey, numerical experiment and scientific research in the chosen direction, it is possible to estimate the investment potential of introducing energy-saving technologies with relatively consolidated indicators.

Using results of a numerical experiment and scientific research on the chosen direction, it is possible to estimate the investment potential of introduction of energy saving technologies with relatively enlarged parameters.

Let for carrying of actions energy modernization housing stock is allocated volume of money of C = 100 000 rub. Let us allocate 4 types of energy saving technologies with relatively enlarged indicators (n = 4). Types of energy saving technologies, which are established systemically, will be considered as a uniform measure. Actions, which can be interchangeable, are considered separately. Basic value has Selection of the major limiting factors. To them concern Amounts of works, financing restriction, the accounting of system of a variation of cost indexes of materials of works. As the most important information for development of model and its decision, we will choose a number of properties: types of actions, specific costs of their carrying out, tariffs for payment of utilities, energy saving and economic efficiency. In addition, we will plan creation of fund of reserve means, which will be used, on carrying out the repair construction works, which are not providing energy-savings, such as finishing works and works on updating of the territory around the considered objects and other works. Accumulation of means will go to the created fund as percent of means from economic effect of energy modernization of housing stock. And additionally, if the result involves the partial implementation of energy-saving measures, then the funds for their implementation are collected in this special fund.

Results of calculations are given in a type of schedules in the Figure 2.

	1	2	3	4
The economic effect	70654.6	25758	21192	4566
Deposits	100000	50000	40000	10000

Figure 2. Distribution of funds between with 4 ET

From these tables and graphs it is clear that any process of the energy modernization consisting of different quantity and quality of energy-saving measures can be based on indicators of the amount of investments by optimizing the allocation of funds that provide the maximum economic effect.

To carry out or not to hold these or those events solves the given management algorithm (figure 2), in the conditions of shortage of funds and relatively low efficiency, an event cannot be conducted. The use of methods of dynamic programming makes it possible to identify those measures that most effectively reduce the cost of housing and utilities and at the same time regulate the available funds for their joint implementation. Calculations were carried out on the basis of a survey of the technical condition of residential buildings in the city of Cherkessk (Table 1) and their energy-saving potential.

Table 1. The main characteristics of survey objects

№	Address	Year of commissioning Property	Type of wall material (House type)	Class of energy efficiency
1	Dovatora street, house number 72	1977	Brick	D
2	Dovatora street, house number 74	1974	Brick	E
3	Dovatora street, house number 76	1979	Claydite concrete panels	D
4	Dovatora street, house number 78	1974	Brick	E
5	Dovatora street, house number 80	1973	Brick	E
6	Dovatora street, house number 82	1980	Brick	D
7	Lobodina street, house number 57	1976	Claydite concrete panels	E
8	Lobodina street, house number 59	1975	Claydite concrete panels	E
9	Lobodina street, house number 59a	1986	Brick	D
10	Lobodina street, house number 61	1981	Claydite concrete panels	D

The Figure 3 given the calculated indicators of payback periods of energy saving measures.

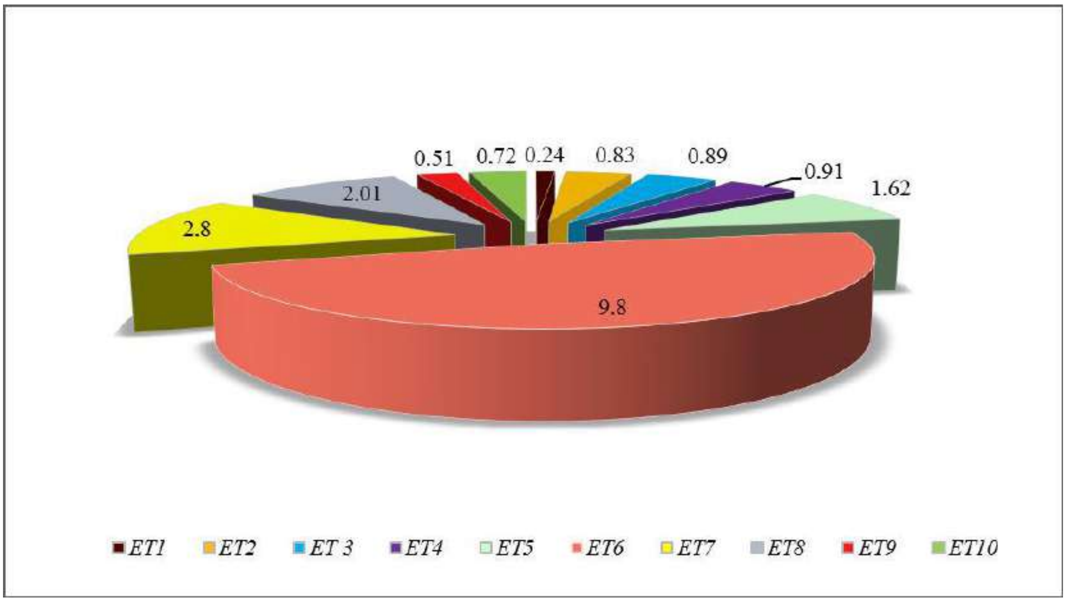

Figure 3. The payback period of energy-saving measures, year

The figure shows that the greatest payback period has kind of a comprehensive modernization housing – warming of external walls. For other technologies, we introduce a reserve fund in charge for the subsequent control, further updating and carrying out other construction works.

The above method of calculation is adequate, and at the expense of computer, technology has the property of efficiency. Dynamic programming techniques allow a certain error to calculate the maximum version of the "income" of the implemented technology.

Conclusions

1. The offered technique of assessment of efficiency of energy saving actions allows to increase quality of decision-making on restoration of housing stock, increase in its energy efficiency; application of

methods of mathematical modeling allows to realize the project of distribution of financial means in such a way that implementation of organizational-technology solutions of consecutive performance of actions will result to maximum possible positive socio-economic effect.

2. Executed economic evaluation of energy saving solutions in the process of a comprehensive energy-modernization, are given results of calculations of distribution of the allocated funds and deadlines of recoupment of holding actions for increase in indicators of energy saving which make 1–3 years for ET1–5, ET 7–10, for ET 6 up to 10 years.

3. Is offered the mathematical model allowing to maximize the number of quality housing due to realization of energy saving and other actions at complex modernization of housing stock.

4. Formulated and considered the theoretical aspects of dynamic programming for solving problems of optimal allocation of allocated funds with minimal loss, which allows calculating the conditions for the implementation of energy-modernization.

5. Is offered the multi-step procedure evaluating the economic efficiency of resource allocation when implementing of energy saving technologies in the process of updating the housing stock. The integrated use of information technology and mathematical descriptions of the processes allows obtaining complex information about the property at different stages of their life cycle, their actual condition and the necessity of modernization and reconstruction. Their joint use during the entire life cycle of buildings will lead to the optimal management of objects, maximizing an economic benefit and, respectively, to social effect.

References

1. Bayramukov S.H., Dolaeva Z.N. Kompleksnyy podkhod k probleme modernizatsii zhilishchnogo fonda [A comprehensive approach to the problem of housing modernization]. *Inzhenernyy Vestnik Dona.* 2013. No. 4. [Online]. System requirements: AdobeAcrobatReader. URL: ivdon.ru/magazine/archive/n4y2013/2048. (date of reference: 09.09.2017). (rus)
2. Larin S.N. Modernizatsiya vosproizvodstva zhilishchnogo fonda regiona na osnove vnedreniya energosberegayushchikh tekhnologiy [Modernization of reproduction of the housing Fund of the region through the introduction of energy saving technologies] *Ekonomicheskiy analiz: teoriya i praktika.* 2013. No. 17(320). Pp. 33–39. (rus)
3. Chukanov S.V. Ekonomicheskoye povedeniye i metod dinamicheskogo programmirovaniya na beskonechnom vremennom intervale [Economic behavior and the method of dynamic programming on an infinite time interval]. *Matematicheskoye modelirovaniye.* 2003. No. 3(15). Pp. 109–121. (rus)
4. Mishchenko V.Ya. *Teoreticheskiye osnovy organizatsii ekspluatatsii i vosproizvodstva obyektov nedvizhimosti* [the Theoretical foundations of exploitation and reproduction of real estate]. Doctoral Thesis: 05.23.08. Voronezh, 2006. 442 p. (rus)
5. Sheina S.G. *Metodologiya strategicheskogo upravleniya tekhnicheskim sostoyaniyem zhilishchnogo fonda putem modelirovaniya i optimizatsii organizatsionno-tekhnologicheskikh resheniy* [Methodology of strategic management of the technical condition of housing stock by modeling and optimization of organizational and technological solutions]. Doctoral Thesis: 05.23.08. Rostov-na-Donu. 2008. 362 p. (rus)
6. Payne G., Majale M. *The Urban Housing Manual*. Earthscan. London, 2004. 134 p.
7. Clapp J.M., Eichholtz P., Lindenthal T. Real option value over a housing market cycle. *Regional Science and Urban Economics.* 2013. Vol. 43. No. 6. Pp. 862–874.
8. Menassa C.C. Evaluating sustainable retrofits in existing buildings under uncertainty. *Energy and Buildings.* 2011. Vol. 43. No. 12. Pp. 3576–3583.
9. Baek C.-H., Park S.-H. Changes in renovation policies in the era of sustainability. *Energy and Buildings.* 2012. Vol. 47. Pp. 485–496

Литература

1. Байрамуков С.Х., Долаева З.Н. Комплексный подход к проблеме модернизации жилищного фонда // Инженерный вестник Дона. 2013. № 4. [Электронный ресурс]. Систем.требования: AdobeAcrobatReader. URL: ivdon.ru/magazine/archive/n4y2013/2048 (дата обращения: 09.09.2017).
2. Ларин С.Н. Модернизация воспроизводства жилищного фонда региона на основе внедрения энергосберегающих технологий // Экономический анализ: теория и практика. 2013. № 17(320). С. 33–39.
3. Чуканов С.В. Экономическое поведение и метод динамического программирования на бесконечном временном интервале // Математическое моделирование. 2003. № 3(15). С. 109–121.
4. Мищенко В.Я. Теоретические основы организации эксплуатации и воспроизводства объектов недвижимости. Дисс. на соиск. учен. степ. д.т.н.: 05.23.08. Воронеж, 2006. 442 с.
5. Шеина С.Г. Методология стратегического управления техническим состоянием жилищного фонда путем моделирования и оптимизации организационно-технологических решений. Дисс. на соиск. учен. степ. д.т.н.: 05.23.08. Ростов-на-Дону, 2008. 362 с.
6. Payne G., Majale M. The urban housing manual. Earthscan. London, 2004. 134 p.
7. Clapp J.M., Eichholtz P., Lindenthal T. Real option value over a housing market cycle // Regional Science and Urban Economics. 2013. Vol. 43. № 6. Pp. 862–874.
8. Menassa C.C. Evaluating sustainable retrofits in existing buildings under uncertainty // Energy and Buildings. 2011. Vol. 43. № 12. Pp. 3576–3583.
9. Baek C.-H., Park S.-H. Changes in renovation policies in the era of sustainability // Energy and Buildings. 2012. Vol. 47. Pp. 485–496
10. Bellman R., Кalaba R. Dynamic Programming and Statistical Communication Theory // Proc. Nat. Acad. Sci. USA, Col. 1957. Vol. 43. Pp. 749–751.
11. Aris R., Nemhauser G.L., Wilde D. Optimization of multistage cyclic and branching system serial procedures // Journal of American Institute of Chemical Engineering. 1964. Vol. 10. № 6. Pp. 913–919.
12. Dreyfus S.E. An appraisal of some shortest-path algorithms // Operations Research. 1969. № 17. Pp. 395–412.

Байрамуков С.Х., Долаева З.Н. Динамическое программирование в оптимизации комплексной модернизации жилищного фонда // Инженерно-строительный журнал. 2017. № 8(76). С. 3–19.

10. Bellman R., Kalaba R. Dynamic Programming and Statistical Communication Theory. *Proc. Nat. Acad. Sci.* USA, Col. 1957. Vol. 43. Pp. 749–751.
11. Aris R., Nemhauser G.L., Wilde D. Optimization of multistage cyclic and branching system serial procedures. *Journal of American Institute of Chemical Engineering.* 1964. Vol. 10. No. 6. Pp. 913–919.
12. Dreyfus S.E. An appraisal of some shortest-path algorithms. *Operations Research.* 1969. No. 17. Pp. 395–412
13. Chen C.L., Sun D.Y., Chang C.Y. Numerical solution of dynamic optimization problems with flexible inequality constraints by iterative dynamic programming. *Fuzzy Sets and Systems.* 2002. Vol. 127. No. 2. Pp. 165–176.
14. Bayramukov S.H., Dolaeva Z.N. O metodakh dinamicheskogo programmirovaniya protsessov kompleksnoy modernizatsii zhilishchnogo fonda [On the methods of dynamic programming processes of comprehensive modernization of the housing stock]. *Vestnik Dagestanskogo gosudarstvennogo tekhnicheskogo universiteta.* 2015. No. 3(38). Pp. 56–63. (rus)
15. Kuhn K.D. Network-level infrastructure management using approximate dynamic programming. *Journal of Infrastructure Systems.* 2010. Vol. 16. No. 2. Pp. 103–111.
16. Flint A., Mei C., Murray D., Reid I. A dynamic programming approach to reconstructing building interiors. *Lecture Notes in Computer Science.* 2010. Vol. 6315 LNCS. P. 5. Pp. 394–407.
17. Noor-E-Alam Md., Doucette J. An application of infinite horizon stochastic dynamic programming in multi-stage project investment decision-making. *International Journal of Operational Research.* 2012. Vol. 13. No. 4. Pp. 423–438.
18. Ovchinnikov V.G. K algoritmam dinamicheskogo programmirovaniya optimalnykh protsessov [Dynamic programming algorithms of optimal processes]. *Vestnik Samarskogo gosudarstvennogo tekhnicheskogo universiteta. Seriya: Fiziko-matematicheskiye nauki.* 2012. No. 3(28). Pp. 215–218. (rus)
19. Popova O.N., Simankina T. L., Sokolovskiy N. D. Planirovaniye periodichnosti remonta zhilykh zdaniy na osnove dinamicheskogo programmirovaniya [Planning the periodicity of repair of residential buildings on the basis of dynamic programming]. *Sovremennaya nauka i innovatsii.* 2017. No. 2(18). Pp.177–191. (rus)
20. Bayramukov S.H., Dolayeva Z.N. Effektivnost energeticheskoy modernizatsii zhilishchnogo fonda. *Inzhenernyy Vestnik Dona.* 2015. No. 4. [Online]. System requirements: AdobeAcrobatReader. URL: ivdon.ru/ru/magazine/archive/n4p2y2015/3452. (date of reference: 09.09.2017). (rus)
21. Dolaeva Z.N., Kidakoeva M.M. Research of residential real estate pricing. *Sciences of Europe.* 2016. No. 8(8). Pp. 85–88.
22. Kolmogorov, O.I. Energoeffektivnaya modernizatsiya pri kapitalnom remonte obyektov zhilishchnogo fonda [Energy efficient modernization and capital repair of objects of housing]. *Vestnik grazhdanskikh inzhenerov*. 2012. No. 6(35). Pp. 234–238. (rus)
23. Venttsel, Ye.S. *Elementy dinamicheskogo programmirovaniya* [Elements of dynamic programming]. Moscow: Nauka, 1964. 176 p. (rus)
24. Popova O.N. *Metod kalendarnogo planirovaniya remonta zhilykh zdaniy na osnove ikh strukturnogo analiza* [The method of calendar planning for the repair of residential buildings on the basis of their structural analysis]. PhD Thesis: 05.23.08. Sankt-Peterburg, 2014. 206 p. (rus)
25. Chentsov A.G., Chentsov A.A. Dinamicheskoye programmirovaniye v zadache marshrutizatsii s ogranicheniyami i stoimostyami, zavisyashchimi ot spiska zadaniy [Dynamic programming in the routing problem with constraints and costs depending on the job list]. *Doklady*

13. Chen C.L., Sun D.Y., Chang C.Y. Numerical solution of dynamic optimization problems with flexible inequality constraints by iterative dynamic programming // Fuzzy Sets and Systems. 2002. Vol. 127. № 2. Pp. 165–176.
14. Байрамуков С.Х., Долаева З.Н. О методах динамического программирования процессов комплексной модернизации жилищного фонда // Вестник Дагестанского государственного технического университета, Технические науки. 2015. № 3(38). С. 56–63.
15. Kuhn K.D. Network-level infrastructure management using approximate dynamic programming // Journal of Infrastructure Systems. 2010. Vol. 16. № 2. Pp. 103–111.
16. Flint A., Mei C., Murray D., Reid I. A dynamic programming approach to reconstructing building interiors // Lecture Notes in Computer Science. 2010. Vol. 6315 LNCS. P.5. Pp. 394–407.
17. Noor-E-Alam Md., Doucette J. An application of infinite horizon stochastic dynamic programming in multi-stage project investment decision-making // International Journal of Operational Research. 2012. Vol. 13. № 4. Pp. 423–438.
18. Овчинников В.Г. К алгоритмам динамического программирования оптимальных процессов // Вестник Самарского государственного технического университета. Серия: Физико-математические науки. 2012. № 3(28). С. 215–218.
19. Попова О.Н., Симанкина Т. Л., Соколовский Н. Д. Планирование периодичности ремонта жилых зданий на основе динамического программирования // Современная наука и инновации. 2017. № 2(18). С. 177–191.
20. Байрамуков С.Х., Долаева З.Н. Эффективность энергетической модернизации жилищного фонда // Инженерный вестник Дона. 2015. № 4. [Электронный ресурс]. Систем.требования: AdobeAcrobatReader. URL: ivdon.ru/ru/magazine/archive/n4p2y2015/3452. (дата обращения: 09.09.2017).
21. Dolaeva Z.N., Kidakoeva M.M. Research of residential real estate pricing // Sciences of Europe. 2016. № 8(8). Pp. 85–88.
22. Колмогоров О.И. Энергоэффективная модернизация при капитальном ремонте объектов жилищного фонда // Вестник гражданских инженеров. 2012. № 6(35). С. 234–238.
23. Вентцель Е.С. Элементы динамического программирования. М.: Наука, 1964. 176 с.
24. Попова О.Н. Метод календарного планирования ремонта жилых зданий на основе их структурного анализа. Дисс. на соиск. учен. степ. к.т.н.: 05.23.08. Санкт-Петербург, 2014. 362 с.
25. Ченцов А.Г., Ченцов А.А. Динамическое программирование в задаче маршрутизации с ограничениями и стоимостями, зависящими от списка заданий // Доклады Академии наук. 2013. № 1 (453). С. 20.
26. ГОСТ 24866-99 «Стеклопакеты клееные строительного назначения».
27. СП 131.13330.2012 «Строительная климатология», актуализированная редакция СНиП 23-01-99*.
28. СП 50.13330.2012 «Тепловая защита зданий», актуализированная редакция СНиП 23-02-2003.
29. Жилищный фонд Карачаево-Черкесской республики в 2014 году/ Статистический бюллетень. Черкесск, 2015. 15 с.
30. СП 52.13330.2011 «Естественное и искусственное освещение», актуализированная редакция СНиП 23-05-95.
31. СП 60.13330.2012 «Отопление, вентиляция и кондиционирование», актуализированная редакция СНиП 41-01-2003.

Akademii nauk. 2013. No. 1(453). 20 p. (rus)

26. GOST 24866-99 *Steklopakety kleyenyye stroitelnogo naznacheniya* [Russian State Standard GOST 24866-99. Glass laminated construction purposes]. (rus)
27. SP 131.13330.2012 Stroitelnaya klimatologiya [Russian Set of Rules SP 131.13330.2012 Building climatology], aktualizirovannaya redaktsiya SNiP 23-01-99*. (rus)
28. SP 50.13330.2012 Teplovaya zashchita zdaniy [Russian Set of Rules SP 50.13330.2012 Thermal protection of buildings], aktualizirovannaya redaktsiya SNiP 23-02-2003. (rus)
29. Zhilishchnyy fond Karachayevo-Cherkesskoy respubliki v 2014 godu [The housing Fund of the Karachay-Cherkess Republic in 2013]. Statisticheskiy byulleten. Cherkessk. 2015. 15 p. (rus)
30. SP 52.13330.2011 Yestestvennoye i iskusstvennoye osveshcheniye [Russian Set of Rules SP 52.13330.2011 Natural and artificial lighting], aktualizirovannaya redaktsiya SNiP 23-05-95. (rus)
31. SP 60.13330.2012 Otopleniye, ventilyatsiya i konditsionirovaniye [Russian Set of Rules SP 60.13330.2012 Heating, ventilation and air conditioning], aktualizirovannaya redaktsiya SNiP 41-01-2003. (rus)

Salis Bayramukov,
+7(8782)29-35-52; salis_pochta@mail.ru

Zurijat Dolaeva,
+7(928)397-10-58; dolaeva.zu@mail.ru

Салис Хамидович Байрамуков,
+7(8782)29-35-52;
эл. почта: salis_pochta@mail.ru

Зурьят Нюзюровна Долаева,
+7(928)3971058; эл. почта: dolaeva.zu@mail.ru

doi: 10.18720/MCE.76.2

Hot metal droplets capture with centrifugal method

Улавливание горячих брызг металла центробежным методом

M.B. Kitain,
K.I. Strelets,
M.V. Petrochenko,
Peter the Great St. Petersburg Polytechnic University, St. Petersburg, Russia

Аспирант М.Б. Китаин,
канд. техн. наук, заместитель директора ИСИ К.И. Стрелец,
канд. техн. наук, ст. преподаватель М.В. Петроченко,
Санкт-Петербургский политехнический университет Петра Великого, г. Санкт-Петербург, Россия

Key words: hot metal droplets filtration; uniflow cyclone; weld spatter; air purification; explosive dust

Ключевые слова: фильтрация капель расплавленного металла; прямоточный циклон; разбрызгивание металла при сварке; воздухоочистка; воспламеняющаяся пыль

Abstract. Weld spatter properties and ways of spatter formation were analyzed in the article. It was deter-mined that solidified spatter can be considered as an active agent in environment pollution due to high dispersion, and there is a mass excess comparing with spatter spray. Hot metal droplets were used to track the flow of jets. The major part of spatter being under solidification has the size of 200 micron by dispersion and can be picked up by modern exhaust devices. The time of droplets solidification reaching heat content magnitudes able to cause firing of cloth filters in dust-tripping devices was determined during the experiment. There was elicited 100 % capture performance of hot metal droplets being under solidification in a uniflow cyclone CP-2500 (ЦП-2500) using marking tracers from particulate matter determination method.

Аннотация. В статье проанализирован механизм образования и свойства брызг металла при сварке. Определено, что застывшие брызги металла в силу высокой дисперсности являются активным загрязнителем окружающей природной среды и превышают по массе сварочный аэрозоль. Большая часть остывающих капель металла по дисперсному составу имеют размер от 200 мкм и улавливаются современными вытяжными устройствами. В эксперименте установлено время остывания капель до величин теплосодержания, способных вызывать загорание тканевых фильтров пылеочистных установок. Установлена 100 % эффективность задержки остывающих капель в прямоточном циклоне ЦП-2500 (CP-2500).

Introduction

Weld spatter is considered to be unfavorable welding wire consumption with low efficiency. It is accompanied by welding of spatters to the material that is used. It is claimed as a safety hazard, which may cause burns and fires. Several authors describe aspects and behavior of welding spatter in studies [1–4].

Also due to high dispersion solidified metal spatter can be considered as an active agent in environment pollution. Because the mass of spatter exceeds the mass of welding aerosol in hundred times. However, the part of metal spatters is not taken into account in estimation of hazardous emissions during welding.

Unfavorable consequences of metal sputtering make difference due to the use of air purifiers made on the basis of nonwoven polymer fabric during welding. Air-intake devices (AID) of filter and ventilation units (FVU) are arranged at a distance of 0.25–0.40 m from welding arc to ensure efficient performance. They take not less than 75 % of welding spray and a part of molten metal spatter flying to the surface of air-intake devices.

Group of scientists carried out CFD simulations and researches of the flow of uniflow cyclone [5]. They verified with the experimental results for different velocities profiles.

Китаин М.Б., Стрелец К.И., Петроченко М.В. Улавливание горячих брызг металла центробежным методом // Инженерно-строительный журнал. 2017. № 8(76). С. 20–27.

Authors from Korea Institute of Energy Research proceed numerical calculation with ANSYS Fluent CFD program to predict pressure loss and internal flow of uniflow cyclone at the plant of coal gasification [6].

Recently, other researchers studied flow pattern in adapted swirl generator and compared with standard design of uniflow cyclone. The description of investigated effect is approved by CFD simulation of the flow profile within the vane channels. They were evaluated by PIV measurements [7].

Other authors studied the effect of flow streams on particle movement in a uniflow cyclone separator. In simulation of movement solid particles in a flow field was used the Eulerian–Lagrangian approach [8].

The studies of hot gas filtration and implementation of different sorbents are described in several articles [9–11]. There was described a problem of explosion and burnings.

Scientists from KTH Royal Institute of Technology, Sweden held investigations of metal droplets on a polished cross section of slag samples by using a Scanning Electron Microscopy (SEM). They have classified all metal droplets in slag samples depending on their morphology. [12]

A number of experiments [13] were carried out to obtain the data on sizes, flying distance and temperature of molten metal spatter.

During the experiments was found out the following:

- Cooling metal droplets have spherical form.
- Solid droplets of sputtering metal with the temperature of + 400 ^{0}C make it possible to melt totally polyester filter fabric. Droplets with the temperature of + 600 ^{0}C contribute to coking of welded edges.
- The major part of solid metal droplets (up to 85 %) with final temperature 400 ÷ 600 ^{0}C fly to the distance of up to one meter from a welding joint. The maximum dispersion accounts to 2 meters.
- Initial velocity of drops flying-off from welding blowpipes is equal to 8 ÷ 14 m/s.
- Average velocity of free settling of drops with the mass of 7.8 g is equal to 4.4 m/s.
- The major mass – 95 % of drops get cold up to the temperature below radiance (less than 600 ^{0}C) within less than 0.25 s.
- Sizes of droplets are their fall diameters, which make it possible to classify them as dust, and are enough to be picked up by exhaust devices and be travelled along ducts.

The aim of this article is characterize the experimental capturing of hot metal droplets in swirling flow. According to the previous articles on metal sputtering [14–18] the fact and the reason are identified, but they do not define initial velocity and rate decreasing of temperature including the context of drops and fractures. To achieve the aim was set a task to make several experiments with highlighted particles.

Methods and Results

Such dry inertial separators as settling chambers, louvered dust collectors and cyclones with centrifugal force are applied in industry to slow down motion of hot solid metal drops produced during welding or cutting processes. [19]

Industrial developers of such devices use the term – spark arrestors. But it is not accessible in the case of noncombustible metal droplets. According to the Russian State Standard GOST 53323-2009 “Flame arresters and spark catchers. General specifications. Testing methods” it is stated that a dry-type spark catcher is a device to be placed on exhaust manifolds of different vehicles and power units, which ensures that spatter of combustibles should be caught and extinguished, which is normally formed by furnace or internal combusting engine operation. A cooling droplet is not combustible. Its extinguishing is considered as heat power decrease up to the define values. That do not cause fire-hazardous materials to catch fire during any contact. This decrease is possible when heat is transferred to air and materials of dust collectors.

Cooling droplets in settling chambers and louvered dust collectors change their direction of rectilinear motion striking surfaces of dust collectors. In the case of cyclones with centrifugal force cooling solid droplets move keeping more complicates and longer tracks and strike cyclone walls.

Change of direction when it comes to rectilinear motion of cooling solid droplets was used by different manufactures in the following units: type “JETCLEAN” ZAO (CJSC) Konsar (Russia) – labyrinth filter, type FILTERCUBE Company TEKA (Germany) – cooper louvered filter, filter and ventilation unit of ZAO (CJSC) SovPlym (Russia) PMSF and others – settling chamber. Centrifugal motion of cooling droplets is used in uniflow cyclone – a spark arrestor “SPARKSHIELD” of the ventilation company “Plymovent Group” (Netherlands) and in cyclones – spark catcher TSG-1 ÷ 20 (ЦГ-1 ÷ 20) ZAO (CJSC) SPACE-MOTOR (Russia). The mechanism of collecting solid metal droplets during welding or cutting in these devices was not described. The effectiveness of temperature decreasing of droplets was not determined.

The experimental research of catching heated droplets of solid metal using centrifugal method was carried out with experimental unit on the basis of uniflow cyclone CP-2500 (ЦП-2500).

The uniflow cyclone CP-2500 (ЦП-2500) that is produced by SovPlym Ltd. since 2003 according to the Specifications (TU) 346-009-05159840-2003. At the entry of the cyclone the air flow is whirled by axial air mover. Large particles of dust are dropped out to the cyclone walls under centrifugal force and are headed to a dust chamber through a side connector. Cylindrical louvered grills inside the cyclone and inertial dust chamber additionally increase separation process and ensure high effectiveness of the cyclone [20]. The overall dust collecting effectiveness of the cyclone is around for 90.4 %.

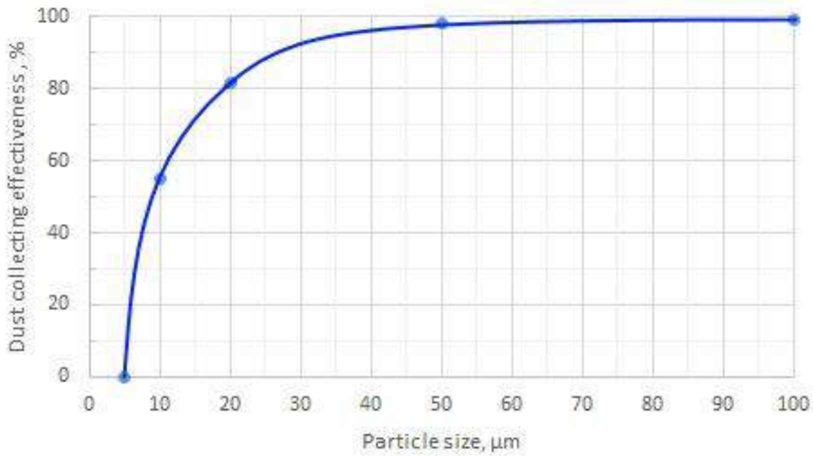

Figure 1. Dust collecting effectiveness in fractures

An estimated time for dust particles staying in the cyclone is equal to 0.15 sec [21, 22].

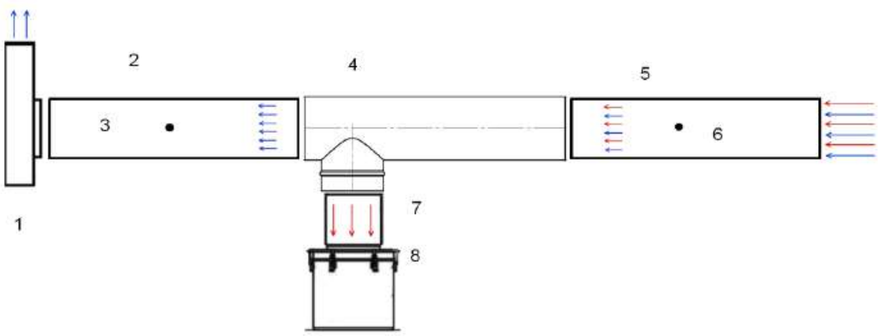

Picture 2. Scheme of the experimental unit

1 – a fan featured by frequency control TEF-600,

2 and 5, 7 – translucent ducts,

3 and 6 – tracers to mark hot particles,

4 – cyclone CP-2500 (ЦП-2500),

8 – dust collector.

← heated metal droplets,

← welding spray.

Metal spatter was formed due to semi-automatic welding. It was used building-up technique in the protective medium: mixture of argon and carbon dioxide; 8mm diameter wire “Св08Г3С”. Current is 120 A, voltage is 19.8 V. Speed of wire feed is 6.6 m/min. Adapters with filters of the type “АФА-ВП-20” were used as tracers to mark hot metal droplets. They were placed in the section center of translucent air ducts. The material “АФА” is based on perchlorovinyl fibre. Perchlorovinyl fibre is not flammable. Decomposition temperature for perchlorovinyl is equal to 130–140 ^{0}C.

Hydraulic resistance of the system was 1645 Pa. It was measured in air ducts before and after cyclone at airflow rate 3400 m^3/h. Parameters were measured using a differential manometer DT-8890 with a receiver of total and static pressure Pitot tube. Results and estimations are shown in the Table.

Table 1.

№	Pressure sensing point	Pd, Pa	Pv, Pa	Ps, Pa	V, m/s	Q, m3/h	∆Pv, Pa
1	before cyclone work	220	530	750	19.1	3382	1645
2	after cyclone work	225	2175	2400	19.3	3420	

Recording was held during experiment where hot droplets flow through translucent air ducts. Continuous light emission in the translucent air duct was seen at the entry of the cyclone, and single tracks of hot droplets were seen before the dust chamber. As a result there were no luminous tracks at the exit of the cyclone.

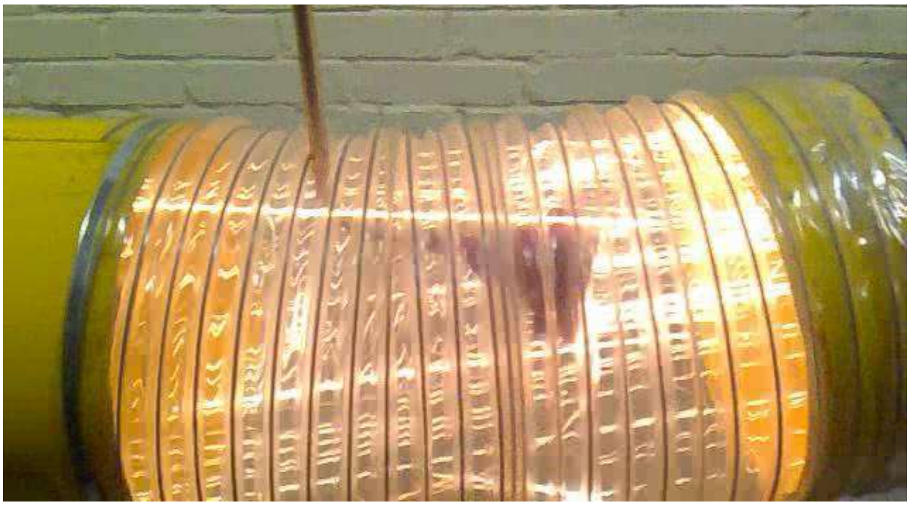

Figure 3. Tracks of hot metal droplets at the entry of the cyclone

The distance to the welding arc is 2 meters. A marking tracer – dust receiving adapter is arranged in the center of the air duct. Tracers to mark hot metal droplets were used to identify whether they appeared or not in the flow before and after cyclone work.

before cyclone work **after cyclone work**

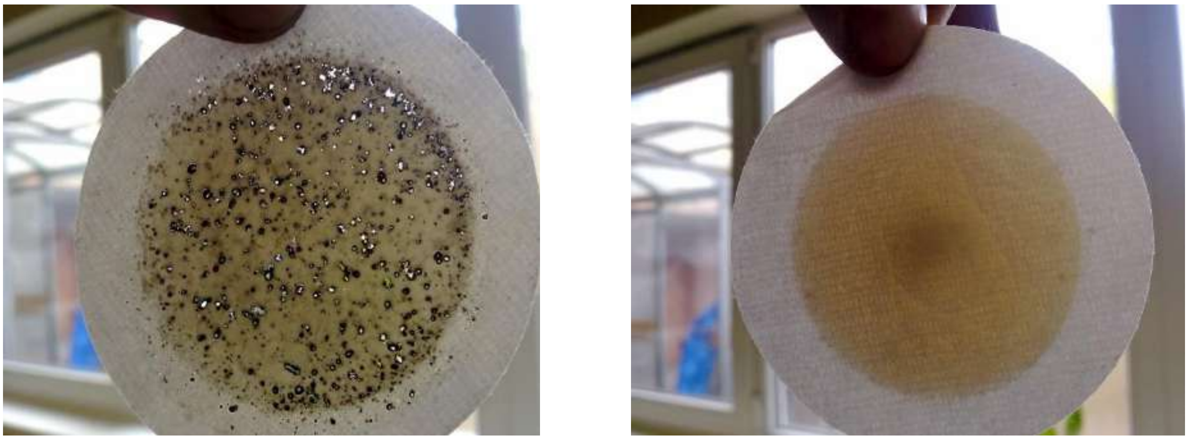

Figure 4. Marking tracers before and after cyclone work (1:1)

Kitain M.B., Strelets K.I., Petrochenko M.V. Hot metal droplets capture with centrifugal method. *Magazine of Civil Engineering*. 2017. No. 8. Pp. 20–27. doi: 10.18720/MCE.76.2.

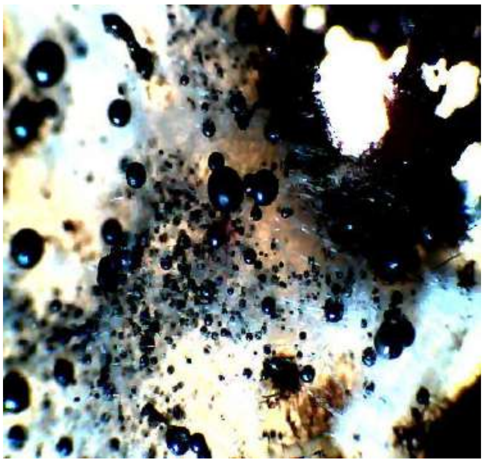

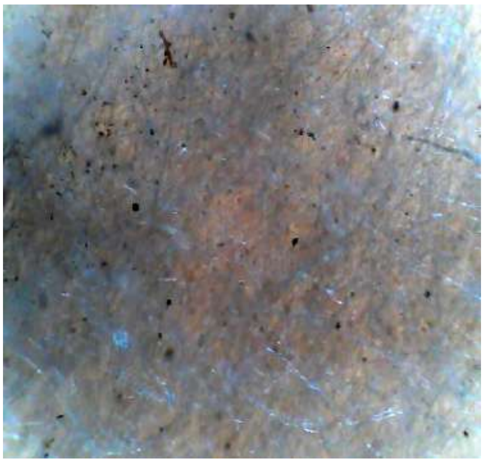

1:50 **1:10**

Picture 5. Solidified droplets of metal spatter, 50μm on filter fiber

Perchlorovinyl fibre that was used as marking tracers, can be melted at the temperature of 130–140 ^{0}C. Droplets with the size of 50 μm in diameter and less, which were suspended of the fiber surface of the first marking tracer, had heat output, which was not enough for melting. Larger droplets went through, burnt in and made fiber charred and darkened. On the second marking tracer we can see single solidified droplets, which sizes are ten times less than were picked up by the first marking tracer. On the marker after the cyclone there were no burning droplets and going through the fiber particles.

During analysis of video snapshots was received additional information about motion of particles in the cyclone (CP) ЦП and motion of hot metal droplets. In the flow entering of device can be already observed the effect of air mover for circular whirled flows. It also can be seen how the air flow changes from rectilinear motion into circular before it enters the cyclone. When the spinning flow goes to the dust receiver single hot particles continue to move in a circular manner going on in the dust receiver. Then leave the traces of their motion to the bottom.

Discussion

Mechanism of metal spatter formation and its danger

Sputtering of liquid electrode metal is caused by gas-dynamic impact. It emerges when a bonding strip between a welding wire and a droplet is broken transferring to a molten pool. The pressure emerged is radially forwarded away from the point of disruption. When this occurs there is a possibility of liquid metal slopping in the area of both a bonding strip and an electrode tip. A liquid droplet rapidly solidifies when flying out of the arc zone. The initial temperature of the solid particle is about 1500 up to 1130 ^{0}C. [5, 6, 23, 24]

The coefficient of electrode metal loss during sputtering ψ is determined by the difference between the masses of metal consumed and metal weld. An actual value of ψ for covered electrodes may vary within the limits 5–20 %. In the case of stable welding processes when carbon dioxide gas with 2 mm diameter electrodes is used, the value ψ accounts for 5–8 % and does not exceed 15 %, and in the case of CO_2+Ar – 5–7 %. About 10–30 % of molten metal spatter formed while welding under average regime depending on physical welding conditions stick and is welded to working area of nozzles, current contact tips (CCT) being part of welding blowpipes, and detecting devices in welding machines and robots. The rest part – much minor droplets – (as drops in a liquid state and as solid spherical particle in a state of crystallization), fly away from a welding seam.

Metal spatter during crystallization has spherical form. Maximum size of spatter is a bit more than the diameter of welding wire, the minimum size may account for tenths or a hundredths of a millimeter. The major part of spatter in the case of stable welding processes can be attributed to the droplets of the size equal to 2/3 of the wire diameter. Depending on technological conditions of welding molten metal spatter can be classified as small (< 0.2 mm), medium (0.2–0.5 mm) and large (> 0.5 mm). [7–9]

The temperature of molten metal droplets (spatter) reaches to 250–500 °C in a second after a contact with the surface. Also temperature depends on the contact diameter of their interaction and the thickness of the metal being welded, and in a 6–7 seconds heat generation is almost equal to 0. [25]

Estimations according to Russian State Standard GOST (ГОСТ) 12.1.004-91 show that the molten metal droplet under crystallization with the size of 5-mm in diameter keeps the temperature of 852 ^{0}C in 1.1 seconds after its formation and may transfer 0.16 Joule of heat to the environment, and that is enough for major part of combustibles to ignite.

When horizontal welding the largest and heaviest droplets of molten metal are welded to the metal and stay on the manufactured object in the area of approximately 200 mm away from the welding seam. Metal droplets which are getting cold fly down during the process of vertical and overhead welding.

Flying droplets of the metal under crystallization appeared to be flying sparks of different radiance. Colors of various gradients like yellow and white or yellow and red indicate that the temperature of the steel, which is getting cold, is 1200–900 ^{0}C. A quenched spark of barely discernible dark brown color has the temperature of 550 degrees ^{0}C. This autoignition temperature of most combustibles is much higher than +70 ^{0}C, and it may cause first-degree burns of skin after the contact with the object heated within over 1 second. [26]

Due to high dispersion solidified metal spatter can be considered an active agent in environment pollution, and there is a mass excess comparing with spatter spray. The major part of spatter being under solidification has the size of 200 micron by dispersion and can be picked up by modern exhaust devices.

Conclusions

1. An experimental installation for research performance of hot metal drops catching was constructed from uniflow cyclone CP-2500 (ЦП-2500) with air swirl generator, inlet louvered grill and dust collecting tank.
2. Experiment was held with marking tracers from particulate matter determination method.
3. The video was recorded to track the flow of jets which were formed by hot metal droplets
4. Was demonstrated that the process to separate hot metal drops in the uniflow cyclone causes the temperature drop of flying droplets from 800 up to 130 ^{0}C and less. Particles get cold in the cycle within 0.15 sec which is less than cooling process when they are idle – 0.25 ÷ 0.5 sec.
5. Was demonstrated that CP-2500 (ЦП-2500) construction ensure that 100 % of fire-hazardous solid hot metal droplets are picked up.

Consequently, it was first described in the research an opportunity to catch hot metal droplets and avoid ignition of explosive dust.

References

1. Yanqiua Y., Jianchun F. Research on fusion characteristics of sulfur dust and risk control of the explosion. *Procedia Engineering.* 2014. Vol. 84. Pp. 449–459.
2. Chang B., Blackburn J., Allen C., Hilton P. Studies on the spatter behaviour when welding AA5083 with a Yb-fibre laser. *The International Journal of Advanced Manufacturing Technology.* 2016. Vol. 84. Pp. 1769–1776.
3. Koseki H. Study and countermeasure of hazard of dust explosion of various toner cartridges. *Procedia Engineering.* 2014. Vol. 84. Pp. 273–279.
4. Taveau J. Application of dust explosion protection systems. *Procedia Engineering.* 2014. Vol. 84. Pp. 297–305
5. Mokni I., Dhaouadi H., Mhiri H., Lepalec G. CFD Simulation Of The Flow Field In A Uniflow Cyclone Separator. *Engineering Letters.* 2009. No. 17. P. 3.
6. Oh J., Choi S., Jin G.T., Kim J., Lee S. Advanced Particle Separation with the Concept of Uniflow Cyclone. *Proceedings of the Twenty-second International Offshore and Polar Engineering Conference*. 2012. Pp. 16–22.
7. Pillei M., Kofler T., Kraxner M. A swirl generator design approach to increase the efficiency of uniflow cyclones. *17th International Symposium on Application of Laser Techniques to Fluid Mechanics.* Lisbon, 2014. P. 3.
8. Oh J., Choi S., Kim J. Numerical simulation of an internal flow field in a uniflow cyclone separator. *Powder Technology.* 2015. Vol. 274. Pp. 135–145.
9. Feng Y., Li Y., Shi L., Wu M., Mi J. Effect of preparation method of active component on the cycling performance of sorbents for hot coal gas clean-up. *Canadian Journal of*

Литература

1. Yanqiua Y., Jianchun F. Research on fusion characteristics of sulfur dust and risk control of the explosion // Procedia Engineering. 2014. Vol. 84. Pp. 449–459.
2. Chang B., Blackburn J., Allen C., Hilton P. Studies on the spatter behaviour when welding AA5083 with a Yb-fibre laser // The International Journal of Advanced Manufacturing Technology. 2016. Vol. 84. Pp. 1769–1776.
3. Koseki H. Study and countermeasure of hazard of dust explosion of various toner cartridges // Procedia Engineering. 2014. Vol. 84. Pp. 273–279.
4. Taveau J. Application of dust explosion protection systems // Procedia Engineering. 2014. Vol. 84. Pp. 297–305.
5. Mokni I., Dhaouadi H., Mhiri H., Lepalec G. CFD Simulation Of The Flow Field In A Uniflow Cyclone Separator // Engineering Letters. 2009. № 17. P. 3.
6. Oh J., Choi S., Jin G.T., Kim J., Lee S. Advanced Particle Separation with the Concept of Uniflow Cyclone // Proceedings of the Twenty-second International Offshore and Polar Engineering Conference. 2012. Pp. 16–22.
7. Pillei M., Kofler T., Kraxner M. A swirl generator design approach to increase the efficiency of uniflow cyclones // 17th International Symposium on Application of Laser Techniques to Fluid Mechanics. Lisbon. 2014. P. 3.
8. Oh J., Choi S., Kim J. Numerical simulation of an internal flow field in a uniflow cyclone separator // Powder Technology. 2015. Vol. 274. Pp. 135–145.
9. Feng Y., Li Y., Shi L., Wu M., Mi J. Effect of preparation method of active component on the cycling performance of sorbents for hot coal gas clean-up // Canadian Journal of Chemical Engineering. 2017. Vol. 95. № 11.

Chemical Engineering. 2017. Vol. 95. No. 11. Pp. 2087–2095.

10. Mertzis D., Koufodimos G., Kavvadas I., Samaras Z. Applying modern automotive technology on small scale gasification systems for CHP production: A compact hot gas filtration system. *Biomass and Bioenergy.* 2017. Vol. 101. Pp. 9–20.
11. Yang L., Ji Z., Wu X., Ma W. Application and operating experience of sintered metal fiber hot gas filters for FCC unit. *Procedia Engineering.* 2015. Vol. 102. Pp. 1073–1082.
12. Yang A., Karasev A., Jönsson G. Characterization of metal droplets in slag after desulfurization of hot metal. *ISIJ International.* 2015. No. 3. Pp. 570–577.
13. Vatin N.I., Strelec K.I., Kitain M.B. Opredelenie harakteristik svarochnyh iskr dlja rascheta ih udalenija v ciklone [Determination of the characteristics of welding sparks to calculate their removal in a cyclone]. *Magazine of Civil Engineering.* 2011. No. 23. Pp. 25–30. (rus)
14. Solodskij S.A., Brunov O.G. Vlijanie gazodinamicheskogo udara na razbryzgivanie jelektrodnogo metalla pri svarke v aktivnyh gazah [Influence of gas-dynamic impact on splashing of electrode metal during welding in active gases]. *XIII Mezhdunarodnaya nauchno-prakticheskaya konferenciya studentov, aspirantov i molodyh uchenyh TPU: tezisy dokladov* [XIII International scientific-practical conference of students, graduate students and young scientists of TPU]. Tomsk: TPU, 2007. Pp. 363–365. (rus)
15. Hejfec A.L., Pinchuk I.S., Postaushkin V.F. Rol' ehlektricheskogo vzryva peremychki i silovogo vozdejstviya dugi v razbryzgivanii metalla pri svarke s korotkimi zamykaniyami [The role of an electric explosion of the web and the power action of the arc in the spattering of metal when welding with short circuits]. *Avtomaticheskaya svarka.* 1978. No. 10. Pp. 26–28. (rus)
16. Potap'evskij G.V., Lavpishchev V.YA. Pazbpyzgivanie pri svapke v uglekislom gaze provolokoj Sv-08G2S. [Disintegration during welding in carbon dioxide gas with a wire Sv-08G2S]. *Avtomaticheskaya svarka.* 1972. No. 8. Pp. 39–42. (rus)
17. Fed'ko V.T. Teorija, tehnologija i sredstva snizhenija nabryzgivanija i trudoemkosti pri svarke v uglekislom gaze [Theory, technology and means of reducing spraying and labor intensity in welding in carbon dioxide]. Tomsk: Tomsk State University, 1998. 432 p. (rus)
18. Dmitrik V.V., Glushko A.V. K obrazovaniju bryzg rasplavlennogo metalla pri dugovoj svarke v srede uglerodistogo gaza [To the formation of sparks of molten metal during arc welding in a carbon dioxide environment]. *Energy saving. Power engineering. Energy audit.* 2011. No. 12. Pp. 43–49. (rus)
19. Strelets K., Petrochenko M., Girgidov A. Energy performance of particle settling in cyclone. *Applied Mechanics and Materials.* 2015. Pp. 1363–1371.
20. Zajcev N.O. *Gidravlicheskij raschet prjamotochnyh ciklonov. Diss. na soisk. uchen. step. kan. tech. nauk: Spets. 23.05.16* [Hydraulic calculation of direct-flow cyclones. Cand. Tech. sci. diss]. Saint-Petersburg. 2007. 116p. (rus)
21. Vatin N.I., Strelec K.I. Ochistka vozduha pri pomoshhi apparatov tipa ciklon [Air cleaning with cyclone type devices]. SPb.: SPbGPU, 2003. 65 p. (rus)
22. Vatin N.I., Strelec K.I. Ochistka vozduha kak vazhnejshee napravlenie jekotehniki vozdushnoj sredy. Metodika rascheta i vozmozhnost' povyshenija jeffektivnosti pyleulavlivanija apparatov tipa ciklon [Air purification as the most important direction of environmental engineering of the air environment. The calculation procedure and the possibility of increasing the efficiency of the dust collection of cyclone type devices]. *Inzhenernye sistemy.* 2005. No. 3 (19). Pp. 63–64. (rus)

Pp. 2087–2095.

10. Mertzis D., Koufodimos G., Kavvadas I., Samaras Z. Applying modern automotive technology on small scale gasification systems for CHP production: A compact hot gas filtration system // Biomass and Bioenergy. 2017. Vol. 101. Pp. 9–20.
11. Yang L., Ji Z., Wu X., Ma W. Application and operating experience of sintered metal fiber hot gas filters for FCC unit // Procedia Engineering. 2015. Vol. 102. Pp. 1073–1082.
12. Yang A., Karasev A., Jönsson G. Characterization of metal droplets in slag after desulfurization of hot metal // ISIJ International. 2015. № 3. Pp. 570–577.
13. Ватин Н.И., Стрелец К.И., Китаин М.Б. Определение характеристик сварочных искр для расчета их удаления в циклоне // Инженерно-строительный журнал. 2011. № 5(23). С. 25–30.
14. Солодский С.А., Брунов О.Г. Влияние газодинамического удара на разбрызгивание электродного металла при сварке в активных газах. // XIII Международная научно-практическая конференция студентов, аспирантов и молодых ученых СТТ: тезисы докладов. Томск: СТТ, 2007. С. 363–365.
15. Хейфец И.С., Пинчук В.Ф., Постаушкин В.Ф. Роль электрического взрыва перемычки и силового воздействия дуги в разбрызгивании металла при сварке с короткими замыканиями // Автоматическая сварка. 1978. № 10. С. 26–28.
16. Потапьевский Г.В., Лаврищев В.Я. Разбрызгивание при сварке в углекислом газе проволокой Св-08Г2С. // Автоматическая сварка. 1972. № 7. С. 39–42.
17. Федько В.Т. Теория, технология и средства снижения набрызгивания и трудоемкости при сварке в углекислом газе. Томск: Изд-во Том. ун-та, 1998. 432 с.
18. Дмитрик В.В., Глушко А.В. К образованию брызг расплавленного металла при дуговой сварке в среде углеродистого газа // Энергосбережение. Энергетика. Энергоаудит. 2011. № 12. С. 43–49.
19. Strelets K., Petrochenko M., Girgidov A. Energy performance of particle settling in cyclone // Applied Mechanics and Materials. 2015. Pp. 1363–1371.
20. Зайцев Н.О. Гидравлический расчет прямоточных циклонов: Дис. на соиск. учен. степ. к.т.н.: Спец. 05.23.16. Санкт-Петербург, 2007. 116 с.
21. Ватин Н.И., Стрелец К.И. Очистка воздуха при помощи аппаратов типа циклон. СПб.: Изд-во СПбГПУ, 2003. 65 с
22. Ватин Н.И., Стрелец К.И. Очистка воздуха как важнейшее направление экотехники воздушной среды. Методика расчета и возможность повышения эффективности пылеулавливания аппаратов типа циклон // Инженерные системы. 2005. № 3(19). С. 63–64.
23. Коновалов Ю.Н. Сравнение свойств универсального инверторного источника питания сварочной дуги «Магма-315» и традиционных выпрямителей для механизированной сварки. // Сварка и диагностика, 2007. № 2. С. 23.
24. Иванова В.П., Аникина А.Д., Брюховец Д.Ф. Основные сведения об изготовлении машин. М.: Машиностроение, 1966. 344с.
25. Сапожков С.Б. Исследование взаимодействия брызг расплавленного металла с поверхностью свариваемого изделия и разработка средств снижения набрызгивания при сварке в СО2. Дис. на соиск. учен. степ. к.т.н.: Спец. 05.03.06. Югра, 1999. 138 с.
26. НИИ ПБ и ЧС. Установление причины пожара. Применяемые методы (определение тепловой энергии и температуры искр). Минск, 2002.

Китаин М.Б., Стрелец К.И., Петроченко М.В. Улавливание горячих брызг металла центробежным методом // Инженерно-строительный журнал. 2017. № 8(76). С. 20–27.

23. Konovalov Y.N. Sravnenie svojstv universal'nogo invertornogo istochnika pitaniya svarochnoj dugi «Magma-315» i tradicionnyh vypryamitelej dlya mekhanizirovannoj svarki [Comparison of the properties of the universal inverter power supply source of the welding arc «Magma-315» and traditional rectifiers for mechanized welding]. *Magazine of Welding and Diagnostics.* 2007. No. 2. P. 23. (rus)
24. Ivanova V. P., Anikina A. D., Bryuhovec D. F. *Osnovnye svedeniya ob izgotovlenii mashin* [Basic information about the manufacture of machines]. Moscow: Mashinostroenie, 1966. 344p. (rus)
25. Sapozhkov S.B. *Issledovanie vzaimodejstvija bryzg rasplavlennogo metalla s po-verhnost'ju svarivaemogo izdelija i razrabotka sredstv snizhenija nabryzgivanija pri svarke v CO2. Diss. na soisk. uchen. step. kan. tech. nauk: Spets. 05.03.06.* [Investigation of the interaction of splashes of molten metal with the surface of the welded product and the development of means for reducing spraying when welding in CO2. Cand. Tech. sci. diss]. Ugra: 1999. 138p. (rus)
26. NII PB i CHS. *Ustanovlenie prichiny pozhara. Primenyaemye metody (opredelenie teplovoj ehnergii i temperatury iskr)* [Determination of the cause of the fire. Applied methods (determination of thermal energy and temperature of sparks)]. Minsk, 2002. (rus)

Mikhail Kitain,
+7(921)934-47-36; mikhail.kitain@gmail.com

Kseniya Strelets,
+7(812)552-94-60; kstrelets@mail.ru

Marina Petrochenko,
+7(812)552-94-60; mpetroch@mail.ru

Михаил Борисович Китаин,
+7(921)934-47-36;
эл. почта: mikhail.kitain@gmail.com

Ксения Игоревна Стрелец,
+7(904)668-76-64; эл. почта: kstrelets@mail.ru

Марина Вячеславовна Петроченко,
+7(812)552-94-60; эл. почта: mpetroch@mail.ru

doi: 10.18720/MCE.76.3

Bearing capacity of rafter systems made of steel thin-walled structures in attic roofs

Несущая способность стропильной системы из стальных тонкостенных конструкций в чердачных крышах

V.A. Rybakov
Peter the Great St. Petersburg Polytechnic University, St. Petersburg, Russia
M. Al Ali
Technical University in Košice, Košice, Slovak Republic
A.P. Panteleev,
K.A. Fedotova,
A.V. Smirnov,
Peter the Great St. Petersburg Polytechnic University, St. Petersburg, Russia

Канд. техн. наук, доцент В.А. Рыбаков
Санкт-Петербургский политехнический университет Петра Великого, г. Санкт-Петербург, Россия
канд. техн. наук, заведующий кафедрой М. Ал Али
Технический университет г. Кошице, г. Кошице, Словакия
студент А.П. Пантелеев,
студент К.А. Федотова,
студент А.В. Смирнов,
Санкт-Петербургский политехнический университет Петра Великого, г. Санкт-Петербург, Россия

Key words: stress strain state; force method; statically indeterminate systems; attic roofs; steel thin-walled structures; timber rafter structures

Ключевые слова: напряженно-деформированное состояние; метод сил; статически неопределимые системы; чердачные крыши; легкие стальные тонкостенные конструкции; деревянные стропильные системы

Abstract. In the article as an alternative of strengthening of existing rafters or replacing them by new timber elements there is an offer to consider the replacing timber rafters by elements of steel thin-walled structures (STWS). The authors have proposed the methodology for calculation the statically indeterminate frame structures with the use of force method. Selected sections of rafters made of STWS and timber for various constructive schemes of pitched roofs were analyzed. The results shown that using of STWS reduces the major repair cost by 13.5 % due to less material consumption compared with a timber structure.

Аннотация. В статье в качестве альтернативы деревянным стропильным конструкциям крыш предлагается рассмотреть вариант устройства стропильной системы из легких стальных тонкостенных конструкций. Предложена методика расчета статически неопределимых стропильных рамных конструкций с использованием метода сил. В результате анализа напряженно-деформированного состояния элементов подобраны сечения стропильных ног из ЛСТК и из дерева для различных конструктивных схем скатных кровель. Показано, что применение ЛСТК позволяет снизить стоимость капитального ремонта скатных крыш на 13,5 % за счет меньшего расхода материалов по сравнению с деревянными стропильными конструкциями.

Introduction

The roof is a construction that transfers the dead load, climatic and other kinds of acting load to the bearing sub-structure. Besides its technical functions, the roof structure creates the most important architectural element of the building.

According to accessible data from the Housing Committee of St. Petersburg, the total roofs area of St. Petersburg is more than 24 million square meters. More than 50 percent of these roofs are in dissatisfactory condition. In the historic center, the roofs area is more than 8 million square meters. The actual unfavourable state of these roofs raise a question of their needed partial and/or overall repairing [1].

Рыбаков В.А., Ал Али М., Пантелеев А.П., Федотова К.А., Смирнов А.В. Несущая способность стропильных систем из стальных тонкостенных конструкций в чердачных крышах // Инженерно-строительный журнал. 2018. № 8(76). С. 28–39.

Nowadays, many researches in the pitched roof repair field are focused on the technologies of roofing. In addition, special attention is paid to repair the roofs for the roofing the operated space (so-called attic). This category is dealt in the work of V.P. Semenikhina, which investigated the causes and factors that reduce the operating parameters of the sloping surfaces of the combined type and formed an effective organizational and technological solutions to reduce the cost and complexity of work on the roofing and repair of combined inclined roofs [2].

Problems of pitched roofs is also dealt in the works of famous scientists: V.B. Belevich [3], N.D. Boyko, Y.G. Krupnik, N.S. Kocharian, and others. Most scientists involved in individual issues related to the defects, damages, roofing, repair and reconstruction of sloping roofs, without considering their complex.

Thus, nowadays, versions of constructive solutions sloping attic pitched roofs with using STWS and how to replace the traditional timber elements by steel thin-walled elements are insufficiently understood.

The construction of buildings, based on steel thin-walled structures (STWS) is a type of innovation fast frame construction. As a direct alternative to timber frame construction, as well as other traditional types of constructions, this technology has a number of advantages, foremost among which are the speed of construction, environmental friendliness and low cost of construction in most cases. is an technology of building erection it is really cheaper. The absence of welding and wet processes makes STWS really quickly erectable technology [4, 8, 23].

The aim of the article is to create an universal calculation procedure, that allows the assessing of stress-strain state of the structures during major repairs and/or replacing of timber structures, that are in an emergency condition.

Recent years, Russia is actively engaged in the development and research of new designs of STWS. Works of E.L. Airumyan, [4], I.I. Vedyakov, [5] and others are focused on the investigation of the designs of bearing frame structures, solid-walls or lattice (truss) crossbars of thin-walled profiles up to 3 mm thick. Numerical and experimental researches of bolted joints, as well as connections to the self-tapping screws are presented by B.I. Belyaev, [6] V.S. Kornienko, and others. N.P. Abovsky and L.V. Endzhievsky proposed a method of sheet elements connection by means of special washers, forming the keyed-bolt connection. B.M. Veynblat and G.I. Buneev found, that the difference of thickness of connected elements has an impact on the carrying capacity of bolted connections. [7]

The theory of steel thin-walled structures with open cross-section was described by the authors of a large number of scientific papers devoted to this subject. The large majority researcments are based on works by V. Z. Vlasov[8].

During the development of this theory many kinds of proposals were presented for its amendment, related to "attempts rejection of the hypothesis lack of progress and take into account the most impact deformation shift work thin-walled bar" in the works of Dzhanelidze and Panovko, [9] Goldenveiser, Vorobyov [10] , Meshcheryakov [11,12].

In Peter the Great St. Petersburg Polytechnic University active research of STWS is conducted. Experiments, computer modeling and simulation of STWS, in particular their local buckling and connections, as well as the implementation of the results into practice are realized within the mentioned research [13–23].

Methods of research

A vast number of constructive schemes could be considered and applied for rafter roofs repair. The exact number depends on rafter distance, span and slope angle variety. Consequently, it is quite difficult to use any software to get solution in general.

That’s why main method, used for achieving the research goals, was t-force method.

Goal of the investigation: expedience rationale of STWS using during major repair of pitched roofs.

The investigation procedure:

1. Solving the static problem in an analytical form for typical construction schemes roof systems developed in album series 1.169.5 " Constructive solutions of timber rafters under metal roof" of "LenzhilNIIproekt" (see Figures 1–5).

2. Choosing the suitable section of STWS rafter.

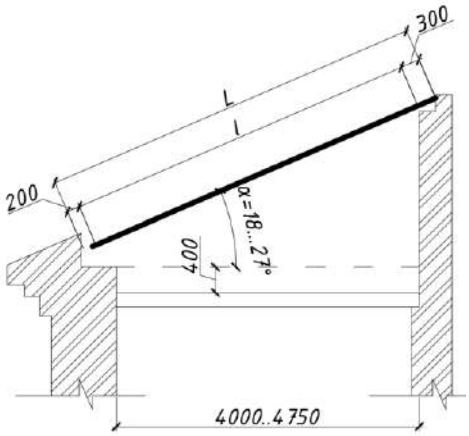

Figure 1. Non-combined rafters without braces

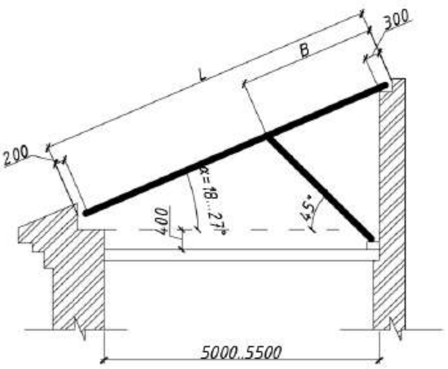

Figure 2. Non-combined rafters with braces

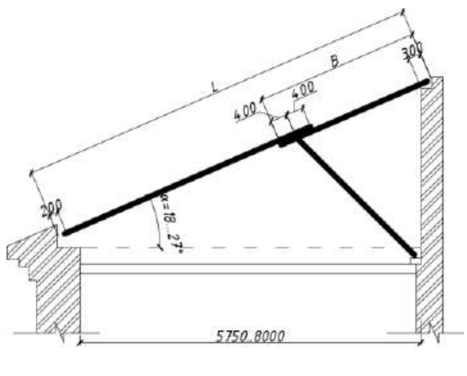

Figure 3. Combined rafters with braces

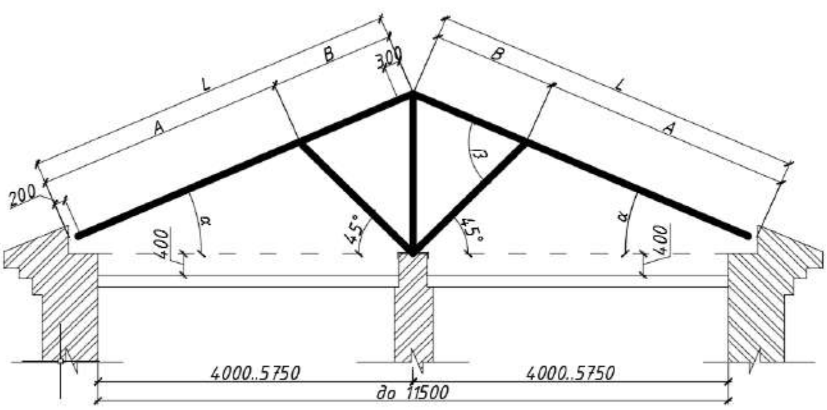

Рыбаков В.А., Ал Али М., Пантелеев А.П., Федотова К.А., Смирнов А.В. Несущая способность стропильных систем из стальных тонкостенных конструкций в чердачных крышах // Инженерно-строительный журнал. 2018. № 8(76). С. 28–39.

Figure 4. Non-combined rafter systems for saddle roofs

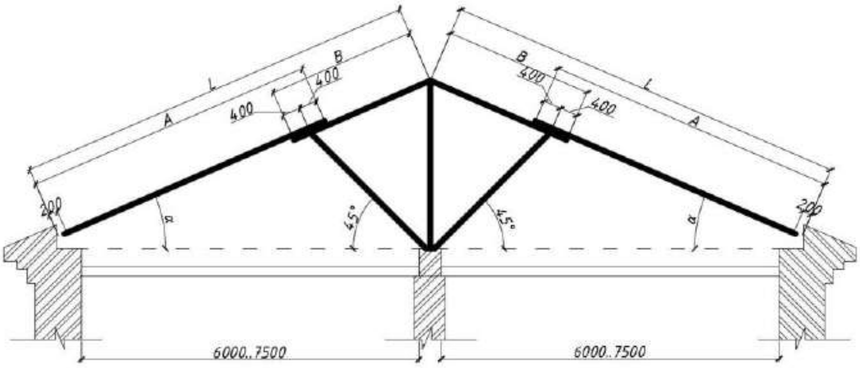

Figure 5. Combined rafter systems for saddle roofs

Rafter section of STWS for combined rafter system of saddle roofs with braces is considered for the applied analyses and calculation. The calculation procedure is the same for non-composite rafter system with bracers having one different connection and larger span values.

Static scheme of the structure is presented on Figure 6.

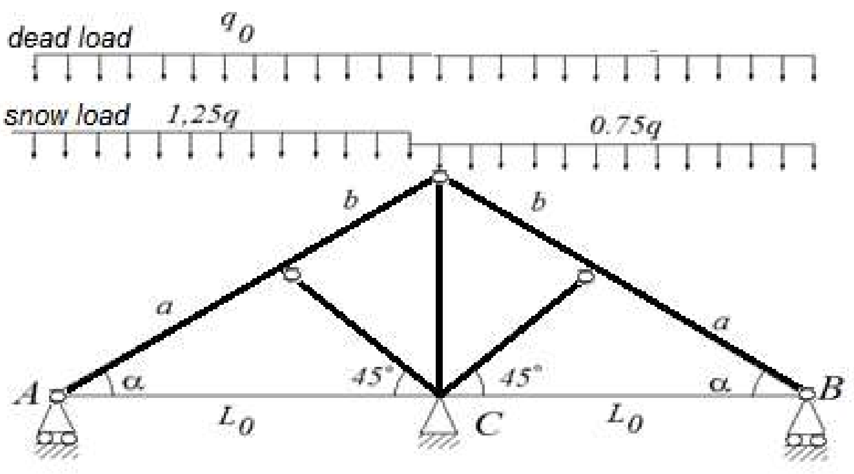

Figure 6. Static scheme of the structure

It is possible to simplify the problem by considering one half of a combined roof system for pitched roofs with braces.

The simplified model of the structure:

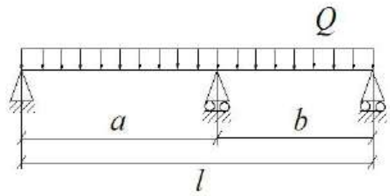

Figure 7. Simplified static scheme of the structure

The reckoning length of rafte:̊

$$l = LO/\cos \propto \tag{1}$$

Rafter step changes is considered 1,000; 1,100; 1,200; 1,300; 1,400 and 1,500mm. Load combination was considered according to table 1, where snow load to the rafter was calculated as:

$$q_1 = q_{snow} * n \tag{2}$$

n – rafter distance.

Table 1. Load cases

i	Type of load		Q_i , kg/m	n, m	Q_i , kg/m
1	Dead load (Self-bearing construction load consisting of rafter weight, lathing and roofing)	$q_{s.b.}$	-		10.1
2	Snow distributed loads, according to SP 20.13330.2011.	q_{snow}	180 kg/m^2	1.0…1.5	180…270

Maximum bending moment may be found by force method using.

Add an additional hinge on the support C and add an additional bending moment (Figure 8).

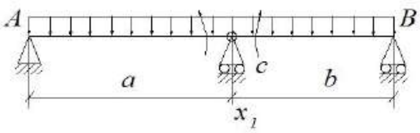

Figure 8. The equivalent system

The main loading is shown in Figure 9.

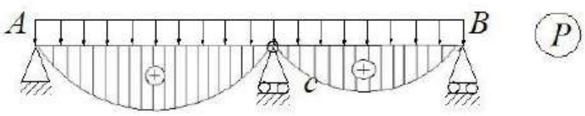

Figure 9. The main loading

The unit loading is shown in Figure 10.

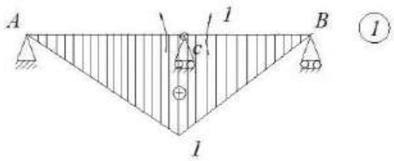

Figure 10. The unit loading

Multiplying of the diagram M_1 on itself:

$$\delta_{11} = \frac{a}{6EI}(0.0 + 4 \times 0.5 \times 0.5 + 1.1) + \frac{b}{6EI}(0.0 + 4 * 0.5 * 0.5 + 0.0) = \frac{2(a+b)}{6EI} \quad (3)$$

Multiplying of diagrams M_1 and M_p:

$$\Delta_{1p} = \frac{a}{6EI}\left(0.0 + 4 * 0.5\frac{Qb^2}{8} + 0.1\right) + \frac{b}{6EI}\left(0.1 + 4 * 0.5\frac{Qb^2}{8} + 0.0\right) = \frac{Q(a^3+b^3)}{24EI} \quad (4)$$

The result of multiplying is coefficients of the equation (5)

$$\delta_{11}x + \Delta_{1p} = 0 \quad (5)$$

By calculating the coefficients of the equation (5) it is able to find the maximum bending moment

$$X = \frac{-Q(a^2 - ab + b^2)}{8} \quad (6)$$

$$M_{max} = \frac{-Q(a^2 - ab + b^2)}{8} \quad (7)$$

The final bending moment diagram M_{max}:

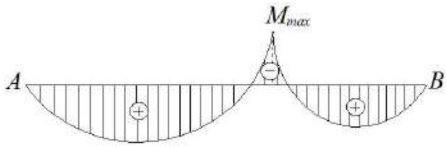

Figure 11. The final bending moment diagram M_{fin}

There is the finding of the reaction of central support (of brace).

Solving static indeterminacy is by force method. The reckoning scheme is the same in Figure 7. Affixing of unit force is in point C.

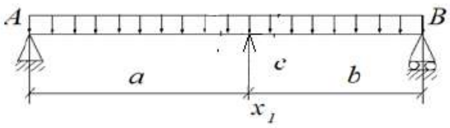

Figure 12. The equivalent system

The main loading is shown in Figure 13.

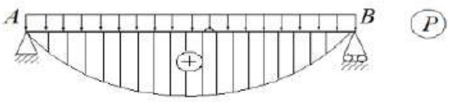

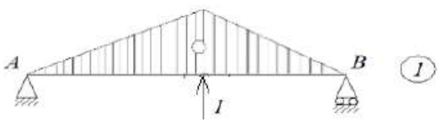

Figure 13. The main loading **Figure 14. The unit loading**

Similarly multiplying of diagrams by formulas (3) and (4) is for support C reaction determination for brace stability checking (compressed diagonal elements).

$$R_C = \frac{-q((a+b)^2 + ab(a+b))}{8ab} \quad (8)$$

Choose the section of the rafter as rectangular with variable width and by accepting of height is h = 175 mm by formula

$$\sigma_{max} = \frac{M_{max}}{I_y} + \frac{N}{A} \leq R \quad (9)$$

R is determined as bending strength of timber from one side and yield stress of steel from other side. Because of identical method there is an ability to compare allowable stress and factual stress.

$$b = \frac{1}{13000000} * \left(\frac{6M_{max}}{175 * 175/_{1000}} + \frac{N}{175 * 175/_{1000}}\right) \quad (10)$$

Rybakov V.A., Al Ali M., Panteleev A.P., Fedotova K.A., Smirnov A.V. Bearing capacity of rafter systems made of steel thin-walled structures in attic roofs. *Magazine of Civil Engineering*. 2017. No. 8. Pp. 28–39. doi: 10.18720/MCE.76.3.

The cross-section of steel thin-walled structures is paired structural channels shape, chosen from Technical requirements. Therefore, there is no considering of bi-moment because of symmetrical shape of cross-section, rafter’s constant step, so eccentricity will not appear.

The static calculation is the same in timber structures.

Finding the maximum bending moment is by loads 1,25Q and 0,75Q

$$M_{1max} = \frac{-1.25Q(a^2 - ab + b^2)}{8} \qquad (11)$$

$$M_{2max} = \frac{-0.75Q(a^2 - ab + b^2)}{8} \qquad (12)$$

Choose the section of the rafter by maximum bending moment according Russian Set of Rules SP 16.13330.2011 and technical requirements of company “BaltProfil”.

Results and Discussion

The Comparative Analysis of the Selection Results of Rafters with Timber structures and STWS

Apply formulas (11) and (12) for the selection of the rafters of STWS.

Compare the obtained results with results for timber structures, received using the formula (10) and the ones from album series 1.169.5 "Constructive solutions of timber rafters under metal roof" of "LenZhilNIIProekt" (1990).

Initial data and the results are represented in Table 2.

Table 2. The results of calculations

<table>
<tr><th rowspan="2">L₀</th><th rowspan="2">α</th><th rowspan="2">b (design)</th><th rowspan="2">step</th><th rowspan="2">Chosen STWS section</th><th rowspan="2">Chosen timber section</th><th colspan="2">Album of technical solutions 1.169.5 (LenZhilNii-Proekt, 1990)</th></tr>
<tr><th>Top rafter</th><th>Bottom rafter</th></tr>
<tr><td>6000</td><td rowspan="7">18</td><td>82</td><td>1500</td><td rowspan="3">2×TN-175-2</td><td rowspan="7">2x50x200</td><td rowspan="7">2x40x125</td><td>2x60x200</td></tr>
<tr><td>6250</td><td>89</td><td>1500</td><td rowspan="4">2x60x225</td></tr>
<tr><td>6500</td><td>96</td><td>1500</td></tr>
<tr><td>6750</td><td>87</td><td>1200</td><td rowspan="2">2×TN-200-1,5</td></tr>
<tr><td>7000</td><td>94</td><td>1200</td></tr>
<tr><td>7250</td><td>94</td><td>1200</td><td rowspan="2">2×TN-200-2</td><td rowspan="2">2x75x225</td></tr>
<tr><td>7500</td><td>82</td><td>1000</td></tr>
<tr><td>6000</td><td rowspan="7">20</td><td>96</td><td>1500</td><td rowspan="3">2×TN-175-2</td><td rowspan="7">2x50x200</td><td rowspan="7">2x40x125</td><td rowspan="2">2x60x200</td></tr>
<tr><td>6250</td><td>84</td><td>1500</td></tr>
<tr><td>6500</td><td>91</td><td>1500</td><td rowspan="3">2x60x225</td></tr>
<tr><td>6750</td><td>98</td><td>1500</td><td rowspan="2">2×TN-200-1,5</td></tr>
<tr><td>7000</td><td>89</td><td>1200</td></tr>
<tr><td>7250</td><td>96</td><td>1200</td><td rowspan="2">2×TN-200-2</td><td rowspan="2">2x75x225</td></tr>
<tr><td>7500</td><td>96</td><td>1200</td></tr>
<tr><td>6000</td><td rowspan="7">22</td><td>92</td><td>1500</td><td rowspan="3">2×TN-175-2</td><td rowspan="7">2x50x200</td><td rowspan="7">2x40x125</td><td rowspan="3">2x60x200</td></tr>
<tr><td>6250</td><td>81</td><td>1500</td></tr>
<tr><td>6500</td><td>87</td><td>1500</td></tr>
<tr><td>6750</td><td>94</td><td>1500</td><td rowspan="2">2×TN-200-1,5</td><td rowspan="3">2x60x225</td></tr>
<tr><td>7000</td><td>86</td><td>1200</td></tr>
<tr><td>7250</td><td>82</td><td>1200</td><td rowspan="2">2×TN-200-2</td></tr>
<tr><td>7500</td><td>98</td><td>1200</td><td>2x75x225</td></tr>
</table>

<table>
<tr><th rowspan="2">L_0</th><th rowspan="2">α</th><th rowspan="2">b (design)</th><th rowspan="2">step</th><th rowspan="2">Chosen STWS section</th><th rowspan="2">Chosen timber section</th><th colspan="2">Album of technical solutions 1.169.5 (LenZhilNii-Proekt, 1990)</th></tr>
<tr><th>Top rafter</th><th>Bottom rafter</th></tr>
<tr><td>6000</td><td rowspan="7">24</td><td>89</td><td>1500</td><td rowspan="3">2×TN-175-2</td><td rowspan="7">2x50x200</td><td rowspan="7">2x40x125</td><td rowspan="4">2x60x200</td></tr>
<tr><td>6250</td><td>96</td><td>1500</td></tr>
<tr><td>6500</td><td>84</td><td>1500</td></tr>
<tr><td>6750</td><td>91</td><td>1500</td><td rowspan="2">2×TN-200-1,5</td></tr>
<tr><td>7000</td><td>98</td><td>1500</td><td rowspan="3">2x60x225</td></tr>
<tr><td>7250</td><td>89</td><td>1200</td><td rowspan="2">2×TN-200-2</td></tr>
<tr><td>7500</td><td>95</td><td>1200</td></tr>
<tr><td>6000</td><td rowspan="7">26</td><td>94</td><td>1500</td><td rowspan="3">2×TN-175-2</td><td rowspan="7">2x50x200</td><td rowspan="7">2x40x125</td><td rowspan="5">2x60x200</td></tr>
<tr><td>6250</td><td>86</td><td>1500</td></tr>
<tr><td>6500</td><td>82</td><td>1200</td></tr>
<tr><td>6750</td><td>89</td><td>1200</td><td rowspan="2">2×TN-200-1,5</td></tr>
<tr><td>7000</td><td>95</td><td>1200</td></tr>
<tr><td>7250</td><td>86</td><td>1000</td><td rowspan="2">2×TN-200-2</td><td rowspan="2">2x60x225</td></tr>
<tr><td>7500</td><td>92</td><td>1000</td></tr>
</table>

Analyzing the results, it is possible to draw the following conclusions:

The section of the upper rafter spar, adopted in the album of technical solutions, is less than the cross-section of the timber structures calculated in this work. This is a consequence of the fact that the album of technical solutions of timber rafters for metal roofing 1.169.5 for calculation there was applied a design scheme, different from the design scheme adopted in this paper.

However, the cross section of the lower rafter spar, adopted in the album of technical solutions, is larger than the cross-section of the timber structures calculated in this work. This is due to the fact that the album of technical solutions adopted different sections for the lower and upper rafter spars. This is also since different loads were applied to the design schemes.

Structures made of STWS or timber were calculated according to Russian Set of Rules SP 20.13330.2011, structures from album series 1.169.5 were calculated according to SNIP 2.01.07-85.

In Russian Construction Norms and Rules SNIP 2.01.07-85 (changes have been made N 1 and N 2, approved by resolutions of the State Construction Committee of Russia dated July 5, 1993 N 18-27 and of 29 May 2003 N 45, respectively) in particular, paragraph 5.2 has been changed, concerning the snow load values. Also, changes have been made to Attachment 3 concerning the schemes of application of snow loads and snow bags.

Based on this, it can be concluded that the use of the calculation scheme adopted in this paper, in calculations based on current standards and changed loads, makes it possible to save material compared to the version from the album of technical solutions.

The of Economic Efficiency Analysis of Application of Steel Thin-walled Structures in Major Repair of Attic Roofs

The economic expediency was made with the major repair of the building of the roof of 8-th mental hospital building in Druzhnoselo. Via software Smeta Wizard 4.0 there were worked out 2 estimates for the major repair. A rafter section from timber structures is 2x50x175; from STWS is the profile 2xTH-175-2.

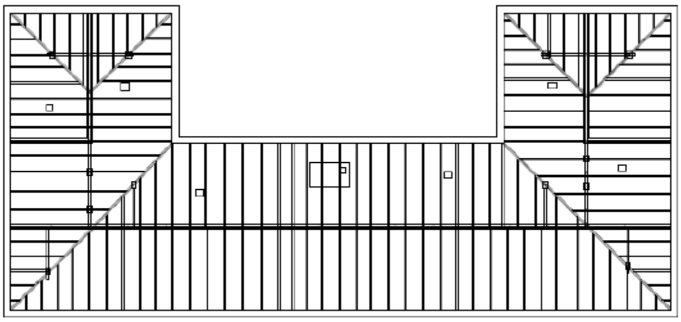

Figure 15. The rafter construction scheme

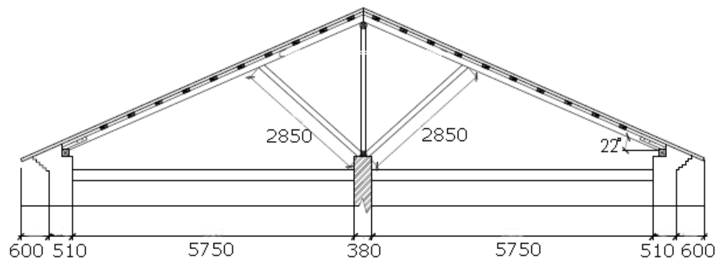

Figure 16. The cross-section construction scheme

The cost of repair is shown in Table 3. The prices are as of April 2015. The estimate is for the territorial unit prices.

Table 3. The hospital repair cost

	Estimate cost, RUR	**Salary, RUR**	**Materials cost, RUR**	**Cost price, RUR**
Timber structures	2 185 637.00	410 966.21	1 106 718.44	1 972 747
STWS	1 879 647.82	353 430.94	951 777.86	1 657 107

The cost comparison is shown in Figure 17.

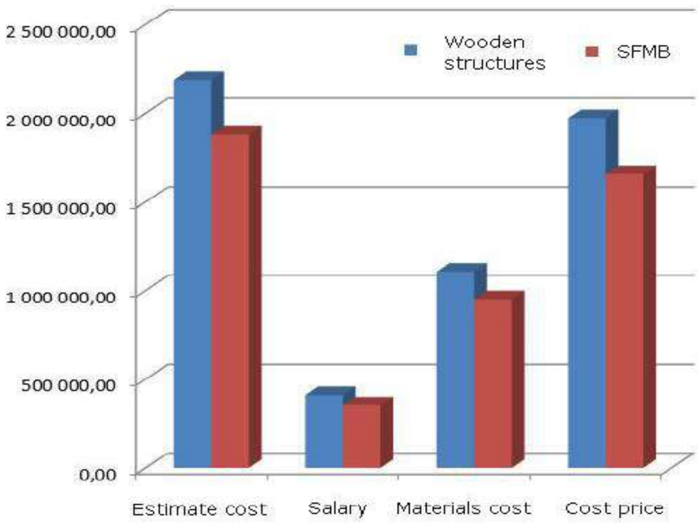

Figure 17. The cost comparison

The major repair by STWS using is cheaper because of less material consumption. The economy is 13 %.

Conclusion

The result of the following conclusions:

1. The authors have proposed the methodology for calculation the statically indeterminate frame structures with the use of force method. The main idea of the proposed methodology is to simplify the design diagram (structural design) to beam and hereafter use the B.P.E. Clapeyron principle system.

2. Universal solutions are obtained for the selection of rafters made of timber or STWS using the proposed method.

3. The expediency of using the same sections of rafters (50 x 200 mm) and (50 x 175mm) for the same reckoning scheme due to their variable pitch.

4. The section select of STWS rafters for various constructive schemes of pitched roofs:

- For non-combined rafter system of one-pitched roof without braces there is 2xTH-200-1,5 for every overlapped span for unification. The rafter step is reducing with span increasing.

- For non-combined rafter system of one-pitched roof with brace there is 2xTH-175-1,5 for every overlapped span because of small difference of the span.

- For combined rafter system of one-pitched roof with brace there are three sections: 2xTH-175-1,5, 2xTH-175-1,5, 2xTH-200-2 for every overlapped span. The section is increasing with span increasing.

- For non-combined rafter system of saddle roof with brace there is 2xTH-175-1,5, 2xTH-175-2 for every overlapped span. The rafter step is reducing with span increasing.

- For combined rafter system of saddle roof with brace there is 2xTH-175-2, 2xTH-200-1,5, 2xTH-200-2 for every overlapped span. The rafter step is reducing with span increasing.

5. The STWS using allows reducing the major repair cost to 13.5 % because of less material consumption.

6. The research results were implemented in the activity of design institute OJSC "LenzhilNIIproyekt". In using for development of album of technical solutions for the attic roof rafter system.

Acknowledgement

This paper is partially prepared within the research project VEGA No. 1/0188/16 supported by the Scientific Grant Agency of the Ministry of Education of Slovak Republic and by the Slovak Academy of Sciences.

Acknowledgment is also expressed to K.A. Sharlygina, G.S. Sharbabchev and A.O. Rodicheva ("LenzhilNIIproekt", Co., Ltd, St. Petersburg, Russia) for providing archive materials and help in research.

References

1. Martynenko E.A., Staritsyna A.A., Rybakov V.A. Rekonstruktsia zhilogo kvartala istoricheskogo tsentra Sankt-Peterburga [The reconstruction of a residential neighborhood of St. Petersburg's historical center]. *Construction of Unique Buildings and Structures*. 2016. No. 1(40). Pp. 32–42. (rus)
2. Semenikhina V.P. *Sovershenstvovanie sposobov ustroistva i remonta skatnykh krysh ekspluatiruemykh cherdakov* [The improving of the installation and repair ways of pitched roofs of unexploited attic]. Ph.D. Thesis. Moscow, 2010. (rus)
3. Belevich V.B. *Progressivnye tekhnologii ustroistva krovel* [The progressive roofing technology]. Ph.D. Thesis. Moscow, 2007. (rus)
4. Airumyan E.L. *Rekomendatsii po proektirovaniyu, izgotovleniyu i montazhu ograzhdauschikh i nesuschikh konstruktsii iz stalnykh gnutykh profilei povyshennoi zhyostkosti.* [The recommendations for the design, fabrication and installation of fencing and supporting structures of increased rigidity steel roll-formed sections]. Moscow, 1999. 32 p. (rus)

Литература

1. Мартыненко Е.А., Старицына А.А., Рыбаков В.А. Реконструкция жилого квартала исторического центра Санкт-Петербурга // Строительство уникальных зданий и сооружений. 2016. № 1(40) С. 32–42.
2. Семенихина В.П. Совершенствование способов устройства и ремонта скатных крыш эксплуатируемых чердаков. Дисс. на соиск. учен. степ к.т.н. Спец.: 05.23.08. М., 2010
3. Белевич В.Б. Прогрессивные технологии устройства кровель. Дисс. на соиск. учен. степ д.т.н. Спец.: 05.23.08. М., 2007.
4. Айрумян Э.Л. Рекомендации по проектированию, изготовлению и монтажу ограждающих и несущих конструкций из стальных гнутых профилей повышенной жёсткости М.,1999. 32 с.
5. Ведяков И.И. Выявление резервов несущей способности стальных строительных конструкций на основе совершенствования методов их расчета и рационального применения современных материалов. Дисс. на соиск. учен. степ д.т.н. Спец.: 05.23.01. М., 2000.

Rybakov V.A., Al Ali M., Panteleev A.P., Fedotova K.A., Smirnov A.V. Bearing capacity of rafter systems made of steel thin-walled structures in attic roofs. *Magazine of Civil Engineering*. 2017. No. 8. Pp. 28–39. doi: 10.18720/MCE.76.3.

5. Vedyakov I.I. *Vyyavlenie rezervov nesuschei sposobnosti stalnykh stroitelnykh konstruktsii na osnove sovershenstvovaniya metodov ikh rastsyota i ratsionalnogo primeneniya sovremennykh materialov* [The reserves revealing of the bearing capacity of steel building structures by improving the methods of their calculation and rational use of modern materials]. Ph.D. Thesis. Moscow, 2000. (rus)
6. Belayev B. Ye. *Prichiny avariy stalnykh konstruktsii i sposoby ikh ustraneniya.* [Reasons of steel structures accidents and their removal methods]. Moscow, 1968. 240 p. (rus)
7. Tarasov A.V. *Eksperimentalno-teoreticheskiye issledovaniya ramnykh konstruktsii iz stalnykh tonkostennykh kholodnognutykh profilei* [Experimental and theoretical researches of frame structures made of steel thin-walled cold-formed profiles]. Tomsk, 2013. 7 p. (rus)
8. Rybakov V.A., Gamayunova O.S. Napryazhyonno-deformirovannoye sostoyaniye elementov karkasnykh sooruzheniy iz tonkostennykh sterzhney [Stress-state elements frame structures from thin-walled rods]. *Construction of Unique Buildings and Structures.* 2013. No. 7(12). Pp. 79–123. (rus)
9. Dzhanelidze G.Yu., Panovko Ya.G. *Statika uprugikh tonkostennykh sterzhney.* [Statics of thin elastic rods]. Moscow, 1948. 208 p. (rus)
10. Vorobyov L.N. Deformatsionnyy rastsyot i ustoytsivost tonkostennykh sterzhney otkrytogo profilya [Deformation calculation and stability of thin-walled open profile bars]. *Novocherkassk polytechnic university's collection.* 1958. No. 69(83). Pp. 3–48. (rus)
11. Mescheryakov V.B. O kruchenii tonkostennykh sterzhney [About torsion of thin-walled bars]. *Moscow railway university's collection.* 1967. No. 236. Pp. 77–85. (rus)
12. Mescheryakov V.B. Obschiye uravneniya teorii tonkostennykh sterzhney otkrytogo profilya s utsetom sdvigov [The general equations of the theory of thin-walled open profile bars taking into account shifts]. *Moscow railway university's collection.* 1967. No. 260. Pp. 82–93. (rus)
13. Trubina D.A., Pichugin E.D., Rybakov V.A., Garifullin M.R., Sokolova O.V. Comprasion of the bearing capacity of lst-profile depending on the thickness of its elements. *Applied Mechanics and Materials.* 2015. No. 725–726. Pp. 752–757. doi: 10.4028/www.scientific.net/AMM.725-726.752
14. Trubina D.A., Abdulaev D.A., Pichugin E.D., Garifullin M.R. The loss of local stability of thin-walled steel profiles. *Applied Mechanics and Materials.* 2014. No. 633–634. Pp. 1052–1057. doi: 10.4028/www.scientific.net/AMM.633-634.1052
15. Vatin N.I., Sinelnikov A.S., Garifullin M.R., Trubina D.A. Simulation of cold-formed steel beams in global and distortional buckling. *Applied Mechanics and Materials.* 2014. No. 633–634. Pp. 1037–1041. doi: 10.4028/www.scientific.net/AMM.633-634.1037
16. Garifullin M.R., Trubina D.A., Vatin N.I. Local buckling of cold-formed steel members with edge stiffened holes. *Applied Mechanics and Materials.* 2015. No. 725–726. Pp. 697–702. doi: 10.4028/www.scientific.net/AMM.725-726.697
17. Garifullin M.R., Nackenhorst U. Computational analysis of cold-formed steel columns with initial imperfections. *Procedia Engineering.* 2015. No. 117. Pp. 1073–1079. doi: 10.1016/j.proeng.2015.08.239
18. Garifullin M.R., Bronzova M., Sinelnikov A.S., Vatin N.I. Buckling analysis of cold-formed c-shaped columns with reticular-stretched perforations. *Interdisciplinarity in Theory and Practice.* 2015. No. 7. Pp. 163–169.
19. Vatin N.I., Havula J., Martikainen L., Sinelnikov A.S.,

6. Беляев Б.Е. Причины аварий стальных конструкций и способы их устранения. М.: Издательство литературы по строительству, 1968. 240 с
7. Тарасов А.В. Экспериментально-теоретические исследования рамных конструкций из стальных тонкостенных холодногнутых профилей: автореферат дис. канд. техн. наук: 05.23.01. Сибирский федеральный ун-т . Томск, 2013. С. 7
8. Рыбаков В.А., Гамаюнова О.С. Напряженно-деформированное состояние элементов каркасных сооружений из тонкостенных стержней // Строительство уникальных зданий и сооружений. 2013. № 7(12). С. 79–123.
9. Джанелидзе Г.Ю., Пановко Я.Г. Статика упругих тонкостенных стержней. М.: Государственное издательство технико-теоретической литературы, 1948. 208 с.
10. Воробьев Л. Н. Деформационный расчет и устойчивость тонкостенных стержней открытого профиля // Сб.научн.тр. Новочеркасского политехнического института. 1958. Т. 69/83. С. 3–48.
11. Мещеряков В. Б. О кручении тонкостенных стержней // Сб. научн. тр. Моск. ин-т. инж. ж-д. тр-та. 1967. № 236. С. 77–85.
12. Мещеряков В. Б. Общие уравнения теории тонкостенных стержней открытого профиля с учетом сдвигов // Сб.научн.тр. Моск. ин-т. инж. ж-д. тр-та. 1967. № 236. С. 77–85.
13. Trubina D.A., Pichugin E.D., Rybakov V.A., Garifullin M.R., Sokolova O.V. Comprasion of the bearing capacity of lst-profile depending on the thickness of its elements // Applied Mechanics and Materials. 2015. No. 725–726. Pp. 752–757. doi: 10.4028/www.scientific.net/AMM.725-726.752
14. Trubina D.A., Abdulaev D.A., Pichugin E.D., Garifullin M.R. The loss of local stability of thin-walled steel profiles // Applied Mechanics and Materials. 2014. No. 633–634. Pp. 1052-1057. doi: 10.4028/www.scientific.net/AMM.633-634.1052
15. Vatin N.I., Sinelnikov A.S., Garifullin M.R., Trubina D.A. Simulation of cold-formed steel beams in global and distortional buckling // Applied Mechanics and Materials. 2014. No. 633–634. Pp. 1037–1041. doi: 10.4028/www.scientific.net/AMM.633-634.1037
16. Garifullin M.R., Trubina D.A., Vatin N.I. Local buckling of cold-formed steel members with edge stiffened holes // Applied Mechanics and Materials. 2015. No. 725–726. Pp. 697–702. doi: 10.4028/www.scientific.net/AMM.725-726.697
17. Garifullin M.R., Nackenhorst U. Computational analysis of cold-formed steel columns with initial imperfections // Procedia Engineering. 2015. No. 117. Pp. 1073–1079. doi: 10.1016/j.proeng.2015.08.239
18. Garifullin M.R., Bronzova M., Sinelnikov A.S., Vatin N.I. Buckling analysis of cold-formed c-shaped columns with reticular-stretched perforations // Interdisciplinarity in Theory and Practice. 2015. No. 7. Pp. 163–169.
19. Vatin N.I., Havula J., Martikainen L., Sinelnikov A.S., Orlova A.V., Salamakhin S.V. Thin-walled cross-sections and their joints: tests and fem-modelling // Advanced Materials Research. 2014. No. 945–949. Pp. 1211–1215.
20. Trubina D.A., Abdulaev D.A., Pichugin E.D., Rybakov V.A. Geometric nonlinearity of the thin-walled profile under transverse bending // Applied Mechanics and Materials. 2014. No. 633–634. Pp. 1133–1139. doi: 10.4028/www.scientific.net/AMM.633-634.1133
21. Trubina D.A., Abdulaev D.A., Pichugin E.D., Rybakov V.A. Effect of constructional measures on the total and local loss stability of the thin-walled profile under transverse bending // Applied Mechanics and Materials. 2014.

Orlova A.V., Salamakhin S.V. Thin-walled cross-sections and their joints: tests and fem-modelling. *Advanced Materials Research.* 2014. No. 945–949. Pp. 1211–1215.

20. Trubina D.A., Abdulaev D.A., Pichugin E.D., Rybakov V.A. Geometric nonlinearity of the thin-walled profile under transverse bending. *Applied Mechanics and Materials.* 2014. No. 633–634. Pp. 1133–1139. doi: 10.4028/www.scientific.net/AMM.633-634.1133
21. Trubina D.A., Abdulaev D.A., Pichugin E.D., Rybakov V.A. Effect of constructional measures on the total and local loss stability of the thin-walled profile under transverse bending. *Applied Mechanics and Materials.* 2014. No. 633–634. Pp. 982–990. doi: 10.4028/www.scientific.net/AMM.633-634.982
22. Rybakov V.A., Panteleev A., Sharbabchev G., Epshtein E. Snow-retaining system as a temporary decision for providing of the suitable temperature and humidity level of pitched roofs. *Applied Mechanics and Materials.* 2014. No. 584–586. Pp. 1876–1880. doi: 10.4028/www.scientific.net/AMM.584-586.1876
23. Rybakov V.A. *Primeneniye polusdvigovoy teorii V.I. Slivkera dlya analiza napryazhenno-deformirovannogo sostoyaniya sistem tonkostennykh sterzhney* [The application of half-shift theory by V.I. Slivker for analysis of stress-strain state of thin-walled systems]. Ph.D. Thesis. Peter the Great St. Petersburg Polytechnic University, Saint-Petersburg, 2012. 184 p. (rus)

No. 633–634. Pp. 982–990. doi: 10.4028/www.scientific.net/AMM.633-634.982

22. Rybakov V.A., Panteleev A., Sharbabchev G., Epshtein E. Snow-retaining system as a temporary decision for providing of the suitable temperature and humidity level of pitched roofs // Applied Mechanics and Materials. 2014. No. 584–586. Pp. 1876–1880. doi: 10.4028/www.scientific.net/AMM.584-586.1876
23. Рыбаков В.А. Применение полусдвиговой теории В.И. Сливкера для анализа напряженно-деформированного состояния систем тонкостенных стержней: дис. канд. техн. наук: 01.02.04. С.-Петерб. гос. политехн. ун-т. Санкт-Петербург, 2012. 184 с.

Vladimir Rybakov,
+7(964)331-29-15; fishermanoff@mail.ru;

Mohamad Al Ali,
+421905359228; mohamad.alali@tuke.sk

Anton Panteleev,
+7(999)041-58-81; a.p.panteleev@mail.ru

Kseniya Fedotova,
+7(921)326-28-76; himole@rambler.ru

Andrei Smirnov,
+7(921)381-80-40; andrewsmirnov@inbox.ru

Владимир Александрович Рыбаков,
+7(964)3312915; эл. почта: fishermanoff@mail.ru

Мохамад Ал Али,
+421905359228;
эл. почта: mohamad.alali@tuke.sk

Антон Павлович Пантелеев,
+7(999)041-58-81;
эл. почта: a.p.panteleev@mail.ru

Ксения Александровна Федотова,
+7(921)326-28-76; эл. почта: himole@rambler.ru

Андрей Вадимович Смирнов,
+7(921)381-80-40;
эл. почта: andrewsmirnov@inbox.ru

doi: 10.18720/MCE.76.4

The simulation models of river flow management by a system of flood control facilities

Имитационные модели регулирования речного стока системой противопаводковых гидроузлов

M.P. Fedorov,
A.N. Chusov,
V.I. Maslikov,
D.V. Molodtsov,
I. Togo
Peter the Great St. Petersburg Polytechnic University, St. Petersburg, Russia

Д-р техн. наук, президент М.П. Фёдоров,
канд. техн. наук, заведующий кафедрой А.Н. Чусов,
д-р техн. наук, профессор В.И. Масликов,
старший преподаватель Д.В. Молодцов,
канд. техн. наук, заведующий кафедрой И. Того.
Санкт-Петербургский политехнический университет Петра Великого, г. Санкт-Петербург, Россия

Key words: hydrotechnical construction; mathematical simulation; flood control; hydro facilities; river flow management; environmental protection

Ключевые слова: гидротехническое строительство; математическое моделирование; защита от наводнений; гидроузлы; управление речным стоком; охрана окружающей среды

Abstract. The authors propose the simulation models of river flow management during extreme river discharges for a hydro complex with a hydroelectric power plant (HPP) on a main river and a flood control facility on its side tributary, including the case of their joint operation as part of a system of flood control facilities distributed on a drainage basin. The possibility of applying the previous years' water-management plans for the choice of flood control facilities locations is considered. In the mathematical model of a hydro complex, operating modes of a HPP are assigned using its reservoir operating rule curves, considering the requirements of safety and environmental protection. In the mathematical model of a flood control facility, the scheme for flood discharge through uncontrolled bottom spillways and an uncontrolled surface spillway is considered. The use of the models makes possible to determine the operating modes of hydro facilities, considering the modern economic and environmental requirements, revision of their parameters, estimation of the energy-economic and environmental effects from the creation of systems of flood control facilities distributed on drainage basins.

Аннотация. В статье предложены имитационные модели регулирования речного стока при экстремальных расходах для комплексного гидроузла с ГЭС на основной реке, противопаводкового гидроузла на боковом притоке, в том числе для случая их совместного функционирования в составе системы распределенных на водосборе гидроузлов. Рассмотрена возможность применения проектных проработок прошлых лет по схемам использования гидроэнергетических ресурсов речного бассейна при выборе створов гидроузлов. В математической модели комплексного гидроузла режимы работы ГЭС назначаются с использованием диспетчерских графиков с учетом требований безопасности и охраны окружающей среды. В математической модели противопаводкового гидроузела рассмотрена схема пропуска паводка через нерегулируемые донные водопропускные сооружения и нерегулируемый поверхностный водослив. Использование моделей позволяет определить режимы работы гидроузлов, с учетом современных хозяйственных и природоохранных требований провести корректировку их параметров, оценить энерго-экономический и экологический эффект от создания распределенной на водосборе системы гидроузлов.

Федоров М.П., Чусов А.Н., Масликов В.И., Молодцов Д.В., Того И. Имитационные модели регулирования речного стока системой распределенных на водосборе противопаводковых гидроузлов // Инженерно-строительный журнал. 2017. № 8(76). С. 40–49.

Introduction

Flood control has always been an important task for many countries, including Russia, as floods cover large areas, lead to many casualties and huge economic losses. It can be noted that, due to the global climate change, the intensity of floods in many regions of the world is increasing. This requires improving the methods of flood control [1–6].

The task of flood management through the creation of a system of flood control facilities distributed on a drainage basin was considered in the article [7]. First, it is advisable to analyze the previous years' water-management plans for the choice of flood control facilities locations and the assessment of their parameters, since they include all the necessary justifications for hydro complexes with hydroelectric power plants. Usually these materials have not lost their significance even now. But it is necessary to revise the flood storage of the main river's reservoir, since considering the current and prospective economic and environmental conditions in its upper pool during flood flows accumulation, it may be necessary to reduce the designed maximum water level. If, at the same time, the reduction of extreme water flow to the maximum allowable value is not ensured in the lower pool, then to reduce the flow entering to the main river's reservoir, the missing volume is redistributed into flood control facilities on side tributaries. Thus, the system of hydro facilities of different functional purposes distributed on the drainage basin will be created (Figure 1).

The goals of this work are revision of flood storage of a reservoir of a hydro complex with a HPP on a main river, determination of flood control effects from flood control facilities on its side tributaries, justification of the structure of the system of flood control facilities distributed on the drainage basin.

The following simulation models were developed for these goals:

- the mathematical model of operating modes of a hydro complex with a HPP;
- the mathematical model of extreme flows management by flood control facilities;
- the integrated model of river flow management by a system of flood control facilities distributed on a drainage basin.

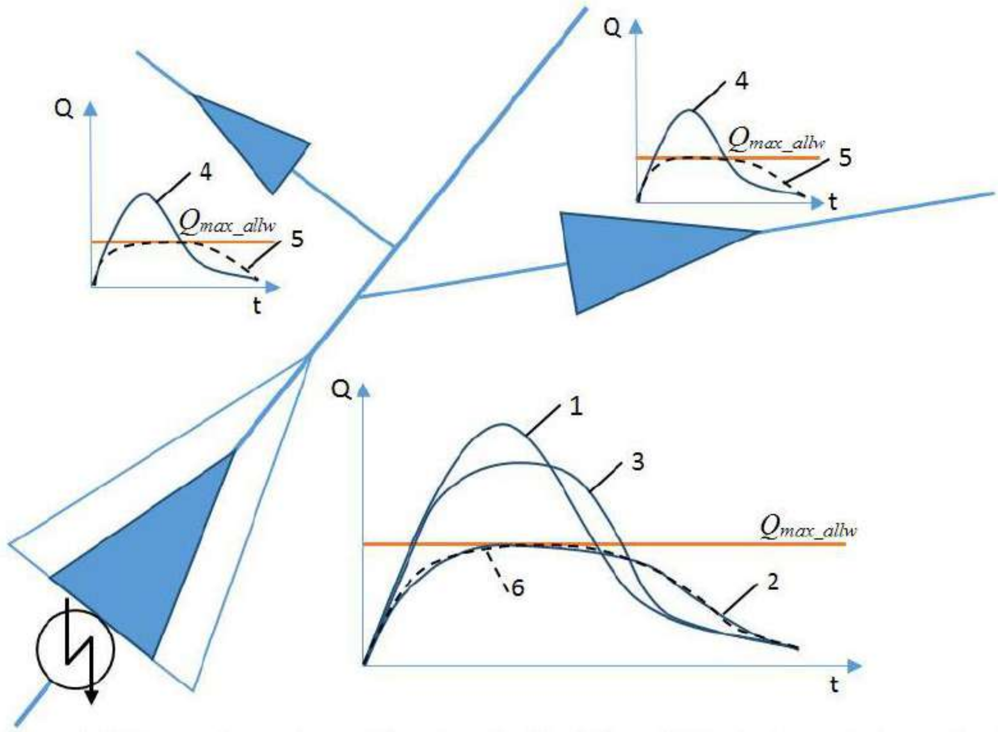

Figure 1. Scheme of a system of flood control facilities distributed on a drainage basin

where:

1 – conditional hydrograph of extreme natural water flow with 1% probability of the main river,

2 – conditional hydrograph of managed water flow in the lower pool of the hydro complex with the designed maximum water level,

3 – conditional hydrograph of managed water flow in the lower pool of the hydro complex with the reduced maximum water level considering the current and prospective environmental and economic conditions,

4 – conditional hydrograph of extreme natural water flow with 1% probability of the *i*-th side tributary,

5 – conditional hydrograph of managed water flow in the lower pool of the flood control facility of the *i*-th side tributary which accepts the missing volume for flood control from the main reservoir,

6 – conditional hydrograph of managed water flow in the lower pool of the hydro complex under the reducing extreme water flow on the side tributaries,

Q_{max_allw} – the maximum allowable river flow considering the current and prospective environmental and economic conditions.

Methods

The mathematical model of operating modes of a hydro complex with HPP

The mathematical model of long-term operation modes of a hydro complex with a HPP is created in accordance with the current recommendations [8] regulating the operation modes of water reservoirs and the use of their water resources, and which are based on the methodology of the integrated approach to river flow management [9]. These recommendations are based on Russian and foreign experience of water management.

As a research object, a hydro complex with a reservoir of annual flow regulation as the most common was chosen [10]. In earlier researches [11], the task of estimating the influence of the creation on a side tributary the flood control facility on the operating regimes and parameters of a hydro complex with a HPP on the main river was considered. In this paper another task of revision of flood storages of HPPs reservoirs (as a rule, in the direction of reducing) is solving, considering the current and prospective economic and environmental conditions and redistributing the missing regulating volume to flood control facilities on side tributaries.

When modeling HPP operating modes, the designed reservoir operating rule curves are applied, that should be periodically revised [12, 13] considering the changing economic and hydrological conditions over time, but the previous researches [14, 15] have shown that in modern conditions, as a rule, existing designed reservoir operating rule curves allow operational services to operate hydropower plants relatively safely.

The river flow management includes the following stages:

- the period of reservoir filling;
- the period of accumulation of flood flows;
- the period of reservoir draw-off.

Stage 1. The period of reservoir filling

Calculations should be made for a high-water year of estimated probability.

Case 1. The water level mark in the upper pool $Z_{UP}^{HPP}(t)$ is above the upper limit of water surface level on the reservoir operating rule curves in the range:

$$DSL \le Z_{UP}^{HPP}(t) \le FRL,$$

where: *DSL* – Dead Storage Level; *FRL* – Full Reservoir Level.

Depending on the water head *H(t)* at the calculated time (*t*), the HPP operates with the power of $N^{HPP}(t)$:

$$N^{HPP}(t) = \begin{cases} N_A^{HPP}(t), & H(t) \le H_R \\ N_R^{HPP}, & H(t) > H_R \end{cases}$$

$$H(t) = Z_{UP}^{HPP}(t) - Z_{LP}^{HPP}(t) - \Delta H,$$

where:

$N_A^{HPP}(t)$ – available power. It is determined using the operating curve $N_A^{HPP}(t) = f_1\big(H(t)\big)$.

N_R^{HPP} – rated power.

$Z_{LP}^{HPP}(t)$ – water level mark in the lower pool.

ΔH – head loss.

H_R – rated head.

According to the conditions of reliability and safety of hydro facilities operation, it is provided the restriction on the rise rate of the water level in the reservoir:

$$\frac{dZ_{UP}^{HPP}(t)}{dt} \leq h,$$

where h – the maximum safe value of the rise of the water level in the reservoir per day.

The water discharge in the lower pool at the time (t) is:

$$Q_{LP}^{HPP}(t) = Q_T^{HPP}(t) + Q_S(t),$$

where:

$Q_T^{HPP}(t)$ – water discharge through the hydro turbines.

$Q_S(t)$ – seepage discharge.

Accordingly, the power of the hydropower plant is determined by:

$$N^{HPP}(t) = k_N * H(t) * Q_T^{HPP}(t),$$
$$k_N = 9.81 \cdot \eta_T \cdot \eta_G,$$

where k_N – correction factor, considering the turbine efficiency (η_T) and the generator efficiency (η_G).

Electricity production is:

$$E(t) = \int_0^{T_1} N^{HPP}(t)dt,$$

where T_1 – estimated time interval.

The volume of water in the reservoir at time (t):

$$V(t) = V(t-1) + \left[Q_{ENT}(t) - \left(Q_T^{HPP}(t) + Q_S(t) + Q_{ID}(t) + Q_{EV}(t) + Q_{EN}(t)\right)\right] \cdot T_1$$

where:

$Q_{ENT}(t)$ – natural water flow, entering the reservoir.

$Q_{ID}(t)$ – idle discharge through the spillways.

$Q_{EV}(t)$ – loss of water due to evaporation from the surface of the reservoir.

$Q_{EN}(t)$ – the water, taken from the upper pool of the hydropower plant for economic needs.

$V(t-1)$ – the volume of water in the reservoir at a previous point in time.

Case 2. The water level mark in the upper pool is below the upper limit of water surface level on the reservoir operating rule curves within:

$$Z_{UP}^{HPP}(t) \leq FRL \text{ and } N^{HPP}(t) \leq N_R^{HPP}.$$

The spillways are closed:

$$n_{SW}(t) = 0,$$

where $n_{SW}(t)$ – the number of open spillways.

The water flow in the lower pool is determined by the requirements of water consumers:

$$Q_{LP}^{HPP}(t) = Q_T^{HPP}(t) + Q_S(t) \cong Q_{WC}(t),$$

where $Q_{WC}(t)$ – water flow according to the requirements of water consumers.

Stage 2. The period of accumulation of flood flows

The water level mark in the upper pool is in the range:

$$FRL \leq Z_{UP}^{HPP}(t) \leq MWL,$$

where *MWL* – Maximum Water Level.

The main requirements for managing flood flows during accumulating extreme flows with low probability (1%):

- The water discharge in the lower pool of the HPP should not exceed the maximum allowable Q_{max_allw} (it is assumed to be equal to the peak natural flow with probability of 10%), providing safety requirements for economic activities. In this case, the flood-alluvial regime of the river is also preserved:

$$Q_{LP}^{HPP}(t) \leq Q_{max\_allw}$$

- The water level mark in the upper pool must not exceed the *MWL*:

$$Z_{UP}^{HPP}(t) \leq MWL.$$

The additional requirements are minimization of socio-economic damage and conservation of biodiversity of ecosystems in the area upstream of the HPP. For this purpose, areas, types of flooded lands and duration of standing water etc. should be analyzed. Using the criteria of not decreasing the diversity and the ratio between anthropogenic and natural ecosystems [16,17], the MWL is corrected. When it decreases, the flood storage ΔV is redistributed into flood control facilities on side tributaries:

$$\Delta V = V_{MWL} - V_{MWL*},$$

where:

V_{MWL} – designed maximum volume of the reservoir.

V_{MWL*} – revised maximum volume of the reservoir in accordance with environmental requirements.

The number of open spillways is determined in accordance with the spillways operating rule curve, depending on the actual water level (*z*). In this case, each spillway is operating in the "full opening" mode.

$0 \leq n_{SW}(t) \leq n_1$ spillways are opened when $FRL = z_1 \leq Z_{UP}^{HPP}(t) \leq z_2$.

$n_2 \leq n_{SW}(t) \leq n_3$ spillways are opened when $z_2 \leq Z_{UP}^{HPP}(t) \leq z_3$.

…

$n_{x-1} \leq n_{SW}(t) \leq n_x$ spillways are opened when $z_{m-1} \leq Z_{UP}^{HPP}(t) \leq z_m = MWL$.

The additional requirement is the restriction on the frequency of opening/closing operations of the spillways – the minimum time between opening and closing according to ensuring reliability of a hydro complex under operating conditions.

Stage 3. The period of reservoir draw-off

$$DSL \leq Z_{UP}^{HPP}(t) \leq FRL$$

Case 1. The water level mark in the upper pool is above the upper limit of water surface level.

The HPP is operating with the rated power.

$$N^{HPP}(t) = N_R^{HPP}$$

Case 2. The water level mark in the upper pool is below the upper limit of water surface level.

The HPP is operating with the guaranteed power.

$$N^{HPP}(t) = N_G^{HPP},$$

where N_G^{HPP} – guaranteed power of the HPP with the rated probability.

The water discharge through the turbines is:

$$Q_T^{HPP}(t) = Q_G^{HPP},$$

where Q_G^{HPP} – guaranteed water discharge with rated probability.

The reservoir is drawing-off to the dead storage level in winter.

Case 3. The water level mark in the upper pool is below the lower limit of water surface level.

The HPP is operating with the reduced power.

$$N^{HPP}(t) = p \cdot N_G^{HPP},$$

where $p < 1$ – reduction ratio of the guaranteed power.

The mathematical model of extreme flows management by flood control facilities

It is noted in the researches [18,19], that flood control facilities with uncontrolled bottom spillways and an uncontrolled surface spillway, characterized by relative reliability and safety in operation, are often used for the flood flow management on side tributaries. The volume of flood water in a reservoir on a side tributary $V^{st}(t)$ at time (*t*) is determined using the following equation:

$$V^{st}(t) = V^{st}(t-1) + (Q_{ent}^{st}(t) - Q_{reg}^{st}(t) - Q_{ev}^{st}(t) - Q_s^{st}(t)) \cdot T_2,$$

where:

$Q_{ent}^{st}(t)$ – natural water flow with rated probability, entering the reservoir.

$Q_{reg}^{st}(t)$ – regulated water flow in the downstream of the flood control facility.

$Q_{ev}^{st}(t)$ – loss of water due to evaporation from the surface of the reservoir.

$Q_s^{st}(t)$ – seepage discharge.

T_2 – estimated time interval.

$V^{st}(t-1)$ – the volume of flood water in a reservoir on a side tributary at a previous point in time.

The main requirements for flood flows management on side tributaries are:

- The reduction of extreme water discharges from values with probability of 1 % to values with probability of 10 % in downstream of a flood control facility. This protects the flood-alluvial regime of the river.
- Not exceed the maximum allowable level of the upper pool (Z_{max_allw}) to minimize the area of land flooding and preserve biodiversity of ecosystems [16].

$$Z_{up}^{st}(t) \le Z_{max\_allw},$$

where $Z_{up}^{st}(t)$ – The water level mark in the upper pool of the flood control facility on the side tributary.

At the initial stage of hydraulic calculations, the design parameters of the flood control facility are taken as the main ones: the accumulating volume, the water level marks, the number of bottom and surface spillways, their sizes, etc.

The operating mode of the flood control facility is determining for the following cases:

1. The low-flow period.

The water level mark in the upper pool is in the range:

$$Z_1 < Z_{up}^{st}(t) \le Z_1 + a,$$

where:

Z_1 – bottom level mark of the uncontrolled bottom spillways.

a – height of the uncontrolled bottom spillways.

The bottom spillways operate in not drowned mode. The equation for water flow through a spillway with a wide crest is used to calculate the water-carrying capacity of the flood control facility [20] (the water-level in the lower pool is not considered).

2. The high-water period.

2.1. The water level mark in the upper pool is in the range:

$$Z_1 + a < Z_{up}^{st}(t) \leq Z_2,$$

where Z_2 – bottom level mark of the uncontrolled surface spillway.

The bottom spillways are operated in the drowned mode with variable pressure [20].

2.2. The water level mark in the upper pool is in the range:

$$Z_2 < Z_{up}^{st}(t) < Z_{max},$$

where Z_{max} – the maximum allowable water level in the upper pool of the flood control facility, considering the safety requirements, minimizing socio-economic damage and preserving the biodiversity of ecosystems.

The bottom spillways are operated in the drowned mode with variable pressure, and the surface spillway is in operated mode. In this case, the water discharge is determined by the water flow through the bottom and surface spillways [20]. The model allows to specify different versions and numbers of spillways (type, size, layout, etc.).

The maximum allowable value of accumulating capacity, the number and sizes of bottom and surface spillways are specified based on the results of calculations.

The integrated model of river flow management by a system of flood control facilities distributed on a drainage basin

The designed flood storage, MWL and the maximum water flow in the lower pool of the HPP should be revised to ensure its projected electricity generation and minimization of economic and environmental damage in the modern and prospective conditions. If they are exceeded, the missing volume (Δ*V*) is determined for redistribution into flood control facilities on side tributaries. The criterion of availability of the required total flood storage of the hydro complex with the HPP on the main river and flood control facilities on side tributaries: the flow in the lower pool of the HPP must not exceed the maximum allowable discharge (Q_{max_allw}).

$$Q_{LP}^{HPP}(t) \leq Q_{max\_allw}$$

The water volume in the reservoir at time (*t*):

$$V(t) = V(t-1) + \left[Q_{ENT}^{*}(t) - \left(Q_{T}^{HPP}(t) + Q_S(t) + Q_{ID}(t) + Q_{EV}(t) + Q_{EN}(t)\right)\right] \cdot T_1,$$

where:

$Q_{ENT}^{*}(t)$ – natural water flow, entering the reservoir of the HPP, when flood control facilities on side tributaries are operating.

$$Q_{ENT}^{*}(t) = Q_{ENT}(t) \pm \sum_{1}^{k} \Delta Q_i^{st}(t),$$

where:

k – number of flood control facilities on side tributaries on the drainage basin.

$\Delta Q_i^{st}(t)$ – the difference between the natural $Q_{nat\_i}^{st}(t)$ and regulated $Q_{reg\_i}^{st}(t)$ discharges in the downstream of the *i*-th flood control facility on the side tributary:

$$\Delta Q_i^{st}(t) = Q_{nat\_i}^{st}(t) - Q_{reg\_i}^{st}(t).$$

The calculations should be carried out considering the delay for travel water flows from a flood control facility to the HPP reservoir.

In river flow management, it is necessary to consider possible asynchrony and locality of rain precipitation in a catchment area [21], that lead to a mismatch in time of maximum water flow on a main river and its side tributaries. It is necessary to perform an analysis of possible combinations of rain-water discharges with different probability in the side tributaries, the effect of their accumulation in flood control facilities in the form of reducing extreme water discharges in downstream side and the corresponding decrease in the flow entering to the HPP reservoir on the main river.

Results and Discussion

At the first stage, using the simulation models, the regulating effect of joint operation of the hydro complex with each flood control facility on side tributaries is estimated. The estimated frequency of the natural flood flow is accepted for hydro complex on the main river and in sequence for each of flood control facilities on side tributaries. The assessment of the operating modes of each flood control facility and the revision of the water flow value entering the reservoir on the main river are carried out. Then the indicators of electricity generation of the HPP, the area of land flooding and the environmental and economic effect should be determined. This makes it possible to determine the main flood control facility (with the maximum regulating effect) from the many variants possible for construction, as well as to make the ranking of them on this basis. Only flood control facilities with positive ecological and economic effect should be selected for the further consideration.

The possibility of distribution of the flood storage to a chain of flood control facilities on each of the side tributaries should be considered.

At the next stage, the regulating effect of the joint operation of the hydro complex on the main river with the selected ones is estimated, for which hydrographs of the flood discharges with different probabilities are used, reflecting asynchrony and locality of rain precipitation on the catchment area.

Test calculations of parameters for one of the representative flood control facilities were performed and showed that its regulated water discharge in the lower pool can be reduced by 30 % compared to the natural with probability of 1% (corresponds to the natural water discharge with probability of 1 %). At the same time, the extreme water discharge in the main river entering the reservoir of the HPP is reduced by approximately 10%. Accordingly, the volume of accumulation of extreme water flow is reduced by ~11%, and the flooding area in the upper pool is reduced by ~11.5 %.

A number of works, for example [22, 23], is devoted to the substantiation of parameters and operating modes of self-regulating flood control facilities on side tributaries, successful experience of their usage for protecting lands from floods by reducing extreme water discharges. The models considered in this article show a similar effect from the use of self-regulating flood control facilities on side tributaries, but they are also aimed at solving a new problem of use of hydro potential of a main river in conditions of necessary revision of a HPP's designed MWL and, accordingly, the flood storage due to changed economic and environmental conditions in the lower and upper pools using flood control facilities on side tributaries.

Conclusions

In this paper, the developed simulation mathematical models of the operation modes and parameters of a system of flood control facilities distributed on a drainage basin are presented. Based on them the algorithm is proposed for solving the task of revision of flood storages of hydro complex reservoirs on main rivers (as a rule, in the direction of reducing), considering the current and prospective economic and environmental conditions. This task achieved by redistributing a missing regulating volume into the self-regulating flood control facilities on side tributaries.

Acknowledgements

The research was supported by Russian Science Foundation (grant №16-17-00050).

References

1. *Statista – Das Statistik-Portal. Unversicherte Schadenssummen bedeutender Hochwasserkatastrophen in Mitteleuropa seit 1993 (in Millionen Euro).* Available at: https://de.statista.com/statistik/daten/studie/2459/umfrage/unversicherte-schaeden-bedeutender-flutkatastrophen-in-europa/ (Accessed 19.10.2017)
2. U*nited Nations Office for Disaster Risk Reduction.* The human cost of weather-related disasters 1995-2015, 2015. 30 p.
3. Alfieri L., Burek P., Feyen L., Forzieri G. Global warming

Литература

1. Statista – Das Statistik-Portal. Unversicherte Schadenssummen bedeutender Hochwasserkatastrophen in Mitteleuropa seit 1993 (in Millionen Euro). [Электронный ресурс]. URL: https://de.statista.com/statistik/daten/studie/2459/umfrage/unversicherte-schaeden-bedeutender-flutkatastrophen-in-europa/ (дата обращения: 19.10.2017)
2. United Nations Office for Disaster Risk Reduction. The human cost of weather-related disasters 1995-2015, 2015. 30 p.

increases the frequency of river floods in Europe. *Hydrology and Earth System Sciences.* 2015. No. 19(5). Pp. 2247–2260.

4. Arnell N.W., Gosling S.N. The impacts of climate change on river flood risk at the global scale. *Climatic Change.* 2016. No. 134(3). Pp. 387–401.
5. Vatin N., Lavrov N., Loginov G. Processes at water intake from mountain rivers into hydropower and irrigation systems. *MATEC Web of Conferences.* 2016. Vol. 73. No. 01006.
6. Vatin N., Lavrov N., Shipilov A. The water intake facility for diversion HPPs in winter operation conditions in an urban area. *Procedia Engineering.* 2015. Vol. 117. Pp. 369–375.
7. Fedorov M.P., Maslikov V.I., Badenko V.L., Chusov A.N., Molodtsov D.V. Reducing the risk of flooding by using hydro complexes distributed on the drainage basin. *Power Technology and Engineering.* 2017. No. 51(4). Pp. 365–370.
8. *The order of the Ministry of Natural Resources and Ecology of the Russian Federation of January 26, 2011, No. 17 " Ob utverzhdenii Metodicheskih ukazanij po razrabotke pravil ispol'zovanija vodohranilishh* [On approving methodological guidelines for the development of rules for the use of reservoirs]". (rus)
9. Reznikovskii A.Sh., Rubinshtein M.I. *Dispetcherskie pravila upravleniya rezhimami vodoxranilishh* [Dispatcher Rules Governing Management of Reservoir Regimes]. Moscow: Energoatomizdat, 1984. 104 p. (rus)
10. Asarin A.E., Bestuzheva K.N. *Vodnoe'nergeticheskie raschety* [Water-energy calculations]. Moscow: Energoatomizdat, 1986. 224 p. (rus)
11. Elistratov V.V., Maslikov V.I., Fyong F.V. Regulirovanie stoka rechnogo bassejna sistemoj raspredeleniya na vodosbrose gidrouzlov. [Runoff regulation of the river basin by the distributed system of hydro systems on the catchment area]. *The collection of papers of the International Scientific and Technical Conference "Hydraulic Engineering and Hydropower: Problems of Construction, Exploitation, Ecology and Training of Specialists"*, ed. M.I. Balzannikov. Samara, 2002. Pp. 63–68 (rus).
12. Reznikovskii A.Sh., Rubinshtein M.I. *Upravlenie rezhimami vodoxranilishh gidroe'lektrostancij: proizvodstvenno-prakticheskoe izdanie* [Management of hydroelectric power stations reservoirs]. Moscow: Energia, 1974. 175 p. (rus)
13. Arsenyev G.S. Sovremennye problemy regulirovaniya e'kstremal'nyh pavodkov vodoxranilishhami gidroe'lektrostancij [Modern problems of the extreme flash floods regulation by the hydropower plant reservoirs]. *Proceedings of the Russian State Hydrometeorological University. A theoretical research journal.* 2009. No. 10. Pp. 13–20. (rus)
14. Elistratov V.V., Maslikov V.I., Sidorenko G.I. Water-power regimes of the HPP in the Volga–Kama cascade. *Power Technology and Engineering.* 2015. No. 49(1). Pp. 6–10.
15. Sidorenko V.I., Maslikov G.I. Analiz vodno-e'nergeticheskih rezhimov zhigulevskoj GE'S i svyaz' vyrabotki e'lektroe'nergii so stokom. [Evaluation of Water Energetic Modes of Zhigulevskaya Hydroelectric Power Station and Correlation between Electric Energy Generation and Water Discharge]. *Vestnik of SSUACE. Town Planning and Architecture.* 2015. No. 2(19). Pp. 73–80. (rus).
16. Chusov A.N. et al. Determination of environmental impact factors of flood control hydrosystems with temporarily filled self-regulating reservoirs. *Advances in Intelligent Systems and Computing.* No. 692. (in press)
17. Fedorov M.P., Bogolyubov A.G., Maslikov V. I. Environmental safety of power plants using renewable sources of energy. *Hydrotechnical Construction.* 1995. No. 29(6). Pp. 353–357.
18. Hornich R. Überwachung und Kontrolle von

3. Alfieri L., Burek P., Feyen L., Forzieri G. Global warming increases the frequency of river floods in Europe // Hydrology and Earth System Sciences. 2015. № 19(5). Pp. 2247–2260.
4. Arnell N.W., Gosling S.N. The impacts of climate change on river flood risk at the global scale // Climatic Change. 2016. № 134(3). Pp. 387–401.
5. Vatin N., Lavrov N., Loginov G. Processes at Water Intake from Mountain Rivers into Hydropower and Irrigation Systems // MATEC Web of Conferences. 2016. Vol. 73. № 01006.
6. Vatin N., Lavrov N., Shipilov A. The water intake facility for diversion HPPs in winter operation conditions in an urban area // Procedia Engineering. 2015. Vol. 117. Pp. 369–375.
7. Fedorov M.P., Maslikov V.I., Badenko V.L., Chusov A.N., Molodtsov D.V. Reducing the risk of flooding by using hydro complexes distributed on the drainage basin // Power Technology and Engineering. 2017. № 51(4). Pp. 365–370.
8. Приказ Министерства природных ресурсов и экологии Российской Федерации от 26 января 2011 г. № 17 «Об утверждении Методических указаний по разработке правил использования водохранилищ».
9. Резниковский А.Ш., Рубинштейн М.И. Диспетчерские правила управления режимами водохранилищ. М.: Энергоатомиздат, 1984. 104 с.
10. Асарин А.Е., Бестужева К.Н. Водноэнергетические расчеты. М.: Энергоатомиздат, 1986. 224 с.
11. Елистратов В.В., Масликов В.И., Фыонг Ф.В. Регулирование стока речного бассейна системой распределения на водосбросе гидроузлов. // Сборник трудов Международной научно-технической конференции "Гидротехника и гидроэнергетика: проблемы строительства, эксплуатации, экологии и подготовки специалистов" под ред. М.И. Бальзанникова. Самара, 2002. С. 63-68.
12. Резниковский А.Ш., Рубинштейн М.И. Управление режимами водохранилищ гидроэлектростанций: производственно-практическое издание. М.: Энергия, 1974. 175 с.
13. Арсеньев Г.С. Современные проблемы регулирования экстремальных паводков водохранилищами гидроэлектростанций. // Ученые записки Российского Государственного Гидрометеорологического Университета. 2009. № 10. С. 13–20.
14. Elistratov V.V., Maslikov V.I., Sidorenko G.I. Water-power regimes of the HPP in the Volga–Kama cascade // Power Technology and Engineering. 2015. № 49(1). Pp. 6–10.
15. Масликов В.И., Сидоренко Г.И. Анализ водно-энергетических режимов жигулевской ГЭС и связь выработки электроэнергии со стоком. // Вестник СГАСУ. Градостроительство и архитектура. 2015. № 2(19). С. 73–80.
16. Chusov A.N. et al. Determination of environmental impact factors of flood control hydrosystems with temporarily filled self-regulating reservoirs // Advances in Intelligent Systems and Computing. № 692. (in press)
17. Fedorov M.P., Bogolyubov A.G., Maslikov V. I. Environmental safety of power plants using renewable sources of energy // Hydrotechnical Construction. 1995. № 29(6). Pp. 353–357.
18. Hornich R. Überwachung und Kontrolle von Hochwasserrückhaltebecken // Österreichische Wasser- und Abfallwirtschaft. 2013. Vol. 65. № 7-8. Pp. 248–252.
19. Lange B., Metz G. Innovative Bauverfahren beim Bau von Hochwasserrückhaltebecken // 35 Dresdner Wasserbaukolloquium 2012 “Staubauwerke - Planen, Bauen, Betreiben”, Technische Universität Dresden – Fakultät Bauingenieurwesen, Institut für Wasserbau und Technische Hydromechanik. 2012. Pp. 493–502.

Hochwasserrückhaltebecken. *Österreichische Wasser- und Abfallwirtschaft.* 2013. Vol. 65. No. 7-8. Pp. 248–252.
19. Lange B., Metz G. Innovative Bauverfahren beim Bau von Hochwasserrückhaltebecken. *35 Dresdner Wasserbaukolloquium 2012 "Staubauwerke - Planen, Bauen, Betreiben", Technische Universität Dresden – Fakultät Bauingenieurwesen, Institut für Wasserbau und Technische Hydromechanik.* 2012. Pp. 493–502.
20. *Gidravlicheskie raschety vodosbrosnyx gidrotexnicheskih sooruzhenij* [Hydraulic calculations of spillway hydrotechnical constructions: reference manual]. Moscow: Energoatomizdat, 1988. 624 p. (rus)
21. *Gidrologicheskie osnovy gidroe'nergetiki* [Hydrological basis of hydropower]. Ed. Reznikovsky A.Sh. Second edition. Moscow: Energoatomizdat, 1989. 263 p. (rus)
22. *Bundesministerium für Land- und Forstwirtschaft, Umwelt und Wasserwirtschaft.* Leitfaden Hochwasserrückhaltebecken. Grundsätze für Planung, Bau und Betrieb bei der Wildbach- und Lawinenverbauung Österreichs. Wien, 2014. 159 p.
23. Winkler N.S. *Optimierung der Steuerung von Hochwasserruckhaltebeckensystemen.* Stuttgart: Inst. für Wasserbau, 2006. 210 p.

20. Гидравлические расчеты водосбросных гидротехнических сооружений. М: Энергоатомиздат, 1988. 624 с.
21. Гидрологические основы гидроэнергетики / под. ред. А.Ш. Резниковский. – 2-е изд., перераб. и доп. М.: Энергоатомиздат, 1989. – 263 с.
22. Bundesministerium für Land- und Forstwirtschaft, Umwelt und Wasserwirtschaft. Leitfaden Hochwasserrückhaltebecken. Grundsätze für Planung, Bau und Betrieb bei der Wildbach- und Lawinenverbauung Österreichs. Wien, 2014. 159 p.
23. Winkler N.S. Optimierung der Steuerung von Hochwasserruckhaltebeckensystemen. Stuttgart: Inst. für Wasserbau, 2006. 210 p.

Mikhail Fedorov,
+7(812)297-16-16; m.fedorov@spbstu.ru

Alexander Chusov,
+7(812)297-59-28; chusov17@mail.ru

Vladimir Maslikov,
+7(812)297-59-28; vmaslikov@list.ru

Dmitry Molodtsov,
+7(812)297-59-28; molodtsov_dv@spbstu.ru

Togo Issa
+7(921)337-37-30; issatogo@mail.ru

Михаил Петрович Фёдоров,
+7(812)297-16-16;
эл. почта: m.fedorov@spbstu.ru

Александр Николаевич Чусов,
+7(812)297-59-28; эл. почта: chusov17@mail.ru

Владимир Иванович Масликов,
+7(812)297-59-28; эл. почта: vmaslikov@list.ru

Дмитрий Владиславович Молодцов,
+7(812)297-59-28;
эл. почта: molodtsov_dv@spbstu.ru

Того Исса,
+7(921)337-37-30; эл. почта: issatogo@mail.ru

Fedorov M.P., Chusov A.N., Maslikov V.I., Molodtsov D.V., Togo I. The simulation models of river flow management by a system of flood control facilities distributed on a drainage basin. *Magazine of Civil Engineering*. 2017. No. 8. Pp. 40–49. doi: 10.18720/MCE.76.4.

doi: 10.18720/MCE.76.5

Indoor environment of a building under the conditions of tropical climate

Внутренняя среда жилых помещений в условиях тропического климата

J.C.L. Castro,
D.D. Zaborova,
T.A. Musorina,
I.E. Arkhipov,
Peter the Great St. Petersburg Polytechnic University, St. Petersburg, Russia

Студент Х. Кастро,
аспирант Д.Д. Заборова,
аспирант Т.А. Мусорина,
студент И.Е. Архипов,
Санкт-Петербургский политехнический университет Петра Великого, г. Санкт-Петербург, Россия

Key words: energy efficiency; sustainability; indoor climate; enclosing structure; building materials; temperature variation

Ключевые слова: энергоэффективность; теплоустойчивость; климат в помещении; ограждающие конструкции; строительные материалы; изменение температуры

Abstract. This paper is focused on having a different approach to energy efficiency and the way it is employed in industry. It considers the real case of Latin-America where normal temperature during day drastically changes from 0 to 25 degrees. Such temperature variation affects the indoor climate and its comfort. Therefore, one of the important tasks in construction of such regions is the correct choice of building materials for the enclosing structures. This article studies the typical construction materials in Colombia by analyzing its energy behavior. Temperature experiments are made for typical reinforced concrete and bricks. As a result of the experiment, it has been obtained that enclosing structures consisting of bicks are more stable to sudden changes in outside air temperature, suggesting it as the most appropriate solution for such climatic conditions.

Аннотация. Данная статья посвящена энергоэффективности в строительной индустрии. Рассматривается существующие жилые здания Латинской Америки, где температура воздуха в течении дня может резко измениться с 0 до 25 градусов Цельсия. Такие температурные колебания влияют на внутренний климат помещений и его комфорт. Поэтому одной из важных задач при строительстве жилых зданий в регионах с таким климатом является правильный выбор строительных материалов для ограждающих конструкций. В статье исследуются типичные строительные материалы в Колумбии с учетом анализа их энергетического поведения. Проводятся температурные эксперименты для таких материалов как железобетон и кирпич. В результате эксперимента было получено, что ограждающие конструкции, состоящие из полнотелого кирпича, более устойчивы к резким изменениям температуры наружного воздуха, что является наиболее подходящим решением для таких климатических условий.

Introduction

Most of the studies analyse conditions of materials for keeping warm the inside facilities because of the extremely low temperatures they must deal with. Furthermore there is comparable little literature about Latin-America and its warm environments. There is a need of analysing materials which can improve living conditions [3]; studies have confirmed the correlation between temperature and human working performance. Moreover, is a priority for governments to give the best possible settings to citizens protecting them from potential illness due to unbearable working and living conditions, all this translates into guaranteeing good Social Health. Typical tropical climates may change in a drastic manner, this makes daily living uncomfortable to citizens which must deal with hot temperatures and cold ones in the same day. In Latin-America most of the principal cities must deal with relatively high temperatures [1, 2]. Colombia is not the exception having cities with more than 25 °C all year long; moreover must be considered the opposite conditions whit cities that have medium-low temperatures which can, inclusively, drop down to 0 °C.

Кастро Х., Заборова Д.Д., Мусорина Т.А., Архипов И.Е. Внутренняя среда жилых помещений в условиях тропического климата // Инженерно-строительный журнал. 2017. № 8(76). С. 50–57.

The climate of Colombia is dominated by its geographical conditions more than stationary regimes, this is due to the proximity to the Equator line (Latitude 0°). Located in the tropic is usual to have a different range of temperatures and conditions; of high influence is the mountain range which divides the country and defines the climatic parameters. In very short distances climatic conditions can change because of the topographic characteristics of each zone. High pressure zones in the sub-tropics and the low pressure in the equatorial line lead to massive air currents. These are located in the called Convergence Inter-tropical Line. Bogotá (the capital city) is located in the mountain ridge, which has average temperatures during the day of 15 °C; during the night temperatures oscillates around 5 °C dropping down to 0 °C. In contrast to Bogotá, almost all the other main cities must deal with high temperatures as shown in the following table.

Table 1. Average temperatures in the main cities of Colombia

Main Cities in Colombia	Average Temperature (C°)	Highest Temp (C°)	Lowest Temp (C°)	Delta Temp (C°)
CARTAGENA	28	32	22	10
SANTA MARTA	27	35	20	15
BOGOTÁ	14	21	0	21
MEDELLIN	21	28	17	11
TUNJA	13	19	1	18
PEREIRA	22	26	18	8
VILLAVICENCIO	25	32	20	12
NEIVA	28	35	23	12
POPAYAN	19	24	12	12
PASTO	13	18	2	16
ARMENIA	23	28	15	13
BUCARAMANGA	23	29	19	10
CALI	24	31	18	13

Climatic conditions demand solutions to deal with high temperatures; for special cases as Neiva it is extremely hot (28 °C). Although low temperatures, in Bogotá and Tunja is necessary to apply a solution which give comfort and good design to residences and commercial structures.

More than 30 countries laying in the tropic suffer the same problematic identified in this article, extreme temperature changes during short periods of time. In this way the purpose is to deliver accurate results for complementing the efforts of improving indoor environments in all the different structures. Moreover the objective is to give values that help understand the differences between both materials, more deeply, is to give suggestions of the predominance of the best one which gather together the best solution to the characteristics of the climatic conditions described.

Typical construction in Colombia

At the present time in Colombia there are mainly 2 types of technologies used in the construction of new buildings and houses:

1) Reinforced concrete structures (Fig. 1);

2) Brick structures (Fig. 2).

Figure 1. Typical concrete structure

Figure 2. Construction with bricks

Bricks / masonry are the typical and most used material in Colombia. It is in direct contact with the outside with no layers that divide it from the inside [4]. The reason of the highly use of bricks in Bogotá is what is called the "Bricks Culture" which has made the identity of the city; new bold and adventurous designs make the city unique over others, furthermore with international recognition [5]. Constructions made of bricks are much more expensive than those in concrete, but what makes the difference is the low prices of labour or workforce. This makes an advantage for allowing big projects to be made out of bricks (Fig. 2). The main reasons for positioning this material in Bogotá was that during the 50´s the best recognized architects used massively bricks for almost all projects, with new designs and textures they gave the actual prestige to the material. Another reason is the abundance of production factories among the country. On the other hand, concrete is mostly used for simple designs and fast construction, moreover concrete is much cheaper than bricks [6].

The indoor climate is one of the main tasks during the construction of residential buildings [7–12]. Therefore, a special attention should be paid to the selection of materials. Although heat moisture conditions of the building envelope have been studied actively during a long time in construction; the final answer for which material is the best one doesn't exist [13–15].

The motivation of this article is under the perspective of having a study to real conditions in a country with similar weather as many southern cities in Russia. In this way is possible to link a global approach under the scope of improving living conditions for people. Furthermore is a tool for governmental entities helping them to understand real problematic and give real solutions and accurate conclusions.

Goal and objectives.

Most of the building in Colombia do not use a heating system or insulation on walls and roofs. Therefore, the main strategy to heat building deals with proper material selection and the orientation of the building. For this purpose the following objectives have been set:

- Detection of the thermal characteristics of materials;

- Analyzing the thermal stability of the most common enclosing structures for non-periodic regime;

- Comparison experimental data and formulation of recommendations for material selections.

Methods and Materials.

For this study were selected two types of the materials used in Colombian construction (Table 2). In laboratory materials were compared for showing appropriate conclusions based on the results. Following are the characteristics of both in accordance to its energy efficiency.

Table 2. Thermal characteristics of materials

№	Material	Thickness δ, [m]	Coefficient of thermal conductivity λ, [W/(m·°C)]	Specific heat c_p, [J/(kg·°C)]	Density ρ, [kg/m^3]	Coefficient of thermal absorption β, [J/($\sqrt{s}$·m^2·°C)]
1	Reinforced concrete	0.12	1.7	840	2500	1889.44
2	Ceramic brick	0.12	0.64	880	1600	949.27

The experiment consists on simulating the real conditions of typical structures in tropical climates, it is by drastic temperature changes in few hours during one same day. It has built a box (imitation of a closed room) for both materials: bricks and reinforced concrete simulating the indoor conditions. Installing the appropriate sensors and equipment inside it is the way to be in accordance with real characteristics of buildings [16, 17]. In addition, for both surfaces (up and down) it was sealed with thermic isolation for simulating roof and floor of a typical internal environment. The initial temperature of the air inside the chamber is 25 °C, followed by a drastic drop down to 0°C and then up to the initial temperature. These is to go in accordance to typical behaviors because in the early morning temperature is 0 °C and proportionally increased until the highest 25 °C during midday. Temperature inside the “box” is registered and collected for both specimens, brick and concrete. In this way is able to compare the behavior which really apply in real life conditions [6, 18] for giving future conclusions about the most appropriate material which guarantees comfort. As explained before and in accordance to the aim of this article, the idea is to simulate with all possible details all conditions of environments in similar climatic conditions tendencies.

Initial data

Consider the periodic regime of a reinforced concrete structure.

It consists of the following: a wooden board, a heater, a reinforced concrete sample. It is represented in Figure 3.

Figure 3. Chamber conditions for reinforced concrete structure

The sample was placed in a chamber (initial temperature inside the structure was approximately 21 °C) and released to an air temperature of 0°C degrees. The sample was at 0 °C degrees for 30 minutes. Then followed an increase of temperature in the chamber to 25 °C degrees. The sample was heated until the sensor inside the structure began to register an increase in temperature. Due to the fact that the material is thermally stable, it continues to cool down, even if the chamber has at plus temperature. Then the material was cooled until the temperature of the sensor began to fall.

The second structure – brickwork.

Similar to the last one, it consists of the following: a wooden board, a heater, a brick sample. The time and temperatures were the same as the experiment of reinforced concrete structure. A sample is shown in Figure 4.

Figure 4. Chamber conditions for brick structure

Results and Discussion

The result of the experiment is shown in Figure 5.

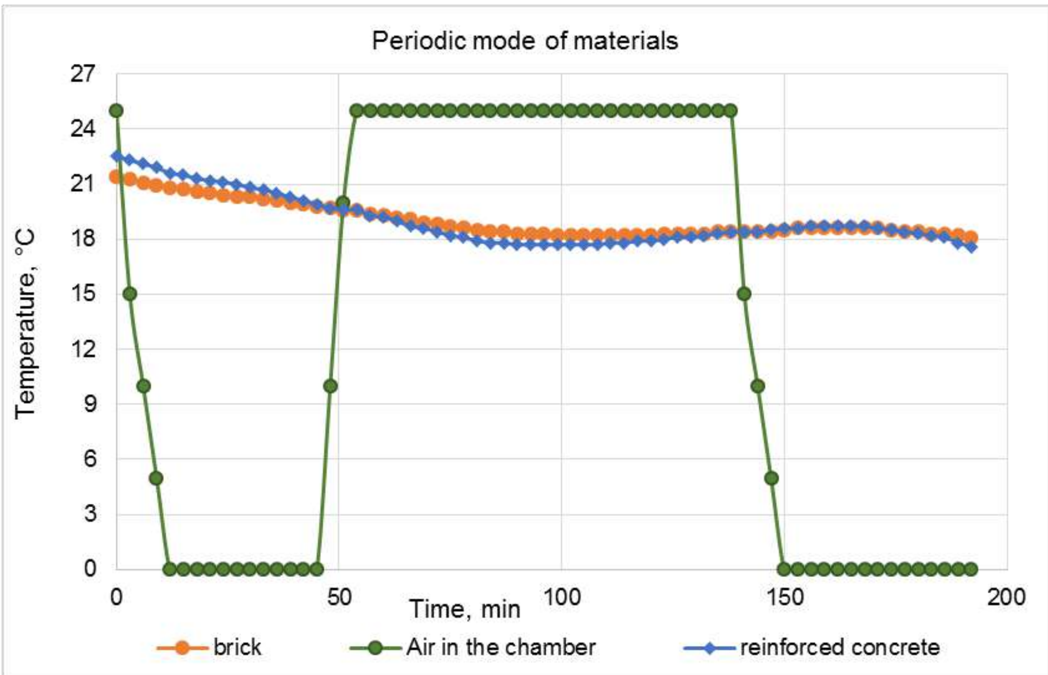

Figure 5. Internal air temperature of the structures

As a result, it is seen that when cooling for the same time, the air inside the brick structure cools down considerably less than in reinforced concrete structure. Furthermore, when heated, the reinforced concrete continues to cool down, the brick reacts more stable to temperature changes. At the second cooling phase the brick keeps an average temperature of 18.5°C. In contrast to the reinforced concrete which continues to give off heat, and then reduces heat.

This is due to the fact that reinforced concrete is considered to be an inhomogeneous material and the reinforcement works as a bridge of cold, which can be clearly seen on the resulting graph.

In consequence of this, it will be most comfortable to stay indoors, under the given conditions, with a reinforced concrete structure because it will be considerably hotter under cold temperatures and colder under high temperatures. But is the brick the one considered to be the most thermally stable material, so for purposes of this paper is recommended brick as the appropriate material due to the fact that keeps temperature in a more stable way than concrete does, is more suitable for keeping indoor conditions in a more unchanging manner.

Analyzing each phase of drastic temperature changes has been found the following. For the first drop down both materials release energy as is expected, the concrete has a considerably steeper slope than brick does in the graph. The second phase is when temperature increases drastically; both materials continue to release until they get a stable point and begin to absorb energy. Concrete shows a changes in its graph´s slope in a more differentiable way than brick does, its slope changes faster. The third phase is the final drop down of temperature; both materials keep increasing temperature until their stable point when they begin to drop down, ones more, is the concrete the one with more pronounced changes of slope in the graph.

Analyzing each phase of the experiment the results show that internal temperature of both structures has the form of a smoothly varying function.

It is shown the good convenience of bricks for guarantee a more suitable condition of comfort inside structures. In article [15] authors also considered behavior of materials and measured temperature of material in different points. This article consider indoor temperature of the air under the condition of different barrier materials.

A point to be taken into account is the humidity factor, the experiment was made with 55 % humidity but in tropical conditions it may reach up to 90%. Humidity does not affect the inside temperature but it affects the human body. For further research it is recommended to install humidity sensors and to consider the effect of heat and humidity regime in the room. As exposed in other articles [3, 9] is highly important the fact of keeping appropriate conditions for residents, both offices and living spaces. Results support the fact that more than considering price of materials should keep in mind also the advantages over long term periods [19–23].

Conclusion

This paper aims to compare the thermal behavior of the typical materials for constructions in tropical weathers, particularly was choose Colombia as a representative to the normal temperature characteristics for these types of regions. Bricks and reinforced concrete were the analyzed materials. The results showed a difference between both materials which can be considered decisive at the moment of taking a decision for choosing the most appropriate construction material. For drastic changes of temperature it has shown the way bricks and concrete behave; been more recommendable to have the first ones as an element of thermal stability material which is translated into more conformability for tropical climates.

According to results, the following conclusions have been done:

1. Full cooling time of the reinforced concrete was 90 minutes, cooling time of the brick was 99 minutes;
2. Then temperature in the chamber was 25 °C again. Materials kept cooling down for 36 minutes (reinforced concrete) and 45 minutes (brick).
3. Full heating time of the reinforced concrete was 66 minutes, brick was 54 minutes;
4. Then temperature in the chamber was changed to 0 °C. Materials kept heating up for 6 minutes (reinforced concrete) and 3 minutes (brick).
5. The lowest internal temperature was for reinforced concrete structure (17.6 °C).
6. Both materials are comparatively resistant to sudden temperature changes, but temperature range of the reinforced concrete (4.9 °C) is bigger, than brick (3.3 °C).

For drastic changes of temperature it has shown the way bricks and concrete behave, been more recommendable to have the first ones as an element of thermal stability material which is translated into more conformability for tropical climates.

As a further study may be conducted an assessment for drastic cooling and heating with a higher percentage of humidity. Moreover would be appropriate to consider the same methodology in 1:1 scale conditions, this is by installing all the equipment and sensors inside concrete and bricks buildings and collect supporting results.

References

1. Mattar S., Morales V., Cassab A., Rodríguez-Morales A. J. Effect of climate variables on dengue incidence in a tropical Caribbean municipality of Colombia, Cerete 2003–2008. *International Journal of Infectious Diseases.* 2013. Vol. 17.

Литература

1. Mattar S., Morales V., Cassab A., Rodríguez-Morales A. J. Effect of climate variables on dengue incidence in a tropical Caribbean municipality of Colombia, Cerete 2003–2008 // International Journal of Infectious Diseases. 2013. Vol. 17.

No. 5. Pp. e358–e359.
2. Franco J.F., Pacheco J., Belalcázar L.C., Behrentz, E. Characterization and source identification of VOC species in Bogotá, Colombia. *Journal Atmosfera.* 2015. Vol. 28. No. 1. Pp. 1–11.
3. Bluyssen P.M., Aries M., van Dommelen P. Comfort of workers in office buildings: the European hope project. *Building and Environment.* 2011. No. 46. Pp. 280–288.
4. Afanador García N., Ibarra Jaime A.C., López Durán C.A. Caracterización de arcillas empleadas en pasta cerámica para la elaboración de ladrillos en la zona de Ocaña, Norte de Santander. Characterization of clays used for bricks in the Ocaña zone, North Santander. *Epsilon Magazine.* 2013. No. 20. Pp. 101–119.
5. Engel J.M., Zhao L., Fan Z., Chen J., Liu C. Smart brick. *Masonry Construction the World of Masonry.* 2005. Vol. 18. No. 8. Pp. 39–41.
6. Kamendere E., Grava L., Zvaigznitis K., Kamenders A., Blumberga A. Properties of brick masonry of historical buildings as a background for safe renovation measures. *International Scientific Conference “Environmental and Climate Technologies”.* 2015. Pp. 119–123.
7. Vatin N., Gamayunova O., Nemova D. An energy audit of kindergartens to improve their energy efficiency. *Advances in Civil Engineering and Building Materials IV - Selected and Peer Reviewed Papers from the 2014 4th International Conference on Civil Engineering and Building Materials, CEBM 2014 4th.* 2015. Pp. 305–308.
8. Vatin N.I., Nemova D.V., Rymkevich P.P., Gorshkov A.S. Influence of building envelope thermal protection on heat loss value in the building. *Magazine of Civil Engineering.* 2012. № 8(34). Pp. 4–14. (rus)
9. Musorina T., Olshevskyi V., Ostrovaia A., Statsenko E. Experimental assessment of moisture transfer in the vertical ventilated channel. *MATEC Web of Conferences.* 2016. Vol. 73. Pp. 02002.
10. Vatin N., Petrichenko M., Nemova D. Hydraulic methods for calculation of system of rear ventilated facades. *Applied Mechanics and Materials.* 2014. Vol. 633–634. Pp. 1007–1012.
11. Petrichenko M., Vatin N., Nemova D., Kharkov N., Korsun A. Numerical modeling of thermogravitational convection in air gap of system of rear ventilated facades. *Applied Mechanics and Materials.* 2014. Vol. 672–674. Pp. 1903–1908.
12. Petrichenko M., Ostrovaia A., Statsenko E. The glass ventilated facades – research of an air gap. *Applied Mechanics and Materials.* 2015. Vol. 725–726. Pp. 87–92.
13. Statcenko E.A., Ostrovaia A.F., Musorina T.A., Kukolev M.I., Petritchenko M.R. The elementary mathematical model of sustainable enclosing structure. *Magazine of Civil Engineering.* 2016. No. 8. Pp. 86–91.
14. Zaborova D.D., Kukolev M.I., Musorina T.A., Petrichenko M.R. The simplest mathematical model of the energy efficiency of layered building envelopes. *Nauchno-tekhnicheskiye vedomosti Sankt-Peterburgskogo gosudarstvennogo politekhnicheskogo universiteta.* 2016. Vol. 4. Pp. 28–33.
15. Zaborova D.D., Musorina T.A., Petrichenko M.R. Termicheskaya neustoychivost stenovykh konstruktsiy s uteplitelem [Thermal imbalance of wall constructions with a heater]. *Stroitelstvo — formirovaniye sredy zhiznedeyatelnosti Elektronnyy resurs: sbornik trudov XX Mezhdunarodnoy mezhvuzovskoy nauchno-prakticheskoy konferentsii studentov, magistrantov, aspirantov i molodykh uchenykh* [Construction - the formation of the environment of life Electronic resource: proceedings XX International Interuniversity Scientific and Practical Conference of students, undergraduates, graduate students and young scientists]. 2017. Pp. 813–815.

№ 5. Pp. e358–e359.
2. Franco J.F., Pacheco J., Belalcázar L.C., Behrentz, E. Characterization and source identification of VOC species in Bogotá, Colombia // Journal Atmosfera. 2015. Vol. 28. № 1. Pp. 1–11.
3. Bluyssen P.M., Aries M., van Dommelen P. Comfort of workers in office buildings: the European hope project // Building and Environment. 2011. № 46. Pp. 280–288.
4. Afanador García N., Ibarra Jaime A.C., López Durán C.A. Caracterización de arcillas empleadas en pasta cerámica para la elaboración de ladrillos en la zona de Ocaña, Norte de Santander. Characterization of clays used for bricks in the Ocaña zone, North Santander // Epsilon Magazine. 2013. № 20. Pp. 101–119.
5. Engel J.M., Zhao L., Fan Z., Chen J., Liu C. Smart brick // Masonry Construction the World of Masonry. 2005. Vol. 18. № 8. Pp. 39–41.
6. Kamendere E., Grava L., Zvaigznitis K., Kamenders A., Blumberga A. Properties of brick masonry of historical buildings as a background for safe renovation measures // International Scientific Conference “Environmental and Climate Technologies”. 2015. Pp. 119–123.
7. Vatin N., Gamayunova O., Nemova D. An energy audit of kindergartens to improve their energy efficiency // Advances in Civil Engineering and Building Materials IV - Selected and Peer Reviewed Papers from the 2014 4th International Conference on Civil Engineering and Building Materials, CEBM 2014 4th. 2015. Pp. 305–308.
8. Ватин Н.И., Немова Д.В. Рымкевич П.П. Горшков А.С. Влияние уровня тепловой защиты ограждающих конструкций на величину потерь тепловой энергии в здании // Инженерно-строительный журнал. 2012. № 8(34). С. 4–14.
9. Musorina T., Olshevskyi V., Ostrovaia A., Statsenko E. Experimental assessment of moisture transfer in the vertical ventilated channel // MATEC Web of Conferences. 2016. Vol. 73. Pp. 02002.
10. Vatin N., Petrichenko M., Nemova D. Hydraulic methods for calculation of system of rear ventilated facades // Applied Mechanics and Materials. 2014. Vol. 633–634. Pp. 1007–1012.
11. Petrichenko M., Vatin N., Nemova D., Kharkov N., Korsun A. Numerical modeling of thermogravitational convection in air gap of system of rear ventilated facades // Applied Mechanics and Materials. 2014. Vol. 672–674. Pp. 1903–1908.
12. Petrichenko M., Ostrovaia A., Statsenko E. The glass ventilated facades – research of an air gap // Applied Mechanics and Materials. 2015. Vol. 725–726. Pp. 87–92.
13. Стаценко Е.А., Островая А.Ф.,Мусорина Т.А., Куколев М.И., Петриченко М.Р. Простая модель теплоустойчивой ограждающей конструкции // Инженерно-строительный журнал. 2016. № 8(68). С. 86–91.
14. Заборова Д.Д., Куколев М.И., Мусорина Т.А., Петриченко М.Р. Математическая модель энергетической эффективности слоистых строительных ограждений // Научно-технические ведомости Санкт-Петербургского государственного политехнического университета. 2016. Т. 4. С. 28–33.
15. Заборова Д.Д., Мусорина Т.А., Петриченко М.Р. Термическая неустойчивость стеновых конструкций с утеплителем // Строительство — формирование среды жизнедеятельности Электронный ресурс: сборник трудов XX Международной межвузовской научно-практической конференции студентов, магистрантов, аспирантов и молодых учёных. 2017. С. 813–815.
16. Keyvanfar A., Shafaghat A., Abd Majid M.Z., Bin Lamit H., Hussin M.W., Ali K.N.B., Saad A.D. User satisfaction adaptive behavior criteria for assessing energy efficient building indoor cooling and lighting qualities // Journal of

16. Keyvanfar A., Shafaghat A., Abd Majid M.Z., Bin Lamit H., Hussin M.W., Ali K.N.B., Saad A.D. User satisfaction adaptive behavior criteria for assessing energy efficient building indoor cooling and lighting qualities. *Journal of Renewable & Sustainable Energy Reviews.* 2014. Vol. 39. Pp. 277-293.
17. Nagy B., Nehme S.G., Szagri D. Thermal properties and modeling of fiber reinforced concretes. *Energy Procedia.* 2015. Vol. 78. Pp. 2742–2747.
18. Bricks - Thermal Conductivity and Thermal Resistance of Extruded and Pressed House Bricks. Sponsored by Austral BrickAug 13. 2002.
19. Pacheco-Torgal F., Shasavandi A., Jalali S. Eco-Efficient Concrete Using Industrial Wastes: A Review. *Materials Science Forum.* 2013. T. 730-732, s. 581-586.
20. 20. Fares, H., Remond, S., Noumowe, A., Cousture, A. High temperature behaviour of self-consolidating concrete. Microstructure and physicochemical properties. *Cement and Concrete Research.* 2010. Vol. 40. No. 3. Pp. 488–496.
21. *NSR 10 – Seismic Norm code for Colombia.* Consulted on April 2017.
22. Zhang L. Production of bricks from waste materials - A review. *Construction and Building Materials.* 2013. Vol. 47. Pp. 643–655.
23. Borovkov V.M., Kalyutik A.A., Sergeyev V.V. *Teplomassoobmennoye oborudovaniye* [Heat-mass exchange equipment]. Izd-vo Politekhnicheskogo un-ta. 2008. 231 p.

16. Keyvanfar A., Shafaghat A., Abd Majid M.Z., Bin Lamit H., Hussin M.W., Ali K.N.B., Saad A.D. User satisfaction adaptive behavior criteria for assessing energy efficient building indoor cooling and lighting qualities // Journal of Renewable & Sustainable Energy Reviews. 2014. Vol. 39. Pp. 277–293.
17. Nagy B., Nehme S.G., Szagri D. Thermal properties and modeling of fiber reinforced concretes // Energy Procedia. 2015. Vol. 78. Pp. 2742–2747.
18. Bricks - Thermal Conductivity and Thermal Resistance of Extruded and Pressed House Bricks. Sponsored by Austral BrickAug 13. 2002.
19. Pacheco-Torgal F., Shasavandi A., Jalali S. Eco-Efficient Concrete Using Industrial Wastes: A Review // Materials Science Forum. 2013. Vol. 730–732. Pp. 581–586.
20. Fares H., Remond S., Noumowe A., Cousture A. High temperature behaviour of self-consolidating concrete. Microstructure and physicochemical properties // Cement and Concrete Research. 2010. Vol. 40. № 3. Pp. 488–496.
21. NSR 10 – Seismic Norm code for Colombia. Consulted on April 2017.
22. Zhang L. Production of bricks from waste materials - A review // Construction and Building Materials. 2013. Vol. 47. Pp. 643–655.
23. Боровков В.М., Калютик А.А., Сергеев В.В. Тепломассообменное оборудование. Изд-во Политехнического ун-та. 2008. 231 с.

Jose Castro,
+7(996)771-50-59;
jose.castro.lozano@hotmail.com

Daria Zaborova,
+7(911)180-60-33; zaborova-dasha@mail.ru

Tatiana Musorina,
+7(952)286-03-76; flamingo-93@mail.ru

Ivan Arkhipov,
+7(967)552-63-91; ivan-arhipov-95@mail.ru

Хосе Кастро,
+7(996)771-50-59;
эл. почта: jose.castro.lozano@hotmail.com

Дарья Дмитриевна Заборова,
+7(911)180-60-33;
эл. почта: zaborova-dasha@mail.ru

Татьяна Александровна Мусорина,
+7(952)286-03-76;
эл. почта: flamingo-93@mail.ru

Иван Евгеньевич Архипов,
+7(967)552-63-91;
эл. почта: ivan-arhipov-95@mail.ru

doi: 10.18720/MCE.76.6

The deflection of spatial coatings with periodic structure

Прогиб пространственного покрытия с периодической структурой

M.N. Kirsanov,
National Research University "Moscow Power Engineering Institute", Moscow, Russia

Д-р физ.-мат. наук, профессор
М.Н. Кирсанов,
Национальный исследовательский университет "МЭИ", г.Москва, Россия

Key words: spatial truss; deflection; Maple; analytical solution; coating

Ключевые слова: пространственная ферма; прогиб; Maple; аналитическое решение; покрытие

Abstract. The scheme of the statically determinate spatial truss is proposed. Rectangular truss has a vertical supports on the sides and loaded uniformly at the nodes by the vertical forces. The forces in the rods and supports are determined using cut nodes method. The dependence of the deflection mid-span on a number of panels is obtained. A generalization of the particular solutions on an arbitrary number of panels obtained by the method of induction. All transformations and solutions are made in the system of computer mathematics Maple. The homogeneous linear recurrence equation satisfied by the members of the sequence of coefficients of the desired formula are derived and solved using the special operators of Maple. The formula for deflection is polynomial type in the number of panels. Plots of the deflection of the number of panels, height and the distribution ratio of cross-sectional areas of the rods are given. Expression of forces in the most stretched and compressed rods are obtained to perform durability and structural stability. The found solutions can be used by practical engineers to assess the performance of the designed construction and its optimization.

Аннотация. Предложена схема статически определимой пространственной фермы. Прямоугольная в плане ферма имеет вертикальные опоры по боковым сторонам и равномерно нагружена в узлах вертикальной нагрузкой. Усилия в стержнях и опорах определяются методом вырезания узлов. Найдена зависимость прогиба середины пролета от числа панелей. Обобщение частных решений на произвольное число панелей получено методом индукции. Все преобразования и решения выполнены в системе компьютерной математики Maple. С помощью специальных операторов Maple выводятся и решаются однородные линейные рекуррентные уравнения, которым удовлетворяют члены последовательностей коэффициентов искомой формулы. Полученная формула для прогиба имеет полиномиальный по числу панелей характер. Построены графики зависимости прогиба от числа панелей, от высоты и от коэффициента распределения площадей поперечных сечений в стержнях. Применительно к анализу прочности и устойчивости конструкции найдены выражения для усилий в наиболее растянутых и сжатых стержнях. Найденные решения могут быть использованы практическими инженерами для оценки работоспособности проектируемой конструкции и для ее оптимизации.

Introduction

One of the urgent problems of structural mechanics is the problem of overlap in large areas. This is required in the construction of hangars for aircraft, modern shopping centers, airports and concert halls. Known variants of the coatings in the form of hanging structures [1–4], the overlap in the membrane [5, 6]. As one of the most simple and easily implemented solutions to cover large areas without the use of intermediate supports is the use of lightweight trusses [7–11].

In this paper, we design and analytical calculation of truss (Fig. 1). The design consists of several gable trusses connected along the long sides. Statically determinate truss with $2n$ panels on one side and $2m$ on the other contains $n_s = 3(4mn + 2m + 2n + 1)$ rods, including three rods, forming a spherical bearing A and cylindrical B. At the sides of the truss located $4(m+n)$ vertical support legs with a length h and $h+c$ (Figs. 2,3). Truss consist $2n(2m+1)$ horizontal rod a long, $4mn$ bracing of length $d = \sqrt{a^2 + b^2 + h^2}$ and $2m(2n+1)$ inclined struts of length $g = \sqrt{b^2 + h^2}$.

Кирсанов М.Н. Прогиб пространственного покрытия с периодической структурой // Инженерно-строительный журнал. 2017. № 8(76). С. 58–66.

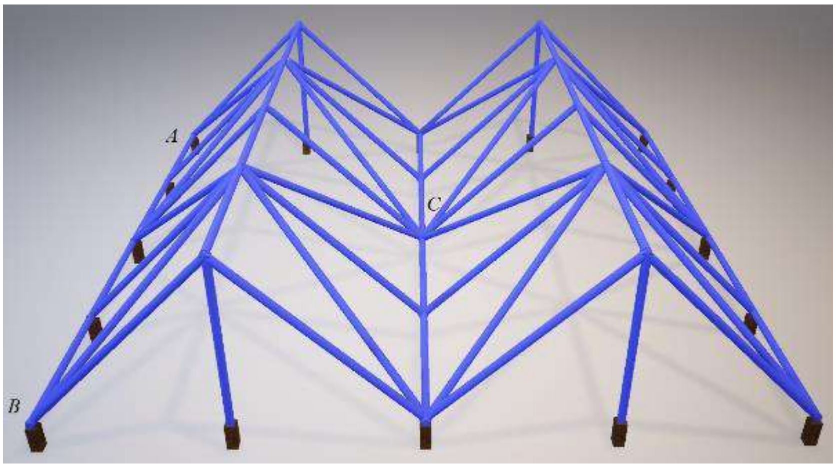

Figure 1. 3D model of the truss, $n = m = 2$

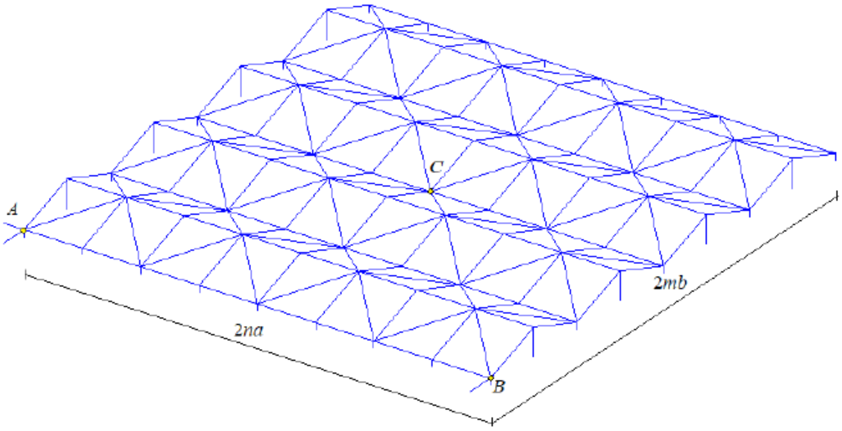

Figure 2. The scheme of the truss, $m = n = 4$

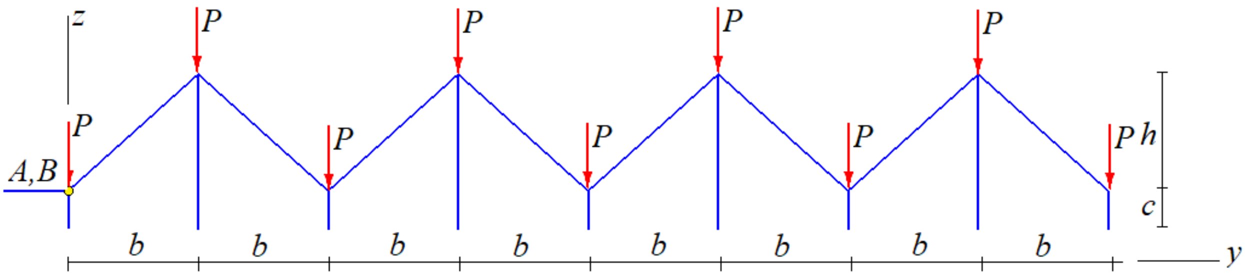

Figure 3. Truss and load in plane $y - z$, m=4

The calculation of the stresses in the rods

The task is to find the analytic dependence of the deflection of the panels under uniform loading of a truss in the joints. A mathematical model of truss has been built in the system of analytical transformations Maple [12]. A similar problem for statically determinate rectangular cover with four nodes in the corners of the structure and an arbitrary number of panels is decided by the author [13, 14]. The analytical dependence of the spatial deflection of the cantilever truss on a number of panels is found in [15]. Beam spatial truss with the construction rise is investigated in an analytical form in [16].

The program [12] is used to determine the stresses in the bars. The algorithm is based on the method of cutting nodes in symbolic form. Therefore, it allows applying the method of induction to generalize the solution for an arbitrary number of panels. The program introduces the coordinates of the nodes of the core mesh

$$x_k = a(i-1), y_k = b(j-1), \ z_k = 0, \ k = i + (j-1)(2n+1), \ i = 1,..,2n+1, \ j = 1,..,2m+1,$$
$$z_{i+(2j-1)(2n+1)} = h, \ i = 1,..,2n+1, \ j = 1,..,m. \quad (1)$$

The order of connection of rods and nodes (joints) is set by the special vectors containing the numbers of the rods ends. Orthogonal mesh of coating is specified, for example, by vectors

$$V_{i+2n(j-1)} = [i + (j-1)(2n+1), i + (j-1)(2n+1) + 1], \ i = 1,..,2n, \ j = 1,..,2m+1,$$

$$V_{i+u+2m(j-1)} = [j + (2n+1)(i-1), \ j + (2n+1)i], \ u = 2n(2m+1), \ i = 1,..,2m, \ j = 1,..,2n+1.$$

Similarly, the braces and support legs are encoded. The matrix of equilibrium equations of the nodes is formed of the guides of the cosines of forces, determined based on the given geometry of the structure and the order of connection of terminals [13–16]. The rows of the matrix with numbers $3i-2, \ i = 1,...,n_s$ corresponding to a projection of the efforts on the axis of *x.* The rows $3i-1$ correspond to the projections on the *y*-axis; rows $3i$ are the projection on a vertical *z*-axis. The load (vertical force *P*) is applied at all nodes of the truss. The right part of the system of equilibrium equations is a vector $B_{3i} = -P, \ i = 1,..,(2n+1)(2m+1).$ The solution of the system equations in symbolic form with specified numbers of panels m and n gives the forces in all members (including supporting members) of the respective truss. Reactions of supports of the vertical struts along the longitudinal side length 2*na* do not depend on the number of panels m the transverse direction: $R_a = -(2n+1)P/2$. This dependence turned out the simplest generalization of the solutions for n=1, 2, 3, ... The reactions of the supports along the lateral sides do not depend on the number n: $R_b = -P$. These supports take the vertical load applied to the corresponding node. The reactions of horizontal connections in the corner hinge *A* and hinge *B* equal to zero.

For the calculation of the stability of rods in the truss according to the calculations of forces in rods with different numbers of panels on the sides of the structure one can be obtained the function of efforts in the most compressed and stretched rods from the values of *n* and *m*. Here depending on the parity of m longitudinal horizontal rods in the middle of the span, connected with the Central node in the truss will either be compressed or stretched. For even *n* these rods are in the stretched lower zone (Figs. 1, 2, 4). These values are independent of number *m*, and the dependence of the number of longitudinal panels n revealed by induction with the help of operators *rgf_findrecur* and *rsolve* of Maple [11-16]: $S^{(+)} = P(2n^2 - 1 - (-1)^n)a/(2h)$, m=2k. For odd *m* (Fig. 5) the corresponding rods are at the top of the truss, and they are compressed, and also the efforts do not depend on m>1. The dependence of the number n has the form $S^{(-)} = -P(2n^2 + (-1)^n - 1)a/(2h)$. Transverse oblique bars (Figs. 4, 5) connected to the central node, depending on the parity of *n* are compressed or stretched at any values of m: $T = -(-1)^n Pg/(2h)$.

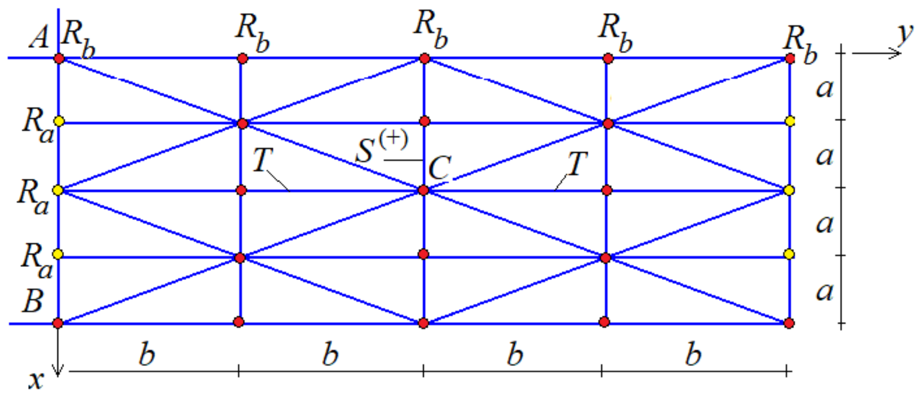

Figure 4. The forces in the rods and the support reaction for the even numbers m, ($n = 2, m = 2$)

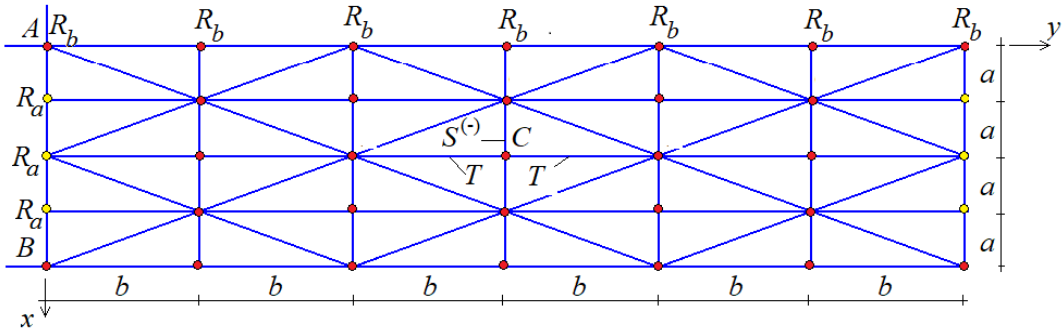

Figure 5. The forces in the rods and the support reaction for odd numbers m, ($n = 2, m = 3$)

Deflection

Figures We use the formula of Maxwell-Mohr for the computation of deflection:

$$\Delta = \Delta_1 + \Delta_2 = \sum_{j=1}^{n_1} \frac{S_j s_j l_j}{EF_j} + \sum_{j=n_1+1}^{n_s} \frac{S_j s_j l_j}{EF_j}, \tag{2}$$

where $n_1 = 2(6mn + m + n)$ – is the number of rods of the covering, E – cthe modulus of elasticity of the rods F_j, l_j and S_j – the cross-sectional area, length and stress in *j*-th core under the action of a given load s_j – forces under a single vertical force applied to the central node *C*. The sum Δ_1 allocated separately by member cover and the sum Δ_2 – of vertical supports. The summ has been conducted on all cores of the truss. In the General case of the square sections of the truss may be different. Let the sections of all the trusses of the truss, in addition to the vertical support posts, have an area $F_j = F$, $j = 1,..,n_1$, and the cross-sectional area of the racks $F_j = \gamma F$, $j = n_1 + 1,..,n_s$. The ratio γ defines the cross-section of the compressed struts and set by the designer. Consider the case $m = n$. A consistent calculation of the deflection of the truss by the formula (2) shows that the formula Δ_1 for all values of *n* did not change (which is a consequence of the regularity of the structure [17–19]):

$$\Delta_1 = P(C_{1,n}a^3 + C_{2,n}d^3 + C_{3,n}g^3)/(8h^2EF). \tag{3}$$

The coefficients in this relationship form a sequence, shared members, which can be determined using operators *rgf_findrecur* and *rsolve* of Maple. For the coefficient at a^3 the operator *rgf_findrecur* returns an equation of the fifth order

$$C_{1,n} = 5C_{1,n-1} - 10C_{1,n-2} + 10C_{1,n-3} - 5C_{1,n-4} + C_{1,n-5}.$$

The initial conditions obtained from the solutions of the problems of deflection of trusses with $n = 2,...,6$, have the form

$$C_{1,2} = 96, C_{1,3} = 552, C_{1,4} = 1728, C_{1,5} = 4200, \; C_{1,6} = 8688.$$

The operator *rsolve* gives the following solution of the recurrence equation

$$C_{1,n} = 6(n^4 + 2n^3 - 13n^2 + 38n - 40).$$

Similarly, there are other coefficients

$$C_{2,n} = 4n^2,$$

$$C_{3,n} = (1 - 2n)((-1)^n - 1),$$

and also, the second term in (2) — the deflection due to deformation of the support pillars:

$$\Delta_2 = P(2n+1)(c + h(1 - (-1)^n)/2)/(\gamma EF). \tag{4}$$

Curves of the dimensionless deflection of the panels (Fig. 6) in the condition of the constancy of the span construction $L = 60\,m$, $b = a = L/(2n)$, and the total load to the truss $P_{sum} = (2n+1)^2 P$ show almost monotonous decrease of the deflection with increasing number of panels. Given the notation: $\Delta_1' = \Delta_1 EF/(P_{sum}L)$.

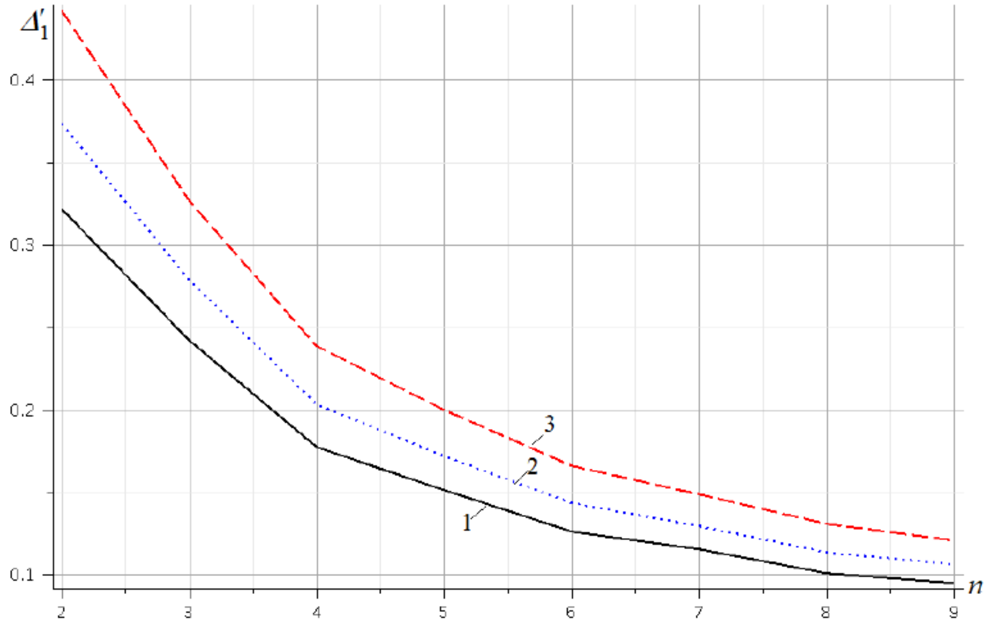

Figure 6. The dependence of the deflection of the panels.
1 – = $12m$, 2 – $h = 11m$, 3 – $h = 10m$

The dependence of the deflection of the height of the truss (in the previous assumptions on the total load and length of span) is more complicated. At sufficiently high altitudes of the truss, curves reveal the minimum (Fig. 7). This fact can be used to optimize stiffness. Analytical expressions for the minimum value cannot be obtained. Simple numerical calculations by formula (3) show that with the increase in the number of panels the critical height decreases.

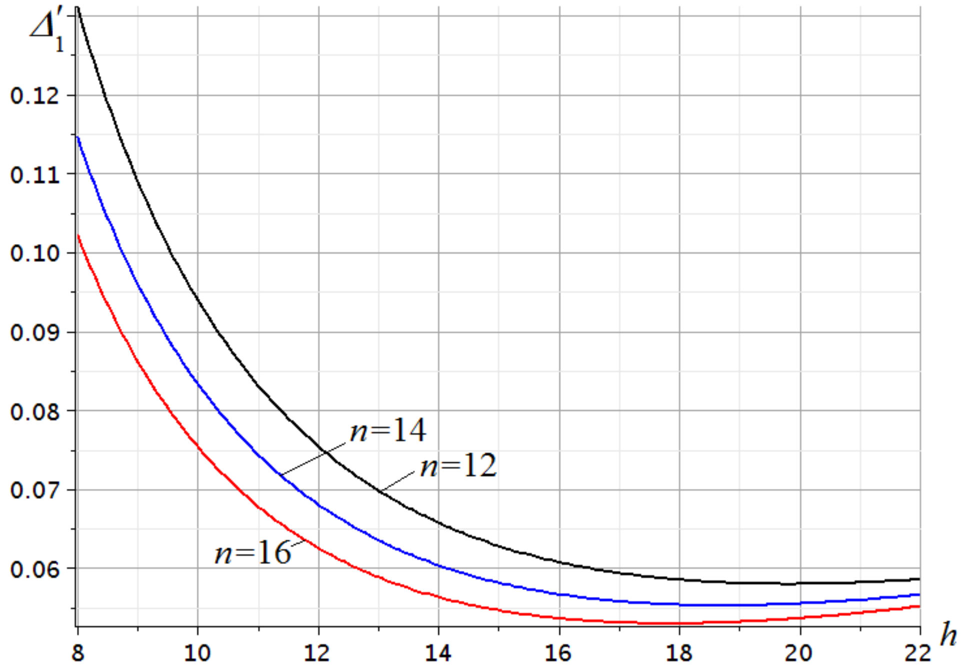

Figure 7. The dependence of the deflection of the height

The effect of the gain of the cross sections of the support racks on the solution is shown in the curves in Figure 8. An interesting and unexpected effect of the intersection of the curves was found for different numbers of panels.

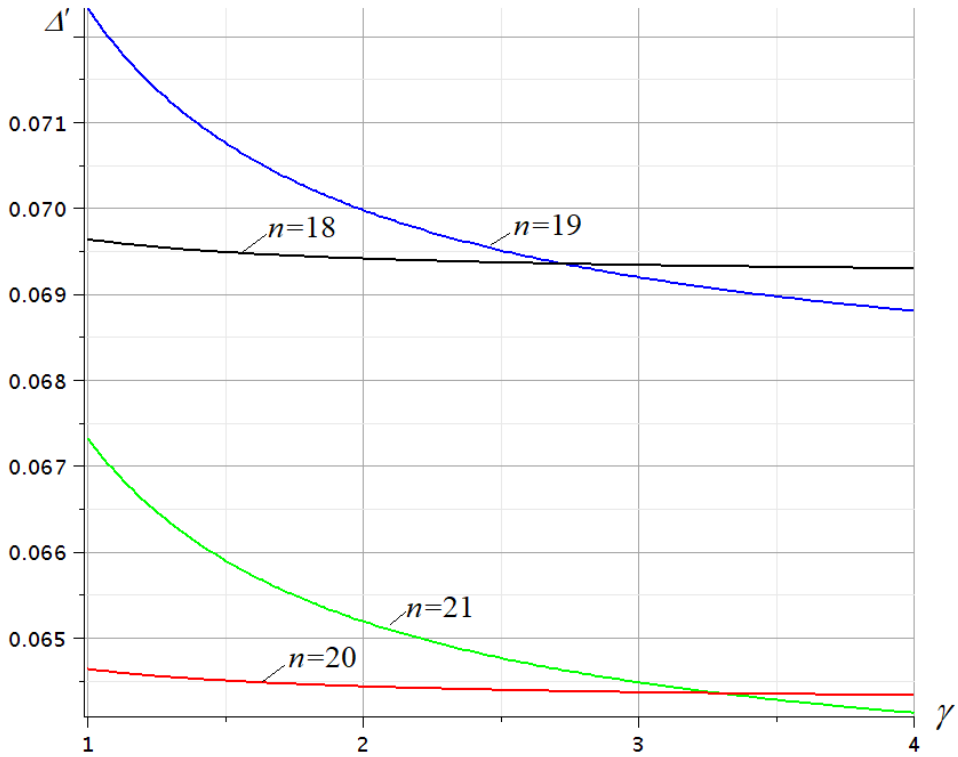

Figure 8. Dependence of the deflection on the cross-section ratio, *h* = 10 m, *L* = 60 m

We also give a formula for deflecting a truss from the action of one concentrated force in the central hinge *C*

$$\Delta_3 = P\left((n^3a^3 + nd^3 + (1-(-1)^n)g^3/2)/h^2 + (2c + h(1-(-1)^n))/\gamma\right)/(4EF). \quad (5)$$

To derive this formula, it was sufficient to use the values of the forces s_j obtained from the action of the unit force used in the derivation of the solution (3). The coefficients here turned out to be quite simple, and the operators of the Maple system did not need to compile and solve recurrence equations. The check of the analytical dependencies (3), (4) and (5) was carried out for different values of *n* according to the same program [12] but in the numerical mode. The speed of numerical transformations in Maple is inferior to specialized programs based on the finite element method, but it is an order of magnitude higher than the rate of symbolic transformations. It is this feature of the symbolic transformations, which does not allow directly obtaining a formula of the form (3) for large numbers of panels, that has caused the development of inductive methods. From the practice of calculating spatial trusses, it was noted that as the number of panels increases, the time of symbolic transformations grows faster than the geometric sequence. If seconds are required to obtain the formula (3) for $n = 2$ with integer coefficients $C_{1,n}$, $C_{2,n}$, $C_{3,n}$ necessary for the initial conditions of the corresponding recurrent equations, then the solution of the same problem for $n = 9$ requires the operating hours of the computer with a high-speed processor i7 and 16 GB memory. However, in this problem, an interesting move has been found that makes it possible to shorten the time of obtaining a sequence with a length sufficient to reveal its common term. It turned out that for $C_{2,n}$, $C_{3,n}$ simpler formulas are obtained based on the calculation of only six trusses with $n = 2, ..., 7$, while the lengths of the corresponding sequence of coefficients $C_{1,n}$ are still insufficient to obtain a common term. The *rgf_findrecur* operator does not give a recursive equation for $C_{1,n}$ if the sequence is not long enough. Therefore, it was decided to obtain a sequence of solutions in a numerical mode that is practically unlimited in counting speed, and subtract the terms $C_{2,n}d^3$ and $C_{3,n}g^3$ from the obtained numerical values of the deflection, and formulas for the coefficients in which have already been obtained. If we take a = 1 in this numerical experiment, then the difference found just gives the coefficient $C_{1,n}$ for n = 2, ..., 10. After this, with the involvement of the operator, one can obtain the desired common term.

Results and Discussion

In [17, 18] R.G. Hutchinson and N.A. Fleck announced the "hunt" for schemes of statically determinate periodic trusses. The number of such constructions is limited [19, 20]. In this paper, we propose new scheme of a spatial construction of this type. The advantages of analytical calculations of such trusses are obvious. By changing only one parameter in the solution, one can obtain and analyze solutions for a fairly wide class of constructions. Sometimes when analyzing such solutions, hidden and quite dangerous features of the trusses are found. For example, in [11] it was found that for an even number of panels the truss becomes a kinematically variable mechanism. The investigated truss (Fig. 1) does not possess similar features, however, when the shape of the surface $z = z(i, j)$ given by function (1) changes, one can obtain the case when the determinant of the system of equations becomes zero. In particular, this is possible if all rods connected to a node are in the same plane. In this case, the load on the node perpendicular to the plane of the rods can not be balanced. We note that it is the easiest method to discover the unique features of the construction and to outline the ways of its optimization from the formal representation of the result. It is the direction of the research chosen by the author and his students [20–23]. Another direction in analytical research can be the solution to problems based on the symbolic form of equilibrium equations or equations of the finite element method. This method has the right to exist, especially for solving problems for irregular (non-periodic) systems. However, it is not possible to obtain any closed compact formulas suitable for analysis and practical use [24]. In [25–27] simple semi-empirical approximate formulas are proposed for the calculation of flat and spatial trusses. It is possible that the linear formulation of the problem, adopted in analytical calculations, does not always yield exact solutions. Non-linear analysis of the trusses [28] is usually performed numerically, but some algorithms used in this study can be useful for a non-linear statement of the problem.

Conclusions

A new periodic core structure of the spatial coverage is proposed and analytically investigated. A formula has been obtained for the dependence of the deflection in the middle part of the span on the number of panels. The solution found, in addition to the magnitude of the load and the characteristics of the material, contains five geometric parameters describing the dimensions and shape of the structure. Therefore, it allows us to apply the desired formula for a fairly wide class of similar trusses, both for a simple estimation of the possibilities of the construction and for testing the numerical solutions found possible with a more general formulation of the problem. The applied algorithm of modeling the cover with supports along its entire perimeter makes it possible to easily generalize the form of the coating to some more complex, possibly non-periodic, surface. However, in this case, the possibility for an analytical calculation of deflection and effort disappears. The experience of modeling and experiments in the Maple system in this direction showed that not all surfaces, even periodic ones, allow the use of the induction method. The limitation here is the time of symbolic transformations. Transformations lasting more than a day and with a result in the form of a formula per page or more lose their practical meaning. Facilities with these properties make sense to calculate numerically, obtaining particular solutions for each specific case

References

1. Kirsanov N.M. *Visyachiye pokrytiya proizvodstvennykh zdaniy* [Hanging covers of industrial buildings]. Moscow: Stroyizdat. 1990. 128 p. (rus)
2. Sophianopoulos D.S., Michaltsos G.T. Nonlinear stability of a simplified model for the simulation of double suspension roofs. *Engineering Structures.* 2001. Vol. 23. No. 6. Pp. 705–714.
3. Diord S., Magalhaes F., Cunha A., Caetano E. High spatial resolution modal identification of a stadium suspension roof: Assessment of the estimates uncertainty and of modal contributions. *Engineering Structures.* 2017. Vol. 135. No. 15. Pp. 117–135.
4. Pyl L., Sitters C.W.M., De Wildea W.P. Design and optimization of roof trusses using morphological indicators. *Advances in Engineering Software.* 2013. Vol. 62–63. No. 8-9. Pp. 9–19.
5. Shimanovskiy A.V., Tsykhanovskiy V.K. *Teoriya i raschet*

Литература

1. Кирсанов Н.М. Висячие покрытия производственных зданий. М.:Стройиздат, 1990. 128 с.
2. Sophianopoulos D.S., Michaltsos G.T. Nonlinear stability of a simplified model for the simulation of double suspension roofs // Engineering Structures. 2001. Vol. 23. №6. Pp. 705–714.
3. Diord S., Magalhaes F., Cunha A., Caetano E. High spatial resolution modal identification of a stadium suspension roof: Assessment of the estimates uncertainty and of modal contributions // Engineering Structures. 2017. Vol. 135. Pp. 117–135.
4. Pyl L., Sitters C.W.M., De Wildea W.P. Design and optimization of roof trusses using morphological indicators // Advances in Engineering Software. 2013. Vol. 62–63. Pp. 9–19.
5. Шимановский А.В., Цыхановский В.К. Теория и расчет

silnonelineynykh konstruktsiy [The theory and analysis of nonlinear structures]. Kiev: Izd-vo "Stal". 2005. 432 p. (rus)
6. Mushchanov V., Gorokhov Y., Vardanyan A., Kashchenko M. Nemova D. Particular features of calculation and design of long-span membrane roofs. *Procedia Engineering.* 2015. Vol. 117. Pp. 990–1000.
7. Cai J., Feng J., Jiang C. Development and analysis of a long-span retractable roof structure. *Journal of Constructional Steel Research.* 2014. Vol. No. 1. Pp. 175–182.
8. Guo Y.-L., Zhao S.-Y., Dou C., Pi Y.-L. Out-of-plane strength design of spatially trussed arches with a rectangular lattice section. *Journal of Constructional Steel Research. 2013*. Vol. 88. No. 9. Pp. 321–329.
9. Guo Y.L., Zhou P., Wang M.Z., Pi Y.L., Bradford M.A., Tong J.Z. Experimental and numerical studies of hysteretic response of tripletruss-confined buckling-restrained braces. *Engineering Structures.* 2017. Vol. 148. No. 1. Pp. 157–174.
10. Nasrollahi A. Optimum shape of large-span trusses according to AISC-LRFD using Ranked Particles Optimization. *Journal of Constructional Steel Research.* 2017. Vol. 134. Pp. 92–101.
11. Kirsanov M.N. Raschet prostranstvennoy sterzhnevoy sistemy, dopuskayushchey mgnovennuyu izmenyayemost [Calculation of spatial bar system that permits variability of instantly]. *Stroitelnaya mekhanika i raschet sooruzheniy*. 2012. No. 3. Pp. 48–51. (rus)
12. Kirsanov M. N. *Maple i Maplet. Resheniya zadach mekhaniki* [Maple, and Maplet. Solving mechanics problems]. Saint Petersburg. Izd-vo Lan'. 2012. 512 p. (rus)
13. Kirsanov M. N. Stress State and Deformation of a Rectangular Spatial Rod Cover. *Scientific Herald of the Voronezh State University of Architecture and Civil Engineering. Construction and Architecture.* 2016. Vol. 31. No. 3. Pp. 71–79.
14. Kirsanov M. N. Analysis of the buckling of spatial truss with cross lattice. *Magazine of Civil Engineering.* 2016. No. 4. Pp. 52–58.
15. Domanov Ye. V. Analiticheskaya zavisimost progiba prostranstvennoy konsoli treugolnogo profilya ot chisla paneley [The analytical dependence of the deflection spatial console triangular profile of the number of panels]. *Science Almanac.* 2016. No. 6-2(19). Pp. 214–217. (rus)
16. Larichev S. A. Induktivnyy analiz vliyaniya stroitelnogo podyema na zhestkost prostranstvennoy balochnoy fermy [Inductive analysis of the impact of the construction hoist on the spatial stiffness of a girder]. *Trends in Applied Mechanics and Mechatronics.* Moscow: Infra-M. 2015. Vol. 1. Pp. 4–8. (rus)
17. Hutchinson R. G., Fleck N.A. Microarchitectured cellular solids – the hunt for statically determinate periodic trusses. *ZAMM Z. Angew. Math. Mech.* 2005. Vol. 85. No. 9. Pp. 607–617.
18. Hutchinson R.G., Fleck N.A. The structural performance of the periodic truss. *Journal of the Mechanics and Physics of Solids.* 2006. Vol. 54. No. 4. Pp. 756–782.
19. Zok F.W., Latture R.M., Begley M.R. Periodic truss structures. *Journal of the Mechanics and Physics of Solids.* 2016. Vol. 96. Pp. 184–203.
20. Tinkov D.V. Sravnitelnyy analiz analiticheskikh resheniy zadachi o progibe fermennykh konstruktsiy [Comparative analysis of analytical solutions to the problem of truss structure deflection]. *Magazine of Civil Engineering.* 2015. No. 5. Pp. 66–73.(rus)
21. Tinkov D.V. Analiz vliyaniya usloviy zakrepleniya na progib ploskoy balochnoy fermy s niskhodyashchimi raskosami [Analysis of the influence of the fixing conditions for the deflection of a flat beam truss with down braces]. *Trends in Applied Mechanics and Mechatronics.* Moscow: Infra-M. 2015. Vol. 1. Pp. 52–56.
22. Smirnova A.A., Rakhmatulina A.R Analytical calculation of the displacement of the truss support. *Science Almanac.* 2017. No. 2-3(28). Pp. 275–278.
23. Rakhmatulina A.R., Smirnova A.A. The dependence of the deflection of the arched truss loaded on the upper belt, on the

сильнонелинейных конструкций. К.: Изд-во "Сталь", 2005. 432 с. (rus)
6. Mushchanov V., Gorokhov Y., Vardanyan A., Kashchenko M., Nemova D. Particular features of calculation and design of long-span membrane roofs // Procedia Engineering. 2015. Vol. 117. Pp. 990–1000.
7. Cai J., Feng J., Jiang C. Development and analysis of a long-span retractable roof structure // Journal of Constructional Steel Research. 2014. Vol. 92. Pp. 175–182.
8. Guo Y.-L., Zhao S.-Y., Dou C., Pi Y.-L. Out-of-plane strength design of spatially trussed arches with a rectangular lattice section // Journal of Constructional Steel Research. 2013. Vol. 88. Pp. 321–329.
9. Guo Y.L., Zhou P., Wang M.Z., Pi Y.L., Bradford M.A., Tong J.Z. Experimental and numerical studies of hysteretic response of tripletruss-confined buckling-restrained braces // Engineering Structures. 2017. Vol. 148. Pp. 157–174.
10. Nasrollahi A. Optimum shape of large-span trusses according to AISC-LRFD using Ranked Particles Optimization // Journal of Constructional Steel Research. 2017. Vol. 134. Pp. 92–101.
11. Кирсанов М.Н. Расчет пространственной стержневой системы, допускающей мгновенную изменяемость // Строительная механика и расчет сооружений. 2012. № 3. С. 48–51.
12. Кирсанов М.Н. Maple и Maplet. Решения задач механики. СПб.: Изд-во Лань, 2012. 512 с. (rus)
13. Kirsanov M. N. Stress State and Deformation of a Rectangular Spatial Rod Cover // Scientific Herald of the Voronezh State University of Architecture and Civil Engineering. Construction and Architecture. 2016. Vol. 31. № 3. Pp. 71–79.
14. Кирсанов М.Н. Анализ прогиба фермы пространственного покрытия с крестообразной решеткой // Инженерно-строительный журнал. 2016. № 4(64). С. 52–58.
15. Доманов Е.В. Аналитическая зависимость прогиба пространственной консоли треугольного профиля от числа панелей // Научный альманах. 2016. № 6-2(19). С. 214–217.
16. Ларичев С.А. Индуктивный анализ влияния строительного подъема на жесткость пространственной балочной фермы // Trends in Applied Mechanics and Mechatronics. М: Инфра-М. 2015. Т. 1. С. 4–8.
17. Hutchinson R.G., Fleck N.A. Microarchitectured cellular solids – the hunt for statically determinate periodic trusses // ZAMM Z. Angew. Math. Mech. 2005. Vol. 85. № 9. Pp. 607–617.
18. Hutchinson R.G., Fleck N.A. The structural performance of the periodic truss // Journal of the Mechanics and Physics of Solids. 2006. Vol. 54. № 4. Pp. 756–782.
19. Zok F.W., Latture R.M., Begley M.R. Periodic truss structures // Journal of the Mechanics and Physics of Solids. 2016. Vol. 96. Pp. 184–203.
20. Тиньков Д.В. Сравнительный анализ аналитических решений задачи о прогибе ферменных конструкций // Инженерно-строительный журнал. 2015. № 5(57). С. 66–73.
21. Тиньков Д.В. Анализ влияния условий закрепления на прогиб плоской балочной фермы с нисходящими раскосами // Trends in Applied Mechanics and Mechatronics. М: Инфра-М. 2015. Т. 1. С. 52–56.
22. Smirnova A.A., Rakhmatulina A.R Analytical calculation of the displacement of the truss support // Научный альманах. 2017. № 2-3(28). С. 275–278.
23. Rakhmatulina A.R., Smirnova A.A. The dependence of the deflection of the arched truss loaded on the upper belt, on the number of panels // Научный альманах.

number of panels. *Science Almanac.* 2017. No. 2-3(28). Pp. 268–271.

24. Rybakov L.S. Linejnaya teoriya ploskoj ortogonal'noj reshetki [Linear theory of a flat orthogonal grid]. *Mekhanika tverdogo tela.* 1999. No. 4. Pp. 174–189. (rus)
25. Marutyan A.S., Pavlenko Yu.I. Priblizhennyy raschet perekrestnykh sistem na staticheskiye vozdeystviya [An approximate calculation of the cross-systems on static exposure]. *Stroitelnaya mekhanika i raschet sooruzheniy*. 2009. No. 4. Pp. 14–20.
26. Marutyan A.S. *Legkiye metallokonstruktsii iz perekrestnykh sistem* [Light metal construction of cross systems]. Pyatigorskiy gosudarstvennyy tekhnologicheskiy universitet. – Pyatigorsk: Izd-vo RIA KMV, 2009. 348 p.
27. Marutyan A.S., Grigoryan M.B., Glukhov S.A. Prostranstvennyye reshetchatyye nesushchiye konstruktsii (moduli tipa «Pyatigorsk»-2)[Spatial lattice supporting structures (modules of type "Pyatigorsk"-2)]. *Stroitelnaya mekhanika i raschet sooruzheniy.* 2014. No. 1. Pp. 64–71.
28. Galishnikova V.V., Dunaiski P., Pahl P.J. *Geometrically Nonlinear Analysis of Plane Trusses and Frames SUN MeDIA,* Stellenbosch (Republic of South Africa). 2009. 382 p.

2017. No. 2-3(28). С. 268–271.

24. Рыбаков Л.С. Линейная теория плоского призматического каркаса // Известия РАН. Механика твердого тела. 2001. № 106-118. (rus)
25. Марутян А.С., Павленко Ю.И. Приближенный расчет перекрестных систем на статические воздействия // Строительная механика и расчет сооружений. 2009. № 4. С. 14–20.
26. Марутян А.С. Легкие металлоконструкции из перекрестных систем. Пятигорск: Изд-во РИА КМВ, 2009. 348 с.
27. Марутян А. С., Григорьян М. Б., Глухов С. А. Пространственные решетчатые несущие конструкции (модули типа «Пятигорск»-2) // Строительная механика и расчет сооружений. 2014. № 1. С. 64–71.
28. Galishnikova V.V., Dunaiski P., Pahl P.J. Geometrically Nonlinear Analysis of Plane Trusses and Frames SUN MeDIA, Stellenbosch (Republic of South Africa), 2009. 382 p.

Mikhail Kirsanov,

+7(495)362-73-14; mpei2004@yandex.ru

Михаил Николаевич Кирсанов,

+7(495)362-73-14;
эл. почта: mpei2004@yandex.ru

Кирсанов М.Н. Прогиб пространственного покрытия с периодической структурой // Инженерно-строительный журнал. 2017. № 8(76). С. 58–66.

doi: 10.18720/MCE.76.7

Earthquake engineering optimization of structures by economic criterion

Оптимизация конструкций сейсмостойких сооружений по экономическому критерию

N.I. Vatin,
Peter the Great St. Petersburg Polytechnic University, St. Petersburg, Russia
A.Yu. Ivanov,
Y.L. Rutman,
St. Petersburg State University of Architecture and Civil Engineering, St. Petersburg, Russia
S.A. Chernogorskiy,
K.V. Shvetsov,
Peter the Great St. Petersburg Polytechnic University, St. Petersburg, Russia

Д-р техн. наук, директор Инженерно-строительного института Н.И. Ватин,
Санкт-Петербургский политехнический университет Петра Великого, г. Санкт-Петербург, Россия
аспирант А.Ю. Иванов,
д-р техн. наук, профессор Ю.Л. Рутман,
Санкт-Петербургский государственный архитектурно-строительный университет, г. Санкт-Петербург, Россия
канд. экон. наук, доцент С.А. Черногорский,
канд. экон. наук, профессор, доцент К.В. Швецов
Санкт-Петербургский политехнический университет Петра Великого, г. Санкт-Петербург, Россия

Key words: construction; civil engineering, economic efficiency; capacity curve; financial curve; life cycle; performance-based earthquake engineering; seismic retrofit; damage state

Ключевые слова: сооружение; проектирование и строительство зданий; экономическая эффективность; кривая несущей способности; финансовая кривая; жизненный цикл; проектирование сейсмостойких зданий на основе рабочих характеристик; сейсмоусиление; ущерб

Abstract. The article deals with an economic optimization problem of structures designed on areas exposed to seismic hazard. Profit (cost-effectiveness) from building usage due its design life-cycle is considered as objective function in this optimization task. Building damage state evaluation procedure and repair cost estimation method are proposed in this study. A criterion and a variable parameter of an optimization problem is suggested here as well. There is an algorithm, which combines seismic computation results with economic performance indicators of damage state. The example of practical use of the algorithm is shown with the help of numerical simulations and economic parameters analysis for industrial building frame designed using different seismic retrofit schemes. Financial costs for each seismic retrofit scheme of a building are determined based on cost estimates, which allows to obtain the near-real estimation of seismic retrofit cost and financial losses from repair works of injured structural elements after various earthquakes.

Аннотация. В данной статье на примере промышленного здания рассмотрена проблема оптимизации конструкций, проектируемых в сейсмически опасных районах. Решается задача оптимизации, за критерий оптимальности в которой принимается экономическая эффективность, при этом исследуется её изменение на протяжении всего жизненного цикла здания в зависимости от определённых варьируемых параметров, принимаемых на этапе проектирования. Полученный алгоритм оптимизации основывается на ранее предложенных методах оценки экономического эффекта сейсмостойкого строительства, доработанных и развитых, а также приведённых к структуре, позволяющей решать конкретные инженерно-экономические задачи сейсмостойкого проектирования. Практическое применение алгоритма продемонстрировано на примере расчёта экономической эффективности антисейсмических мероприятий при выборе того или иного варианта несущего каркаса здания, которая оценивалась на разных временных этапах его срока

Ватин Н.И., Иванов А.Ю., Рутман Ю.Л., Черногорский С.А., Швецов К.В. Оптимизация конструкций сейсмостойких сооружений по экономическому критерию // Инженерно-строительный журнал. 2017. № 8(76). С. 67–83.

службы. Рассматривается подход по определению суммарного конструктивного ущерба, который может быть нанесён зданиям различными землетрясениями за весь ожидаемый срок службы. Также приведены некоторые методы по определению подобного рода ущерба, рассматриваемого как результат нелинейной работы материала элементов здания. Финансовые затраты на возведение каждого варианта здания определены на основании сметных расчётов, что позволяет получить близкое к действительности представление о стоимости строительства и ремонтов после землетрясений.

Introduction

The article deals with the algorithm to optimize design projects of earthquake resistant buildings by an economic criterion, which is subject to research.

Optimization based on economic criterion is a widespread type of optimization. Such problems can be generalized as follows: choose an option at the lowest cost out of varied options for design structures to meet certain requirements. In most cases it is about how to minimize weight, dimensions and labor intensity. Most recently a notion of life-cycle, including service life of a building, has started to be commonly used [1, 2]. In case of earthquake-resistance structures optimized by cost-effective indicators it is necessary to consider changes of its state (failure, partial failure, repair) due to seismic impacts, i.e. consider life cycle of a building. The article is concerned with the method to choose an optimal project solution for an earthquake resistant building based on the analysis of cost to profit ratio during the whole life cycle of a building.

The problem under consideration has been intensively discussed in the different studies over the last 15 years. Optimization problem by an economic criterion in earthquake engineering has been defined in [2, 3]. There are suggestions how to perform economic analysis of prospective seismic damages in these research works as well. There is a number of approaches how to identify defects and damages in buildings, changes in service characteristics, idle period in the articles [4–10]. The works [1, 2] are also concerned on this problem. It is important to mention the research work [11], where the problem of economic damage forecast and seismic structural optimization were considered for the first time.

However, the algorithm which combines seismic estimation results with economic performance indicators of damage value has not been suggested. Optimization criteria have not been specified to full extent. The algorithm to vary structural characteristics suggested in these works is complex and time consuming. The task of the present article is to eliminate these drawbacks. And the authors objective was to develop such an optimization procedure (criteria, variables and algorithm) which could correspond to the design provisions and codes specified for earthquake engineering in Russian Federation.

Methods

Optimization problem. Objective function

Economic criterions suggested in [1] is considered as the most algorithmically solvable. These criterions are based on the ideas developed in [11]. The proposed in this study optimization criterion makes it possible to combine two different economic parameters developed in [1]. The criterion suggested below makes an optimization procedure more visual form a physical standpoint. When the construction site is located on areas exposed to seismic hazard, structural analysis must be provided with consideration of seismic load. Therefore, extra activities are stipulated to sustain seismic retrofit of the frame in accordance with the computation results. If there is an earthquake due the life-cycle of the building it will cause some damages, and the damage in the retrofitted frame after earthquake will be less than in the frame without seismic retrofit. That is to say, if to compare the frame with seismic retrofit and the one without it, a prevented damage will be found, but some damage will be caused anyway. Thus, when the number of anti-seismic measures are considered along with the one, which excludes these measures, the damage can be shown as a sum of two components:

$$D(I)=D_{pr}(I)+D_{rel}(I), \quad (1)$$

where D_{pr} – the prevented damage, D_{rel} – the real damage, D – the damage that could occur in the frame without retrofit, I – the intensity[1] of earthquake.

[1] Earthquake intensity is scaled by MSK-64 in terms of a rate.

Vatin N.I., Ivanov A.Yu., Rutman Y.L., Chernogorskiy S.A., Shvetsov K.V. Earthquake engineering optimization of structures by economic criterion. *Magazine of Civil Engineering*. 2017. No. 8. Pp. 67–83. doi: 10.18720/MCE.76.7.

Damage estimations can be explicated in the following way. Let's assume that there are n types of structural elements (columns, trusses, beams and bracing elements) which may fail. If the frame is not retrofitted, all these structural elements fail (or partially fail). If the frame is retrofitted, then just a few structural elements fail (or partially fail). Consequently, the cost of structural members which have not failed is the prevented damage D_{pr}. The cost (repair costs) of structural elements which have failed (or partially failed) is the real damage D_{rel}.

Having modified the formula (5.10) proposed in [1] with consideration of Eq. (1) for calculation the cost effectiveness of the manufacturing building during the considering life-cycle equal to N years we obtain the economic effect

$$E_{eff}=\left[\sum_{n=1}^{N} P(n) - K_{build}\right] - K_{ant} - f(k,N)\sum_{I=I_{min}}^{I=I_{max}} L(I)\cdot\Big(D(I)-D_{pr}(I)\Big), \tag{2}$$

where $P(n)$ – profit (total by N year); K_{build} – investments into construction of the building (cost of the entire building including costs to equip manufacturing lines); K_{ant} – seismic retrofit cost (if there are no such costs the building will fail due to seismic impacts and there either will be no profit or minor profit as damages will limit production output); $f(k,N)$ – cost adjustment factor in accordance with recommendations given in [1] under the formula $f(k,N)=\left(\frac{1}{k}-1\right)[1-(1-k)^N]$. Here $k=\frac{d+d^*}{1+d}$, where d^* – depreciation rate (the parameter which determines reduction of the building value over the time inverse to its maintenance period) d – annual profitability of production; $L(I)$ – average number of rate I earthquakes on construction site; N – time after the maintenance start (years).

In the formula (1) $D-D_{pr}=D_{rel}$ the real damage as well as the prevented damage contain the following:

- repair and replacement cost of injured structural elements;
- losses of the equipment inside facility;
- losses in profit due to idle period when repairing.

Since the manufacture must be financially justified the value E_{eff} must be positive. The Eq. (2) is clear. If there are no anti-seismic measures taken then K_{ant} = 0 and D_{pr}=0. Thus financial losses due to earthquakes are determined by the damage $D(I)$ taken into account a number of earthquakes with intensity I and damage costs adjustment from year to year. If anti-seismic measures have been taken the real damage $D(I)_{rel}=D(I)-D(I)_{pr}$ is less than $D(I)$ but on the other hand financial losses increase owing to K_{ant}. Correlation of all these variables determines optimization E_{eff}.

If we keep in the Eq. (2) only those variables which depend on anti-seismic measures then we obtain

$$E=-K_{ant}+f(k,N)\sum_{I=I_{min}}^{I=I_{max}} L(I)\cdot D_{pr}, \tag{2}$$

which corresponds to the formula (5.9) in [1]. Thus introduction of the variable D made it possible to demonstrate that two different (as it is stated in [1]) approaches to compute cost-effectiveness of anti-seismic measures are identical as a matter of fact.

In economic optimization problem the variable E should be taken as an objective function. An optimization criterion in the formula (3) is a certain one and allows for seismic characteristics of a construction site. And we cannot say the same about the criteria suggested in the article [2].

Optimization problem. A variable. Constraints

Taking into account standards and regulations of the Russian Federation [12] and design practice based on the linear and spectral theory and the concept which considers plastic deformation of buildings using the reduction factor K_1 regarding seismic loads then while optimizing a project the factor K_1 should be taken as the variable. With such a variable there is no need to vary structural members (beam cross sections, columns, coefficient of reinforcement, etc.). While setting the value K_1 there is an opportunity to automatically select these variables using the design software (SCAD Office, Ing + MicroFe, SOFiSTiK and others). Requirements of standards are automatically met as well. In other words the value set for K_I determines an option of seismic retrofit. As to previous reasons and formulas it is apparent that it is not always the case when reduction of K_1 factor in total reduction costs (it is often assumed as a norm) since reduction of capital costs is correlated with increase in repair costs.

A constraint matrix in a variation problem is a constraint matrix for estimation results in accordance with standards and regulations.

It is assumed that the frame keeps its structural stability due the seismic ground shakings [13–17]. If the requirement is met it secures life safety and no serious injuries for people inside a building due the seismic event. That is why the criterion (3) does not include costs associated with rehabilitation of injured people and casualties.

Financial loss determination

Suggestions to determine financial losses corresponding to the earthquake with the intensity should be considered as the weakest point in the methods meant for optimization of the seismic building design suggested in [1, 2]. As a matter of fact this problem is avoided in these articles owing to a formal introduction of different definitions and notions. Naturally, the problem stated can be solved regarding only one certain structure, and not as a general case. However the algorithm which combines engineering computations and financial indicators can be suggested.

Nowadays the nonlinear static Pushover analysis is recommended to be used for nonlinear analysis in earthquake engineering by a major part of regulations. The method is based on the use of the curve describing load-bearing capacity of a structure [13, 15, 17]. This curve depicts dependence of the structure roof displacement and the base shear. It is suggested to use assumptions, software and methods that is considered by the structural engineer as adequate to obtain this curve. In the Pushover method this curve is transformed into the spectrum describing structural capacity which correlates roof displacements and seismic accelerations of the structure. If we determine the damage state as a function of the roof displacement then we will obtain an opportunity for analysis of successive destruction of structural elements with the increasing of seismic load. Said another way, we can obtain the building performance objective as a function of seismic shaking intensity. This performance objective is actively used in regulations and guidelines [13, 15–17] in foreign seismic structural design practice. It represents a certain damage state or performance level of a building after a certain earthquake, which is applied at the stage of a new building design or seismic rebuilding operations of the existing one. For instance, the chapter 3 of ATC-40 [17] (Applied Technology Council of California Seismic Safety Commission) is concerned to the problem of building performance objective selection based on standard performance levels. This approach is named “performance based earthquake engineering” (design of structures with specified seismic characteristics). It should be noted that damage state of load-carrying structures are classified in national guidelines of structural reliability assessment [4].

We can do a successive transformation of the capacity curve having plotted financial indicators of damage loss for different values of roof displacement instead of performance characteristics. We can name such a curve as financial curve**.** Having applied the nonlinear static analysis to the seismic structural behavior we can suggest the following algorithm to compute the cost-effectiveness of seismic retrofit schemes:

1. Set the intensity of seismic ground motion I.

2. By the value I determine maximum accelerations A.

3. With the help of pushover determine maximum roof displacement of a structure u.

4. By the value u, using financial curve**,** determine the damage D_{rel}.

5. Using I and D_{rel}, make computations under the formula (3).

Computation of displacement u can be provided in different ways, which a designer considers to be sufficient regarding accuracy of source data. For instance, with rough estimations it is possible to apply an energy method [6].

There is a wide range of tools to create the capacity curve:

- increment nonlinear analysis using FEM in ANSYS, SOFiSTiK etc.;

- extended finite element method (XFEM) for reinforced concrete structures [18];
- pseudo-stiffness method [19];

and others.

Calculation example. Numerical analysis

A. Load-bearing framing description

The building, considering as the example in this study, is a one-story rectangular shaped frame with plan dimensions $43.0\ x\ 108.0$ m and the height equal to 10.5 m. A two-story outbuilding with office and utility rooms is arranged inside the building. Roof coverage consists of truss rafters spaced at 4 m and mounted on supporting trusses which are assembled on columns through pillar sections. Top and bottom truss chords are unbraced with horizontal longitudinal girders, diagonal girders are set between top chords. Trusses are designed as 24 m span with 2 sloping surfaces and 12 m span with one sloping surface and uniform triangular grid with lowering diagonals. Supporting truss are designed 24 m span and 12 m with horizontal parallel chords and uniform triangular grid with lowering diagonals. Top chords of supporting truss ST2 and ST6 as well as pillar sections are designed from steel C345, all the rest metal structures are made from steel C245. Framing columns are precast reinforced ones, column section К1 – $600\ x\ 600$ mm, columns К2 – $400\ x\ 400$ mm. Strength grade of concrete B25 and reinforcing bars A500 are taken for columns. The layout for load-bearing structures is shown in the Figure 1.

B. Project types and computations

Computation is executed for three options[2] of load-bearing framing: typical S_{tip}, partially-reinforced Frame S_{PS} and maximum reinforced Frame S_{MS}. A finite element model of the frame was developed using SCAD Office and a seismic load was set in accordance with requirements [12]. The first type Frame S_{tip} is a building designed for a basic combination of design loads, dead weight and anticpated live loads without any seismic considerations. Sections for steel elements and column reinforcement are set in accordance with the computation results.

A fragment of analytical model with the results of reinforcement computation for columns which are not vertically braced are shown in the Figure 2. The bending moment value at the foundation level of these columns achieves the peak, therefore, the area of longitudinal reinforcement required to be the maximum. Color scale depicts total area of reinforcement bars (cm^2) placed along longitudinal axis of a bar next to the edge of a member section under ultimate tension.

The second type S_{PS} is represented as the frame of the same configuration but designed for rate 8 earthquake with the coefficient $K_1=0.5$. The task of the coefficient K_1 correction in the linear spectral method, which is the basis for this computation, have been considered in the works [20–23]. Seismic retrofit is confined the strengthening of load-bearing structures by increasing the area of longitudinal reinforcement in reinforced columns and increasing sections of steel structures elements section in accordance with computations.

The fragment of the analytical model with the results of reinforcement computation for columns, which are not vertically unbraced, are shown in the Figure 3.

The third type S_{MS} is the maximum reinforced frame. The coefficient $K_1=1$ is taken numerical simulations. The design seismic shaking intensity corresponds the rate 9 earthquake in this case. Seismic retrofit is executed as it is done for the option S_{PS} by increasing the section areas of longitudinal reinforcement of the reinforced columns and increasing sections of steel structures elements to a greater extent. Reinforcement in sections of the reinforced columns is selected with no regard crack resistance.

[2] Option of load-bearing framing implies the seismic retrofit scheme.

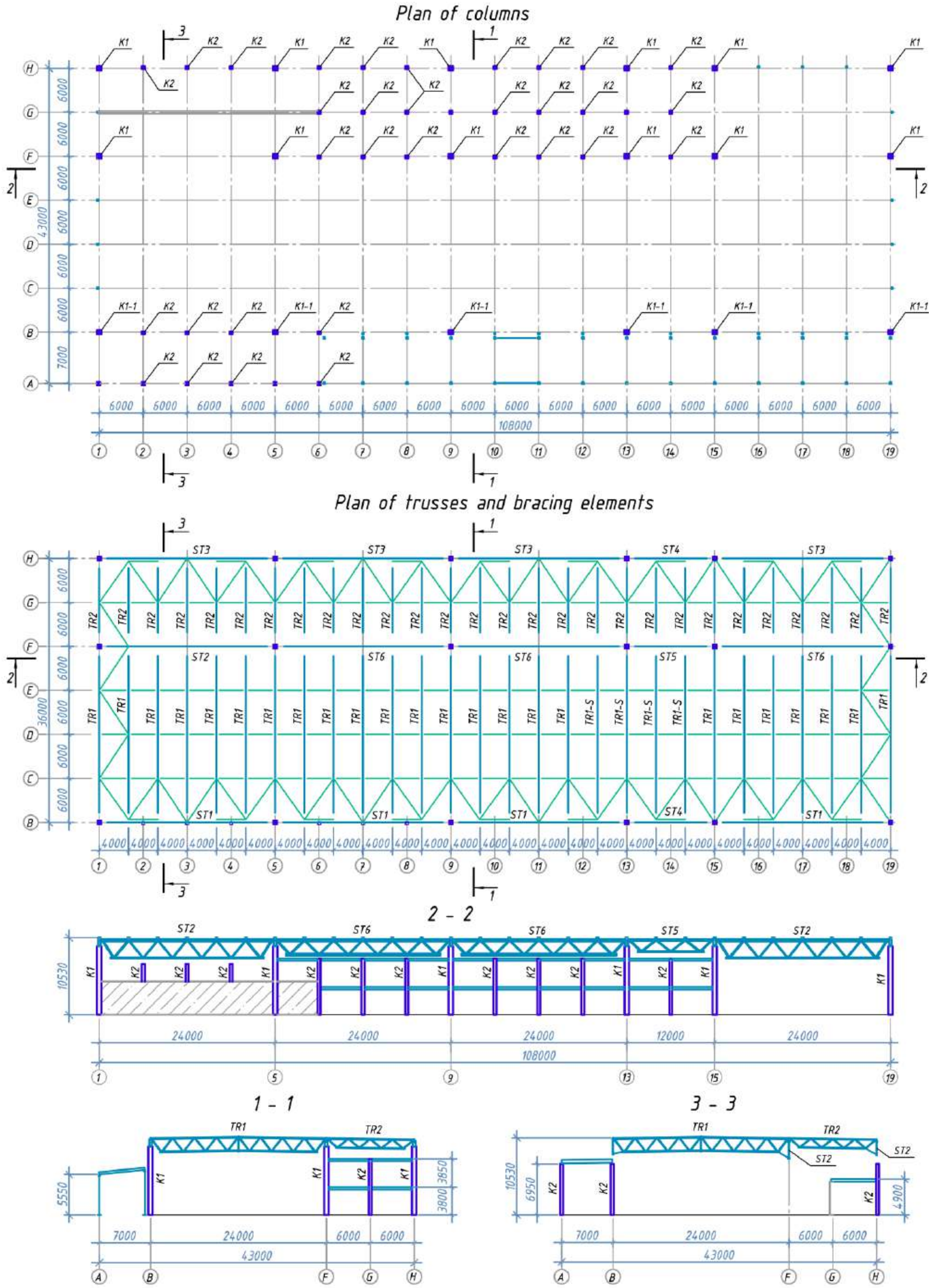

Figure 1. Layout for load-bearing structures

Vatin N.I., Ivanov A.Yu., Rutman Y.L., Chernogorskiy S.A., Shvetsov K.V. Earthquake engineering optimization of structures by economic criterion. *Magazine of Civil Engineering*. 2017. No. 8. Pp. 67–83. doi: 10.18720/MCE.76.7.

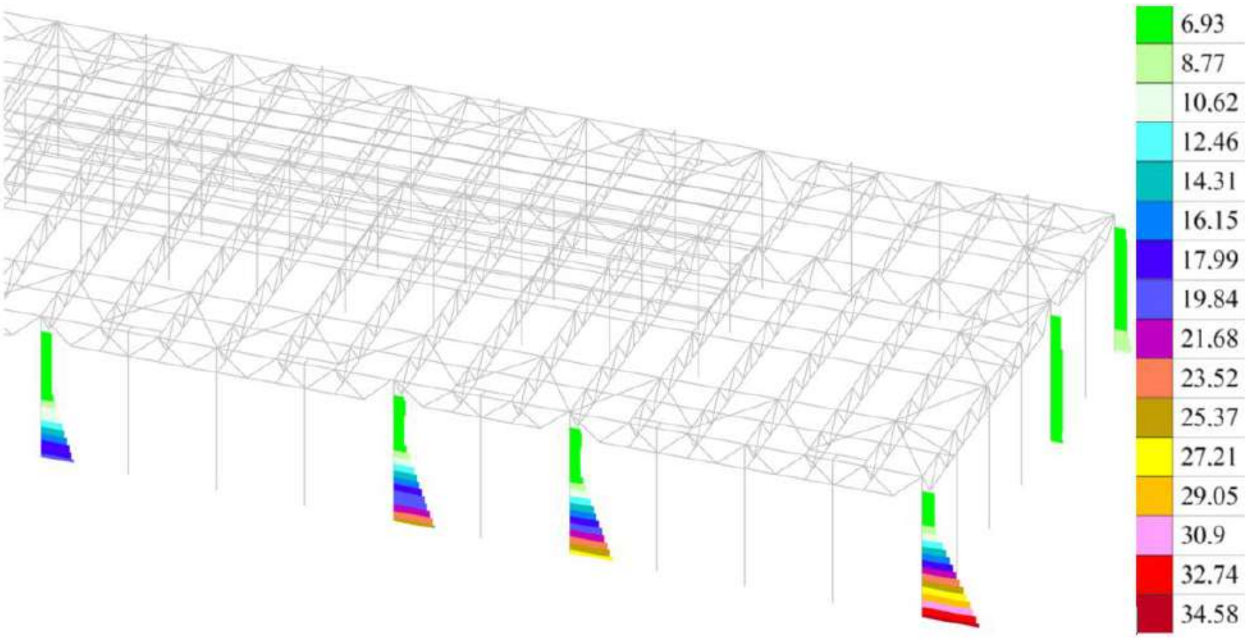

Figure 2. Reinforcement colored distribution diagram in sections of the reinforced columns members of Frame S_{tip}

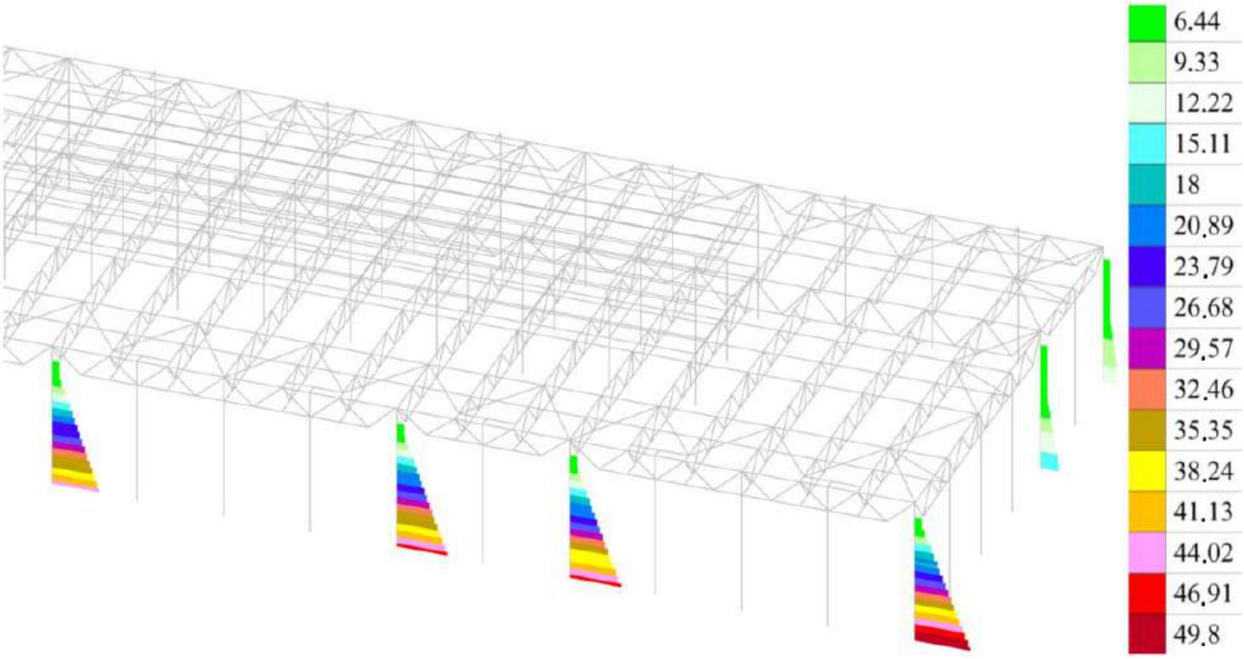

Figure 3. Reinforcement coloured distribution diagram in sections of the reinforced columns members of Frame S_{PS}

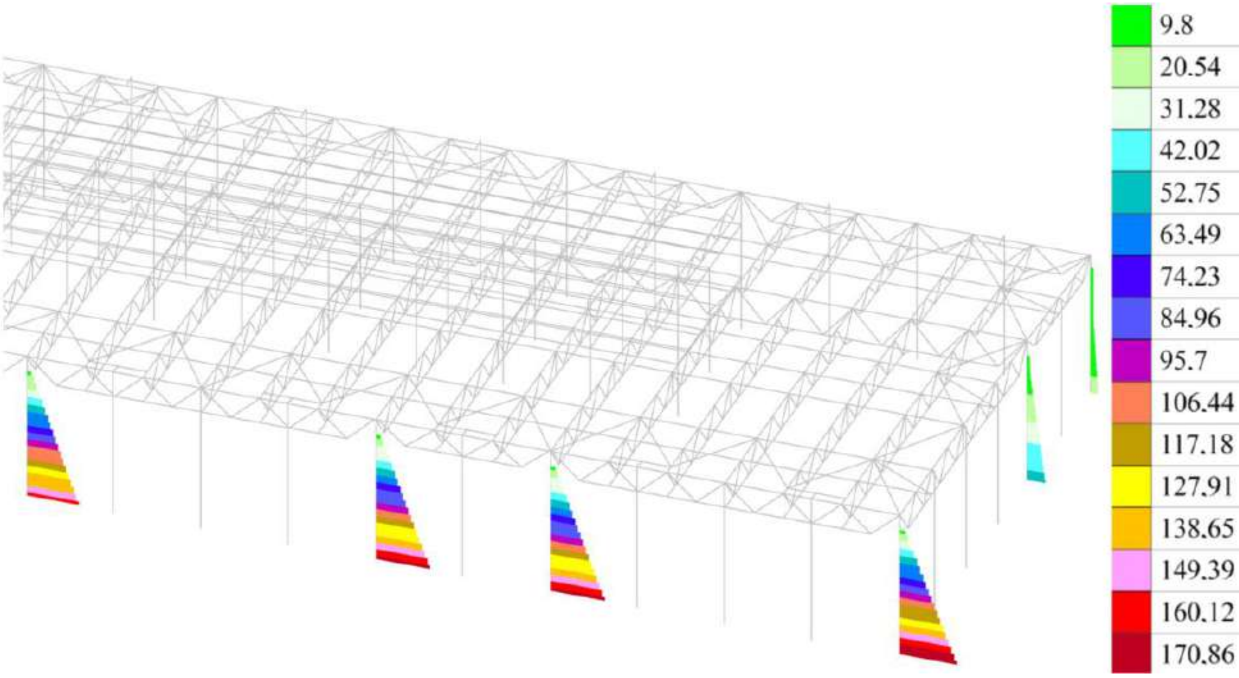

Figure 4. Reinforcement coloured distribution diagram in sections of the reinforced concrete columns members of the Frame S_{MS}

On the basis of these computational data three options of structural frames were designed for this object, technical specifications of steel were worked out, specification worksheets considering steel consumptions were elaborated. Data for reinforced concrete columns sections obtained for each option are shown in the Figure 5.

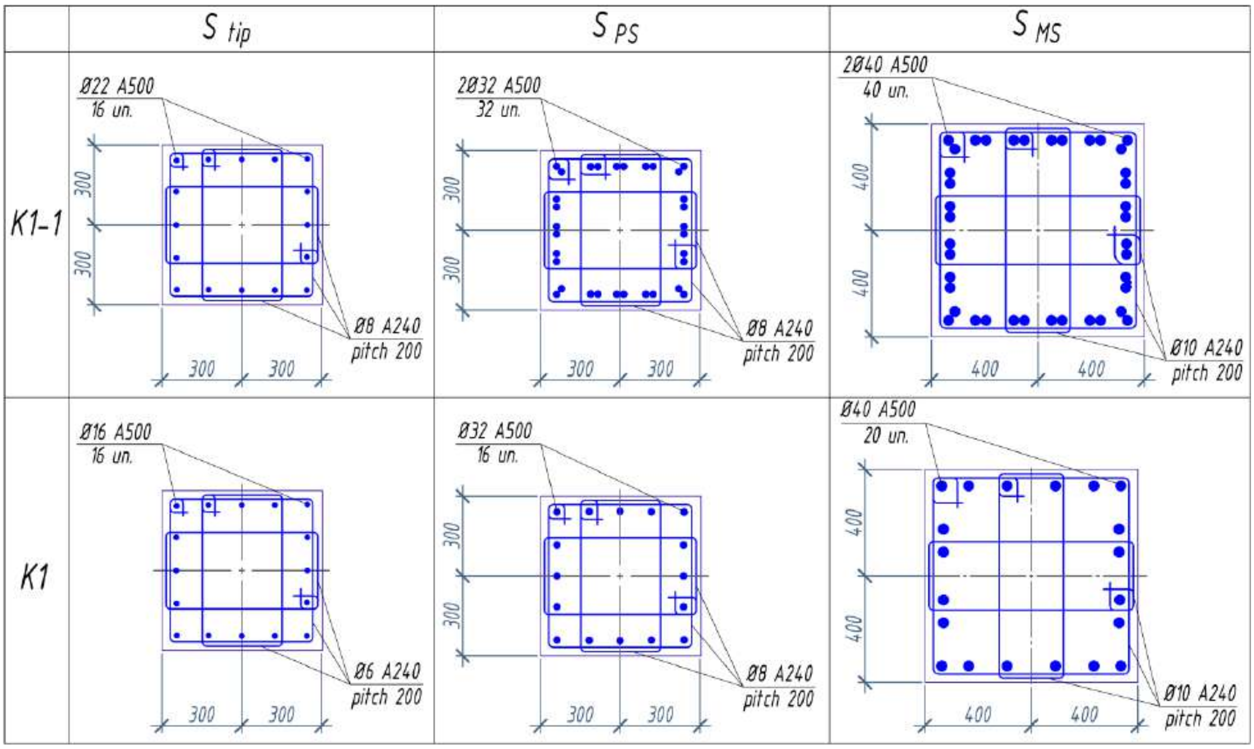

Figure 5. Data on reinforcement for sections of the reinforced concrete columns K1, K1-1

C. Costs of load-beraing framing works and seismic retrofit measures

Costs of structural framing works regarding a manufacturing building C based on technical specifications C were estimated for each of these three options. Costs associated with framing works for the option S_{tip} is equal to $C_{tip}=15.9$ mln rubles. Framing costs for the option S_{PS} are equal to $C_{PS}=20.19$ mln rubles, and framing costs for the option S_{MS} are equal to $C_{MS}=30.8$. A contractor allocates investments in the amount of $C_{tot}=200.0$ mln rubles to cover total construction costs. This value is taken as 1, and then we obtain

- Frame S_{tip} costs on the per-unit basis is equal to $C_{tip}=\frac{15.90}{200.0}=0.08$;
- partially reinforced Frame S_{PS} costs on the per-unit basis is equal to $C_{PS}=\frac{20.19}{200.0}=0.101$;
- maximum reinforced Frame S_{MS} costs on the per-unit basis is equal to $C_{MS}=\frac{30.80}{200.0}=0.154$;

Then costs associated with seismic retrofit for each of two options can be determined under the formulas:

- $K_{ant,\ PS}=C_{PS}-C_{tip}=0.101-0.08=0.021;$
- $K_{ant,\ MS}=C_{MS}-C_{tip}=0.154-0.08=0.074.$

D. Buildings capacity curves creation

As it was noticed before it is suggested to take assumptions, computation methods and software, which a designer considers to be appropriate, to get a capacity curve (which describes building capacity under load). Hereafter, a certain approach is suggested to create this curve based on the example of the building under consideration. The approach implies estimation of horizontal shear at the base (Base shear) and horizontal displacement of the building's top (roof displacement) and creation of the curve based on the data obtained.

A number of points to create the capacity curve according to the guidelines [17] should correspond to the number of performance levels set due the object design, which is relevant to the idea of performance based earthquake engineering, what is mentioned in [2, 5, 22]. Thus, the performance objective of this building is based on 2 requirements:

1) When the rate 6 and smaller earthquakes occur the frame should behave elastically, and its maintenance should not be terminated ("Operational" performance level in accordance with the guidelines [17]);

2) When the rate 9 earthquake occurs failures of load-bearing structures should not exceed ultimate ones, which may cause a collapse failure of the frame; the building should be suitable for repairs; life safety and no injures should be secured ("Life Safety" performance level in accordance with [17]).

Capacity curves should be developed for each frame. Firstly, computation for the option S_{MS} – the building with the maximum reinforced load-bearing framing – should be done. The value of horizontal base shear, which corresponds to the first point, is suggested to be determined by exerting lateral force on longitudinal load-bearing column – truss joints, which is not going to cause inelastic behavior of any structural members

$$V_1=\sum_{i=1}^{K} V_i,$$

where V_1 - horizontal base shear, which corresponds to the first point of capacity curve;

V_i – value of the lateral force exerted on the point of intersection between an *i* column and roof truss;

K – the number of main load-bearing columns supporting the roof structures (18 columns).

Lateral forces V_i are set in SCAD, then linear computation is executed and reinforcement for column sections is selected, which value after a number of iterations aimed at setting the value V_i should be close to the data in Figure 5 to the greatest extent. In accordance with the method indicated for the option S_{MS} the value of the lateral force V_1 = 5827 kN is obtained, under which action a bending moment at the base of columns is taken up by the reinforcement close to its elastic behavior. Displacement of the structure's top Δ_{roof1} corresponding to its base shear is equal to 0.094 m.

The value of the horizontal base shear which corresponds to the second point is determined on the following assumption: after a maximum bending moment in the column under maximum load is reached inelastic deformations will start to emerge and develop, and it will pull up all the rest columns due to force redistribution. It is necessary to sum up all the ultimate bending moments in the load-bearing columns and divide this sum by the column height taken in the Figure 1.

$$V_2 = \frac{\sum_{i=1}^{K} M_{pr,i}}{h}$$

where V_2 – horizontal base shear, which corresponds to the second point of the capacity curve;

$M_{pr,\,i}$ – the value of the failure bending moment at the base of an *i* column;

K – the number of basic load-bearing columns supporting the roof equal to 18 (for columns K and K-1 the values of the failure bending moment will be different);

h – column height.

According to computations we obtain $V_2 = 11085$ kN. The value Δ_{roof2} can be found multiplying by 2.2, then $\Delta_{roof2} = 0.207$ m. Based on these data we may create the capacity curve for the option S_{MS}. Points 1 and 2 for the option S_{PS} and S_{tip} can be found in a similar way, corresponding capacity curves are created on the basis of these points shown in Figure 6.

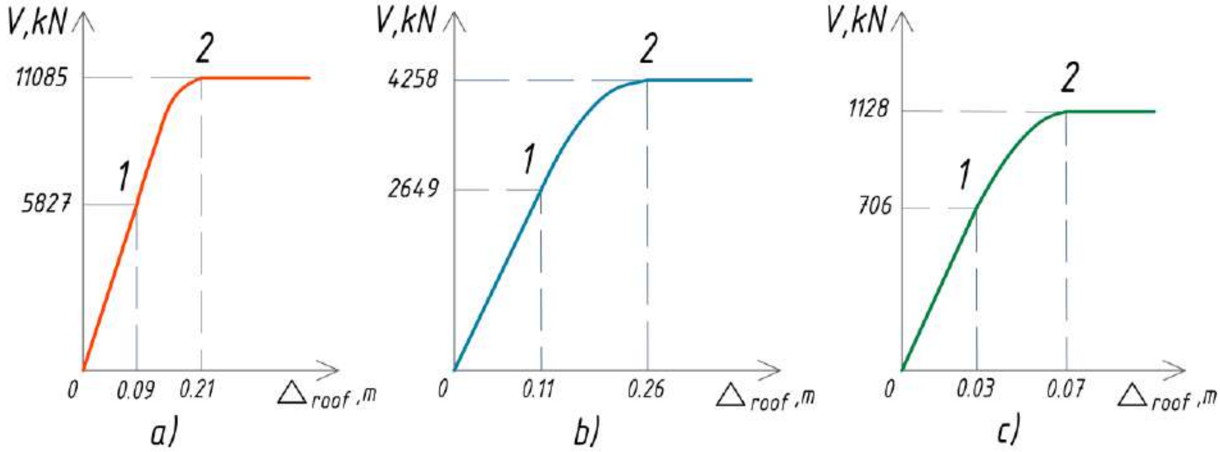

Figure 6. Curves describing load-bearing capacity for buildings
a – S_{MS} with maximum reinforced load-bearing framing;
b – S_{PS} with partially-reinforced load-bearing framing;
c – S_{tip} typical

E. Estimations of the damages for each seismic impact

It is necessary to set source data to estimate damages and solve an economic problem:

1. Life cycle of a building T is equal to 50 years.
2. Within these life cycle timings there will be a number of earthquakes with different intensity

Earthquake intensity	**Number of earthquakes**	**Average annual number of earthquakes $\overline{L}$**
Rate 6	5	0.10
Rate 7	4	0.08
Rate 8	3	0.06
Rate 9	1	0.02

To estimate the damages in each frame type caused by each earthquake specified there is computation based on time history analysis using the software Nonlin taking the range of rate 9, 8, 7 and 6 impacts, and the maximum displacement is determined, which allows estimating the value of damages once it is plotted on the relevant curve describing load-bearing capacity. Thus, there is an opportunity to represent curves describing load-bearing capacity in a form of the ratio “horizontal base shear – roof displacement /value of real structural damage". The value of structural damage emerged within the 0 – 1 spacing of the curve is equal to 0 since buildings behave elastically and there no damages in structural members. As the point 2 corresponds to the failure collapse of the columns due to an ultimate bending moment then from the financial point of view it represents total costs of all 18 load-bearing columns К1 and К1-1 with due account for works associated with disassembly of damaged ones and mounting new ones on their spots. These data can be obtained from cost estimates for each type of a building. In the financial curves obtained by distance values based on time history analyses it is possible to evaluate the damage state in the fractions of building costs per each impact. Estimation results for each type of buildings are given in corresponding tables.

Table 1. Time history analysis results for Frame S_{tip} (typical)

Earthquake intensity	Accelerogram	Acceleration max/min, g	Displacement, m	Real Damage D_{rel}
Rate 6	IMPERIAL VALLEY 10/15/79 2319, BONDS CORNER, 140 (USGS STATION 5054)	0.050 -0.084	0.009	0
	KOBE 01/16/95 2046, SHIN-OSAKA, UP (CUE)	0.059 -0.042	0.013	0
	KOCAELI 08/17/99, ARCELIK, DWN (KOERI)	0.086 -0.084	0.009	0
	IMPERIAL VALLEY 10/15/79 2319, BONDS CORNER, 230	0.100 -0.087	0.015	0
	IMPERIAL VALLEY 10/15/79 2319, BONDS CORNER, UP (USGS STATION 5054)	0.052 -0.042	0.015	0
Rate 7	LANDERS 06/28/92 1158, YERMO FIRE STATION, 270 (CDMG STATION 22074)	0.169 -0.245	0.042	0.0045
	KOCAELI 08/17/99, IZMIT, 180 (ERD)	0.147 -0.152	0.036	0.0023
	CHI-CHI 09/20/99, TCU045, V	0.181 -0.361	0.036	0.0023
	SUPERSTITION HILLS 11/24/87 13:16, EL CENTRO IMP CO CENTER, 090 (CDMG STATION 01	0.136 -0.258	0.031	0.0004
Rate 8	FRIULI, ITALY 05/06/76 2000, TOLMEZZO, 270	0.299 -0.315	0.083	1
	DUZCE 11/12/99, DUZCE, 180 (ERD)	0.307 -0.348	0.071	1
	CHI-CHI 09/20/99, TCU065, N	0.362 -0.603	0.092	1
Rate 9	CAPE MENDOCINO 04/25/92 1806, RIO DELL OVERPASS FF, 360 (CDMG STATION 89324)	0.549 -0.479	0.140	1

Based on the data from this Table we can deduce that when there is the rate 6 earthquake for this type of frame there are no structural damages. When there is the rate 7 earthquake the columns undergo to inelastic deformations and few of them are subject to be replaced. When there are the rate 8 and the rate 9 earthquake displacements exceed ultimate ones, and the building is forecasted to fail. Replacement costs for all the columns of Frame S_{tip} in the fractions from total building costs amounts to 0.015 in accordance with cost estimations.

Table 2. Time history analysis results for Frame S_{PS}

Earthquake intensity	Accelerogram	Acceleration max/min, g	Displacement, m	Real Damage D_{rel}
Rate 6	IMPERIAL VALLEY 10/15/79 2319, BONDS CORNER, 140 (USGS STATION 5054)	0.050 -0.084	0.007	0
	KOBE 01/16/95 2046, SHIN-OSAKA, UP (CUE)	0.059 -0.042	0.007	0
	KOCAELI 08/17/99, ARCELIK, DWN (KOERI)	0.086 -0.084	0.007	0
	IMPERIAL VALLEY 10/15/79 2319, BONDS CORNER, 230	0.100 -0.087	0.008	0
	IMPERIAL VALLEY 10/15/79 2319, BONDS CORNER, UP (USGS STATION 5054)	0.052 -0.042	0.001	0
Rate 7	LANDERS 06/28/92 1158, YERMO FIRE STATION, 270 (CDMG STATION 22074)	0.169 -0.245	0.034	0
	KOCAELI 08/17/99, IZMIT, 180 (ERD)	0.147 -0.152	0.028	0
	CHI-CHI 09/20/99, TCU045, V	0.181 -0.361	0.026	0
	SUPERSTITION HILLS 11/24/87 13:16, EL CENTRO IMP CO CENTER, 090 (CDMG STATION 01	0.138 -0.258	0.036	0
Rate 8	FRIULI, ITALY 05/06/76 2000, TOLMEZZO, 270	0.299 -0.315	0.064	0
	DUZCE 11/12/99, DUZCE, 180 (ERD)	0.307 -0.348	0.069	0
	LOMA PRIETA 10/18/89 00:05, CAPITOLA, 090 (CDMG STATION 47125)	0.368 -0.443	0.054	0
Rate 9	CAPE MENDOCINO 04/25/92 1806, RIO DELL OVERPASS FF, 360 (CDMG STATION 89324)	0.549 -0.479	0.140	0.004

From the time history analysis results for Frame S_{MS} it is clearly seen that there are no structural damages for all impacts except the rate 9 earthquake. When there is rate 9 earthquake the columns undergo to inelastic deformations and few of them are subject to be replaced. Replacement costs for all the main columns K1 and K1-1 of Frame S_{PS} in the fractions from total building costs amounts to 0.018 in accordance with cost estimations.

Table 3. Time history analysis results Frame S_{MS}

Earthquake intensity	Accelerogram	Acceleration max/min, g	Displacement, m	Real Damage D_{rel}
Rate 6	IMPERIAL VALLEY 10/15/79 2319, BONDS CORNER, 140 (USGS STATION 5054)	0.050 -0.084	0.007	0
	KOBE 01/16/95 2046, SHIN-OSAKA, UP (CUE)	0.059 -0.042	0.008	0
	KOCAELI 08/17/99, ARCELIK, DWN (KOERI)	0.086 -0.084	0.008	0
	IMPERIAL VALLEY 10/15/79 2319, BONDS CORNER, 230	0.100 -0.087	0.009	0
	IMPERIAL VALLEY 10/15/79 2319, BONDS CORNER, UP (USGS STATION 5054)	0.052 -0.042	0.001	0
Rate 7	LANDERS 06/28/92 1158, YERMO FIRE STATION, 270 (CDMG STATION 22074)	0.169 -0.245	0.035	0
	KOCAELI 08/17/99, IZMIT, 180 (ERD)	0.147 -0.152	0.028	0
	CHI-CHI 09/20/99, TCU045, V	0.181 -0.361	0.028	0
	SUPERSTITION HILLS 11/24/87 13:16, EL CENTRO IMP CO CENTER, 090 (CDMG STATION 01	0.138 -0.258	0.036	0
Rate 8	FRIULI, ITALY 05/06/76 2000, TOLMEZZO, 270	0.299 -0.315	0.065	0
	DUZCE 11/12/99, DUZCE, 180 (ERD)	0.307 -0.348	0.070	0
	CHI-CHI 09/20/99, TCU067, N	0.325 -0.302	0.071	0
Rate 9	CAPE MENDOCINO 04/25/92 1806, RIO DELL OVERPASS FF, 360 (CDMG STATION 89324)	0.549 -0.479	0.085	0

Estimation time history analysis results for Frame S_{MS} show no structural damages and the building behaves elastically for all the earthquake intensities specified in the Table 3. So we may deduce that there is no necessity to carry out repair works after earthquakes have been emerged.

Cost plots are given in Figure 7a-c. Repair costs after each earthquakes (i.e. damage state) can be determined doing interpolation by the value of displacement obtained from time history analysis estimations in accordance with corresponding intensity. Having all the damage state values obtained by the values of displacement corresponding to different impacts (rate 6, 7, 8 and 9) and given on the Tables1-3, we may evaluate cost-effectiveness for each retrofit scheme and determine strengths and drawbacks considering different life-cycle timings for different objects. Thereat, it is assumed that maximum structural roof displacements, which exceed ultimate values, can cause a collapse and the damage will amount the total cost of the building equal to 1.

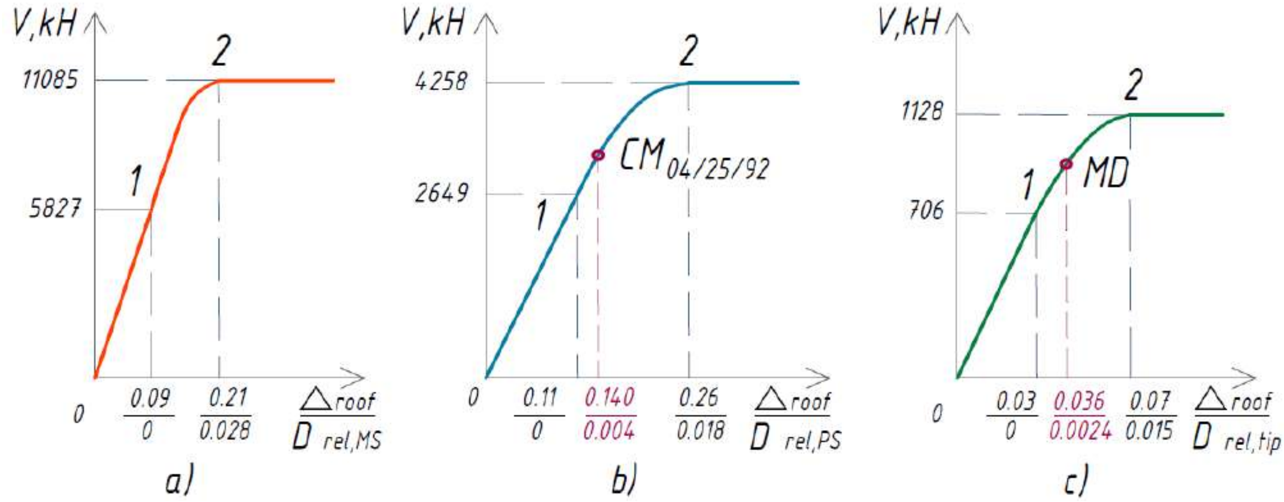

Figure 7. Financial curves for frames
a – S_{MS} with maximum-reinforced;
b – S_{PS} partially reinforced (the point $CM_{04/25/92}$ corresponds to rate 9 earthquake CAPE MENDOCINO 04/25/92 1806, RIO DELL OVERPASS FF, 360 (CDMG STATION 89324) (see Table 2), where the displacement specified and the corresponding damages are obtained);
***c* – S_{tip} typical (the point *MD* corresponds to the average displacement value specified on the basis of four rate 7 impacts (see Table 1) and the corresponding damage)**

F. Computation of cost-effectiveness due to anti-seismic measures

With the values of the damage state for each building due to each seismic impact there is an opportunity to compute the cost-effectiveness E with the help of the Eq (2). Whereas the first term can be eliminated as it accounts for the income profit. In this case, the most beneficial option is selected with regard to the value size of costs associated with seismic retrofit, and the difference $D - D_{pr}$ can be represented as D_{rel}. Then the equation for the cost-effectiveness E will be as follows:

$$E=-K_{ant}\text{-}f(k,N)\sum_{I=I_{min}}^{I=I_{max}} L(I)\cdot D_{rel}, \tag{4}$$

The value E is estimated for each frame at seven points which specify a certain period of the building life-cycle. Results are presented as plots depicting the ratio “cost-effectiveness E – building life-cycle N”, a peculiar curve corresponds to each frame. When computing the parameter $f(k, N)$ the variable representing the profitability is considered equal to d=0.1, and d^*=0.03, but the value may change depending on the value of the profit.

Results and Discussion

G. Analysis of the results obtained

It is clearly seen from the plot in Figure 8 that the curves for frames S_{PS} and S_{MS} which correspond to the value E are parallel. It can be explained by the fact that when computing the value E for the building S_{PS} the only structural damage is considered, which is equal to 0.004 from total costs of the considered building. However, as a matter of fact, after an earthquake has been emerged there will be the damages associated with both structural members and non-structural ones (partition walls, suspended ceiling and etc.), members of utility services, engineering and manufacturing equipment, and site improvements can be damaged as well. As it is seen from the capacity curve (Figure 6b) and financial curve (Figure 7b) created for Frame S_{PS}, the damage state characterized by the displacement obtained from the computation made for the rate 9 time history, are beyond the level of standard “Operational” performance, which indicates the necessity to terminate operation of manufacturing until the damages are fixed. Termination incurs losses due to production downtime and loss of revenue, which estimation methods are suggested in the works [2, 8, 9, 10]. If we do an approximation and increase the structural damage value, for example, twice, then it is seen from the plot in Figure 9 that the cost-effectiveness curves for the frames S_{PS} and S_{MS} by the end of 50-years life-cycle period considered coming close to each other. Nevertheless, from investor point of view, it is economically feasible to execute partial reinforcement, since repair costs may not realized. It should be noted that the cost-effectiveness of the Frame S_{tip} with account of all types of damages, is dramatically going down with the time passed.

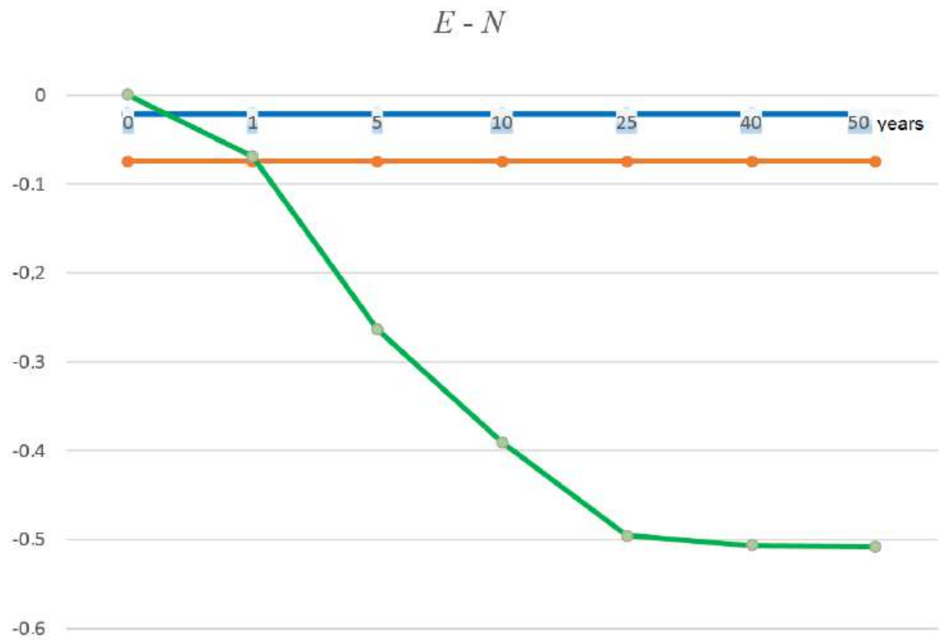

Figure 8. Dependence Plot
"cost-effectiveness E – life-cycle of the building N" considering only structural damage
– S_{PS} partially reinforced; – S_{MS} maximum reinforced; – S_{tip} typical

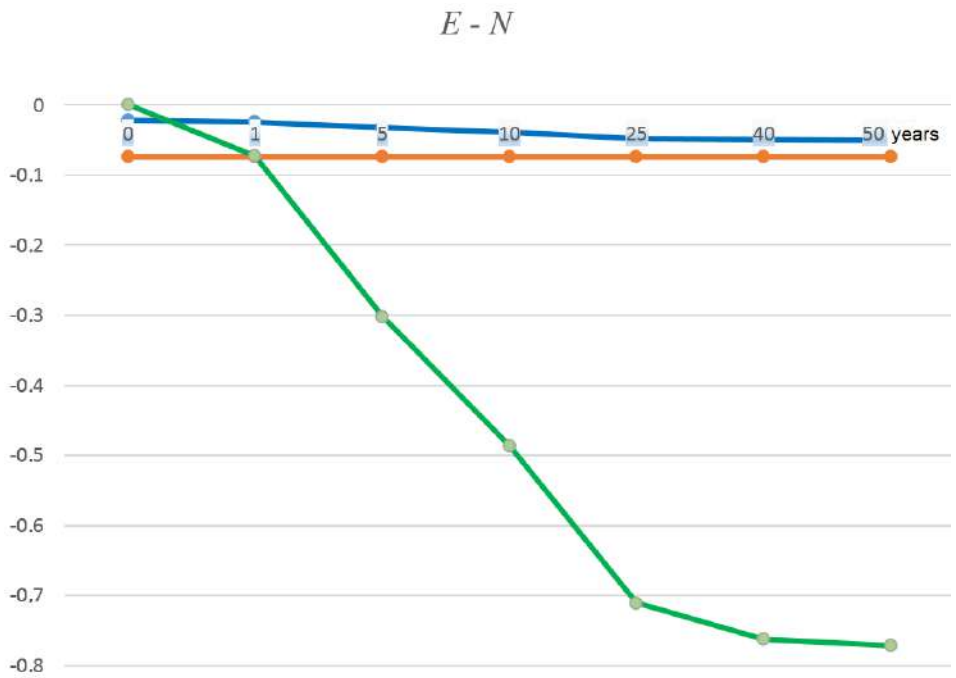

Figure 9. Dependence Plot
"cost-effectiveness E – life-cycle of the building N" considering total damage
– S_{PS} partially reinforced; – S_{MS} maximum reinforced; – S_{tip} typical

Thus, the higher cost-effectiveness E over the whole period can be achieved, as it seen, when designing the building with partially-reinforced frame. The cost-effectiveness value depending on the structural strengthening can be determined using procedure proposed in this study. At the same time, maintenance of Frame S_{tip} implies risks associated with high cost of repairs after each rate 7 earthquake or complete recovery after rate 8 and 9 earthquakes.

Conclusions

The method of comparative economic analysis for the range traditional seismic retrofit schemes of frames is developed in the article. The method provides the economic effect evaluation algorithm of applying a certain seismic retrofit scheme for the building designed on areas of seismic hazard.

References

1. Uzdin A.M., Yelizarov S.V., Belash T.A. *Seysmostoykiye konstruktsii transportnykh zdaniy i sooruzheniy* [Earthquake engineering of transport buildings and structures]. M.: 2012. 501 p. (rus)
2. Lagaros N.D., Fragiadakis M. Evaluation of ASCE – 41, ATC – 40 and N2 static pushover methods based on optimally designed buildings. *Soil Dynamics and Earthquake Engineering.* 2011. No. 31. Pp. 77–90.
3. Lagaros N.D. Life-cycle cost analysis of construction practices. *Bulletin of Earthquake Engineering.* 2007. No. 5. Pp. 425–442.
4. *Rekomendatsii po otsenke nadezhnosti stroitelnykh konstruktsiy zdaniy i sooruzheniy po vneshnim priznakam* [Reliabilty assessmnet guidlines of structures]. Moscow: TsNIIPromzdaniy, 2001. 53 p.
5. Nemchinov Yu.I., Maryenkov N.G., Khavkin A.K., Babik K.N. *Proyektirovaniye zdaniy s zadannym urovnem obespecheniya seysmostoykosti (s uchetom rekomendatsiy Yevrokoda 8, mezhdunarodnykh standartov i trebovaniy DBN)* [Performance-based earthquake engineering (taking into account Eurocode 8 recommends and DBN international standarts]. Kiyev: GP GNIISK, 2012. 53 p. (rus)
6. Rutman Yu.L., Shivua A.Dzh. Otsenka seysmicheskoy energii, postupivshey v uprugoplasticheskuyu sistemu s odnoy stepenyu svobody [Seismic energy assessment in elasto plastic response in single degree of freedom system]. *Vestnik grazhdanskikh inzhenerov.* 2015. No. 2(49). Pp. 64–74. (rus)
7. Chopra A.K. *Dynamic of structures. Theory and Applications to Earthquake Engineering.* New Jersey: Prentice-Hall, 2006. 794 p.
8. Kang Y.J., Wen Y.K. *Minimum life-cycle cost structural design against natural hazards.* Structural Research Series No. 629. Department of Civil and Environmental Engineering, University of Illinois at Urbana-Champaign, Urbana, IL, 2000.
9. Wen Y.K., Kang Y.J. Minimum building life-cycle cost design criteria. I. Methodology. *Journal of Structural ngineering New York.* 2001. No. 127(3), Pp. 330–337.
10. Wen Y.K., Kang Y.J. Minimum building life-cycle cost design criteria. II. Applications. *Journal of Structural ngineering New York.* 2001. No. 127(3), Pp. 338–346.
11. Keylis-Borok V.I., Nersesov I.A., Yaglom A.M. *Metody otsenki ekonomicheskogo effekta seysmostoykogo stroitelstva* [Vethods of assessment of economic effect in earthquake design]. Moscow: AN SSSR, 1962. 46 p. (rus).
12. *SP 14.13330.2014. SNiP II-7-81* Stroitelstvo v seysmicheskikh rayonakh* [Russian Set of Rules SP 14.13330.2014. SNiP II-7-81* Construction in seismic regions]. TsNIISK im. V.A. Kucherenko, OAO «NITs «Stroitelstvo». M.: OAO «TsPP», 2014. 126 p.
13. *ASCE/SEI Standard 41-06. Seismic Rehabilitation of Existing Buildings.* Prepublication edition. Structural Engineering Institute, American society of civil engineers, 2006.
14. *FEMA 273. NEHRP Guidelines for the Seismic Rehabilitation of Buildings.* Washington, DC. Building

Литература

1. Уздин А.М., Елизаров С.В., Белаш Т.А. Сейсмостойкие конструкции транспортных зданий и сооружений. М.: 2012. 501 с.
2. Lagaros N.D., Fragiadakis M. Evaluation of ASCE – 41, ATC – 40 and N2 static pushover methods based on optimally designed buildings // Soil Dynamics and Earthquake Engineering. 2011. № 31. Pp. 77–90.
3. Lagaros N.D. Life-cycle cost analysis of construction practices // Bulletin of Earthquake Engineering. 2007. № 5. Pp. 425–442.
4. Рекомендации по оценке надёжности строительных конструкций зданий и сооружений по внешним признакам. М.: ЦНИИПромзданий, 2001. 53 с.
5. Немчинов Ю.И., Марьенков Н.Г., Хавкин А.К., Бабик К.Н. Проектирование зданий с заданным уровнем обеспечения сейсмостойкости (с учётом рекомендаций Еврокода 8, международных стандартов и требований ДБН). Киев: ГП ГНИИСК, 2012. 53 с.
6. Рутман Ю.Л., Шивуа А.Дж. Оценка сейсмической энергии, поступившей в упругопластическую систему с одной степенью свободы // Вестник гражданских инженеров. 2015. № 2 (49). С. 64–74.
7. Chopra A.K. Dynamic of structures. Theory and Applications to Earthquake Engineering. New Jersey: Prentice-Hall, 2006. 794 p.
8. Kang Y.J., Wen Y.K. Minimum life-cycle cost structural design against natural hazards. Structural Research Series No. 629. Department of Civil and Environmental Engineering, University of Illinois at Urbana-Champaign, Urbana, IL, 2000.
9. Wen Y.K., Kang Y.J. Minimum building life-cycle cost design criteria. I. Methodology // Journal of Structural Engineering New York. 2001. № 127(3). Pp. 330–337.
10. Wen Y.K., Kang Y.J. Minimum building life-cycle cost design criteria. II. Applications // Journal of Structural Engineering New York. 2001. № 127(3). Pp. 338–346.
11. Кейлис-Борок В.И., Нерсесов И.А., Яглом А.М. Методы оценки экономического эффекта сейсмостойкого строительства. М.: АН СССР, 1962. 46 с.
12. СП 14.13330.2014. СНиП II-7-81* Строительство в сейсмических районах / ЦНИИСК им. В.А. Кучеренко, ОАО «НИЦ «Строительство». М.: ОАО «ЦПП», 2014. 126 с.
13. ASCE/SEI Standard 41-06. Seismic Rehabilitation of Existing Buildings. Prepublication edition. Structural Engineering Institute, American society of civil engineers, 2006.
14. FEMA 273. NEHRP Guidelines for the Seismic Rehabilitation of Buildings. Washington, DC. Building Seismic Safety Council for the Federal Emergency Management Agency, 1997.
15. EC8. Eurocode 8: Design of structures for earthquake resistance. European Committee for Standardisation: Brussels, Belgium, The European Standard EN 1998-1, 2004.
16. FEMA 356. Prestandard and Commentary for the Seismic Rehabilitation of Buildings. Washington, DC. ASCE

Seismic Safety Council for the Federal Emergency Management Agency, 1997.

15. *EC8. Eurocode 8: Design of structures for earthquake resistance.* European Committee for Standardisation: Brussels, Belgium, The European Standard EN 1998-1, 2004.
16. *FEMA 356. Prestandard and Commentary for the Seismic Rehabilitation of Buildings.* Washington, DC. ASCE Standards Committee on Seismic Rehabilitation, 2000.
17. *Seismic Evaluation and Retrofit of Concrete Buildings.* Vol. 1: ATC-40 Report. – Applied Technology Council. Redwood City, California. 1996. 334 p.
18. Yermakova A.V. *Metod dopolnitelnykh konechnykh elementov dlya nelineynogo rascheta zhelezobetonnykh konstruktsiy po predelnym sostoyaniyam* [Extended finite element method (XFEM) for reinforced concrete structures]. Moscow: ASV, 2017. 61 p. (rus).
19. Rutman Yu.L. *Metod psevdozhestkostey dlya resheniya zadach o predelnom ravnovesii zhestkoplasticheskikh konstruktsiy* [Pseudo-stiffness method for the problem of balance limit state of rigid plastic structures]. Saint-Petersburg, 1998. 53 p. (rus).
20. Simbort E.Kh.S. *Opredeleniye koeffitsiyenta reduktsii s uchetom dinamicheskikh kharakteristik seysmicheskikh vozdeystviy* [Reduction coefficient assessment with consideration of dynamic characteristics of seismic events]: dis. kand. tekhn. nauk. Sankt-Peterburg, 2012. 168 p. (rus).
21. Simbort E. Selection procedure of seismic-load reduction factor K1 at a given level of ductility factor. *Magazine of Civil Engineering.* 2012. No. 1(27). Pp. 44–52.
22. Sosnin A.V. Ob utochnenii koeffitsiyenta dopuskayemykh povrezhdeniy K1 i yego soglasovannosti s kontseptsiyey reduktsii seysmicheskikh sil v postanovke spektralnogo metoda (v poryadke obsuzhdeniya) [About specification of seismic force reduction factor K1 and it coherence with response modification technique to the spectrum method formulation (in order of discussion)]. *Vestnik grazhdanskikh inzhenerov.* 2017. No. 1(60). Pp. 92–114.

Standards Committee on Seismic Rehabilitation, 2000.

17. Seismic Evaluation and Retrofit of Concrete Buildings. Vol. 1: ATC-40 Report. – Applied Technology Council. Redwood City, California. 1996. 334 p.
18. Ермакова А.В. Метод дополнительных конечных элементов для нелинейного расчета железобетонных конструкций по предельным состояниям. М.: АСВ, 2017. 61 с.
19. Рутман Ю.Л., Шивуа А.Дж. Оценка сейсмической энергии, поступившей в упругопластическую систему с одной степенью свободы // Вестник гражданских инженеров. 2015. № 2 (49). С. 64–74.
20. Симборт Э.Х.С. Определение коэффициента редукции с учетом динамических характеристик сейсмических воздействий: дис. канд. техн. наук. Санкт-Петербург, 2012. 168 с.
21. Симборт Э.Х.С. Методика выбора коэффициента редукции сейсмических нагрузок K1 при заданном уровне коэффициента пластичности // Инженерно–строительный журнал. 2012. № 1. С. 44–52.
22. Соснин А.В. Об уточнении коэффициента допускаемых повреждений K1 и его согласованности с концепцией редукции сейсмических сил в постановке спектрального метода (в порядке обсуждения) // Вестник гражданских инженеров. 2017. № 1 (60). С. 92–114.

Nikolai Vatin,
+79219643762; vatin@mail.ru

Andrei Ivanov,
+(950)0318162; andreyivanov4@gmail.com

Yury Rutman,
+79219548479; 605fractal@mail.ru

Sergey Chernogorskiy,
+7(911)9177816; chernog_sa@spbstu.ru

Konstantin Shvetsov,
+7(921)922-54-30; shvetsov@inbox.ru

Николай Иванович Ватин,
+7(921)964-37-62; эл. почта: vatin@mail.ru

Андрей Юрьевич Иванов,
+7(950)031-81-62;
эл. почта: andreyivanov4@gmail.com

Юрий Лазаревич Рутман,
+7(921)954-84-79; эл. почта: 605fractal@mail.ru

Сергей Александрович Черногорский,
+7(911)917-78-16;
эл. почта: chernog_sa@spbstu.ru

Швецов Константин Владимирович
+7(921)922-54-30;
эл. почта: shvetsov@inbox.ru

Ватин Н.И., Иванов А.Ю., Рутман Ю.Л., Черногорский С.А., Швецов К.В. Оптимизация конструкций сейсмостойких сооружений по экономическому критерию // Инженерно-строительный журнал. 2017. № 8(76). С. 67–83.

doi: 10.18720/MCE.76.8

Technical normalization of working processes in construction based on spatial-temporal modeling

Техническое нормирование рабочих процессов в строительстве на основе пространственно-временного моделирования

T.V. Bobrova,
P.M. Panchenko,
Siberian State Automobile and Highway University (SibADI), Omsk, Russia

Д-р техн. наук, профессор Т.В. Боброва,
магистрант П.М. Панченко,
Сибирский государственный автомобильно-дорожный университет, г.Омск, Россия

Key words: BIM+4D framework; rate setting; visualization; flowsheets of operational sequence; synchronization; ceiling slabs mounting

Ключевые слова: BIM+4D технологии; техническое нормирование; визуализация; карты трудовых процессов; синхронизация; монтаж плит перекрытия

Abstract. Application of spatial-time modeling to the rate setting of operational sequence is a practical way to reduce the labor required for this work without losing any accuracy and authenticity of the results was analyzed. The methodology provided the analytical algorithm of rate calculation in MS Excel is synchronized with the visualization of operational sequence in Cinema 4D. The sequence of visualization of rate setting is considered with the example of a common operational sequence for mounting reinforced-concrete ceiling slabs of a five-storey brick apartment building. A peculiarity of the framework shows in the variable parameters of production activities. During the animation the calculated standards of working time were corrected in order to provide a safe working environment. The application of visual modeling and computational and analytical method for designing the flowsheets of operational sequence proved the given method to be effective and appropriate for extensive use in rate setting for various sequences in construction with the base of improves software, such as Synchro Pro, SOMOKS.CMR and a number of other tools for automated scheduling of construction operational sequence.

Аннотация. Рассмотрено использование пространственно-временного моделирования для технического нормирования рабочих процессов как реальный путь к снижению трудоемкости этой работы без потерь в точности и достоверности результатов. В предлагаемой методике алгоритм расчета норм аналитическим методом в MS Excel синхронизирован с визуализацией рабочих процессов в среде Cinema 4D. Порядок визуализации технического нормирования рассмотрен на примере технологического процесса на монтаж железобетонных плит перекрытия пятиэтажного кирпичного жилого дома. Характерная особенность технологии – постоянно меняющиеся параметры производственных операций. В процессе анимации выполнялась корректировка расчетных норм времени для обеспечения безопасности на фронте работ. Опыт применения визуального моделирования и расчетно-аналитического метода для разработки карт трудовых процессов доказал эффективность предлагаемого метода и возможность его широкого применения для технического нормирования различных процессов в строительстве на основе более совершенных программных продуктов, к которым можно отнести Synchro Pro, СОМОКС.СМР и ряд других инструментов по автоматизации процессов планирования строительных работ.

Introduction

The principles of spatial-time modeling, known as BIM+4D framework (Building Information Model), have produced new approaches and possibilities in construction design [1–6]. The benefit of this type of modeling is determined by the combination and integrity of architectural, constructional engineering, executive and economical elements of construction industry in a single dynamic unit. At first the main goal of BIM was the 3D presentation of design concepts of venues. Later the informational technologies were developed for visualization of the construction operational sequence by means of combining the schedules designed in MS Project, Oracle Primavera etc, with the 3D models of the venues.

Боброва Т.В.,Панченко П.М. Техническое нормирование рабочих процессов в строительстве на основе пространственно-временного моделирования // Инженерно-строительный журнал. 2017. № 8(76). С.84–97.

At present this method, sometimes called the method of visual planning (MVP) [7–9] becomes more and more widespread. The crucial elements of the method in question, according to many authors, are the well-thought and organized structure of venues and operational sequences, modular decomposition of systems of production logistics, relevance and authenticity of used data, availability of multivariable element libraries for determination of the most effective project alternative based of the multicriteria rating [10–12].

The methods of visualization have gone through a revolutionary advance in comparatively short time, allowing the broadening of functional opportunities of construction modeling in various fields of construction industry [13–16]. New inventions in information modeling provide solutions for the matter of higher safety of construction, analysis for clashing operational activities at the construction site, informational support to choose an optimal solution [17–20]. Different companies utilize specialized software complexes Synchro Pro, SOMOKS.CMP, focused on effective informational management of operational lifetime of a construction at every stage of engineering design development:

- designing engineering documentation;
- arrangement of construction operations;
- construction, reconstruction, overhaul;
- operation;
- decommissioning.

For the construction of the most complex venues of nuclear power industry a special standard has been developed: “Visualization of the construction management sequence. In-process control testing.” (Standard of Organization STO SRO-S 60542960 00042 – 2015) [21].

The matters of visual modeling, which could be solved with the given system, concern a wide scope of specialists in construction industry. At the same time, the more the peculiarities of preproduction planning and scheduling are taken into account, the more relevant models and reliable terms of project execution we shall achieve [22–24].

The importance of BIM+4D framework in the matters of providing the safety of workplaces, minimizing the losses of time, human and technological resources, improving the energy efficiency of the project solutions, optimizing the duration of construction is mentioned by the researchers, involved in the given field [25–28].

It is well-known, that the real duration of construction of many venues exceed the terms, set by the schedule of construction master plans (CMP) and work production plans (WPP) [29, 30]. One of significant reasons for such a discrepancy is the lack of reliable information about the standard terms of certain classes of work, about synchronization of operational sequence while combining the lateral and temporal operational activities.

The use of current informational technologies for automated planning of construction management in MS Project, Oracle Primavera etc minimizes many technical complexities of scheduling, reduces the labor required for designing executive documentation, but does not solve the matter of setting an optimal term of operational sequence execution, based on the current regulatory system.

This problem of construction engineering is mentioned by a number of authors [31–33], considering the vulnerability of current informational technology application to be the transference of rate setting and following scheduling, which are not efficient enough, into automated project management mode. M.M. Kalyzhniyk [31] points out the lack of works among the current papers on scheduling, which are devoted to the problems of rate setting of basic operational activities. Insufficient specificity and standardization of operational sequence cannot be compensated only by utilizing temporal probability parameters of isolated work classes. Thus, Y.B. Kalugin [34, 35] has shown, that the calculation of project network with the highly recommended system PERT provides the boosted positive results and therefore confuses project managers. The reliability of scheduling may be achieved with a number of measures, one of which would be the improvement of accuracy and authenticity of standards for operational activities and operational periods within flowsheets.

The importance of facilitating construction with the flowsheets during the automatization of designing work WPP is specified by professor S.A. Sinenko [36]. According to him, the crucial principles of the work in question are:

1. Goal statement and development of the project tasks structure;

2. Preparation and development of a knowledge database based on regulatory, methodology and reference tools;

3. Automatization of individual task solution, including the bulk of scheduling.

All the above mentioned principles, most of all the latter, are corresponding to the goals of the given paper. Executive technological modeling is the foundation for automated designing of CMP and WPP. The documents in question use the flowsheets, software and regulatory databases to determine the correlation of the main elements of construction: the scopes of workload, agents, technological and physical resources [37–39].

Officially active standards of work load and operating time for corresponding work class operations, issued as Unified Norms and Prices, are ethically and practically outdated.

The system of budgeted pricing currently employs State Itemized Cost Estimate Standards. These documents determine the standards of requirements for human, technological and physical resources predominantly in the complex operational sequences. New issues of Standards do not reflect current innovations and changes in equipment and technology on time. More relevant to the needs of rate setting and automated construction management planning are the standards of the flowcharts of operational sequence (FOS). Current issues of the documents in question are the updated versions of the previous ones, while new developments are rare. Sometimes regulatory documentation for operational sequences is issued as company standards.

Development of this documentation requires a lot of labor, and is carried out after the commissions of engineering and construction companies. Engineering solutions in these documents are not variable-oriented in case of use of interchangeable equipment. The matter of technical standards for determining the operational duration of activities in construction schedule is still of vital importance. Well-organized and scientifically valid rate setting is at the same time one of the crucial conditions of better performance, saving physical, technological and financial resources. The use of current informational technologies for rate setting is the most likely way to reduce the labor required for the work in question without losing accuracy and authenticity of results. It is especially important to rate the standard duration of operational activities when utilizing new equipment and technologies.

The goal of rate setting is to determine scientifically valid standards of expedience of labor, equipment and physical resources per unit of production. Operational standards can be developed via two main methods of rate setting: computational research and computational analysis [40].

For calculations of physical and operational capacity of equipment and time standards for performance we have developed the software based on MS Excel [33, 41]. Our experience in rate setting of road construction plants, including the modern plants of high efficiency, has shown that changes in environment cause the efficiency of mechanical units vary within a broad range. For example, the operational rates for excavation by Caterpillar 320L, set by means of computational analysis, take the following into account: the conditions of dumping (to spoil, or into a vehicle); type of ground (six types, graded by complexity of excavation); type of scoop (shovel bucket, back hoe, dragline), steering angle, deg. (90, 110, 135, 150, 180).

Considering the given factors, it is possible to calculate 150 types за operational rates for excavation of 100 m^3 of ground by Caterpillar 320L. Within the range of the easiest to the hardest environment time rates vary from 0.3 to 4.9 veh/hr.

The method in question is rather broad-based, applicable for efficiency calculation and for comparison of operational losses of different types of leading equipment during operational activity [38, 42]. At the same time automated calculations in MS Excel would not improve the authenticity of rate setting or analyze the availability of working area and the probability of safe combining of the operations.

The models for testing work areas during the construction, providing safe work environment were presented in paper [25]. As a result of the given research the method of software integration was evaluated for visualization of work areas and determining the conflicting zones of the human and technical resources in these areas.

According to S.A. Bolotin [43] the application of current methods of visualization and informational technologies in rate setting is the most valid way to reduce the labor required for the given work without losing accuracy and authenticity of rate results.

The goal of developing of visual flowsheets of operational sequence (VFOS) is to graphically present the operational sequence of activities, the plan of work area setting, (dimensions, arrangement of workers, physical resources, equipment and tools).

Flowsheets reflect all the components of operational sequence: availability and condition of work area, material, construction, production handling, preliminary work. The final document includes the schedule of operational sequence by the elements (operations, activities) with the agents, labor required for certain elements, terms of operation, rest and routine breaks at work.

The algorithm of spatial-time modeling is presented in Figure 1.

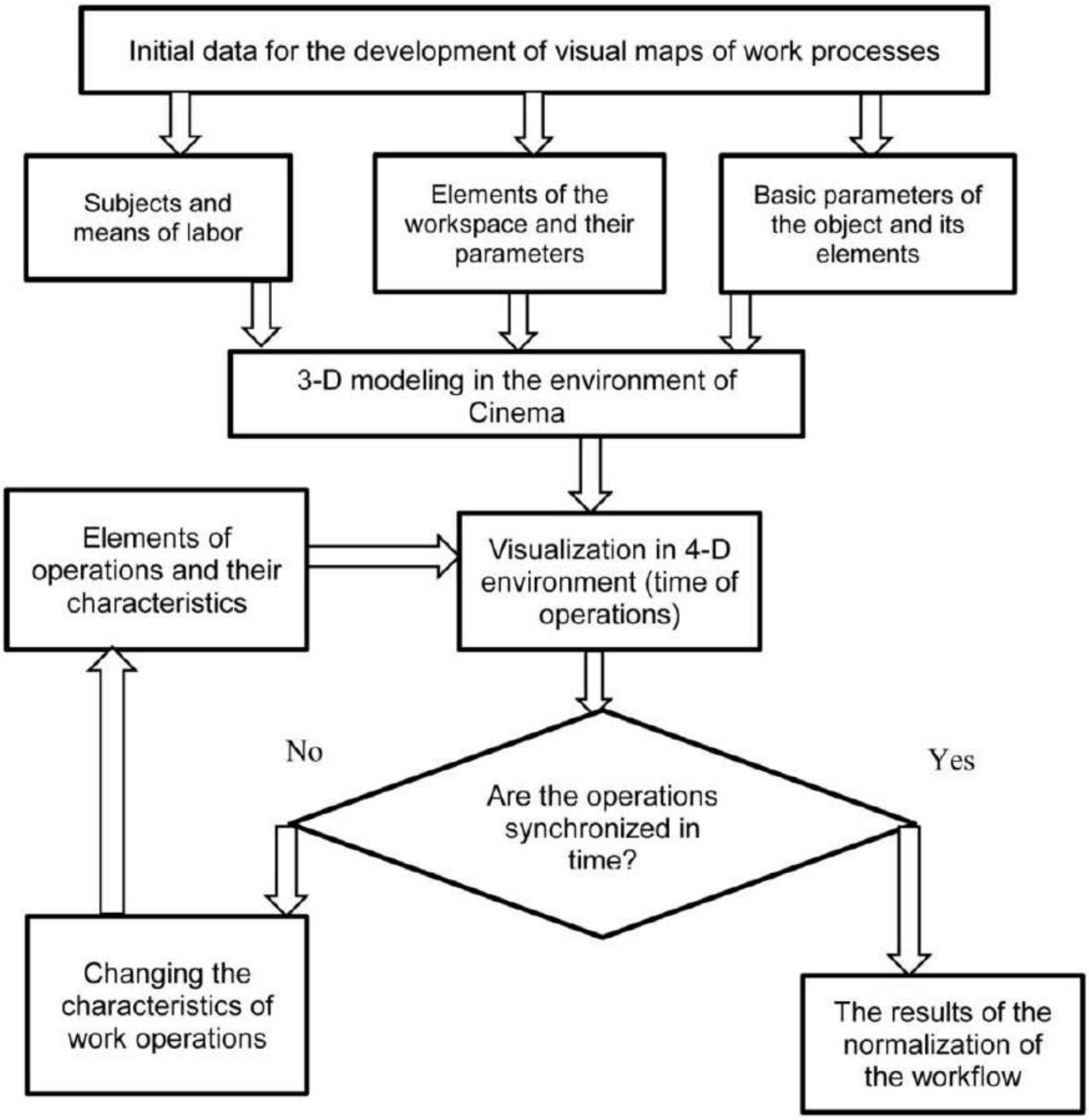

Figure 1. Algorithm of spatial-time modeling of operational sequence

Methodology of visualization the rate setting is shown with the example of developing VFOS for arranging reinforced-concrete ceiling slabs of a five-storey brick apartment building. The object is chosen due to a number of reasons: the specialty training of the graduate student being carried out in the construction of the given type of residential buildings; the request of a construction enterprise to develop the flowsheets of operational sequence; engineering documentation available for the research. The experience in rate setting for transport construction has been useful, while the algorithm for time rates calculation has the foundation in the general approach based on computational analisys [40].

The complexity of operational process is determined by constant variation of operational parameters (the height of slabs handling, angle of boom swing, etc). The visualization is carried out in Cinema 4D software, which is a general-purpose package program, meant for spatial modeling as well as for animation [44]. At the present stage of research the crucial benefit of the program was its relative simplicity and availability. Before working in the “space + time” coordinates, the preliminary technicalities were solved:

1. 3-D models were designed for a building, mounting crane, ceiling slabs storage site, crane ways. 3-D models preserve the correspondence of real dimensions of sites and work area, taking operational safety into consideration.

2. Movement of objects was described with spline functions: for a crane, load weight, bogey, workers (sling-operator and two adjustors), and equipment [45].

3. Connection layout of ceiling slabs was designed, gravity centers of slabs marked, sequence of mounting and distance of handling from stacks to the mounting site, considering the variation of stack height during the mounting, determined; crane staging area marked. These measures are described in details in paper [46]. The given work is not concerned with the details of animation process, immediately related to Cinema 4D software. However, the instructions of the program let the user, familiar with MS Excel, AutoCAD, prepare the necessary data.

Cinema 4D software, using the calculations in Excel spreadsheets, records the moments of beginning and end of every operation of the system elements via the recording of "active objects" (according to Cinema terminology). When the input data is changed in MS Excel, Cinema 4D software is changed automatically, which is immediately reflected in the operational duration during the visualization.

Visualization of manual operations is carried out by moving the figures of the sling-operator and adjusters along certain trajectories (splines). For example, for the sling operator circling the slab a rectangular spline was used. The moments of beginning and end of the manual operations are set by changes in elements of figures of workers (raising and lowering hands).

All the motion plans of the system are presented in animation, factoring real trajectories. The motion of the hook at the rotation of the swing and its simultaneous rise or descent goes by a rather complex trajectory, that is, by a three-dimensional spiral. Circular alignment determines the circular trajectory of an object, instead of a chord, and this way of rotation setting is used for the bogey and the hook, as well as for the slab. The variation of handling radius has also been set.

Detailed development of the flowcharts of operational sequence for slabs mounting cycles makes it necessary to describe these cycles spatially and temporally. The calculations of terms of operational activities for a given machine was carried out with the method of analytical calculation using passport specifications and motion distances in MS Excel, with and without the load weight. Terms of manual labor were estimated with the data from chronometer reviewing of similar operations [47]. Time of manual labor, simultaneous to crane operation, is not included into the general cycle, but is used for working hours calculation. The model of the site and work conditions is shown in Figure 2.

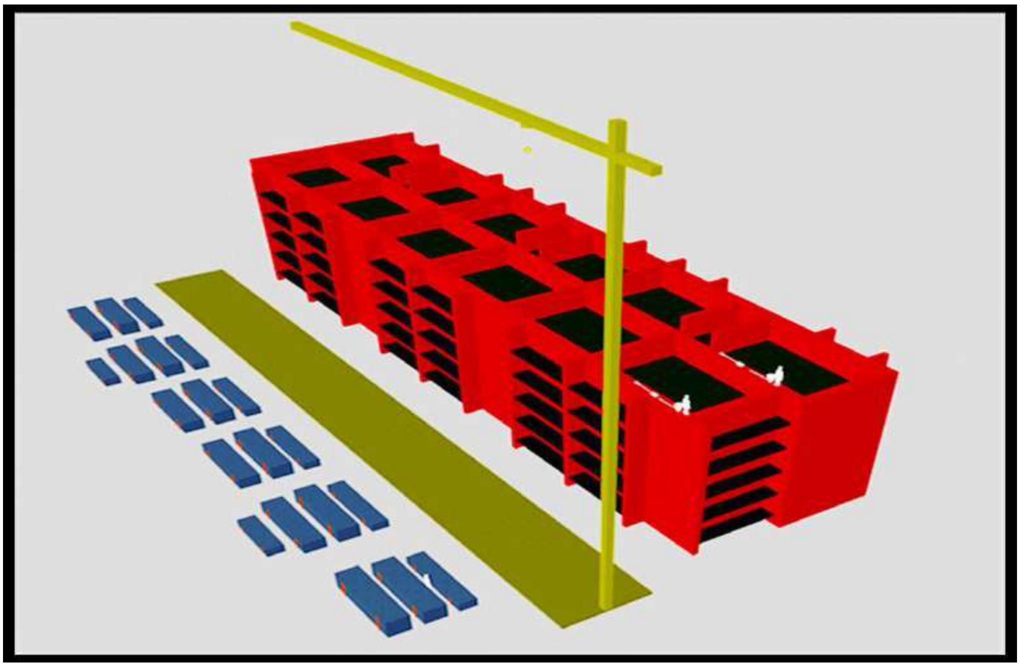

Figure 2. Model of the site and work conditions

Principal passport specifications of various cranes, used for the animation of mounting, are shown in table 1.

Cycle duration was determined according to the following sequence:

1 – slab strapping;

2 – rising the slab to the mounting height;

3 – modification of the operating radius for mounting;

4 – rotation of the swing to the mounting site;

5 – setting the load weight;

6 - leveling;

7 – unstrapping the slab;

8 – modification of the operating radius to strap the next slab;

9 – rotation of the swing to the site of strapping the next slab;

10 – descent of the hook.

Table 1. Passport specifications of machines

№	Name	Reference	Unit	KB-403B	KB-474A	KBM-401P	KBSM-503B
1	Speed of load rise (descent)	U_{lh}	m/min	40	22	30	19
2	Speed of unloaded hook rise (descent)	U_{uh}	m/min	50	45	46	50
3	Speed of loaded bogey	U_{lb}	m/min	7	30	30	8.4
4	Speed of unloaded bogey	U_{ub}	m/min	30	45	45	25.2
5	Rate of tower rotation	n	rpm	0.65	0.75	0.72	0.64
6	Speed of the crane	U_{cr}	m/min	18	14	20	19.2

Routine breaks were calculated by adding standard time per every 1.5 h of actual work, at the beginning of the work there is time set for preliminary operations.

Calculation of machine operations takes into account tolerable temporal combinations, for example, the motion of the crane and bogey.

Then, via the plan, tower cranes passport specifications and connection layout the duration of mounting cycles of building slabs was calculated, taking the space of height marks into account,

Rating formulae for determining the time of crane operations are shown in Table 2.

Table 2. Rating formulae for the crane operations

Operation name	Operation time rating formula, min	Notes
Raising the slab to the mounting height	$(H_{hm1} - H_{hs1}) / U_{lh}$	H_{hm1} и H_{hs1} – hook marks for mounting and strapping, m
Modifying the operating radius for mounting	$(Z_{m1} - Z_{s1}) / U_{lb}$	Z_{m1} и Z_{s1} – operating radius at mounting and strapping of the slab, accordingly, m
Rotation of the swing to the mounting site	$\alpha_1 / (360n)$	α_1 – angle of swing rotation from the strapping site to the mounting site, deg.
Modification of the operating radius to strap the next slab	$(Z_{m1} - Z_{s2}) / U_{ub}$	Z_{s2}- operating radius for strapping the next slab, m
Rotation of the swing to the site of strapping the next slab	$\alpha_2 / (360n)$	α_2 – angle of swing rotation to the site of strapping, deg
Descent of the hook.	$(H_{hm1} - H_{hs2}) / U_{uh}$	H_{hm2}- hook mark for strapping the next slab, m

Cinema 4D software works not with seconds, but with frames. The default animation speed is 25 frames per second, therefore, to present the operational process in real-time mode the duration of all operations is multiplied by 25. For the faster overview the speed can be modified.

The duration of manual labor in the program, measured in frames, is determined with a formula:

$$D_{rk} = D_r S_v \tag{1}$$

where D_r is the duration of manual labor, sec; S_v is the speed of video (25 fps).

The duration of mechanized operations for the process visualization (with the frame number) is calculated the following way:

$$D_{mk} = \frac{\Delta F}{V_F} 60 S_v \tag{2}$$

where ΔF is the variation of operation parameters, parameter units; V_F is the speed of parameter variation according to the crane passport, parameter units/min;

For example let us examine in detail the animation of mounting the first slab with KB-403B crane. Getting to the first site, the crane stops and starts simultaneously rotating the swing and descending the hook to the site of strapping the first slab. Swing rotation angle is 90 degrees, the height of hook descent is 32.3 m. KB-403B crane has the tower rotation rate of 0.65 rotations per minute (that is, 234 degrees), therefore, the swing rotation takes 23 seconds. The speed of rising (descending) the unloaded hook is 55 m/min, therefore, descent duration is 35 seconds. It is worth mentioning that in the model swing rotation and hook descent are coinciding, and the duration of such a combined operation is determined by the maximum time. It practice such a combination may be not possible, it depends on the professionalism of the crane operator. To take this factor into account, the coefficient of combination is introduced, equaling 0.95. Crane rotation is designed by recording the operating agents. Strapping takes 90 seconds. Strap height is 3 meters.

Setting the slab lasts for 30 seconds. Animation consists of slab rotation around its vertical axis, linear motion of the mounters and the variation of their arm positions at the beginning and the end of operations. During operational synchronization availability of the work area and the operating agents is taken into account. Thus, the setting of mortar bedding is started simultaneously with the strapping. Setting the slab by the mounters starts from the moment of its proximity of 1 m to the wall surface. Combining manual and machine labor factored the routine breaks in operational process to provide safety in the work area. For example, crane operator, after getting the hook to the site of strapping the next slab, does not descent it, as the sling operator does not have enough time to prepare the second slab to strapping (check for defects and cleanse the surface).

During the animation the calculated time rates for slab mounting was corrected for different stores for different crane sites. Various options of mounting plans were considered. Cycle repetition for the next slabs took the variations of operation parameters into account, operational time, number of frames, frame numbers for beginning and the end of each operation were calculated.

Figures 3, 4 show isolated work moments of spatial-time modeling.

Figure 5 shows the situation during the ceiling slabs mounting at the mark of 14.000 meters with KB-403B crane.

Picture shows the location of all the workers, the crane, the slabs at the stack site. The table in the upper part of the screen records the data on every cycle of mounted plate. Model allows managing the construction storage facilities more efficiently, in particular, unloading the constructions and materials for the next operational activities.

Application of MS Excel and visualization in Cinema 4D allowed to determine the rate of duration for mounting cycle of every slab of the house, slab mounting duration for the individual floors and the total duration for the whole building. The calculations were carried out for four types of cranes for every height marks.

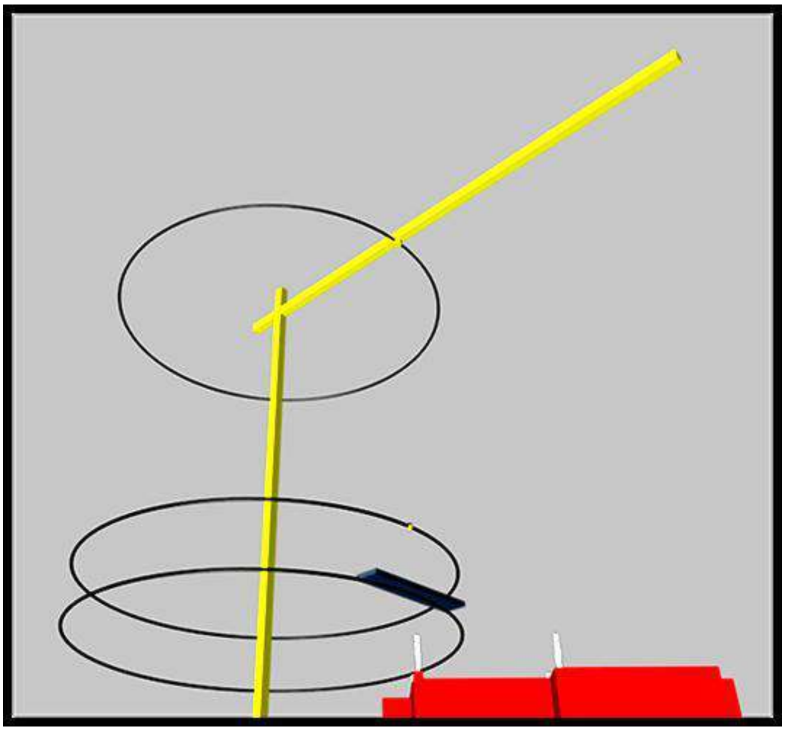

Figure 3. Swing rotation with the operational radius variation

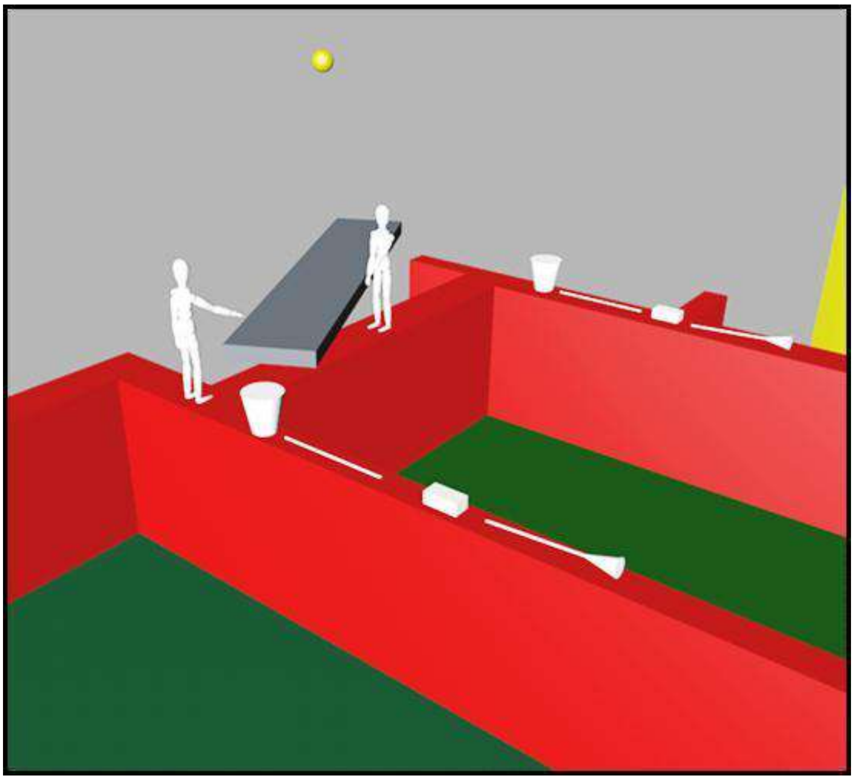

Figure 4. Setting the first slab on the mortar bedding

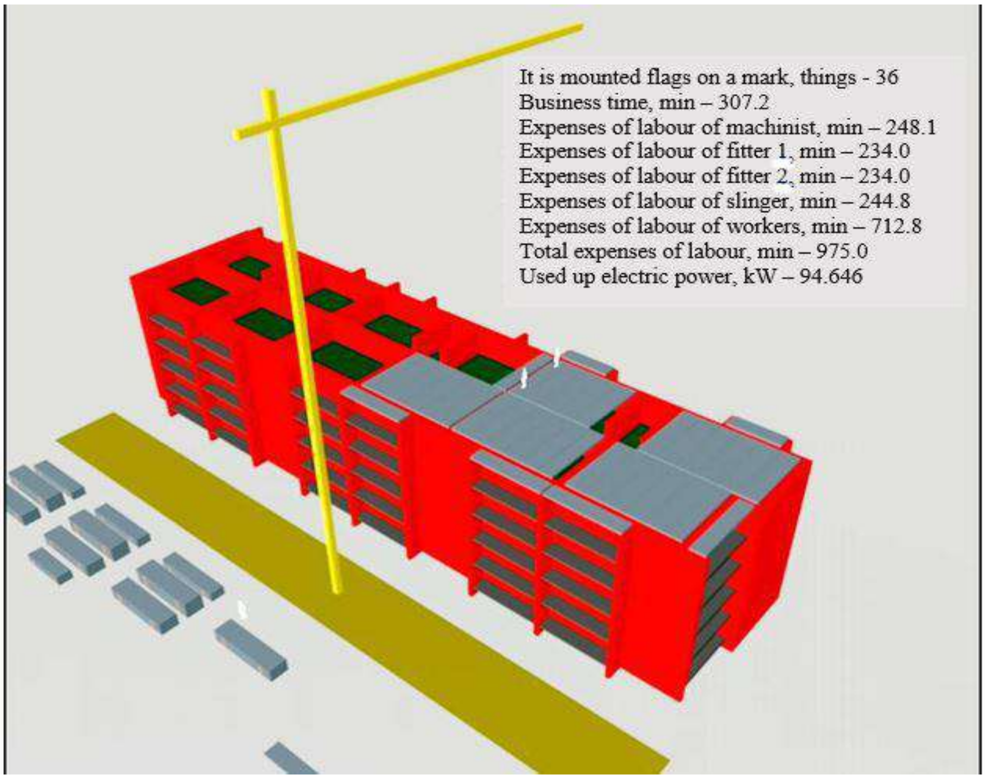

Figure 5. 4D-model of mounting the ceiling slabs

Results and Discussion

Aside from machine and human labor time rates FOS provides the calculation of power consumption, kWt, based on the passport specifications of the cranes. The results of varying labor requirements for the slab mounting on different floors are shown in graphs in Figure 6 (a, b, c). The comparative analysis of work of different cranes allows estimating their efficiency and making a valid choice of crane facilities, referencing the projected construction environment. Naturally, the methods in question may be used not only for ceiling slabs mounting, but for any operational sequence, one only needs to prepare the relevant input data, plan of constructions, types and properties of equipment.

Let us compare the calculated results of mounting duration for 80 slabs of one floor of the building, obtained with the designed FOS and the previously calculated rates without visualization, obtained in MS Excel. The duration in accordance with FOS is on the average 27 % longer. The reason for this is the inclusion of rated routine breaks within the operational activities, as well as the impediments in the crane operation at the collisions at the work area, providing work safety.

Method of computational analysis, carried out in MS Excel, combined with Cinema 4D visualization, reflects the “normal rate” of the operational sequence, that is, considers the current level of equipment and technology, occupational safety rules, complete procedural nomenclature, compliance of workmanship to the rates of work activity regulations. The influence of external factors, complicating the operational activity, may me taken into account with additional coefficients [48].

The provided method of rate setting is a supplement and development of several applications for the visualization software for construction operations. The authors of works, focused on the given matter, point out the drawbacks of regulatory framework for production engineering and organization in construction [10, 11, 14, 16] and propose a number of solutions for its perfection by means of informational technologies: grading and analysis of work activity structure in operational sequence using the graph theory [31, 32]; providing safe work environment for machine operations in the overall work area [20, 25]; reducing the risks of project execution in ambiguous conditions [34, 35, 36, 43], and so on. These propositions were partially considered and would be examined additionally within the improvement of the given method.

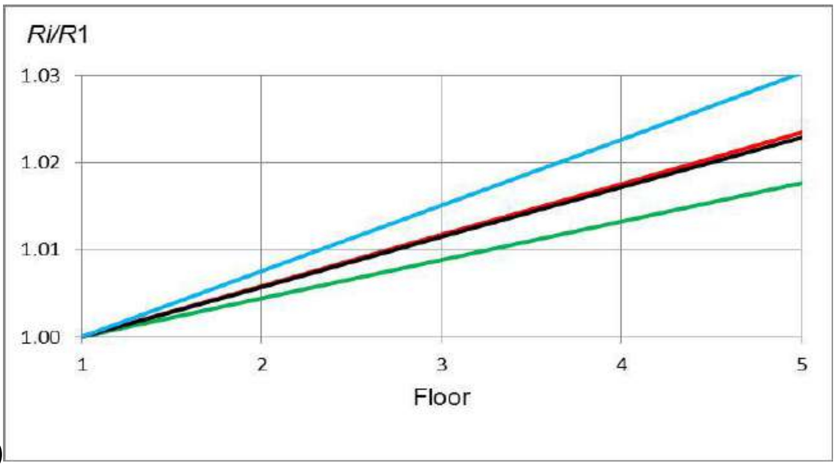

a)

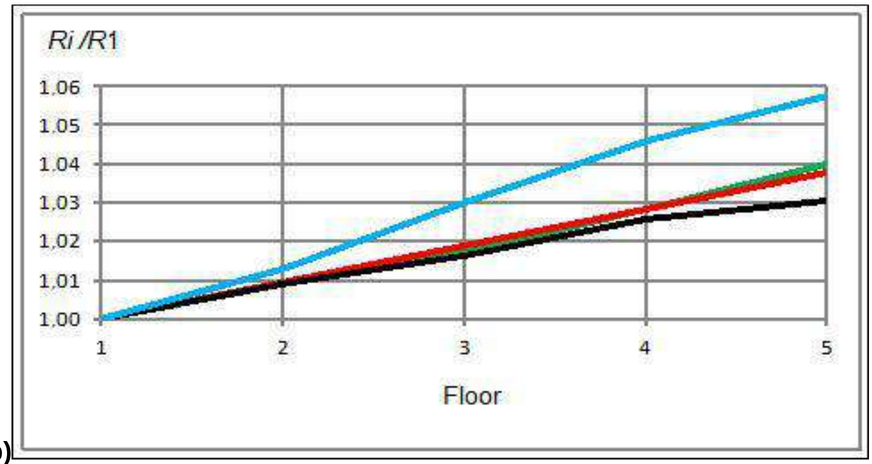

b)

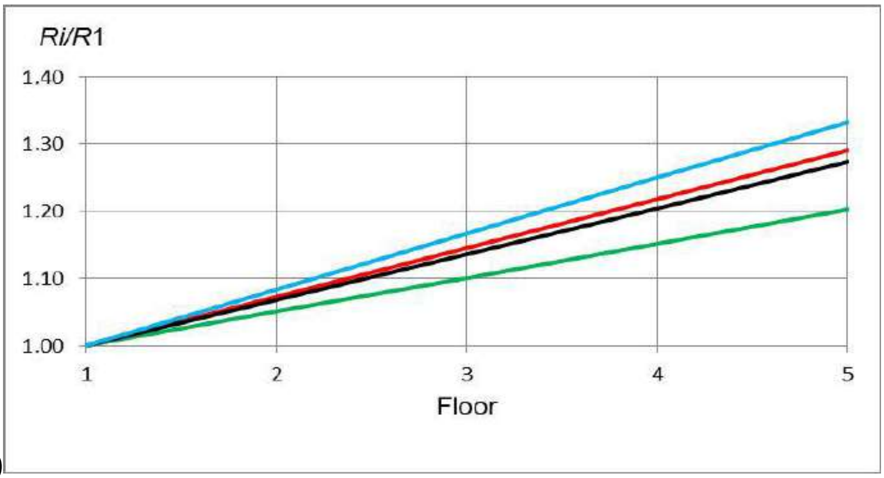

c)

Figure 6. Relative variation of resources R_i required for ceiling slabs mounting on *i*-th floors to the respective resources R_1 required for slab mounting on the ground floor:
a) duration of crane operation;
b) labor required for mounting;
c) power consumption

The approach, laid out in the given paper, allows to use the tools of virtual reality for examination of work activity parameters, their qualitative and quantitative assessment at the construction site. The given suggestion provides new possibilities for rate setting and raising the efficiency of engineering and organization of construction.

Conclusion

The use of spatial-time modeling method in rate setting solves the following problems:

1. Improve the accuracy and reliability of rate setting based on synchronized calculations in MS Excel and software for operational sequence visualization, analyze the possibilities of safe combining the operational activities at the work area;

2. Improve the efficiency of executive solutions within CMP and WPP on the foundation of scientifically valid choice of the options for operating activities realization in flowsheets, using innovational technologies;

3. Reduce the labor required to develop the flowcharts of operational sequence at chronometer works and reviews at the immediate construction sites;

4. Improve the regulatory database of construction scheduling on the base of reference and methodical electronic databases;

Without doubt, the methodology of FOS is to be developed, first of all, with the use of specialized software, secondly, due to consideration of probability parameters of machine and human labor activities. The developing of FOC would allow the broadening of regulatory database for automated scheduling and improve the reliability of venue construction within the deadline.

References

1. Krinitskiy Ye.V. Building Information Model (BIM). *Magazine of Civil Engineering.* 2010. No. 2(12). Pp. 16–18 (rus)
2. Ginzburg A.V. Informacionnaya model zhiznennogo cikla stroitelnogo obekta [Information model of the life cycle of a building object]. *Promyshlennoe i grazhdanskoe stroitelstvo.* 2016. No. 9. Pp. 61–65. (rus)
3. Chavada R., Dawood N., Kassem M. Construction workspace management: the development and application of a novel nD planning approach and tool. *J. Inform. Technol. Constr. (ITcon).* 2012. Vol. 17. Pp. 213–236.
4. Ting W., Ying Y., Xiao L. The impact of BIM application to the project organizational process. *3rd International Conference on Civil Engineering, Architecture and Building Materials.* Jinan, 2013. No. 357. Pp. 2524–2528.
5. Skvorcov A.V. Trudnosti perehoda ot avtomatizirovannogo proektirovaniya k informacionnomu modelirovaniyu dorog [Difficulties of transition from computer-aided design to information modeling of roads]. *SAPR i GIS avtomobilnyh dorog.* 2015. No. 2(5). Pp. 4–12. (rus)
6. Moon H., Dawood N., Kang L. Development of workspace conflict visualization system using 4D object of work schedule. *Advanced Engineering Informatics.* 2014. Vol. 28. No. 1. Pp. 50–65.
7. Nesterov I.V. Informacionnoe modelirovanie v stroitelstve [Information modeling in construction] [Online]. URL: http://www.cadgis.ru/2014/3/CADGIS-2014-2(3)-05.Nesterov(IM-in-building).pdf (date of reference: 07.07.2017). (rus)
8. Feng C.W., Chen Y.J., Huang J.R. Using the md cad model to develop the time-cost integrated schedule for construction projects. *Automation in Construction.* 2010. Vol.19. No. 3. Pp. 347–356.
9. Sarker B.R., Egbelu p.J., Liao T.W., Yu J. Planning and design models for construction industry: a critical survey. *Automation in Construction.* 2012. Vol. 22. Pp. 123–134.
10. Talapov V.V. O nekotoryh principah, lezhaschih v osnove BIM [About some of the principles underlying BIM]. *Izvestiya vuzov. Stroitelstvo.* 2016. No. 4. Pp. 108–114. (rus)
11. Popov V., Juocevicius V., Migilinskas D., Ustinovichius L., Mikalauskas S. The use of a virtual building design and construction model for developing an effective project concept in 5d environment. *Automation in Construction.* 2010. Vol. 19. No. 3. Pp. 357–367.
12. Volkov A.A., Petrova S.N., Dubovkina A.V. Modulnaya dekompoziciya proizvodstvenno-logisticheskih processov v stroitelstve [Modular decomposition of production and logistics processes in construction]. *Vestnik MGSU.* 2014. No. 10. Pp. 212–218. (rus)

Литература

1. Криницкий Е.В. Информационная модель здания (BIM) // Инженерно-строительный журнал. 2010. № 2. С. 16–18.
2. Гинзбург А.В. Информационная модель жизненного цикла строительного объекта // Промышленное и гражданское строительство. 2016. № 9. С. 61–65.
3. Chavada R., Dawood N., Kassem M. Construction workspace management: the development and application of a novel nD planning approach and tool // J. Inform. Technol. Constr. (ITcon). 2012. Vol. 17. Pp. 213–236.
4. Ting W., Ying Y., Xiao L. The impact of BIM application to the project organizational process//3rd International Conference on Civil Engineering, Architecture and Building Materials. Jinan, 2013. No. 357. Pp. 2524–2528.
5. Скворцов А.В. Трудности перехода от автоматизированного проектирования к информационному моделированию дорог // САПР и ГИС автомобильных дорог. 2015. № 2(5). С. 4–12.
6. Moon H., Dawood N., Kang L. Development of workspace conflict visualization system using 4D object of work schedule // Advanced Engineering Informatics. 2014. Vol. 28. № 1. Pp. 50–65.
7. Нестеров И.В. Информационное моделирование в строительстве [Электронный ресурс]. URL: http://www.cadgis.ru/2014/3/CADGIS-2014-2(3)-05.Nesterov(IM-in-building).pdf (дата обращения 07.07.2017).
8. Feng C.W., Chen Y.J., Huang J.R. Using the md cad model to develop the time-cost integrated schedule for construction projects // Automation in Construction. 2010. Vol. 19. No. 3. Pp. 347–356.
9. Sarker B.R., Egbelu P.J., Liao T.W., Yu J. Planning and design models for construction industry: a critical survey // Automation in Construction. 2012. Vol. 22. Pp. 123–134.
10. Талапов В.В. О некоторых принципах, лежащих в основе BIM // Известия вузов. Строительство. 2016. № 4. С. 108–114.
11. Popov V., Juocevicius V., Migilinskas D., Ustinovichius L., Mikalauskas S. The use of a virtual building design and construction model for developing an effective project concept in 5d environment // Automation in Construction. 2010. Vol. 19. No. 3. Pp. 357–367.
12. Волков А.А., Петрова С.Н., Дубовкина А.В. Модульная декомпозиция производственно-логистических процессов в строительстве // Вестник МГСУ. 2014. № 10. С. 212–218.
13. Sacks R., Koskela L., Dave B.A., Owen R. Interaction of lean and building information modeling in construction // Journal of Construction Engineering and Management – ASCE. 2010. Vol. 136. No. 9. Pp. 968–980.

13. Sacks R., Koskela L., Dave B.A., Owen R. Interaction of lean and building information modeling in construction. *Journal of Construction Engineering and Management – ASCE.* 2010. Vol. 136. No. 9. Pp. 968–980.
14. Khosrowshahi F., Alani A. Visualisation of impact of time on the internal lighting of a building. *Automation in Construction.* 2011. Vol. 20. No. 2. Pp. 145–154.
15. Wu W., Li Q., Yang H., Yang S.H., Chew D.A.S., Gibb A.G.F. Towards an autonomous real-time tracking system of near-miss accidents on construction sites. *Automation in Construction.* 2010. Vol. 19. No. 2. Pp. 134–141.
16. Kang I.S., Moon H.S., Dawood N., Kang M.S. Development of methodology and virtual system for optimised simulation of road design data. *Automation in Construction.* 2010. Vol. 19. No. 8. Pp. 1000–1015.
17. Zhang J.P., Hu Z.Z. BIM and 4D-based integrated solution of analysis and management for conflicts and structural safety problems during construction: 1. Principles and methodologies. *Automation in Construction.* 2011. Vol. 20. No. 2. Pp. 167–180.
18. Hu Z., Zhang J. BIM- and 4D-based integrated solution of analysis and management for conflicts and structural safety problems during construction: 2. Development and site trials. *Automation in Construction.* 2011. Vol. 20. No. 2. Pp. 155–166.
19. Arayici Y., Coates P., Koskela L., Kagioglou M., Usher C., O'Reilly K. Technology adoption in the BIM implementation for lean architectural practice. *Automation in Construction.* 2011. Vol. 20. No. 2. Pp. 189–195.
20. Sharmanov V.V., Simankina T.L., Mamaev A.E. BIM in the assessment of labor protection. *Magazine of Civil Engineering.* 2017. No. 1. Pp. 77–88.
21. Standart organizacii: obekty ispolzovaniya atomnoj energii. Vizualizaciya processov upravleniya stroitelstvom. Proizvodstvennyj analiz i kontrol. *STO SRO-S 60542960 00042 -2015* [Standard of organization: objects of use of atomic energy. Visualization of building management processes. Production analysis and control. SRT SPRO-S 60542960 00042 -2015]. Moscow. (rus)
22. Marinenkov D.V. Experience of applying information modeling technologies when executing infrastructure projects of fuel and energy complex. *Vestnik MGSU.* 2016. No. 1. Pp. 181–191. (rus)
23. Lebedeva I.M., Sinenko S.A. Problemy realisticheskoj vizualizacii organizacionno-tehnologicheskih reshenij v srede AutoCAD [Problems of realistic visualization of organizational and technological solutions in the AutoCAD environment]. *Vestnik MGSU.* 2011. No. 8. Vol. 2. Pp. 451–458. (rus)
24. Lebedeva I.M., Sinenko S.A. Algoritm programmy vizualizacii proektnyh reshenij v srede AutoCAD [Algorithm for visualization of design solutions in the AutoCAD environment]. *Tehnologiya i organizaciya stroitelnogo proizvodstv.* 2012. No.1-1(1). Pp. 43–47. (rus)
25. Elshejh A.M. 4D vizualizaciya rabochih prostranstv v hode stroitelstva [4D visualization of workspaces during construction]. *Sovremennye problemy nauki i obrazovaniya.* 2014. No. 6. P. 276. (rus)
26. Bolotin S.A., Gurinov A.I., Dadar A.Kh., Oolakay Z.H. An energy efficiency evaluation of architectural and construction solutions of an initial design stage in Autodesk REVIT Architecture. *Magazine of Civil Engineering.* 2013. No. 8(43). Pp. 64–73. (rus)
27. Bovteev S.V., Kanyukova S.V. Development of methodology for time management of construction projects *Magazine of Civil Engineering.* 2016. No. 2. Pp. 102-112.
28. Morozova T.F., Khe Tyanfu, Petrova Ye.M. Building side area minimization at the expense of optimization the displacement time diagram of workers. *Magazine of Civil Engineering.* 2011. No. 7(25). Pp. 76–81. (rus)

14. Khosrowshahi F., Alani A. Visualisation of impact of time on the internal lighting of a building // Automation in Construction. 2011. Vol. 20. No. 2. Pp. 145–154.
15. Wu W., Li Q., Yang H., Yang S.H., Chew D.A.S., Gibb A.G.F. Towards an autonomous real-time tracking system of near-miss accidents on construction sites // Automation in Construction. 2010. Vol. 19. № 2. Pp. 134–141.
16. Kang I.S., Moon H.S., Dawood N., Kang M.S. Development of methodology and virtual system for optimised simulation of road design data // Automation in Construction. 2010. Vol. 19. № 8. Pp. 1000–1015.
17. Zhang J.P., Hu Z.Z. BIM and 4D-based integrated solution of analysis and management for conflicts and structural safety problems during construction: 1. Principles and methodologies // Automation in Construction. 2011. Vol. 20. № 2. Pp. 167–180.
18. Hu Z., Zhang J. BIM- and 4D-based integrated solution of analysis and management for conflicts and structural safety problems during construction: 2. Development and site trials // Automation in Construction. 2011. Vol. 20. № 2. Pp. 155–166.
19. Arayici Y., Coates P., Koskela L., Kagioglou M., Usher C., O'Reilly K. Technology adoption in the BIM implementation for lean architectural practice // Automation in Construction. 2011. Vol. 20. № 2. Pp. 189–195.
20. Шарманов В.В., Симанкина Т.Л., Мамаев А.Е. BIM технологии в оценке уровня охраны труда // Инженерно-строительный журнал. 2017. № 1(69). С. 77–88.
21. Стандарт организации: объекты использования атомной энергии. Визуализация процессов управления строительством. Производственный анализ и контроль. СТО СРО-С 60542960 00042 -2015. Москва. Разработан ООО «Центр технических компетенций атомной отрасли».
22. Мариненков Д.В. Опыт применения технологий информационного моделирования при реализации инфраструктурных проектов топливно-энергетического комплекса // Вестник МГСУ. 2016. № 1. С. 181–191.
23. Лебедева И.М., Синенко С.А. Проблемы реалистической визуализации организационно-технологических решений в среде AutoCAD // Вестник МГСУ. 2011. Т. 2. № 8. С. 451–458.
24. Лебедева И.М., Синенко С.А. Алгоритм программы визуализации проектных решений в среде AutoCAD // Технология и организация строительного производства. 2012. №1-1(1). С. 43–47.
25. Эльшейх А.М. 4D визуализация рабочих пространств в ходе строительства // Современные проблемы науки и образования. 2014. № 6. С. 276.
26. Болотин С.А. Оценка энергоэффективности архитектурно-строительных решений начального этапа проектирования в программе Revit Architecture / С.А.Болотин, А.И.Гуринов, А.Х.Дадар, З.Х. Оолакай // Инженерно-строительный журнал. 2013. № 8. С. 64–91.
27. Бовтеев С.В., Канюкова С.В. Развитие методики контроля сроков инвестиционно-строительного проекта// Инженерно-строительный журнал. 2016. № 2(62). С.102–112.
28. Морозова Т.Ф., Тяньфу Хэ, Петрова Е.М. Сокращение площади строительной площадки за счет оптимизации графиков движения рабочих // Инженерно-строительный журнал. 2011. № 7(25). С. 76–81
29. Величкин В.З. Управление и надежность реализации строительных программ // Инженерно-строительный журнал. 2014. № 7(51). С. 74–79.
30. Калугин Ю.Б. Моделирование воздействия дестабилизирующих факторов на технологический комплекс // Известия вузов. Строительство. 2013. № 7. С. 93–102.
31. Калюжнюк М. М., Калюжнюк А. В. Упорядочение рабочих операций простых технологических процессов в

29. Velichkin V.Z. Management and reliability of construction programs. *Magazine of Civil Engineering.* 2014. No. 7(51). Pp. 74–79. (rus)
30. Kalugin Yu.B. Modelirovanie vozdejstviya destabiliziruyuschih faktorov na tehnologicheskij kompleks [Modeling the impact of destabilizing factors on the technological complex]. *Izvestiya vuzov. Stroitelstvo.* 2013. No. 7. Pp. 93–102. (rus)
31. Kalyuzhnyuk M.M., Kalyuzhnyuk A.V. Working operations of simple technological processes in construction industry ordering. *Magazine of Civil Engineering.* 2011. No. 7(25). Pp. 87–99. (rus)
32. Kalyuzhnyuk M.M., Kalyuzhnyuk A.V. Automated organization production and mounting of glass curtain walls. *Magazine of Civil Engineering.* 2013. No. 7(42). Pp. 58–66. (rus)
33. Ozernoj A.V., Bobrova T.V., Dubenkov A.A. Povyshenie urovnya organizacii dorozhnogo proizvodstva na osnove vnedreniya i tehnicheskogo normirovaniya innovacionnyh tehnologij [Increase in the level of organization of road production based on the introduction and technical standardization of innovative technologies]. *Mater. Mezhd. 66-j nauch.-prakt. konf.* [Proceedings of International 66th scientific-practice conference]. Omsk: SibADI, 2012. Vol. 1. Pp. 106–110. (rus)
34. Kalugin Yu.B. Universal method for calculation of reliable completion times. *Magazine of Civil Engineering*. 2016. No. 7. Pp. 70–80. (rus)
35. Kalugin Yu.B. Universal method of computing finish time for networks with imprecise durations. *News of Higher Educational Institutions.*. 2015. No. 1. Pp. 44–52. (rus)
36. Sinenko S.A. Primenenie sovremennyh informacionnyh tehnologij dlya formirovaniya tehnologicheskih kart vypolneniya stroitelnyh processov [Application of modern information technologies for the formation of technological maps for the execution of construction processes]. *Eurasian Union of Scientists.* 2015. No. 5-3(14). Pp. 149–151. (rus)
37. Bobrova T.V., Dubenkov A.A., Tytar I.V. Improvement of organizational and technological design of linear transport objects by modeling their spatial decomposition. *Systems. Methods. Technologies.* 2016. No. 4. Pp. 169–175. (rus)
38. Bobrova T.V., Bedrin E.A., Dubenkov A.A. *Modelirovanie proektnyh reshenij zemlyanogo polotna v usloviyah kriolitozony: monografiya* [Modeling of design solutions of the roadbed in conditions of cryolithozone: monograph]. Omsk: SibADI. 2016. 164 p. (rus)
39. Sultanova I.P. Analysis of planning, management and development methodsof organizational and technological solutions in infrastructure projects. *Vestnik MGSU.* 2015. No. 7. Pp. 127–136. (rus)
40. Balova E.F., Bakerman R.S. i dr. *Normirovanie truda rabochih v stroitelstve* [Normalization of labor of workers in construction]. Moscow: Strojizdat, 1985. 440 p. (rus)
41. Bobrova T.V., Dubenkov A.A. Kraeva E.I. Normirovanie tehnologicheskih processov kak faktor energosberezheniya pri stroitelstve zemlyanogo polotna avtomobilnyh dorog v slozhnyh prirodnyh usloviyah [Normalization of technological processes as a factor of energy saving in the construction of the roadbed of highways in difficult natural conditions]. *Materialy III Mezhvuz. Nauch. konf. Stud. i asp."Prirodnye i intellektualnye resursy Omskogo regionga"* [Proceedings of III interuniversity scientific conference of students and graduate students “Natural and intellectual resources of Omsk region]. Omsk: Izd-vo OmGTU. 2013. Pp. 167–169. (rus)
42. Dubenkov A.A. Variantnoe proektirovanie dorozhnyh konstrukcij s ispolzovaniem funkcionalno-stoimostnogo analiza [Variant design of road structures using functional-cost analysis]. *Materialy VII Mezhdunarodnoj nauch.-tehn. konf. studentov, aspirantov i molodyh uchenyh*

строительстве // Инженерно-строительный журнал. 2011. № 7(25). С. 87–99.

32. Калюжнюк М.М., Калюжнюк А.В. Организационная подготовка автоматизированного производства и монтажа элементов конструкций светопрозрачных фасадов // Инженерно-строительный журнал. 2013. № 7(42). С. 58–66
33. Озерной А.В., Боброва Т.В., Дубенков А.А. Повышение уровня организации дорожного производства на основе внедрения и технического нормирования инновационных технологий // Ориентированные фундаментальные и прикладные исследования – основа модернизации и инновационного развития архитектурно-строительного и дорожно-транспортного комплексов России. Матер. Межд. 66-й науч.-практ. конф. Омск : СибАДИ, 2012. Кн. 1. С. 106–110.
34. Калугин Ю.Б. Универсальный метод вычисления достоверных сроков реализации проекта // Инженерно-строительный журнал. 2016. № 7(67). С. 70–80.
35. Калугин Ю.Б. Универсальный метод оценки сроков выполнения проекта с вероятностными временными параметрами // Известия вузов. Строительство. 2015. № 1. С. 44–52.
36. Синенко С.А. Применение современных информационных технологий для формирования технологических карт выполнения строительных процессов // Евразийский Союз Ученых. 2015. № 5-3(14). С. 149–151.
37. Боброва Т.В., Дубенков А.А., Тытарь И.В. Совершенствование организационно-технологического проектирования линейных транспортных объектов на основе моделирования их пространственной декомпозиции // Системы. Методы. Технологии. 2016. № 4. С. 169–175.
38. Боброва Т.В., Бедрин Е.А., Дубенков А.А. Моделирование проектных решений земляного полотна в условиях криолитозоны: монография. Омск: СибАДИ. 2016. 164 с.
39. Султанова И.П. Анализ методов планирования, управления и разработки организационно-технологических решений в проектах капитального строительства // Вестник МГСУ. 2015. № 7. С. 127–136.
40. Балова Е. Ф., Бакерман Р. С. и др. Нормирование труда рабочих в строительстве. М.: Стройиздат, 1985. 440 с.
41. Боброва Т.В., Дубенков А.А., Краева Е.И. Нормирование технологических процессов как фактор энергосбережения при строительстве земляного полотна автомобильных дорог в сложных природных условиях // Материалы III Межвуз. Науч. конф. Студ. и асп. ОмГТУ-Омск: Изд-во ОмГТУ. 2013. С. 167–169.
42. Дубенков А.А. Вариантное проектирование дорожных конструкций с использованием функционально-стоимостного анализа // Материалы VII Международной науч.-техн. конф. студентов, аспирантов и молодых ученых. Волгоград : ВолГАСУ, 2013. С. 311–315.
43. Болотин С.А., Дадар А.Х., Птухина И.С. Имитация календарного планирования в программах информационного моделирования зданий и регрессионная детализация норм продолжительностей строительства // Инженерно-строительный журнал. 2011. № 7(25). С. 82–86.
44. Зеньковский В.А. Cinema 4D. Практическое руководство. Солон-Пресс. 2008. 376 с.
45. Шикин Е.В., Плис Л.И. Кривые и поверхности на экране компьютера. Руководство по сплайнам для пользователей. М.: ДИАЛОГ-МИФИ, 1996. 240 с.
46. Панченко П.М., Боброва Т.В. Оценка продолжительности выполнения монтажных работ при строительстве зданий на основе нормирования технологических операций // Архитектурно-строительный и дорожно-транспортный комплексы:

[Proceedings of VII International scientific-technical conference of students, post graduate students and young scientists]. Volgograd: VolGASU, 2013. Pp. 311–315. (rus)
43. Bolotin S.A., Dadar A.Kh., Ptuhina I.S. Simulation of calendar planning in Building information modelling programms and regression detailing of construction period rules. *Magazine of Civil Engineering*. 2011. No. 7(25). Pp. 82–86. (rus)
44. Zenkovskij V.A. *Cinema 4D. Prakticheskoe rukovodstvo*. [Cinema 4D. Practical guide]. Solon-Press, 2008. 376 p. (rus)
45. Shikin E. V., Plis L. I. *Krivye i poverhnosti na ekrane kompyutera. Rukovodstvo po splajnam dlya polzovatelej* [Curves and surfaces on the computer screen. A guide to splines for users]. Moscow: DIALOG-MIFI, 1996. 240 p. (rus)
46. Panchenko P.M., Bobrova T.V. Ocenka prodolzhitelnosti vypolneniya montazhnyh rabot pri stroitelstve zdanij na osnove normirovaniya tehnologicheskih operacij [Estimating the duration of the installation work during the construction of buildings based on the normalization of technological operations]. *Materialy Mezhdunarodnoj nauchno-prakticheskoj konferencii "Arhitekturno-stroitelnyj i dorozhno-transportnyj kompleksy: problemy, perspektivy, novacii"* [Proceedings of International scientific-practical conference "Architectural-building and road-transport complexes: problems, perspectives, innovations"]. Omsk: Izd-vo SibADI, 2016. (rus)
47. *Karta trudovogo processa stroitelnogo proizvodstva. Montazh plit perekrytij lodzhij ploschadyu do 5 m2 : (vzamen KT-4.1-7.23-75) : KT-4.1-7.23-77* [Map of the labor process of construction. Installation of floor slabs of loggias with area up to 5 m2]. Moscow: Minstroj, 2008. 10 p. (rus)
48. Romanovich M.A. *Povyshenie organizacionno-tehnologicheskoj nadezhnosti monolitnogo domostroeniya na osnove modelirovaniya parametrov kalendarnogo plana: avtoref. dis.…kand. tehn. nauk: 05.23.08* [Improving the organizational and technological reliability of monolithic housing construction on the basis of modeling the parameters of the calendar plan. Abstract of PhD Thesis 05.23.08]. Saint-Petersburg, 2015. 21 p. (rus)

проблемы, перспективы, новации: материалы Международной научно-практической конференции. Омск: Изд-во СибАДИ, 2016.
47. Карта трудового процесса строительного производства. Монтаж плит перекрытий лоджий площадью до 5 м2 : (взамен КТ-4.1-7.23-75) : КТ-4.1-7.23-77. М.: Минстрой, 2008. 10 с.
48. Романович М.А. Повышение организационно-технологической надежности монолитного домостроения на основе моделирования параметров календарного плана: автореф. дис.…канд. техн. наук: 05.23.08. СПб. 2015. 21 с.

Tatyana Bobrova,
+7(965)980-00-86; bobrova.tv@gmail.com

Pavel Panchenko,
+7(908)795-38-26; pach121092@mail.ru

Татьяна Викторовна Боброва,
+7(965)980-00-86;
эл. почта: bobrova.tv@gmail.com

Павел Михайлович Панченко,
+7(908)795-38-26;
эл. почта: pach121092@mail.ru

doi: 10.18720/MCE.76.9

Seismic input models for tuned mass damper designing

Расчетное сейсмическое воздействие для сооружения с динамическим гасителем колебаний

Y.U. Albert,
JSC "VNIIG im.B.E.Vedeneeva", Saint Petersburg, Russia
A.A. Dolgaya ,
JSC "Transmost", St. Petersburg, Russia
T.V. Ivanova,
JSC "VNIIG im.B.E.Vedeneeva", Saint Petersburg, Russia
O.P. Nesterova,
A.M. Uzdin,
Petersburg State Transport University, St. Petersburg, Russia
J. Guan,
China University of Petroleum, Huadong, China
D.A. Ivashintzov,
O.K. Voronkov,
V.B. Shtilman,
S.G. Shulman,
A.A. Khrapkov,
JSC "VNIIG im.B.E.Vedeneeva", Saint Petersburg, Russia

Д-р техн. наук, ст. науч. сотрудник И.У. Альберт,
АО "ВНИИГ им. Б.Е. Веденеева", г. Санкт-Петербург, Россия
канд. техн. наук, инженер А.А. Долгая,
ОАО «Трансмост», г. Санкт-Петербург, Россия
канд. техн. наук, ученый секретарь Т.В. Иванова,
АО "ВНИИГ им. Б.Е. Веденеева", г. Санкт-Петербург, Россия
аспирант О.П. Нестерова,
д-р техн. наук, профессор А.М. Уздин,
Петербургский государственный университет путей сообщения Императора Александра I, г. Санкт-Петербург, Россия
PhD Ю. Гуань,
Нефтяной Университет Китая, Циндао, КНР
д-р техн. наук, профессор, гл. науч. сотрудник-консультант Д.А. Ивашинцов,
д-р техн. наук, гл. науч. сотрудник-консультант О.К. Воронков,
д-р техн. наук, ст. науч. сотрудник В.Б. Штильман,
д-р техн. наук, профессор, гл. науч. сотрудник С.Г. Шульман,
д-р техн. наук, профессор, гл. науч. сотрудник А.А. Храпков,
АО "ВНИИГ им. Б.Е. Веденеева", г. Санкт-Петербург, Россия

Key words: tuned mass damper; seismic input; mathematical modeling

Ключевые слова: динамический гаситель колебаний; сейсмическое воздействие; математическое моделирование

Abstract. The subject of investigations is seismic input models for tuned mass damper designing. Some features of simulating design accelerograms for estimating seismic stability of a structure with a mass damper are considered. The method of accelerogram modeling, proposed by Dolgaya A.A., approved by the Building Ministry of Russian Federation and included and in the corresponding Recommendations in 1996, is considered as the basic one. In accordance with this method, an accelerogram is modeled by a sum of three damped sinusoids. The sinusoid frequencies are chosen as dangerous for the structure, and the amplitudes and damping parameters are chosen so that the kinematic and energy characteristics of the model input correspond to the actual ones. The main feature of MD designing is the presence of close frequencies, and the choice of a dangerous frequency is not unambiguous. Features of choosing a dangerous frequency and the influence of various characteristics of real accelerograms on the generated synthetic accelerogram are considered.

Альберт И.У., Долгая А.А., Иванова Т.В., Нестерова О.П., Уздин А.М., Гуань Ю., Ивашинцов Д.А., Воронков О.К., Штильман В.Б., Шульман С.Г., Храпков А.А. Расчетное сейсмическое воздействие для сооружения с динамическим гасителем колебаний // Инженерно-строительный журнал. 2017. № 8(76). С. 98–105.

Аннотация. Рассматриваются особенности моделирования расчетных акселерограмм для оценки сейсмостойкости сооружения с динамическим гасителем колебаний. В качестве базового рассмотрен метод А.А.Долгой, вошедший в Рекомендации Госстроя РСФСР, утвержденные в 1996 году. В соответствии с этим методом акселерограмма моделируется набором из трех затухающих синусоид. Частоты синусоид подбираются опасными для сооружения, а амплитуды и показатели затухания выбираются так, чтобы кинематические и энергетические характеристики модельного воздействия соответствовали натурным. Основной особенностью конструкций с ДГК является наличие близких частот, и выбор опасной частоты не является однозначным. Рассматриваются особенности выбора опасной частоты и влияние различных характеристик воздействия на вид синтетической акселерограммы.

Introduction

Tuned mass dampers (MD) were proposed by H. Fram in 1911 [1, 2]. In the years that followed, many well-known specialists were engaged in optimizing the MD tuning and damping [3–5]. The summing up of studies on the MD problems is given in a well-known monograph by B.G. Korenev and L.M. Reznikov [6]. Since the end of the 70-s of the last century proposals to use the MD for seismic protection of buildings and structures have been made [7–11]. In the recent 20 years the MD began to be widely used for structure protection, i.e. for high-rises building protection against winds and earthquakes in Taipei, Shanghai and other countries [13, 14]. At present, the MD are produced by leading firms in the field of vibration protection such as Maurer Söhnes, FIP Industrial and others. Not long ago investigations on applying the MD in designing non-symmetrical buildings of complicated configuration [15, 16] as well as for non-linear systems [17] and bridges [18] are begun. In order to increase the MD efficiency for seismic protection of structures, it was proposed to use the MD of large mass with a part of the structure itself, being used in the MD [6, 7]. In particular, in [7], it was discovered that there exists the critical mass of the MD, above which the dynamic damping effect disappears, and the MD turns into Lanchester damper. The description of the MD for seismic protection of structures is included in textbooks and teaching aids, as well as in the Guidlines [20, 21]. In the presence of a large number of studies and the apparent simplicity of the problem, attempts to use the MD still bring surprises for scientists. For example, in 2016-17 the essential dependence of the MD tuning, damping and the critical mass on damping in the structure was found [12]. Foreign specialists also found the necessity of taking into account damping in the construction [23, 24]. However, analyzing systems with heterogeneous damping faced with certain difficulties. The normative version of the response spectra method (RSM) cannot be used for inhomogeneous damping. A complete version of the RSM of damped systems was proposed in [15, 25], but has not been used in designing practice yet. The main method of assessing seismic resistance of heavily damped systems remains time-history calculation using accelerograms of earthquakes. Such calculations give designers some freedom, which can result in completely different estimates of seismic resistance. One can see this sort of results in paper [19]. In the authors' opinion, the main problem here is to set seismic input.

The study aim is founding seismic input features for estimating the seismic stability of structures with the MD, in order to exclude errors and ambiguous results of such assessment.

Two approaches to generating design accelerograms have been developed in the earthquake engineering practice. These approaches are described in detail in scientific [16] and educational [8] literature. The first approach is generating design accelerograms for the building site. It can be used when reliable seismological information is available and if the authors of the design accelerograms are ready to bear financial and legal responsibility for them, which is possible when designing highly responsible structures. For mass and especially typical designing it is necessary to use the second method of generating accelerograms, i.e. generating accelerograms for the structure. In this case, the input spectral composition is chosen as dangerous for the structure, and the generated process parameters are chosen so that the characteristics of the model input correspond to the actual ones. In its turn, generating accelerograms for a structure includes 5 methods as follows:

1. Using a package of accelerograms of past earthquakes
2. Choosing a set of narrowband processes
3. Setting a single broadband process
4. Generating a process with a spectrum that coincides with the normative response spectrum
5. Generating a narrowband process dangerous for the structure

Albert Y.U., Dolgaya A.A. Ivanova T.V., Nesterova O.P., Uzdin A.M., Guan J., Ivashintzov D.A., Voronkov O.K., Shtilman S.G., Shulman V.B., Khrapkov A.A, Seismic input models for tuned mass damper designing. *Magazine of Civil Engineering*. 2017. No. 8. Pp. 98–105. doi: 10.18720/MCE.76.9.

These methods are considered in detail in [17]. We only note that the use of this or that technique is always a trade-off between ensuring the danger of the design input for the structure and the similarity of the input to real accelerograms. Thus, for the oscillator, the input in the form of a rectangular sine with the natural oscillator frequency is the most dangerous. For the structure it is possible to set the input in the form of successive harmonics so that each oscillation mode of the structure passes through resonance. Such inputs are dangerous for the construction, but are not like real accelerograms at all. If deliberately dangerous input led to acceptable technical solutions, their further specification and approximation to the real ones would not be necessary. However, as a rule, this does not occur, and the task of specifying the design input is rather urgent. Below, the authors consider setting the abovementioned narrow-band process to be dangerous for the building in calculating structures with the tuned mass damper (MD).

Materials and methods of research

At the description statement of input model a multiparameter narrow-band process can be defined in various ways [18–20]. Below, the model proposed in [18] is considered, but the conclusions obtained on its basis are valid for other models of this type. In accordance with [18], the velosigram of the model input is presented as the sum of three damped sinusoids

$$\dot{y}(t)=\sum_{i=1}^{3} A_i e^{-\varepsilon_i t}\cdot\sin\omega_i t \tag{1}$$

In the process under consideration frequencies ω_i are chosen as dangerous (resonant) for the structure. The amplitude A_2 is determined by the condition $\dot{y}(t)=0$. The rest 5 parameters A_1, A_3, ε_1, ε_2, ε_3 are set so that the characteristics of the model process correspond to the field data. In [19] peak ground accelerations (PGA), depending on the frequency of oscillations, and Arias intensity I_A were accepted as the input characteristics. Recent studies make it possible to take into account a wider range of seismic input characteristics. The analysis of these characteristics is given in [21]. When generating the impact, the authors took into account 5 characteristics of real accelerograms.

1. Peak ground acceleration, $\ddot{y}_0^{(\max)}$, PGA.

2. Coefficient of process harmonicity κ,

$$\kappa=\frac{\ddot{y}_0^{(\max)}\cdot y_0^{(\max)}}{\left(\dot{y}_0^{(\max)}\right)^2} \tag{2}$$

where $y_0^{(\max)}$ is the maximum displacement of the base, and $\dot{y}_0^{(\max)}$ is the maximum velocity of the base.

3. Arias intensity I_A

$$I_A=\frac{\pi}{2g}\int_0^T \ddot{y}_0^2 dt. \tag{3}$$

4. Absolute cumulative velocity CAV

$$CAV=\int_0^T \left|\ddot{y}_0\right| dt \tag{4}$$

5. Seismic energy density SED

$$SED=\int_0^T \dot{y}_0^2 dt \tag{5}$$

The first two characteristics are referred to kinematic ones, and the next three are attributed to energy characteristics.

The foregoing approach is aimed at generating a dangerous design input and taking into account important features of actual impacts.

Two features of the method of input generating under consideration, which are not taken into account in [18, 19] should be noted.

First, the parameters of the input are determined approximately, parameter weighting factors are given for each parameter and the difference between the characteristics of the model and the actual input is minimized taking into account these parameters. Thus, it is possible to construct the infinite number of model processes with a given spectral composition. Secondly, in [19, 20] the first component of the process is considered as the main one. It is assumed that it accounts for minimum half of the SED value, i.e. the following condition takes place.

$$A_1^2 > A_2^2 + A_3^2 \tag{6}$$

The foregoing statement of the problem of seismic input generating is suitable for calculating structures with a rarefied spectrum in which the main part of the seismic load is provided by the first oscillation mode. Meanwhile, in design practice, one has to deal with structures having a dense spectrum. In this case, a dangerous mode is not known in advance. The simplest object of this type is the construction with the MD. The specifics of the input setting for such structures are discussed below.

Results and Discussion

Setting the seismic input to assess the effectiveness of MD. When calculating systems with the MD, it is necessary to deal with at least three characteristic frequencies. This fact is illustrated in Fig. 1, which shows the gain-frequency characteristic of an oscillator with eigen frequency k_0 and with static displacement A_{st}. For the structure without the MD the dangerous frequency is ω_0, and for the structure with the MD there are two dangerous frequencies ω_1 and ω_2, and the amplitudes of oscillations at these frequencies coincide. In this regard, for the example under consideration it is necessary to generate three design accelerograms: the basic one, for calculating a structure without the MD, and two accelerograms dangerous for a structure with the MD. This means that algorithmically in the first generation the frequency ω_1 should be used as the first main frequency, and in the second generation the first main frequency must be ω_2.

For example, let us consider a bridge pier with two spans, for which the second span of the system acts as the MD due to its connection with the pier by an elastic-damping joint (Fig. 2). Such technical solutions are considered in the literature [7–9, 22]. The pier has dense sandy soils in the base with a deformation modulus E_0 = 300 kg/cm^2 (30 MPa). The dynamic characteristics of the pier are given in Table 1. The MD under consideration is the MD of big mass and its optimum damping, i.e. inelastic resistant ratio γ, exceeds the critical value. The letter is difficult to achieve, therefore, in this example γ = 0.5 (25 % of critical value) is considered.

Table 1. Dynamic characteristics of the structure for which the calculated accelerogram is generated

Mode characteristics	**Pier with one span**			**Pier with two spans with the second span used as the MD**		
	The mode number			The mode number		
	1	2	3	1	2	3
Period, T, s	0.425	0.0433	0.0142	1.767	0.412	0.0433
Frequency, ω, s^{-1}	14.80	145.03	441.8	3.556	15.246	145.03
Inelastic resistant ratio, γ	0.167	0.228	0.141	0.478	0.165	0.185

Table 2. Characteristics of generated inputs

Object to be calculated		**Structure without the MD**	**Structure with the MD**	
			Dominance on the first mode	Dominance on the second mode
Input characteristics	PGA, м/с^2	5.415	2.074	5.383
	I_A, м/с	2.874	0.303	3.911
	CAV, м/с	11.230	3.459	14.072
	SED, м^2/с	0.053	0.122	0.181
	κ	3.465	3.00	2.378

The results of calculating structures using generated accelerograms are shown in Figures 3–5 and in Table 3.

Table 3. Some results of structure calculations

Characteristics of structure calculations		**Design accelerograms**		
		For the structure without the MD	For the structure with the MD	
			At the first mode tuning	At the second mode tuning
displacements, m	The first span (structure top)	0.0587	0.011	0.0374
	The second span (MD)	-	0.001	0.0027
accelerations, m/s^2	The first span (structure top)	12.80	2.462	8.89
	The second span (MD)	-	0.123	0.534

Note, that the calculating the system with the MD using the accelerogram dangerous for the structure without the MD, gives an incorrect estimate of the MD efficiency. In this case, the maximum shift of the MD is 0.002 m, the maximum displacement of the structure is 0.027 m and the corresponding maximum accelerations are 0.385 m/s^2 and 6.605 m/s^2.

Conclusions

The abovementioned investigations made it possible to discover some peculiarities of seismic input setting for structures with tuned mass dampers. Among them one can stress the following

1) When generating seismic input in the form of a narrow-band process dangerous for a structure, several inputs corresponding to several resonant frequencies should be generated. In the example considered, the second natural frequency of the structure with the MD turned out to be dangerous.

2) It should also be stressed that when evaluating the effectiveness of the MD using accelerograms of earthquakes, the calculation of the structure without the MD and with the MD should be carried out using different accelerograms

Acknowledgements

The work has been carried out with the support of RFBR grant № 16-58-53095 "Development of the theory of limit states to ensure seismic stability of operated railway bridges and those under constriction".

References

1. Frahm H., *Schlingertanks zur Abdämpfung von Schiffsrollbewegungen, Jahrbuch d.* Schiffbautechnick Ges.. 1911. Bd. 12.
2. Frahm H *Device for damping vibrations of bodies.* U.S. Patent 0989958. 1909.
3. Warburton G.V. Optimum absorber parameters for various

Литература

1. Frahm H. Schlingertanks zur Abdämpfung von Schiffsrollbewegungen, Jahrbuch d. Schiffbautechnick Ges.. 1911. Bd. 12.
2. Frahm H Device for damping vibrations of bodies. U.S. Patent 0989958. 1909.
3. Warburton G.V. Optimum absorber parameters for various

Альберт И.У., Долгая А.А., Иванова Т.В., Нестерова О.П., Уздин А.М., Гуань Ю., Ивашинцов Д.А., Воронков О.К., Штильман В.Б., Шульман С.Г., Храпков А.А. Расчетное сейсмическое воздействие для сооружения с динамическим гасителем колебаний // Инженерно-строительный журнал. 2017. № 8(76). С. 98–105.

combinations of response and excitation parameters. *Earthquake Engineering and Stucture Dynamics.* 1982. Vol. 10. No. 3. Pp. 381–401.

4. Timoshenko S.P. *Kolebaniya v inzhenernom dele* [Fluctuations in engineering]. Moscow: Nauka. 1976. Pp. 209–216. (rus)
5. Savinov O.A. O primenenii dinamicheskogo gasitelya kolebaniy [On the application of a dynamic vibration damper]. *Trudy nauchno-issled. sektora L.O. tresta glubinnykh rabot* [Proceedings of the Research Sector of the Leningrad Branch of the Trust of the Deep Works]. 1940. No. 2. Leningrad, Moscow: Gosizdat stroitelnoy literatury. Pp. 30–35. (rus)
6. Korenev B.G., Reznikov L.M. *Dinamicheskiye gasiteli kolebaniy* [Dynamic vibration absorbers]. Moscow: Nauka, 1988. 303 p. (rus)
7. Korenev B.G., Polyakov V.S. Optimalnyye parametry dinamicheskogo gasitelya kolebaniy pri vozdeystviyakh tipa seysmicheskogo [Optimal parameters of the dynamic vibration damper under the action of the seismic type]. *Seysmostoykoye stroitelstvo.* 1977. No. 3. Pp. 37–42. (rus)
8. Tseytlin A.I., Kim L.I. Seysmicheskiye kolebaniya mnogoetazhnogo zdaniya s "gibkim" verkhnim etazhom. Snizheniye materialoyemkosti i trudoyemkosti seysmostoykogo stroitelstva [Seismic vibrations of a multi-storey building with a "flexible" upper floor. Reduction of the material consumption and labor intensity of earthquake-resistant construction]. *Tezisy dokladov Vsesoyuznogo soveshchaniya* [Theses of the reports of the All-Union Conference]. Moscow: Stroyizdat. 1982. 85 p. (rus)
9. Nikitin A.A., Uzdin A.M. Primeneniye dinamicheskikh gasiteley kolebaniy dlya seysmozashchity mostov. Ekspress-informatsiya VNIIIS. Ser.14 [Application of dynamic vibration dampers for seismic protection of bridges. Express information VNIIIS]. *Seysmostoykoye stroitelstvo.*1986. No. 9. Pp. 20–24. (rus)
10. Aldemir U., Yanik A., Bakiogl M.U. Control of structural response under earthquake excitation. *Comput-Aided Civil Infrastructure Engineering.* 2012. No. 27(8). Pp. 620–638.
11. Nikitin A.A., Tsibarova M.Yu., Uzdin A.M. K voprosu o primenenii dinamicheskikh gasiteley kolebaniy bolshoy massy dlya energeticheskikh sooruzheniy [To the question of the application of dynamic absorbers for large-scale oscillations for power structures]. *Materialy konferentsiy i soveshchaniy po gidrotekhnike: Povysheniye nadezhnosti energeticheskikh sooruzheniy pri dinamicheskikh vozdeystviyakh* [Materials of conferences and meetings on hydraulic engineering: Increasing the reliability of power structures under dynamic influences]. Leningrad: Energoatomizdat. 1989. Pp. 242–245. (rus)
12. Castelliano M.G., Kuznetsova I.O., Nikitin A.A., Verholin V.V., Uzdin A.M. The study of FIP-INDUSTRIALE devices for the earthquake protection of bridges in Russia. *Proceedings of 8-th world Seminar on Seismic Isolation, Energy Dissipation and Active Vibration Control of Structures.* Yerevan, Armenia. 2003. Pp. 407–416.
13. Tamboli A., Joseph L., Vadnere U., Xu X., Tall buildings: sustainable design opportunities. *Council on Tall Buildings and Urban Habitat. 8th World Conference.* Dubai, 2008.
14. Tuan A.Y., Shang G.Q. Vibration control in a 101-storey building using a tuned mass damper. *Journal of Applied Science and Engineering.* 2014. Vol. 17. No. 2. Pp. 141–156.
15. Lin J.-L., Tsai K.-C., Yu Y.-J. Coupled tuned mass dampers for the seismic control of asymmetric-plan buildings. *Earthquake Spectra*. 2010. No. 26(3). Pp. 749–778.
16. Lavan O., Daniel Y. Full resources utilization seismic design of irregular structures using multiple tuned mass

combinations of response and excitation parameters // Earthquake Engineering and Stucture Dynamics. 1982. Vol. 10. № 3. Pp. 381–401.

4. Тимошенко С.П. Колебания в инженерном деле. М.: Наука. 1976. С. 209–216.
5. Савинов О.А. О применении динамического гасителя колебаний // Труды научно-исслед. сектора Л.О. треста глубинных работ. 1940. № 2. Л., М.: Госиздат строительной литературы. С. 30–35.
6. Коренев Б.Г., Резников Л.М. Динамические гасители колебаний. М.: Наука, 1988. 303 с.
7. Коренев Б.Г., Поляков В.С. Оптимальные параметры динамического гасителя колебаний при воздействиях типа сейсмического // Сейсмостойкое строительство. 1977. № 3. С. 37–42.
8. Цейтлин А.И., Ким Л.И. Сейсмические колебания многоэтажного здания с "гибким" верхним этажом. Снижение материалоемкости и трудоемкости сейсмостойкого строительства // Тезисы докладов Всесоюзного совещания. М.: Стройиздат. 1982. 85 с.
9. Никитин А.А., Уздин А.М. Применение динамических гасителей колебаний для сейсмозащиты мостов. Экспресс-информация ВНИИИС. Сер.14. // Сейсмостойкое строительство.1986. № 9. С. 20–24.
10. Aldemir U., Yanik A., Bakiogl M.U. Control of structural response under earthquake excitation // Comput-Aided Civil Infrastructure Engineering. 2012. № 27(8): Pp. 620–638.
11. Никитин А.А., Цибарова М.Ю., Уздин А.М. К вопросу о применении динамических гасителей колебаний большой массы для энергетических сооружений // Материалы конференций и совещаний по гидротехнике: Повышение надежности энергетических сооружений при динамических воздействиях. Л.: Энергоатомиздат, 1989. С. 242–245.
12. Castelliano M.G., Kuznetsova I.O, Nikitin A.A., Verholin V.V, Uzdin A.M. The study of FIP-INDUSTRIALE devices for the earthquake protection of bridges in Russia // Proceedings of 8-th world Seminar on Seismic Isolation, Energy Dissipation and Active Vibration Control of Structures. Yerevan, Armenia. 2003. Pp. 407–416.
13. Tamboli A., Joseph L., Vadnere U., Xu, X. Tall buildings: sustainable design opportunities // Council on Tall Buildings and Urban Habitat. 8th World Conference. Dubai, 2008.
14. Tuan A.Y., Shang G.Q. Vibration control in a 101-storey building using a tuned mass damper // Journal of Applied Science and Engineering. 2014. Vol. 17. № 2. Pp. 141–156.
15. Lin J.-L., Tsai K.-C., Yu Y.-J. Coupled tuned mass dampers for the seismic control of asymmetric-plan buildings // Earthquake Spectra. 2010. № 26(3). Pp. 749–778.
16. Lavan O., Daniel Y. Full resources utilization seismic design of irregular structures using multiple tuned mass dampers // Structure Multidiscip Optim. 2013. № 48(3). Pp. 517–532.
17. Mohebbi M., Joghataie A. Designing optimal tuned mass dampers for nonlinear frames by distributed genetic algorithms // Struct Des Tall Spec Buildiungs. 2012. № 21(1). Pp. 57–76.
18. Hoang T., Ducharme K.T., Kim Y., Okumus P. Structural impact mitigation of bridge piers using tuned mass damper // Engineering Structures. 2016. Vol. 112. Pp. 287–294.
19. Elias S., Matsagar V. Effectiveness of tuned mass dampers in seismic response control of isolated bridges including soil-structure interaction // Latin American Journal of Solids and Structures. 2017. № 14. Pp. 1–18.
20. Инструкция по оценке сейсмостойкости эксплуатируемых мостов на сети железных и автомобильных дорог (на территории Туркменской ССР). Ашхабад:Ылым,1988.106 с.
21. Рекомендации по проектированию гасителей колебаний для защиты зданий и сооружений, подверженных

dampers. *Structure Multidiscip Optim*. 2013. No. 48(3). Pp. 517–532.

17. Mohebbi M, Joghataie A Designing optimal tuned mass dampers for nonlinear frames by distributed genetic algorithms. *Struct Des Tall Spec Buildiungs*. 2012. No. 21(1). Pp. 57–76.
18. Hoang T., Ducharme K.T., Kim Y., Okumus P. Structural impact mitigation of bridge piers using tuned mass damper. *Engineering Structures.* 2016. Vol. 112. Pp. 287–294.
19. Elias S., Matsagar V. Effectiveness of tuned mass dampers in seismic response control of isolated bridges including soil-structure interaction. *Latin American Journal of Solids and Structures.* 2017. No. 14. Pp. 1–18.
20. *Instruktsiya po otsenke seysmostoykosti ekspluatiruyemykh mostov na seti zheleznykh i avtomobilnykh dorog (na territorii Turkmenskoy SSR)* [Instruction on the assessment of seismic resistance of operated bridges on the network of railways and highways (on the territory of the Turkmen SSR)]. Ashkhabad:Ylym,1988.106 p. (rus)
21. *Rekomendatsii po proyektirovaniyu gasiteley kolebaniy dlya zashchity zdaniy i sooruzheniy, podverzhennykh gorizontalnym dinamicheskim vozdeystviyam ot tekhnologicheskogo oborudovaniya i vetra* [Recommendations for the design of vibration dampers for the protection of buildings and structures subject to horizontal dynamic influences from process equipment and wind]. Moscow: TsNIISK im. V.A.Kucherenko,1978. 68 p. (rus)
22. Nesterova O.P., Uzdin A.M. Osobennosti raboty dinamicheskikh gasiteley kolebaniy pri silovom i kinematicheskom vozmushchenii dempfirovannykh sooruzheniy [Features of the operation of dynamic vibration dampers in the case of force and kinematic perturbations of damping structures]. *Izvestiya rossiyskoy Akademii raketnykh i artilleriyskikh nauk.* Moscow. 2016. No. 2(92). Pp. 84–89.
23. Hori Y., Kurino H., Kurokawa Y. Development of large tuned mass damper with stroke control system for seismic upgrading of existing high-rise building. *International Journal of High-Rise Buildings.* 2016. Vol. 5. No. 3. Pp. 167–176.
24. Shayeghi A., Shayeghi H., Eimani Kalasar H. Application of PSO technique for seismic control of tall building. *International Journal of Intelligent Systems and Technologies.* 2009. No. 4. Pp. 28–35.
25. Nesterova O.P., Vorobyeva K.V.,Uzdin A.M. Otklik na statyu A.G.Tyapina «Neklassicheskoye dempfirovaniye v sisteme «osnovaniye-sooruzheniye» i vopros primenimosti spektralnogo metoda rascheta usiliy» [Response to the article of A.G. Tyapin "Non-classical damping in the" foundation-construction "system and the question of the applicability of the spectral method of calculating the effort"]. *Seysmostoykoye stroitelstvo. Bezopasnost sooruzheniy.* 2017. No. 2. Pp. 60–63. (rus)

горизонтальным динамическим воздействиям от технологического оборудования и ветра. М.: ЦНИИСК им. В.А.Кучеренко,1978. 68 с.

22. Нестерова О.П., Уздин А.М. Особенности работы динамических гасителей колебаний при силовом и кинематическом возмущении демпфированных сооружений // Известия российской Академии ракетных и артиллерийских наук. 2016. № 2(92). С. 84–89.
23. Hori Y., Kurino H., Kurokawa Y. Development of Large Tuned Mass Damper with Stroke Control System for Seismic Upgrading of Existing High-Rise Building // International Journal of High-Rise Buildings. 2016. Vol. 5. № 3. Pp. 167–176.
24. Shayeghi A., Shayeghi H., Eimani Kalasar H. Application of PSO technique for seismic control of tall building // International Journal of Intelligent Systems and Technologies. 2009. № 4. Pp. 28–35.
25. Нестерова О.П., Воробьева К.В., Уздин А.М. Отклик на статью А.Г. Тяпина «Неклассическое демпфирование в системе «основание-сооружение» и вопрос применимости спектрального метода расчета усилий» // Сейсмостойкое строительство. Безопасность сооружений. 2017. № 2.С. 60–63.

Альберт И.У., Долгая А.А., Иванова Т.В., Нестерова О.П., Уздин А.М., Гуань Ю., Ивашинцов Д.А., Воронков О.К., Штильман В.Б., Шульман С.Г., Храпков А.А. Расчетное сейсмическое воздействие для сооружения с динамическим гасителем колебаний // Инженерно-строительный журнал. 2017. № 8(76). С. 98–105.

Yuliy Albert
+7(812)493-93-18; AlbertYU@vniig.ru

Anzhelika Dolgaya,
+7(921)992-58-99; anzhelika-dolgaya@yandex.ru

Tatiana Ivanova,
+7(812)493-93-63; IvanovaTV@vniig.ru

Olga Nesterova,
+7(960)280-59-75; Neona975@yandex.ru

Aleksandr Uzdin,
+7(921)788-33-64; uzdin@mail.ru

Youhai Guan,
329953890@qq.com

Sergey Shulman,
493-93-40;

Oleg Voronkov,
493-93-90; VoronkovOK@vniig.ru

Vladimir Shtilman,
493-93-78; ShtilmanVB@vniig.ru

Anatoliy Khrapkov,
493-93-30; khrapkovaa@vniig.ru
Ivashintzov D.A.
535-26-04; IvashintsovDA@vniig.ru

Июля Ушерович Альберт,
+7(812)493-93-18; эл. почта: AlbertYU@vniig.ru

Анжелика Александровна Долгая,
+7(921)992-58-99;
эл. почта: anzhelika-dolgaya@yandex.ru

Татьяна Викторовна Иванова,
+7(812)493-93-63; эл. почта: IvanovaTV@vniig.ru

Ольга Павловна Нестерова,
+7(960)280-59-75;
эл. почта: Neona975@yandex.ru

Александр Моисеевич Уздин,
+7(921)788-33-64; эл. почта: uzdin@mail.ru

Юхай Гуань,
эл. почта: 329953890@qq.com

Ивашинцов Дмитрий Александрович
+7(812)535-26-04;
эл. почта: IvashintsovDA@vniig.ru

Олег Константинович Воронков,
+7(812)493-93-90;
эл. почта: VoronkovOK@vniig.ru

Владимир Борисович Штильман,
+7(812)493-93-78;
эл. почта: ShtilmanVB@vniig.ru

Сергей Георгиевич Шульман,
+7(812)493-93-40

Храпков Анатолий Александрович
+7(812)493-93-30;
эл. почта: khrapkovaa@vniig.ru

Albert Y.U., Dolgaya A.A. Ivanova T.V., Nesterova O.P., Uzdin A.M., Guan J., Ivashintzov D.A., Voronkov O.K., Shtilman S.G., Shulman V.B., Khrapkov A.A, Seismic input models for tuned mass damper designing. *Magazine of Civil Engineering*. 2017. No. 8. Pp. 98–105. doi: 10.18720/MCE.76.9.

doi: 10.18720/MCE.76.10

Critical section and critical depth in open flows finding device

Устройство для нахождения критического сечения и критической глубины в открытых потоках

N.K. Yerzhanova,
M.Kh. Dulaty Taraz State University, Taraz, Republic of Kazakhstan
Zh.A. Mussin,
The Kazakh scientific research institute of water economy, Taraz, Republic of Kazakhstan
S.K. Dzholdasov,
M.Kh. Dulaty Taraz State University, Taraz, Republic of Kazakhstan
A.D. Altynbekova,
M.Kh. Dulaty Taraz State University, Taraz, Republic of Kazakhstan

***Докторант Н.К. Ержанова**,*
Таразский государственный университет им. М.Х. Дулати, г.Тараз, Республика Казахстан
канд. техн. наук, ведущий науч. сотрудник Ж.А. Мусин,
КазНИИ водного хозяйства, г. Тараз, Республика Казахстан
канд. техн. наук, доцент С.К. Джолдасов,
Таразский государственный университет им. М.Х. Дулати, г.Тараз, Республика Казахстан
магистрант А.Д. Алтынбекова,
Таразский государственный университет им. М.Х. Дулати, г.Тараз, Республика Казахстан

Key words: flow rate; average speed; dynamic head; specific energy; spitzen scale; measuring needle; Pitot tube; stock; critical section; critical depth

Ключевые слова: расход потока; средняя скорость; динамический напор; удельная энергия; шпитцен-масштаб; мерная игла; трубка Пито; шток; критическое сечение; критическая глубина

Abstract. There is theoretically shown that pressure is equal to half of flow depth at state of speed flow, i.e .It is equal to half of critical depth. Knowing it, authors offer a device that is designed to finding critical section and critical depth in open flows which are defined by consecutive measurements of dynamic pressure and depth of flow by means of the device in various cross sections and section findings where the dynamic pressure is equal to a half of flow depth, and depth is critical depth, i.e. equality is observed. As a result of the use of such a device increases information density due to the direct determination of the critical section and the critical depth of flow and increase ease of operation.

Аннотация. В статье теоретически показывается, что при критическом состоянии потока скорости напор равен половине глубины потока, т.е. половине критической глубины. Авторами предлагается устройство предназначенное для нахождения критического сечения и критической глубины в открытых потоках, которые определяются путем последовательных замеров динамического напора и глубины потока с помощью устройства в различных поперечных сечениях и нахождения сечения, где динамический напор равен половине глубины потока, а глубина – критической глубине, т.е. равенство соблюдается. В результате применении такого устройства повышается информативность за счет возможности непосредственного определения критического сечения и критической глубины потока и повышение удобства эксплуатации.

Introduction

Finding the critical section and critical depth is necessary not only for estimation the flow state but also for the performance of a number of hydraulic calculations and analysis of the dimensionless coordinate research results. In addition, the critical depth is a unique function of speed and consumption, which enables to determine the velocity and flow rate of the fluid. For example, N.P. Lavrov and M.K. Toropov proposed a way for determining the water discharge at the head sections of the fleeting canals at a critical depth [1]. Consequently, the questions raised are of practical importance.

In hydrometric practice, as well as in the laboratory to measure the depth of the flow widespread measuring needle or Scale-Spitze, hydrometric tube piezometers [2-9]. It allows you to measure the level in the adjustment and calibration of flowmeters variable level.

The main part of the needle measuring rod is coated with it privileges. On the stock strengthened toothed strap and body are based on rack and vernier. Produce vernier reading on the moment of contact needle attached to the stem, or the liquid surface at the time of separation of the needle from the surface [10–16].

To fix the exact moment of contact dimensional needles used electro-contact way to display the time needle touch the liquid surface [2, 17].

Application dimensional needles can measure the level with great precision. Absolute error of measurement is almost independent of range. These advantage dimensional needles formed the basis for measuring the parameters of liquid flow in open flows. However, none of them is able to determine the critical section and a direct measurement of the critical depth.

Examine critical state of flow [18–25]. At the critical state of flow when h=hкр, and the specific energy section has a minimum value E = Emin, therefore,

$$\frac{dE}{dh} = 1 - \frac{\alpha Q^2}{g\omega^3}\frac{d\omega}{dh} = 1 - \frac{\alpha \upsilon^2}{g\omega}\frac{d\omega}{dh} = 0, \quad (1)$$

where E – the specific energy of the cross section; Q – flow rate; ω – open area flow; h – the depth of the flow in the living section; g – acceleration of gravity; α – the coefficient of kinetic energy (Coriolis); *u* – the average speed in the living section.

Since $d\omega = bdh$ and $h = \frac{\omega}{b}$ equation (1) can be written as

$$\frac{dE}{dh} = 1 - \frac{\alpha \upsilon^2 b}{g\omega} = 1 - \frac{\alpha \upsilon^2}{gh} = 0, \quad 2)$$

From here you can get

$$\frac{\alpha \upsilon^2}{2g} = \frac{h}{2} \quad (3)$$

Equation (3) can be written in the parameter of kinetism $\alpha = 1$ how

$$\frac{\upsilon}{\sqrt{gh}} = 1 \quad (4)$$

or $F_r = 1$ that meets the definition of a critical mode, i.e.,

$$F_r = \frac{\upsilon^2}{gh} = 1, \quad (5)$$

Here

$$\upsilon^2 = gh, \quad (6)$$

where F_r – froude number.

If both sides of (6), we multiply to $\frac{\rho}{2\gamma}$, we get

$$\frac{\rho \upsilon^2}{2\gamma} = \frac{\rho g h}{2\gamma} \quad \text{or} \quad \frac{\upsilon^2}{2g} = \frac{h}{2} \quad (7)$$

where ρ – density of the fluid; γ – the proportion of liquid.

This is the criteria for the critical state of flux, therefore, the critical state of flow rate pressure is equal to half the depth of the stream, i.e., half of the critical depth.

The purpose of the work is to increase the informative due to the possibility of finding the critical section and measuring the critical depth of the fluid flow, which is achieved by using a device, based on the equation of the dynamic head in the critical section of the flow half of its depth, which makes it is very easy to find the critical section of the liquid flow and measure the critical depth.

To achieve this objectives the following tasks:

– to conduct a theoretical analysis of the critical state of the open flow;

– select the conditions and justification devices for critical cross-section of the fluid flow and measuring the critical depth;

– collecting model to determine the critical cross-section of the fluid flow and measuring the critical depth;

– experiments on the measurement of critical depth;

– conclusions.

Materials and methods of research

A device is offered for finding critical section and critical depth in open flows. As a result of the application of such device the informative value increases due to the possibility of direct determination of the critical section, and critical depth of flow and flexibility in application increases too.

The goal is achieved by successive measurements of the dynamic pressure and flow depth using the device in different cross sections and finding the section where the dynamic pressure is half the depth of the flow and the depth - critical depth. This device performs the method of finding the critical section and measuring the critical depth in open flows. It contains measuring needle Pitot tube, the signal system in which the stem-dimensional needle designed for the measurement of fluid flow. It is equipped with two series-connected and arranged symmetrically with respect to the liquid surface of the same hinge diamonds, mounted one on top of the sleeve slid ably fitted on the rod, and the other - the lower part resting on the bottom of the channel. Wherein a portion of the vertical extension of a diagonal rod which is installed pitot tube, wherein the fluid level is fixed at the throat of the other dimensional position of the needle through rod rigidly connected to the first measuring needle, wherein the end of the needle is mounted on a level with the upper horizontal diagonal of the rhombus which effect mobility rhombuses constantly, regardless of the cross section will be located at a height $\frac{3}{2}h$ relative to the bottom of the channel. Two upper side of the lower extension of the rhombus are the two lower side of the top of the rhombus, constituting one unit with it, and their intersection point is fixed to the needle hub dimensional fixing fluid flow rate via a hinge whose axis is flush with the end of the needle. Horizontal diagonal rhombus are executed in the form of rods, one ends fixed to the left side hinges, and other moving freely on the sleeves mounted on the right side of the hinges. Two lower side of the lower rumba pulled an elastic member (spring) to prevent spontaneous alignment of the parties. Figure 1 is a schematic diagram of a device, Figure 2 – the same, as seen from the incident flow.

The device consists of two dimensional needles 1 and 2, the two articulated lozenges is the upper 3 and lower 4 forming the pantograph mechanism, the receiver of the velocity head in the form of a Pitot tube 5, consisting of a suction connection of the measuring tube, and the indicator 6. Measuring the needle 1 is rigidly fixed to the hub 7 is fixedly fitted on the guide rod 8, and is connected to the signaling device 6. On the rod 8 has two serially connected and arranged symmetrically with respect to the liquid surface of the rhombus hinge 3 and 4, one of which is fixed on the upper part of the sleeve 9 is movably fitted on the rod 8 and the other – the lower part rests on the bottom of the channel. The articulated lozenges 3 and 4 two upper sides 10 and 11 of the lower rhombus 4 are a continuation of the two lower sides 12 and 13 of the upper three rhombus, making them integral, and their intersection point is fixed to the hub 7 through a hinge 14, whose axis is at one measuring the level of the end of needle 1, and horizontal diagonals 15 and 16, made in the form of rods, one ends are fixed to the left side hinges 17 and 18 and the other ends are free to move along the sleeves 19 and 20 attached to the right side hinges 21 and 22. The lower side 23 and 24 of the lower rhombus tightened elastic member 4 (spring) 25.

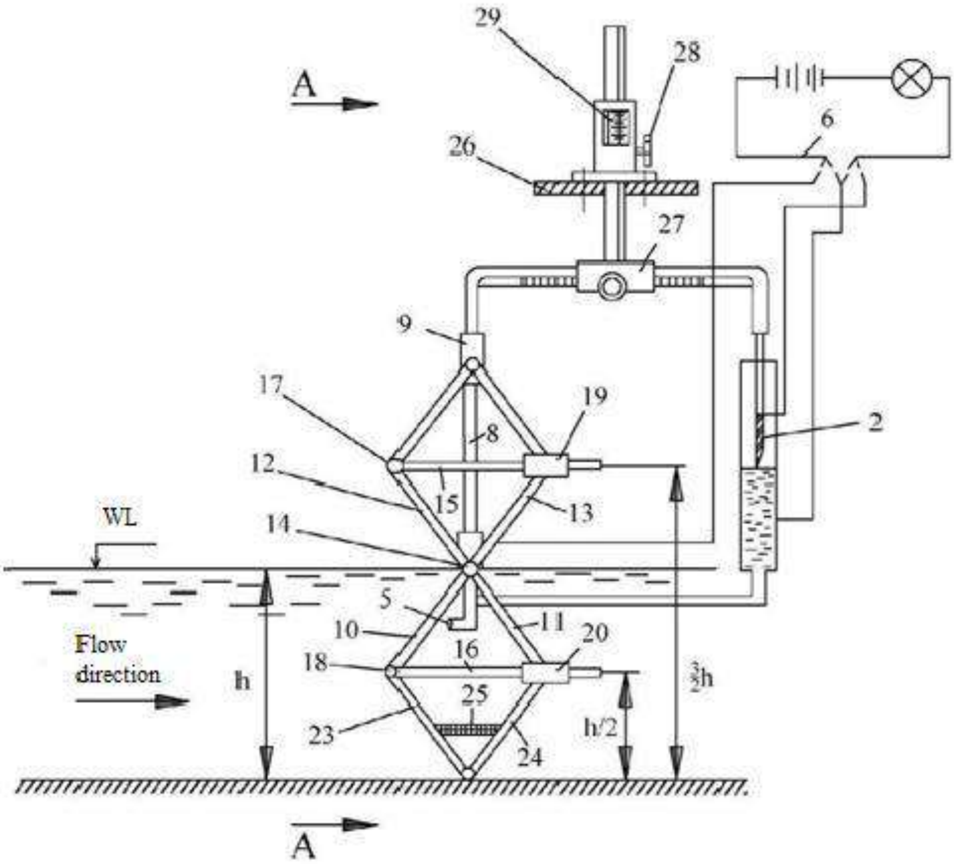

Figure 1. Schematic diagram of a device for measuring parameters of fluid flow in open flow

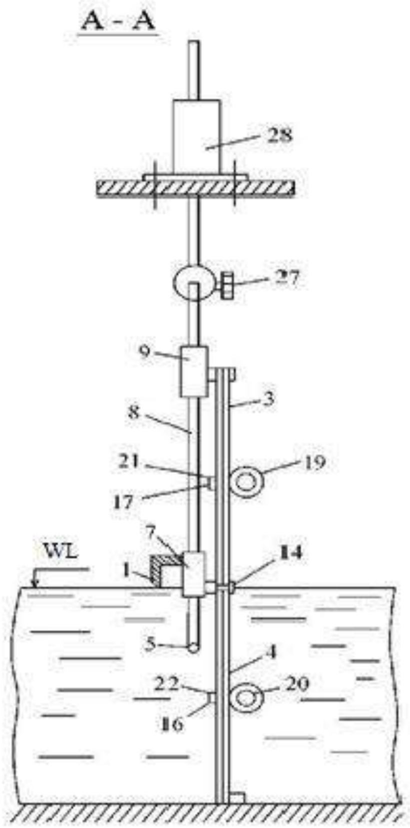

Figure 2. Device type from the incoming flow

On the lower part of the vertical diagonal rhombus 4, which is an extension rod 8, set Pitot tube 5 for measuring the mean dynamic pressure where the fluid level in the critical section is fixed dimensional needle 2 rigidly connected through the rod with measuring needle 1 is also connected to the signaler 6 wherein the needle tip is mounted flush with the upper horizontal diagonal of the rhombus 15 3, which by virtue of the mobility of rhombuses continuously and independently of the cross section will be located at a height of 3/2 h relative channel bottom. The entire installation is fixed on the bridge 26 and is moved horizontally by means of screws 27 and 28 coordinate mechanism. The critical depth is removed on a scale of 29.

Results and Discussion

For a channel of arbitrary shape in general form, it is solved by selection or graph analytical method, for the channel of the correct cross section, simple solutions are possible.

The well-known formulas are given for determining the critical depth for a channel of a regular section:

for a rectangular channel

$$h_{cr} = \sqrt[3]{\alpha \frac{q^2}{g}}, \tag{8}$$

where $q = \frac{Q}{b}$ – the specific consumption, i.e. flow per unit width of a rectangular channel.

for a trapezoidal channel, it is determined by the analytical method, proposed by Agroskin I.I., according to the formula

$$h_{cr.t.} = h_{cr} \frac{\sqrt[3]{1+2z_t}}{1+z_t}, \tag{9}$$

where $h_{cr} = \sqrt[3]{\alpha \frac{q^2}{g}}$ – the critical depth in a rectangular channel for a given flow rate (Q) and a width along the bottom (b); $z_т = mh_{кр.т}/b$ $z_t = mh_{cr.t.}/b$ – dimensionless ratio; $m = ctg\theta$ – slope coefficient of the trapezium.

The notation is introduced by $z_r = mh_{cr}/b$ for a rectangular channel and after some transformation, it is obtained from

$$z_r = \frac{z_t(1+z_t)}{\sqrt[3]{1+2z_t}}, \tag{10}$$

here $\frac{hcr.t}{h_{cr}} = \frac{z_t}{z_r}$.

Substituting different values of z_t, it can obtain from (10) the corresponding z_r and then the values of the ratio $h_{cr.t} = h_{cr}$.

for a triangular channel

$$h_{cr.tr} = \sqrt[5]{\frac{2\alpha}{g}\left(\frac{Q}{m}\right)^2}; \tag{11}$$

for a parabolic channel

$$h_{cr.par} = \sqrt[4]{\frac{27\alpha Q^2}{64gp}}, \tag{12}$$

where p – parabola parameter;

for a weir with a wide threshold, the critical depth of the flow is determined taking into account its curvature [20–22]

$$h_{cr.w} = \sqrt[3]{\frac{\alpha q^2}{g}} \cdot \sqrt[3]{1+\frac{ka}{\alpha}} = h_{cr}\sqrt[3]{1+\frac{ka}{\alpha}}, \tag{13}$$

where $\upsilon = \frac{1}{R_{av}}$ – the curvature of a trickle with dimension $[L]^{-1}$; $a = \upsilon h$ – the dimensionless curvature of the trickle; R_{av} – the value is calculated indirectly from the hydrodynamic pressure of the flow to the bottom; h – the depth of flow.

According to the dependencies shown above, the critical depth is determined analytically, and there is no direct determination of the critical section and the measurement of the critical depth using the device in any of the papers [21–25]. Direct measurement of the critical depth and the critical section in situ is not currently available.

There is described how the devise works and given an example of finding the critical depth. The device operates as follows.

Using 27 screws attached moves horizontally in the direction of flow. In the selected section using the screw 28 descends vertically setting up until the end of the needle 1 will not touch the surface of the liquid flow and not warning light at the first switch position. Then, the key signaling 6 is transferred to the second position and, if the warning light does not light up, the setting moves to the next position and the process is repeated as long as the warning light lights up in the second position of the key, which is fixed by contact dimensional needle 2 with the level of liquid in the tube Pitot 5. This will be the position of the critical section. On a scale with 29 divisions relieve the critical depth.

Essentially the process location of the critical section of flow is determined at equal velocity (dynamic) pressure of the fluid in millimeters of the column of fluid, such as millimeters of water column equal to half the depth of the liquid in the sectional view taken in the same units (millimeters). In other words, it must satisfy the relation

$$\frac{\rho\upsilon^2}{2} = \frac{\rho g h}{2}, \tag{14}$$

where $\frac{\rho\upsilon^2}{2}$ – speed pressure fluid in the flow; h – the depth of the flow in this section; ρ – density of the fluid; υ – velocity of liquid flow; g – acceleration of free fall.

If equality is not respected, the experiment was repeated in the other section to perform this equality, and in the case of compliance conclude according to the measured depth of the flow of critical value in this section, which is the critical section.

For example. Divide the flow - uneven. Rectangular tray at flow rates of 8.83 l/s, 13.37 l/s, 19.77 l/s. h_{cr} should be measured.

Consumption is 8.83 l/s. Installation is moved horizontally in the direction of flow until the first section by means of 27 screws. In the first section by means of screw 28 descends in the vertical installation position as long as one end of the needle 1 touches the liquid surface. Warning light switches in the first position of the key. Then, the key of signaling system translates to the second position - bulb does not light up. Installation is moved to the second section. The process is repeated. The warning light in the second position of key does not light up again. Move the installation to the third section. In this section the warning light at the second position of the key lights up, indicating the critical section. Measure the critical depth which is 5.22 cm and so on, the experiment is curried out when consumptions are 13.37 l/s, 19.77 l/s. The results of the experiments are given in the table.

Table 1. Measuring of critical depth

Tests	Section	Bottom mark	The level of fluid flow	The flow depth, cm	The warning light in the first key position	The warning light in the second switch position	Critical depth cm
1	2	3	4	5	6	7	8
1	1	14.21	19.86	5.65	Lights up	No lights	–
	2	14.00	19.40	5.40	–//–	–//–	–
	3	13.80	19.02	5.22	–//–	Lights up	5.22
2	1	14.02	21.34	7.32	Lights up	No lights	–
	2	13.80	20.82	7.02	–//–	–//–	–
	3	13.60	20.45	6.85	–//–	Lights up	6.85
3	1	13.80	23.12	9.32	Lights up	No lights	–
	2	13.49	22.50	9.01	–//–	–//–	–
	3	13.34	22.21	8.87	–//–	Lights up	8.87

Conclusions

1. Theoretical analysis of the critical state of the flow shows that in the critical state of the flow, the velocity head is equal to half the depth of the stream, i.e. half the critical depth.
2. In a rectangular cross section, where the condition $\frac{\rho\vartheta^2}{2} = \frac{\rho g h}{2}$ is observed, the measured flow depth corresponds to the critical value in this section, i.e. in the critical section.
3. The use of the device, based on the equality of the dynamic pressure in the critical flow cross section is half of its depth, allows you quite simply to find the critical cross-section of the fluid flow and measure the critical depth.
4. The device makes it possible to determine the critical section and critical depth flow by direct measurement in real conditions correspond to reality, no additional calculations, which increases the accuracy of determination of the critical depth and greatly reduces the time (if necessary measurement process is automated).

References

1. Lavrov N.P., Toropov M.K. Izmerenie raskhoda vody na golovnyh uchastkah bystrotechnyh kanalov [Measurement of water discharge at head sections of the fleeting canals]. *Meteorologiya i gidrologiya v Kyrgyzstane.* 2002. No. 2. Pp. 31–36. (rus)
2. Kosichenko N.V. Analiz izucheniya i utochneniya metodov svobodnogo rastekaniya potoka za beznapornymi vodopropusknymi otverstiyami [The analysis of studying and specification of methods of free spreading of a stream behind free-flow water throughput openings]. *Vestnik SGAU.* 2011. No. 9. Pp. 27–33. (rus)
3. Giancoli D.C. *Physics for Scientists & Engineers.* Third Edition. Prentice Hall. Upper Saddle River. New Jersey. 2000. 1024 p.
4. Liptak B. *Instrument Engineers' Handbook, Vol. 1: Process Measurement and Analysis.* CRC Press. 4 edition. 2003. 1920 p.
5. Biryukov B.V., Danilov M.A., Kivilis S.S. *Tochnyye izmereniya raskhoda zhidkostey* [Accurate measurement of liquid flow rate]. Moscow: Mashinostroyeniye. 1977. 144 p. (rus)
6. Kokhanenko N.V. Opredeleniye parametrov potoka na beskonechnosti, vdol' krayney linii toka i postoyannoy A [Determination of parameters of a stream on infinity, along the extreme line of current and permanent]. *Cherez innovatsii v nauke i obrazovanii k ekonomicheskomu rostu APK: materialy mezhdunar. nauch.– prakt. konf.* [Through innovations in science and education to the economic

Литература

1. Лавров Н.П., Торопов М.К. Измерение расхода воды на головных участках быстротечных каналов // Метеорология и гидрология в Кыргызстане. 2002. №2. С. 31–36
2. Косиченко Н.В. Анализ изучения и уточнения методов свободного растекания потока за безнапорными водопропускными отверстиями // Вестник СГАУ. 2011. № 9. С. 27–33.
3. Giancoli D.C. Physics for Scientists & Engineers. Third Edition. Prentice Hall. Upper Saddle River. New Jersey. 2000. 1024 p.
4. Liptak B. Instrument Engineers' Handbook, Vol. 1: Process Measurement and Analysis. CRC Press. 4 edition. 2003. 1920 p.
5. Бирюков Б.В., Данилов М.А., Кивилис С.С. Точные измерения расхода жидкостей. М.: Машиностроение, 1977.144 с.
6. Коханенко Н.В. Определение параметров потока на бесконечности, вдоль крайней линии тока и постоянной А // Через инновации в науке и образовании к экономическому росту АПК: материалы междунар. науч. – практ. конф. ДонГАУ: Персиановский. 2008. Т. 2. С. 198–200.
7. Коханенко Н.В., Баленко Е.Г., Ширяев В.В. Определение аналитической зависимости распределения глубин и скоростей вдоль продольной оси симметрии в задаче свободного растекания бурного потока // Изв. вузов. Сев.-Кавк. регион. Техн. науки. 2006. № 2. С. 14-16.

growth of the agro-industrial complex. Proceedings of international research and practical conference]. DonGAU. Persianovskiy. 2008. Vol. 2. Pp. 198–200. (rus)

7. Kokhanenko N.V., Balenko Ye.G., Shiryayev V.V. Opredeleniye analiticheskoy zavisimosti raspredeleniya glubin i skorostey vdol prodolnoy osi simmetrii v zadache svobodnogo rastekaniya burnogo potoka [Determination of the analytical dependence of the depth distribution and velocities along the longitudinal symmetry axis in the problem of free rapid flow]. *Izv. vuzov. Sev.Kavk. region. Tekhn. nauki.* 2006. No. 2. Pp. 14–16. (rus)
8. Kosichenko N.V., Mitsik M.F., Lemeshko M.A. Metod s ispolzovaniyem godografa skorosti primenitelno k raschetu parametrov burnogo dvukhmernogo potoka [Method using the velocity hodograph as applied to the parameter calculation of a turbulent two-dimensional flow]. *Matematicheskoye i kompyuternoye modelirovaniye yestestvennonauchnykh i sotsialnykh problem: sb. st. IV Mezhdunar. nauchn.tekhn. konf. molodykh spetsialistov, aspirantov i studentov* [Mathematical and computer modeling of natural and social problems: proceedings IV Intern. scientific-techn. conf. young specialists, post-graduate students and students]. Penza: Privolzhskiy Dom znaniy, 2010. Pp. 130–141. (rus)
9. Miller R.W. *Flow Measurement Engineering Handbook.* Second Edition. McGraw-Hill Publishing Compan.New York. NY. 1989.
10. Bobrovnikov G.N., Katkov A.G. *Metody izmereniya urovney* [Methods of level measurement]. Moscow. Mashinostroyeniye. 1977. 167 p. (rus)
11. Dedrick A.R., Clemmens A.J. Instrumentation for monitoring water levels. *Proc. Of Agri-Mation Conference and Exposition. ASAE.* Chicago. IL, 1986. Pp. 148–152.
12. Compton P.R., Kulin G. *A Guide to Methods and Standards for the Measurement of Water Flow.* Washington. National Bureau of Standards Special Publication 421. Institute for Basic Standards 1975. 97 p.
13. Grant D.M. *Open Channel Flow Measurement Handbook.* 1st edition, Lincoln. Instrument. Instrumentation Specialties Company. 1979.
14. Park J., Mackay S., Wright E. *Practical Data Communications for Instrumentation and Control.* IDC Technologies, 2003. 402 p.
15. Reynders D., Mackay S., Wright E. *Practical Industrial Data Communications. Best Practice Techniques.* IDC Technologies, 2005.
16. Bakshtanin A.M. *Gidravlicheskoye obosnovaniye metodov rascheta vodoboynykh kolodtsev s bokovym otvodom potoka* [Hydraulic study of the methods for the calculation of the stilling basin wells with a lateral diversion of flow]. PhD Thesis. Moscow. 2006. 154 p. (rus)
17. Kuphaldt T.R. *Lessons in Industrial Instrumentation* Version 0.2. 2008.
18. Andreyev A.Ye. Osobennosti upravleniya okolokriticheskimi potokami v nizhnikh byefakh nizkonapornykh vodopropusknykh sooruzheniy i otsenka yego effektivnosti [Management features of near-critical flows in the lower pools of low-head culverts and evaluation of its effectiveness]. *Gidravlika vodokhozyaystvennykh obyektov: Sb.nauchn.tr.:Trudy LPI* [Hydraulics of water management objects: Proceedings of LPI]. No. 424. Leningrad. 1983. Pp. 49–52. (rus)
19. Garanina Ye.B., Ponomarev N.K., Rabkova Ye.K. K voprosu o kinematicheskoy strukture otkrytykh potokov [To the question about the kinematic structure of open flows]. *Gidrotekhnicheskoye stroitelstvo.* 1995. No. 19. Pp. 30–33. (rus)
20. Gur'yev A.P., Khanov N.V., Yershov K.S. Vliyaniye planovogo rasshireniya vodosliva s gorizontal'noy vstavkoy na yego propusknuyu sposobnost' [Influence of planned expansion of a spillway with a horizontal insert on its bandwidth]. *Prirodoobustroystvo.* Moscow. 2010. No. 5.

8. Косиченко Н.В., Мицик М.Ф., Лемешко М.А. Метод с использованием годографа скорости применительно к расчету параметров бурного двухмерного потока // Математическое и компьютерное моделирование естественнонаучных и социальных проблем: сб. ст. IV Междунар. научн.-техн. конф. молодых специалистов, аспирантов и студентов. Пенза: Приволжский Дом знаний, 2010. С. 130–141.
9. Miller R.W. Flow Measurement Engineering Handbook. Second Edition. McGraw-Hill Publishing Compan.New York. NY. 1989.
10. Бобровников Г.Н., Катков А.Г. Методы измерения уровней. М: Машиностроение, 1977. 167 с.
11. Dedrick A.R., Clemmens A.J. Instrumentation for monitoring water levels // Proc. Of Agri-Mation Conference and Exposition. ASAE. Chicago. IL. 1986. Pp. 148–152.
12. Compton P.R., Kulin G. A Guide to Methods and Standards for the Measurement of Water Flow, Washington. National Bureau of Standards Special Publication 421. Institute for Basic Standards 1975. 97 p.
13. Grant D.M. Open Channel Flow Measurement Handbook. 1st edition, Lincoln. Instrument. Instrumentation Specialties Company. 1979.
14. Park J., Mackay S., Wright E. Practical Data Communications for Instrumentation and Control. IDC Technologies, 2003. 402 p.
15. Reynders D., Mackay S., Wright E. Practical Industrial Data Communications. Best Practice Techniques. IDC Technologies, 2005.
16. Бакштанин А.М. Гидравлическое обоснование методов расчета водобойных колодцев с боковым отводом потока: дис. канд. техн. наук. М., 2006. 154 с.
17. Kuphaldt T.R. Lessons in Industrial Instrumentation Version 0.2. 2008.
18. Андреев А.Е. Особенности управления околокритическими потоками в нижних бьефах низконапорных водопропускных сооружений и оценка его эффективности.// Гидравлика водохозяйственных объектов: Сб.научн.тр.: Труды ЛПИ № 424. Л., 1983. С. 49–52.
19. Гаранина Е.В., Пономарев Н.К., Рабкова Е.К. К вопросу о кинематической структуре открытых потоков // Гидротехническое строительство. 1995. № 19. С. 30–33.
20. Гурьев А.П., Ханов Н.В., Ершов К.С. Влияние планового расширения водослива с горизонтальной вставкой на его пропускную способность // Природообустройство. 2010. № 5. С. 42–46.
21. Гурьев А.П., Козлов В.Д., Ханов Н.В., Ершов К.С. Расчёт водосливов с переменной шириной пролёта в плане/ // Природообустройсво. 2010. № 3. С. 47–50.
22. Гурьев А.П., Хайруллин Р.А. Определение кинематических характеристик безнапорного потока в вертикально расположенных сопрягающих коленах // Природообустройсво. 2013. № 1. С. 42–50.
23. Ершов К.С. Формирование свободной поверхности потока на водосливе практического профиля криволинейного очертания с горизонтальной вставкой и непараллельными боковыми стенками // Природообустройсво. 2011. № 4. С. 51–54.
24. Бакштанин А.М. Теоретическое обоснование работы водобойного колодца с боковым отводом потока // Природообустройсво. Ч. III. «Гидротехническое строительство». 2008. № 5. С. 57–62.
25. Гурьев А.П. Совершенствование конструкции шахтного водосброса полигонального поперечного сечения // Сборник научных трудов «Известия ВНИИГ им. Б.Е.Веденеева». 2009. Т. 256. С. 35–45.

Pp. 42–46. (rus)

21. Guryev A.P., Kozlov V.D., Khanov N.V., Yershov K.S. Raschet vodoslivov s peremennoy shirinoy proleta v plane [Calculation of weirs with variable span width in a plan]. *Prirodoobustroysgvo.* Moscow. 2010. No.3. Pp. 47–50. (rus)
22. Gur'yev A.P., Khayrullin R.A. Opredeleniye kinematicheskikh kharakteristik beznapornogo potoka v vertikal'no raspolozhennykh sopryagayushchikh kolenakh [Definition of kinematic characteristics of a free-flow stream in vertically located interfacing knees]. *Prirodoobustroysgvo.* Moscow. 2013. No. 1. Pp. 42–50. (rus)
23. Yershov K.S. Formirovaniye svobodnoy poverkhnosti potoka na vodoslive prakticheskogo profilya krivolineynogo ochertaniya s gorizontal'noy vstavkoy i neparallel'nymi bokovymi stenkami [Formation of a free surface of a stream on a spillway of a practical profile of a curvilinear outline with a horizontal insert and nonparallel the side walls]. *Prirodoobustroysgvo.* Moscow. 2011. No. 4. Pp. 51–54. (rus)
24. Bakshtanin A.M. Teoreticheskoye obosnovaniye raboty vodoboynogo kolodtsa s bokovym otvodom potoka [Theoretical study of the stilling basin with side outlet flow. Nature conservation]. *Prirodoobustroysgvo.* Ch. III. «Gidrotekhnicheskoye stroitelstvo». 2008. No. 5. Pp. 57–62. (rus)
25. Gur'yev A.P. Sovershenstvovaniye konstruktsii shakhtnogo vodosbrosa poligonal'nogo poperechnogo secheniya [Improvement of the design of the spillway dug polygonal cross section]. *Sbornik nauchnykh trudov «Izvestiya VNIIG im. B.Ye.Vedeneyeva».* 2009. Vol. 256. Pp. 35–45. (rus)

Nurliza Yerzhanova,
+7(777)965-31-65; nurliza66@mail.ru

Zhassulanbay Mussin,
+7(726)242-55-40; musin_jasulan@mail.ru

Saparbek Dzholdasov,
+7(726)256-85-82; Arnur_68@mail.ru

Aliya Altynbekova,
+7(747)667-67-38; kleo-14@mail.ru

Нурлиза Киякбаевна Ержанова,
+7(777)965-31-65; эл. почта: nurliza66@mail.ru

Жасуланбай Аккаирович Мусин,
+7(726)242-55-40;
эл. почта: musin_jasulan@mail.ru

Сапарбек Куракбаевич Джолдасов,
+7(726)256-85-82; эл. почта: Arnur_68@mail.ru

Алия Досжанкызы Алтынбекова
+7(747)667-67-38; эл. почта: kleo-14@mail.ru

Ержанова Н.К., Мусин Ж.А., Джолдасов С.К., Алтынбекова А.Д. Устройство для нахождения критического сечения и критической глубины в открытых потоках // Инженерно-строительный журнал. 2017. № 8(76). С. 106–114.

doi: 10.18720/MCE.76.11

Dynamic interaction of high-speed trains with span structures and flexible support

Динамическое взаимодействие высокоскоростных поездов с пролетными строениями и гибкими опорами

V.N. Smirnov,
E.B. Shestakova,
S.V. Chizhov,
A.A. Antonyuk,
L.A. Lediaev,
I.A. Indeykin ,
Petersburg State Transport University,
St. Petersburg, Russia
E.S. Evtukov,
Saint-Petersburg State University of Architecture and Civil Engineering, St. Petersburg, Russia

Д-р техн. наук, заведующий кафедры В.Н. Смирнов,
канд. техн. наук, доцент Е.Б. Шестакова,
канд. техн. наук, доцент С.В. Чижов,
аспирант А.А. Антонюк,
д-р техн. наук, профессор А.П. Ледяев,
д-р техн. наук, заведующий кафедры А.В. Индейкин,
Петербургский государственный университет путей сообщения Императора Александра I, г. Санкт-Петербург, Россия
д-р техн. наук, профессор С.А. Евтюков,
Санкт-Петербургский государственный архитектурно- строительный университет, г. Санкт-Петербург, Россия

Key words: railway bridge; train; supports; high-speed railway mainline (HSRM)

Ключевые слова: железнодорожный мост; поезд; опоры; высокоскоростная железная магистраль (ВСМ)

Abstract. To ensure reliable and safe operation of the bridge structure throughout the life cycle, it is necessary to analyze and take into account many important factors, including the interaction of the main load-bearing structures. The presented work has new theoretical information, which gives the main provisions in the field of design of artificial structures for high-speed railroads. To analyze the system of a multi-span split bridge design using flexible intermediate supports of a flyover type, the Newton method (algorithm) is used. The basic data on the interaction of span structures and the design of flexible supports that are not taken into account in the design of facilities are not specified or regulated in the basic normative space, either by domestic JV standards or by foreign European EN standards, including national normative bases of the CIS countries. Harmonic analysis of the recording of the interaction of high-speed rolling stock and the joint operation of the main bridge structures of man-made structures is necessary for the design of high-speed railroads of transport infrastructure, especially in conditions of high-speed rolling stock. The article proposes a methodology for taking into account the interaction of the elements of the "bridge-train" system and determines the directions for further research to take into account the joint work and optimization of the basic designs of modern bridges and rolling stock in the region of high train speeds.

Аннотация. Для обеспечения надежной и безопасной работы мостового сооружения на протяжении всего жизненного цикла необходим анализ и учет многих важных факторов, в том числе и учет взаимодействия основных несущих конструкций. Представленная работа обладает новыми сведениями теоретического характера, дающими основные положения в области проектирования искусственных сооружений для скоростных железнодорожных магистралей. Для анализа системы многопролетной разрезной конструкции моста с применением гибких промежуточных опор эстакадного типа используется метод (алгоритм) Ньютона. Представлены основные данные о взаимодействии пролетных строений и конструкции гибких опор, которые не учитываются при проектировании сооружений, не оговариваются и не регламентированы в базовом нормативном пространстве, как отечественными нормами СП, так и зарубежными европейскими нормами EN, включая национальные нормативные базы стран СНГ. Гармонический анализ учета взаимодействия высокоскоростного подвижного состава и совместной работы основных мостовых конструкций искусственных сооружений необходим для проектирования скоростных железнодорожных магистралей транспортной инфраструктуры, особенно в условиях

Смирнов В.Н., Шестакова Е.Б., Чижов С.В., Антонюк А.А., Ледяев Л.А., Индейкин И.А., Евтюков Е.С. Динамическое взаимодействие высокоскоростных поездов с пролетными строениями и гибкими опорами // Инженерно-строительный журнал. 2017. № 8(76). С. 115–129.

высокоскоростного движения подвижного состава. В статье предложена методика учета взаимодействия элементов системы «мост-поезд» и определены направления дальнейших исследований для учета совместной работы и оптимизации основных конструкций современных мостов и подвижного состава в области высоких скоростей движения поездов.

Introduction

According to preliminary forecast, the total length of high-speed mainlines (HSRM) will reach 60 thousand kilometers until 2020 in the world. Nowadays, China possesses the densest and developed network of high-speed railway mainlines in the world, holds first place in the world – 40% of total length of HSRM, will hold this position until 2020 increasing the length till 30 thousand kilometers, and 38 thousand kilometers until 2025. As a rule, more than half of the total length HSRM consists of elevates, 48-80% tunnels and bridges.

The normative documents used in the design of bridges operating in the Russian Federation [1, 2] and the countries of the near and far abroad [2, 3] formulate only general basic requirements for the corresponding projected structure that is part of the railway network. The above normative documents do not take into account and do not reflect the effect of the interaction of high-speed rolling stock and basic structures of bridges (towers and span structures), these norms do not apply at all to the design of bridges intended for high-speed traffic – HSRM. The main drawback is that the regulatory framework is not updated for the design of high-speed railways.

In compliance with the program for creating national standards, leading project Institute Gyprostroymost (The largest organization of total bridge engineering design in Russian Federation), there was prepared first redaction of Project for set of rules “Artificial constructions of high-speed railway lines. The rules of projecting and building” [5, 6].

To develop project-specific design codes (PSDC) for designing and building the infrastructure of the Moscow to Kazan high-speed long-distance railway line in order to create an up-to-date regulatory document for designing bridges on high-speed long-distance railway lines [7, 8].

In the works dedicated to analysis of bridge construction works of HSRM, as a rule, the dynamical reaction of the bridge is not evaluated on longitudinal train action that is necessary for constructions with (flexible) supports, characterized for high-speed mainlines.

Dynamic interaction of train loading on bridges usually either brings to analysis of span fluctuations or is considered as a interaction of spans and trains, as in 60-70s years [9, 10]; 80-90s years [11,12]; and 2000s [13–15].

Method

Influence of solid characteristics support of various types of railway bridges while constructing “bridge-train” models is not practically taken into account.

With the development of high-speed railways, the dynamic behaviour of trains and bridges has been studied more thoroughly. However, it is difficult to find papers in the scientific, normative and technical literatures about the lateral response of high-speed trains travel over long viaducts with pier.

The dynamic interaction between high-speed train and bridge is studied by theoretical analysis and field experiment. The main purpose of this paper is to develop a simple-model moving wheel/rail contact element, so that the sticking, sliding, and separation modes of the wheel/rail contact can be appropriately simulated. The three-dimensional (3D) contact finite element analysis for a realistic wheel and rail was used to accurately model the wheel/rail contact stiffness [16].

A computational model of train-bridge system with 24 m-span PC box girders are simulated. The dynamic responses of the bridge such as dynamic deflections, lateral amplitudes, lateral and vertical accelerations, lateral pier amplitudes, and the vehicle responses such as derail factors, offload factors, wheel/rail forces and car-body accelerations are calculated [17, 18]. Experimental and theoretical studies have been performed to determine the dynamic behavior of bridges crossed by the Korean high-speed train (KHST) [19, 20].

In the article of Russian authors deals with peculiar features of dynamic interaction of high-speed train loading and beam superstructures of bridges on the basis of numerical experiment. It also presents dependence of the quan tity of dynamic influence of trains on bridges from the speed of their movement, dynamic characteristics of the superstructures (more than 10 basic types and their lengths from 2.55 m to

90 m), as well as the results of pilot studies of the operation of steel superstructures at 250 km/h speed of movement of the high-speed train “Sapsan” [21].

In the article of Spain authors influence of pier height on the response of train and bridge is also studied. Continuous bridges, straight and constant section deck viaducts with variable height and tapered piers are the structures which have been considered. The height of the tested viaduct ranges between 60 and 120 m [22–25].

To solve the problem of oscillations of a railway beam bridge in its plane, taking into account the work of the bridge, the following assumptions were made.

1. A multi-span bridge is viewed as a system with a finite number of degrees of freedom.

2. The bases of the supports are perfectly elastic (the movements of the foundation of the support and the reaction of the base are connected by a linear dependence).

3. The bridge cloth is modeled by an elastic bar fixed to the elastic at the ends of the structure and lying on the base, elastic in the longitudinal direction. The last assumption is based, first, on the fact that, with terminal fasteners and elastic gaskets, it is possible for the track to work elastically at relatively large longitudinal displacements of the rails, and secondly because the values of the experimental relative displacements of the rails on the bridges at longitudinal effects of trains are very small.

4. When simulating a temporary mobile longitudinal load, the latter is assumed to be a one-dimensional system with one degree of freedom, which simplifies the solution of the problem, making it possible to obtain reliable results.

5. Dynamic impact on the bridge along the track axis is realized with a change in the time of traction forces or braking of the train f_π. For example, the traction force of a locomotive can be expressed as

$$f_\Pi(t) = F_0(1 - e^{-t\gamma}); \tag{1.1}$$

and the intensity of the brake load

$$\tau(t) = \tau(1 - e^{-\delta t}). \tag{1.2}$$

Here F_0, τ – the maximum values of the relevant factors (for example, for the freight train $\tau = 0.1q$, where q – the uniformly distributed vertical train load), γ, δ – coefficients, t – time.

It is assumed that at the time of the longitudinal load on the structure the train is on the bridge, and the transmission of the horizontal longitudinal force in the case of split beam bridges is carried out through the fixed support parts of the beams and the path. Thus, between the rolling stock and the rail way of the bridge, a frictional coupling that varies in time is assumed. Between the beams of span structures and the supports in the places where the beams are supported on the movable bearing parts, friction bonds are also provided.

Under the assumed assumptions, the calculation scheme of, for example, the four-span bridge will have the form shown in Figure 1. In accordance with the design scheme, the bridge is an elastic system with elastic connections between track rails and span structures and with frictional connections in the moving support parts.

Equations of free vibrations of a bridge as a conservative system can be obtained by making Lagrange equations of the second kind, which have the form

$$\frac{d}{dt}\left(\frac{d\tau_w}{dq_j}\right) + \frac{d\pi_w}{dq_j} = 0; \tag{1.3}$$

where q_j – displacement in the direction of the j-th generalized coordinate;

π_w – potential energy of deformation of the bridge;

τ_w – kinetic energy of the structure oscillations.

To determine π_w, τ_w it is necessary to establish the dependence of the crossings of the sections of the track $u(x)$ from generalized coordinate’s q_j. Vertical displacements of the centers and longitudinal displacements of the ends of span beams, vertical and longitudinal displacements of the top of supports, as well as displacement along the axis of the path of points located in the middle part of each intermediate support are accepted as generalized coordinates.

We will determine the desired displacements of the points of the track as a function of the displacement of the top of the beams of the span structures. To compose the differential equation of motion of the elastic rod (on the elastic in the direction along the bridge base), which simulates the rail track on the bridge, consider the element of the rod with the stiffness EA_P of length dx. It can be seen from the figure that

$$dN = r(u - v)dx;$$

where

$$\frac{dN}{dx} = r\left[u(x) - v(x)\right]. \tag{1.4}$$

Here *r[u(x) - v(x)]* is the linear resistance of the track to the shear; *r* – coefficient of proportionality, characterizing the elastic properties of the path in the direction along the axis of the bridge (longitudinal modulus of elasticity of the under-rail base). Taking into account that, according to Hooke's law, the elementary displacement of a bar from a pair of rails with rigidity EA_P is determined by expression

$$du = \frac{Ndx}{EA_p};$$

$$\frac{du}{dx} = \frac{N}{EA_p}; \tag{1.5}$$

$$\frac{d^2u}{dx^2} = \frac{dN}{dx} \cdot \frac{1}{EA_p}. \tag{1.6}$$

Equating the expressions for *dN/dx*, obtained by (1.4) and (1.6), we obtain the required differential equation:

$$\frac{d^2u}{dx^2} = \frac{r}{EA_p}(u - v). \tag{1.7}$$

We represent the resulting equation in the following form

$$u^{//}(x) - \gamma^2 \cdot u(x) = -\gamma^2 \cdot v(x); \tag{1.8}$$

where, $\gamma^2 = \dfrac{r}{EA_p}$.

The boundary conditions for equation (1.7) are obtained by writing down the relations for the normal stresses at the ends of the rail track:

$$\sigma(0) = \frac{R \cdot u(0)}{A_p}; \qquad \sigma(L) = \frac{-R \cdot u(L)}{A_p}. \tag{1.9}$$

Representing the equation (1.9) in the form

$$\sigma(0) = E\frac{du}{dx_{x=0}}, \qquad \sigma(L) = E\frac{du}{dx_{x=L}}, \tag{1.10}$$

we find the following parameters

$$\frac{du}{dx}\Big|_{x=0} = \frac{R\cdot u(0)}{EA_p}; \quad \frac{du}{dx}\Big|_{x=L} = \frac{-R\cdot u(L)}{EA_p}. \tag{1.11}$$

The solution of equation (1.7) taking into account condition (1.11) has the form

$$u(\xi) = -\gamma^2 \cdot \int_0^L G(x,\xi)\cdot v(x)dx; \tag{1.12}$$

where $G(x,\xi)$ – the Green's function, taking into account the boundary conditions (1.11), has the form

$$G(x,\xi) = \begin{cases} A(\xi)\cdot U(x) \text{ if } 0\le x\le \xi \\ B(\xi)\cdot V(x) \text{ if } \xi \le x \le L \end{cases}. \tag{1.13}$$

Here

$$A(\xi) = a_1 \cdot sh\,\gamma\xi + a_2 \cdot ch\,\gamma\xi; \tag{1.14}$$

$$B(\xi) = b_1 \cdot sh\,\gamma\xi + b_2 \cdot ch\,\gamma\xi; \tag{1.14}$$

Where

$$a_1 = \frac{\gamma\cdot sh\gamma L + h\cdot ch\gamma L}{D};\ a_2 = -\frac{h\cdot sh\gamma L + \gamma\cdot ch\gamma L}{D}; \tag{1.15}$$

$h=R/(EA_p)$;

$b_1 = h/D$; $b_2 = \gamma/D$, $D = \gamma(\gamma^2+h^2)sh\gamma L + 2\gamma^2 h.ch\gamma L$;

$U(x) = hsh\,\gamma\, x + \gamma\, ch\,\gamma\, x$;

$V(x) = (h.ch\,\gamma\, L + \gamma .sh\,\gamma\, L)\, sh\,\gamma\, x - (h.sh\,\gamma\, L + \gamma\ ch\,\gamma\, L)ch\,\gamma\, x.$

As regards the second factor of the integrand in equation (1.12), which represents the displacement of the points of the top of the i-th span structure $v_i(x)$, it is determined on the basis of the following considerations. We will assume that the span structure is bent along the half-wave of the sinusoid, that is, the vertical displacement of the point of the *i*-th span structure with abscissa *x* is expressed by the dependence

$$y(x) = y_{max}\, sin\frac{\pi x}{l_i}.$$

It is clear that the longitudinal displacement of the lower belt of the movable end of the beam from its deflection y will amount to is $2\varphi e$. Moving the movable end of the beam along the upper fiber will be

$$2\varphi e - \varphi H_B = (\frac{2\pi}{l}e - \frac{\pi H_B}{l})y = \frac{2\pi}{l}(e - \frac{H_B}{2})y;$$

$$\varphi = \frac{\pi}{l}y.$$

where *e*, H_b – the eccentricity and height of the span of the span structure, respectively.

Longitudinal displacements of the points of the top of the beam of the *i*-th span during its deflection are given by

$$v_i^B(x) = (A + B\cos\frac{\pi}{l_i}x);$$

$$x\, E\,\{\,0,\, 1_i\,\}. \tag{1.16}$$

where:

$$A + B = \varphi_i H_{Bi};\tag{1.17}$$

$$A - B = 2\varphi_i e_i - \varphi_i H_{Bs}.$$

By solving the system of equations (1.17), we find

$$A = \varphi_i e_i, \qquad B = -\varphi_i e_i + \varphi_i H_{Bi}.\tag{1.18}$$

Substituting equation (1.18) into (1.16), we obtain the current displacement of the top of the i-th beam from its sagging along the sinusoid:

$$v_i^{*B}(x) = \frac{\pi}{l_i} y_i (e_i - (e_i - H_{Bi})\cos\frac{\pi}{l_i}x) = v_i^{B}(x) y_i.\tag{1.19}$$

Accordingly, the longitudinal displacement of the beam bottom is determined by the expression

$$v_i^{*H} = v_i^{*B}(x) - \varphi_i H_{Bi}\cos\frac{\pi}{l_i}x.\tag{1.20}$$

The expression for the total longitudinal displacement of the top of the i-th beam (taking into account its deformation both under the action of longitudinal forces and the compliance of the supports in the vertical direction) will have the form

$$v_i(x) = v_i^{B}(x)(y_i - (\frac{y_i^{right}}{2} + \frac{y_i^{left}}{2})) + y_i^{H} + \frac{y_i^{\Pi} - y_i^{H}}{l_i}x;\tag{1.21}$$

where y^{right}, y^{left} – vertical displacement of the right and left ends of the beam of the i-th span, respectively; y_i^{Π}, y_i^{H} – longitudinal displacement, respectively, of the movable and fixed end of the beam of the i-th span in the level of the centers of gravity of the section; y_i – vertical deflection of the middle of the beam of the i-th span.

Now, in the case of a multi-span bridge or viaduct (see, for example, Fig. 2), the solution of equation (1.7) can be written in the form

$$-\frac{1}{\gamma^2}u(\xi) = \int_0^{L_1} G(x,\xi)v_1(x)dx + \int_{L_1}^{L_2} G(x,\xi)v_2(x)dx + \int_{L_2}^{L_3} G(x,\xi)v_3(x)dx + \ldots \int_{L_{k-1}}^{L_k} G(x,\xi)v_k(x)dx\tag{1.22}$$

$(0 \le x \le k_1)$, k – number of spans.

Figure 1 shows

$$v_1(x) = v_1^B(x)\left(q_1 - \frac{q_3}{2}\right) + \frac{q_2}{l_1}x \qquad (0 \le x \le L_1);$$

$$v_2(x) = v_2^B(x)\left(q_6 - \frac{q_3 - q_8}{2}\right) + q_4 + \frac{q_7 - q_4}{l_2}x \qquad (L_1 \le x \le L_2);$$

$$v_3(x) = v_3^B(x)\left(q_{11} - \frac{q_{13} - q_{18}}{2}\right) + q_{9+}\frac{q_{12} - q_9}{l_3}x \qquad (L_2 \le x \le L_3).$$

$$v_i^B(x) = \frac{\pi}{l_i}\left[e_i - (e_i - H_{Hi})\cos\frac{\pi}{l_i}(x - L_{i-1})\right].\tag{1.23}$$

Considering, as an example, a four-span viaduct as a system with seventeen degrees of freedom (see Figure 1), we can, based on the above, write an expression for the displacement of the S point of the railroad track of the bridge in the form

$$-\frac{1}{\gamma^2}u(\xi s)=q_1\int_0^{L_1}G(x,\xi_S)v_1^B(x)dx+q_2\int_0^{L_1}G(x,\xi_S)\frac{x}{l_1}dx-$$
$$-\frac{1}{2}q_3\int_0^{L_1}G(x,\xi_S)v_1^B(x)dx-\frac{1}{2}q_3\int_{L_1}^{L_2}G(x,\xi_S)v_2^B(x)dx+$$
$$+q_4\int_{L_2}^{L_3}G(x,\xi_S)\left(1-\frac{x-L_1}{L_2}\right)dx+q_6\int_{L_1}^{L_2}G(x,\xi_S)v(x)dx+q_7\int_{L_1}^{L_2}G(x,\xi_S)\frac{x-L_1}{L_2}dx-$$
$$-\frac{1}{2}q_8\int_{L_1}^{L_2}G(x,\xi_S)v_2^B(x)dx-\frac{1}{2}q_8\int_{L_2}^{L3}G(x,\xi_S)v_3^B(x)dx+q_9\int_{L_2}^{L3}G(x,\xi_S)\left(1-\frac{x-L_2}{l_3}\right)dx+ \tag{1.24}$$
$$+q_{11}\int_{L_2}^{L3}G(x,\xi_S)v_3^B(x)dx+q_{12}\int_{L_2}^{L3}G(x,\xi_S)\frac{x-L_2}{l_3}dx-\frac{1}{2}q_{13}\int_{L_2}^{L3}G(x,\xi_S)v_3^B(x)dx-$$
$$-\frac{1}{2}q_{13}\int_{L3}^{L4}G(x,\xi_S)v_4^B(x)dx+q_{14}\int_{L_3}^{L4}G(x,\xi_S)\left(1-\frac{x-L_3}{l_4}\right)dx+$$
$$+q_{16}\int_{L_3}^{L4}G(x,\xi_S)v_4^B(x)dx+q_{17}\int_{L_3}^{L4}G(x,\xi_S)\frac{x-L_3}{l_3}dx.$$

where L_{1-1}, L_1 – the abscissa of the initial and final reference sections of the i-th span structure, respectively (Figure 1).

We divide the rail whip with a length equal to the length of the viaduct into m sections and we will consider its displacements at m + 1 boundary points of these sections (Figure 1). We introduce the vector {u} of displacements of the rail track at these points

$$\{u(\xi)\}=\{u(\xi_1=0)\ \ u(\xi_2)\ ...\ u(\xi_{m+1})\}=\{u_1\ u_2\ ...\ u_{m+1}\}; \tag{1.25}$$

then the equation (1.24) for a system with n degrees of freedom in the matrix form is written in the form

$$u=-\gamma^2\sum G(x,\xi)\,a_i(x)d(x)q \tag{1.26}$$

where $q = \{q_1\ q_2\ ...\ q_n\}$ – column of generalized coordinates of the system;

u – a column of offsets of track points within the structure;

$a_i(x)$ – i-th matrix-string, given for the calculation scheme in Figure 2.

Finally, the equation 1.24 for a system with n degrees of freedom in the matrix form is written in the form

$$u = \Phi\cdot q; \tag{1.27}$$

where Φ – the matrix of coefficients j determined from expression

$$\varphi_j^{(S)}=-\gamma^2\cdot\sum_{1=1}^{k}G(x,\xi_S)\cdot f_{ij}(x)dx \tag{1.28}$$

(S=1, 2 ..., m+1; i=1, 2 …, k; j=1, 2 …, n).

where $G(x,\xi_s)$ – function of the effect of the movements of the base on the displacements of the rails of the bridge web, resiliently fixed at the ends of the bridge (Green's function);

ξ_S – abscissa of the s-th point of the track;

f_{ij} – a function that determines the longitudinal displacement of the top of the i-th span when the qj of the system is moved;

m – number of sections of railroad lashing on the bridge;

k – number of spans;

n – number of degrees of freedom of the system.

The matrix Φ can be represented in the form

$$\Phi = \begin{bmatrix} \varphi_1^{(1)} & \varphi_2^{(1)} & .....\varphi_j^{(1)} & ....\varphi_n^{(1)} \\ \varphi_1^{(2)} & \varphi_2^{(2)} & .....\varphi_j^{(2)} & ....\varphi_n^{(2)} \\ \dots & \dots & \dots & \dots \\ \varphi_1^{(m+1)} & \varphi_2^{(m+1)} & .....\varphi_j^{(m+1)} & ......\varphi_{n1}^{(m+1)} \end{bmatrix} \quad (1.29)$$

The coefficients $\varphi_j^{(S)}$ for the example of the four-span bridge (Fig. 2) have the form

$$\varphi_1^{(1)} = -\gamma^2 \int_0^{L_1} G(x,\xi_1) v_1^B(x) dx;$$
$$\varphi_2^{(1)} = -\gamma^2 \int_0^{L_1} G(x,\xi_1) v_1^B(x) \frac{1}{l_1} x dx; \quad (1.30)$$

and so on in accordance with equation (1.24).

Returning to the Lagrange equations (1.36), we note that the potential strain energy of the railway bridge can be expressed by the formula

$$\pi_w = \pi_r + \pi_{ec} + \pi_b + \pi_{pier}; \quad (1.31)$$

where, π_r, π_{ec}, π_b, π_{pier} – the potential energy of deformation, respectively, of the rails of the track, elastic connections between rails and beams of span structures, beams of span structures, supports.

The kinetic energy of the oscillations of the bridge can be expressed by the dependence

$$\tau_w = \tau_b + \tau_{pier}; \quad (1.32)$$

where τ_b, τ_{pier} – kinetic energy of oscillations, respectively, of span structures and supports.

In the matrix form, expression (1.31) can be represented in the form

$$\pi_w=(1/2)q^T \Pi\, q; \quad (1.33)$$

where Π – matrix of coefficients under generalized coordinates q of the system.

The expression (1.33) can be written in the matrix form

$$\tau_w=(1/2)q^{*T} T\, q^*; \quad (1.34)$$

where T – matrix of coefficients for the vector q*.

Substituting the expressions (1.33) and (1.34) into the Lagrange equations (1.36), we obtain a system of ordinary differential equations of the form

$$Tq^{**}+\Pi q=0. \quad (1.35)$$

For $q = z \cdot sinwt$, instead of (1.35), we have

$$Tz - (1/w^2)\Pi z =0. \quad (1.36)$$

It is known that the shapes and the corresponding frequencies of free oscillations described by the system of equations (1.36) are obtained by analyzing the eigenvectors z and the corresponding frequencies of their own problem

$$(T - \lambda \Pi)z = 0; \quad (1.37)$$

where in $\lambda = 1/w^2$, w – frequency of free oscillations.

On the basis of the above methodology, it is possible to obtain a solution to the problem of free oscillations of a beam rail bridge structure in its plane, taking into account the influence of the track.

Analysis of forced oscillations of bridges with longitudinal effects of a train

In non-stationary (transient) modes of train traffic movement, characteristic for real operating conditions, there are forced oscillations of the structure in its plane.

The oscillations of the train-bridge system from the longitudinal effects of the train under the assumptions made earlier will be described by a system of nonlinear differential equations of the form

$$
\begin{gathered}
Mp^{**} + \frac{M_B g}{m} f_\Pi I^T\{ I \, sign\, [\,(v+p^*) - \Phi q^*]\} + (M-M_B)\cdot g\cdot f_\Pi \cdot sign(v+p^*)=0; \\
T^{-1}\, T\, q^{**} + T^{-1} B\, q^* + T^{-1}\Pi q + T^{-1} Q = T^{-1} w \frac{M_B g}{m} f_\Pi I^T\{ I \;\, sign\, [(v+p^*) - \Phi\, q^*]\}.
\end{gathered}
\tag{2.1}
$$

where q, q^*, q^{**} – the column of the generalized coordinates, velocities and accelerations of the bridge, respectively, as a system with n degrees of freedom (see Figure 1);

T, B, and P – the matrix of the coefficients of inertia, resistance and rigidity, respectively;

Q – column of generalized frictional forces in the movable supporting parts of span beams;

I – column of the form $\{0{,}7 \;\; 1 \;\; 1 \ldots 0{,}7\}\; m + 1$, reflecting the discreteness of the mobile load;

v – the speed of the moving load relative to the fixed path;

p – the longitudinal displacement of the moving load band caused by the bridge oscillations;

g – the acceleration due to gravity;

M, M_B – the mass of the temporary mobile load is respectively common and on the bridge;

f_Π – function describing the impact on the bridge on the side of the train longitudinal load (for example, braking);

Φ – the matrix characterizing the elasticity of the under-rail base along the axis of the path, formed from expression (1.29);

w – column of the form $\{1\;1\;1 \ldots 1\}_n$.

As a result of the calculation, the movements of the points of the structure along the directions of the generalized coordinates q are determined, the values of the forces acting on the structure and applied along the directions of the generalized coordinates are determined for any instant of time by the formula

$$s = \Pi\cdot q; \tag{2.2}$$

and the longitudinal forces at the $m + 1$ point of the track on the bridge according to formula

$$N_{m+1} = R_o\cdot \Phi\cdot q; \tag{2.3}$$

where

$$R_o = \frac{EA_p}{L/m}\, K. \tag{2.4}$$

where EA_P – the linear rigidity of rail track sections on a bridge of length L;

$$
K = \begin{bmatrix}
-1 & 1 & & & & \\
1 & -2 & 1 & & & \\
& \ldots\ldots & 1 & -2 & 1 & \\
& & & \ldots\ldots & & \\
& & & & 1 & -1
\end{bmatrix}_{m+1}
\tag{2.5}
$$

Thus, the proposed method of dynamic calculation of a beam rail bridge on the longitudinal effects of a train includes the following steps.

1. We construct the matrices *T, П*, *Ф* (according to 1.29),

2. A matrix of coefficients of resistance B is formed.

3. The columns of external loads are determined, as well as the generalized friction forces Q in the moving support parts.

4. The system of non-linear differential equations (2.1), which describes the oscillations of the interacting "train-bridge" system, is solved numerically, as a result of which the displacements along directions of the generalized coordinates qj are determined.

5. According to the expression (2.2), the forces acting on the structure along the directions of the generalized coordinates are determined for the longitudinal action of the rolling stock (braking or starting from the place).

6. According to the formula (2.3), axial dynamic forces are sought in the rails of the track on the bridge, which arise when braking or starting from the place of temporary loading.

7. The values of the dynamic coefficients to the longitudinal loads on the supports are determined by the formula $1 + \mu = \dfrac{q_j^{dyn}}{q_j^{st}}$.

Where q_j^{dyn}, q_j^{st} – the dynamic and static displacement of the support, respectively, in the direction of the corresponding generalized coordinate (static displacements q_j^{st} are obtained, for example, by assuming a coefficient $\gamma = 0$ for the function f_P determined by (2.1), which ensures a "quasistatic" effect of the train load).

According to the methodology outlined above, a dynamic calculation of a four-span railway bridge with reinforced concrete beams of span structures of 27.6 m in length, intermediate supports of 17.85 m in height and ballast rides (see Figure 1) is performed when the train brakes with a vertical load equal to 80 kN / m of the way. The module of longitudinal elasticity of the under-rail base was adopted *U* = 0 (the work of the rail track for longitudinal actions is not taken into account), as well as *U* = 4.5 MPa and *U* = 26 MPa (in the case of bridges with riding on wooden cross bars with crutches and riding on reinforced concrete sleepers with crushed stone ballast and separate fasteners).

The resistance of the path along the ends of the bridge was not taken into account (in Figure 1 *R* = 0). Integration of the system equations (2.1) was carried out numerically by the Runge-Kutta method using a special program. Some results of the calculations are given below. The role of the connections between the rail and the sub-rail base on the dynamic reaction of supports is evaluated. In Figure 2 is a graph of the dynamic movements of the top of the support along the axis of the path under the longitudinal action of the rolling stock. The vibrational nature of the motion of the support is seen, and in the absence of elastic bonds between the rails and beams of the span structures (*U* = 0), the support oscillations are realized at a frequency of about 3.5 Hertz (circular frequency *w* = 22.5 1 / s), and in the presence of such bonds (*U* = 26 MPa) the frequency increases to 9.7 Hertz. The values of the dynamic displacements of the support, calculated with the account of the work of the bridge cloth for longitudinal forces, are several times smaller than the corresponding displacements found by the traditional method - without taking into account the work of the path on the bridge (at *U* = 0).

In Fig. 2, it is shown that the largest values of the amplitude of the oscillations of the top of the support are observed in the step-like form of the longitudinal action function, when the resistivity of the train increases almost instantaneously (from $f_П$ = 0.01 to $f_П$ = 0.1), which is theoretically possible and sometimes adopted in dynamic calculations. However, the practical implementation of the $f_П$ transition from the minimum to the regulated by the norms is stretched in time, which is confirmed experimentally.

In order to reflect this circumstance in the computational model, the coefficient of friction $f_П$ in exponential calculations varied exponentially (in practice, changing discrete values of fn were determined at different instants of time).

Due to the gradual increase in the value of $f_П$ in time, the dynamic displacements of the top of the supports with longitudinal actions of the rolling stock are significantly reduced in comparison with the case of instantaneous changes in the values of $f_П$.

As can be seen from the figure, with static application of the braking force, the amount of displacement of the top of the support (without taking into account the path) was 1.2 mm. The dynamic nature of the process of interaction between the train and the bridge caused an increase in movement by 10-12% (Figure 1). This circumstance gives grounds to assume in the future (with the accumulation of a pachet and experimental material) the possibility of introducing corresponding dynamic coefficients to the longitudinal loads on the supports, the values of which depend on the dynamic properties of the system and the nature of the interaction of the temporary load and the structure. The recommendations of the norms for assigning the values of the dynamic coefficient for the supports appear to be poorly grounded.

Result and Discussion

While passing of train by bridges sprung crew experience the dynamic interaction specified with rebound deflection of spans and other irregularities on roads. Especially, adverse conditions are created while passing of rolling-stock by multi-span bridge with equal spans. Spans can experience in this case essential vertical fluctuations, especially in case of one-type crew. On these occasions dynamic processes, leaked into system “train-bridge”, in substantial measure may depend on solid, inertial and dissipative characteristic intermediate support which are projected for moderns elevates in the form of eased constructions of reduced rigidity. To define dynamic forces in supports as elements of the system is becoming more controversial task.

Calculating scheme of the system “bridge-train” is shown on the Figure 1. Elevate is presented in the view of system of discrete lumps, each of them has 2 levels of freedom. Every crew in case of this dynamic task also owns 2 levels of freedom, having an opportunity of vertical moving (bumping) and turning (galloping). Foundations are accepted absolutely hard.

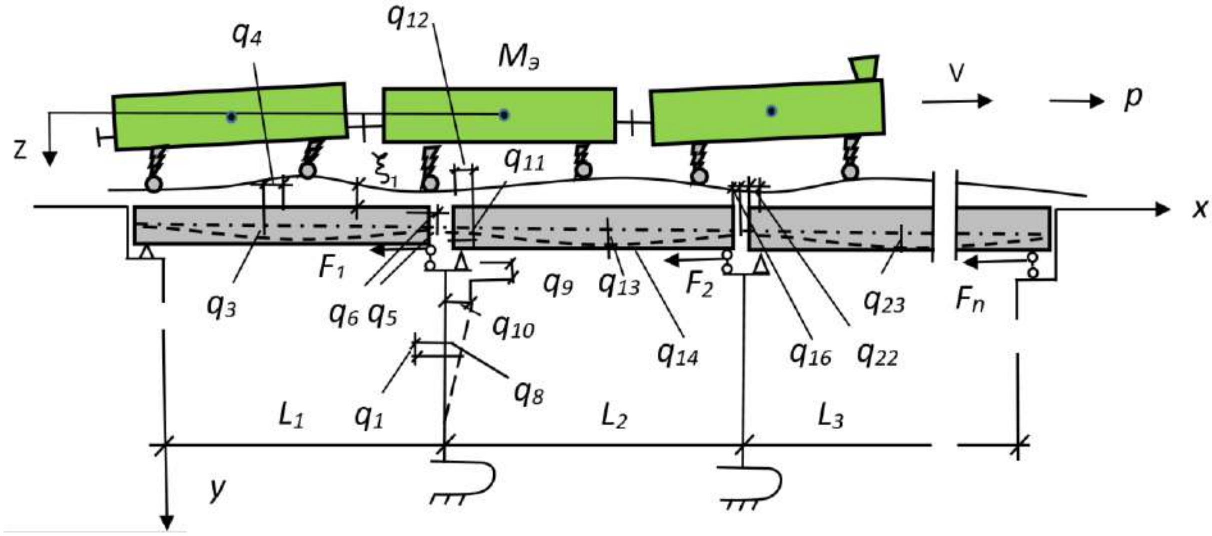

Figure 1. Calculating scheme of the system “bridge-train”

By accepted assumptions differential equations of system’s fluctuations “bridge-train” may be considered as:

$$\left\{\begin{aligned} q_3 = &-\left(M_3\ddot{q}_3+\beta_3\dot{q}_3\right)\left(\delta_{33}+\frac{\delta_{55}}{2}\right)-M_5\ddot{q}_5\delta_{35}-M_7\ddot{q}_7\delta_{37}-M_9\ddot{q}_9\delta_{39}-\\ &-\sum_1^m\frac{M\text{э}}{2}(\ddot{z}_1-g)\delta_{31(i)}-\sum_1^n\frac{M\text{э}}{2}(\ddot{z}_2-g)\delta_{32(i)}+S_1F_1 sign\left(S_1\dot{q}_3+\dot{q}_6-\dot{q}_{12}\right)\\ &\ldots\ldots\ldots\ldots\ldots\ldots\ldots\ldots\ldots\ldots\ldots\ldots\ldots\ldots\ldots\ldots\ldots\ldots\ldots\ldots\ldots\ldots \end{aligned}\right\}$$

$$q_{10} = -\left(M_{10}\ddot{q}_{10} + \beta_{10}\dot{q}_{10} \right)\delta_{10,10} - M_8\ddot{q}_8\delta_{10,8} - M_{12}\ddot{q}_{12}\delta_{10,12} - M_{14}\ddot{q}_{14}\delta_{10,14} -$$

$$M_{16}\ddot{q}_{16}\delta_{10,16} + F_1 sign\left(S_1\dot{q}_3 + \dot{q}_6 - \dot{q}_{12} \right) + F_2 sign\left(S_2\dot{q}_{13} + \dot{q}_{16} - \dot{q}_{22} \right)$$

Here Z_1 – absolute movement of body i-th crew on point 1 (first by passing in a run), defined by rigidity spring and irregularities of passage.

q_j – movement of j-th point of the bridge by directions of summing coordinations.

δ_{kl} – solitary movement of the point “k” of the bridge from force, given on point *l*;

$M_Э$ – mass i-th crew;

M_i –th discrete lump of construction;

F_1- friction force of movable bearing parts, put on i-th support, from permanent and temporary loading;

$$\delta_{31,i} = \delta_{33i}\sin \pi u_1 + \frac{\delta_{55}}{2}u_1 \qquad \left(u_1 = \frac{x_1}{l_1} = \frac{vt}{l_1} \right);$$

$$\delta_{32,i} = \delta_{33}\sin \pi u_2 + \frac{\delta_{55}}{2}u_2 \qquad \left(u2 = \frac{x2}{l2} = \frac{vt}{l2} \right);$$

v – speed of train’s running;

S – coefficient of passing from vertical movement in the middle of spans to longitudinal movement of construction on joint hinge’s level of support part.

The solution of nonlinear differential equation system provides to get the image of dynamic interaction elements of the system “bridge-train” on conditions of high-speed running and to reveal the influence of support parameters on construction’s dynamical work.

Conclusions

1. To ensure reliable and safe operation of a bridge structure under conditions of high-speed movement within the limits of long-term operation throughout the life cycle, it is necessary to take into account the joint operation of the rolling stock and the main load-bearing bridge structures: span structures and supports.
2. Harmonic analysis of the recording of the interaction of high-speed rolling stock and the joint operation of the main bridge structures of man-made structures is necessary from the point of view of optimal design of high-speed railroads of transport infrastructure, especially in conditions of high-speed rolling stock movement.
3. As a result of using the above methodology for calculating the interaction of the elements of the "bridge-train" system, the dependence of the dynamic characteristics of bridge structures on the inertial and rigid parameters of the supports is revealed, which makes it possible to design the supports of the flyover with the provision of their minimum possible massiveness (and, consequently, material capacity). This significantly reduces the material consumption of the support and the laboriousness of its erection and, as a consequence, increases the economy of the structure, ensuring operational reliability and durability.
4. The proposed method for the bridge design makes it possible to determine the stress-strain state of the elements of the structure (including the rail unshackled path) with longitudinal influences to avoid the appearance of unacceptable efforts in the rails and at the same time to ensure the design of non-material-intensive economical supports, avoiding excessive reserves of massive railroad bridge supports, and with optimal geometric parameters and ensuring the necessary operational parameters of the structure for reliability and durability awns. Thus, by varying the geometric parameters of the supports, the designer can evaluate the dynamic response under the influence of the railway train load under different initial data and choose the optimal design solution for the bridge structure taking into account economic indicators.

5. The results of the calculation procedure presented in this article can be used in the future for practical applications and for a deeper study:

– It is recommended to update the current standards taking into account the interaction of the elements of the "bridge-train" system and the criterion of the economics of the support of bridge structures;
– Development of recommendations and an album of technical solutions for new railroad bridge supports operated at high speeds of railway transport;
– It is recommended to apply this method in software tools Revit and SOFiSTiK or others to expand the basic kit for modeling the dynamic effects on a bridge structure from high-speed trains.

References

1. *Stroitelnyye pravila SP 35.13330.2011.* Mosty i truby [Construction rules SP 35.13330.2011. Bridges and pipes]. Moscow, 2011. (rus)
2. *Stroitelnyye normy i pravila SNiP 2.05.03-84*.* Mosty i truby [Construction Norms and Rules SNiP 2.05.03-84*. Bridges and pipes]. Gosstroy Rossii. Moscow, GUP TsPP, 1998. 214 p. (rus)
3. *EN 1990.* Eurocode: Basis of structural design. Annex A2 application for bridges. European Committee for Standardization. 2002.
4. *EN 13848-5.* Railway applications – track – track geometry quality – Part 5: geometric quality assessment. European Committee for Standardization. 2009.
5. *Ofitsialnyy sayt Proyektnogo Instituta Giprostroymost* [Official site of the Project Institute Giprostroymost.]. [Online]. URL: http://www.giprostroymost.ru/news/events/432-vsm. (date of reference: 31.05.2017). (rus)
6. Ivanchenko I.I. Dynamic interaction of bridges and high-speed trains. *Mechanics of Solids.* 2011. No. 46(455).
7. Benin A.V. Dyachenko L.K., Smirnov V.N. Osobennosti proyektirovaniya i stroitelstva mostov vysokoskorostnoy zheleznodorozhnoy magistrali «Moskva - Kazan» [Features of designing and building bridges of the high-speed railway "Moscow - Kazan"]. *Izvestiya Peterburgskogo universiteta putey soobshcheniya*. 2015. No. 4(45). Pp. 15–20. (rus)
8. Wu Y.S., Yang Y.B., Yau J.D. Three-dimensional analysis of train–rail–bridge interaction problems. *Vehicle Syst Dyn.* 2001. No. 36(1). Pp. 1–35.
9. Doronin F.A., Indeykin A.V. Issledovaniye dinamiki proletnykh stroyeniy mosta s uchetom yego sovmestnoy raboty s oporami [Investigation of the dynamics of span structures of a bridge, taking into account its joint work with supports]. *Byulleten rezultatov nauchnykh issledovaniy.* 2012. No. 4(3). Pp. 131–136. (rus)
10. Kozmin Yu.G. *Vzaimodeystviye balochnykh proletnykh stroyeniy zheleznodorozhnykh mostov i podvizhnogo sostava pri vysokikh skorostyakh dvizheniya* [Interaction of beam span structures of railway bridges and rolling stock at high speeds]. Doc. Thesis: 05.23.17. LIIZhT, 1973. 356 p. (rus)
11. Zhang N., Tian Y., Xia H. A train-bridge dynamic interaction analysis method and its experimental validation. *Engineering.* 2016. Vol. 2(4). Pp. 528–536.
12. Bondar N.G. Kozmin Yu.G., Roytburd Z.G. et al. *Vzaimodeystviye zheleznodorozhnykh mostov s podvizhnym sostavom* [Interaction of railway bridges with rolling stock]. Moscow: Transport, 1984. 272 p.
13. Fridkin V.M., Arkhipenko Yu.V. Iteratsionnyy metod resheniya uravneniy dvizheniya yedinoy dinamicheskoy sistemy «mostovoye sooruzheniye podvizhnoy sostav» [Iterative method for solving the equations of motion of a single dynamic system "bridge structure rolling stock"]. Nauchnyye trudy OAO TsNIIS. Moscow, OAO TsNIIS, 2006. № 230. Pp. 32–39. (rus)
14. Chen Z.W., Zhai W.M., Cai C.B., Sun Y. Safety threshold of high-speed railway pier settlement based on train-track-

Литература

1. Строительные правила СП 35.13330.2011. Мосты и трубы. Актуализированная редакция Строительные нормы и правила СНиП 2.05.03-84*. (утв. Приказом Минрегиона РФ от 28.12.2010 N 822). М., 2011.
2. Строительные нормы и правила СНиП 2.05.03-84*. Мосты и трубы/ Госстрой России. М., ГУП ЦПП, 1998. 214 с.
3. EN 1990. Eurocode: Basis of structural design. Annex A2 application for bridges. European Committee for Standardization; 2002.
4. EN 13848-5. Railway applications – track – track geometry quality – Part 5: geometric quality assessment. European Committee for Standardization; 2009.
5. Официальный сайт проектного Института Гипростроймост. [Электронный ресурс]. URL: http://www.giprostroymost.ru/news/events/432-vsm. (дата обращения: 31.05.2017)
6. Ivanchenko I.I. Dynamic interaction of bridges and high-speed trains // Mechanics of Solids. 2011. № 46(455).
7. Бенин А.В. Дьяченко Л.К., Смирнов В.Н. Особенности проектирования и строительства мостов высокоскоростной железнодорожной магистрали «Москва - Казань» // Известия Петербургского университета путей сообщения. 2015. № 4(45). С. 15–20.
8. Wu Y.S., Yang Y.B., Yau J.D. Three-dimensional analysis of train–rail–bridge interaction problems // Vehicle Syst Dyn. 2001. № 36(1). Pp. 1–35.
9. Доронин Ф.А., Индейкин А.В. Исследование динамики пролетных строений моста с учетом его совместной работы с опорами // Бюллетень результатов научных исследований. 2012. № 4(3). С. 131–136.
10. Козьмин Ю.Г. Взаимодействие балочных пролетных строений железнодорожных мостов и подвижного состава при высоких скоростях движения. Дис. докт. техн. наук: 05.23.17. ЛИИЖТ, 1973. 356 с.
11. Zhang N., Tian Y., Xia H. A train-bridge dynamic interaction analysis method and its experimental validation // Engineering. 2016. Vol. 2(4). Pp. 528–536.
12. Бондарь Н.Г., Козьмин Ю.Г., Ройтбурд З.Г. и др. Взаимодействие железнодорожных мостов с подвижным составом. М.: Транспорт, 1984. 272 с.
13. Фридкин В.М., Архипенко Ю.В. Итерационный метод решения уравнений движения единой динамической системы «мостовое сооружение подвижной состав» // Научные труды ОАО ЦНИИС. М.: ОАО ЦНИИС, 2006. № 230. С. 32–39.
14. Chen Z.W., Zhai W.M., Cai C.B., Sun Y. Safety threshold of high-speed railway pier settlement based on train-track-bridge dynamic interaction // Science China Technological Sciences. 2015. Vol. 58(2). Pp. 202–210.
15. Смирнов В.Н. Динамическая работа мостов высокоскоростных железнодорожных магистралей при продольных воздействиях поездной нагрузки: моногр. СПб. : Петербург. гос. ун-т путей сообщения, 2013. 65 с.
16. Ju S.H. A frictional contact finite element for wheel/rail

bridge dynamic interaction. *Science China Technological Sciences.* 2015. Vol. 58(2). Pp. 202–210.

15. Smirnov V.N. *Dinamicheskaya rabota mostov vysokoskorostnykh zheleznodorozhnykh magistraley pri prodolnykh vozdeystviyakh poyezdnoy nagruzki* [Dynamic work of bridges of high-speed railways with longitudinal forces of train load]. Saint-Petersburg: Peterburg. gos. un-t putey soobshcheniya, 2013. 65 p. (rus)
16. Ju S.H. A frictional contact finite element for wheel/rail dynamic simulations. *Nonlinear Dynamics.* 2016. No. 85(1). Pp. 365–374.
17. Xia H., Zhang N. Dynamic analysis of railway bridge under high-speed trains. *Computers and Structures.* 2005. No. 83(23-24). Pp. 1891–1901.
18. Claus H, Schiehlen W. Modeling and simulation of railway bogie structural vibrations. *Vehicle Syst Dyn.* 1997. No. 29(1). Pp. 538–552.
19. Kwark J.W., Choi E.S., Kim Y.J., Kim B.S., Kim S.I. Dynamic behavior of two-span continuous concrete bridges under moving high-speed train. *Computers and Structures.* 2004. No. 82(4-5). Pp. 463–474.
20. Iwnicki S.D. The Manchester benchmarks for rail vehicle simulation. *Vehicle Syst Dyn Suppl.* 1999. No. 31. Pp. 41–48.
21. Kondratov V.V. Osobennosti dinamicheskogo vzaimodeystviya vysokoskorostnykh poyezdov s proletnymi stroyeniyami mostov [Features of dynamic interaction of high-speed trains with span structures of bridges]. *Izvestiya Peterburgskogo universiteta putey soobshcheniya.* 2013. No. 3(36). Pp. 28–37. (rus)
22. Olmos J.M., Astiz M.A. Analysis of the lateral dynamic response of high pier viaducts under high-speed train travel. *Engineering Structures.* 2013. No. 56. Pp. 1384–1401.
23. Chen G., Zhai W.M. A new wheel/rail spatially dynamic coupling model and its verification. *Vehicle Syst Dyn.* 2004. No. 41. Pp. 301–322.
24. Vatin N.I., Havula J., Martikainen L., Sinelnikov A.S., Orlova A.V., Salamakhin S.V. Thin-walled cross-sections and their joints: tests and FEM-modelling. *Advanced Materials Research.* 2014. Vol. 945. Pp. 1211–1215.
25. Vatin N.I., Rybakov V.A. Raschet metallokonstruktsiy: sedmaya stepen svobody [Calculation of metal structures: the seventh degree of freedom]. *Stroyprofil.* 2007. No. 2. Pp. 60–63. (rus)
26. Grebowski K., Zielińska M. Dynamic analysis of historic railway bridges in Poland in the context of adjusting them to Pendolino trains. *International Journal of Applied Mechanics and Engineering.* 2015. No. 20(2). Pp. 283–297.
27. Xia F., Cole C., Wolfs P. The dynamic wheel–rail contact stresses for wagon on various tracks. *Proceeding of the 7th international conference on contact mechanics and wear of rail/wheel systems.* Brisbane, Australia, 2006. Pp. 33–39.
28. Iwnicki S.D. The Manchester benchmarks for rail vehicle simulation. *Vehicle Syst Dyn.* 1998. No. 30. Pp. 295–313.
29. Xia H., De Roeck G., Zhang N., Maeck J. Experimental analysis of a high-speed railway bridge under Thalys trains. *J Sound Vib.* 2003. No. 268. Pp. 103–113.
30. Lin X., Zhang L., Guo Q., Zhang Y. Dynamic finite element model updating of prestressed concrete continuous box-girder bridge. *Earthq Eng Eng Vib.* 2009. No. 8. Pp. 399–407.
31. Xia H., Zhang N., Guo W. Analysis of resonance mechanism and conditions of train–bridge system. *J Sound Vib.* 2006. No. 297. Pp. 810–822.
32. Xia H., Zhang N., De Roeck G. Dynamic analysis of high speed railway bridge under articulated trains. *Comput Struct*. 2003. No. 81. Pp. 2467–2478.

dynamic simulations // Nonlinear Dynamics. 2016. № 85(1). Pp. 365–374.

17. Xia H., Zhang N. Dynamic analysis of railway bridge under high-speed trains // Computers and Structures. 2005. № 83(23-24). Pp. 1891–1901.
18. Claus H, Schiehlen W. Modeling and simulation of railway bogie structural vibrations // Vehicle Syst Dyn. 1997. № 29(1). Pp. 538–552.
19. Kwark J.W., Choi E.S., Kim Y.J., Kim B.S., Kim S.I. Dynamic behavior of two-span continuous concrete bridges under moving high-speed train // Computers and Structures. 2004. № 82(4-5). Pp. 463–474.
20. Iwnicki S.D. The Manchester benchmarks for rail vehicle simulation // Vehicle Syst Dyn Suppl. 1999. № 31. Pp. 41–48.
21. Кондратов В.В. Особенности динамического взаимодействия высокоскоростных поездов с пролетными строениями мостов // Известия Петербургского университета путей сообщения. 2013. № 3(36). С. 28–37.
22. Olmos J.M., Astiz M.A. Analysis of the lateral dynamic response of high pier viaducts under high-speed train travel // Engineering Structures. 2013. № 56. Pp. 1384–1401.
23. Chen G, Zhai W.M. A new wheel/rail spatially dynamic coupling model and its verification // Vehicle Syst Dyn. 2004. № 41. Pp. 301–322.
24. Vatin N.I., Havula J., Martikainen L., Sinelnikov A.S., Orlova A.V., Salamakhin S.V. Thin-walled cross-sections and their joints: tests and FEM-modelling // Advanced Materials Research. 2014. Vol. 945. Pp. 1211–1215.
25. Ватин Н.И., Рыбаков В.А. Расчет металлоконструкций: седьмая степень свободы // Стройпрофиль. 2007. № 2. С. 60–63.
26. Grebowski K., Zielińska M. Dynamic analysis of historic railway bridges in Poland in the context of adjusting them to Pendolino trains // International Journal of Applied Mechanics and Engineering. 2015. № 20(2). Pp. 283–297.
27. Xia F., Cole C., Wolfs P. The dynamic wheel–rail contact stresses for wagon on various tracks // Proceeding of the 7th international conference on contact mechanics and wear of rail/wheel systems. Brisbane, Australia, 2006. Pp. 33–39.
28. Iwnicki S.D. The Manchester benchmarks for rail vehicle simulation // Vehicle Syst Dyn. 1998. № 30. Pp. 295–313.
29. Xia H., De Roeck G., Zhang N., Maeck J. Experimental analysis of a high-speed railway bridge under Thalys trains // J Sound Vib. 2003. № 268. Pp. 103–113.
30. Lin X., Zhang L., Guo Q., Zhang Y. Dynamic finite element model updating of prestressed concrete continuous box-girder bridge // Earthq Eng Eng Vib. 2009. № 8. Pp. 399–407.
31. Xia H., Zhang N., Guo W. Analysis of resonance mechanism and conditions of train–bridge system // J Sound Vib. 2006. № 297. Pp. 810–822.
32. Xia H., Zhang N., De Roeck G. Dynamic analysis of high speed railway bridge under articulated trains // Comput Struct. 2003. № 81. Pp. 2467–2478.

Smirnov V.N., Shestakova E.B., Chizhov S.V., Antonyuk A.A., Lediaev L.A., Indeykin I.A., Evtukov E.S. Dynamic interaction of high-speed trains with span structures and flexible support. *Magazine of Civil Engineering*. 2017. No. 8. Pp. 115–129. doi: 10.18720/MCE.76.11.

Vladimir Smirnov,
+7(812)572-61-19; svn193921@rambler.ru

Ekaterina Shestakova,
+7(921)094-51-06; ekaterinamost6@gmail.com

Sergei Chizhov,
+7(921)793-53-21; sergchizh@yandex.ru

Anatoly Antonyuk,
+7(999)025-18-33; aaa.12.03.1992@mail.ru

Alexander Lediaev,
+7(812)457-86-29; Tunnels@pgups.ru

Andrey Indeykin,
+7(812)457-82-49; andrey.indeykin@mail.ru

Sergey Evtukov,
+7(911)258-85-55; s.a.evt@mail.ru

Владимир Николаевич Смирнов,
+7(812)572-61-19;
эл. почта: svn193921@rambler.ru

Екатерина Борисовна Шестакова,
+7(921)094-51-06;
эл. почта: ekaterinamost6@gmail.com

Сергей Владимирович Чижов,
+7(921)793-53-21;
эл. почта: sergchizh@yandex.ru

Анатолий Анатольевич Антонюк,
+7(999)025-18-33;
эл. почта: aaa.12.03.1992@mail.ru

Александр Петрович Ледяев,
+7(812)457-86-29; эл. почта: Tunnels@pgups.ru

Андрей Викторович Индейкин,
+7(812)457-82-49;
эл. почта: andrey.indeykin@mail.ru

Сергей Аркадьевич Евтюков,
+7(911)258-85-55; эл. почта: s.a.evt@mail.ru

doi: 10.18720/MCE.76.12

Normal stresses of frost heaving as function of excess moisture

Нормальные напряжения морозного пучения как функция избыточной влажности

O.V. Tretiakova,
Perm National Research Polytechnic University, Perm, Russia

Аспирант О.В. Третьякова,
Пермский национальный исследовательский политехнический университет, г. Пермь, Россия

Key words: frost heave; water sucking up; normal stress; soil interstices; soil interstitial volume; ice-cement; disjoining action of water films

Ключевые слова: морозное пучение; миграция воды из талой зоны; нормальное напряжение; поры грунта; свободное поровое пространство; замерзшая поровая вода; расклинивающее действие водных пленок

Abstract. Tangential and normal stresses are arises foundation area from the frost heave process. Currently known is the analysis of the tangential stresses based on adfreezing of the frozen soil to the lateral surface of foundation. However, the differences in values of normal stresses may be due to the fact that no single approach to normal stress evaluation has been developed yet. The purpose of our research is to work out the analysis method of the frost heave normal stresses. The stresses appear perpendicular to the surfaces of structures not allowing increase in the soil volume when cooled and frozen. Based on the author's research and other investigators' experience, analytical dependences for normal stresses of soil frost heaving were obtained. The stresses were calculated as a function of excess moisture, which volume exceeds the soil interstitial volume under freezing. The results obtained took into account such factors causing heaving process as ice formation during water freezing, accumulation of ice resulting from sucking up water and influence of unfrozen water. The proposed formulas allow for calculation of stresses in any kind soil.

Аннотация. При морозном пучении грунта, вблизи фундаментов развиваются касательные и нормальные напряжения. В настоящее время известен метод расчета касательных напряжений, основанный на определении сил смерзания грунта с боковыми поверхностями фундаментов. Однако значения нормальных напряжений морозного пучения в различных исследованиях имею большой разброс. Это говорит об отсутствии единого подхода к их расчету. Целью данной работы является разработка метода расчета нормальных напряжений морозного пучения. Последние возникают и действуют по нормали к поверхностям конструкций, которые ограничивают увеличение грунтов в объеме при охлаждении и промерзании. На основании исследований автора и опыта существующих работ получены аналитические зависимости для нормальных напряжений морозного пучения грунта в открытой системе. Значения напряжений вычислены как функция избыточной влажности, превышающей свободный объем пор грунта при промерзании. В полученных зависимостях учтены факторы, обуславливающие процесс пучения: льдовыделение при замерзании свободной поровой воды, влияние миграции влаги. Предложенные выражения позволяют выполнять расчет нормальных напряжений пучения для любого вида грунта.

Introduction

The seasonal decrease in temperature causes soil freezing leading to its volume increase. Uniform volume increase in a vast homogeneous bed does not usually result in occurrence of forces. However, any obstacle to volume increase can cause significant normal stress resulting in negative impact on embedded structures and foundations, which, in its turn, leads to heaving, deformation and cracks of structures. It has been studied by many authors [1–4]. Unbalanced loading of structures can cause horizontal shear and building tilt.

To prevent these negative effects, it is necessary to design structures capable of enduring the frost heaving stress based on the calculation [5–8] and modeling [9–12] or the frost heave stress must be partially or completely neutralized [13–15]. Proper evaluation of the frost heave stress can help solve the problem, which is possible after its detailed study. In Russia, N.A. Tsytovich gave basic theory of frost heave [16]. This research was carried out by many other authors. J.-M. Konrad [17, 18], R.L Harlan [19], S.S.L. Peppin, R.W. Style [20] studied physics of frost heave. R.L. Michalowski [21] and Y. Zhang [22, 23] made some frost heave theoretical models.

The components of the frost heave process, being tangential and normal forces, are of different value and direction. V.S. Sazhin [24], V.I. Puskov [25], R.Sh. Abzhalimov [26] described mechanism of this process. This study is concerned with frost heave normal stresses.

The normal stresses of frost heaving are perpendicular to limiting surface, that is, lateral sides of foundations, which resist the increase in volume. Normal stresses acting on foundation bed occasion vertical uplift of foundation. Normal stresses acting on lateral surface causes the tangential forces.

Existing methods of studying the normal stresses of soil frost heaving comprise those used under laboratory conditions (in a closed and open system) [27–31] and under natural conditions (in open system) [32–36]. In a closed system normal stress values are determined by the pressure ice crystals under constrained water freezing and depend on the moisture properties of soil freezing. They may be significant and do not reflect the actual soil behaviour under natural freezing. When designing embedded structures, the stress-strain-state of the freezing soil in an open system is of great importance. The purpose of this study was to give a method of normal stresses under natural conditions in open system. The objectives were to study components of heaving stress in the open system, to determine mechanism the heaving normal stress and to develop a formula of the stress.

Methods

The open system is a soil body freezing under natural conditions. These conditions are formed on the experimental area, a construction site or in the soil body next to embedded structures built before. The open system is characterized by water sucking up from adjacent soil layers. In addition, this system is exposed to the influence of the stress-strain state of the adjacent layers subject to the shrinkage or increase in volume. In most cases, water sucking up in the unfrozen zone causes soil shrinkage in adjacent unfrozen layers.

Therefore, in the open system the normal heaving forces are caused by the pressure of ice-cement, influence of ice created by sucked up water, disjoining action of unfrozen water films and shrinkage of adjacent soil layers. In addition to soil properties, the values of normal heaving forces in the open system depend on the hydraulic conductivity of soil, compressibility of the underlying layers, structural rigidity and sensing forces of frost heaving.

Schematically heaving normal stress for the open system is shown in Figure 1. As can be seen in the figure, heaving stress in the open system consists of the following components,

- volumetric heaving stresses caused by accumulation of ice-cement resulting from crystallization of interstitial water;
- heaving stresses caused by influence of water sucking up due to
  a) crystallization of free capillary water,
  b) crystallization of bound water,
  c) disjoining action of unfrozen water films;
- shrinkage stress.

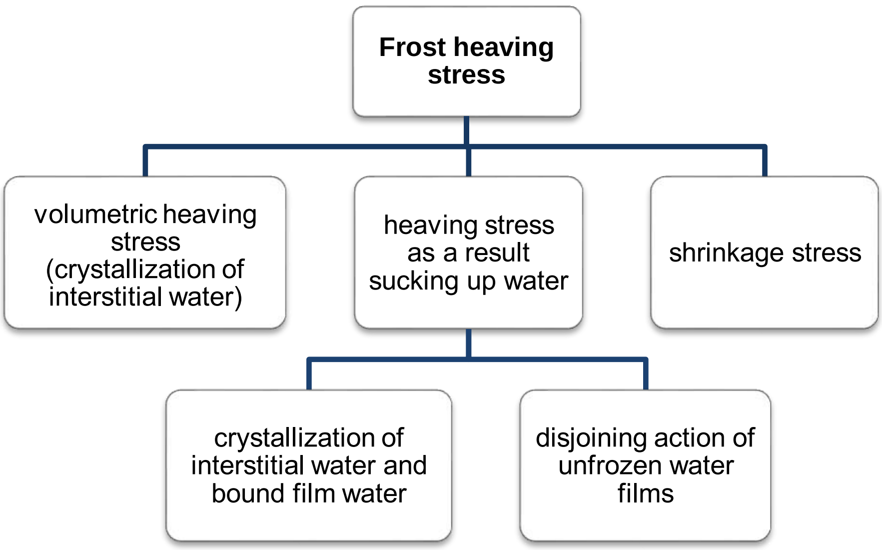

Figure 1. Components of heaving stress in the open system

Tretiakova O.V. Normal stresses of frost heaving as function of excess moisture. *Magazine of Civil Engineering*. 2017. No. 8. Pp. 130–139. doi: 10.18720/MCE.76.12.

The ice and unfrozen water whose overall amount is less than the soil interstices volume does not usually affect the walls of interstices and cause internal stresses in the soil. Accordingly there is no increase in the soil volume. Frost heave occurs if the amount of the frozen and unfrozen water exceeds the volume of the soil interstices. Unfrozen film water fed by sucking up, has a disjoining action on the freezing soil and is similar to swelling. In addition, “excess ice” acts as a “wedge” between the ice in the interstice volume and the walls of interstices. This results in stress in the soil causing displacement of the soil interstices, which in its turn, leads to increase in the soil volume. The normal stresses of frost heaving are developed due to foundations constraining action on the soil volume increase. Thus frost heaving stresses are, on one hand, the function of the soil porosity, on the other hand, the function of “excess moisture” resulting in the formation of “excess ice”, which the normal stresses reflect. “Excess ice” is the amount of ice exceeding the free interstice volume not filled by frozen and unfrozen film water. The normal stress value is also characterized by the rigidity of the foundation structure.

Condition under which soil heaving pressure occurs can be presented as follows

$$v_{ice} + v_{unfrouz.\,water} > v_{pore} \,, \tag{1}$$

where v_{ice}, $v_{unfroz.water}$ and v_{pore} are the ice-cement volume, volume of unfrozen film water and soil interstices, respectively.

Based on this, the expression for normal heaving stresses in the open system can be written as

$$\sigma_{heave} = \left(\sigma_{excess\ \ ice} + \sigma_{unfrouz.\,water} - \sigma_{shrincage.} \right) \cdot k_{an.} \,, \tag{2}$$

where “$\sigma_{excess\ \ ice}$, $\sigma_{uvfroz.\ water}$” are the ice pressure and unfrozen water pressure due to water sucking up;

“$\sigma_{shrincage}$” is an unloading effect resulting from the soil shrinkage in the adjacent layers due to water sucking up;

“$k_{an.}$” is the anisotropy factor taking into account the direction of heaving forces.

To define the pressure of “excess ice”, we considered the distribution of water phase states in frozen soil (Figure 2). The total actual ice pressure results from two values, i.e.

a) ice-cement pressure together with 9 percent volumetric gain;

b) ice pressure caused by capillary and bound film water freezing due to water sucking up.

The (b) parameter (ice pressure) is a variable.

The $\sigma_{excess\ \ ice}$ (site 4b in Figure 2) reflects the difference between ice pressure due to total water sucked up (site 4a and 4b in Figure 2) and that of water sucked up in the interstitial volume (site 4a in Figure 2). The interstitial volume is the space free of ice-cement (site1 and 2 in Figure 2) and unfrozen film water (site 3 in Figure 2).

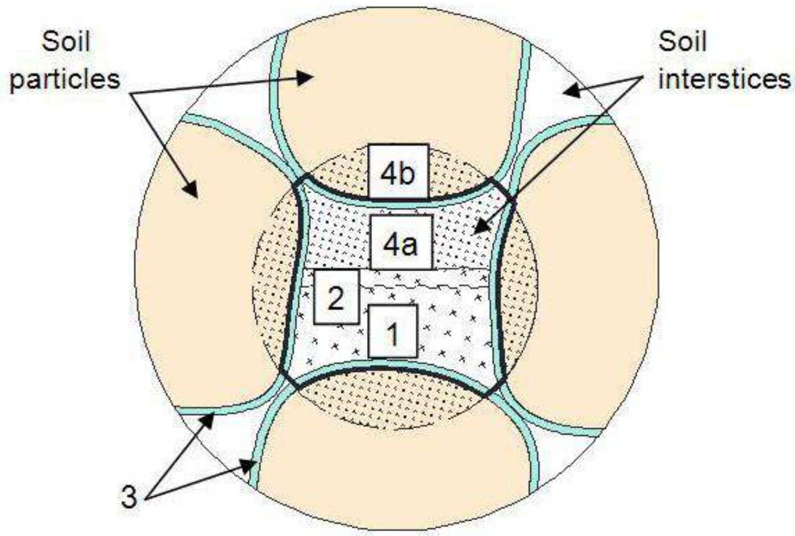

Figure 2. Water phase states in frozen soil
1 – ice-cement; 2 – 9 percent volumetric gain of interstitial water; 3 – unfrozen film water
4a and 4b – frozen sucked up water together with 9 percent volumetric gain (4a – in a soil interstices volume, 4b – in excess of soil interstices volume - "excess ice")

We deduced the expression of "excess ice pressure"

$$\sigma_{excess\ \ ice} = \sigma_{ice}^{migr.} - \sigma_{ice.}^{migr.} \cdot e \cdot (1 - w_w - 1.09 \cdot w)\,, \tag{3}$$

where "*w*" is the natural moisture of soil and "w_w" is the water content due to unfrozen water, *e* – porosity ratio.

Upon rearrangement, expression (3) is as follows

$$\sigma_{excess\ \ ice} = \sigma_{ice}^{migr} \cdot [1 - e \cdot (1 - w_w - 1.09 \cdot w)]\,, \tag{4}$$

Stresses due to the "excess ice pressure" in soil were expressed in terms of the Hook's law

$$\sigma_{ice}^{migr.} = h_{heave} \frac{E_M}{z}\,, \tag{5}$$

where "h_{heave}" is the displacement of soil under frost heave (cm), "E_M" is the deformation modulus of frozen soil (кN/cm^2) [37, 38], "*z*" is the depth of soil freezing vertically, soil thickness horizontally (cm).

Substituting the expression (5) in the expression (4), we obtained the formula for excess ice pressure

$$\sigma_{excess\ \ ice} = h_{heave} \cdot \frac{E_M}{z} \cdot [1 - e \cdot (1 - w_w - 1.09 \cdot w)]\,, \tag{6}$$

Using the A.L. Nevzorov's formula [39], we expressed the displacement of soil under frost heave resulting from water sucking up as follows

$$h_{heave} = 1.09 \cdot SP \cdot \tau \cdot grad\ t\,, \tag{7}$$

where "*SP*" is the segregation soil potential (cm^2/hour· Celsius degree), "*t*" is the frost heaving time (hour) and "*grad t*" is the temperature gradient (Celsius degree/cm).

The expression (7) was substituted into the (6). By combining (6) and (7), we obtained the equation (8). The formula for excess ice pressure taking into account soil properties and frost soil thickness without regard to shrinkage and unfrozen water was transformed into

$$\sigma_{excess\ ice} = 1.09 \cdot SP \cdot \tau \cdot grad\ t \cdot \frac{E_M}{z} \cdot \left[1 - e \cdot \left(1 - w_w - 1.09 \cdot w\right)\right] \qquad (8)$$

The value of frost heave normal stresses equals the ‘excess ice’ pressure that results from «excess moisture» exceeding soil interstitial volume under freezing. We neglected the small pressure of unfrozen film water sucked up in frozen soil. The heave stress expression (2) was rewritten without regard to shrinkage and unfrozen film water as follows:

$$\sigma_{heave} = \sigma_{excess\ ice} \cdot k_{an}. \qquad (9)$$

Then, the expression (8) was substituted into the expression (9). Gravity water content was conversed to the volumetric water content. As a result the formula of normal stress as the function of moisture that resulted in formation of “excess ice” was obtained.

$$\sigma_{heave} = 1.09 \cdot SP \cdot \tau \cdot grad\ t \cdot \frac{E_M}{z} \cdot \left[1 - e \cdot \left(1 - w_w \cdot \frac{\rho_d}{\rho_w} - 1.09 \cdot w \cdot \frac{\rho_d}{\rho_w}\right)\right] \cdot k_{an}, \qquad (10)$$

where “ ρ_d / ρ_w” *is the* gravity water content to volumetric water content conversion factor.

The “excess ice” reflects the difference between ice pressure due to total water sucked up and that of water sucked up in the interstitial volume.

The formula of normal stress as the function of excess ice under total moisture capacity was written as

$$\sigma_{heave} = 1.09 \cdot SP \cdot \tau \cdot grad\ t \cdot \frac{E_M}{z} \cdot \frac{w_{sat} - w_w}{n \cdot \left(1 - w_w\right)} \cdot k_{an}, \qquad (11)$$

where “w_{sat}” – total moisture capacity, n – soil porosity.

Results

Table 1. The normal stresses calculated by formula

№ formula	Evaluation	σ_{heave} кN/m^2
10	$\sigma_{heave} = 1.09 \cdot SP \cdot \tau \cdot grad\ t \cdot \frac{E_M}{z} \cdot \left[1 - e \cdot \left(1 - w_w \cdot \frac{\rho_d}{\rho_w} - 1.09 \cdot w \cdot \frac{\rho_d}{\rho_w}\right)\right] \cdot k_{an}$	134
11	$\sigma_{heave} = 1.09 \cdot SP \cdot \tau \cdot grad\ t \cdot \frac{E_M}{z} \cdot \frac{w_{sat} - w_w}{n \cdot \left(1 - w_w\right)} \cdot k_{an}$	165

Table 1 displays calculation of frost heaving stress in clay by formula (10) and (11). The normal stresses of frost heaving in the open system were calculated as a function of “excess moisture” exceeding the free soil interstitial volume under freezing.

Table 2. The comparison of stresses calculated by formula to Guidance on design of substructures and foundations on heaving soil (1979)

	Methods	Thickness of frozen layer under the foundation base or on the lateral surface of foundation, *m*	Direction of frost heave normal stress	The frost heave normal stress, *kH/m^2*
The research	Formula evaluation	1.0	Horizontal lateral	134 – 165
Guidance on designing of substructures and foundations on heaving soil (1979)	Tabular date	1.0	Vertical	100 – 600

Table 3. The comparison of stresses calculated by formula to other authors' result

	Methods	Foundation depth, m	Thickness of frozen layer under the foundation base or on the lateral surface of foundation, m	Temperature of soil	Rate of heave mm/day	Direction of frost heave normal stress	The frost heave normal stress, kH/m^2
This research (2016)	Formula evaluation	1.0	1.0	-4.0	1.7	Horizontal	134-165
A.E. Fedosov (1935)	Laboratory test					Vertical and horizontal	150-180
N.N. Morareskul, N.A. Tsytovich (1950)	Laboratory test					Vertical and horizontal	500-800
B.I. Dalmatov (1954)	Field test	0.9 – 1				Horizontal	30 – 35
		1.45 – 1.72					64 – 66
V O. Orlov (1958) (frost zone out of contact with permafrost embedding on 4,5m)	Field test	1.09	0.18	–0.9	0.95	Vertical	160
			0.33	–1.4	1.36		510
			0.41	–2.4	1.35		950
			0.51	–4.4	1.22		3100
			0.6	–4.7	1.12		3800
			0.67	–4.9	0.96		4700
N.A. Tolkachev (1964)	Field test					Vertical	310-430
B.E. Slavin (1969)	Field test	1 – 6				Vertical and horizontal	182 – 322
E.A. Marov (1970-1971)	Field test	0.3	2.4			Vertical	760
V.S. Sazhin, V.Ia. Shishkin (1982)	Field test	1.2	0 – 1.2			Horizontal	1400 - 1600
E.D. Ershov (1985)	Laboratory test		0.5			Vertical and horizontal	220 - 620
Guidelines for accounting and preventing strains and forcers of frost heaving soils (Production and Research Institute for Survey and Construction) (1986)	Formula evaluation		0.9	–2		Vertical	63.9
				–4			183
A.G. Alekseev (2006)	Field test	2.0	1 - 2			Horizontal	20-190

Tretiakova O.V. Normal stresses of frost heaving as function of excess moisture. *Magazine of Civil Engineering*. 2017. No. 8. Pp. 130–139. doi: 10.18720/MCE.76.12.

The comparison of stresses calculated by formula with tabular data of RF Code is displayed in Table 2. As can be seen in Table 2, the normal stresses, calculated by formula (10, 11), agree with the tabular data of RF Code provided the anisotropy factor is taken into consideration.

The comparison of stresses calculated by formula with the results obtained by other researchers is displayed in Table 3.

So, the formula values of frost heave normal stress for layers of seasonal freezing proved true when compared with those, obtained by numerous researchers. The differences in values may be due to the fact that no single approach to normal stress evaluation has been developed yet.

Discussion

Division of frost heave stress into tangential and normal seems to be reasonable. Currently widely known is the analysis of the tangential stresses based on adfreezing of the frozen soil to the lateral surface of foundation. Research of academic specialists into frost heave direction led us to infer that it is possible to work out an analysis method of the heave normal stresses.

Research into frost heave normal stresses in open and closed systems seems to be representative. The normal stresses in the open system prove to be more reasonable as they take into account such factors causing heaving process as accumulation of ice due to sucking up water and influence of unfrozen water and stress-strain behaviour of soil below. Based on the research we can conclude that the normal stresses of frost heaving in the open system are a function of porosity and “excess moisture” whose volume exceeds the soil interstitial volume under freezing.

Soil and sucking up water that exceeds the soil interstitial volume after freezing causes increase in soil volume, which together with expansion constraint of foundations results in the heave normal stresses.

The comparison of stresses in Table 3 is worth mentioning that the normal stress values obtained in our research are comparable to those of other researchers. They correlate most with the results of B.I. Dalmatov (1954) [32] it taking into account the deformation modulus of the frozen soil. According to Table 3 our results can be associated with stress values obtained by A.E. Fedosov (1935) [40], B.E. Slavin (1969) [41], E.D. Ershov (1985) [28], A.G. Alekseev (2006) [35] and researchers from Production and Research Institute for Survey and Construction (1986). Our results agree with N.N. Morareskul’ [27] and V.S. Sazhin’ stresses [24] allowing for the anisotropy factor. Field tests carried out by E.A. Marov indicated significant increase of stresses depending on the thickness of the soil layer frozen [33]. Marov’s results are comparable with our data under reduced layer soil thickness. Stress testing under the close system, i.e. in laboratory conditions, shows the high value stresses, which do not reflect the actual soil behaviour under natural freezing. In addition, research into the normal stresses in the permafrost region suggests these conditions be different from the seasonal freezing conditions (V.O. Orlov 1958) [42].

To make the analysis method work, several objectives need to be achieved:

- Statistical data on temperature and moisture of the soil at various depths within autumn-winter seasons should be provided, information on the freezing soil velocity is needed, which requires cartographic reference material.
- The method supposes revision of deformation modulus of frozen soil.
- To confirm the results obtained, a certain number of experiments should be carried out in different kinds of soil.
- The analysis method needs further interpretation in design programs.

Conclusion

As, a result of the research carried out it was found that

1. Frost heave occurs if the amount of the frozen and unfrozen water exceeds the volume of the soil interstices. Thus frost heaving normal stress is, on one hand, the function of the soil porosity on the other hand, it is the function of “excess moisture” resulting in the formation of “excess ice”. “Excess ice” is the amount of ice exceeding the free interstice volume not filled with frozen and unfrozen film water after freezing.
2. The normal stresses in the open system prove to be more reasonable.
3. The formulas (10, 11) for the normal stresses of frost heaving in the open system as a function of excess moisture exceeding the free soil interstitial volume under freezing, and their results appear to

be relevant to the tabular data of RF Code available and other authors' results. The expression obtained make it possible to define normal stress in any hydrogeological and climatic conditions.

References

1. Modisette J.P., Modisette J.L. Pipe Line Frost Heave. *Pipeline Simulation Interest Group*. 2014. Vol. 1421. Pp. 1–8.
2. Kibriya T., Tahir L. Adfreeze forces on Lightly Loaded Pile foundations of Solar PV Farms in Gold Regions. *American journal of Civil Engineering and Architecture.* 2015. Vol. 3. No. 4. Pp. 109–117.
3. Babaei M., liu J., Staseff D. Numerical analysis of freezing and thawing influence on soil nail walls. *Conference: CGS GeoVancouver Conference.* Vancouver, October 2016.
4. Karlov V. D. *Sezonno promerzayushchie grunty kak osnovaniya sooruzheniy* [Seasonal freezing soils as a base of construction]: Doctorial Thesis: 05.23.02 Saint-Petersburg: SPbGASU, 1998. 349 p. (rus)
5. Golli O.R. *Integral'nye zakonomernosti moroznogo pucheniya gruntov i ikh ispol'zovanie pri reshenii inzhenernykh zadach v stroitel'stve* [Integral mechanism of frost heaving of soils and application of them in the performance of the engineering challenges in building]: Doctorial abstract: 05.23.02. Saint-Petersburg: VNIIG im. Vedeneeva B.E., 2000. 45 p. (rus)
6. Matveeva M.V. *Razrabotka algoritma chislennogo issledovaniya moroznogo pucheniya gruntov* [Logical design of frost heave numerical simulation]: Doctorial abstract: 05.13.18. Yakutsk. Yakutskiy gosudarstvennyy universitet im. M.K. Ammosova, 2009. 15 p. (rus)
7. Abzhalimov R.Sh. Printsipy rascheta maloetazhnykh zdaniy i podzemnykh sooruzheniy na puchinistykh gruntovykh osnovaniyakh [Calculation principles of low-storey buildings and underground structures on heaving foundation beds]. *Geotekhnika.* 2009. No.1. Pp. 25–33. (rus)
8. Zhou J. Z., Li D.Q. Numerical analysis of coupled water, heat and stress in saturated freezing soil. *Gold Regions Science and Technology.* 2012. Vol. 72. Pp. 43–49.
9. Cao H. Z., Liu S., Jiang F., Liu J. The theoretical study on frost heave for saturated granular soil-numerical simulation of 1-d ice segregating model based on equilibrium of force and phase. *Chinese Journal of Theoretical and Applied Mechanics.* 2007. Vol. 39. No. 6. Pp. 848–857.
10. Zhou G.-g., Hu K., Shang X.-y., Zhou J.-s. Test and numerical simulation on frost heave in frozen soils in intermittent freezing mode. *Procedia Earth and Planetary Science 1*. 2009. Pp. 512–518.
11. Michalowski R.L., Zhu M. Modeling of Freezing in Frost-Susceptible Soils. *Computer Assisted Mechanics and Engineering Sciences.* 2006. No. 13. Pp. 613–625.
12. Rotta Loria A.F., Frigo B., Chiaia B. A non – linear constitutive model for describing the mechanical behavior of frozen ground and permafrost. *Gold regions Science and technology.* 2016. Vol. 133. Pp. 63–69.
13. Kiselev M.F. *Meropriyatiya protiv deformatsiy zdaniy i sooruzheniy ot deystviya sil moroznogo vypuchivaniya fundamentov* [Protective measures against deformations building and construction due to frost uplift foundations]. Moscow: Stroyizdat, 1971. 104 p. (rus)
14. Babaei M., liu J. *Soil nailing for highway construction in Ontario – freezing and thawing effects on soil nail walls in Ontario.* Technical report. July 2016.
15. Guo R., Wang Z., Niu Y. Anti – frost heave of lining channel with concrete composite insulation based on TCR principle. *Chinese Society of Agricultural Engineering.* October 2015.
16. Tsytovich N. A. *Mekhanika merzlykh gruntov* [Mechanics of frozen soil]. Moscow: Vysshaya shkola, 1973. 636p. (rus)
17. Konrad J.- M. *Frost heave mechanics.* Ph. D. Thesis. Dept. of Givil. Eng. Univ. Edmonton Alberta, 1980. 472 p.
18. Konrad J.- M., Morgenstern N. R. A mechanistic theory of

Литература

1. Modisette J.P., Modisette J.L. Pipe Line Frost Heave // Pipeline Simulation Interest Group. 2014. Vol. 1421. Pp. 1–8.
2. Kibriya T., Tahir L. Adfreeze forces on Lightly Loaded Pile foundations of Solar PV Farms in Gold Regions // American journal of Civil Engineering and Architecture. 2015. Vol. 3. № 4. Pp. 109–117.
3. Babaei M., liu J, Staseff D. Numerical analysis of freezing and thawing influence on soil nail walls // Conference: CGS GeoVancouver Conference. Vancouver. 2016.
4. Карлов В.Д. Сезонно промерзающие грунты как основания сооружений: дис. д-ра тех. наук: 05.23.02 Санкт-Петербург: СПбГАСУ, 1998. 349 с.
5. Голли О.Р. Интегральные закономерности морозного пучения грунтов и их использование при решении инженерных задач в строительстве: автореф. д-ра техн. наук: 05.23.02 Санкт-Петербург: ВНИИГ им. Веденеева Б.Е., 2000. 45 с.
6. Матвеева М. В. Разработка алгоритма численного исследования морозного пучения грунтов: автореферат дис. канд. физ.-мат.наук: 05.13.18 Якутск: Якутский государственный университет им. М.К. Аммосова, 2009. 15 с.
7. Абжалимов Р. Ш. Принципы расчета малоэтажных зданий и подземных сооружений на пучинистых грунтовых основаниях // Геотехника. 2009. №1. С. 25–33.
8. Zhou J.Z, Li D.Q. Numerical analysis of coupled water, heat and stress in saturated freezing soil // Gold Regions Science and Technology. 2012. Vol. 72. Pp. 43–49.
9. Cao H. Z., Liu S., Jiang F., Liu J. The theoretical study on frost heave for saturated granular soil-numerical simulation of 1-d ice segregating model based on equilibrium of force and phase // Chinese Journal of Theoretical and Applied Mechanics. 2007. Vol. 39. № 6. Pp. 848–857.
10. Zhou G.-g., Hu K., Shang X.-y., Zhou J.-s. Test and numerical simulation on frost heave in frozen soils in intermittent freezing mode // Procedia Earth and Planetary Science 1. 2009. Pp. 512–518.
11. Michalowski R. L., Zhu M. Modeling of Freezing in Frost-Susceptible Soils // Computer Assisted Mechanics and Engineering Sciences. 2006. №13. Pp. 613–625.
12. Rotta Loria A.F, Frigo B., Chiaia B. A non – linear constitutive model for describing the mechanical behavior of frozen ground and permafrost // Gold regions Science and technology. October 2016.
13. Киселев М.Ф. Мероприятия против деформаций зданий и сооружений от действия сил морозного выпучивания фундаментов. М.: Стройиздат, 1971. 104 с.
14. Babaei M., liu J. Soil nailing for highway construction in Ontario – freezing and thawing effects on soil nail walls in Ontario // Technical report. July 2016.
15. Guo R., Wang Z., Niu Y. Anti – frost heave of lining channel with concrete composite insulation based on TCR principle // Chinese Society of Agricultural Engineering. October 2015.
16. Цытович Н. А. Механика мерзлых грунтов. М.: Высшая школа, 1973. 636 с.
17. Konrad J. - M. Frost heave mechanics. Ph. D. Thesis. Dept. of Givil. Eng. Univ. Edmonton Alberta, 1980. 472 p.
18. Konrad J.- M., Morgenstern N. R. A mechanistic theory of ice lens formation in fine-grained soils // Canadian Geotechnical Journal. 1980. Vol. 17. № 4. Pp. 473–486.
19. Harlan R.L. Analysis of coupled heat-fluid transport in frozen soil // Water Resources Research 9(5). 1973. № 5.

ice lens formation in fine-grained soils. *Canadian Geotechnical Journal.* 1980. Vol. 17. No. 4. Pp. 473–486.

19. Harlan R. L. Analysis of coupled heat-fluid transport in frozen soil. *Water Resources Research*. 1973. No. 5. Pp. 1314–1323.
20. Peppin S.S.L., Style R.W. *The physics of frost heave and ice-lens growth.* Oxford, 2012. 35 p.
21. Michalowski R.L, Zhu M. Frost heave modeling using porosity rate function. *International Journal for Numerical and Analytical Methods in Geomechanics.* 2006. No. 30(8). Pp. 703–722.
22. Zhang Y., Michalowski R. Thermal – Hydro – Mechanical Analysis of Frost Heave and Thaw Settlement. *Journal of Geotechnical and Geoenvironmental Engineering.* 2015. Vol. 141(7).
23. Zhang Y. *Thermal – Hydro – Mechanical Model for Freezing and Thawing of Soils.* Author's abstract of Civil Engineering doctoral thesis. University of Michigan, 2014. 201 p.
24. Sazhin V.S. *Vzaimodeystvie puchinistogo grunta s fundamentami, rabotayushchimi sovmestno s konstruktsiyami sooruzheniy* [Interaction of heaving soil with foundations that operates together with building]: Doctorial abstract: 05.23.02 Moscow: NIIOSP im. N.M. Gersevanova, 1989. 45 p. (rus)
25. Puskov V.I. *Silovye vozdeystviya moroznogo pucheniya gruntov na fundamenty sooruzheniy i metody ikh rascheta* [Force action of frost heave on building foundations and analysis methods]: Doctorial abstract: 05.23.02 Novosibirsk: Sibirskaya Gosudarstvennaya akademiya putey soobshcheniya, 1993. 37 p. (rus)
26. Abzhalimov R.Sh. *Zakonomernosti vzaimodeystviya puchinistogo gruntovogo osnovaniya s fundamentami maloetazhnykh zdaniy i podzemnymi sooruzheniyami i metody ikh rascheta* [Interaction mechanism of heaving ground bed with foundations of low-storey building and underground structures and its calculation principles]: Doctorial abstract: 05.23.02 Moscow: Mos. gos. un-t. putey soobshcheniya, 2011. 47 p. (rus)
27. Morareskul N.N. *Issledovanie normal'nykh sil pucheniya gruntov* [Investigation of frost heave normal forces]. Doctorial abstract. Leningrad: LISI, 1950. 26 p. (rus)
28. *Deformatsii i napryazheniya v promerzayushchikh i ottaivayushchikh porodakh* [Strains and stresses into freezing and thawing solid] ed. Ershova E. D. Moscow: Izd-vo Mosk. un-ta., 1985. 167 p. (rus)
29. Thomas H., Cleall P., Li Y.C., Harris C., Kern-Luetschg. Modelling of cryogenic processes in permafrost and seasonally frozen soils. *Geotechnique.* 2009. No. 59(3). Pp. 173–184.
30. Hyang Y.–H., Cai Z.–Y., Zhang C. Development of centrifugal model test facility for frost heave of channels. *Yantu Gongcheng Huebao / Chinese Journal of Geotechnica l Engineering*. 2015. No. 37(4). Pp. 615–621.
31. Ming F., Li D.-g. Experimental and theoretical investigations on frost heave in porous media. *Mathematical Problems in Engineering.* Vol. 2015. ID 198986. Pp. 1–9.
32. Dalmatov B.I. *Issledovaniya kasatel'nykh sil pucheniya i vliyaniya ikh na fundamenty sooruzheniy* [Investigation of frost heave tangential forces and their effect on foundations]. AN SSSR: Institut merzlotovedeniya, 1954. 60 p. (rus)
33. Marov E.A. Opredelenie normal'nykh i kasatel'nykh moroznogo pucheniya v polevykh usloviyakh [Definition of frost heave normal and tangential forces in the field]. *Sb. nauch. tr. Fundamentproekt vyp. 14: Materialy po proektirovaniyu slozhnykh fundamentov i osnovaniy i po proizvodstvu izyskaniy* [Design proceedings of elaborate foundations and survey]. Moscow: Fundamentproekt, 1974. Pp. 40-49. (rus)

Pp. 1314–1323.

20. Peppin S.S.L, Style R.W. The physics of frost heave and ice-lens growth. Oxford, 2012. 35 p.
21. Michalowski R.L, Zhu M. Frost heave modeling using porosity rate function // International journal for numerical and analytical methods in geomechanics. 2006. № 30(8). Pp. 703–722.
22. Zhang Y., Michalowski R. Thermal – Hydro – Mechanical Analysis of Frost Heave and Thaw Settlement // Journal of Geotechnical and Geoenvironmental Engineering. 2015. № 141(7).
23. Zhang Y. Thermal – Hydro – Mechanical Model for Freezing and Thawing of Soils. Author's abstract of Civil Engineering doctoral thesis. University of Michigan, 2014. 201 p.
24. Сажин В.С. Взаимодействие пучинистого грунта с фундаментами, работающими совместно с конструкциями сооружений: автореф. дис. д-ра тех. наук: 05.23.02 М.: НИИОСП им. Н.М. Герсеванова, 1989. 45 с.
25. Пусков В.И. Силовые воздействия морозного пучения грунтов на фундаменты сооружений и методы их расчета: автореф. дис. д-ра тех. наук: 05.23.02 Новосибирск: Сибирская Государственная академия путей сообщения, 1993. 37 с.
26. Абжалимов Р.Ш. Закономерности взаимодействия пучинистого грунтового основания с фундаментами малоэтажных зданий и подземными сооружениями и методы их расчета: авторефер. дис. д-ра тех. наук: 05.23.02 М.: Мос. гос. ун-т. путей сообщения, 2011. 47 с.
27. Морарескул Н.Н. Исследование нормальных сил пучения грунтов. автореф. дис. к-та тех. наук. Ленинград: ЛИСИ, 1950. 26 с.
28. Деформации и напряжения в промерзающих и оттаивающих породах / под ред. Ершова Э. Д. М.: Изд-во Моск. ун-та. 1985.167 с.
29. Thomas H., Cleall P., Li Y.C., Harris C., Kern-Luetschg. Modelling of cryogenic processes in permafrost and seasonally frozen soils // Geotechnique. 2009. № 59(3). Pp. 173–184.
30. Hyang Y.–H., Cai Z.–Y., Zhang C. Development of centrifugal model test facility for frost heave of channels // Yantu Gongcheng Huebao / Chinese Journal of Geotechnical Engineering. 2015. № 37(4). Pp. 615–621.
31. Ming F., Li D-g. Experimental and theoretical investigations on frost heave in porous media // Mathematical Problems in Engineering. 2015. ID198986. Pp. 1–9.
32. Далматов Б.И. Исследования касательных сил пучения и влияния их на фундаменты сооружений. АН СССР: Институт мерзлотоведения, 1954. 29 с.
33. Маров Э.А. Определение нормальных и касательных сил морозного пучения в полевых условиях // Сб. науч. тр. Фундаментпроект вып. 14 Материалы по проектированию сложных фундаментов и оснований и по производству изысканий. М.: Фундаментпроект, 1974. С. 40–49.
34. Толкачев Н. А. Определение относительных нормальных сил морозного пучения грунтов // сб. науч. тр. НИИ оснований и подземных сооружений вып. 54 Основания и фундаменты. М.: Стройиздат, 1964. С. 165–170.
35. Алексеев А.Г. Определение горизонтального давления грунта на подпорные стены при сезонном промерзании-оттаивании: дис. к-та тех. наук: 05.23.02 М.: ОАО ПНИИИС, 2006. 190 с.
36. Jiang H., Tian Y. Test for frost heaving damage mechanism of rigid – soften composite trapezoidal canal in seasonally frozen ground region // Nongye Gongcheng Xyebao /Transactions of the Chinese Society of Agricultural Engineering. 2015. № 31(16). Pp. 145–151.

34. Tolkachev N.A. Opredelenie otnositel'nykh normal'nykh sil moroznogo pucheniya gruntov [Definition of frost heave relative normal forces]. *Sb. nauch. tr. NII osnovaniy i podzemnykh sooruzheniy vyp. 54: Osnovaniya i fundamenty* [Foundation engineering]. Moscow: Stroyizdat, 1964. Pp. 165–170 (rus)
35. Alekseev A.G. *Opredelenie gorizontal'nogo davleniya grunta na podpornye steny pri sezonnom promerzanii-ottaivanii* [Definition of frost heave horizontal pressure on retaining walls under seasonal freeze-thaw]: PhD Thesis: 05.23.02. Moscow: OAO PNIIIS, 2006. 190 p. (rus)
36. Jiang H., Tian Y. Test for frost heaving damage mechanism of rigid – soften composite trapezoidal canal in seasonally frozen ground region. *Nongye Gongcheng Xyebao/Transactions of the Chinese Society of Agricultural Engineering.* 2015. No. 31(16). Pp. 145–151.
37. Roman L.T., Kotov P.I. Modul' deformatsii merzlykh gruntov pri kompressionnykh ispytaniyakh [Deformation modulus of frozen soil under compression tests]. *Osnovaniya, fundamenty i mekhanika gruntov*. 2016. No. 5. Pp. 35–40. (rus)
38. Azmatch T.F, Sego D.C, Arenson L.U, Biggar K.W. Tensile strength and stress-strain 33ehaviour of Devon silt under frozen fringe conditions. *Gold Regions Science and Technology.* 2011. Vol. 68. No. 1–2. Pp. 85–90.
39. Nevzorov A.L. *Fundamenty na sezonnopromerzayushchikh gruntakh* [Foundations on seasonal freezing soil]. Moscow: Izd-vo ASV, 2000. 152 p. (rus)
40. Fedosov A.E. *Fiziko-mekhanicheskie protsessy v gruntakh pri ikh zamerzanii i ottaivani.* [Physico-mechanical process in soils under its freezing-thawing]. Moscow: Transzheldorizdat, 1935. 48 p. (rus)
41. *Tonneli* [Tunnels]: ed. D.I. Fedorova. Moscow: Transport, 1979. 176 p. (rus)
42. Orlov V.O. *Kriogennoe puchenie tonkodispersnykh gruntov* [Cryogenic heaving of finaly-dispersed soils]. Moscow: Izd-vo Akad. Nauk SSSR, 1962. 187p. (rus)

37. Роман Л.Т., Котов П.И. Модуль деформации мерзлых грунтов при компрессионных испытаниях // Основания, фундаменты и механика грунтов. 2016. № 5. С. 35–40.
38. Azmatch T.F., Sego D.C., Arenson L.U., Biggar K.W. Tensile strength and stress-strain 33ehaviour of Devon silt under frozen fringe conditions // Gold Regions Science and Technology. 2011. Vol. 68. № 1–2. Pp. 85–90.
39. Невзоров А.Л. Фундаменты на сезоннопромерзающих грунтах. М.: Изд.- во АСВ, 2000. 152 с.
40. Федосов А.Е. Физико-механические процессы в грунтах при их замерзании и оттаивании. М.: Трансжелдориздат, 1935. 48 с.
41. Тоннели: под ред. Д. И. Федорова. М.: Транспорт, 1979. 176с.
42. Орлов В.О. Криогенное пучение тонкодисперсных грунтов. М.: Изд-во Акад. Наук СССР, 1962. 187 с.

Olga Tretiakova,
+7(908)276-71-48; olga_wsw@mail.ru

Ольга Викторовна Третьякова,
+7(908)276-71-48; эл. почта: olga_wsw@mail.ru

Tretiakova O.V. Normal stresses of frost heaving as function of excess moisture. *Magazine of Civil Engineering*. 2017. No. 8. Pp. 130–139. doi: 10.18720/MCE.76.12.

doi: 10.18720/MCE.76.13

Energy performance of domestic hot water systems

Энергетические характеристики систем бытовой горячей воды

Dz. Grasmanis,
Riga Technical University, Riga, Latvia
D.O. Sovetnikov,
D.V. Baranova,
Peter the Great St. Petersburg Polytechnic University, St. Petersburg, Russia

Д-р техн. наук, профессор Д. Грасманис,
Рижский технический университет, г. Рига, Латвия
студент Д.О. Советников,
студент Д.В. Баранова,
Санкт-Петербургский политехнический университет Петра Великого, г. Санкт-Петербург, Россия

Key words: domestic hot water; energy performance; apartment building; water consumption; calculation

Ключевые слова: бытовая горячая вода; энергоэффективность; жилые дома; потребление воды; расчет

Abstract. Residential sector consumes 70 % of the district heat. The domestic hot water system consumes 27 % of the total thermal energy consumption in these buildings in Riga. According to the mandate of the European Committee for Standardization (CEN) European standards for assessment of the energy performance of buildings have been developed. CEN standards give different methods and default values for calculations and procedures for energy performance assessment. Taking into account national or regional regulations and climatic conditions for all CEN standards application a national annex is required. CEN standards adapted to the status of Latvian standards (LVS) are not complemented with national annexes that are required for high grade use of standards at the national level. The target of this paper is assessment the suitability of CEN standards for the calculation of energy performance of the domestic hot water systems and search for the optimal solutions (methods and default values) for Latvian conditions. In this study there is performed assessment of the consumption of the heat energy in the apartment buildings for heating and hot water system, including: 1) assessment of the DHW volume and necessary energy amount; 2) assessment of the heat losses in the hot water distribution system during heating and non-heating seasons; 3) assessment of the auxiliary energy of the DHW system. The results of this paper give possible evaluation of economic feasibility and energy impact for improvements of domestic hot water systems. The method corresponding to CEN standards suitable for Latvian conditions is proposed.

Аннотация. Жилой сектор потребляет 70 % тепловой энергии. Внутренняя система горячего водоснабжения потребляет 27 % от общего потребления тепловой энергии в этих зданиях в Риге. В соответствии с документом Европейского комитета по стандартизации были разработаны европейские стандарты оценки энергетических характеристик зданий. Данные стандарты содержат принятые по умолчанию методы и значения для расчетов и процедур оценки эффективности использования энергии. Принимая во внимание национальные или региональные правила и климатические условия для применения стандартов, требуется национальное приложение. Стандарты, адаптированные под статус латвийских стандартов, не дополняются национальными приложениями, которые необходимы для высококачественного использования стандартов на национальном уровне. Целью настоящего документа является оценка пригодности стандартов, принятых Европейским комитетом, для расчета энергетических характеристик бытовых систем горячего водоснабжения и поиск оптимальных решений (методов и значений по умолчанию) для латвийских условий. В этом исследовании проводится оценка потребления тепловой энергии в многоквартирных домах для систем отопления и горячего водоснабжения, в том числе: 1) оценка объема ГВС и необходимого количества энергии; 2) оценка потерь тепла в системе распределения горячей воды во время нагрева и ненагрева; 3) оценка вспомогательной энергии системы ГВС. Результаты этой работы дают возможность оценить экономическую осуществимость и энергетическое воздействие для улучшения бытовых систем горячего водоснабжения. Предложен метод, соответствующий стандартам Европейского комитета, подходящий для латвийских условий.

Грасманис Д., Советников Д.О., Баранова Д.В. Энергетические характеристики систем бытовой горячей воды // Инженерно-строительный журнал. 2017. № 8(76). С. 140–155.

Introduction

Multi-apartment buildings are one of the largest group of district heat users in Latvia. The residential sector consumes 70 % from the total heat produced in district heating systems in Latvia. The amount of energy consumed in domestic hot water (DHW) systems represents an average of 51 kWh per square meter of apartment's heated area annually or 27 % of the total heat energy consumption in those buildings.

To implement the goals of the European energy policy has adopted the Energy Performance of Buildings Directive that introduced energy performance certification of the buildings. According to European Commission mandate M480 there are a lot of developed and adopted European standards (CEN) for assessment of the energy performance of buildings – EPBD standards. The EPBD standards prescribe that EU member states shall adopt the standards on national or regional level, taking into consideration local climatic conditions. The EPBD standards adopted for Latvia (LVS) are not supplemented with national annexes necessary for full application of the standards on national level.

Previous studies [1–4] carried out in various European countries, China, Japan, USA, Canada point out many differences in DHW usage and consumption as well the tendency to change over time due to a global increase of energy prices, changes in technologies, introducing of individual metering, as well as wide variety of other factors that may appear on local or regional level.

Researches in Estonia [5] show that household hot water consumption has decreased for more than three times during last 30 years, which is caused by the implementation of the water consumption metering, increase in energy price and implementation of energy efficiency measures in the buildings.

The Latvian researchers study [6–13] on DHW consumption profiles in apartment buildings found that the actual consumption of DHW is twice lower than the normative. Energy needs for the DHW represents significant part of energy balance of residential and some other sectors of buildings. Significant amount of energy demand can be formed by both – DHW consumption needs as well DHW circulation losses.

The scientific and technical articles [14–18] provide wide and overall information on DHW systems, consumption profiles, technologies and technical solutions. Taking into consideration changeable political, economic, technological circumstances and legal conditions as well as local or regional factors the necessity for more and more new researches on DHW systems investigation still exists.

In articles [19–21] the analysis and solutions of problems of hot water systems were produced. The authors offer various methods of studying of problems of domestic hot waters in residential buildings.

Research studies [22–25] present the main architectural-planning, spatial and constructive solutions aimed at energy saving and enhancing energy efficiency of residential buildings. It is shown that the determining factors for low-level consumption in buildings thermal energy for heating are: high level of thermal insulation of external enclosing structures, integrity of the outer shell of the building and its compactness. Lists the possible measures to reduce costs for DHW.

The goal of this paper is to assess the applicability of EPBD standards for Latvian conditions and to find the right solutions for calculation the energy performance indicators of the DHW system for energy certification of the building.

Materials and Methods

Within this study, there are analyzed heat energy and hot water consumption in multi-apartment buildings with many apartments. This approach smoothes out the differences and gives higher validity of results to characterize the apartment housing sector. Selected multi-apartment buildings have a typical annual heat consumption for Latvian climate conditions. The buildings have been operating for a long time without any reconstruction, except automatic heating units that improved about 10 to 15 years ago in most buildings. The annual thermal energy consumption in the analyzed buildings ranges from 164 to 225 kWh/m^2 in Riga and from 155 to 245 kWh/m^2 in Bauska (both calculated on total dwelling area). The investigated buildings are built according to standard type designs from sixties to nineties of 20th century. Usually apartment buildings have a single heat meter for both heating and DHW in Latvia. Therefore, to calculate energy performance indicators of the building it is necessary to assess the volumes of the DHW, the energy required for DHW heat at the required temperature and thermal losses in the DHW distribution and circulation pipelines. Estimated indicators of residential areas are presented in Table 1.

Table 1. Indicators of residential areas

	Riga	Bauska
Number of buildings	39	57
Number of stores	3–12	
Total heated area (m^2)	158 194	91 001
Number of dwellings	3359	3167
Number of inhabitants	7139	no reliable information

All investigated buildings are connected to the district heating network. All buildings have the automatic heating unit equipped with the single heat meter for heating and DHW as well as hot water and cold-water meters. Automatic heating control unit ensures DHW temperature of about 50 to 55 °C during the water taping. The draw of DHW distribution systems with circulation is shown on Figure 1. For most of the standard design type buildings (except for 12 storied destine type No 104) the DHW distribution system have several circulation loops with bottom distribution supply pipes from basement, branch pipes from supply pipes in dwellings and downward return pipes.

The DHW distribution system of 12 storied destine type No 104 buildings have one upwards supply pipe from basement to building top (attic) and several downward return pipes with branch pipes in dwellings.

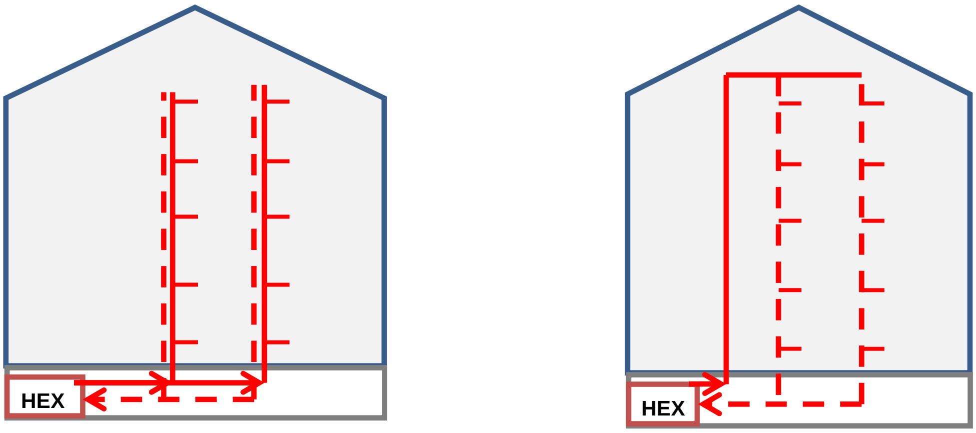

Figure 1. DHW distribution system with circulation loop. The bottom distribution (on the left), the upper distribution (on the right).

The CEN standards for energy performance of buildings provide concept and common methods for preparing energy performance certification and energy inspections of buildings. Calculation model for energy performance assessment of DHW systems described by the standards:

1) EN 15316-1 – Heating systems in buildings - Method for calculation of system energy requirements and system efficiencies – Part 1: General (EN 15316-1);

2) EN 15316-3-1 – Heating systems in buildings - Method for calculation of system energy requirements and system efficiencies – Part 3-1: Domestic hot water systems, characterization of needs (tapping requirements) (EN 15316-3-1);

3) EN 15316-3-2 – Heating systems in buildings - Method for calculation of system energy requirements and system efficiencies – Part 3-2: Domestic hot water systems, distribution (EN 15316-3-2).

Results and discussion

Assessment of energy performance of the DHW systems of the apartment buildings

Characteristics of the domestic water consumption

The assessment of the consumption data per dwelling area in 22 buildings in Riga shows that average annual consumption of water in the investigated buildings is 3.64 liters per m^2 daily, of which

2.12 liters cold water and 1.52 liters hot water. The average daily consumption of domestic cold water and DHW per m^2 per day shown in Fig. 2. The chart shown that consumption of the hot water decreased but consumption cold water increased during the summer.

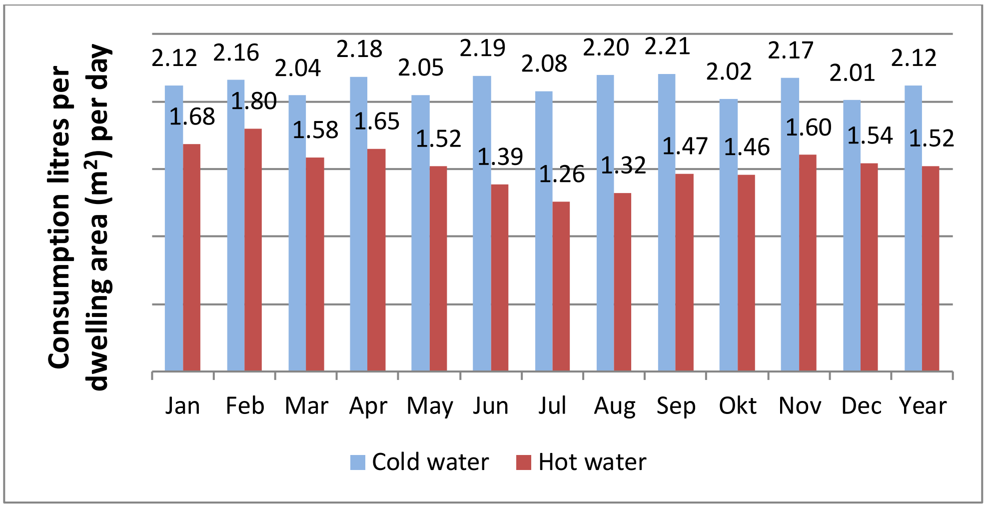

Figure 2. Average daily consumption of domestic cold water (DCW) and domestic hot water (DHW) in apartment buildings (liters per m^2 per day) by months and yearly

The average DHW consumption ratio is 41.8 % of total annual water consumption while seasonally it is 43.9 % during heating season and 39.4 % during non-heating season. The Figure 3 shows DHW consumption ratios of total and inlet water average temperature variations per months. The monthly differences of hot water consumption ratio are caused by variation of temperature of inlet cold water during a year. When supplied cold-water temperate increases (in summer) necessary hot water amount decreases whereas when supplied cold-water temperature decreases (in winter) the necessary hot water amount increases. DHW consumption is 94 % of annual average in the non-heating season and 106 % of annual average in the heating season.

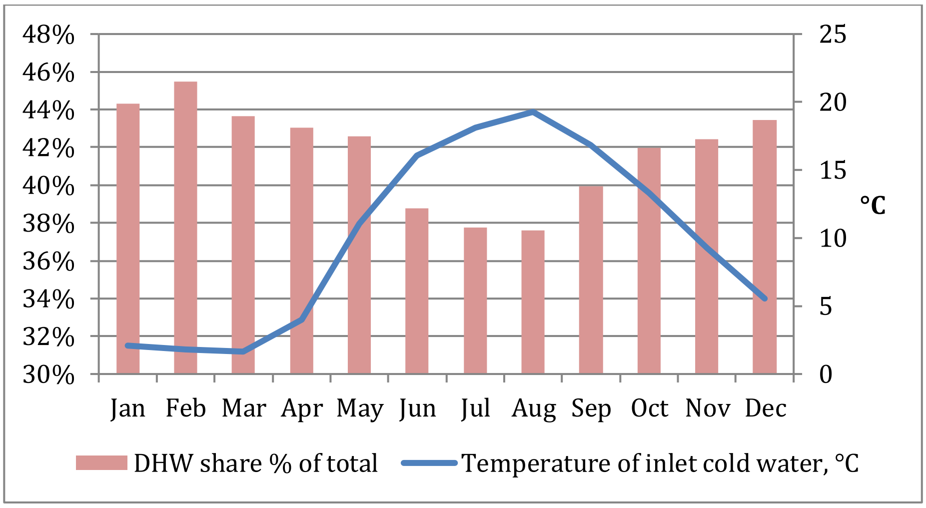

Figure 3. The ratio (%) of consumption of DHW to the total consumption in apartment buildings and average temperature of inlet cold water per month

The study shows specific indicators for a better understanding of DHW consumption (Table 2).

The coefficient of determination R has used to explain how much variability of one factor can be caused by its relationship to another factor (if the coefficient is closer to 1 then the relationship is closer). Consequently, the DHW consumption per one inhabitant has the highest coefficient of determination (R^2=0.94).

Table 2. DHW consumption indicators

		Minimum	Maximum	Average	Coefficient of determination R^2
Consumption of DHW, liters per day					
Per m^2 of dwelling area	Riga	1.10	2.73	1.86	0.90
	Bauska	1.01	3.53	1.54	0.84
per dwelling (household)	Riga	55.7	142.6	94.0	0.88
	Bauska	40.0	121.3	73.1	0.81
per person	**Riga**	24.2	60.2	41.0	**0.94**

By comparing DHW consumption indicators in the investigated buildings to default values set out in Annex A of standard EN 15316-3-1 the authors found out that average DHW consumption of 41.0 liters per person per day is close to the default value 36 liters per person per day in Table A.1 'Tapping program No. 1'. In addition, DHW consumption significantly differs from the values set out in Latvian Construction standard LBN 221-15 "Internal Water-main and Sewage of Buildings". The paragraphs 1.6 to 1.8 of Annex 4 of LBN 221-15 set out DHW consumption normative values 85 until 105 liters per person per day.

The average values of DHW consumption 94.0 litres per dwelling in Riga and 73.1 litres per dwelling in Bauska are less than default values of 100.2 liters per dwelling, determined in Table A.2 ('Tapping program No. 2.') and is very different from the default value of 199.8 liters per dwelling, determined in Table A.3 ('Tapping program No. 3.').

Assessment of energy consumption for DHW subsystems

To calculate energy used for DHW needs and DHW circulation, there is used data on heat energy consumption in the buildings during non-heating season (May to September).

In general, the total heat energy consumption Q in the analyzed building is the sum of energy for heating, DHW needs and heat losses in the DHW distribution circulation loop.

$$Q = Q_H + Q_W + Q_{W,cirk}, \tag{1.2.1}$$

where Q – the total energy consumption for heating and for DHW system, kWh;

Q_H – the energy consumption for space heating, kWh;

Q_W – the energy consumption for DHW needs, kWh;

$Q_{W,\, cirk}$ – the thermal losses from pipes of DHW distribution circulation loop, kWh.

The energy need for DHW heating Q_w is calculated as follows:

$$Q_W = V_W \frac{\rho_W c_W}{3600} \cdot \left(\theta_{w,dbl} - \theta_{w,o}\right), \tag{1.2.2}$$

where Q_w – the energy need for DHW, kWh;

V_w – the volume of water (in the respective period), m^3;

ρ_w – the density of water, kg/m^3;

C_w – the specific heat capacity, J/(kg·K);

$\theta_{w,del}$ – the average cold water inlet temperature, °C;

$\theta_{w,o}$ – the average DHW delivery temperature, °C;

3600 – the factor of conversion from megajoules to kilowatt-hours.

The calculations on the study based on actual monthly average cold water temperatures. For comparison, the calculations based on seasonal (heating and non-heating season) average cold water temperatures or default cold water temperatures from LBN 221, have impact the results within 2%. The calculation with average annual default cold-water temperature (either LBN 221 or EN 15316-3-1) affect the results more higher and error may exceed 10 %.

Based on data of necessary energy for DHW needs during non -heating season it is possible to calculate the energy losses on DHW distribution circulation loop. The calculated monthly data of energy consumption for DHW needs (consumption), the thermal loses on DHW circulation loop and the energy for heating system per dwelling area of buildings in Riga shown in Figure 4.

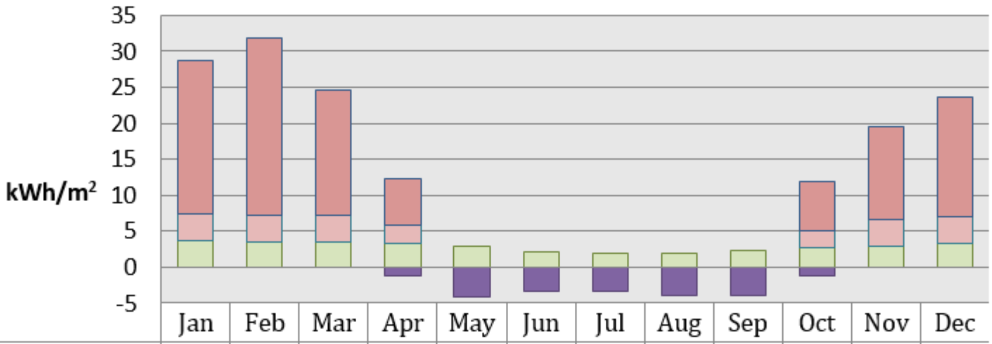

	Jan	Feb	Mar	Apr	May	Jun	Jul	Aug	Sep	Oct	Nov	Dec
Heating needs	21.29	24.68	17.29	6.49						6.77	12.98	16.59
Recoverable DHW circulation losses (heat gains)	3.74	3.74	3.74	2.49						2.49	3.74	3.74
Non-recoverable DHW circulation losses				-1.25	-4.12	-3.40	-3.37	-3.93	-3.88	-1.25		
DHW needs	3.66	3.42	3.55	3.26	2.82	2.19	1.95	2.00	2.23	2.63	2.89	3.32

Figure 4. Heat energy average values per m^2 of heated dwelling area per month for heating, DHW needs, DHW circulation (data on 39 building in Riga)

The total thermal losses of a DHW distribution circulation loop range from 28.9 to 65.2 kWh per m^2 per dwelling area annually for different standard design buildings. The average thermal losses of a DHW distribution circulation loop is 45.4 kWh per m^2 dwelling area annually for buildings in Riga and 53.5 kWh per m^2 dwelling area annually for buildings in Bauska.

The assessment of thermal losses in DHW circulation loop in different standard design buildings per apartment give values ranges from 1.1 to 3.0 MWh per annum or 0.1 to 0.25 MWh per month. For buildings in Riga the average value is 2.28 MWh per apartment per annum or 0.18 MWh per month, for buildings in Bauska the average value is 2.58 MWh per apartment per annum or 0.21 MWh per month. In most buildings, monthly thermal losses in DHW circulation loop significantly exceed default value (0.1 MWh per apartment per month) recommended for settlement calculations in Riga city.

During heating season, the heat losses from the DHW circulation loop are recoverable for heating needs. Thus, during the heating season the heat losses in DHW circulation system are heat gains as part of total heating balance of the building.

During non-heating season, all thermal energy consumption used only in DHW system of building. The study shows that share of heat losses in DHW circulation loop ranges from 35 % till 79 % (in average 56 %) from total energy consumption or from 14.9 till 25.6 (in average 20.2) kWh per m^2 annually during non-heating season in investigated buildings in Riga.

Heat losses in the DHW circulation system have close correlation to the heated area of the building, but there is also a correlation in relation to the number of apartments, as well as number of circulation loops. Simultaneously the study shows that there is no correlation between heat loss in DHW circulation loop and such characteristic of building as: dwelling area, number of apartments, number of inhabitants (Fig. 5), i.e. the variables that have a close correlation to DHW consumption.

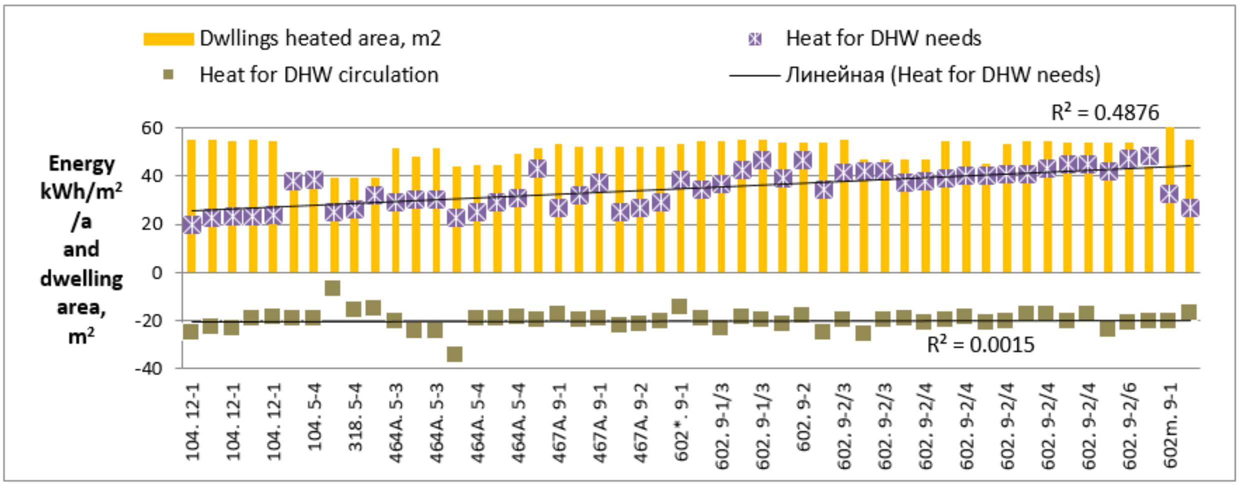

Figure 5. Heat consumption for DHW needs and DHW circulation losses and average space area of households (data on 39 buildings in Riga arranged by heat consumption for DHW needs)

Calculation of the heat energy losses based on DHW pipes actual physical characteristics

Estimation of the thermal energy losses in the DHW distribution system (experimental data), which assessed based on actual measured data for heating and DHW volume consumption in the building (see the section 1.2), in the study compared with the results obtained according to the methods:

1. Calculation of thermal losses based on the DHW pipeline physical characteristics according to 6.3.3. of the standard EN 15316-3-2;

2. Calculation of thermal losses based on DHW pipeline physical characteristics according to 6.3.3. of the standard EN 15316-3-2 using standard values provided in Annex D of the standard.

The general determination of thermal losses of a circulation loop comprising several pipe sections *I* is given by:

$$Q_{w,dis,ls,col} = \sum_i Q_{w,dis,ls,col,i} = \sum_i \Psi_{W,i} \cdot L_{W,i} \cdot \left(\theta_{W,dis,avg,i} - \theta_{amb,i}\right) \cdot t_W; \qquad (1.3.1.)$$

where $Q_{w,dis,ls,col,i}$ – specific energy losses of the distribution of pipe section *i*, Wh;

$\Psi_{w,i}$ – linear thermal transmittance of the respective pipe section *I*, W/(m·K);

$L_{w,i}$ – length of the distribution pipe section *i* (m);

$\Theta_{w,dis,avg,i}$ – mean inner temperature (water temperature) of pipe section *i* (°C);

$\Theta_{amb,i}$ – ambient temperature for the pipe section *i* (°C);

t_w – period of the time that the heat loss shall be calculated for $\Theta_{w,dis,avg,i}$ (hours).

The DHW circulation system of investigated buildings has the following features:

a) vertical distribution with known number of circulation loops in building section for each building type;

b) he circulation loops run continuously all the time; c) each apartment has one towel rail on the circulation loop.

The DHW distribution system comprises three different pipe sections:

V – distribution pipes from heat exchanger to the vertical supply pipes on basement;

S – main supply pipes on building heated area comprise: vertical pipes (S1) and individual tower rails in the apartments (S2);

I – individual branching pipes to the user outlets on dwellings. Heat losses from individual branching pipes are not affect overall circulation losses. Heat losses from individual branching pipes is part of the heat energy for DHW consumption needs.

The authors have worked out unified formulas for calculation of length of circulation loop sections for investigated buildings. The values and unified formulas for calculation of pipe length of each DHW circulations loop section based on technical design of different standard buildings are shown in Table 3.

For comparison in the Table 3. are shown default values and formulas of Annex D of standard EN 15316-3-2. To compare different calculation models the calculations use equal temperature characteristics for both the DHW temperature in the pipe sections and the ambient temperate around pipe sections. This approach allows in more accurately compare the authors' calculation method with the methods of standard EN 151316-3-2.

Table 3. The values and formulas for calculation of thermal losses of the domestic hot water distribution pipe sections

Author's calculation model	**Default values from Annex D of standard EN 15316-3-2**
Technical characteristics of distribution pipes	
V - insulated, steel, Ψ=0.4 (W/(m·K)) S_1, $S_{1,up}$, $S_{1,down}$ – non insulated, steel, Ψ=1.0 (W/(m·K)) S_2 – non-insulated, steel towel rails, Ψ=1.0 (W/(m·K))	V – insulated, Ψ=0.4 (W/(m·K)) S – non-insulated, external, Ψ=1.0 (W/(m·K))
Length of pipe section (m)	
FOR ALL TYPE OF STANDARD DESIGN, EXCEPT DESIGN NO 104 OF 12-STORE BUILDINGS: $L_V = 2 \times L_B + B_B \times n_{B,dis,col}$ $L_{S,1} = 2 \times L_B \times n_f \times h_f \times n_{B,dis,col}$ $L_{S,2} = n_{dwelling} \times L_{towel\,rail}$ 12-store 104. serial: $L_V = L_B + B_B \times n_{B,dis,col}$ (One) up distribution pipe $L_{S1,up}$ $L_{S1,up} = L_B \times n_f \times h_f \times 1$ Down distribution pipes $L_{S1,down}$ $L_{S1,down} = L_B \times n_f \times h_f \times n_{B,dis,col}$ $L_{S2} = n_{dwelling} \times L_{towel\,rail}$	For all buildings: $L_V = 2 \times L_B + 0.0125 \times L_B \times B_B$ $L_S = 0.075 \times L_B \times B_B \times n_f \times h_f$
Ψ – linear thermal transmittance of pipe section W/(m·K); L_B – the largest extended length of the building (m), B_B – the largest extended width of the building (m), N_F – the number of heated stores; $N_{B,DIS.COL}$ – the number of circulation loops in building; H_F – the height of the heated stores (m); $D_{WELLING}$ – the number of dwellings in building; $L_{TOWEL\,RAIL}$ – average length of the towel rails in dwellings (m).	
The following conditions are used in calculations: the average temperature of DHW circulation system +52°C, ambient temperature around DHW pipes +20°C, calculation time period: 162 days per 24 hours. *The CEN standards define the following default values: the average temperature of DHW circulation system +60°C, ambient temperature around DHW pipes +22°C. The standard values not been used on calculations.*	

According to the standard, the default linear thermal transmittance of pipe section should show respect to building area. The calculations with default values of the linear thermal transmittance (3.0 W/(m·K)) of main supply circulation pipe section on heated area of building give results which significantly (more than 4 times) differ from the result of actual assessment.

The results demonstrate that default values of the linear thermal transmittance set in standard EN 15316-3-2 is not applicable for assessment of the heat loss of DHW circulation subsystem. Thereby authors used input value 1.0 W/(m·K) as the closest to the actual value for calculation of the linear thermal transmittance of main supply circulation pipe section on heated area of investigated building. The comparison of the length of pipe sections by the actual and standard model shown that differences are less significant – length of the pipes located in the basement (section V) according to the standards have a length from 50% to 90% from the actual, while for other sections (S) the difference range from 110% to 320%. The calculation results for circulation losses by different assessment methods differs for standard type buildings with different technical design (Fig. 6)

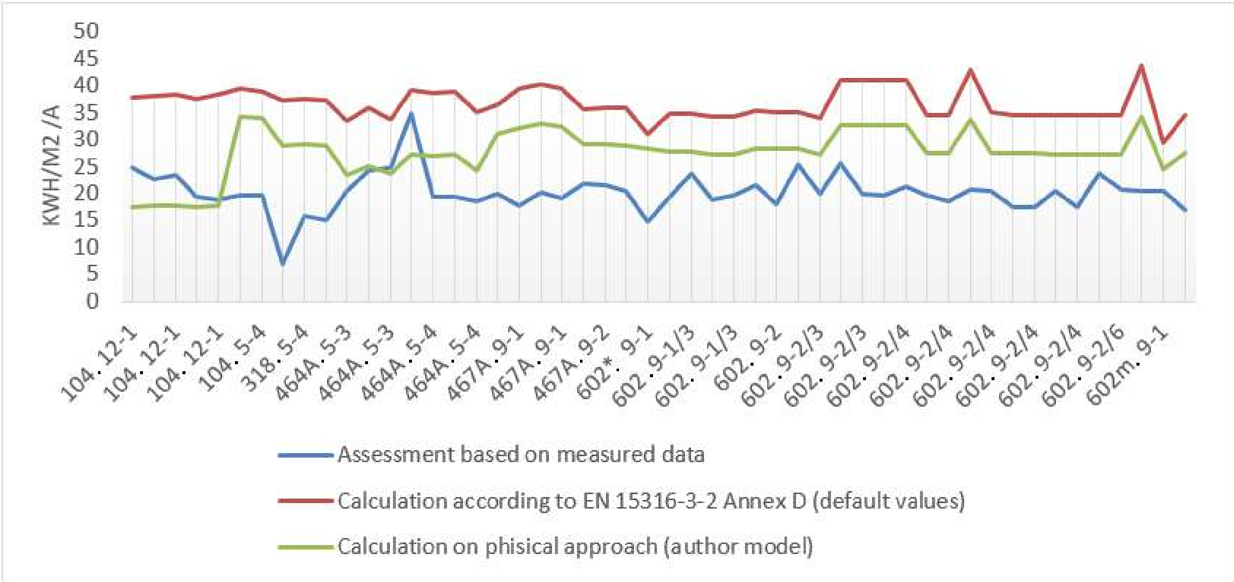

Figure 6. Calculation results for circulation losses by different assessment methods

The authors believe that most accurate results based on actual measured data of heat energy and DHW volume consumption. The calculations based on metered data shown that thermal losses of a circulation loop ranges from 14.9 to 25.6 (in average 20.1) kWh/m^2 per non-heating period (162 days) for buildings in Riga and from 12.8 to 36.7 (in average 23.7) kWh/ m^2 per non-heating period for buildings in Bauska.

Based on the default values of technical characteristics of DHW system the calculation results in most cases significantly differ from the actual data (obtained during experiments).

The calculation of thermal losses based on the actual DHW pipeline physical characteristics and calculation using standard values of the standard EN 15316-3-2 gives highest results than experimentally based.

Theoretical calculations according to the authors methods gives closer results to the experimentally results that obtained on measured heat energy and DHW consumption. The assessment results based on authors' model differs from the experimental results range from 1 % to 88 % (in average 44 %) for different standard design buildings. In comparison, using default values and formulas for calculation, the difference is between 13 % and 147 % (in average 81 %) for buildings in Riga and from 11 % until 274 % (in average 98 %) for buildings in Bauska.

The authors consider that the biggest differences between the calculation results based on physical approach and metered results caused by the inappropriate default values of linear heat transmittance coefficient of pipe sections. Inaccuracy has formed, for example, due to embedding of pipes in the internal structures of the building. Therefore, the actual difference of the temperature of the pipeline and ambient temperature may significantly differ from the default data set up on standard. It is also known that some technical design of standard buildings has shared duct openings for DHW pipes and close sewage pipes that affect the surrounding temperature around the circulation pipes. Those errors can be prevented with correction (reduction) of the default linear heat transmittance coefficient for vertical pipe sections.

The breakdown of heat loss by DHW circulation loop sections

Additionally, the authors assessed circulation heat loss ratio of the DHW circulation systems by pipe sections during non-heating and heating seasons in different standard design buildings. This assessment based on physical approach with actual technical characteristics of DHW circulation system. The equal conditions used for calculations for heating and for non-heating seasons, with exception for average ambient temperature (+20 °C for the non-heating season and +10 °C for the heating season) around pips in the basement.

The heat losses of domestic water circulation loop outside the heating space (section V) are not recoverable during all the year (on heating and non-heating season), while it is acceptable that the heat losses from towels rails (S2 section) are useful heat gains for comfort in the bathrooms throughout the year. However, heat losses from the vertical distribution circulation pips (section S1) are useful heat gains (recoverable heat losses) during the heating season but not recoverable during non-heating season.

Based on the calculation model, the following rates obtained for different pipe sections of the DHW system:

1) for pipes in non-heated basement: from 10 % to 13 % during non-heating season and from 12% to 16 % during heating season for 5 to 12 storied buildings, from 19 % to 24 % during non-heating season and from 24 % to 29 % during heating season for 3 storied buildings and modified 4 storied buildings of standard design type No 103 in Bauska;

2) vertical distribution pipes: from 50 % to 60 % for 3-storied buildings, and from 55 % to 60 % for in 5-storied buildings, from 64 % to 67 % for 9 storied buildings, and from 48 to 49 % for 12-storied buildings;

3) for individual towel rails in dwellings: from 16 % to 27 % in 3-storied buildings, from 30 % to 33 % for 5-storied buildings, from 22 % to 24 % for 9 storied buildings, 38 % for 12-storied buildings.

The calculations shows that representative non-recoverable energy losses of DHW circulation loop ranges from 16 to 24 and in average 20 kWh per m^2 per year in investigated apartment buildings. The result is representative according to considerations that non-recoverable energy losses are in the basement during whole year, in vertical distribution pipes during non-heating season, but heat energy losses from towel rails are useful (not losses) during whole year.

The assessment of the auxiliary energy for DHW system

Auxiliary energy is one of the indicators that should be calculate during assessment of energy performance of the building. The auxiliary energy of DHW system can be calculated according to methods given in CEN or DIN[1] standards:

1) DIN V 18599-8:2007-02;

2) EN 15316-3-2:2008 (standard gives two methods: simplified and detailed);

3) European draft standards prEN 15316-1:2014 and prEN 15316-3:2014.

In the investigated buildings, the auxiliary energy for the DHW emission sub-system, generation sub-system and storage sub-system is zero. Thus, the study detailed calculations done only for auxiliary energy for DHW distribution sub-system.

According to the simplified calculation method, the auxiliary energy for the pump can be calculated by multiplying the pump power with the pump operational running time. According to the detailed calculation method, the assessment of the auxiliary energy of the DHW system takes into account hydraulic energy requirements during the operation, performance characteristics of the circulation pump as well as more than 20 other technical characteristics of the buildings and DHW system.

Results calculated according to both methods are shown in Table 4.

Table 4. Auxiliary energy by different calculation methods

	Auxiliary energy, kWh/m^2 per year					
	For DHW circulation system		For Heating system		**Total**	
Calculation method	Detailed	Simplified*	Detailed	Simplified	Detailed	Simplified
Average	0.44	*0.63/0.46*	1.18	*0.56/0.92*	**1.62**	***1.02/1.54***

* The auxiliary energy by simplified method calculated with the nominal power and maximum power of the pumps.

Discussion

The author S.V. Korniyenko in his work [26] find that actual DHW consumption represents an average of 71.5 kWh per square meter of apartment's heated area annually or 34 % of the total heated consumption at 23-storey multi-apartment building in Russia.

[1] DIN – Deutsches Institut für Normung (German Institute for standartization)

In the study [27] it is mentioned that data based on static studies of the modes of operation of heating systems for DHW consumption of 10-storey building in Cheboksary is an average 32.2 kWh per heating period and 53.1 kWh per year and from 32 to 54 liters per inhabitant per day.

Research paper [28] concludes that DHW consumption of 32-storey building in Chogqing, a cooling dominated region in China, is 132 kWh per year. In case of DHW compouned with ground-source heat pump the simulation showed that the operation of DHW system could effectively reduce the ground temperature and improve the system performance to 89 kWh per year.

In the article [29] autors present the results of domestic hot water consumption measurements, which were done in a 32-appartament house in Riga. The results were worked up using the prescribed formulas of building normative LBN 221-98 and compose in average 44 liters per inhabitant per day.

The average value of the energy consumption for DHW system, obtained by the authors of this article, is 45.4 kWh per m^2 dwelling area annually for buildings in Riga and 53.5 kWh per m^2 dwelling area annually for buildings in Bauska The resulting discrepancy can be explained with heat losses from 50 % to 70 % for vertical distribution pipe sections and the fact that the present study covers building up to 12 floors.

In comparison with normative documents the actual DHW consumption (from 24.2 to 60.2 liters per inhabitant per day and in average 91.4. liters per households in Riga and 71.5 liters per housholds in Bauska) is less than specified in standard EN 15316-3-1 (from 100.2 to 199.8 liters per day per household) and in the Latvian Construction regulation LBN 221-15 (from 85 to 105 liters per inhabitant per day).

The actual DHW consumption from the energy point of view is significantly less that specified in Russian standard (135 kWh/m^2 per year).

Recommendations for energy performance calculation model for the DHW system

The study confirms that energy consumption of DHW system of apartment building have two distinctly independent correlative relationships:

1) Consumed volume of DHW and the required energy depend on number of inhabitants, dwelling area and number of apartments;

2) The thermal losses of DHW system circulation loop depend on heated areas of dwellings, number of apartments, number of circulation loop sections in dwellings.

The study shows and typical values the typical range for both correlative relationships. Nevertheless, the study shows differences for different standard design type buildings as well for buildings with the same design. In view of the findings authors suggest the method for energy performance assessment of DHW system of the building with unified accounting for heating and DHW needs. Detailed calculation should be carried out this way:

1. the accounting data shall be determined as:
a. the duration of the non-heating time period for month with no heating $t_{non\text{-}heating,count}$;
b. the total length of non-heating season $t_{non\text{-}heating}$,
c. the energy consumption Q_m for non-heating months *m* and the sum of energy consumption during months with no heating $Q_{non\text{-}heating,count} = \Sigma Q_m$;
d. the volume of DHW V_m consumed during non-heating months *m* and the sum of DHW volume consumed during months with no heating $V_{non\text{-}heating,count} = \Sigma V_m$;
(It is preferable to use the metering data from DHW meter of whole building instead of total sum of individual consumption data provided by the inhabitants of apartments);

2. The next step is the calculation of monthly energy consumption $Q_{W,m}$ necessary for DHW use during months with non-heating (see the formula 1.2.2. in section 1.2) and the sum for the months with non-heating

$$Q_{W,non-heating.count} = \sum Q_{W,m};$$

3. The next is the calculation of thermal losses in the DHW circulation loops $Q_{W,dis,non\text{-}heating.count}$ for non-heating months according the formula:

$$Q_{W,dis,non-heating.count} = Q_{non-heating.count} - Q_{W,non-heating.count}; \quad (2.1)$$

4. The energy for DHW needs $Q_{w,non\text{-}heating}$ and thermal energy losses in DHW circulation loop $Q_{W,dis,non\text{-}heating}$ for full non-heating season shall calculated as linear interpolation from the relevant data from months with non-heating according the formula:

$$Q_{W,non-heating} = Q_{W,non-heating.count}\frac{t_{non-heating}}{t_{non-heating.count}}; \quad (2.2)$$

$$Q_{W,dis,non-heating} = Q_{W,dis,non-heating.count}\frac{t_{non-heating}}{t_{non-heating.count}} \quad (2.3)$$

5. The difference of the DHW temperature ($\theta_{w,o}$) and inlet cold water temperature during heating ($\theta_{w,del,\ heating}$) and non-heating season ($\theta_{w,del,non\text{-}heating}$) should be taken into account to calculate the energy for DHW needs during heating season $Q_{w,heating}$ according to the formula:

$$Q_{W,heating} = Q_{W,non-heating.count}\frac{t_{heating}}{t_{non-heating.count}} \cdot \frac{(\theta_{W,o} - \theta_{w,del,heating})}{(\theta_{W,o} - \theta_{w,del,non-heating})} \quad (2.4)$$

6. The thermal losses of the DHW circulation loop $Q_{W,del,heating}$ depend on the temperature of the DHW in pipes sections i ($\Theta_{w,dis,avg,i}$) and the ambient temperature around the relevant DHW pipes sections i ($\Theta_{amb,i}$) during heating and non-heating seasons. Usually the temperature of the DHW in pipes have fixed value during heating and non-heating season. The average temperature around the pipes of sections on heated area of the building have equal value during heating and non-heating season, but the difference is caused by the pips outside the heated areas i.e. in non-heated basements and attics.

$$\begin{aligned} Q_{W,del,heating} &= Q_{W,dis,non-heating.count}\frac{t_{heating}}{t_{non-heating.count}} \\ &\cdot \frac{\sum_i \Psi_{W,i} \cdot L_{W,i} \cdot (\theta_{W,cirk,i} - \theta_{amb,i,heating})}{\sum_i \Psi_{W,i} \cdot L_{W,i} \cdot (\theta_{W,cirk,i} - \theta_{amb,i,non-heating})}; \end{aligned} \quad (2.5)$$

The calculations of the thermal losses in of the DHW circulation loop for the investigated buildings shows that the difference of ambient temperature during heating and non-heating season for the pipes outside the heating area affect the total circulation losses from 2% for twelve storied buildings, to 5 % for five storied buildings. This conclusion allows us to simplify the formula with substitution of the multiplier with differences of ambient temperatures with empiric coefficient K (with the values from 1.02 to 1.05).

$$Q_{W,dis,heating} = Q_{W,non-heating.count}\frac{t_{heating}}{t_{non-heating.count}} \cdot K; \quad (2.6)$$

The calculations according to the described method gives accurate energy performance indicators of the DHW system and gives the base to evaluate benefits of possible measures for the DHW system of the building.

To improve energy performance of the DHW system during energy audit of the building shall be considered implementation of the following measures:

- optimization of the operational settings by set up the day and night mode conditions, which include switching off during the night hours (for certain types of buildings switching off is possible also during holidays/weekends), the reduction of the temperature of DHW during the night hours;
- replacement of metal (steel or copper) pipes with the pipes with lower thermal conductivity;
- thermal insulation of the distribution pipes (effective for all uninsulated pipes);
- optimization of distribution network of the circulation pipes, for example, replacement of all or part of distribution pipes with one well insulated larger diameter central pipeline;
- installation of the hydraulic flow controllers (thermostatic, self-acting, proportional valves) on each section of the DHW circulation loop to ensure a balanced flow;
- replacement of the fixed power pump with demand controlled variable-speed pump that automatically adjusts to the hydraulic power needs and temperature settings;
- installation the waste water heat recovery system can be cost effective for the buildings with significant DHW consumption.

Economic impact of DHW system heat loss

The thermal losses of the DHW distribution circulation pipes system of the building consists of: thermal losses in the basement pipes during the whole year, thermal losses in the vertical distribution loop pipes during non-heating seasons. The thermal losses from the towel rails of the DHW distribution system gives comfort on bathrooms and may be useful throughout the whole year. As concluded in the section 1.4. characteristic thermal losses from the DHW circulation loop is average 20 kWh/m^2 per year for standard design type apartment buildings with originally installed DHW system steel pipes.

For a standard design type apartment building with total area of 4000 m^2 and typical thermal losses of the DHW systems (20 kWh/m^2 per year) the total thermal losses of the DHW systems is 80 MWh yearly and costs for the apartment owners is €4062 ([2]). After insulation (10 to 20 mm thickness with a thermal conduction 0.04 W/(m^2·K)) of the DHW pipes the linear thermal characteristic value of pipes range from 0.1 to 0.2 W/(m·K) or less. Such activities reduce the thermal losses from the DHW system for 70% or about 14 kWh/m^2/per year therefore yearly savings are 56 MWh of heat energy and costs € 2843.

According to the data of JSC “Ragas siltums” about 4000 apartment buildings with total heating area of 12 million m^2 connected to district heating network in Riga use heat energy for heating and DHW needs. Most of these buildings and their heating and DHW systems not improved since the building construction. The assessed thermal losses of DHW systems of these buildings are 240 GWh per year that cost € 12.2 million annually to apartment owners. The insulation of distribution pipes of the DHW systems of these buildings can save 168 GWh of heat energy and cost € 8.5 million annually.

As, a result of the research carried out it was found that

1. Frost heave occurs if the amount of the frozen and unfrozen water exceeds the volume of the soil interstices. Thus frost heaving normal stress is, on one hand, the function of the soil porosity on the other hand, it is the function of “excess moisture” resulting in the formation of “excess ice”. “Excess ice” is the amount of ice exceeding the free interstice volume not filled with frozen and unfrozen film water after freezing.

2. The normal stresses in the open system prove to be more reasonable.

3. The formulas (10, 11) for the normal stresses of frost heaving in the open system as a function of excess moisture exceeding the free soil interstitial volume under freezing, and their results appear to be relevant to the tabular data of RF Code available and other authors' results. The expression obtained make it possible to define normal stress in any hydrogeological and climatic conditions.

Conclusions

The DHW systems of the apartment buildings has the following typical characteristics:

- DHW consumption
  - ranges from 24.2 to 60.2 (in average 41.0) liters per inhabitant per day;
  - ranges from 40.0 to 142.6 liters per day per household (dwelling), in average 91.4. liters for buildings in Riga and 71.5 liters for buildings in Bauska;
  - 1.52 liters per day per one square meter of dwelling;
- DHW share of the total domestic water consumption varies during a year: it is 41,8% in average during whole year, 43,9% during heating season, 39,4% during non-heating season;
- DHW consumption is 94% from the annual average consumption during non-heating season and 106% from the annual average consumption during heating season;
- the energy consumption for DHW system ranges from 19.8 to 48.2 (in average 34.5) kWh/m^2 annually.
- the actual DHW consumption is less than specified in standard EN 15316-3-1 (from 100.2 to 199.8 liters per day per household) and in the Latvian Construction regulation LBN 221-15 (from 85 to 105 liters per inhabitant per day). Therefore, the appropriate national annexes of standard EN 15316-3-1 should developed with DHW consumption characteristics suitable for Latvian conditions.

[2] JSC “Rīgas Siltums” heat energy prise was 45.33 € per MWh On March 2017 (www.sprk.gov.lv), 12% VAT rete for heat energy for housing, heat energy bruto prise 50.77 € per MWh.

The comparison of correlations of DHW consumption to miscellaneous technical indicators shows that closest correlation is between the DHW consumption to the number of the inhabitants (R^2=0.94), however close coloration (R^2=0.88) is to the housing area and to the number of the households (R^2=0.85). There is no correlation between the DHW consumption and thermal losses in the DHW circulation loop.

The temperature of inlet cold water for heating and non-heating seasons (or months) used in the calculations have impact to the energy consumption of the DHW system. The study shows that the most accurate result can be achieve if the mean monthly value of inlet cold water temperature or seasonal mean value cold water temperatures (+5°C on heating season, +15°C on non-heating season) from Latvian Construction regulation LBN 221-15 are used in calculations. The calculation using mean annual cold-water temperature (either LBN 221 (+10°C) or EN 15316-3-1 (+13°C)) may cause error more than 10%.

The thermal energy loses of DHW circulation loop varies from 0.1 to 0.28 MWh per month per dwelling for different standard design type buildings, in average 0.18 MWh per month for buildings in Riga and 0.21 MWh per month for buildings in Bauska. The study shows that actual thermal energy loses of DHW circulation loop significantly exceed 0.1 MWh – the value recommended by Riga city council for one dwelling per month (24 of August 2010 Instruction No.9).

The heat losses of the DHW circulation loop has the following typical characteristics on apartment buildings:

- Representative non-recoverable energy losses of DHW circulation loop ranges from 16 to 24 and in average 20 kWh per m^2 per year investigated apartment buildings. The result is representative according to considerations that non-recoverable energy losses are in the basement during whole year, in vertical distribution pipes during non-heating season, but heat energy losses from towel rails are useful (not losses) during whole year.

- The thermal losses of t from total heat energy consumption of the DHW system ranges from 35% to 79% (in average 56%) during non-heating season;

- The thermal losses in the DHW distribution system differs by different standard design types of buildings;

- The share of heat losses for different pipe sections breakdown is:

  - from 10% to 25% for 5 and more storied buildings up to 28% for 3 storied buildings on pipe sections on non-heated basement;
  - from 50% to 70% for vertical distribution pipe sections;
  - from 20% to 30% for individual tower rails in dwellings.

The calculation of the auxiliary energy of the DHW system of the building by different CEN standard methods (simplified and detailed) gives similar results. The calculation according to simplified method shows that auxiliary energy of the DHW system ranges from 1.07 to 1.93 (in average 1.54) kWh/m^2 per year for different standard design type buildings, while calculation according to detailed method gives results from 1.54 to 1.82 (in average 1.62) kWh/m^2 per year. The authors find that detailed calculation method is too complicate and time consuming. Therefore, the simplified method is recommended for use for the buildings energy performance certification. As an alternative, the default value (for example, 2.0 kWh/m^2 per year) may adopted on national level.

References

1. Zhang L., Xia J., Thorsen J., Gudmundsson O., Li H., Svendsen S. Technical, economic and environmental investigation of using district heating to prepare domestic hot water in Chinese multi-storey buildings. *Energy.* 2016. Vol. 116. Pp. 281–292.
2. An J., Yan D., Deng G., Yu R. Survey and performance analysis of centralized domestic hot water system in China. *Energy and Buildings.* 2016. Vol. 133. Pp. 321–334.
3. Aki H., Wakui T., Yokoyama R. Development of a domestic hot water demand prediction model based on a bottom-up approach for residential energy management systems. *Applied Thermal Engineering.* 2016. Vol. 108. Pp. 697–708.
4. George D., Pearre N.S., Swan L.G. High resolution measured domestic hot water consumption of Canadian

Литература

1. Zhang L., Xia J., Thorsen J., Gudmundsson O., Li H., Svendsen S. Technical, economic and environmental investigation of using district heating to prepare domestic hot water in Chinese multi-storey buildings // Energy. 2016. Vol. 116. Pp. 281–292.
2. An J., Yan D., Deng G., Yu R. Survey and performance analysis of centralized domestic hot water system in China // Energy and Buildings. 2016. Vol. 133. Pp. 321–334.
3. Aki H., Wakui T., Yokoyama R. Development of a domestic hot water demand prediction model based on a bottom-up approach for residential energy management systems // Applied Thermal Engineering. 2016. Vol. 108. Pp. 697–708.
4. George D., Pearre N.S., Swan L.G. High resolution measured domestic hot water consumption of Canadian

homes. *Energy and Buildings.* 2015. Vol. 109. Pp. 304–315.

5. Koiv T.A., Kovshikov A. Changes in the heating load of domestic hot water and its impact on the design of the district heating network. *WSEAS transactions on environment and development.* 2015. Vol. 11. Pp. 108–115.
6. Grasmanis Dz., Mālnieks A., Jēkabsons A. Implementation of the EPBD in Latvia. Implementation of the Energy Performance of Building Directive (EPBD). *Construction Science.* 2011. Vol. 5. Pp. 223–234.
7. Grasmanis Dz. EPBD implementation in Latvia. 2013. Vol. 9. Pp. 237–246.
8. Tumanova K., Cimbale A. The technical-economic analysis of hot water supply systems for residential buildings // *Proceedings of REHVA Annual Conference 2015 "Advanced HVAC and Natural Gas Technologies".* 2015. Pp. 177–183.
9. Grasmanis Dz., Talcis N., Greķis A. Heat consumption assessment of the domestic hot water systems in the apartment buildings. *Construction Science.* 2013. Vol. 5. Pp. 38–43.
10. Ovchinnikov P., Borodiņecs A., Strelets K. Utilization potential of low temperature hydronic space heating systems: a comparative review. *Building and Environment.* 2017. Vol. 112. Pp. 88–98.
11. Tumanova K., Borodiņecs A. Heat consumption for hot water supply in residential buildings. *Innovations for Sustainable Future.* 2016. Vol. 3. Pp. 331–337.
12. Kalamees T., Lupíšek A., Sojková K., Mørck O., Borodiņecs A., Almeida M., Rovers R. What kind of heat loss requirements NZEB and deep renovation sets for building envelope? *Innovations for Sustainable Future.* 2016. Vol. 1. Pp. 137–144.
13. Grasmanis Dz., Talcis N., Greķis A. Heat consumption assessment of the domestic hot water systems in the apartment buildings. *Proceedings of REHVA Annual Conference.* 2015. Pp. 167–176.
14. Ovchinnikov P., Borodiņecs A., Millers R. Utilization potential of low temperature hydronic space heating systems in Russia. *Journal of Building Engineering.* 2017. Vol. 13. Pp. 1–10.
15. Liu F., Tian Z., Dong F., Yan C., Zhang R., Yan A. Experimental study on the performance of a gas engine heat pump for heating and domestic hot water. *Energy and Buildings.* 2017. Vol. 152. Pp. 273–278.
16. Lomet A., Suard F., Chèze D. Statistical modeling for real domestic hot water consumption forecasting. *Energy Procedia.* 2015. Vol. 70. Pp. 379–387.
17. Efimov A.Yu., Markov V.A. Analiz i ocenka problem sistem goryachego vodosnabzheniya [Analysis and evaluation of problems in hot water systems]. *Energoeffektivnye i resursosberegayushhie texnologii i sistemy mezhvuzovskij sbornik nauchnyx trudov.* 2016. No. 1. Pp. 167–173. (rus)
18. Efimov A.Yu., Krylov A.Yu. Analiz i reshenie problem sistem goryachego vodosnabzheniya [Analysis and solution of problems of hot water systems]. *Sovremennye tendencii razvitiya nauki i texnologij.* 2017. No. 3-4. Pp. 34–39. (rus)
19. Moore A.D., Urmee T., Bahri P.A., Rezvani S., Baverstock G.F. Life cycle assessment of domestic hot water systems in Australia. *Renewable Energy.* 2017. Vol. 103. Pp. 187–196.
20. Ahmed K., Pylsy P., Kurnitski J. Monthly domestic hot water profiles for energy calculation in Finnish apartment buildings. *Energy and Buildings.* 2015. Vol. 97. Pp. 77–85.
21. Belz K., Kuznik F., Werner K.F., Schmidt T., Ruck W.K.L. Thermal energy storage systems for heating and hot water in residential buildings. *Advances in Thermal Energy Storage Systems.* 2015. Vol. 4. Pp. 441–465.
22. Biryuzova E.A., Ogurcova K.I. Issledovanie meropriyatij po

homes // Energy and Buildings. 2015. Vol. 109. Pp. 304–315.

5. Koiv T.A., Kovshikov A. Changes in the heating load of domestic hot water and its impact on the design of the district heating network // WSEAS transactions on environment and development. 2015. Vol.11. Pp. 108–115.
6. Grasmanis Dz., Mālnieks A., Jēkabsons A. Implementation of the EPBD in Latvia. Implementation of the Energy Performance of Building Directive (EPBD) // Construction Science. 2011. Vol. 5. Pp. 223–234.
7. Grasmanis Dz. EPBD implementation in Latvia. 2013. Vol. 9. Pp. 237–246.
8. Tumanova K., Cimbale A. The technical-economic analysis of hot water supply systems for residential buildings // Proceedings of REHVA Annual Conference 2015 "Advanced HVAC and Natural Gas Technologies". 2015. Pp. 177–183.
9. Grasmanis Dz., Talcis N., Greķis A. Heat consumption assessment of the domestic hot water systems in the apartment buildings // Construction Science. 2013. Vol. 5. Pp. 38–43.
10. Ovchinnikov P., Borodiņecs A., Strelets K. Utilization potential of low temperature hydronic space heating systems: a comparative review // Building and Environment. 2017. Vol. 112. Pp. 88–98.
11. Tumanova K., Borodiņecs A. Heat consumption for hot water supply in residential buildings // Innovations for Sustainable Future. 2016. Vol. 3. Pp. 331–337.
12. Kalamees T., Lupíšek A., Sojková K., Mørck O., Borodiņecs A., Almeida M., Rovers R. What kind of heat loss requirements NZEB and deep renovation sets for building envelope? // Innovations for Sustainable Future. 2016. Vol.1. Pp. 137–144.
13. Grasmanis Dz., Talcis N., Greķis A. Heat consumption assessment of the domestic hot water systems in the apartment buildings // Proceedings of REHVA Annual Conference. 2015. Pp. 167–176.
14. Ovchinnikov P., Borodiņecs A., Millers R. Utilization potential of low temperature hydronic space heating systems in Russia // Journal of Building Engineering. 2017. Vol. 13. Pp. 1–10.
15. Liu F., Tian Z., Dong F., Yan C., Zhang R., Yan A. Experimental study on the performance of a gas engine heat pump for heating and domestic hot water // Energy and Buildings. 2017. Vol. 152. Pp. 273–278.
16. Lomet A., Suard F., Chèze D. Statistical modeling for real domestic hot water consumption forecasting // Energy Procedia. 2015. Vol. 70. Pp. 379–387.
17. Ефимов А.Ю., Марков В.А. Анализ и оценка проблем систем горячего водоснабжения // Энергоэффективные и ресурсосберегающие технологии и системы межвузовский сборник научных трудов. 2016. № 1. С. 167–173.
18. Ефимов А.Ю., Крылов А.Ю. Анализ и решение проблем систем горячего водоснабжения // Современные тенденции развития науки и технологий. 2017. № 3-4. С. 34–39.
19. Moore A.D., Urmee T., Bahri P.A., Rezvani S., Baverstock G.F. Life cycle assessment of domestic hot water systems in Australia // Renewable Energy. 2017. Vol. 103. Pp. 187–196.
20. Ahmed K., Pylsy P., Kurnitski J. Monthly domestic hot water profiles for energy calculation in Finnish apartment buildings // Energy and Buildings. 2015. Vol. 97. Pp. 77–85.
21. Belz K., Kuznik F., Werner K.F., Schmidt T., Ruck W.K.L. Thermal energy storage systems for heating and hot water in residential buildings // Advances in Thermal Energy Storage Systems. 2015. Vol. 4. Pp. 441–465.
22. Бирюзова Е.А., Огурцова К.И. Исследование мероприятий по повышению энергоэффективности системы ГВС // Вестник гражданских инженеров. 2012.

povysheniyu energoeffektivnosti sistemy GVS [A study of measures to improve the energy efficiency of the domestic hot water system]. *Vestnik grazhdanskix inzhenerov.* 2012. No. 4(33). Pp. 188–192. (rus)

23. Nemova D.V., Vatin N.I., Gorshkov A.S., Kashabin A.V., Rymkevich P.P. Tekhniko-ekonomicheskoye obosnovaniye meropriyatiy po utepleniyu ograzhdayushchikh konstruktsiy individualnogo zhilogo doma [Feasibility study of measures for insulation of the enclosing structures of individual houses]. *Construction of Unique Buildings and Structures.* 2014. No. 8(23). Pp. 93–115. (rus)
24. Gorshkov A.S., Nemova D.V., Vatin N.I. Formula energoeffektivnosti [The formula of energy efficiency]. *Construction of Unique Buildings and Structures.* 2013. No. 7(12). Pp. 49–63. (rus)
25. Sovetnikov D.O. Stroitelstvo zdaniya, otvechayushchego standartam passivnogo doma [Construction of building in accordance with passive house standards]. *Construction of Unique Buildings and Structures.* 2014. No. 9(24). Pp. 11–25. (rus)
26. Korniyenko S.V. Monitoring of energy efficiency in buildings at the Russian construction norms. *BST — Bulletin of Construction Equipment.* 2017. Vol. 6(994). Pp. 46–49.
27. Afanasyev V.V., Kovalev V.G., Tarasov V.A., Tarasova V.V., Fedorov D.G. Issledovaniye raskhoda teplovoy energii na otopleniye zdaniy [Statistical analysis of the heat flow in heating]. *Vestnik Chuvashskogo universiteta.* 2014. No. 2. Pp. 10–18. (rus)
28. Zhou S., Cui W., Zhao S., Zhu S. Operation analysis and performance prediction for a GSHP system compounded with domestic hot water (DHW) system. *Energy and Buildings.* 2016. Vol. 119. Pp. 153–163.
29. Budhko Z., Zebergs V. Investigation of the domestic hot water consumption in the apartment building. *Construction Science.* 2009. Vol. 10. No. 10. Pp. 42–50.

№ 4(33). С. 188–192.

23. Немова Д.В., Ватин Н.И., Горшков А.С., Кашабин А.В., Рымкевич П.П., Цейтин Д.Н. Технико-экономическое обоснование мероприятий по утеплению ограждающих конструкций индивидуального жилого дома // Строительство уникальных зданий и сооружений. 2014. № 8(23). С. 93–115.
24. Горшков А.С., Немова Д.В., Ватин Н.И. Формула энергоэффективности // Строительство уникальных зданий и сооружений. 2013. № 7(12). С. 49–63.
25. Советников Д.О. Строительство здания, отвечающего стандартам пассивного дома // Строительство уникальных зданий и сооружений. 2014. № 9(24). С. 11–25.
26. Korniyenko S.V. Monitoring of energy efficiency in buildings at the Russian construction norms // BST — Bulletin of Construction Equipment. 2017. Vol. 6(994). Pp. 46–49.
27. Афанасьев В.В., Ковалёв В.Г., Тарасов В.А., Тарасова В.В., Федоров Д.Г. Исследование расхода тепловой энергии на отопление зданий // Вестник Чувашского университета. 2014. № 2. С. 10–18.
28. Zhou S., Cui W., Zhao S., Zhu S. Operation analysis and performance prediction for a GSHP system compounded with domestic hot water (DHW) system // Energy and buildings. 2016. Vol. 119. Pp. 153–163.
29. Budhko Z., Zebergs V. Investigation of the domestic hot water consumption in the apartment building // Construction Science. 2009. Vol. 10. № 10. Pp. 42–50.

Dzintars Grasmanis,
+7(911)111-11-11; dzintars.grasmanis@gmail.com

Daniil Sovetnikov,
+7(911)901-90-58; sovetnikov.daniil@gmail.com

Daria Baranova,
+7(921)640-12-00; baranova-d@mail.ru

Дзинтарс Грасманис,
+7(911)111-11-11;
эл. почта: dzintars.grasmanis@gmail.com

Даниил Олегович Советников,
+7(911)901-90-58;
эл. почта: sovetnikov.daniil@gmail.com

Дарья Вадимовна Баранова,
+7(921)640-12-00;
эл. почта: baranova-d@mail.ru

doi: 10.18720/MCE.76.14

Stress-strain state of three-layered shallow shells under conditions of nonlinear creep

Напряженно-деформированное состояние трехслойных пологих оболочек в условиях нелинейной ползучести

A.S. Chepurnenko,
Don State Technical University, Rostov-on-Don, Russia

Канд. техн. наук, ст. преподаватель А.С. Чепурненко,
Донской государственный технический университет, г.Ростов-на-Дону, Россия

Key words: nonlinear creep; three-layer constructions; plates; shells; numerical methods

Ключевые слова: нелинейная ползучесть; трехслойные конструкции; пластины; оболочки; численные методы

Abstract. The resolving equations were obtained and a calculation technique was developed with allowance for the nonlinear creep of three-layer plates and shallow shells with a lightweight filler. The problem was reduced to a system of three differential equations with respect to the stress function, displacement and deflection function. An example is given of calculating a rectangular planar shell in the form of an elliptical paraboloid. The solution was performed numerically by the finite difference method in combination with the Euler method for determining creep strains. The linear Maxwell-Thompson equation and the Maxwell-Gurevich nonlinear equation were used as the creep law. There were no significant discrepancies between the results obtained on the basis of the linear and nonlinear theory. It was established that, as the curvature of the shell increases, the creep of the aggregate has a lesser effect on the deflection value. It was revealed that for shells of greater curvature with constant displacements a redistribution of stresses and internal forces occurs. The bending and twisting moments decrease, and the longitudinal and shearing forces increase. In the aggregate, the tangential stresses relax, while in the sheaths the normal and tangential stresses increase.

Аннотация. Получены разрешающие уравнения и разработана методика расчета с учетом нелинейной ползучести трехслойных пластин и пологих оболочек с легким заполнителем. Задача свелась к системе из трех дифференциальных уравнений относительно функции напряжений, функции перемещений и прогиба. Приведен пример расчета прямоугольной в плане пологой оболочки в форме эллиптического параболоида. Решение выполнялось численно методом конечных разностей в сочетании с методом Эйлера для определения деформаций ползучести. В качестве закона ползучести использовано линейное уравнение Максвелла-Томпсона и нелинейное уравнение Максвелла-Гуревича. Существенных расхождений между результатами, полученными на основе линейной и нелинейной теории, не выявлено. Установлено, что с увеличением кривизны оболочки ползучесть заполнителя оказывает меньшее влияние на величину прогиба. Выявлено, что для оболочек большей кривизны при постоянных перемещениях происходит перераспределение напряжений и внутренних усилий. Изгибающие и крутящие моменты убывают, а продольные и сдвигающие силы возрастают. В заполнителе происходит релаксация касательных напряжений, а в обшивках нормальные и касательные напряжения возрастают.

Introduction

Three-layer structures with lightweight filler are widely used in various industries, including civil and industrial construction, aircraft construction, shipbuilding, etc. With the same flexural rigidity, such structures are much lighter then single-layer panels. As a filler of three-layered structures, polymeric materials are widely used, for which, in addition to elastic properties, viscoelasticity is characteristic. Therefore, to adequately describe the stress-strain state of three-layer structures, it is necessary to involve the apparatus of the theory of creep. There is a large number of papers devoted to the calculation taking into account the creep of three-layer beams, including [1–7]. As for the plates and shells, in most papers the calculation is considered only in the elastic stage [8–10]. In [11–12] the solution of the problem of axisymmetric bending of circular plates with a nonlinear elastic filler is given. In this case, only instantaneous nonlinearity is taken into account. In [13], a three-layered shell model with a lightweight filler is used to describe the linear creep of a reinforced concrete structure. The linear creep of three-layer plates and shells is also investigated in the author's papers [14–16].

In this paper, we will consider the technique for calculating plates and shallow shells, suitable for arbitrary creep laws, including nonlinear ones.

Methods

The element of the three-layered shallow shell is shown in Figure 1. In the calculation, we will use the technical theory of three-layer structures, according to which the bending and twisting moments, as well as the shear and longitudinal forces are completely perceived by the carrier layers. The filler only works on shear, taking transverse forces. The thickness of the carrier layers δ is the same and small compared to the total shell thickness h.

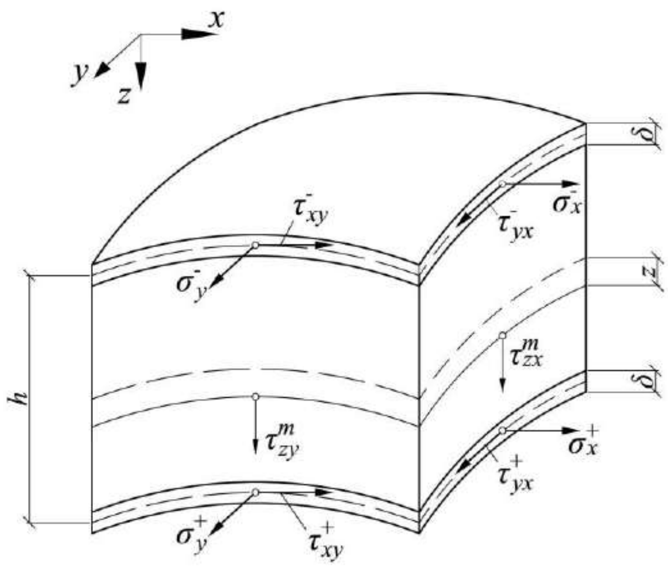

Figure 1. Element of a three-layered shallow shell

Equilibrium equations for the element of a three-layered shallow shell are written in the form:

$$\frac{\partial N_x}{\partial x}+\frac{\partial S}{\partial y}=0;\ \frac{\partial S}{\partial x}+\frac{\partial N_y}{\partial y}=0;$$
$$\frac{\partial M_x}{\partial x}+\frac{\partial H}{\partial y}-Q_x=0;\ \frac{\partial M_y}{\partial y}+\frac{\partial H}{\partial x}-Q_y=0; \qquad (1)$$
$$\frac{\partial Q_x}{\partial x}+\frac{\partial Q_y}{\partial y}-k_xN_x-k_yN_y+q=0,$$

where N_x, N_y – longitudinal forces; S – shear force; M_x, M_y – bending moments; H – torque; Q_x, Q_y – transverse forces; q – surface load, $k_x \approx -\frac{\partial^2 z}{\partial x^2}, k_y \approx -\frac{\partial^2 z}{\partial y^2}$ – principal curvatures.

To satisfy the first two equilibrium equations in (1), we introduce the stress function according to the formulas:

$$N_x=\frac{\partial^2\Phi}{\partial y^2},\qquad N_y=\frac{\partial^2\Phi}{\partial x^2},\qquad S=-\frac{\partial^2\Phi}{\partial x\partial y}. \qquad (2)$$

Bending moments and torque are related to the stresses in the carrier layers as follows:

$$M_x=(\sigma_x^+-\sigma_x^-)\delta\frac{h}{2};\ M_y=\left(\sigma_y^+-\sigma_y^-\right)\delta\frac{h}{2};\ H=\left(\tau_{xy}^+-\tau_{xy}^-\right)\delta\frac{h}{2}. \qquad (3)$$

Longitudinal and shear forces are written as:

$$N_x=(\sigma_x^++\sigma_x^-)\delta;\ N_y=\left(\sigma_y^++\sigma_y^-\right)\delta;\ S=\left(\tau_{xy}^++\tau_{xy}^-\right)\delta. \qquad (4)$$

For tangential stresses in the aggregate, a uniform thickness distribution is adopted:

$$Q_x=\tau_{zx}^m h;\ Q_y=\tau_{zy}^m h. \qquad (5)$$

Deformations of the carrier layers can be written as:

$$\varepsilon_x^{+(-)} = \frac{\partial u^{+(-)}}{\partial x} + k_x w;$$
$$\varepsilon_y^{+(-)} = \frac{\partial v^{+(-)}}{\partial y} + k_y w; \qquad (6)$$
$$\gamma_{xy}^{+(-)} = \frac{\partial u^{+(-)}}{\partial y} + \frac{\partial v^{+(-)}}{\partial x},$$

where $u^{+(-)}$, $v^{+(-)}$ – displacements of the lower (upper) skin along the axes x and y, w – deflection.

For the displacements of the filler, a linear thickness distribution is adopted:

$$u^m = \frac{u^- + u^+}{2} + \frac{u^+ - u^-}{h} z = u + \alpha z;$$
$$v^m = \frac{v^- + v^+}{2} + \frac{v^+ - v^-}{h} z = v + \beta z. \qquad (7)$$

Shear strains of the filler are defined as follows:

$$\gamma_{zx}^m = \frac{\partial u^m}{\partial z} + \frac{\partial w}{\partial x} = \alpha + \frac{\partial w}{\partial x};$$
$$\gamma_{zy}^m = \frac{\partial v^m}{\partial z} + \frac{\partial w}{\partial y} = \beta + \frac{\partial w}{\partial y}. \qquad (8)$$

When calculating, we assume that the carrier layers work elastically, and the middle layer is viscoelastic. The stresses in the carrier layers of the shell are determined as follows:

$$\sigma_x^{+(-)} = \frac{E}{1-\nu^2}\left(\varepsilon_x^{+(-)} + \nu\varepsilon_y^{+(-)}\right);$$
$$\sigma_y^{+(-)} = \frac{E}{1-\nu^2}\left(\varepsilon_y^{+(-)} + \nu\varepsilon_x^{+(-)}\right); \qquad (9)$$
$$\tau_{xy}^{+(-)} = \frac{E}{2(1+\nu)}\gamma_{xy}^{+(-)}.$$

Deformations of the filler represent the sum of elastic deformations and creep strains:

$$\gamma_{zx}^m = \frac{\tau_{zx}^m}{G_m} + \gamma_{zx}^*; \; \gamma_{zy}^m = \frac{\tau_{zy}^m}{G_m} + \gamma_{zy}^*, \qquad (10)$$

where G_m – shear modulus of the middle layer, γ_{zx}^* and γ_{zy}^* – creep strains of the middle layer.

We express from (9) the stresses through deformations:

$$\tau_{zx}^m = G_m(\gamma_{zx}^m - \gamma_{zx}^*) = G_m\left(\alpha + \frac{\partial w}{\partial x} - \gamma_{zx}^*\right);$$
$$\tau_{zy}^m = G_m(\gamma_{zy}^m - \gamma_{zy}^*) = G_m\left(\beta + \frac{\partial w}{\partial y} - \gamma_{zy}^*\right). \qquad (11)$$

Then the transverse forces will take the form:

$$Q_x = G_m h\left(\alpha + \frac{\partial w}{\partial x} - \gamma_{zx}^*\right);$$
$$Q_y = G_m h\left(\beta + \frac{\partial w}{\partial y} - \gamma_{zy}^*\right). \qquad (12)$$

Substituting (6) into (9) and then (9) into (3), we obtain:

$$M_x = D\left(\frac{\partial \alpha}{\partial x} + \nu\frac{\partial \beta}{\partial y}\right);$$
$$M_y = D\left(\nu\frac{\partial \alpha}{\partial x} + \frac{\partial \beta}{\partial y}\right); \qquad (13)$$
$$H = \frac{D(1-\nu)}{2}\left(\frac{\partial \alpha}{\partial y} + \frac{\partial \beta}{\partial x}\right),$$

where $D = \frac{E\delta h^2}{2(1-\nu^2)}$ – cylindrical rigidity of a three-layer shell.

For longitudinal forces, taking into account (9) and (4), we can write:

$$N_x = \frac{E\delta}{1-\nu^2}\left(\varepsilon_x^+ + \varepsilon_x^- + \nu(\varepsilon_x^+ + \varepsilon_x^-)\right) = \frac{E\delta}{1-\nu^2}\Big(\frac{\partial u^+}{\partial x} + \frac{\partial u^-}{\partial x} +$$
$$+2\left(k_x + \nu k_y\right)w + \nu\left(\frac{\partial v^+}{\partial y} + \frac{\partial v^-}{\partial y}\right)\Big) = \frac{2E\delta}{1-\nu^2}\left(\frac{\partial u}{\partial x} + \nu\frac{\partial v}{\partial y} + \left(k_x + \nu k_y\right)w\right);$$
$$N_y = \frac{2E\delta}{1-\nu^2}\left(\frac{\partial v}{\partial y} + \nu\frac{\partial u}{\partial x} + \left(k_y + \nu k_x\right)w\right); \tag{14}$$
$$S = \frac{E\delta}{1+\nu}\left(\frac{\partial u}{\partial y} + \frac{\partial v}{\partial x}\right).$$

By analogy with the average displacements u and v, we introduce the values of the average deformations of the carrier layers by the formulas:

$$\varepsilon_x^0 = \frac{\partial u}{\partial x}; \quad \varepsilon_y^0 = \frac{\partial w}{\partial y}; \quad \gamma_{xy}^0 = \frac{\partial u}{\partial y} + \frac{\partial v}{\partial x}. \tag{15}$$

For the values introduced by formulas (15), the deformation compatibility equation is valid:

$$\frac{\partial^2 \varepsilon_x^0}{\partial y^2} + \frac{\partial^2 \varepsilon_y^0}{\partial x^2} = \frac{\partial^2 \gamma_{xy}^0}{\partial x \partial y}. \tag{16}$$

We express from the relations (14) the values ε_x^0, ε_y^0 и γ_{xy}^0:

$$\varepsilon_x^0 = \frac{1}{2E\delta}\left(N_x - \nu N_y\right) - k_x w = \frac{1}{2E\delta}\left(\frac{\partial^2\Phi}{\partial y^2} - \nu\frac{\partial^2\Phi}{\partial x^2}\right) - k_x w;$$
$$\varepsilon_y^0 = \frac{1}{2E\delta}\left(N_y - \nu N_x\right) - k_y w = \frac{1}{2E\delta}\left(\frac{\partial^2\Phi}{\partial x^2} - \nu\frac{\partial^2\Phi}{\partial y^2}\right) - k_y w; \tag{17}$$
$$\gamma_{xy}^0 = \frac{1+\nu}{E\delta}S = -\frac{1+\nu}{E\delta}\frac{\partial^2\Phi}{\partial x \partial y}.$$

Substituting (17) into the deformation compatibility equation (16), we obtain the first resolving equation:

$$\frac{1}{2E\delta}\nabla^4\Phi - k_x\frac{\partial^2 w}{\partial y^2} - k_y\frac{\partial^2 w}{\partial x^2} = 0. \tag{18}$$

To obtain the second resolving equation, we substitute the formulas of the transverse forces (12) into the last equation of equilibrium in (1):

$$G_m h\left(\frac{\partial\alpha}{\partial x} + \frac{\partial\beta}{\partial y} + \nabla^2 w - \frac{\partial\gamma_{zx}^*}{\partial x} - \frac{\partial\gamma_{zy}^*}{\partial y}\right) = -q + k_x\frac{\partial^2\Phi}{\partial y^2} + k_y\frac{\partial^2\Phi}{\partial x^2}. \tag{19}$$

We introduce the displacement function F by the formula:

$$F = \frac{\partial\alpha}{\partial x} + \frac{\partial\beta}{\partial y}. \tag{20}$$

Then equation (19) takes the form:

$$\nabla^2 w - \frac{1}{G_m h}\left(k_x\frac{\partial^2\Phi}{\partial y^2} + k_y\frac{\partial^2\Phi}{\partial x^2}\right) = -\frac{q}{G_m h} - F + \frac{\partial\gamma_{zx}^*}{\partial x} + \frac{\partial\gamma_{zy}^*}{\partial y}. \tag{21}$$

We exclude the transverse forces from the last three equilibrium equations in (1):

$$\frac{\partial^2 M_x}{\partial x^2} + 2\frac{\partial^2 H}{\partial x \partial y} + \frac{\partial^2 M_y}{\partial y^2} - k_x N_x - k_y N_y + q = 0. \tag{22}$$

The third resolving equation is obtained by substituting (13) into (22):

$$D\nabla^2 F = -q + k_x\frac{\partial^2\Phi}{\partial y^2} + k_y\frac{\partial^2\Phi}{\partial x^2}. \tag{23}$$

Thus, the problem of calculating a shallow three-layer shell reduces to a system of three differential equations (18), (21), and (23). Instead of two second-order equations (21) and (23) with respect to the functions w, F and Φ, we can obtain a fourth-order equation with respect to the deflection and stress function. For this we express from (21) the value F:

$$F = -\nabla^2 w + \frac{1}{G_m h}\left(k_x \frac{\partial^2 \Phi}{\partial y^2} + k_y \frac{\partial^2 \Phi}{\partial x^2} - q\right) + \frac{\partial \gamma_{zx}^*}{\partial x} + \frac{\partial \gamma_{zy}^*}{\partial y}. \qquad (24)$$

Further we substitute (24) into (23):

$$\begin{gathered}\nabla^4 w - \frac{1}{G_m h}\nabla^2\left(k_x \frac{\partial^2 \Phi}{\partial y^2} + k_y \frac{\partial^2 \Phi}{\partial x^2}\right) + \frac{1}{D}\left(k_x \frac{\partial^2 \Phi}{\partial y^2} + k_y \frac{\partial^2 \Phi}{\partial x^2}\right) = \\ = \frac{q}{D} - \frac{1}{G_m h}\nabla^2 q + \nabla^2\left(\frac{\partial \gamma_{zx}^*}{\partial x} + \frac{\partial \gamma_{zy}^*}{\partial y}\right).\end{gathered} \qquad (25)$$

The solution of the system of equations (18) and (25) makes it possible to determine the deflection, as well as longitudinal and shearing forces. However, to calculate the bending moments, torque and shear forces, it is required to find the functions α and β. To obtain the resolving equations for α and β, we substitute (13) in the third and fourth equation (1):

$$\begin{gathered}Q_x = \frac{\partial M_x}{\partial x} + \frac{\partial H}{\partial y} = D\left(\frac{\partial^2 \alpha}{\partial x^2} + \frac{1+\nu}{2}\frac{\partial^2 \beta}{\partial x \partial y} + \frac{1-\nu}{2}\frac{\partial^2 \alpha}{\partial y^2}\right); \\ Q_y = \frac{\partial M_y}{\partial y} + \frac{\partial H}{\partial x} = D\left(\frac{\partial^2 \beta}{\partial y^2} + \frac{1+\nu}{2}\frac{\partial^2 \alpha}{\partial x \partial y} + \frac{1-\nu}{2}\frac{\partial^2 \beta}{\partial x^2}\right).\end{gathered} \qquad (26)$$

Using the displacement function F, we exclude the function β from the first equation in (26), and the function α from the second:

$$\begin{gathered}Q_x = \frac{D}{2}\left((1-\nu)\nabla^2 \alpha + (1+\nu)\frac{\partial F}{\partial x}\right); \\ Q_y = \frac{D}{2}\left((1-\nu)\nabla^2 \beta + (1+\nu)\frac{\partial F}{\partial y}\right).\end{gathered} \qquad (27)$$

Equating (27) to (12), we obtain:

$$\begin{gathered}\nabla^2 \alpha - \frac{2G_m h}{D(1-\nu)}\alpha = \frac{2G_ь h}{D(1-\nu)}\left(\frac{\partial w}{\partial x} - \gamma_{zx}^*\right) - \frac{1+\nu}{1-\nu}\frac{\partial F}{\partial x}. \\ \nabla^2 \beta - \frac{2G_m h}{D(1-\nu)}\beta = \frac{2G_m h}{D(1-\nu)}\left(\frac{\partial w}{\partial y} - \gamma_{zy}^*\right) - \frac{1+\nu}{1-\nu}\frac{\partial F}{\partial y}.\end{gathered} \qquad (28)$$

Thus, to determine the functions α and β, it is necessary to first find the displacement function F, therefore, the use of Eq. (25) instead of (21) and (23) is inexpedient.

After calculating the longitudinal forces, bending and twisting moments stresses in the carrier layers can be found by the formulas:

$$\begin{gathered}\sigma_x^+ = \frac{N_x}{2\delta} + \frac{M_x}{h\delta}; \quad \sigma_x^- = \frac{N_x}{2\delta} - \frac{M_x}{h\delta}; \\ \sigma_y^+ = \frac{N_y}{2\delta} + \frac{M_y}{h\delta}; \quad \sigma_y^- = \frac{N_y}{2\delta} - \frac{M_y}{h\delta}; \\ \tau_{xy}^+ = \frac{S}{2\delta} + \frac{H}{h\delta}; \quad \tau_{xy}^- = \frac{S}{2\delta} - \frac{H}{h\delta}.\end{gathered} \qquad (29)$$

We consider the calculation technique using the example of a three-layered shallow shell rectangular in plan, the surface of which is an elliptical paraboloid (Fig. 2). The equation of the shell surface is:

$$z = f\left[\frac{f_1}{f}\left(2\frac{x}{a} - 1\right)^2 + \frac{f_2}{f}\left(2\frac{y}{b} - 1\right)^2 - 1\right], \qquad (30)$$

where $f = f_1 + f_2$ – shell elevation.

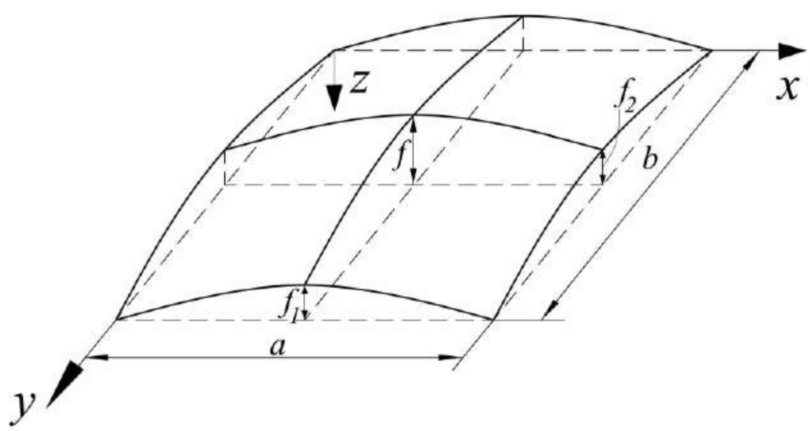

Figure 2. Rectangular in the plan shallow shell in the form of an elliptical paraboloid

The principal curvatures of the considered shell are determined as follows:

$$k_x = -\frac{\partial^2 z}{\partial x^2} = -\frac{8f_1}{a^2};$$
$$k_y = -\frac{\partial^2 z}{\partial y^2} = -\frac{8f_2}{b^2}. \tag{31}$$

In the calculations, we assume that along the contour the shell is connected to diaphragms absolutely rigid in their plane and flexible from it. The boundary conditions on the edges have the form:

at $x = 0$, $x = a$:

$$w = 0;\ M_x = 0;\ N_x = \frac{\partial^2 \Phi}{\partial y^2} = 0;\ v^+ = v^- = 0. \tag{32}$$

at $y = 0$, $y = b$:

$$w = 0;\ M_y = 0;\ N_y = \frac{\partial^2 \Phi}{\partial x^2} = 0;\ \ u^+ = u^- = 0. \tag{33}$$

From the last equality in (32) it follows that at the edges $x = 0$ and $x = a$:

$$\beta = \frac{v^+ - v^-}{h} = 0. \tag{34}$$

Then on these edges the derivative $\frac{\partial \beta}{\partial y}$ automatically vanishes. In order for the bending moment M_x to be zero it is necessary that the derivative $\frac{\partial \alpha}{\partial x}$ is equal to zero. Then for the edges $x = 0$, $x = a$ we can write:

$$w = 0;\ \frac{\partial^2 \Phi}{\partial y^2} = 0;\ F = \frac{\partial \alpha}{\partial x} + \frac{\partial \beta}{\partial y} = 0. \tag{35}$$

Similarly for the edges $y = 0$ and $y = b$:

$$w = 0;\ \frac{\partial^2 \Phi}{\partial x^2} = 0;\ F = 0. \tag{36}$$

To solve the system of differential equations (18), (21) and (23), one more boundary condition is necessary with respect to the stress function Φ. As this condition we use the equality of Φ function to zero at the edges.

The boundary conditions for the α function have the form:

at $x = 0, x = a$: $\frac{\partial \alpha}{\partial x} = 0$;

at $y = 0, y = b$: $\alpha = 0$.

For the function β, the boundary conditions are written as:

at $x = 0, x = a$: $\beta = 0$;

at $y = 0, y = b$: $\frac{\partial \beta}{\partial y} = 0$.

The system of equations (18), (21) and (23) was solved numerically by the finite difference method in combination with Euler's method for determining creep strains. Calculations were performed in the Matlab package. The time interval at which the creep process was considered we divided into n steps Δt. The first step was the solution of the elastic problem with $t = 0$, $\gamma_{zx}^* = 0$, $\gamma_{zy}^* = 0$. After defining the functions Φ, w and F the numerical solution of equations (28) was performed. Next, the stresses in the shells and filler were determined. If the creep law is given in differential form, then the stresses can be used to calculate the growth rates of creep strains, as well as creep strains at time $t + \Delta t$ by linear approximation:

$$\gamma_{t+\Delta t}^* = \gamma_t^* + \frac{\partial \gamma^*}{\partial t}\Delta t. \tag{37}$$

Note that for three-layered plates in comparison with shells, the calculation is much simpler, since instead of a system of three differential equations, it is sufficient to solve successively the following two equations:

$$D\nabla^2 F = -q;$$
$$\nabla^2 w = -\frac{q}{G_m h} - F + \frac{\partial \gamma_{zx}^*}{\partial x} + \frac{\partial \gamma_{zy}^*}{\partial y}. \tag{38}$$

The first equation in (38) does not include creep strains, which implies that the displacement function F for a three-layer plate does not depend on time, and it is not necessary to solve this equation at every time step, but only once. After determining the functions F and w, the functions α and β are determined from Eqs. (28).

Results and Discussion

The calculation was made for a rectangular shell with dimensions $a = b = 3$ m, overall thickness $h = 8$ cm, loaded by uniformly distributed over the area the load q. Carrier layers of the shell were steel with thickness of 1 mm ($E = 2 \cdot 10^5$ MPa, $\nu = 0.3$). The middle layer is a rigid polyurethane foam ($G_m = 4.85$ MPa).

As the creep law, the Maxwell-Thompson linear equation was used, as well as the nonlinear Maxwell-Gurevich equation. For uniaxial tension (compression), the Maxwell-Thompson equation has the form [17]:

$$nE\frac{\partial \varepsilon}{\partial t} + H\varepsilon = n\frac{\partial \sigma}{\partial t} + \sigma, \tag{39}$$

where E and H – respectively, instantaneous and long-term elastic moduli, n – relaxation time, σ – normal stress, ε – full strain.

For the case of pure shear, equation (39) can be written in the form:

$$nG_m\frac{\partial \gamma}{\partial t} + H\gamma = n\frac{\partial \tau}{\partial t} + \tau. \tag{40}$$

Here G_m and H are respectively the instantaneous and long-term shear moduli, τ is the tangential stress, and γ is the total shear deformation.

Representing the total deformation as the sum of elastic deformation and creep deformation, we can express from (40) the growth rate of creep strains in the following form:

$$\frac{\partial \gamma_i^*}{\partial t} = \frac{1}{\kappa}\left[\left(1 - \frac{H}{G_m}\right)\tau_i - H\gamma_i^*\right], \tag{41}$$

where $\kappa = nG_m$ – coefficient of viscosity of the filler.

To determine the deformations γ_{zx}^* and γ_{zy}^* it suffices to substitute the corresponding indices in (41) instead of i.

The Maxwell-Gurevich equation in the case of a triaxial stress state is written in the form [18]:

$$\frac{\partial \varepsilon_{ij}^*}{\partial t} = \frac{f_{ij}^*}{\eta^*}, \qquad i = x, y, z, \qquad j = x, y, z, \tag{42}$$

where f_{ij} – stress function, η^* – relaxation viscosity.

$$f_{ij}^* = \frac{3}{2}\left(\sigma_{ij} - p\delta_{ij}\right) - E_\infty \varepsilon_{ij}^*;$$
$$\eta^* = \eta_0^* \ \exp\left(-\frac{|f_{max}^*|}{m^*}\right), \qquad (43)$$

where δ_{ij} – Kronecker symbol, $p = (\sigma_x + \sigma_y + \sigma_z)/3$ – mean stress, m^* – the relaxation constant, called the velocity modulus, η_0^* – initial relaxation viscosity, E_∞ – high elasticity modulus.

When using equation (43), it is necessary to bear in mind that $\varepsilon_{zx}^* = \frac{1}{2}\gamma_{zx}^*$ and $\varepsilon_{zy}^* = \frac{1}{2}\gamma_{zy}^*$.

The results of tests of rigid polyurethane foam in shear creep are presented in [1–2]. The creep curves in the above studies are approximated by the Findley power law, which in the case of uniaxial tension is:

$$\varepsilon = \sigma\left(\frac{1}{E_e} + \frac{1}{E_t}t^n\right), \qquad (44)$$

where E_e and E_t – respectively, elastic and viscoelastic modulus of deformation of the material.

The disadvantage of this law is that the time in it is contained in an explicit form, which can lead to contradictory results. A method for determining the relaxation constants of a material on the basis of the Maxwell-Gurevich equation is given in [19–20]. Using this technique, as well as the results presented in [1–2], the author obtained the following values of the relaxation constants: $E_\infty = 27.38\ \mathrm{MPa}$, $\eta_0^* = 1.43 \cdot 10^4\ \mathrm{MPa \cdot h}$, $m^* = 0.0218\ \mathrm{MPa}$.

When processing creep curves on the basis of the Maxwell-Thompson equation, the relaxation parameters were chosen so that at the end of the creep process the solution using this equation coincided with the solution based on the Maxwell-Gurevich equation. As a result we obtained the values $\kappa = 1118\ \mathrm{MPa \cdot h}$, $H = 3.17\ \mathrm{MPa}$.

The magnitude of the load was assumed constant: $q = 2\ \mathrm{kPa}$. The curvature of the shell was varied by varying the amount of elevation f. The growth curves of the largest deflection relative to the deflection at $t = 0$ with different values of the ratio $f\ /\ a$ are shown in Fig. 3. The dashed lines correspond to the result based on the Maxwell-Gurevich equation, continuous - to the Maxwell-Thompson equation.

In his Ph.D. thesis, the author studied the influence of the curvature of the shell on the growth of deflection under linear creep by the example of a spherical three-layer shell. For the analysis, finite element modeling was used. As a result, it was found that with increasing curvature, the creep effect decreases, and for shells of large curvature, the creep of the aggregate has no effect on the amount of deflection. Similar results are observed in Figure 3. Creep of the aggregate does not have a noticeable effect on the deflection already at $f/a = 1/15$. We recall that it is customary to refer to shallow shells such that have $f/a \leq 1/5$. The results obtained on the basis of the linear and nonlinear theory differ insignificantly, especially for shells with greater curvature.

If the displacements in time practically do not change, then in the presence of viscoelastic properties of the material, the stresses can not be constant. Figure 4 is a graph of the change in time of the greatest value of tangential stresses τ_{zx}^m at $f/a = 1/15$. As before, the dashed line corresponds to the result based on the Maxwell-Gurevich equation, continuous - to the Maxwell-Thompson equation. It is seen from the presented graph that in the aggregate with constant shear deformations the stress relaxation occurs. Bending and twisting moments also decrease in time. The graphs of their changes are shown in Figure 5. The greatest bending moment in the creep process decreased by 32.7 %, and the torque – by 27 %.

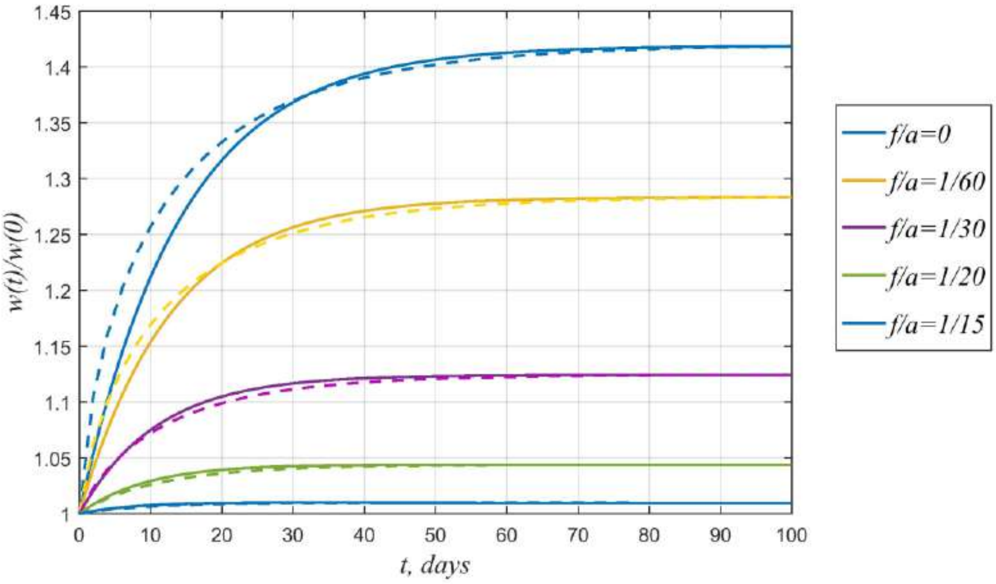

Figure 3. Graphs of the growth of the deflection for different values of the shell elevation: solid lines – Maxwell-Thompson equation, dashed lines – Maxwell-Gurevich equation

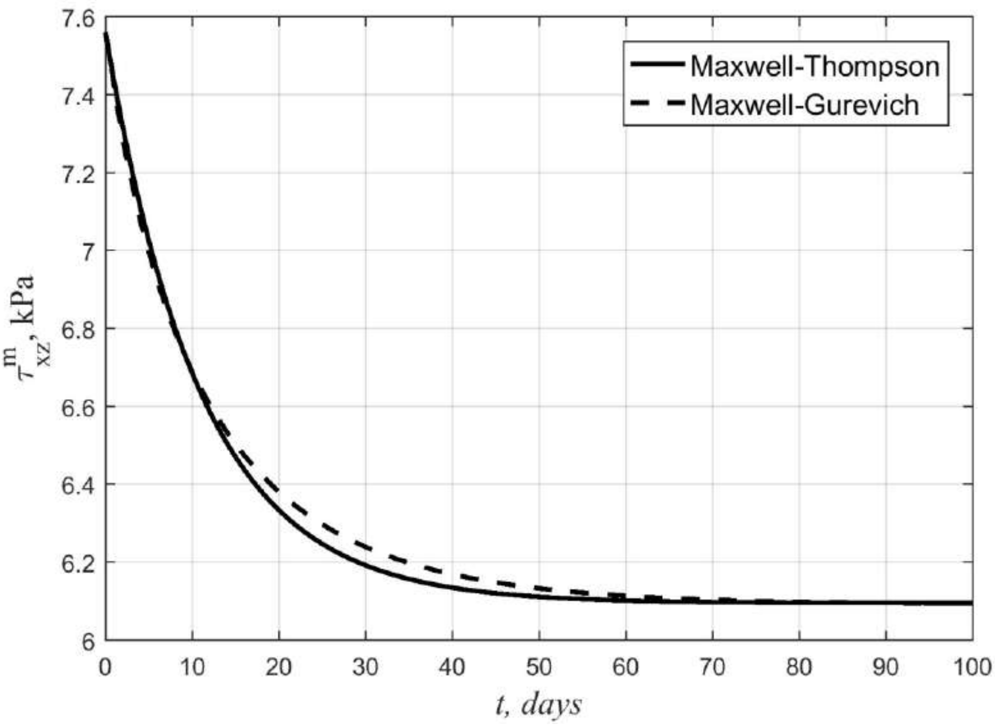

Figure 4. Change in time of the greatest tangential stresses in the aggregate

Longitudinal and shear forces increase during the creep process. The graphs of their growth are shown in Figure 6. The longitudinal force N_x increased by 8.33 %, and the shear force S – by 12.4 %. Figure 7 is a graph of the change in time of the largest values of the normal stresses σ_x in the upper and lower skin. In the upper skin, the stresses are practically constant, and in the lower skin they increase by 17.4 %. The tangential stresses increase both in the upper and the lower skin, as it can be seen from Figure 8. In the upper skin, the stresses τ_{xy} increased by 18.8 %, and in the lower skin by 7.71 %.

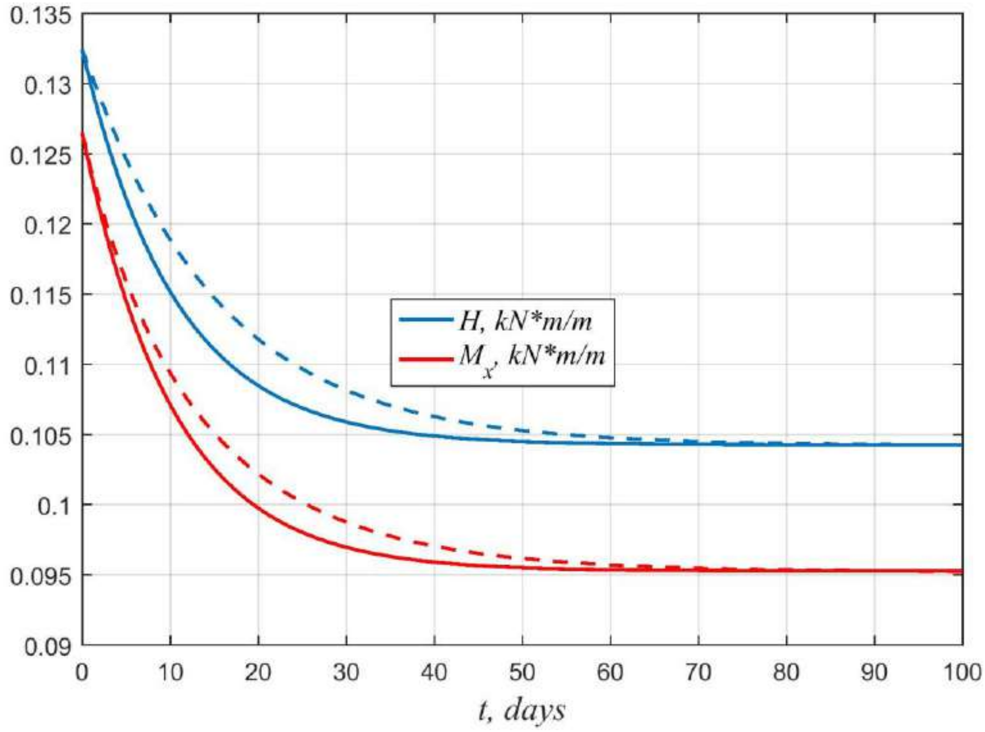

Figure 5. Change in time of the greatest bending and twisting moments: solid lines – Maxwell-Thompson equation, dashed lines – Maxwell-Gurevich equation

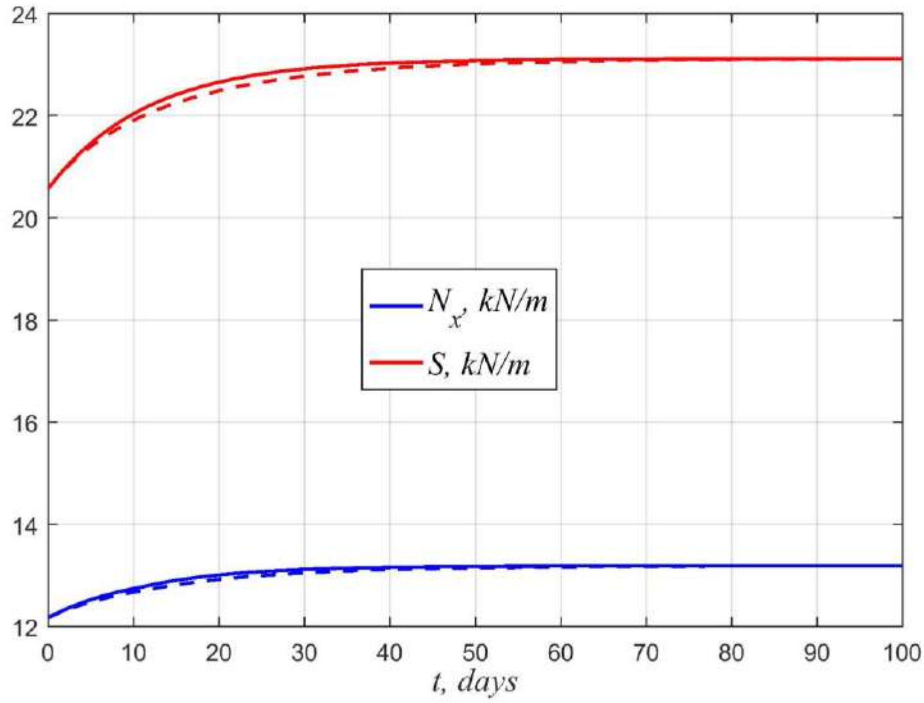

Figure 6. Change in time of the greatest longitudinal and shear forces

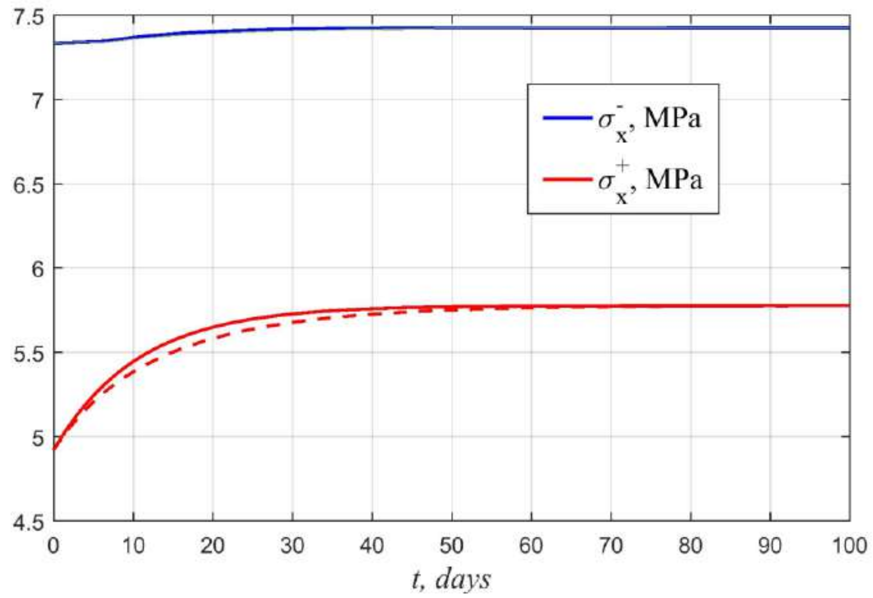

Figure 7. Change in time of the greatest normal stresses in the carrier layers

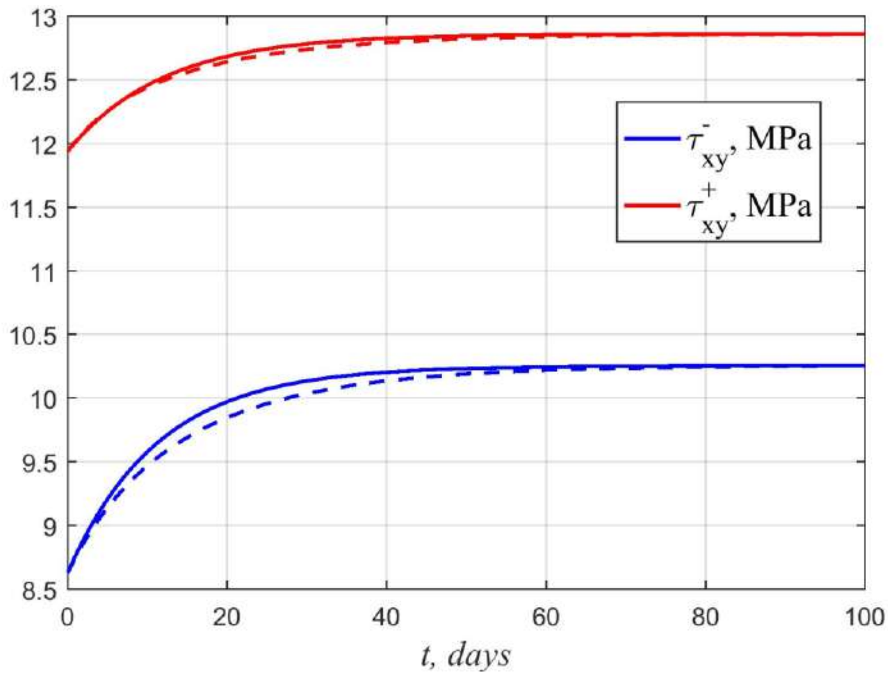

Figure 8. Change in time of the greatest tangential stresses in the shells

Conclusions

The obtained resolving equations are universal and allow to calculate three-layer plates and shallow shells under an arbitrary creep law. Using the example of a three-layer shell in the form of an elliptical paraboloid, it was shown that, with increasing of curvature, the effect of creep of the aggregate on the deflection amount decreases and is practically absent even at $f\ /\ a\ =\ 1/15$. At the same time, with constant displacements, redistribution of stresses and internal forces occurs. The bending and twisting moments decrease, and the longitudinal and shear forces increase. As for stresses, in the middle layer relaxation occurs, and in carrier layers stresses increase.

References

1. Garrido M. et al. Creep behaviour of sandwich panels with rigid polyurethane foam core and glass-fibre reinforced polymer faces: Experimental tests and analytical modelling. *Journal of Composite Materials.* 2014. Vol. 48. No. 18. Pp. 2237–2249.
2. Correia J. R. et al. GFRP sandwich panels with PU foam

Литература

1. Garrido M. et al. Creep behaviour of sandwich panels with rigid polyurethane foam core and glass-fibre reinforced polymer faces: Experimental tests and analytical modeling // Journal of Composite Materials. 2014. Vol. 48. № 18. Pp. 2237–2249.
2. Correia J. R. et al. GFRP sandwich panels with PU foam

and PP honeycomb cores for civil engineering structural applications: Effects of introducing strengthening ribs. *International Journal of Structural Integrity.* 2012. Vol. 3. No. 2. Pp. 127–147.

3. Li J. et al. Analysis on time-dependent behavior of laminated functionally graded beams with viscoelastic interlayer. *Composite Structures.* 2014. Vol. 107. Pp. 30–35.
4. Du Y., Yan N., Kortschotb M. T. An experimental study of creep behavior of lightweight natural fiber-reinforced polymer composite/honeycomb core sandwich panels. *Composite Structures.* 2013. Vol. 106. Pp. 160–166.
5. Ramenazi M., Hamed E. On the influence of temperature on the creep response of sandwich beams with a viscoelastic soft core. *Proceedings of the 6th international composites conference (ACUN-6).* Melbourne, Australia, 2012
6. Ramezani M., Hamed E. Coupled thermo-mechanical creep behavior of sandwich beams–Modeling and analysis. *European Journal of Mechanics-A/Solids.* 2013. Vol. 42. Pp. 266–279.
7. Hamed E., Frostig Y. Geometrically nonlinear creep behavior of debonded sandwich panels with a compliant core. *Journal of Sandwich Structures & Materials.* 2016. Vol. 18. No. 1. Pp. 65–94.
8. Lukashevich E.B., Sergeyev S.N. Sistema differentsialnykh uravneniy dlya svodchatoy trekhsloynoy obolochki s legkim zapolnitelem [A system of differential equations for a vaulted three-layer shell with a lightweight aggregate]. *Internet-zhurnal Naukovedeniye.* 2012. No. 4(13). [Online]. System requirements: AdobeAcrobatReader. URL: http://naukovedenie.ru/PDF/56trgsu412.pdf (date of reference: 09.10.2017). (rus)
9. Osadchiy N.V., Shepel V.T. Analiticheskiy i konechno-elementnyy raschet pryamougolnykh trekhsloynykh paneley na poperechnyy izgib [Analytical and finite-element calculation of rectangular three-layer panels for transverse bending]. *Vestnik IrGTU.* 2014. No. 10(93). Pp. 53–59. (rus)
10. Kogan Ye.A., Yurchenko A.A. O deformirovanii trekhsloynoy sfericheskoy obolochki s szhimayemym zapolnitelem pod deystviyem akusticheskoy volny davleniya [About the deformation of a three-layer spherical shell with a compressible aggregate under the action of an acoustic pressure wave]. *Izvestiya MGTU.* 2013. No. 1(15). Pp. 61–68. (rus)
11. Kudin A.V., Choporov S.V. Kompyuternoye modelirovaniye izgiba krugloy trekhsloynoy plastiny s ispolzovaniyem analiticheskogo i chislennogo podkhodov [Computer modeling of the bending of a circular three-layer plate using analytical and numerical approaches]. *Radioyelektronika, informatika, upravlinnya.* 2014. No. 1(30). Pp. 75–81. (rus)
12. Kudin A.V., Choporov S.V., Gomenyuk S.I. Osesimmetrichnyy izgib kruglykh i koltsevykh trekhsloynykh plastin s nelineyno-uprugim zapolnitelem [Axisymmetric bending of round and annular three-layer plates with nonlinear elastic filler]. *Matematicheskoye modelirovaniye.* 2017. Vol. 29. No. 2. Pp. 63–78. (rus) .
13. Bezoyan E.K. K voprosu o napryazhennom sostoyanii trekhsloynoy pologoy obolochki s uchetom polzuchesti srednego sloya [To the question of the stressed state of a three-layered shallow shell with allowance for the creep of the middle layer]. *Izvestiya natsionalnoy akademii nauk Armenii.* 2013. No. 4. Pp. 23–28. (rus)
14. Andreyev V.I., Yazyyev B.M., Chepurnenko A.S., Litvinov S.V. Raschet trekhsloynoy pologoy obolochki s uchetom polzuchesti srednego sloya [Calculation of a three-layered shallow shell, taking into account the creep of the middle layer]. *Vestnik MGSU.* 2015. No. 7. Pp. 17–24. (rus)
15. Yazyyev B.M., Chepurnenko A.S., Litvinov S.V., Yazyyev S.B. Raschet trekhsloynoy plastinki metodom

and PP honeycomb cores for civil engineering structural applications: Effects of introducing strengthening ribs // International Journal of Structural Integrity. 2012. Vol. 3. № 2. Pp. 127–147.

3. Li J. et al. Analysis on time-dependent behavior of laminated functionally graded beams with viscoelastic interlayer // Composite Structures. 2014. Vol. 107. Pp. 30–35.
4. Du Y., Yan N., Kortschotb M.T. An experimental study of creep behavior of lightweight natural fiber-reinforced polymer composite/honeycomb core sandwich panels // Composite Structures. 2013. Vol. 106. Pp. 160–166.
5. Ramenazi M., Hamed E. On the influence of temperature on the creep response of sandwich beams with a viscoelastic soft core // Proceedings of the 6th international composites conference (ACUN-6). Melbourne, Australia, 2012
6. Ramezani M., Hamed E. Coupled thermo-mechanical creep behavior of sandwich beams–Modeling and analysis // European Journal of Mechanics-A/Solids. 2013. Vol. 42. Pp. 266–279.
7. Hamed E., Frostig Y. Geometrically nonlinear creep behavior of debonded sandwich panels with a compliant core // Journal of Sandwich Structures & Materials. 2016. Vol. 18. № 1. Pp. 65–94.
8. Лукашевич Э.Б., Сергеев С.Н. Система дифференциальных уравнений для сводчатой трехслойной оболочки с легким заполнителем // Интернет-журнал Науковедение. 2012. № 4(13). [Электронный ресурс]. Сист.требования: AdobeAcrobatReader. URL: http://naukovedenie.ru/PDF/56trgsu412.pdf (дата обращения: 09.10.2017).
9. Осадчий Н.В., Шепель В.Т. Аналитический и конечно-элементный расчет прямоугольных трехслойных панелей на поперечный изгиб // Вестник ИрГТУ. 2014. № 10(93). С. 53–59.
10. Коган Е.А., Юрченко А.А. О деформировании трехслойной сферической оболочки с сжимаемым заполнителем под действием акустической волны давления // Известия МГТУ. 2013. № 1(15). С. 61–68.
11. Кудин А.В., Чопоров С.В. Компьютерное моделирование изгиба круглой трехслойной пластины с использованием аналитического и численного подходов // Радіоелектроніка, інформатика, управління. 2014. № 1(30). С. 75–81.
12. Кудин А.В., Чопоров С.В., Гоменюк С.И. Осесимметричный изгиб круглых и кольцевых трехслойных пластин с нелинейно-упругим заполнителем // Математическое моделирование. 2017. Т. 29. № 2. С. 63–78 .
13. Безоян Э.К. К вопросу о напряжённом состоянии трёхслойной пологой оболочки с учётом ползучести среднего слоя // Известия национальной академии наук Армении. 2013. № 4. С. 23–28.
14. Андреев В.И., Языев Б.М., Чепурненко А.С., Литвинов С.В. Расчет трехслойной пологой оболочки с учетом ползучести среднего слоя // Вестник МГСУ. 2015. № 7. С. 17–24.
15. Языев Б.М., Чепурненко А.С., Литвинов С.В., Языев С.Б. Расчёт трёхслойной пластинки методом конечных элементов с учётом ползучести среднего слоя // Вестник Дагестанского государственного технического университета. Технические науки. 2014. Т. 33. № 2. С. 47–55.
16. Chepurnenko A.S., Mailyan L.R., Jazyev B.M. Calculation of the three-layer shell taking into account creep // Procedia Engineering. 2016. Vol. 165. Pp. 990–994.
17. Litvinov S.V., Klimenko E.S., Kulinich I.I., Yazyeva S.B. Longitudinal bending of polymer rods with account taken of creep strains and initial imperfections // International Polymer Science and Technology. 2015. Vol. 42.

konechnykh elementov s uchetom polzuchesti srednego sloya [Calculation of a three-layer plate by the finite element method taking into account the creep of the middle layer]. *Vestnik Dagestanskogo gosudarstvennogo tekhnicheskogo universiteta. Tekhnicheskiye nauki.* 2014. Vol. 33. No. 2. Pp. 47–55. (rus)

16. Chepurnenko A.S. Mailyan L.R., Jazyev B.M. Calculation of the three-layer shell taking into account creep. *Procedia Engineering*. 2016. Vol. 165. Pp. 990–994.
17. Litvinov S.V., Klimenko E.S., Kulinich I.I., Yazyeva S.B. Longitudinal bending of polymer rods with account taken of creep strains and initial imperfections. *International Polymer Science and Technology.* 2015. Vol. 42. Pp. 23–25.
18. Litvinov S.V., Trush L.I., Yazyev S.B. Flat axisymmetrical problem of thermal creepage for thick-walled cylinder made of recyclable PVC. *Procedia Engineering.* 2016. Vol. 150. Pp. 1686–1693.
19. Dudnik A.Ye., Chepurnenko A.S., Litvinov S.V. Opredeleniye reologicheskikh parametrov polivinilkhlorida s uchetom izmeneniya temperatury [Determination of the rheological parameters of polyvinyl chloride taking into account the temperature change]. *Plasticheskiye massy.* 2016. No. 1-2. Pp. 30–33.
20. 2Chepurnenko A.S., Andreev V.I., Beskopylny A.N., Jazyev B.M. Determination of Rheological Parameters of Polyvinylchloride at Different Temperatures. *MATEC Web of Conferences.* 2016. Vol. 67. P. 06059.

Pp. 23–25.

18. Litvinov S.V., Trush L.I., Yazyev S.B. Flat axisymmetrical problem of thermal creepage for thick-walled cylinder made of recyclable PVC // Procedia Engineering. 2016. Vol. 150. Pp. 1686–1693.
19. Дудник А.Е., Чепурненко А.С., Литвинов С.В. Определение реологических параметров поливинилхлорида с учетом изменения температуры // Пластические массы. 2016. № 1-2. С. 30–33.
20. Chepurnenko A.S., Andreev V.I., Beskopylny A.N., Jazyev B.M. Determination of Rheological Parameters of Polyvinylchloride at Different Temperatures // MATEC Web of Conferences. 2016. Vol. 67. P. 06059.

Anton Chepurnenko,
+7(918)571-87-38; anton_chepurnenk@mail.ru

Антон Сергеевич Чепурненко,
+7(918)571-87-38;
эл. почта: anton_chepurnenk@mail.ru

doi: 10.18720/MCE.76.15

Burnt rock of the coal deposits in the concrete products manufacturing

Горелая порода угольных месторождений в производстве изделий из бетона

M.P. Kuz'min,
L.M. Larionov,
V.V. Kondratiev,
M.Yu. Kuz'mina,
V.G. Grigoriev,
A.S. Kuz'mina,
Irkutsk National Research Technical University, Irkutsk, Russia

Канд. техн. наук, доцент М.П. Кузьмин,
ведущий инженер Л.М. Ларионов,
канд. техн. наук, руководитель центра В.В. Кондратьев,
канд. хим. наук, доцент М.Ю. Кузьмина,
канд. техн. наук, заведующий кафедрой В.Г. Григорьев,
инженер А.С. Кузьмина,
Иркутский национальный исследовательский технический университет, г. Иркутск, Россия

Key words: burnt rock; slagheaps ash; mine dumps; coal deposits; active mineral addition; concrete; cement; cement stone; fly ash

Ключевые слова: горелая порода; зола терриконов; шахтные отвалы; угольные месторождения; активная минеральная добавка; бетон; цемент; цементный камень; зола уноса

Abstract. The paper presents the results of the comprehensive study of the composition, properties and structure of the burnt rock found at the mining dumps of Cheremkhovo coal deposit (Irkutsk region, Russia). In the course of laboratory research, which included optical crystallography, there have been established the reasons accounting for the extent of burnt rock activity when in contact with cement during the cement stone formation. The benefit of the burnt rock as an active mineral additive, compared to the fly ash used by the cement plants, was confirmed as well. The optimal ratio of cement and burnt rock in concrete mixtures was determined experimentally. Likewise, the most effective method of using burnt rock as an active mineral additive was developed as the result of semi-industrial tests when the sample was subjected to the pressing and steam treatment. Finally, the impact such an additive can have on the production cost have been calculated.

Аннотация. В работе представлены результаты исследований состава, свойств и структуры горелой породы шахтных отвалов Черемховского угольного месторождения, расположенного в Иркутской области. В ходе лабораторных исследований и кристаллооптического анализа установлены причины, объясняющие степень активности горелой породы в контакте с цементом, при формировании цементного камня. Показано преимущество использования горелой породы в качестве активной минеральной добавки, по сравнению с золой уноса, традиционно применяемой цементными заводами. Опытным путём определены оптимальные соотношения цемента и горелой породы в бетонных смесях. В ходе полупромышленных испытаний в режиме прессования и тепловлажностной обработки определён наиболее эффективный способ использования горелой породы в качестве активной минеральной добавки. Установлены границы её влияния на себестоимость продукции.

Introduction

At present time, concrete products lay the foundation for the construction industry. Hence, improving the quality of the concrete products while reducing the cost of their manufacturing is a task of the utmost importance. An extensive number of theoretical research as well as applied studies are dedicated to this issue [1–4].

The prime cost of the concrete (up to 70%) depends on the price of its main component – the cement, as it is the qualities of the cement that account for the strength and durability of the concrete constructions [5].

Кузьмин М.П., Ларионов Л.М., Кондратьев В.В., Кузьмина М.Ю., Григорьев В.Г., Кузьмина А.С. Горелая порода угольных месторождений в производстве изделий из бетона // Инженерно-строительный журнал. 2017. № 8(76). С. 169–180.

The use of active mineral additives in the cement production can reduce the energy and material costs associated with the commercial output. Moreover, it allows to improve both construction and technical properties of the product [6]. When cement is mixed with water, active mineral additives (AMA) react with calcium hydroxide, which is released as the result of hydration of tricalcium silicate, and form water-insoluble calcium hydrosilicates. Thus, together with conservation of the clinker part, mineral additives provide the cement with a number of special properties such as increased impact strength, reduced water permeability and efflorescence, and so on [7].

It is also worth noting that as technogenic AMA are inherently wastes and by-products of various mining and processing industries, they are of considerable interest in terms of accessibility, cost and environmental safety [8, 9].

Based on the extent of AMA activity, special attention should be paid to the burnt rock of the coal deposits, as that is one of the most widespread types of technogenic waste. During the mine exploitation of the coal deposits, dead rock containing traces of coal is stored in the artificial mounds called the slag heaps [10, 11] (Figure 1).

Figure 1. Slag Heap

Spontaneous coal combustion in slag heaps with temperatures ranging from 600°C to 850°C results in the formation of ash rich in active ingredients [6,12,13]. Such combustion processes inside the slag heap tend to last for 35–40 years. During that time, the entire internal massif reaches a homogeneous state (i.e. the chemical composition of the samples is identical to those collected at all sampling points of the slag heap).

Nine slag heaps of a total volume of about three million cubic meters are located in the Cheremkhovo area of Irkutsk region, Russia. Multiple slag heaps of similar appearance and chemical composition are located in the regions where coal was extracted via deep mining technique (Russia, Ukraine, China, Czech Republic, Spain, etc.) [14–17].

The paper presents the results of the profound study of the burnt rock of the Cheremkhovo coal deposit. It also sets to propose technologies for the use of the burnt rock of the aforementioned mine dumps as an acidic active mineral additive to the cement and the concrete products based on it.

The study is intended to provide a comprehensive explanation of the increased extent of the burnt rock activity, develop a technology for its use as an active mineral additive in the concrete production, and determine the optimum quantity of the cement to be replaced with the burnt rock without reducing the strength parameters of the end product.

To achieve this goal, accomplished tasks include the following:

– research of the physical properties and chemical composition, and the structure of the burnt rock;

– measurement of the extent of the burnt rock activity as well as its place in the range of active mineral additions;

– determination of the effect the burnt rock has on the formation of the cement stone as well as its subsequent qualitative characteristics; establishing of the optimum degree of replacement of cement by burnt rock under normal conditions of hardening;

– conducting crystal optical studies of the structure of the cement stone formed with the addition of the burnt rock to identify the possibility of new formations, namely, the forms and the types of replacement as well as interaction of the formed phases in the general structure;

– conducting semi-industrial tests with a view to replace the cement with the burnt rock at the operating plant; determination of the optimum degree of cement substitution under the conditions of vibrocompression and stream treatment.

Materials and Methods of research

Crystal-optical studies of the burnt rock as well as the cement stone with the burnt rock additive were performed with a digital polarizing microscope Altami Polar 1. X-ray diffraction analysis was conducted to study the phase composition of the burnt rock, with the help of the Shimadzu X-ray diffractometer XRD-7000. Qualitative and quantitative analyses of the chemical composition of the samples was carried out by the Bruker AXS S4 PIONEER X-ray fluorescence spectrometer.

To conduct laboratory tests of the burnt rock activity as well as its mechanical properties in the cement composition, the following regulatory documents were referred to:

– Russian State Standard GOST 310.1–76* “Cements. Test methods. General” (EN 197–1);

– Russian State Standard GOST 310.2–76* “Cements. Methods of grinding fineness determination” (EN 196–6);

– Russian State Standard GOST 25094–94 “Active mineral additions for cements. Methods of testing” (EN 934–2);

– Russian State Standard GOST 310.4–81 “Cements. Methods of bending and compression strength determination” (EN196–1).

All samples were dried to achieve stationary weight. Burnt rock drying was carried out at the temperature of 105 ± 5 °C; gypsum stone drying (as to prevent its dehydration) was completed at the temperature of 68 ± 2 °C. Further, the materials were pebbled together. To study their grindability, the grinding time in the mill was altered (30, 60 and 100 min). The grinding quality was evaluated based on the specific surface and screen sizing (sieve No. 0071 was used). The surface area of the grains was 5500-6500 cm^2/g (to compare, the surface area of the cement grains subjected to the same grinding technique lies in the range of 3000–4000 cm^2/g).

The materials milled to the desired fineness were dried again for one hour period and then placed in hermetically sealed vessels. The vessels with the powdered substance, prior to their use in the compositions, were stored in a chamber where calcium chloride was layered on the oven-tray to maintain the low level of relative air humidity.

Water-to-cement ratio was determined in accordance with Russian State Standard GOST 30744 “Cements. Methods of testing with using polyfraction standard sand”. The samples were prepared from the mortar mixtures based on Russian State Standard GOST 310.4–81 (EN 196–1). Until the testing, the samples were stored in the chamber with a relative air humidity of 95–98 %.

Results and discussion

Research into the composition, properties and the structure of the burnt rock

The burnt rock is comprised of a loose granular material; the color varies from crimson to light orange. The grains of the rock are gravelly shaped and structured in a layered or lamellar way (Figure 2).

Figure 2. Burnt rock facies

Tables 1 and 2 show the chemical composition and the properties of the burnt rock found at the mine dumps of the Cheremkhovo coal deposit.

Table 1. Average chemical composition of the burnt rock of mining dumps of the Cheremkhovo coal basin deposits

Oxides content, (wt%)									
SiO_2	Al_2O_3	Fe_2O_3	CaO	MgO	K_2O	Na_2O	MnO	TiO_2	SO_2
65.60	18.70	6.03	2.20	2.60	1.90	0.35	0.03	0.30	0.29

Note: the chemical composition of the slag heaps ash is reproduced from the analysis performed in the analytical department of the Vinogradov Institute of Geochemistry – Siberian Branch of the Russian Academy of Sciences

Table 2. Averaged physical and mechanical properties of the burnt rock of mine dumps of the Cheremkhovo coal basin deposits as determined by Russian State Standard GOST 8269.0–97

Characteristics, dimension	**Values**
Natural humidity, (wt%)	8.80
Bulk density, kg/m^3	1085
Grain content, size 0-5 mm (wt%)	58.60
Grain content, size 5-70 mm (wt%)	41.40
True density, g/cm^3	2.58
Strength in a cylinder, g/cm^2	17.70
Water saturation, (wt%)	15.30
Softening coefficient	0.69

According to X-ray diffraction and crystal-optical analyses, the burnt rock is mainly comprised of crystal quartz SiO_2, sillimanite Al_2SiO_5, gypsum $CaSO_4 \cdot 2H_2O$, magnetite Fe_3O_4, and limonite $Fe_2O_3 \cdot nH_2O$ (Figures 3,4).

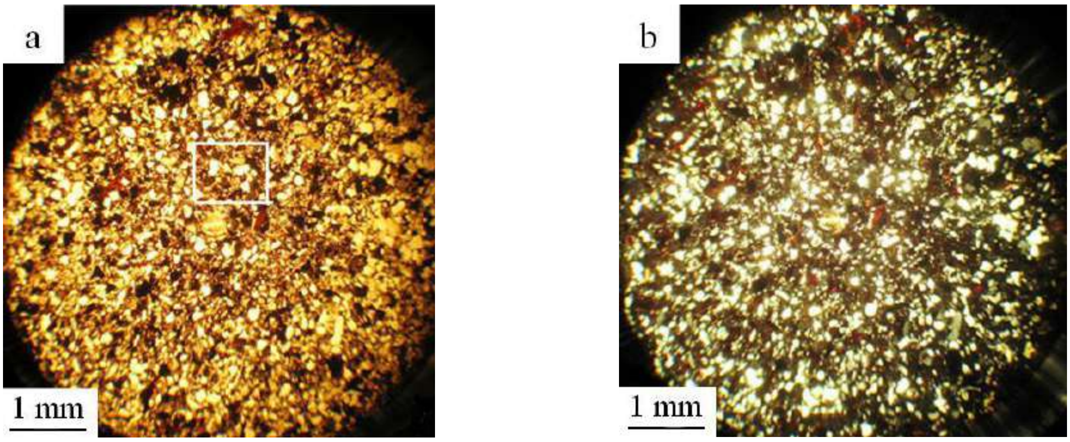

Figure 3. Burnt rock view
a – in transmitted light; b – in polarized light

Quartz in the burnt rock is present both in the form of an independent phase and as a component of the cementing mass. Likewise, quartz is observed in the form of transparent colorless or yellowish-brown grains. The yellowish-brown shade of the quartz indicates the presence of ocherized limonite. The grains of quartz are irregularly shaped – the size of grains can vary from 0.2 to 0.4 mm while individual grains can reach 5 mm - and characterized by undulose extinction (Figure 4).

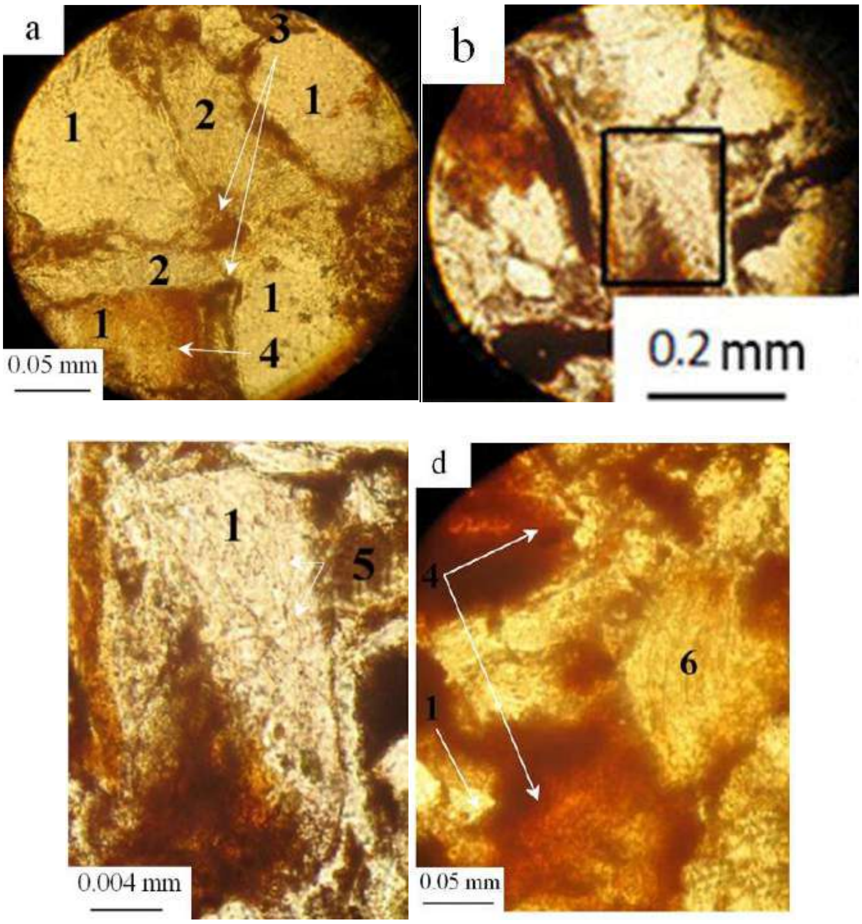

Figure 4. Images of the burnt rock (in a transmitted light):
a – the selected fragment of the figure 1 (grains of quartz and fine-grained mass which cements the clastic material); b – general facies of the burnt rock; c – fragment of the Figure 2, b (quartz with inclusions of acicular and sillimanite pointlike grains); d – gypsum grains among the fragments of quartz (1 – quartz, 2 - cementing mass, 3 – magnetite, 4 – limonite, 5 – sillimanite, 6 – gypsum)

In addition to the limonite streaks in the quartz grains, the inclusions of barely discernible sillimanite acicular grains – size of less than 0.01 mm – can be observed (Figure 4, c).

Gypsum is present both in the form of an independent phase and as a component of the cementing mass. Likewise, a significant amount of gypsum is visible among the quartz fragments – in the form of irregular grains up to 0.5 mm in size (Figure 4, d). Gypsum in the burnt rock is recognized by either columnar colorless or brownish aggregates.

The cementing mass is comprised of quartz, gypsum, sillimanite, magnetite and limonite (Figure 5).

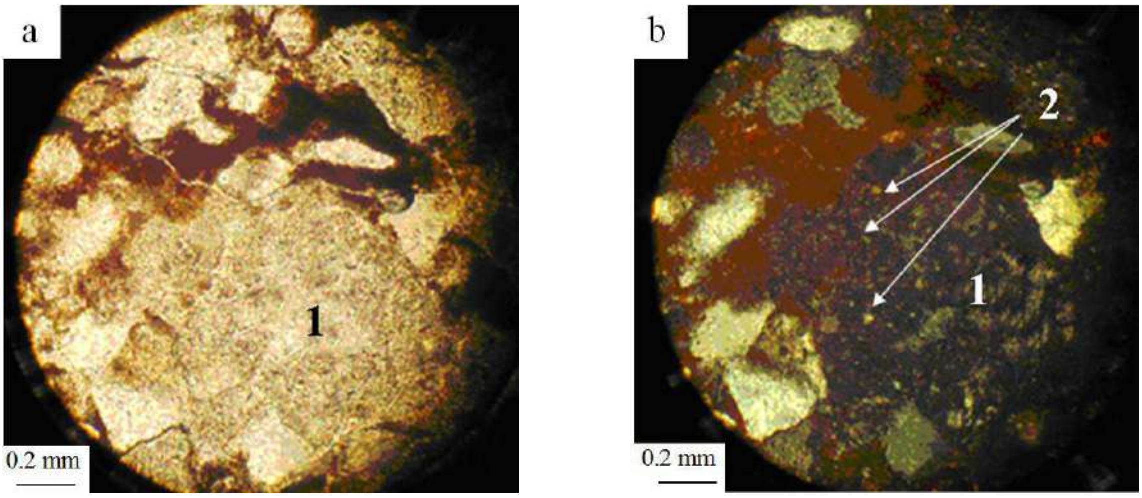

Figure 5. Images of the cementing mass:
a – in the transmitted light, b - in polarized light (1 – cementing mass, 2 – quartz grains, which are part of the cementing mass)

In the total volume of the cement mass, quartz is easily distiguished by its grains size (up to 0.01 mm). Gypsum and sillimanite form a fine-grained aggregate, which makes it difficult to identify them even at high resolution (×400 and ×600). Magnetite is represented by cubic crystals of 0.2–0.5 mm in size and is characterized by an opaque brown tint (caused by the buildup of limonite).

It should be noted that such a detailed optical crystallography of the burnt rock as well as the cement stone formed with its addition was carried out for the first time. However, the very application of the burnt rock as an aluminum silicate additive to the cements has been known about since the 50s of the XX century [2, 7, 10, 18]. Both theoretical and applied research into the issue was conducted in the regions where coal was extracted via deep mining technique. The results of those studies are presented in detail [5–8].

Laboratory studies of cements

For illustrative purposes, during the laboratory studies the burnt rock activity was compared to the activity of TPP fly ash generally used as an active mineral in the additive cement production. The evaluation of the mechanical properties of the laboratory grinding cement was carried out by substituting fly ash with the burnt rock. For this reason, five different compositions were prepared, in which a third, a half, two thirds and all fly ash were replaced by the burnt rock. That being said, the total amount of AMA constituted 18 % of the Portland-cement clinker weight. The addition of gypsum stone to all compositions remained constant and equaled 5.2 (wt%) of the clinker weight.

Preparation of the mortar mixtures and the samples for mechanical testing was based on the cement compositions and single-fraction sand in accordance with Russian State Standard GOST 310.4–81 (EN 196–1). Some samples were tested immediately after steaming, other samples were left to harden in water, and then tested on the 7th and the 28th days. The average values of the mechanical properties of composite cement with burnt rock and fly ash additives are presented in Table 3.

Table 3. Mechanical properties of the composite cement with additions of the burnt rock and fly ash

Mechanical properties		Strength of the sample, MPa
Composition 1: PCC + 0 % BR + 18 % FA + 5.2 % GS		
Steamed, day 1	at bending	3.57
	at compression	19.28
Hardened in water, day 7	at bending	3.61
	at compression	23.02
Hardened in water, days 28	at bending	6.35
	at compression	40.23
Composition 2: PCC + 5.5 % BR + 12.5 % FA + 5.2 % GS		
Steamed, day 1	at bending	3.80
	at compression	20.56
Hardened in water, day 7	at bending	3.77
	at compression	23.58
Hardened in water, day 28	at bending	6.33
	at compression	40.56
Composition 3: PCC + 9 % BR + 9 % FA + 5.2 % GS		
Steamed, day 1	at bending	4.14
	at compression	22.15
Hardened in water, day 7	at bending	3.90
	at compression	24.58
Hardened in water, day 28	at bending	6.64
	at compression	41.89
Composition 4: PCC + 12.5 % BR + 5.5 % FA + 5.2 % GS		
Steamed, day 1	at bending	4.28
	at compression	24.23
Hardened in water, day 7	at bending	4.41
	at compression	26.22
Hardened in water, day 28	at bending	6.92
	at compression	43.56
Composition 5: PCC + 18 % BR + 0 % FA + 5.2 % GS		
Steamed, day 1	at bending	4.37
	at compression	28.98
Hardened in water, day 7	at bending	4.58
	at compression	29.56
Hardened in water, day 28	at bending	7.22
	at compression	45.24
Composition 6: PCC + 25 % BR + 0 % FA + 5.2 % GS		
Steamed, day 1	at bending	4.28
	at compression	27.05
Hardened in water, day 7	at bending	4.40
	at compression	28.80
Hardened in water, day 28	at bending	7.02
	at compression	44.09

Note: PCC is a Portland-cement clinker; BR – burnt rock; FA –fly ash; GS – gypsum stone.

Based on the obtained data, it can be deduced that the optimal amount of AMA to be added to the cement composition is 18 %. This Portland cement satisfies the requirements of Russian State Standard GOST 10178-85 “Portland cement and portland blastfurnace slag cement. Specifications” (EN 196–1) and Russian State Standard GOST 2532882 “Masonry cement. Specifications” (EN 2061).

Thus, one can conclude that the increase in the amount of the burnt rock (the AMA output is constant and equals 18%) corresponds with the increase in the cement stone strength when bending or compressing despite the hardening and the steaming time of the samples vary. The maximum strength property is observed in the Portland cement composition where the AMA consists solely of the burnt rock.

Thereby, the replacement of cement by the burnt rock in the amount of 18 % under normal conditions during the cement stone formation should be considered optimal, since in this case it is possible to achieve maximum strength of the samples. Likewise, it leads to the significant savings of the clinker.

Table 4 shows comparative quality characteristics of the cement produced with addition of the burnt rock and the fly ash of TPP.

Table 4. Qualitative characteristics of the cement with active mineral additives in the form of burnt rock and fly ash of TPP

Characteristics, dimension	Cement quality indicators: AMA in the form of:	
	burnt rock	fly ash of TPP
True density, g/cm^3	3.00	3.03
Bulk density, g/cm^3	1.08	1.10
Grinding fineness: residue on a sieve 0.08, %	13.80	13.10
Grinding fineness: specific surface area, m^2/kg	326	375
Normal density, %	28.50	25.75
Setting start, min.	220	200
Setting end, min.	430	470
Water separation coefficient, %	14.1	32.0

Portland-cement produced with the burnt rock additive belongs to the first steaming efficiency group while the one produced with the fly ash additive reside the third one [18]. Furthermore, the cement produced with the fly ash has a much higher water separation coefficient.

Crystallo-optical studies of the cements samples with AMA

Preparation of the solution mixtures for the crystallo-optical studies was based on the use of single-fraction quartz sand in accordance with Russian State Standard GOST 310.4–81 (EN 196–1).

The samples were made with the cement containing 18 % of the burnt rock as AMA. The grinds were prepared from the plates located in three mutually perpendicular planes of the test bar. The tested sections were identical to each other with regard to their composition and structural features. The resultant description of the studied material is presented below.

Figures 6, 7, 8 show the samples consisting of the quartz sand and the cement with the burnt rock added as AMA. The samples are compounded with the clastic material. The aggregate grains are heterogeneous in composition (gypsum, quartz, plagioclase, etc.), are irregularly shaped. The average size of the grain is up to 4 mm. The clastic fragments are completely moistened with the binder material (Figure 6).

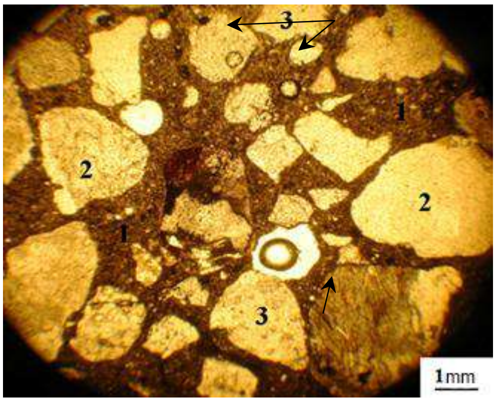

Figure 6. Cement composition with the burned rock as AMA (general view): 1 – fine-grained binding mass; 2 – large clastic material; 3 – voids

Kuz'min M.P., Larionov L.M., Kondratiev V.V., Kuz'mina M.Yu., Grigoriev V.G., Kuz'mina A.S. Burnt rock of the coal deposits in the concrete products manufacturing. *Magazine of Civil Engineering*. 2017. No. 8. Pp. 169–180. doi: 10.18720/MCE.76.15.

Uniformly distributed isometric voids of 0.01–0.03 mm in size, as well as acicular neoplasms, penetrating fine-grained material, were registered in the cementing fine-grained mass. Besides, the units grouped in a certain order while creating the contours of elongated new formations were found in the sample.

It is crucial to note that the new formations are present not only in the cohesive fine-grained mass, but also on its border together with the large clastic grains. This indicates the chemical interactions between the compounds. Figure 7 captures the columnar gypsum grain where its substitution by the needle-like crystals can be traced from the cementitious material deep into the grain across its columnarity.

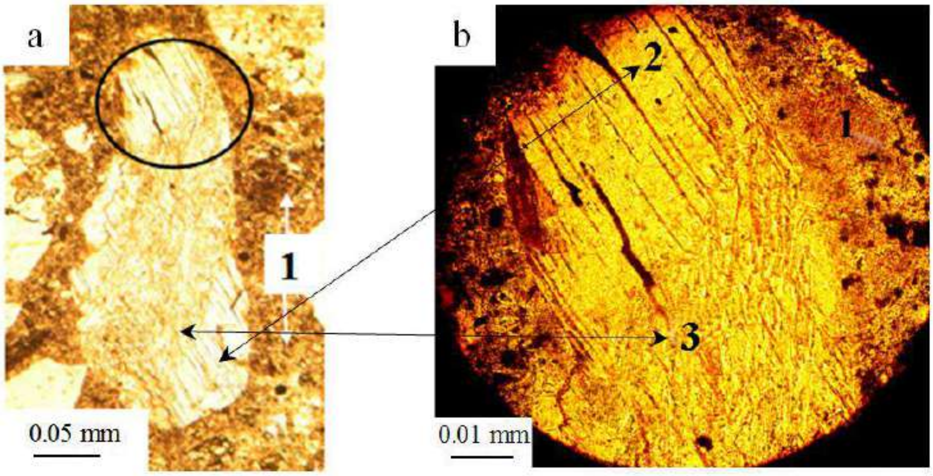

Figure 7. Nature of grain substitution:
a – columnar-fiber grain of gypsum in cementing mass;
b – detail (a) – needle-shaped new formations in gypsum, oriented across the grain columnarity
(1 – cementing material, 2 – columnar gypsum, 3 – needle-shaped new formations)

Figure 8 shows the nature of the replacement of plagioclase grains. The contours of the crystal are blurred and pitted (with the buildup of the binder material). This indicates the presence of a chemical interaction between the crystal and the binder. On some parts of the grain surface, the substitution process can be traced from the edge of the grain to its inside. There, the new formations develop across the polysynthetic twins of plagioclase.

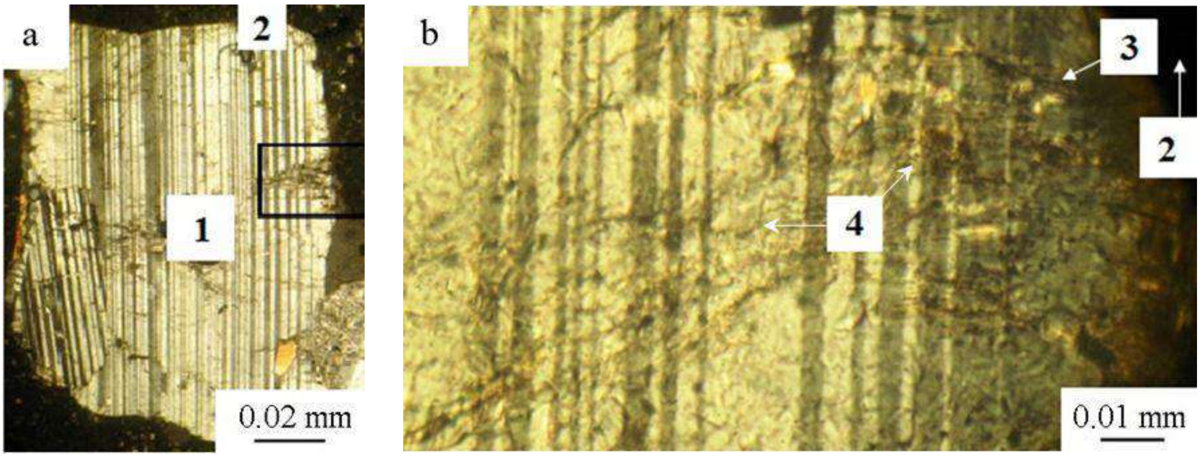

Figure 8. The Nature of grain substitution:
a – plagioclase crystal (1), which is completely encircled by the cementing mass (2);
b –the fragment of the figure (a) – cementing material (2), the pitted edges of the crystal (3),
new formations, developing deep into the crystal across the polysynthetic twins of plagioclase (4)

According to the data obtained by the X-ray structural analysis, the new formations in the samples made from the cement with the burnt rock addition are comprised of calcium hydrosilicate $4CaO \cdot SiO_2 \cdot 13H_2O$, $3CaO \cdot SiO_2 \cdot 2H_2O$.

The use of concretes with the burnt rock additives in the manufacturing of products by methods of pressing and steam treatment in the steaming chamber

The results of laboratory and crystallo-optical studies of the impact of the burnt rock additives on the quality of the cement stone suggest that the burnt rock additives are primarily beneficial for the samples manufactured by pressing and subsequent steaming treatment.

New formations, obtained in the result of the research, their structure and interaction with each other, as well as the nature of the replacement the grains and the binder were subjected to, prove the undeniable industrial potential of the combination (cement-burnt rock) [18–23]. Mechanical impact and steam treatment of the sample during the cement stone formation can only contribute to the case [20].

For that purpose, semi-industrial tests were carried out at the operational plant, which manufactures concrete products (“Stroitechnik”, LLC, Irkutsk, Russia).

The task of the tests was to determine the degree of the possible replacement of "M–500" cement by the burnt rock under the real conditions of the masonry units production. The main criterion to be followed was the preservation of all strength characteristics of the commercial output.

The Units (dimensions: 200×200×400) were produced by the method of vibrocompression on the Condor 1 press of “Stroitechnik Plant”, LLC. Then they were placed in a steaming chamber at a temperature of 60-80 °C for a day. The composition of the concrete mixture was prepared on the basis of the approved regulations. The standard output of the "M-500" cement was 280 kg per 1 m^3 of the mixture. The cement in prototypes was replaced by the burnt rock in a different percentage ratio. The compressive strength of the samples was measured on the 28 day. The results of tests of the compressive strength limit depending on the degree of burnt rock cement replacement are presented in Table 5.

Table 5. Tests of the compressive strength limit depending on the degree of substitution of cement by the burnt rock

Substitution of cement by the burnt rock, %	The compressive strength, day 28, MPa
0 % – standard	29.6
18	32.8
25	30.1
35	29.4
50	23.6

It can be seen that in the blocks production according to the technology described above, it is possible to replace up to 35 % of the cement by the burnt rock.

Thus, the hypothesis about the effectiveness of the burnt rock use along with cement, or as its partial replacement, was confirmed in practice. In addition, the replacement of cement by the burnt rock in the concrete products manufacturing can lead to a significant reduction of the end product price.

Conclusions

1. The research of the chemical compounds, physical properties and structure of the burnt rock have shown high efficiency of its application as active mineral additive.

2. The tests of the mechanical properties of the mixture “cement – burnt rock” and “cement - fly ash” allowed to estimate the extent of the burnt rock activity and determine the optimal amount of active mineral addition (18 %). At this rate, physical and mechanical characteristics of the "M-500" cement are preserved in accordance with Russian State Standard GOST 10178–85, which complies with the 32.5 N strength class standard.

3. Crystal-optical studies with a view to determine the structural features of the burnt rock samples made it possible to establish that the burnt rock activity when in contact with the cement during the formation of cement stone is predicated by the presence of the new needle-shaped formations and their chemical interaction - both with the binder of fine-grained mass and with the large clastic grains.

4. Semi-industrial tests conducted with intent to apply the burnt rock into the concrete mixture by vibrocompression method followed by steaming treatment allowed to determine the optimum value of substitution of cement by the burnt rock. It has been established that it is possible to replace up to 35 % of cement without reducing the strength properties of the end products.

References

1. Kusuma G.H., Budidarmawan J., Susilowati A. Impact of concrete quality on sustainability. *Procedia Engineering.* 2015. Vol. 125. Pp. 754–759.
2. Kim Y.-J. Quality properties of self-consolidating concrete mixed with waste concrete powder. *Construction and Building Materials.* 2017. Vol. 135. Pp. 177–185.
3. Koper A., Koper W., Koper M. Influence of raw concrete material quality on selected properties of recycled concrete aggregates. *Procedia Engineering.* 2017. Vol. 172. Pp. 536–543.
4. Hasan-Nattaj F., Nematzadeh M. The effect of forta-ferro and steel fibers on mechanical properties of high-strength concrete with and without silica fume and nano-silica. *Construction and Building Materials.* 2017. Vol. 137. Pp. 557–572.
5. Chistov L.M. *Ekonomika stroitelstva* [Economy of construction]. Saint-Petersburg: Piter, 2003. 637 p. (rus)
6. Stracher G.B., Prakash A., Sokol E.V. Coal and Peat Fires: A global perspective: Vol. 1: Coal-geology and combustion. United Kingdom : Elsevier, 2011. 358 p.
7. Nagrockienė D., Girskas G., Skripkiūnas G. Properties of concrete modified with mineral additives. *Construction and Building Materials.* 2017. Vol. 135. Pp. 37–42.
8. Liu Q., Tong T., Liu S., Yang D., Yu Q. Investigation of using hybrid recycled powder from demolished concrete solids and clay bricks as a pozzolanic supplement for cement. *Construction and Building Materials.* 2014. Vol. 73. Pp. 754–763.
9. Seredin V.V., Dai S., Sun Y., Chekryzhov I.Yu. Coal deposits as promising sources of rare metals for alternative power and energy-efficient technologies. *Applied Geochemistry.* 2013. Vol. 31. Pp. 1–11.
10. Salikhzyanov R.G. O sisteme kontrolya teplovogo sostoyaniya terrikonov i porodnykh otvalov [On the control system for the thermal state of waste heaps and waste heaps]. *Marksheyderskiy vestnik.* 2002. No. 1. Pp. 26–28. (rus)
11. Kohfahl C., Graupner T., Fetzer C., Holzbecher E., Pekdeger A. The impact of hardpans and cemented layers on oxygen diffusivity in mining waste heaps: Diffusion experiments and modelling studies. *Science of the Total Environment.* 2011. Vol. 59. No. 17. Pp. 3197–3205.
12. Kruszewski Ł. Supergene sulphate minerals from the burning coal mining dumps in the Upper Silesian Coal Basin, South Poland. *International Journal of Coal Geology.* 2013. Vol. 105. Pp. 91–109.
13. Torresa A., Bartlett L., Pilgrim C. Effect of foundry waste on the mechanical properties of Portland Cement Concrete. *Construction and Building Materials.* 2017. Vol. 135. Pp. 674–681.
14. Ribeiro J., Suárez-Ruiz I., Flores D. Geochemistry of self-burning coal mining residues from El Bierzo Coalfield (NW Spain): Environmental implications. *International Journal of Coal Geology.* 2016. Vol. 159. Pp. 155–168.
15. Querol X., Izquierdo M., Monfort E., Alvarez E., Font O., Moreno T., Alastuey A., Zhuang X., Lu W., Wang Y. Environmental characterization of burnt coal gangue banks at Yangquan, Shanxi Province, China. *International Journal of Coal Geology.* 2008. Vol. 75. Pp. 93–104.
16. Sharygin V.V. Mayenite-supergroup minerals from burned dump of the Chelyabinsk Coal Basin. *Russian Geology and Geophysics.* 2015. Vol. 56. Pp. 1603–1621.
17. Křìbek B., Sýkorová I., Veselovský F., Laufek F., Malec J., Knésl I., Majer V. Trace element geochemistry of self-burning and weathering of a mineralized coal waste dump: The Novátor mine, Czech Republic. *International Journal of Coal Geology.* 2017. Vol. 173. Pp. 158–175.
18. Nath S.K., Kumar S. Evaluation of the suitability of ground

Литература

1. Kusuma G.H., Budidarmawan J., Susilowati A. Impact of concrete quality on sustainability // Procedia Engineering. 2015. Vol. 125. Pp. 754–759.
2. Kim Y.-J. Quality properties of self-consolidating concrete mixed with waste concrete powder // Construction and Building Materials. 2017. Vol. 135. Pp. 177–185.
3. Koper A., Koper W., Koper M. Influence of raw concrete material quality on selected properties of recycled concrete aggregates // Procedia Engineering. 2017. Vol. 172. Pp. 536–543.
4. Hasan-Nattaj F., Nematzadeh M. The effect of forta-ferro and steel fibers on mechanical properties of high-strength concrete with and without silica fume and nano-silica // Construction and Building Materials. 2017. Vol. 137. Pp. 557–572.
5. Чистов Л.М. Экономика строительства. Спб: Питер, 2003. 637 с.
6. Stracher G.B., Prakash A., Sokol E.V. Coal and Peat Fires: A global perspective: Vol. 1: Coal-geology and combustion. United Kingdom : Elsevier, 2011. 358 p.
7. Nagrockienė D., Girskas G., Skripkiūnas G. Properties of concrete modified with mineral additives // Construction and Building Materials. 2017. Vol. 135. Pp. 37–42.
8. Liu Q., Tong T., Liu S., Yang D., Yu Q. Investigation of using hybrid recycled powder from demolished concrete solids and clay bricks as a pozzolanic supplement for cement // Construction and Building Materials. 2014. Vol. 73. Pp. 754–763.
9. Seredin V.V., Dai S., Sun Y., Chekryzhov I.Yu. Coal deposits as promising sources of rare metals for alternative power and energy-efficient technologies // Applied Geochemistry. 2013. Vol. 31. Pp. 1–11.
10. Салихзянов Р.Г. О системе контроля теплового состояния терриконов и породных отвалов // Маркшейдерский вестник. 2002. № 1. С. 26–28.
11. Kohfahl C., Graupner T., Fetzer C., Holzbecher E., Pekdeger A. The impact of hardpans and cemented layers on oxygen diffusivity in mining waste heaps: Diffusion experiments and modelling studies // Science of the Total Environment. 2011. Vol. 59. № 17. Pp. 3197–3205.
12. Kruszewski Ł. Supergene sulphate minerals from the burning coal mining dumps in the Upper Silesian Coal Basin, South Poland // International Journal of Coal Geology. 2013. Vol. 105. Pp. 91–109.
13. Torresa A., Bartlett L., Pilgrim C. Effect of foundry waste on the mechanical properties of Portland Cement Concrete // Construction and Building Materials. 2017. Vol. 135. Pp. 674–681.
14. Ribeiro J., Suárez-Ruiz I., Flores D. Geochemistry of self-burning coal mining residues from El Bierzo Coalfield (NW Spain): Environmental implications // International Journal of Coal Geology. 2016. Vol. 159. Pp. 155–168.
15. Querol X., Izquierdo M., Monfort E., Alvarez E., Font O., Moreno T., Alastuey A., Zhuang X., Lu W., Wang Y. Environmental characterization of burnt coal gangue banks at Yangquan, Shanxi Province, China // International Journal of Coal Geology. 2008. Vol. 75. Pp. 93–104.
16. Sharygin V.V. Mayenite-supergroup minerals from burned dump of the Chelyabinsk Coal Basin // Russian Geology and Geophysics. 2015. Vol. 56. Pp. 1603–1621.
17. Křìbek B., Sýkorová I., Veselovský F., Laufek F., Malec J., Knésl I., Majer V. Trace element geochemistry of self-burning and weathering of a mineralized coal waste dump: The Novátor mine, Czech Republic // International Journal of Coal Geology. 2017. Vol. 173. Pp. 158–175.
18. Nath S.K., Kumar S. Evaluation of the suitability of ground granulated silico-manganese slag in Portland slag cement // Construction and Building Materials. 2016. Vol. 125.

granulated silico-manganese slag in Portland slag cement. *Construction and Building Materials.* 2016. Vol. 125. Pp. 127–134.

19. Tavakoli D., Tarighat A. Molecular dynamics study on the mechanical properties of Portland cement clinker phases. *Computational Materials Science.* 2016. Vol. 119. Pp. 65–73.
20. Bassani M., Bertola F., Bianchi M., Canonico F., Marian M. Environmental assessment and geomechanical properties of controlled low-strength materials with recycled and alternative components for cements and aggregates. *Cement and Concrete Composites.* 2017. Vol. 80. Pp. 143–156.
21. Chousidis N., Ioannou I., Rakanta E., Koutsodontis C., Batis G. Effect of fly ash chemical composition on the reinforcement corrosion, thermal diffusion and strength of blended cement concretes. *Construction and Building Materials.* 2016. Vol. 126. Pp. 86–97.
22. Taha Y., Benzaazoua M., Hakkou R., Mansori M. Coal mine wastes recycling for coal recovery and eco-friendly bricks production. *Minerals Engineering.* 2017. Vol. 107. Pp. 123–138.
23. Saljnikov A., Vucˇic´evic´ B., Komatina M., Gojak M., Goricˇanec D., Zoran Stevanovic´ Spectroscopic research on infrared emittance of coal ash deposits. *Experimental Thermal and Fluid Science.* 2009. Vol. 33. Pp. 1133–1141.

Pp. 127–134.

19. Tavakoli D., Tarighat A. Molecular dynamics study on the mechanical properties of Portland cement clinker phases // Computational Materials Science. 2016. Vol. 119. Pp. 65–73.
20. Bassani M., Bertola F., Bianchi M., Canonico F., Marian M. Environmental assessment and geomechanical properties of controlled low-strength materials with recycled and alternative components for cements and aggregates // Cement and Concrete Composites. 2017. Vol. 80. Pp. 143–156.
21. Chousidis N., Ioannou I., Rakanta E., Koutsodontis C., Batis G. Effect of fly ash chemical composition on the reinforcement corrosion, thermal diffusion and strength of blended cement concretes // Construction and Building Materials. 2016. Vol. 126. Pp. 86–97.
22. Taha Y., Benzaazoua M., Hakkou R., Mansori M. Coal mine wastes recycling for coal recovery and eco-friendly bricks production // Minerals Engineering. 2017. Vol. 107. Pp. 123–138.
23. Saljnikov A., Vucˇic´evic´ B., Komatina M., Gojak M., Goricˇanec D., Zoran Stevanovic´ Spectroscopic research on infrared emittance of coal ash deposits // Experimental Thermal and Fluid Science. 2009. Vol. 33. Pp. 1133–1141.

Mikhail Kuz'min,
+7(914)885-83-87; Mike12008@yandex.ru

Leonid Larionov,
+7(902)513-95-06; larionov59@rambler.ru

Victor Kondratiev,
+7(902)568-77-02; kvv@istu.edu

Marina Kuz'mina,
+7(914)891-16-94; kuzmina.my@yandex.ru

Vyacheslav Grigoriev,
+7(983)401-65-01; grigorievvg@istu.edu

Alina Kuz'mina,
+7(950)052-35-00; zhuravlyova-alina@yandex.ru

Михаил Петрович Кузьмин,
+7(914)885-83-87;
эл. почта: Mike12008@yandex.ru

Леонид Михайлович Ларионов,
+7(902)513-95-06;
эл. почта: larionov59@rambler.ru

Виктор Викторович Кондратьев,
+7(902)568-77-02; эл. почта: kvv@istu.edu

Марина Юрьевна Кузьмина,
+7(914)891-16-94;
эл. почта: kuzmina.my@yandex.ru

Вячеслав Георгиевич Григорьев,
+7(983)401-65-01;
эл. почта: grigorievvg@istu.edu

Алина Сергеевна Кузьмина,
+7(950)052-35-00;
эл. почта: zhuravlyova-alina@yandex.ru

Kuz'min M.P., Larionov L.M., Kondratiev V.V., Kuz'mina M.Yu., Grigoriev V.G., Kuz'mina A.S. Burnt rock of the coal deposits in the concrete products manufacturing. *Magazine of Civil Engineering*. 2017. No. 8. Pp. 169–180. doi: 10.18720/MCE.76.15.

doi: 10.18720/MCE.76.16

Flat rod systems: optimization with overall stability control

Плоские стержневые системы: оптимизация с контролем общей устойчивости

I.N. Serpik,
Bryansk State University of Engineering and Technology, Bryansk, Russia
A.V. Alekseytsev,
National Research Moscow State Civil Engineering University, Moscow, Russia
P.Yu. Balabin,
N.S. Kurchenko,
Bryansk State University of Engineering and Technology, Bryansk, Russia

Д-р техн. наук, заведующий кафедрой И.Н. Серпик,
Брянский государственный инженерно-технологический университет, г. Брянск, Россия
канд. техн. наук, доцент А.В. Алексейцев,
Национальный исследовательский Московский государственный строительный университет, г. Москва, Россия
без степени, аспирант П.Ю. Балабин,
канд. техн. наук, доцент Н.С. Курченко,
Брянский государственный инженерно-технологический университет, г. Брянск, Россия

Key words: steel structures; flat rod systems; optimization; genetic algorithms; finite element method; strength; stiffness; overall stability

Ключевые слова: стальные конструкции; плоские стержневые системы; оптимизация; генетические алгоритмы; метод конечных элементов; прочность; жесткость; общая устойчивость

Abstract. An algorithm for discrete optimization of steel flat rod systems was developed on the basis of an evolutionary search. The task is to minimize the weight of the bars via taking into account constraints on stresses, displacements, and overall stability. The cross-sectional dimensions of the bars and the coordinates of their node connections were varied. Buckling is taken into account when stability is lost both in the object plane and out of the plane. Analysis of deformations of the considered structure variants was performed via the displacement-based finite element method. An iterative procedure for solving the task was formulated by using an auxiliary elite population, combined approaches to selection and mutation, and single-point crossover. The primary feature of the proposed computing scheme is simplified structure stability verification by determining stress-strain conditions with a tangent stiffness matrix and the additional self-balanced system of small fictitious forces. Assessment as to how constraint on stability was met was performed based on the results of the considered convergence of the internal iteration cycle used for analyzing load-carrying system behavior by taking into account the influence of longitudinal forces on the bars while bending. It was calculated that it is sufficient to perform only 3–5 iterations of this procedure to verify structure stability. Efficiency of the proposed algorithm is illustrated via the example of optimization of bar system with two supports and a frame with a girder truss.

Аннотация. Разработан алгоритм дискретной оптимизации изготовленных из стали плоских стержневых систем на основе эволюционного поиска. Ставится задача минимизации веса стержней с учетом ограничений по напряжениям, перемещениям и общей устойчивости. Варьируются размеры поперечных сечений стержней и координаты узлов их соединения. Учитывается выпучивание при потере устойчивости как в плоскости, так и из плоскости объекта. Анализ деформаций рассматриваемых вариантов конструкции выполняется методом конечных элементов в форме метода перемещений. Сформулирована итерационная процедура решения поставленной задачи с использованием вспомогательной элитной популяции, комбинированных подходов к селекции и мутации, одноточечного кроссинговера. Основной особенностью предлагаемой вычислительной схемы является упрощенная проверка устойчивости конструкций путем расчета их напряженно-деформированного состояния с использованием касательной матрицы жесткости и дополнительной самоуравновешенной системы малых фиктивных сил. Оценка удовлетворения ограничения по устойчивости выполняется по результатам рассмотрения сходимости внутреннего итерационного цикла, реализующего анализ поведения несущей системы при учете влияния для стержней продольных сил на изгиб. Расчетным путем установлено, что для проверки устойчивости конструкции достаточно выполнить только 3–5 итерации этой процедуры.

Работоспособность предлагаемого алгоритма иллюстрируется на примере оптимизации двухопорной стержневой системы и рамы с ферменным ригелем.

Introduction

For newly designed building systems, the percentage of buildings and constructions with steel bearing structures is increasing. These being the case, flat rod systems are in wide usage. The process of optimally designing such objects often includes the choice of bar profile dimensions and the arrangement of their connecting nodes, taking into account constraints on stresses, displacements, and stability. To verify the provision of strength and stiffness of flat rod systems included in steel framework systems, one should usually implement two-dimensional computational models. At the same time, a stability analysis of such objects, in many cases, is required to be performed while taking into account the possibility of buckling out of the structure plane.

The issue of optimally designing bar systems is given great attention in scientific literature. The most universal approaches to solving these problems have been obtained via the use of meta-heuristic methods [1–10], which allow performing an effective search using discrete sets of variable parameters taking into account a set of standard requirements as the conditions for a building structure design. In particular, the use of genetic algorithms in such issues was considered [1, 4]. At the same time, meta-heuristic procedures for the optimal synthesis of frameworks are often related to the need for performing a significant number of working capacity checks of structure solution variants taken into consideration. A significant volume of work hours for such checks to be spent, particularly for taking into account the necessity of ensuring conditions of stability, to a certain extent restrains the use of such algorithms for practical purposes. In a number of papers that represent optimization methods of various types, stability constraints were considered only for separate bars [11–15], which greatly simplifies the task, but reduces the possibilities of application in real design practice. In [16, 17], compliance with constraints on a structure's overall stability was verified on the basis of the classical solution of the eigenvalue problem within the framework of the Euler approach. In [18, 19], the condition of ensuring stability at size optimization of the flat rod systems unfolded from displacements from the plane of the structure was approximately taken into account by considering the effect of longitudinal forces on bending.

It should be noted that during the optimization process, it is usually not necessary to determine the critical load values and buckling shapes, but only to check structure stability. To do so, it is sufficient to confirm that the determinant of the tangent stiffness matrix of the system is positive [20]. Such a criterion was taken into account for optimization of bar structures in [21, 22]. In this paper, to optimize flat rod systems, even a simpler assessment of in-plane and out-of-plane stability is realized, including analysis of convergence of the iterative process of the structure calculation via the finite element method using a tangent stiffness matrix and a self-balanced system of small auxiliary forces. In this case, the stability test is combined with the analysis of the stress-strain condition of the bar system.

Minimization of the rods' weight is performed with a set of strength, stiffness, and overall stability constraints by varying rod profiles and coordinates of nodal points on discrete sets of permissible variants. Constructive and technological requirements are all taken into account when assigning sets of permissible values of variable parameters. The structure of the optimization scheme is carried out by using the general provisions for genetic algorithm of work [23].

The purpose of this paper is to develop an evolutionary algorithm for optimization of flat rod systems considering with acceptable computational complexity the overall stability as one of the active constraints. To this effect the problem of creating a simplified iteration scheme of overall stability evaluation of rod structures without defining the critical load level for intermediate alternatives of a deformable object is solved.

Methods

Statement of the optimization problem

We believe that the plane steel structure is made of rectilinear bars with constant cross-sections along their lengths. The axes of bars and one of the main axes of bar cross-sections are located in plane XY of the Overall Cartesian coordinate system XYZ (Fig. 1). We set the task of minimizing the weight W of all the bars of the structure:

$$W(H_1, H_2, ..., H_N, R_1, R_2, ..., R_M) \rightarrow \min \,, \quad (1)$$

where $H_n\,(n=1,.2,...,N)$ – set of permissible combinations of sizes of independently varied cross-sections of the bar n, N – total number of such sections, R_m $(m=1,2,...,M)$ – set of permissible values for the independently varied nodal coordinate m, M – the total number of such coordinates.

We take into account that the bars with variable cross-sectional dimensions can be combined into groups in which such parameters are assumed to be the same. Accordingly, variable coordinates can be combined into groups, the values of which are required to be the same.

We assume that the structure is subject to loading in its plane. The stress-strain condition of the object is calculated using the finite element method within the framework of the displacement method. This being the case, the possibility of structure spatial deformation should be taken into account, considering the need to assess compliance with stability requirements both in the framework plane and out of the plane. To ensure the possibility of stability testing of separate bars, each of them is divided into not less than 5–6 finite elements.

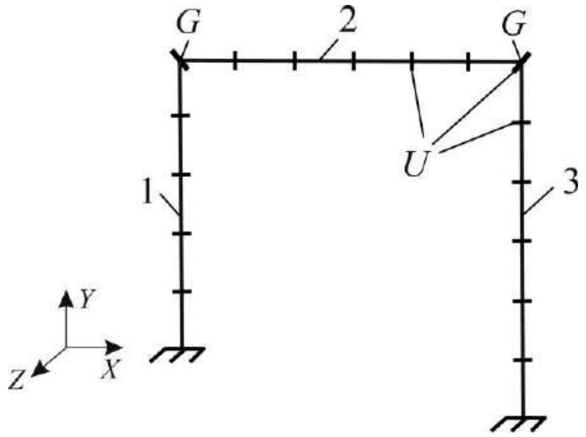

Figure 1. Example of the bar system with separation into bars and finite elements: 1–3 are bar numbers, *G* – bar connection nodes, *U* – nodes of the finite element model

A set Ω of all coordinates of the finite-element model nodes can be represented as follows

$$\Omega=\{\Omega_X,\ \Omega_Y\}, \tag{2}$$

where $\Omega_X=\{X_1, X_2,..., X_I\}$, $\Omega_Y=\{Y_1, Y_2,..., Y_I\}$ – sets of values of the node coordinates along axis X and Y, respectively, I – total number of nodes.

We expand the set Ω into nonoverlapping subsets:

$$\Omega=\Omega_A+\Omega_B+\Omega_D, \tag{3}$$

where Ω_A – set of independently changeable coordinates, Ω_B – set of changeable coordinates being linear functions of the coordinates belonging to the set Ω_A, Ω_D – set of unchangeable coordinates.

Each of sets $R_m\,(m=1,2,...,M)$ is given for one coordinate of set Ω_A. In this case, if the position of the rectilinear structural element varies in the plane, each coordinate of nodes G_1, G_2 of its marginal sections (Fig. 2) may belong only to sets Ω_A or Ω_D only. Then, coordinates X_k, Y_k of a certain internal node k of such a structural element for the current configuration of the structure can be determined using equations

$$X_k=X_1+x_k(X_2-X_1)/l,\ Y_k=X_2+x_k(X_2-X_1)/l, \tag{4}$$

where X_1, Y_1, X_2, Y_2 – coordinates for nodes G_1 and G_2 in the current configuration, respectively, x_k and l – value of coordinate x of node k and the length of the structural element for the basic configuration, respectively.

We believe that, in the general case, the following constraints can be taken into account:

A) *Strength condition:*

$$\sigma_m \leq R_y \,, \tag{5}$$

where σ_m – Mises stress; R_y – design steel resistance assigned with regard to the yield strength [24].

B) S*tiffness requirements.* For each node i of the discretizable structure, inequations should be met

$$\left|u_j\right| \leq [u]_j \,, \; \left|v_j\right| \leq [v]_j \,, \tag{6}$$

where u_j, v_j – projections of j node displacement on X *and* Y axis, respectively, $[u]_j$, $[v]_j$ – permissible values for such displacements.

C) *Overall stability of bar system structure, including stability of individual bars.*

D) *Stability of side flanges and walls of profiles.*

E) Stability of plane bending *of bars.*

F) *Provision of local structural strength.*

G) *Unification regarding topologies and parameters.*

H) *Design constraints (possibility of determining layout of nodal connections, support conditions, etc.).*

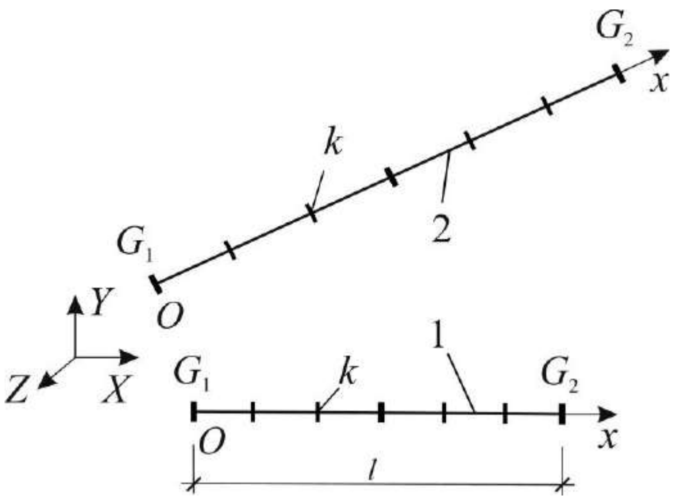

Figure 2. Straight-line structural element in plane XY : 1, 2 – basic and current configurations

Principles of constraints accounting

Constraints A, B, and C are considered active and are directly taken into account during the optimization process. Other constraints are taken into account when choosing the initial prerequisites for optimal design and are controlled after the optimal search has been performed. In general, it is understood that the result of optimization, a variant of the design solution, in any case, should be checked for compliance with all the constraints imposed, by applying certain adjusted schemes. If necessary, the initial prerequisites for optimization can be adjusted and the optimization process performed again.

We assume that the structure material operates under conditions of linear elasticity. In general, we take into account that bars are subject to deformations caused by tension/compression, bending in both main planes, and pure torsion. The finite element model of the bar system is formed in accordance with known provisions [25].

We will check compliance with active constraints based on an analysis of the stress-strain condition of the design variants using the method of a step-by-step approach. We consider the system deformations under conditions of small displacements, while taking into account longitudinal-transverse bending of the bars. For each standard combination of loads, during the first iteration, we perform calculations by applying conventional stiffness matrices of the finite element method and the actual load, and, in iteration $r \geq 2$, we solve the following system of linear algebraic equations:

$$[K]_\tau \{\delta\}^{(r)} = \{Q\} + \{\Delta\}, \qquad (7)$$

where $[K]_\tau$ – tangent of the stiffness matrix [20] of the spatial finite element model, $\{\delta\}^{(r)}$ – vector of nodal displacements calculated in iteration r, $\{Q\}$ – vector of nodal forces that takes into account the standard impact, $\{\Delta\}$ – randomly generated vector of a self-balanced system of small nodal forces that can take non-zero values for any nodal degree of freedom.

The tangent matrix of stiffness can be represented as [20]

$$[K]_\tau = [K] + \left[K_G\left(\{N\}^{(r-1)}\right)\right], \qquad (7)$$

where $[K]$ – stiffness matrix of the finite element model, $\left[K_G\left(\{N\}^{(r-1)}\right)\right]$ – geometric matrix of the finite element system [25] expressed through longitudinal bar forces found in iteration $r-1$ that are combined into vector $\{N\}^{(r-1)}$.

Vector $\{\Delta\}$ should not have any significant influence on the task solution if the load does not approach the Euler critical level. In this case, additional fictitious displacements associated with this vector should allow creating the conditions for the manifestation of stability loss by a planar or spatial scheme. Then, according to the theory of stability [26], as the load approaches the critical level, the energy of the object deformation obtained through the effect of longitudinal forces on the bars bending will tend to infinity. We introduce an estimate of structure stability based on the premise that when implementing the iterative process on a computer in accordance with equation (7), the absence of the convergence of solutions indicates non-fulfillment of constraint C. We control the approach to the condition of instability by verifying the following condition for the preset iteration number $r_o \geq 3$:

$$\left|1 - \frac{U^{(r_o)}}{U^{(r_o-1)}}\right| \leq \alpha, \qquad (9)$$

where $U^{(r_o)}$, $U^{(r_o-1)}$ – discretized object deformation energies obtained in iterations r_o and $r_o - 1$, respectively, α – fixed small positive number.

According to calculations, a sufficiently effective verification of this type is ensured if $r_o = 5$, $\alpha = 0.001$. If all the standard requirements are met for the bar system, then practically 3–5 iterations are required for the iterative process to be implemented.

Management of the optimal search process on the basis of genetic algorithm

In our case, an individual is the variant of the structure obtained by choosing values of parameters from predefined discrete sets. Each of such sets shall be arranged in descending order: by area of cross-sections for sets H_n and the values of the coordinates for sets R_m.

We believe that during each iteration of the genetic algorithm, the following two populations (sets) of individuals shall be considered:

1. *Current population* Φ_1. It has the fixed size N_1 and is used for individuals that can be processed by genetic operators.

2. *Elite population* Φ_2. It is introduced to save the best variants of solutions in the search process. The genetic material of this population can be used in the modification of population Φ_1. It is envisaged that the number of individuals in population Φ_2 should not exceed preset value N_2.

Initially, population Φ_1 is formed. N_1 identical projects based on the first elements of sets H_n $(n = 1,2,...,N)$, R_m $(m = 1,2,...,M)$ are introduced. Next, an iterative procedure is performed, each iteration of which includes the following steps:

1. *Check of the individuals' fitness for work.* The stress-strain condition is calculated for each variant of the structure related to population Φ_1. This population is divided into groups: Φ_1' and Φ_1''. If for an individual belonging to group Φ_1', any of the active constraints is not met, then such individual is replaced by the best individual from the elite population Φ_2 not available in population Φ_1. If there are no such individuals in population Φ_2, then, for this purpose, random information is generated about parameters for a new variant of the structure not considered in population Φ_1. For an individual from group Φ_1'', constraint (9) is taken into account in the same way. At the same time, if only constraints A and B are violated for individuals belonging to this group, a significant penalty shall be introduced by multiplying the value of the objective function by a factor

$$k_p = (1 + \xi_\sigma \chi(\alpha_\sigma))(1 + \xi_\delta \chi(\alpha_\delta)), \tag{10}$$

where ξ_σ, ξ_δ – set positive numbers, $\chi(x)$ – heaviside function of some argument ω ($\chi(\omega) = 0$, if $\omega < 0$ and $\chi(\omega) = 1$, if $\omega \geq 0$),

$$\alpha_\sigma = \max_t \left(\max_i \left(\frac{\sigma_m^{(i\max)}}{R_{yi}} - 1 \right) \right), \alpha_\delta = \max_t \left(\max \left(\max_j \left(\frac{|u_j|}{[u]_j} - 1 \right), \max_j \left(\frac{|v_j|}{[v]_j} - 1 \right) \right) \right), \tag{11}$$

t – number of load combination variants, $\sigma_m^{(i\max)}$ – maximum value σ_m for i bar, R_{yi} – value R_y for this bar material.

2. *Modification of the elite population.* For each individual φ_{1l} of population Φ_1, the objective function value $W(\varphi_{1l})$ is calculated and the following condition shall be verified:

$$(\neg((\varphi_{1l} = \varphi_{2j}) \vee (\varphi_{2j} \in \Phi_2))) \vee (W(\varphi_{1l}) < W_{2\max}), \tag{12}$$

where φ_{2j} – j individual from population Φ_2, $W_{2\max}$ – the maximum value of the objective function for this population individuals.

If the criterion (12) is met, the individual from population Φ_1 is copied into population Φ_2. This being the case, if the elite population already contains individuals N_2, then the individual with the largest value of the objective function is removed from it.

3. *Check of conditions for the optimization completion.* Calculations show that in the absence of changes in population Φ_2, throughout 200-300 iterations, further continuation of the search, as a rule, does not lead to a change in the best value of the objective function. It was assumed that, providing that the elite population is stable for 300 iterations, the solution of the optimization problem is complete.

4. *Mutation.* For individuals of population Φ_1, where in each generation there exists the possibility of random change in part of the parameters in several individuals. The following mixed scheme for changing the position of parameter j in the discrete set T_j of its permissible values is used. Suppose that this set has w_j elements. On the interval (0; 1), with the help of a random number generator, values m_a, m_b are selected by applying the uniform distribution law to be compared with the control numbers of mutation f, f_1, f_2, f_3. If $m_a > f$, then the number of the parameter value in set T_i shall be chosen randomly with equal probability. When $m_a \leq f$, the choice shall be made in accordance with Table 1,

where r_j is the number of the parameter value in set T_i before mutation, $\tilde{r}$ is the value by which this number changes as a result of mutation.

Table 1. Values of additions to the parameter number at $m_a \le f$

r_j	$\tilde{r}$			
	$m_b < f_1$	$f_1 \le m_b < f_2$	$f_2 \le m_b < f_3$	$m_b \ge f_3$
1	0	0	1	2
2	-1	-1	1	2
3	-2	-1	1	2
4	-2	-1	1	2
…	…	…	…	…
w_{j-2}	-2	-1	1	2
w_{j-1}	-2	-1	1	1
w_j	-2	-1	0	0

5. *Selection and crossover.* The selection operator is applied to all individuals from population Φ_1 by applying the roulette method [27, 28] on the basis of the obtained objective function values in accordance with the mixed scheme used in [22]. Crossover was performed using the single-point operator [27, 28].

Results

The use of a developed computational scheme is considered for examples of a bar structure with two supports and a frame with a girder truss. It was assumed that the optimized objects were made of S235 steel [24]. The following was taken into account: modulus of elasticity $E = 2.06 \cdot 10^5 \text{MPa}$, weight density $\rho = 77 \text{kN/m}^3$. The following was set out: $N_1 = N_2 = 20$, $r_o = 5$, $\xi_\sigma = 10$, $\xi_\delta = 100$, $f = 0.9$, $f_1 = 0.5$, $f_2 = 0.75$, $f_3 = 0.9$. Compliance with constraints on strength, stiffness, and stability were confirmed for the obtained optimization task solutions by applying the Autodesk NEi Nastran software package (License FGBOU VO "BGITU" N PR-05918596) and with regard to the existing standards [24].

Example 1 considered the bar structure with two supports consisting of six bars 1–6 of equal length (Fig. 3a) with an H-shaped cross-section (Fig. 3b) at $z \parallel Z$. Dimensions of each bar 1–3 cross-section of the symmetric system were varied independently. Permissible combinations of bar cross-sections are indicated in Table 2. Coordinates of the central node C also varied, provided that straightness of segments $D_\text{I}C$ и $D_\text{II}C$ remain unchanged. The following set of permissible values was specified for this coordinate: {-20, -17.5, -15, -12.5, -10, -7.5, -5, -4, -3, -2, -1, 0, 1, 2, 3 4, 5, 7.5, 10, 12.5, 15, 17.5, 20} (cm). The uniform finite element mesh was introduced (see Fig. 3a). Independently, three cases of optimization were implemented with the following loading conditions: $P_1 = 2.5 \text{ MN}$, $P_2 = P_3 = P_4 = 0$; 2) $P_1 = 2.5 \text{MN}$, $P_2 = P_3 = P_4 = 0.5 \text{MN}$ и 3) $P_1 = 2.5 \text{MN}$, $P_2 = P_3 = 1.25 \text{MN}$, $P_4 = 0$. It was assumed that $[u]_i = [v]_i = 8 \text{ cm}$, $R_y = 230 \text{ MPa}$. Optimization results are shown in Figure 4, where k_{st} – safety factor of stability by the Euler method obtained through the use of Autodesk NEi Nastran software. These design parameters were achieved in no more than 60 generations.

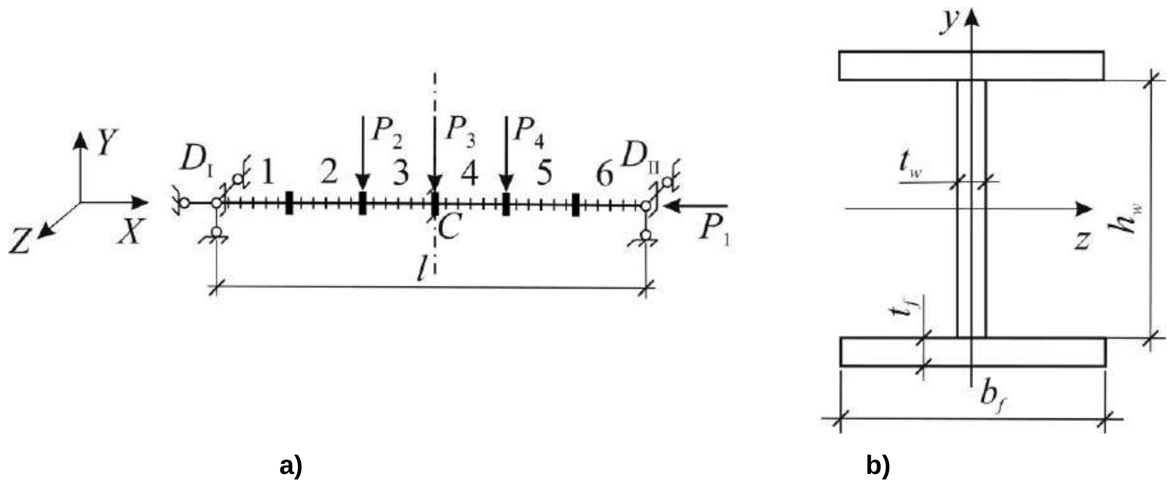

Figure 3. Bar system with two supports: a – design diagram applying the basic geometry of the object with subdivision on finite elements: 1–6 – bar numbers, b – bar cross-section in local system of axes

Table 2. Permissible combinations of cross-section variable parameters for Example 1

Combination number	b_f, cm	t_f, cm	h_w, cm	t_w, cm
1	16	1	15	0.6
2	20	1.5	18	0.8
3	25	2	20	1
4	28	2	25	1.2
5	30	2.2	30	1.2
6	34	2.2	35	1.4
7	38	2.4	40	1.4
8	42	2.6	45	1.6
9	46	2.8	50	1.6
10	50	3	55	1.8

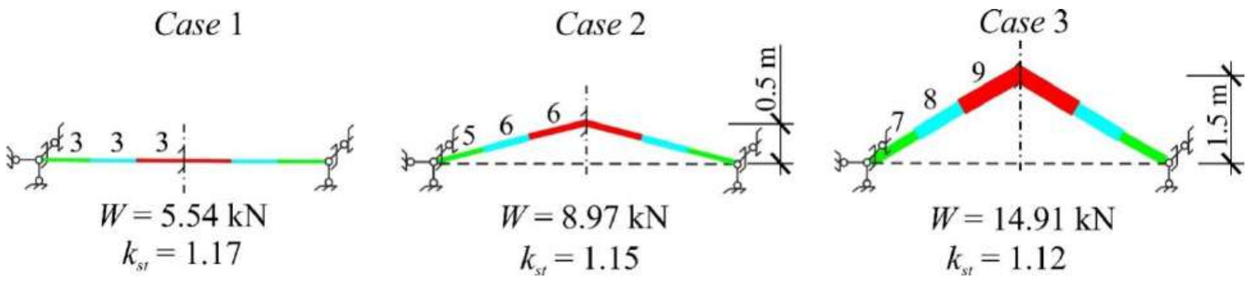

Figure 4. Results of an optimal search for a bar system with two supports with numbers of bar cross-section combinations (see Table 2)

Example 2 demonstrates the object of optimization represented by a symmetrical plane frame with a girder truss, span $L = 36\,\text{m}$ (Fig. 5). In the basic configuration of the object $H_1 = 10\,\text{m}$, $H_2 = 3.5\,\text{m}$, $H_3 = 1.75\,\text{m}$. The frame has rigid supports A, B and is fixed in the nodes of the upper chord of the truss from displacement in the direction of axis Z. The operational load of the weight of the structure and snow in the form of the system of forces P_1, P_2, wind pressure represented by distributed loads q_1 - q_4, and bars weight adjusted during the process of optimization according to the varied parameters, was taken into account. Values of loads were determined considering the structure location in Bryansk (Russian Federation). The following was set out: $P_1 = 108\,\text{kN}$, $P_2 = 54\,\text{kN}$, $q_1 = 1.38\,\text{kN/m}$, $q_2 = 4.42\,\text{kN/m}$, $q_3 = 1.035\,\text{kN/m}$, $q_4 = 3.31\,\text{kN/m}$, $[u]_i = 9\,\text{cm}$, $[v]_i = 12\,\text{cm}$, $R_y = 234\,\text{MPa}$.

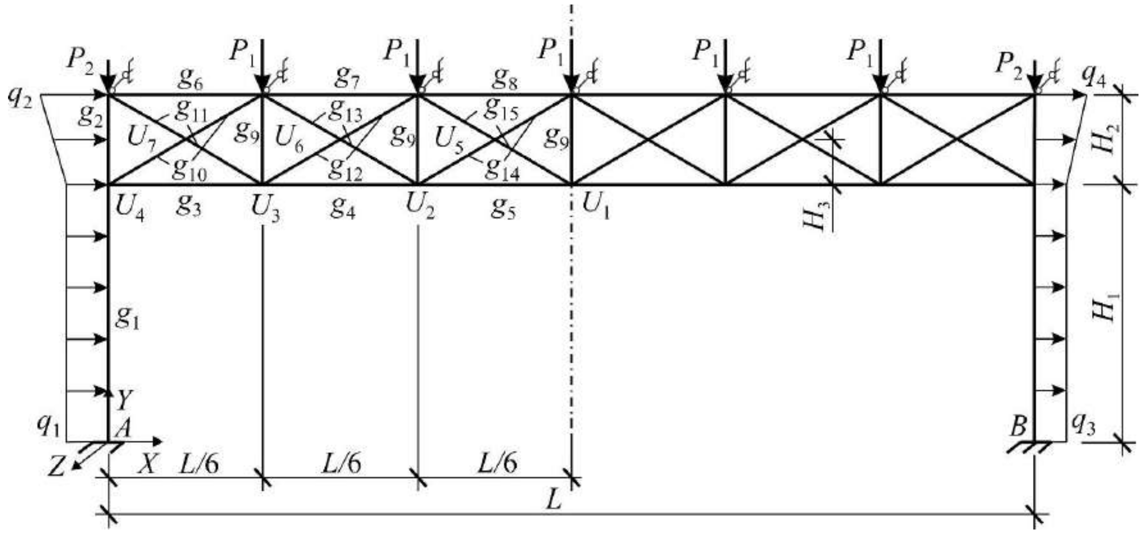

Figure 5. Frame basic configuration

All in all, 22 variables were varied independently: 15 combinations of cross-section dimensions and 7 coordinates. This being the case, provisions were made to ensure structure symmetry. In Figure 5, for the left half of the object, $g_1 - g_{15}$ groups of bars are shown with independently varied combinations of cross-section dimensions and nodes $U_1 - U_7$ with independently variable coordinates Y. It was supposed that the bars have an H-beam cross-section (see Fig. 3b), provided that $z \parallel Z$. For each group $g_1 - g_{15}$ of bars, the search was performed with reference to the combinations of dimensions indicated in Table 3. For Y coordinates of $U_1 - U_4$ nodes, a set of permissible values {700; 800; 900; 1000; 1050 1100} (cm) was taken into account, and for $U_5 - U_7$ nodes – the set {1150; 1175; 1200; 1225; 1250} (cm).

Table 3. Permissible combinations of bar cross-sections in Example 2

Number of combination	b_f, cm	t_f, cm	h_w, cm	t_w, cm
1	10	1	8	0.6
2	20	1.2	18	0.6
3	25	1.6	23	0.8
4	30	1.8	28	0.8
5	35	1.8	33	0.8
6	40	2	38	1
7	43	2	40	1
8	45	2.2	43	1
9	50	2.4	48	1.2
10	55	2.4	52	1.4
11	60	2.6	58	1.6
12	70	2.8	68	1.8

In performing the structure discretization, each bar was divided into five finite elements. As a result of the optimal search, the solution was obtained and shown in Fig. 6 with the value of the objective function $W = 88.50\,\text{kN}$, where digits indicate the number of combinations of bar cross-section dimensions (see Table 3). In this case, 300 iterations of the outer cycle were required with less than $6 \cdot 10^4$ structure variant analysis. The optimization process took 37 hours of computer time by using an Intel Core i7 Processor. For this project, coefficient $k_{st} = 1.19$. From Figure 6, it is clear that during the course of optimization, for the most important bar cross-sections, an arch configuration was reproduced approximately.

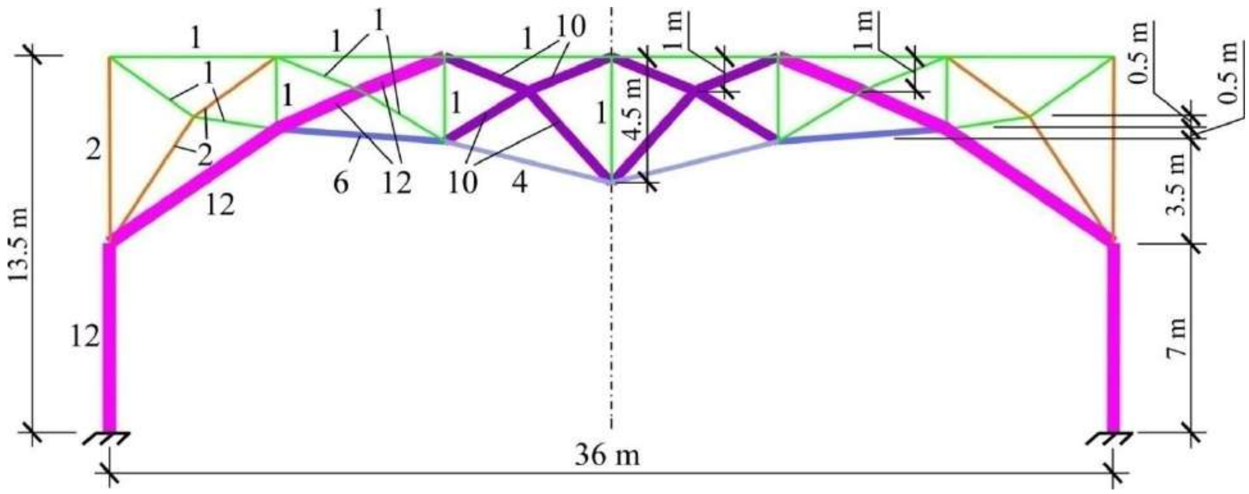

Figure 6. Result of frame optimization

Discussion

It should be noted that in the presented algorithm used for the performance of optimal search iterations, an object stability assessment is provided for, including the stability of individual bars according to a spatial pattern. The introduction of a random self-balanced system of small forces can be considered as a practical means to reduce complexity of calculations when there is an opportunity to approximately reproduce buckling corresponding to the Euler mode of stability loss in the case where a normative load does not allow it to be done. Such conditional additional loading cannot lead to rejection of an efficient structure variant. At the same time, it is presumed that, in any case, the solution of an optimization task must be analyzed in detail, including by applying widely-distributed software for finite element analysis.

In the considered examples, the proposed procedure provided for obtaining the resulting framework variants and stability conditions both via the Euler method and in accordance with standard requirements [24]. The values of the Euler stability coefficient for such project solutions did not exceed 1.19. Since the search was performed using discrete sets of parameters, the stability coefficients are quite acceptable for practical purposes. In this case, in assessing the structure variant stability combined with the calculation of stress and strain of the bar system. This approach does not require intermediate search stages of multiple consideration of the generalized problem of eigenvalues or the performance of calculating the stress-strain structure in a geometrically nonlinear setting, and allows solving, with an acceptable level of requirements to the complexity of the calculations, complex optimization problems of bar systems.

Conclusion

1. A computational scheme is proposed which allows optimization of flat rod systems made of steel, on discrete sets of bar cross-section dimensions and geometrical parameters defining the shape of a structure.

2. An optimal search is performed using the genetic algorithm procedures earlier proposed by the authors for effectively solving complex tasks with a large number of constraints.

3. In the optimization process, verification of the structure variants for stresses, displacements, and overall stability is provided for. Assessment of compliance with requirements for stability is performed both for buckling in the structure plane and out of plane by applying an approximate approach providing for the implementation of 5 iterations of the object deformation analysis via the finite element method based on the tangent of the stiffness matrix. In this case, no multiple generalized eigenvalue problems require solving.

4. Examples of steel load-bearing structures were used to make it possible, due to the proposed approach, to find solutions for flat rod systems optimization. Verification of compliance with stability constraints based on the adjusted schemes showed that factors of safety for the obtained constructive solutions were within the interval [1.12, 1.19].

Acknowledgement

This paper was executed under the auspices of the Russian Fundamental Research Fund: grant 16-38-00041 "Evolutionary optimization of steel load-bearing structures of buildings and structures of the normal and high levels of responsibility".

References

1. Yang X.-S. *Engineering Optimization: An Introduction with Metaheuristic Applications.* Wiley. Hoboken. NJ. USA, 2010. 347 p.
2. Goncalves M.S., Lopez R.H., Miguel L.F.F. Search group algorithm: A new metaheuristic method for the optimization of truss structures. *Computers and Structures.* 2015. No. 153. Pp. 165–184.
3. Ho-Huu V., Nguyen-Thoi T., Vo-Duy T., Nguyen-Trang T. An adaptive elitist differential evolution for optimization of truss structures with discrete design variables. *Computers and Structures.* 2016. No. 165. Pp. 59–75.
4. Erbatur F., Hasançebi O., Tütücü I., Kılıç H. Optimal design of planar and space structures with genetic algorithms. *Computers and Structures.* 2000. No. 75(2). Pp. 209–224.
5. Sonmez M. Discrete optimum design of truss structures using artificial bee colony algorithm. *Structural and Multidisciplinary Optimization.* 2011. No. 43(1). Pp. 85–97.
6. Lamberti L. An efficient simulated annealing algorithm for design optimization of truss structures. *Computers and Structures.* 2008. No. 86(19-20). Pp. 1936–1953.
7. Perez R.E., Behdinan K. Particle swarm approach for structural design optimization. *Computers and Structures.* 2007. No. 85. Pp. 1579–1588.
8. Kaveh A., Talatahari S. Size optimization of space trusses using big bang-big crunch algorithm. *Computers and Structures.* 2009. No. 87(17-18). Pp. 1129–1140.
9. Kaveh A., Khayatazad M. A new meta-metaheuristic method: ray optimization. *Computers and Structures.* 2012. No. 112-113. Pp. 283–294.
10. Kaveh A., Mahdavi V.R. Colliding bodies optimization method for optimum design of truss structures with continuous variables. *Advances in Engineering Software.* 2014. No. 70. Pp. 1–12.
11. Hasançebi O., Erbatur F. On efficient use of simulated annealing in complex structural optimization problems. *Acta Mechanica.* 2002. No. 157(1). Pp. 27–50.
12. Kaveh A., Kalatjari V. Size/geometry optimization of trusses by the force method and genetic algo-rithm. *ZAMM Journal of Applied Mathematics and Mechanics.* 2004. No. 84(5). Pp. 347–357.
13. Dedea T., Ayvaz Y. Combined size and shape optimization of structures with a new meta-heuristic algorithm. *Applied Soft Computing.* 2015. No. 28. Pp. 250–258.
14. Kaveh A., Ahmadi B. Sizing, geometry and topology optimization of trusses using force method and supervised charged system search. *Structural Engineering and Mechanics.* 2014. No. 50(3). Pp. 365–382.
15. Rahami H., Kaveh A., Gholipour Y. Sizing, geometry and topology optimization of trusses via force method and genetic algorithm. *Engineering Structures.* 2008. No. 30. Pp. 2360–2369.
16. Gao X., Ma H. Topology optimization of continuum structures under buckling constraints. *Computers and Structures.* 2015. No. 157. Pp. 142–152.
17. André J., Torii R.H.L., Leandro F.F.M. Modeling of global and local stability in optimization of truss-like structures using frame elements. *Structural and Multidisciplinary Optimization.* 2015. No. 51(6). Pp. 1187–1198.
18. Serpik I.N., Alekseytsev A.V. Optimizatsiya ramnykh konstruktsiy s uchetom vozmozhnosti zaproyektnykh vozdeystviy. Inzhenerno-stroitelnyy zhurnal [Optimization of

Литература

1. Yang X.-S. Engineering Optimization: An Introduction with Metaheuristic Applications. Wiley. Hoboken. NJ. USA, 2010. 347 p.
2. Goncalves M.S., Lopez R.H., Miguel L.F.F. Search group algorithm: A new metaheuristic method for the optimization of truss structures // Computers and Structures. 2015. № 153. Pp. 165–184.
3. Ho-Huu V., Nguyen-Thoi T., Vo-Duy T., Nguyen-Trang T. An adaptive elitist differential evolution for optimization of truss structures with discrete design variables // Computers and Structures. 2016. № 165. Pp. 59–75.
4. Erbatur F., Hasançebi O., Tütücü I., Kılıç H. Optimal design of planar and space structures with genetic algorithms // Computers and Structures. 2000. № 75(2). Pp. 209–224.
5. Sonmez M. Discrete optimum design of truss structures using artificial bee colony algorithm // Structural and Multidisciplinary Optimization. 2011. № 43(1). Pp. 85–97.
6. Lamberti L. An efficient simulated annealing algorithm for design optimization of truss structures // Computers and Structures. 2008. № 86(19-20). Pp. 1936–1953.
7. Perez R.E., Behdinan K. Particle swarm approach for structural design optimization // Computers and Structures. 2007. № 85. Pp. 1579–1588.
8. Kaveh A., Talatahari S. Size optimization of space trusses using big bang-big crunch algorithm // Computers and Structures. 2009. № 87(17-18). Pp. 1129–1140.
9. Kaveh A., Khayatazad M. A new meta-metaheuristic method: ray optimization // Computers and Structures. 2012. № 112-113. Pp. 283–294.
10. Kaveh A., Mahdavi V.R. Colliding bodies optimization method for optimum design of truss structures with continuous variables // Advances in Engineering Software. 2014. № 70. Pp. 1–12.
11. Hasançebi O., Erbatur F. On efficient use of simulated annealing in complex structural optimization problems // Acta Mechanica. 2002. № 157(1). Pp. 27–50.
12. Kaveh A., Kalatjari V. Size/geometry optimization of trusses by the force method and genetic algorithm // ZAMM Journal of Applied Mathematics and Mechanics. 2004. № 84(5). Pp. 347–357.
13. Dedea T., Ayvaz Y. Combined size and shape optimization of structures with a new meta-heuristic algorithm // Applied Soft Computing. 2015. № 28. Pp. 250–258.
14. Kaveh A., Ahmadi B. Sizing, geometry and topology optimization of trusses using force method and supervised charged system search // Structural Engineering and Mechanics. 2014. № 50(3). Pp. 365–382.
15. Rahami H., Kaveh A., Gholipour Y. Sizing, geometry and topology optimization of trusses via force method and genetic algorithm // Engineering Structures. 2008. № 30. Pp. 2360–2369.
16. Gao X., Ma H. Topology optimization of continuum structures under buckling constraints // Computers and Structures. 2015. № 157. Pp. 142–152.
17. André J., Torii R.H.L., Leandro F.F.M. Modeling of global and local stability in optimization of truss-like structures using frame elements // Structural and Multidisciplinary Optimization. 2015. № 51(6). Pp. 1187–1198.
18. Серпик И.Н., Алексейцев А.В. Оптимизация рамных конструкций с учетом возможности запроектных воздействий // Инженерно-строительный журнал. 2013. № 9(44). С. 38–46.

frame structures taking into account the possibility of emergency actions]. *Magazine of Civil Engineering.* 2013. No. 9(44). Pp. 38–46. (rus)

19. Serpik I.N., Alekseytsev A.V. Optimization of flat steel frame and foundation posts system. *Magazine of Civil Engineering*. 2016. No. 1. Pp. 14–24. (rus)
20. Wriggers P. *Nonlinear Finite Element Methods.* Springer-Verlag, Berlin-Heidelberg, 2008. 560 p.
21. Kucherenko A.A. Optimizatsiya topologii sterzhnevykh sistem i ikh ustoychivost [Optimization of the topology of the rod and their stability]. *Sistemnyye tekhnologii.* 2015. No. 4(99). Pp. 23–30. (rus)
22. Sergeyev O.A., Kiselev V.G., Sergeyeva S.A. Obshchaya poterya ustoychivosti i optimizatsiya sterzhnevykh konstruktsiy so sluchaynymi nesovershenstvami pri ogranicheniyakh na veroyatnost bezotkaznoy raboty [Overall instability and optimization of bar structures with random defects in case of constraints on faultless operation probability]. *Magazine of Civil Engineering.* 2013. No. 9(44). Pp. 30–41. (rus)
23. Serpik I.N., Alekseytsev, A.V., Balabin, P.Y. Mixed approaches to handle limitations and execute mutation in the genetic algorithm for truss size, shape and topology optimization. Periodica Polytechnica Civil Engineering. 2017. No. 61(3). Pp. 471–482.
24. *SP 16.13330.2011. Stalnyye konstruktsii.* Aktualizirovannaya redaktsiya SNiP II-23-81* [Russian Set of Rules SP 16.13330.2011. Steel structures. Updated version of SNiP II-23-81 *]. Moscow: Ministerstvo regionalnogo razvitiya RF, 2011. 173 p. (rus)
25. Zienkiewicz O.C., Taylor R.L., Fox D. *The finite element method for solid and structural mechanics.* Elsevier. Oxford, 2014. 672 p.
26. Alfutov N.A. *Osnovy rascheta na ustoychivost uprugikh system* [Basics of calculating the stability of elastic systems]. Moscow: Mashinostroyeniye, 1978. 312 p. (rus)
27. Rutkovskaya D., Pilinskiy M., Rutkovskiy L. *Neyronnyye seti, geneticheskiye algoritmy i nechetkiye sistemy* [Neural networks, genetic algorithms and fuzzy systems]. Moscow: Goryachaya liniya-Telekom, 2008. 452 p. (rus)
28. Gladkov L.A., Kureychik V.V., Kureychik V.M. *Geneticheskiye algoritmy* [Genetic algorithms]. Moscow: Fizmatlit, 2010. 368 p. (rus)

19. Серпик И.Н., Алексейцев А.В. Оптимизация системы стальной плоской рамы и столбчатых фундаментов // Инженерно-строительный журнал. 2016. № 1(61). С. 14–24.
20. Wriggers P. Nonlinear Finite Element Methods. Springer-Verlag, Berlin-Heidelberg, 2008. 560 p.
21. Кучеренко А.А. Оптимизация топологии стержневых систем и их устойчивость // Системные технологии. 2015. № 4(99). С. 23–30.
22. Сергеев О.А., Киселев В.Г., Сергеева С.А. Общая потеря устойчивости и оптимизация стержневых конструкций со случайными несовершенствами при ограничениях на вероятность безотказной работы // Инженерно-строительный журнал. 2013. № 9(44). С. 30–41.
23. Serpik I.N., Alekseytsev, A.V., Balabin, P.Y. Mixed approaches to handle limitations and execute mutation in the genetic algorithm for truss size, shape and topology optimization // Periodica Polytechnica Civil Engineering. 2017. № 61(3). Pp. 471–482.
24. СП 16.13330.2011. Стальные конструкции. Актуализированная редакция СНиП II-23-81*. М.: Министерство регионального развития РФ, 2011. 173 с.
25. Zienkiewicz O.C., Taylor R.L., Fox D. The finite element method for solid and structural mechanics. Elsevier. Oxford, 2014. 672 p.
26. Алфутов Н.А. Основы расчета на устойчивость упругих систем. М.: Машиностроение, 1978. 312 с.
27. Рутковская Д., Пилиньский М., Рутковский Л. Нейронные сети, генетические алгоритмы и нечеткие системы. М: Горячая линия-Телеком, 2008. 452 с.
28. Гладков Л.А., Курейчик В.В., Курейчик В.М. Генетические алгоритмы. М.: Физматлит, 2010. 368 с.

Igor Serpik,
+7(4832)64-88-00; iserpik@online.debryansk.ru

Anatoly Alekseytsev,
+7(960)564-33-58; aalexw@mail.ru

Pavel Balabin,
7(919)196-53-92; pavelbalabin90@yandex.ru

Natalia Kurchenko,
+7(920)602-32-40; inserpik@gmail.com

Игорь Нафтольевич Серпик,
+7(4832)64-88-00;
эл. почта: iserpik@online.debryansk.ru

Анатолий Викторович Алексейцев,
+7(960)564-33-58; эл. почта: aalexw@mail.ru

Павел Юрьевич Балабин,
+7(919)196-53-92;
эл. почта: pavelbalabin90@yandex.ru

Наталья Сергеевна Курченко,
+7(920)602-32-40; эл. почта: inserpik@gmail.com

doi: 10.18720/MCE.76.17

Thermal cracking resistance in massive foundation slabs in the building period

Термическая трещиностойкость массивных фундаментных плит в строительный период

A.V. Bushmanova,
Yu.G. Barabanshchikov,
K.V. Semenov,
A.Ya. Struchkova,
S.S. Manovitsky,
Peter the Great St. Petersburg Polytechnic University, St. Petersburg, Russia

Студент А.В. Бушманова,
д-р техн. наук, профессор Ю.Г. Барабанщиков,
канд. техн. наук, доцент К.В. Семенов,
студент А.Я. Стручкова,
студент С.С. Мановицкий,
Санкт-Петербургский политехнический университет Петра Великого, г. Санкт-Петербург, Россия

Key words: modulus of deformation; massive concrete and reinforced concrete structures; thermal stressed state; thermal cracking resistance; hardening temperature

Ключевые слова: модуль деформации; массивные бетонные и железобетонные конструкции; термонапряженное состояние; термическая трещиностойкость; температура твердения

Abstract. The article deals with the research of the thermal cracking resistance of massive concrete and reinforced foundation slabs of buildings and structures in the building period. The article examines the results of the analysis of the thermal stress state of a massive foundation slab with a fixed thickness of thermal insulation as well as the results of changing the minimum thickness of the insulation on a surface, providing the cracking resistance of the structures on different plate heights, with and without taking into account the hardening temperature influence on the concrete modulus of the deformation. The article authors determined that the solution of the problem of definition the thermal stress state of the massive foundation slab in the building period without the hardening temperature influence on the modulus of deformation may cause a significant distortion of the real diagram of the thermal stresses and elongation deformations in the structures body. It was indicated that the calculation error essentially depends on the height of the foundation slab. Additionally it was established that in case the slab height exceeds 1.25 m the problem should be solved in a strict setting, which would allow to minimize the insulation layer.

Аннотация. Работа посвящена исследованию термической трещиностойкости массивных бетонных и железобетонных фундаментных плит зданий и сооружений в строительный период. В статье рассматриваются результаты анализа термонапряженного состояния массивной фундаментной плиты при фиксированной толщине теплоизоляции, а также результаты изменения минимальных толщин поверхностной теплоизоляции, обеспечивающих трещиностойкость конструкции, при различных высотах плиты с учетом влияния температуры твердения смеси на модуль деформации бетона и без данного учета. Авторами установлено, что решение задачи определения термонапряженного состояния массивных фундаментных плит в строительный период без учета влияния температуры твердения бетона на модуль деформации может привести к существенному искажению действительных эпюр распределения термонапряжений и деформаций удлинения в теле конструкции. Показано, что погрешность в расчетах существенно зависит от высоты фундаментной плиты. Также определено, что при высотах плит, превышающих 1,25 м, расчеты необходимо проводить только в строгой постановке задачи, что приводит к существенной экономии необходимой специальной теплоизоляции.

Introduction

In general practice the calculation of thermal fields is often based on the heat equation solution as well as thermal stresses definition [1–7], linked with calculation of cracking resistance massive of concrete in construction period. A change in the thermal state of such structures occurs due to the heat

Бушманова А.В., Барабанщиков Ю.Г., Семенов К.В., Стручкова А.Я., Мановицкий С.С. Термическая трещиностойкость массивных фундаментных плит в строительный период // Инженерно-строительный журнал. 2017. № 8(76). С. 193–200.

liberation from cement hydration during the concrete hardening process, as well as outside temperature fluctuations, solar exposure, various technological factors, etc. [8–13]. Emerging thermal stresses may cause damage to the structural integrity [14–20].

Due to a number of technological and manufacturing reasons, it is preferable to concrete massive foundation mats and other massive structures as a single block of equal height. However, it causes a considerable heat rise in the mass concrete as the result of an exothermic reaction during the concrete hardening. Consequently, the irregular temperature distribution arises along with the block height, which leads to the dangerous tensile strain first on the surface of the foundation slab and then in its central zones [21–29].

Deal with a problem of cracking it applied a complex of technological measures (the heat enclosure, a peripheral electric heating, cooling of concrete mix, tubing cooling of concrete etc.). However, before setting the optimal complex of measures it necessary to calculate the thermal stressed state of construction in a strict definition of the problem. Such a formulation presupposes taking into account the hardening temperature influence on thermophysical [30] and deformation characteristics of concrete.

The modulus of deformation is important characteristic of concrete, which has a significant running value in the building period. Many researches explored the modulus of deformation [31–37].

Modulus of elasticity is part of many static calculations and has close relation to other physical and mechanical characteristics of concrete as are creeping, shrinking, frost resistance etc. Final value of the modulus of elasticity of concrete depends on many influences [37], for example concrete aggregate [35–36]. One of the most important factors influencing the modulus of elasticity is the ambient temperature during concrete setting and hardening [31–34].

Nowadays in practice of calculating the thermal stressed state of the building period used function [17]:

$$E(t) = E_{max}\left(1 - e^{\alpha t^{\gamma}}\right) \tag{1}$$

where E_{max} – is the limit value of deformation of concrete, setting by rules;

α, γ – are functional dependency parameters;

t – current time.

The paper [31] deal that modulus of deformation significant depend on temperature of hardening. There is also suggested to take into account the dependency of «reduced time» hypothesis, which a real time replaced on reduced time a function of hardening temperature. The temperature function is of the form:

$$f_T = 2^{\frac{(T_1 - T_2)}{\varepsilon}} \tag{2}$$

where ε – is the characteristic temperature difference.

For the foregoing reasons, estimation of hardening temperature influence on modulus of concrete deformation in calculating the thermal cracking resistance of massive reinforced concrete structured in the building period is the vital task. Since the solution of the problem of definition the thermal stress state of the massive foundation slab in the building period without the hardening temperature influence on the modulus of deformation may cause a significant distortion of the real diagram of the thermal stresses.

The purpose of article is estimation of hardening temperature influence on modulus of concrete deformation in calculating the thermal cracking resistance of massive reinforced concrete structured in the building period and calculated validity of the necessity of such accounting.

As initial data (thermophysical and stress-related characteristics of concrete, cement heat radiation) the results or research, obtained in laboratory “Polytech-SKiM-Test” in CUBS department by professor Barabanschikov Y.G. were accepted.

Methods and Materials

This paper demonstrates calculation of the foundation mat thermal stressed state with the help of TERM software developed by the Institute of Civil Engineering at the Peter the Great St.Petersburg Polytechnic University [18]. This software calculates nonstationary fields of temperature and thermal stresses in slabs. An essential feature of the TERM software is the consideration of temperature influence on thermophysical and stress-related concrete characteristics.

Considering horizontal mats sizes significantly exceed their height, we can study a one-dimensional structural model for the mat central part with the reasonable degree of accuracy. In this model, stress and temperature are functions of the vertical coordinate space [38].

In order to estimate the cracking resistance of the foundation mat, we would use the deformation criterion suggested by P.I. Vasiliev [21]. According to this criterion, concrete elongation deformations, determined in view of the concrete creep factor and variable deformation modulus, should not exceed the ultimate concrete elongation.

The article examines the results of the analysis of the thermal stress state of a massive foundation slab with a fixed thickness of thermal insulation as well as the results of changing the minimum thickness of the insulation on a surface, providing the cracking resistance of the structures on different plate heights, with and without taking into account the hardening temperature influence on the concrete modulus of the deformation.

Consider B35 foundation slab 2 m high with the cement consumption of 340 kg/m^3 constructed in summer. The foundation slab is supported by the concrete bedding layer B12.5 with the grade foundation.

Thermal and physical characteristics of the concrete B35 are defined by the concrete thermal conductivity $\boldsymbol{\lambda}$ = 2.67 W/(m·^{0}C) and thermal capacity c = 1.0 kJ/(kg·^{0}C). For modulus of concrete deformation E_{max} = 34500 Мпа, $\alpha = -0.37$, $\gamma = 0.72$ [17].

Concrete creep account according to straight line inherited theory of aging using the relaxation function:

$$R(t,\tau) = A\left(1 - e^{-\beta\tau^{\alpha}}\right) + \left(B_1 + D_1 e^{-\beta\tau^{\alpha}}\right)e^{-\gamma_1(t-\tau)} + \left(B_2 + D_2 e^{-\beta\tau^{\alpha}}\right)e^{-\gamma_2(t-\tau)} \quad (3)$$

Where functional dependency parameters are as follows: A = 0.7; B_1 = 0.2; D_1 = 0.4; B_2 = 0.1; D_2 = 0.3; α = 0.67; $\beta = 3.61\times10^{-6}$ c^{-1}; $\gamma_1 = 1.17\times10^{-5}$ c^{-1}; $\gamma_2 = 2.33\times10^{-7}$ c^{-1}.

The heat dissipation process follows the I.D. Zaporozhets equation [16].

$$Q_T(\tau) = Q_{max}\left\{1 - \left[1 + A_{20}\int_0^t F_Q[T(\tau)d\tau]\right]\right\}^{-\frac{1}{m-1}} \quad (4)$$

The equation parameters I.D. Zaporozhets gets from experimental evidence on concrete heat dissipation [20] Q_{max} = 157500 kJ/m^3, $A_{20}=4.1\times10^{-6}$ c^{-1}.

The following technological specifications of concrete pouring were taken into account: inside the heat enclosure, the concrete mix is poured as a single 2.0 m high block with the concrete mix temperature is 20 ^{0}C and air temperature is 20 ^{0}C. After concreting the surface is covered with insulation, which thickness is determined by the cracking prevention condition.

Results

Evaluation of thermal stressed state with a fixed thickness of thermal insulation

Calculations of this paragraph provide for the same thickness of thermal insulation layer for the case with influence of hardening temperature on modulus of concrete deformation and without such influence. Figure 1 shows graphs of variation in time the thermal stresses in the control points of the base slab without the special insolation. Solid line is the thermal stresses determined with the influence of temperature of hardening on modulus of deformation. Dash line is the thermal stresses without of such influence.

Analyze of a result show us:

1. Character of changing the thermal stresses with time is the same in cases with and without temperature influence on modulus of deformation;
2. The maximum stresses without taking into account the influence of temperature on the modulus deformation for exothermal heating moment (3 days) is: tensile on the surface of the slab is 2.25 MPa, compressive in the center of the slab is 0.86 MPa;
3. Similarly, in the case with taking into account the influence of temperature: tensile stresses on the surface is 3.41 MPa, compressive in the center is 1.38 MPa;

In such a way, problem solution in the simple definition leads to decrease of tensile stresses on the surface to 1.16 MPa (or to 34 %), but compressive tensile to 0.52 MPa (or to 38 %).

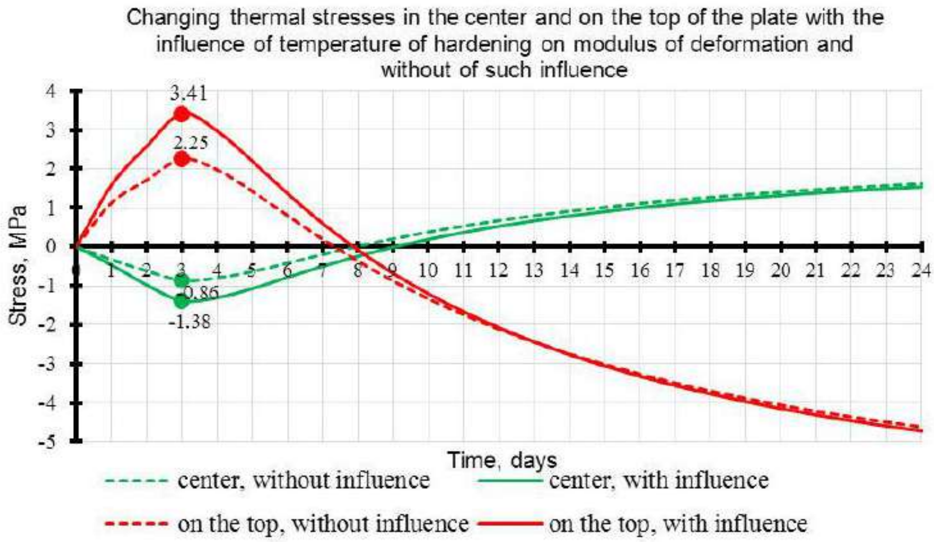

Figure 1. Graph of changing thermal stresses in the center and on the upper surface of the slab (solid line with the influence of temperature of hardening, dash line without of such influence)

With a special heat insulation on the surface of the foundation slab the relative elongation deformations changed not so obviously (Fig. 2). Deformations calculated with the hardening temperature influence on the modulus become less than deformation determined without such influence. If a thickness of insulation layer is 4.7 cm than such reducing is 3.9×10^{-4} (or 8 %). This is effect because relative deformations calculate as stresses divided by modulus of deformation. Using of the heat insulation reduce the temperature difference “center-surface of the slab” and accordingly the stresses themselves. Reducing of numerator (that is stresses) equally for methods with taking into account temperature influence and without that. At the same if we use the hypothesis of “reduced time” than denominator (modulus of deformation) increase in a greater degree.

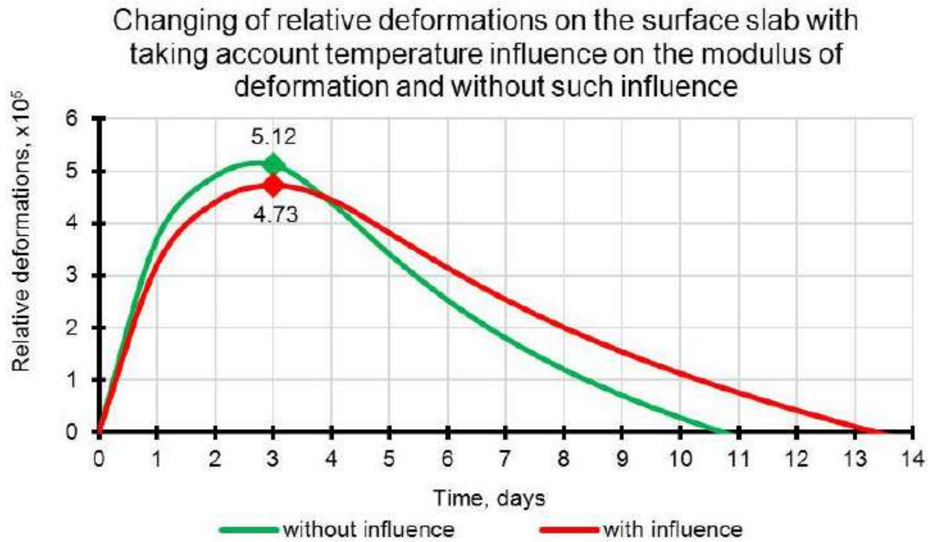

Figure 2. Dependency graph of relative deformations on the surface slab by time with taking account temperature influence on the modulus of deformation and without such influence (thickness of heat insulation 4.7 cm)

Selection of the required insulation thickness

Calculation is performed for the thermal insulation of foam polystyrene density 40 kg/m^3, with a coefficient of heat conductivity: λ = 0.030 W/m×^{o}C. In this part of the work for more information thicknesses of the foundation slabs varied in the range from 1.0 to 2.5 m at a pitch of 0.5 m. Figure 3 shows graphs of the minimum safe (in terms of cracking) surface insulation thicknesses depending on the thickness of the foundation slab.

Bushmanova A.V., Barabanshchikov Yu.G., Semenov K.V., Struchkova A.Y., Manovitsky S.S. Thermal cracking resistance in massive foundation slabs in the building period. *Magazine of Civil Engineering*. 2017. No. 8. Pp. 193–200. doi: 10.18720/MCE.76.17.

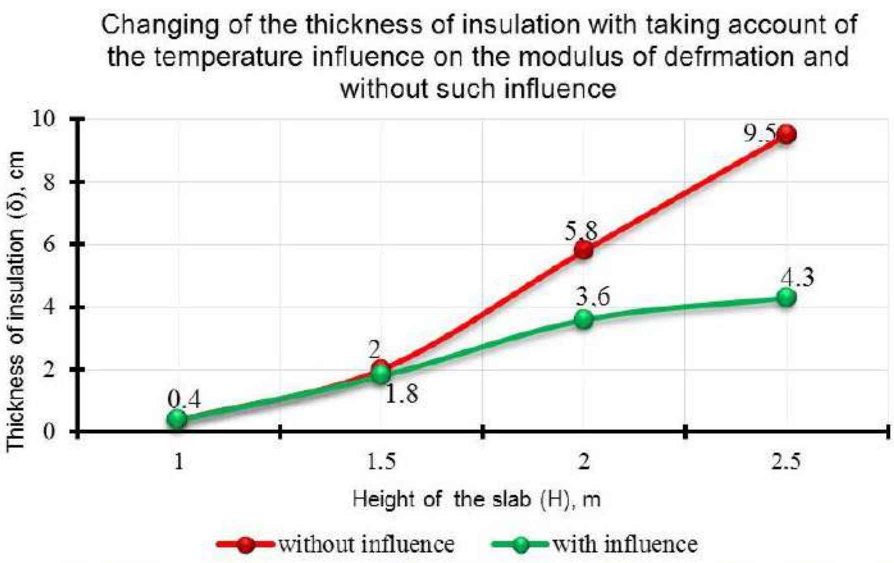

Figure 3. Graph of changing the required thickness of insulation on the surface of the slab

Analyze of a results show us:

1. At low heights of the foundation slab (1.0–1.25 m) the effect of the hardening temperatures on the thickness safety insulation layer is not significant, solve the problem in a simplified variant will cause an error not exceeding the accuracy of the base line (5 %);
2. For the thickness of the slabs from 1.5 m the effect of hardening temperature becomes very significant: so for a foundation slab thickness of 2.0 m not taking into account the hardening temperature influence leads to an overestimation of the necessary thickness of thermal insulation by 2.2 cm (or by 38 %) and for a foundation slab thickness of 2.5 m by 5.2 cm (or 55 %).

Discussion

According to the work [31–37] the elastic modulus is not a constant, in fact, it can reach very different values in concrete of the same strength class. It is thus important to have knowledge of aspects, which have the greatest influence on it. According to studies, the solution of the problem of definition the thermal stress state of the massive foundation slab in the building period without the hardening temperature influence on the modulus of deformation may cause a significant distortion of the real diagram of the thermal stresses and elongation deformations in the structures body. Thereby one of the most important factors influencing the modulus of elasticity is the hardening temperature during concrete setting and hardening [31–34].

Conclusion

The results of the conducted experiments allow us to make following conclusions:

1. Solving the problem of thermal stressed state of the massive foundation slabs in the building period without taking into account the influence of concrete hardening temperature on the modulus of deformation may cause to significant deviation of the real diagram of the thermal stresses and elongation deformations in the structures body;
2. The calculation error significant depends on the heights of the foundation slab. At the heights from 1 to 1.5 m calculations of thermal cracking resistance can make in the simple definition without taking into account the influence of the hardening temperature on the modulus of deformation. At heights of slabs large 1.5 m calculations must be carried out only in the strict definition of problem;
3. Calculation of thermal cracking resistance of foundation slab with taking into account the influence of hardening temperature on the modulus of concrete deformation leads to (for the slabs higher than 1.5 m) significant economy of the special required heat insolation. Volume of economy depends on thickness of the foundation slab because for a slab of 2.0 m height it is 38 %.

References

1. Vatin N.I., Nemova D.V., Rymkevich P.P., Gorshkov A.S. Vliyanie urovnya teplovoy zashchity ograzhdayushchikh konstruktsiy na velichinu poter' teplovoy energii v zdanii

Литература

1. Ватин Н.И., Немова Д.В., Рымкевич П.П., Горшков А.С. Влияние уровня тепловой защиты ограждающих конструкций на величину потерь тепловой энергии в

[Influence of building envelope thermal protection on heat loss value in the building]. *Magazine of Civil Engineering*. 2012. No. 8. Pp. 4–13. (rus)

2. Petrosova D.V., Kuzmenko N.M., Petrosov D.V. Eksperimental'noe issledovanie teplovogo rezhima legkoy ograzhdayushchey konstruktsii v naturnykh usloviyakh [A field experimental investigation of the thermal regime of lightweight building envelope construction]. *Magazine of Civil Engineering.* 2013. No. 8. Pp. 31–37. (rus)
3. Vatin N.I., Gorshkov A.S., Nemova D.V. Energoeffektivnost' ograzhdayushchikh konstruktsiy pri kapital'nom remonte [Energy efficiency of envelopes at major repairs]. *Construction of Unique Buildings and Structures*. 2013. No. 3(8). Pp. 1–11. (rus)
4. Nemova D.V., Vatin N.I., Gorshkov A.S., Kashabin A.V., Rymkevich P.P., Tseytin D.N. Tekhniko-ekonomicheskoe obosnovanie meropriyatiy po utepleniyuograzhdayushchikh konstruktsiy individual'nogo zhilogo doma [Technical and economic assessment on actions for heat insulation of external envelops of an individual house]. *Construction of Unique Buildings and Structures.* 2014. No. 8(23). Pp. 93–115. (rus)
5. Vatin N.I., Nemova D.V. Povyshenie energoeffektivnosti zdaniy detskikh sadov [Increase of power efficiency of buildings of kindergartens]. *Construction of Unique Buildings and Structures.* 2012. No. 3. Pp. 1–11. (rus)
6. Gorshkov A.S., Rymkevich P.P., Vatin N.I. Modelirovanie protsessov nestatsionarnogo perenosa tepla v stenovykh konstruktsiyakh iz gazobetonnykh blokov [Simulation of non-stationary heat transfer processesin autoclaved aerated concrete-walls]. *Magazine of Civil Engineering.* 2014. No. 8. Pp. 38–48. (rus)
7. Platonova M.A., Vatin N.I., Nemova D.V., Matoshkina S.A., Iotti D., Togo I. Vliyanie vozdukhoizolyatsionnogo sostava na teplotekhnicheskie kharakteristiki ograzhdayushchikh konstruktsiy [The influence of the airproof composition on the thermo technical characteristics of the enclosing structures]. *Construction of Unique Buildings and Structures.* 2014. No. 4(19). Pp. 83–95. (rus)
8. Teplova Z.S., Solovyeva K.I., Nemova D.V., Trubina D.A., Petrosova D.V. Teplotekhnicheskiy raschet ograzhdayushchey konstruktsii obshcheobrazovatel'noy shkoly [Thermo technical calculation of enclosure structure of comprehensive school]. *Construction of Unique Buildings and Structures.* 2014. No. 4(19). Pp. 96–108. (rus)
9. Gorshkov A., Vatin N., Nemova D., Tarasova D. The Brickwork Joints Effect on the Thermotechnical Uniformity of the Exterior Walls from Gas-Concrete Blocks. *Applied Mechanics and Materials.* 2015. Vol. 725–726. Pp. 3–8.
10. Vatin N., Petrichenko M., Nemova D., Staritcyna A., Tarasova D. Renovation of educational buildings to increase energy efficiency. *Applied Mechanics and Materials.* 2014. Vol. 633–634. Pp. 1023–1028.
11. Korsun V., Korsun A. The influence of precompression on strength and strain properties of concrete under the effect of elevated temperatures. *Applied Mechanics and Materials.* 2015. Vol. 725–726. Pp. 469–474.
12. Korsun V., Vatin N., Korsun A., Nemova D. Physical-mechanical properties of the modified fine-grained concrete subjected to thermal effects up to 200 ˚С. *Applied Mechanics and Materials.* 2014. Vol. 633–634. Pp. 1013–1017.
13. Korsun V., Korsun A. The influence of precompression on strength and strain properties of concrete under the effect of elevated temperatures. *Applied Mechanics and Materials.* 2015. Vol. 725–726. Pp. 469–474.
14. Barabanshchikov Y.G., Sokolov V.A., Vasiliev A.S., Shevelev M.V. Regulirovanie srokov skhvatyvaniya tsementa khimicheskimi dobavkami [Adjustment of cement setup time with chemical admixtures]. *ALITINFORM: Tsement, Beton, Sukhie smesi.* 2012. No. 3(25).

здании // Инженерно-строительный журнал. 2012. № 8(34). С. 4–14.

2. Петросова Д.В., Кузьменко Н.М., Петросов Д.В. Экспериментальное исследование теплового режима легкой ограждающей конструкции в натурных условиях // Инженерно-строительный журнал. 2013. № 8(43). С. 31–37.
3. Ватин Н.И., Горшкв А.С., Немова Д.В. Энергоэффективнсть ограждающий конструкций при капитальном ремонте // Строительство уникальных зданий и сооружений. 2013. № 3(8). С. 1–11.
4. Немова Д.В., Ватин Н.И., Горшков А.С., Кашабин А.В., Рымкевич П.П., Цейтин Д.Н. Технико-экономическое обоснование мероприятий по утеплению ограждающих конструкций индивидуального жилого дома // Строительство уникальных зданий и сооружений. 2014. № 8(23). С. 93–115.
5. Ватин Н.И., Немова Д.В. Повышение энергоэффективности зданий детских садов // Строительство уникальных зданий и сооружений. 2012. № 3. С. 1–11.
6. Горшков А.С., Рымкевич П.П., Ватин Н.И. Моделирование процессов нестационарного переноса тепла в стеновых конструкциях из газобетонных блоков // Инженерно-строительный журнал. 2014. № 8. С. 38–48.
7. Платонова М.А., Ватин Н.И., Немова Д.В., Матошкина С.А., Иотти Д., Того И. Влияние воздухоизоляционного состава на теплотехнические характеристики ограждающих конструкций // Строительство уникальных зданий и сооружений. 2014. № 4(19). С. 83–95.
8. Теплова Ж.С., Соловьева К. И., Немова Д.В., Трудина Д.А., Петросова Д.В. Теплотехнический расчет ограждающей конструкции общеобразовательной школы // Строительство уникальных зданий и сооружений. 2014. № 4(19). С. 96–108.
9. Gorshkov A., Vatin N., Nemova D., Tarasova D. The Brickwork Joints Effect on the Thermotechnical Uniformity of the Exterior Walls from Gas-Concrete Blocks // Applied Mechanics and Materials. 2015. Vol. 725–726. Pp. 3–8.
10. Vatin N., Petrichenko M., Nemova D., Staritcyna A., Tarasova D. Renovation of educational buildings to increase energy efficiency // Applied Mechanics and Materials. 2014. Vol. 633–634. Pp. 1023–1028.
11. Korsun V., Korsun A. The Influence of Precompression on Strength and Strain Properties of Concrete under the Effect of Elevated Temperatures // Applied Mechanics and Materials. 2015. Vol. 725–726. Pp. 469–474.
12. Korsun V., Vatin N., Korsun A., Nemova D. Physical-mechanical properties of the modified fine-grained concrete subjected to thermal effects up to 200 ˚С // Applied Mechanics and Materials. 2014. Vol. 633–634. Pp. 1013–1017.
13. Korsun V., Korsun A. The Influence of Precompression on Strength and Strain Properties of Concrete under the Effect of Elevated Temperatures // Applied Mechanics and Materials. 2015. Vol. 725–726. Pp. 469–474.
14. Барабанщиков Ю.Г., Соколов В.А., Васильев А.С., Щевелев М.В. Регулирование сроков схватывания цемента химическими добавками // ALITINFORM: Цемент, бетон, сухие смеси. 2012. № 3(25). С. 32–41.
15. Александровский С.В. Расчёт бетонных и железобетонных конструкций на изменения температуры и влажности с учётом ползучести. М.: Стройиздат, 1973. 444 с.
16. Запорожец И.Д., Окороков С.Д., Парийский А.А. Тепловыделение бетона. М.: Стройиздат, 1966. 316 с.
17. Малинин Н.А. Исследование термонапряженного состояния массивных бетонных конструкций с переменными деформативными характеристиками: Дис. на соиск. учен. степ. к. т. н.: Спец. 05.23.01. Л.,

Pp. 32–41. (rus)
15. Aleksandrovskiy S.V. *Raschet betonnykh i zhelezobetonnykh konstruktsiy na izmeneniya temperatury i vlazhnosti s uchetom polzuchesti* [Calculation of temperature change and humidity in terms of concrete creep in concrete and reinforced concrete structures]. Moscow: Stroyizdat, 1973. 444 p. (rus)
16. Zaporozhets I.D., Okorokov S.D., Pariyskiy A.A. Teplovydeleniye betona [Heat Liberation by Concrete]. Moscow: Stroyizdat, 1966. 316 p. (rus)
17. Malinin N.A. *Issledovaniye termonapryazhennogo sostoyaniya massivnykh betonnykh konstruktsiy s peremennymi deformativnymi kharakteristikami.* Diss. na soisk. uchen. step. kan. teh. nauk: Spets 05.23.01 [Research of thermal stressed state of mass concrete structures with changing deformations characteristics. Cand. tech. sci. diss.]. Leningrad, 1977. 186 p. (rus)
18. Semenov K.V. *Temperaturnoye i termonapryazhennoye sostoyaniye blokov betonirovaniya korpusa vysokogo davleniya v stroitelnyy period: Dis. na soisk. uchen. step. kan. teh. nauk: Spets 05.23.01* [Temperature and thermal stressed state of concreting blocks in a high pressure shell during the building period]. Leningrad, 1990. 156 p. (rus)
19. Barabanshchikov Y.G., Semenov K.V. Increasing the plasticity of concrete mixes in hydrotechnical construction. *Power Technology and Engineering.* 2007. No. 41(4). Pp. 197–200.
20. Barabanshchikov Y.G., Semenov K.V., Shevelev M.V. Termicheskaya treshchinostoykost betona fundamentnykh plit [Thermal cracking resistance of concrete foundation mats]. *Popular Concrete Science.* 2009. No. 1. Pp. 70–76.
21. Vasilyev P.I., Ivanov D.A., Kononov Yu.I., Semenov K.V., Starikov O.P. Raschetnoye obosnovaniye razmerov blokov i posledovatelnosti betonirovaniya korpusa reaktora VG-400 s proverkoy na modeli 1/5 naturalnoy velichiny [Calculation analysis of concreting blocks and VG-400 reactor shell concreting sequence using a 1/5 scale model]. *Problems of Atomic Science and Technology.* 1988. No. 1. Pp. 62–68. (rus)
22. Trapeznikov L.P. *Temperaturnaya treshchinostoykost massivnykh betonnykh sooruzheniy* [Thermal cracking resistance of mass concrete structures]. Moscow: Energoatomizdat, 1986. 272 p. (rus)
23. Semenov K.V., Barabanshchikov Y.G. Termicheskaya treshchinostoykost massivnykh betonnykh fundamentnykh plit i yeye obespecheniye v stroitelnyy period zimoy [Maintenance of thermal cracking resistance in massive concrete base slabs during winter concreting]. *Construction of Unique Buildings and Structures.* 2014. No. 2(17). Pp. 125–135. (rus)
24. Semenov K., Barabanshchikov Y. Thermal cracking resistance in massive concrete structures in the winter building period. *Applied Mechanics and Materials.* 2015. Vol. 725–726. Pp. 431–441.
25. Russian State Standards SP 41.13330.2012. *Concrete and reinforced concrete structures of hydroengineering facilities.*
26. Larson M. *Thermal crack estimation in early age concrete - models and methods for practical application.* Division of Structural Engineering, Lulea University of Technology, Doctoral Thesis, 2003. 190 p.
27. Miyazawa S., Koibuchi K., Hiroshima A., Ohtomo T., Usui T. Control of thermal cracking in mass concrete with blast-furnace slag cement. *Concrete Under Severe Conditions*. 2010. No. 7–9. Pp. 1487–1495.
28. Shengxing W., Donghui H. Estimation of cracking risk of concrete at early age based on thermal stress analysis. *Journal of Thermal Analysis and Calorimetry.* 2011. Vol. 105. No. 1. Pp. 171–186.
29. Zhang Z., Zhang X., Wang X., Zhang T., Zhang X. Merge concreting and crack control analysis of mass -concrete

1977. 186 с.
18. Семенов К.В. Температурное и термонапряженное состояние блоков бетонирования корпуса высокого давления в строительный период: Дис. на соиск. учен. степ. к. т. н.: Спец. 05.23.01. Л., 1990. 156 с.
19. Barabanshchikov Y.G., Semenov K.V. Increasing the plasticity of concrete mixes in hydrotechnical construction // Power Technology and Engineering. 2007. № 41(4). Pp. 197–200.
20. Барабанщиков Ю.Г., Семенов К.В., Шевелев М.В. Термическая трещиностойкость бетона фундаментных плит // Популярное бетоноведение. 2009. № 1. С. 70–76.
21. Васильев П.И., Иванов Д.А., Кононов Ю.И., Семенов К.В., Стариков О.П. Расчетное обоснование размеров блоков и последовательности бетонирования корпуса реактора VG-400 с проверкой на модели 1/5 натуральной величины // Вопросы атомной науки и техники. 1988. № 1. С. 62–68.
22. Трапезников Л.П. Температурная трещиностойкость массивных бетонных сооружений. М.: Энергоатомиздат, 1986. 272 с.
23. Семенов К.В., Барабанщиков Ю.Г. Термическая трещиностойкость массивных бетонных фундаментных плит и ее обеспечение в строительный период зимой // Строительство уникальных зданий и сооружений. 2014. № 2(17). С. 125–135.
24. Semenov K., Barabanshchikov Y. Thermal Cracking Resistance in Massive Concrete Structures in the Winter Building Period // Applied Mechanics and Materials. 2015. Vol. 725–726. Pp. 431–441.
25. СП 41.13330.2012. Бетонные и железобетонные конструкции гидротехнических сооружений.
26. Larson M. Thermal crack estimation in early age concrete - models and methods for practical application. Division of Structural Engineering, Lulea University of Technology, Doctoral Thesis, 2003. 190 p.
27. Miyazawa S., Koibuchi K., Hiroshima A., Ohtomo T., Usui T. Control of thermal cracking in mass concrete with blast - furnace slag cement // Concrete Under Severe Conditions. 2010. № 7–9. Pp. 1487–1495.
28. Shengxing W., Donghui H. Estimation of cracking risk of concrete at early age based on thermal stress analysis // Journal of Thermal Analysis and Calorimetry. 2011. Vol. 105. № 1. Pp. 171–186.
29. Zhang Z., Zhang X., Wang X., Zhang T., Zhang X. Merge concreting and crack control analysis of mass -concrete base slab of nuclear power plant // Applied Mechanics and Materials. 2011. № 94–96. Pp. 2107–2110.
30. Барабанщиков Ю.Г., Семенов К.В., Стручкова А.Я., Мановицкий С.С. Оценка учёта влияния температуры твердения на процесс тепловыделения в расчетах термонапряженного состояния массивных бетонных и железобетонных конструкций в строительный период // Приволжский научный вестник. 2017. № 1(65). С. 11–17.
31. Кононов Ю.И. Зависимость модуля мгновенных деформаций от температуры твердения и ее влияние на термонапряженное состояние ебтонных массивов гидротехнических сооружений: Автореф. дис. … канд. тех. наук. Л., 1963. 16 с.
32. Maruyama I., Sasano H., Nishioka Y., Igarashi G. Strength and Young's modulus change in concrete due to long-term drying and heating up to 90 °C // Cement and Concrete Research. 2014. Vol. 66. Pp. 48–63.
33. Kocab D., Danek P., Misak P., Topolar L., Pőssl P. Experimental analysis of the development of elastic properties and strength under different ambient temperature during the hardening of concrete // Procedia Engineering. 2017. Vol. 195. Pp. 102–107.
34. Kocab D., Kucharczykova B., Misak P., Zitt P., Kralikova M. Development of the elastic modulus of concrete under

base slab of nuclear power plant. *Applied Mechanics and Materials.* 2011. No. 94–96. Pp. 2107–2110.

30. Barabanshchikov Y.G., Semenov K.V., Struchkova A.Y., Manovitsky S.S. Otsenka ucheta vliyaniya temperatury tverdeniya na protsess teplovydeleniya v raschetakh termonapryazhennogo sostoyaniya massivnykh betonnykh i zhelezobetonnykh konstruktsiy v stroitelnyy period [Estimate of hardening temperature impact on the heat dissipation process in the calculations of thermal stressed state of massive concrete and reinforced concrete structures in the building period]. *Privolzhsky scientific newsletter.* 2017. No. 1(65). Pp. 11–17
31. Kononov Yu.I. *Zavisimost modulya mgnovennykh deformatsiy ot temperatury tverdeniya i yeye vliyaniye na termonapryazhennoye sostoyaniye betonnykh massivov gidrotekhnicheskikh sooruzheniy: Avtoref. dis. kan. teh. nauk* [Dependence of the instantaneous strain modulus on the hardening temperature and its effect on the thermal stressed state of concrete massifs of hydraulic structures]. Leningrad, 1963. 16 p. (rus)
32. Maruyama I., Sasano H., Nishioka Y., Igarashi G. Strength and Young's modulus change in concrete due to long-term drying and heating up to 90 °C. *Cement and Concrete Research.* 2014. Vol. 66. Pp. 48–63.
33. Kocab D., Danek P., Misak P., Topolar L., Pőssl P. Experimental analysis of the development of elastic properties and strength under different ambient temperature during the hardening of concrete. *Procedia Engineering.* 2017. Vol. 195. Pp. 102–107.
34. Kocab D., Kucharczykova B., Misak P., Zitt P., Kralikova M. Development of the elastic modulus of concrete under different curing conditions. *Procedia Engineering.* 2017. Vol. 195. Pp. 96–101.
35. Piasta W., Góra J., Budzyński W. Stress-strain relationships and modulus of elasticity of rocks and of ordinary and high performance concretes. *Construction and Building Materials.* 2017. Vol. 153. Pp. 728–739.
36. Yıldırım H., Sengul O. Modulus of elasticity of substandard and normal concretes. *Construction and Building Materials. 2011.* Vol. 25. No. 4. Pp. 1645–1652.
37. Hunka P., Kolisko J., Vokac M., Rehacek S. Test and technological influences on modulus of elasticity of concrete – recapitulation. *Procedia Engineering*. 2013. Vol. 65. Pp. 266–272.
38. Bushmanova A.V., Videnkov N.V, Semenov K.V., Barabanshchikov Yu.G., Dernakova A.V., Korovina V.K. The thermo-stressed state in massive concrete structures. *Magazine of Civil Engineering.* 2017. No. 3. Pp. 51–60.

different curing conditions // Procedia Engineering. 2017. Vol. 195. Pp. 96–101.

35. Piasta W., Góra J., Budzyński W. Stress-strain relationships and modulus of elasticity of rocks and of ordinary and high performance concretes // Construction and Building Materials. 2017. Vol. 153. Pp. 728–739.
36. Yıldırım H., Sengul O. Modulus of elasticity of substandard and normal concretes // Construction and Building Materials. 2011. Vol. 25. № 4. Pp. 1645–1652.
37. Hunka P., Kolisko J., Vokac M., Rehacek S. Test and technological influences on modulus of elasticity of concrete – recapitulation // Procedia Engineering. 2013. Vol. 65. Pp. 266–272.
38. Бушманова А.В., Виденков Н.В., Семенов К.В., Барабанщиков Ю.Г., Дернакова А.В., Коровина В.К. Термонапряженное состояние массивных бетонных конструкций // Инженерно-строительный журнал. 2017. № 3(71). С. 51–60.

Aleksandra Bushmanova,
+7(981)822-34-63; nicealexa@mail.ru

Yuriy Barabanshchikov,
+7(812)534-12-86; ugb@mail.ru

Kirill Semenov,
+7(921)781-19-57; kvsemenov@bk.ru

Ayyyna Struchkova,
+7(999)229-56-01; ayyyna_struchkova93@mail.ru

Sergey Manovitsky,
+7(981)980-37-34; sergeimanovitsky@mail.ru

Александра Васильевна Бушманова,
+7(981)822-34-63; эл. почта: nicealexa@mail.ru

Юрий Германович Барабанщиков,
+7(812)534-12-86; эл. почта: ugb@mail.ru

Кирилл Владимирович Семенов,
+7(921)781-19-57; эл. почта: kvsemenov@bk.ru

Айыына Яковлевна Стручкова,
+7(999)229-56-01;
эл. почта: ayyyna_struchkova93@mail.ru

Сергей Сергеевич Мановицкий,
+7(981)980-37-34;
эл. почта: sergeimanovitsky@mail.ru

Bushmanova A.V., Barabanshchikov Yu.G., Semenov K.V., Struchkova A.Y., Manovitsky S.S. Thermal cracking resistance in massive foundation slabs in the building period. *Magazine of Civil Engineering*. 2017. No. 8. Pp. 193–200. doi: 10.18720/MCE.76.17.

doi: 10.18720/MCE.76.18

Purification of hot water by zeolite modified with manganese dioxide

Очистка горячей сетевой воды цеолитом, модифицированным диоксидом марганца

A.V. Chechevichkin,
N.I. Vatin,
Peter the Great St. Petersburg Polytechnic University, St. Petersburg, Russia
V.V. Samonin,
St. Petersburg Institute of Technology (Technical University), St. Petersburg, Russia
M.A. Grekov,
Peter the Great St. Petersburg Polytechnic University, St. Petersburg, Russia

Инженер А.В. Чечевичкин,
д-р техн. наук, директор Инженерно-строительного института Н.И. Ватин,
Санкт-Петербургский политехнический университет Петра Великого, г. Санкт-Петербург, Россия
д-р техн. наук, заведующий кафедрой В. В. Самонин,
Санкт-Петербургский государственный технологический институт (технический университет), г. Санкт-Петербург, Россия
главный инженер М.А. Греков,
Санкт-Петербургский политехнический университет Петра Великого, г. Санкт-Петербург, Россия

Key words: hot water; natural zeolite; manganese dioxide; hydrogen sulfide; buildings; constructions; energy efficiency

Ключевые слова: горячая сетевая вода; природный цеолит; диоксид марганца; сероводород; здания; сооружения; энергетическая эффективность

Abstract. A new material is proposed for complex purification of hot water from iron and hydrogen sulphide – natural zeolite modified by manganese dioxide. It has been shown experimentally that this filtering material has high efficiency of water purification from iron and hydrogen sulphide, low mechanical degradability during operation, as well as low water consumption for washing during regeneration of the filtration media. The complex cleaning of hot water is proposed to carry out by means of two stages: the first – filtration cleaning from insoluble iron compounds with linear water velocity of 10–12 m/h, and the second – oxidation-catalytic purification from hydrogen-sulphide with velocity 1–2 m/h. Regeneration of a filtering material based on a manganese-modified natural zeolite can be carried out by back washing and chemical treatment with an oxidizer solution.

Аннотация. Для комплексной очистки горячей сетевой воды от железа и сероводорода предложен новый материал – модифицированный диоксидом марганца природный цеолит. Экспериментально показано, что данный фильтрующий материал имеет высокую эффективность очистки воды от железа и сероводорода, низкую механическую разрушаемость в процессе эксплуатации, а также малый расход воды на промывку при проведении регенерации загрузки. Предложено комплексную очистку горячей сетевой воды проводить в два этапа: первого – фильтрационной очистки от нерастворимых соединений железа с линейной скоростью движения воды 10–12 м/час, и второго – окислительно-каталитической очистки от сероводорода со скоростью 1–2 м/час. Регенерация фильтрующего материала на основе модифицированного диоксидом марганца природного цеолита может проводиться методом обратной промывки и химической обработки раствором окислителя.

Introduction

Installations and systems for preparation and transportation of hot water, as well as for distribution to use objects form a technical base of network hot water supply of buildings and structures.

Hot water systems are inextricably linked to the heat supply systems of buildings and structures. There are closed and open heat supply systems [1, 2], whose equipment for various reasons undergoes severe corrosion. For a closed system, corrosion reduction is achieved by addition various chemical reagents into the water and minimizing the entry of oxygen into the water [1, 3–6].

Чечевичкин А.В., Ватин Н.И., Самонин В.В., Греков М.А. Очистка горячей сетевой воды цеолитом, модифицированным диоксидом марганца // Инженерно-строительный журнал. 2017. № 8(76). С. 201–213.

Closed heat supply system provides higher energy efficiency of heat supply and hot water supply of buildings. Recently, closed heat supply systems [7, 8] have been used for the purposes of hot water supply [7, 8], in which cold drinking water is heated in heat exchangers of local heat points in buildings (including residential ones).

Both in closed and open systems of hot water supply [7, 9], due to a variety of physicochemical and microbiological processes [7, 9], there is a significant contamination of water with corrosion products [1], which can make it unsuitable for both practical use . Water contamination with corrosion products is very significant [3] and therefore complex cleaning of network hot water is currently extremely urgent.

One of the main measures to reduce corrosion in hot water and heat supply networks is to reduce dissolved oxygen in the water. This leads to the creation of anaerobic conditions in which microbiological corrosion plays an important role.

Anaerobic bacteria (mainly from Desulfovibrio and Desulfomaculum [1, 10]) intensively develop in anoxic environment at pH 5-9 when sulphates, organically substances and phosphorus are present in water (especially at elevated temperature) and hydrogen sulphide is released [1, 10].) Sulphure, in turn (in the form of hydrosulphide ions) is involved in the formation of an insoluble iron (II) sulphide corrosion product having a loose structure. This structure facilitating the development of sulfate-reducing bacteria is the basis for the formation of massive deposits in the pipelines and equipment elements. Even more anaerobic conditions are created between the surfaces of the metal and deposits, which ensure a high rate of microbiological corrosion, not only of steel, but also of aluminum and its alloys and even of brass [2, 12].

Corrosion products (mainly insoluble iron compounds) not only reduce the efficiency of the use of heating equipment, but also greatly impair the quality of the hot water consumed. This making hot water less suitable for use in domestic and industrial uses [12].

There are methods of removing iron from waters of various classes [13–20] which are not use for cleaning network hot water for various reasons:

- addition of chemical reagents (treatment with oxidants and coagulants) is unacceptable when water is disassembled by consumers;

- mesh filters, hydrocyclones and magnetic separators have low cleaning efficiency;

- fibrous filter media are difficult to regenerate.

The most suitable way, from the point of view of the ratio of cleaning efficiency, cost and ease of operation, is the filtration of hot water through the feed of fine-grained materials. These materials (quartz sand, natural zeolite, etc.) have high adhesion to suspended and insoluble iron compounds (iron III hydroxide, carbonate and iron sulphide II). Filtering through these materials allow to reduce such indicators of contamination of hot water, as turbidity, color and iron concentration, but practically does not affect the water content of substances that cause its unpleasant smell (primarily hydrogen sulphide).

To purify waters from various pollutants, natural zeolite is widely used [21–29], and filtering materials based on which have a number of advantages over traditionally used quartz sand loads: low bulk density, which helps to reduce the water consumption for regeneration by backwashing, high mud capacity (i.e., the amount of obtain suspended matter per unit volume of the layer), ion exchange capacity, etc.

Hydrogen sulphide have a high toxity to animals and humans, and high corrosive activity to plumbing equipment [1, 30]. In blood hydrogen sulphide is rapidly redused the oxidized power of haemoglobin and can act upon the central nervous system. Humans exposed to high concentration of hydrogen sulphide show simptoms of gastro-intestinal upset, anorexia, nausea, amnesia, delirium, hallucinations, low blood pressure and epileption convulsions [30, 31].

There are several techniques for removing the hydrogen sulphide from different types of water, including, aeration, ozonation, ion exchenge, reverse osmosis, biological treatment and chemical oxidation [11, 13, 14, 25, 31–34].

This methods of water purification from hydrogen sulphide and other sulfur compound (except reverse osmosis and ion exchange, witch are extremely expending), are not also use for hot water supply, since they are associated with the dosage of reagents in water and the removal of chemical reaction products, as well as with technical difficulties.

It is very promising to use filter materials based on natural manganese-containing ores (mainly pyrolusite) for this purpose [11, 34], but these materials have low mechanical strength and they are very expensive.

Recently, filtering materials modified by manganese dioxide [35–43], including those based on natural zeolites [44–46], have been developed and are being used for deionization and demanganation of natural waters. Such materials combine the advantages of manganese dioxide (high oxidation-catalytic capacity) and natural zeolite (good filtration and mechanical characteristics). The use of these materials for the complex (filtration-catalytic) purification of hot water from the compounds of iron and hydrogen sulphide is very promising.

The purpose of this work was testing of a modified by manganese dioxide natural zeolite for complex cleaning of network hot water. For its implementation the following tasks were solved:

- comparison of physical and chemical properties and performance characteristics of various granular filter materials;

- determination of parameters of hot water treatment from iron and hydrogen sulphide by various granular materials, including materials modified by manganese dioxide;

- study of the optimizing possibility of the technology of complete cleaning of hot water in real operation conditions.

Methods

Experimental studies of the processes of cleaning hot water were carried out on the installation, the scheme of which is presented in Fig.1.

The installation considered of a cylindrical stainless steel filter, having drainage slottedflow distributorsin the upper and lower parts of the filter.

Filtering granular materials were loaded inside the filter housing to a height of 750 mm, with a 250 mm height space provided for top loading for regeneration by backwashing. The filter had a water flow control system, in the forward (up-down) and reverse directions, consisting of the corresponding tapes, valves for precise adjustment of the flow rate of water during operation and during washing, as well as water sampling tapes for analysis before and after purification.

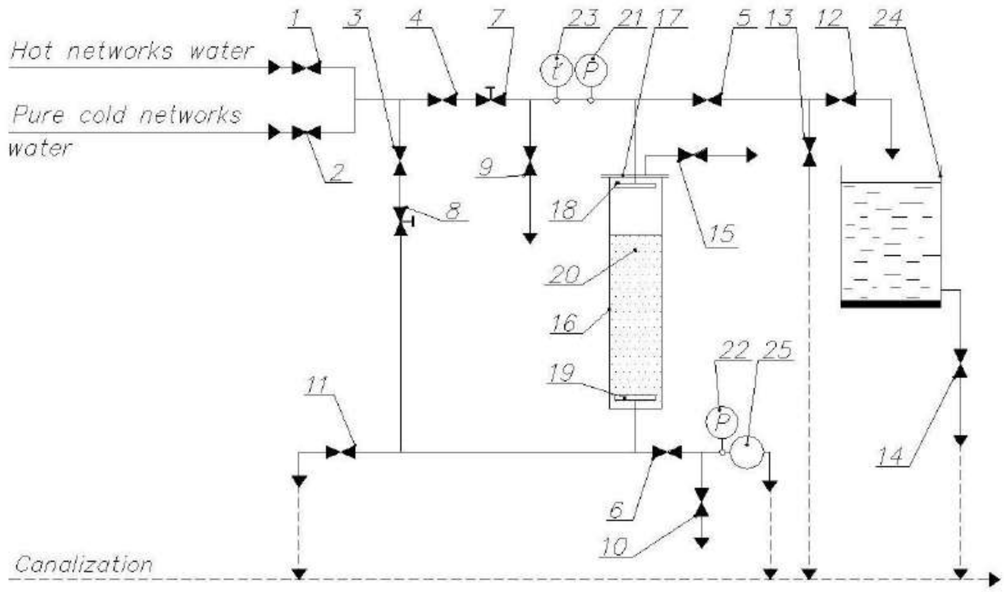

Figure 1 Experimental installation for studying filtering-catalytic properties of granular materials. 1, 2 – network taps; 3, 4, 5, 6 – taps controlling the operation of the filter; 7, 8 – control valves; 9, 10 – sampling taps; 11, 12, 13, 14 – draining taps; 15 – the cock of air release; 16 – filter housing; 17 – removable filter cover; 18, 19 – upper and lower slotted distributors; 20 – filtering material; 21, 22 – model manometers; 23 – thermometer; 24 – tank for collection of wash water; 25 – flowmeter

What is more, the unit was equipped with a thermometer to monitor the water temperature, a flowmeter and standard manometers to monitor the pressure before and after the filter. Moreover the installation had a tank 200 dm^3 volume to collect water during the backwashing of the filter. The accuracy of the determination was: the volume of the transmitted water ± 0.5 x 10^{-3} m^3, temperature ± 0.5 °C, pressure ± 0.01 bar.

The linear velocity of water flow through the filter media was the same in all experiments and was 10 ± 0.4 m/h. The linear velocity of backwash V_{bw} (m/h) for each filter material was defined as the rate of start of the entrainment of the particulate material in a separate experiment with a visual control of the light opening in the glass column.

Filtering granular materials were used in the form of identical fractions of 0.8 ÷ 1.2 mm, which were obtained with the help of a set of appropriate certified sieves and analyzer AP-20 (manufactured by "Vibrotechnik", RF).

Loss of materials during the backwashing was determined after passing through the filter loaded (in the direction from bottom to top) 120 liters (≈ 22 filter volumes) of cold purified tap water that was collected in a suitable tank (see Fig. 1) and settled in it within three days. After draining the water from the vessel, the precipitate was removed, concentrated, dried at a temperature of 70 ± 5 °C and weighed. The losses in washing P, (% mass) were determined by the formula:

$$P = \frac{m1}{M1} \cdot 100\% \qquad (1)$$

where m1 – mass of air-dry sludge, g

M1 – mass of air-dry granular material in the filter, g

The dirt capacity of the burden layer of granular material GE (g / kg, mg / dm3) was determined similarly after the filter operation and washing were completed and calculated by formula (1).

The mechanical strength of the samples of granular materials was estimated as the mechanical destructibility of MD, (% mass), which was determined by the formula:

$$\mathrm{MD} = 100\% - \mathrm{MR}\,(\mathrm{s}) \qquad (2)$$

where MR (s) – mechanical abrasion resistance determined according to Russian State Standard GOST 16188-70 4 [47].

The iron content in the filtration media of the granular material, C_{Fe},, (mg / g) was calculated after processing of its sample with 20% nitric acid and the determination of the total iron content in the resulting solution by the photocolorimetric method with thiocyanate ion [48] using the formula:

$$\mathrm{C_{Fe}} = \frac{m2}{M2} \qquad (3)$$

where *m2* is the mass (mg) of dissolved iron in the sample *M2* (g) of the filtration media of granular material.

The residual iron content in the filtration media RC_{Fe} (mg / g) after the filter operation cycle was determined:

$$RC_{Fe}=C_{Fe}-C^0_{Fe} \qquad (4)$$

where C_{Fe} – iron content in the filtration media of granular filter material after the cycle of its operation and backwashing, mg/g;

C^0_{Fe} – iron content in a pure filtration media before the filter starts to work mg/g.

The studies used hot network water of a closed heating system of an industrial facility with a water temperature of 55±5 °C, in which the concentration of iron (total) was 0.35–0.57 mg/dm^3, and hydrogen sulphide 0.18-0.23 mg/dm^3. This water had a redox potential of -18 ± 5 mV (for the cold water it was 123 ± 15 mV). Determination of hydrogen sulphide content in water was carried out by reaction with NN-dimethyl-n-phenylenediamine by photocolorimetric method [49].

The efficiency of water purification by the main polluting components (total iron and hydrogen sulphide) E_{Fe} (mass %) and E_{H2S} (mass %), respectively, was calculated by the formula:

$$E = \frac{Cin - Cpur}{Cin} \cdot 100\% \qquad (5)$$

where E-efficiency of water purification by iron and hydrogen sulphide, respectively,% mass;

“Cin”, “Cpur” – concentration of pollutants in the initial (before cleaning) and purified (after purification) water, mg/dm^3.

The content of manganese dioxide in the studied materials was determined by the oxalate method [46, 50].

Quartz sand (veined crushed quartz, Karelia), zeolite sand (the breed of the Badinskoye deposit, Eastern Siberia), the same zeolite sand, but modified with manganese dioxide, as well as a number of commercial materials based on manganese dioxide were used as research objects. The latter were investigated: MnO2-coated semi-burnt dolomite (brand MZHF, RF), synthetic deferrizing material (Birm brand, USA), and manganese ore-pyrolusite (Pirolox brand, USA) which used to remove iron and manganese from groundwater.

Results and discussion

Evaluation of possibility of using for the complex treatment of hot water of various granular filtering materials was carried out according to a number of indices take a great importance in the actual operation of filters.

Table 1 compares the various characteristics of the materials studied in the work.

Table 1. Comparison of the properties of the studied granular filter materials

№	Filter material	Bulk density kg/dm^3	MD, % mass	P, % mass	RC Fe, mg/g	DC		E, % mass		V_{bw}, m/hour
						g/ kg	g/ dm^3	for iron-ion	for hydro-gen sulphide	
1	Gangue quartz (Karelia)	1.30	0.02	0.03	0.53	0.37	0.75	45.00	3.00	53.00
2	Zeolite (Badinskoye deposit)	1.00	0.31	0.18	2.87	1.09	1.09	67.00	8.00	37.00
3	Modified MnO_2 zeolite	1.07	0.07	0.03	0.36	1.04	1.11	67.00	68.00	39.00
4	MZHF	1.38	3.36	0.16	0.41	0.63	0.87	56.00	15.00	58.00
5	Birm	0.75	1.82	0.08	1.23	1.61	0.21	61.00	64.00	25.00
6	Pirolox	1.98	2.64	0.07	0.48	0.59	0.16	65.00	70.00	75.00

It can be seen from the table that the use of zeolite sand has advantages over the use of quartz sand, namely: lower bulk density and more efficient iron purification. Zeolite sand, in contrast to quartz and manganese-modified zeolite sand, has a higher mechanical destructibility. This is evidenced by higher losses during backwashing.

Modified by manganese dioxide, zeolite has high water purification efficiency on iron and hydrogen sulphide. The quartz and zeolite sands are not removed the hydrogen sulphide from hot water.

Commercial materials based on manganese dioxide (except for MZHF, for which practically all the indicators are the worst) have values of the efficiency of iron purification and mud capacity close to the modified zeolite. These materials also have higher values of mechanical breakdown rates, washing losses and backwashing rates. This makes their practical use for a real cleaning of network hot water very problematic. In addition, these materials have high cost.

Figure 2 shows dependence of change in purification efficiency on the iron and hydrogen sulphide content indicators for the three materials studied during one filter cycle, which corresponded to a transmission of 20 m^3 (3640 filter volumes) of water.

These dependences confirm the foregoing, and also indicate that at the end of the filter cycle, the efficiency of purification by iron on the manganese dioxide-modified zeolite reaches its maximum value, and by hydrogen sulphide falls to 25 %. The loss of head pressure at a linear rate of water filtration through a load of 10 ± 0.4 m/h at the end of the first filter cycle was not more than 0.1 bar. Thus, the values of filter cycle with high purification efficiency for loading with the manganese-modified zeolite is different for removing iron and hydrogen sulphide.

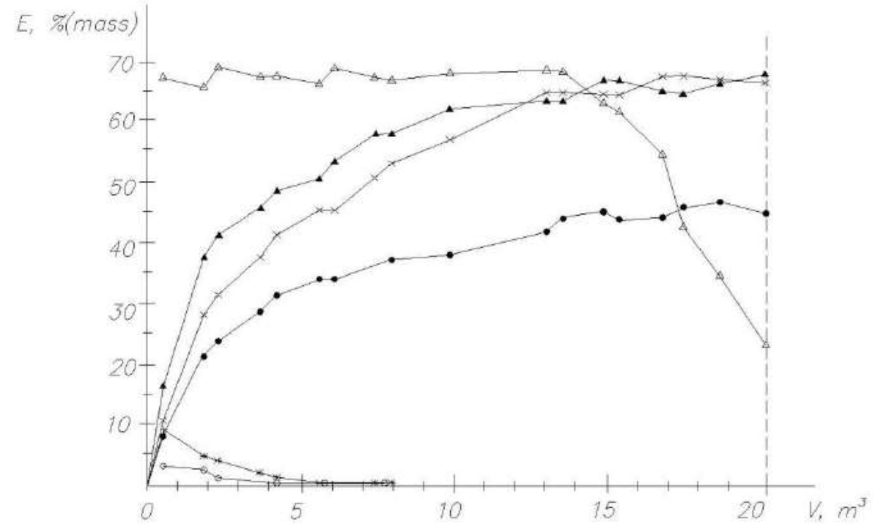

Figure 2 Dependence of iron and hydrogen sulphide purification efficiency (E) on time for one filter cycle.
- ● -, -x-, - ▲ - – by iron, -o-, - * -, -Δ- – by hydrogen sulphide, -o-, - ● - – quartz sand, -x-, - * - – natural zeolite, -Δ-, - ▲ - – manganese dioxide modified natural zeolite.
V, (m^3) – the volume of transmission water

Figure 3 shows the same dependencies as in Figure 2, but over the time of operation corresponding to 5 filter cycles, i.e. passing through the filter ≈ 100 m^3 (or 18 200 filter volumes) of water without carrying out regeneration. The efficiency of purification from iron in this case grew and amounted to 90–91 % at the end of the work, and from hydrogen sulphide it fell to 10 %. The loss of head pressure at the end of the filter operation period was no more than 0.5–0.6 barr, which is a satisfactory result.

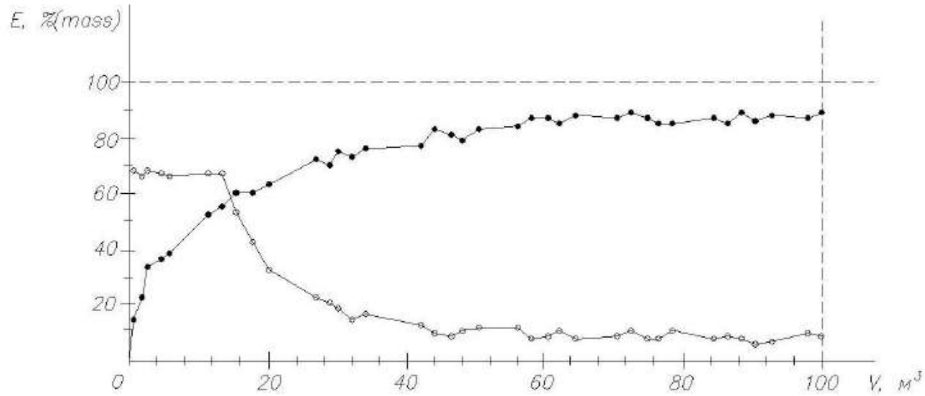

Figure 3.Dependence of iron and hydrogen sulphide purification efficiency (E) on time for five filter cycles without filter regeneration.
- ● - – by iron, -o- – by hydrogen sulphide.
Manganese-modified natural zeolite of Badinskoye deposit

Figure 4 shows the dependencies, similar to those shown in Figure 3, but for the mode of operation of the filter with periodic regeneration of the filtration media from the manganese-modified zeolite both from iron purification (backwash) and from hydrogen sulphide (chemical treatment + backwashing) for five filter cycles of 20 m^3 each. The efficiency of purification from hydrogen sulphide in this case is restored after each filter cycle by treatment of the filtration media with a solution of potassium permanganate. The average iron cleaning efficiency during each filter cycle in this case is lower due to a strong decrease in the retention of iron capacity, after washing the filtration media of the filter.

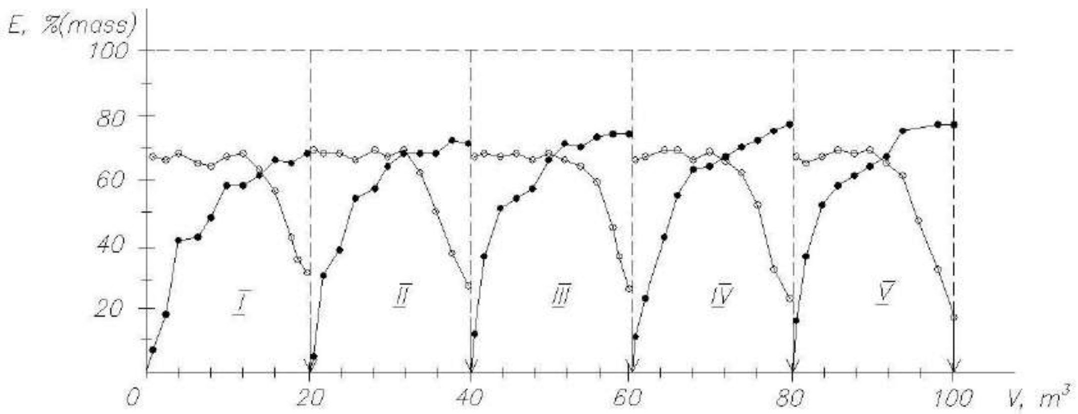

Figure 4 Dependence of iron (- ● -) and hydrogen sulphide (-o-) purification efficiency (E) on time for modified manganese dioxide natural zeolite with periodic regeneration of filter load

Thus, in the case of a real continuous operation of the filter with a modified zeolite material, the restoration of its iron cleansing ability (backwash at a linear speed of 40 ± 1 m/h) can be carried out after passing water in an amount of 18,000–15,000 filter volumes (or 17.0 m^3 of water per kilogram of loading). For hydrogen sulphide, the restoration of its cleaning capacity (chemical treatment with oxidant solution + backwashing) must be carried out after passing 3 600 filter volumes (or 3.4 m^3 water per kilogram of filtration media). Comprehensive cleaning of hot water must be carried out in two stages: the first – mechanical cleaning of iron and the second – contact oxidation of hydrogen sulphide. Regeneration of the filter load of the second stage of purification is five times more often than the first one.

Figure 5 shows the dependence of the purification efficiency on hydrogen sulphide during one filter cycle for different linear velocities of water flow through the filter loading. As a filtering material, the natural zeolite of the Badinskoye deposit, modified with manganese dioxide, was used. At low linear velocities of water movement (1–2 m/h), the efficiency of purification by hydrogen sulphide is 92–96 % mass, and will be maintained throughout the filter cycle (20 m^3 of water). At high velocities (5–10 m/h), the cleaning efficiency is lower (81–76 % by weight) and decreases significantly towards the end of the filter cycle.

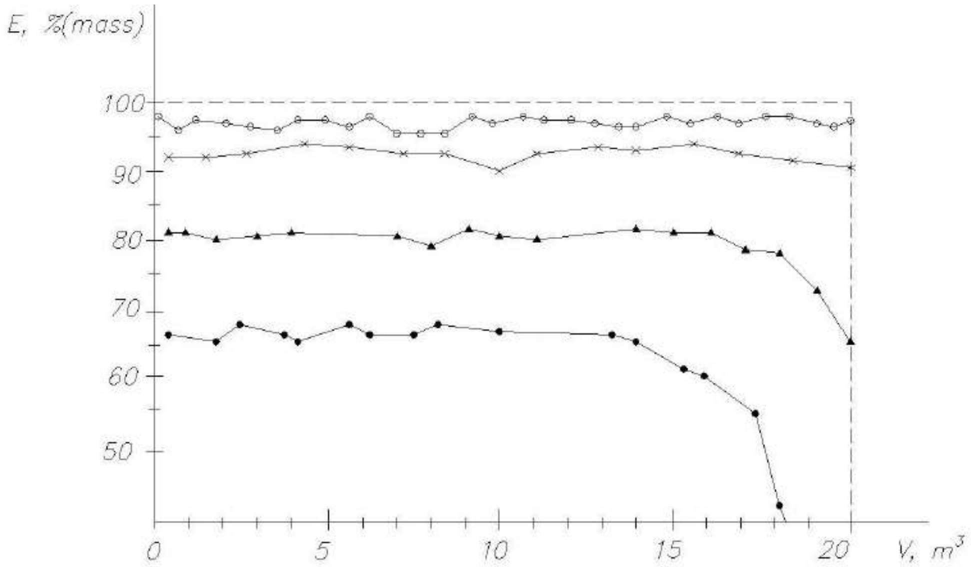

Figure 5. Influence the linear velocity of water flow in the filterefficiency of hydrogen sulphide purification efficiency (E) for loading the filter from the modified manganese dioxide of natural zeolite (Badinskoye deposit).
Linear velocitys: - ● - – 10 m/h, - ▲ - – 5 m/h, -x- – 2 m/h, -o- – 1 m/h.

The properties of materials modified by manganese dioxide based on clinoptilolit – containing rocks of various deposits in Russia were also studied. The appearance of one of these materials is presented in Figure 6.

Figure 6 Appearance of the manganese-modified filter-catalyzed materials based on the natural zeolite of the Badinskoye deposit (Russia)

Table 2 shows the results of comparative tests of these materials for cleaning hot water from iron and hydrogen sulphide. The studied materials have high values of the efficiency of purification from iron and hydrogen sulphide at a high rate of passage of water through the loading of the filter, as well as similar rates of backwashing.

Table 2. Comparison of the properties of MnO_2 – modified materials obtained on the basis of clinoptilolite-containing rocks of various deposits

№	The deposit of zeolite rocks	MnO_2, content % (mass)	MD, % (mass)	RC Fe mg/g	E, %mass		V_{50}, m^3	V_{bw}, m/h
					for iron-ion	for hydrogen sulphide		
1	Badinskoe (East Siberia)	0.36	0.07	0.36	67.00	68.00	17.50	40.00
2	Chuguevskoe (PrimorskyKrai)	0.42	0.11	0.42	61.00	70.00	23.00	46.00
3	Sokirnitskoe (Ukraine)	0.30	1.81	0.55	65.00	62.00	4.50	35.00
4	Shivirtuiskoe (East Siberia)	0.49	6.05	0.91	70.00	61.00	7.50	30.00
5	Kholinskoe (East Siberia)	0.46	4.24	0.74	69.00	69.00	8.00	34.00

From Table 2 it can also be seen that effective water purification from hydrogen sulphide for materials obtained from the rocks of the Shivirtuysky, Kholinsky and Sokirnitsky deposits is less prolonged than for materials based on the Badinskoye and Chuguevskoye deposits. The materials of the first group are characterized by a value of V50, (the volume of purified water with an efficiency of at least 50 %) is 4.5–8.0 m^3, and for the second group it is 17.5–23.0 m^3. All samples have similar values of the total content of manganese dioxide, but its spatial distribution within the material particles for these two groups is different. For samples of material based on rocks Badinskoye and Chuguyevskoye deposits, the manganese dioxide phase is located on the surface of particles of these materials [46] and is maximally available. For other samples of materials, manganese dioxide is distributed throughout the grain and its surface concentration is much lower.

Materials obtained on the basis of zeolite rocks of the Shivirtuysky, Kholinsky and Sokirnitsky deposits in addition have high values of mechanical destructibility (MD), which will lead to a faster grinding and carrying away of the load in conditions of actual operation of the filters. The same samples also have an increased ability to accumulate iron inside of filtration media particles (RCFC index, Table 2). Insoluble iron compounds that are not removed by backwashing the filter with water will greatly reduce the oxidizing ability of these materials by hydrogen sulphide due to the blocking by iron compounds of the surface of the active layer of manganese dioxide.

The high efficiency of water hydrogen sulphide purification for material on base natural piroluzite ("Pirolox") corresponds the information [11, 14] about it application for this purposes.

The process of hydrogen sulphide removing from network hot water on MnO_2-modified natural zeolite (on condition that dissolved oxygen is not present) was similar to process of chemical fixation [25, 27]. Moreover the non-catalitic oxidation process with "active oxygen" of MnO_2 and formation manganese oxides of low valency also was possible [11, 14, 23].

To summarize, in this work for the experimental conditions similar such as real hot water networks conditions [3, 5, 10] good results on purification network hot water from suspended ferrum oxides and hydrogen sulphide was obtained.

The filtering materials base on MnO_2-modified natural zeolites may be use for this purposes, as well as, materials traditionally used in groundwater purification practice [11, 13, 14]. This circumstance increases the possibilities of network hot water complex purification with use the standard filtering equipment.

Conclusion

The work has evaluated the possibilities of hot water cleaning with materials based on manganese dioxide-modified zeolite rocks in comparison with other filtering materials (including those containing manganese dioxide). Based on the results of the studies, the following conclusions are drawn:

Filtering materials based on manganese dioxide-modified zeolite rocks (from the most accessible deposits in Russia) provide good cleaning of hot water from its main pollutants – iron compounds and hydrogen sulphide.

In comparison with other granular filtering materials (quartz sand, unmodified natural zeolite), manganese dioxide-modified zeolite materials have a higher retention capacity for insoluble iron compounds and oxidative activity for hydrogen sulphide, as well as low mechanical breakdown during operation.

The advantage of manganese dioxide -modified zeolite rocks over commercial manganese dioxide-containing materials, traditionally used for deironing and demanganation of groundwater, lies in their less mechanical destructibility (MD) during operation, as well as in the lower cost of water using for washing the load in the filter during its regeneration.

The complex purification of hot network water should be carried out in the form of a two-stage process: filtration and mechanical treatment of water from iron compounds with a linear rate of movement in the apparatus of 10–12 m/h, and sorption-oxidative purification from hydrogen sulphide at a linear speed of no more than 1–2 m/hour.

To ensure the consistency of the oxidation capacity of the filtering of manganese dioxide-modified zeolite rocks by hydrogen sulphide, it must be periodically regenerated with an oxidizer solution.

References

1. Sukhotin A.M., Bogachev A.F., Palmskiy V.G. et al. *Korrozionnaya stoykost oborudovaniya khimicheskikh proizvodstv. Korroziya pod deystviyem teplonositeteley, khladogentov i rabochikh tel* [Corrosion resistance of chemical production equipment. Corrosion under the influence of heat carriers, coolants and working bodies]. Leningrad: Khimiya, 1988. 360 p. (rus)
2. Grishkova A.V., Gavrilov V.B. K voprosu o vliyanii vodno-khimicheskogo rezhima sistem tsentralizovannogo teplosnabzheniya na rabotu sistem otopleniya i goryachego vodosnabzheniya [On the impact of the water-chemical regime of district heating systems on the operation of heating and hot water supply systems]. *Vestnik PNIPU. Stroitelstvo i arkhitektura.* 2014. No. 1. Pp. 63–71. (rus)
3. Mezenova D.V., Starodubceva O.S. Analiz prichin nesootvetstviya kachestva goryachej vody trebovaniyam sanitarnyh pravil [Analysis of the reasons for the inconsistency of the quality of hot water with the requirements of sanitary regulations]. *Mediko-social'nye i psihologicheskie aspekty bezopasnosti promyshlennyh aglomeracij: materialy mezhdunarodnoj nauchno-prakticheskoj konferencii* [Proceedings of international scientific and practical conference]. Ekaterinburg: UrFU, 2016. Pp. 42–47. (rus)
4. Kukushkin A.N., Vinogradov V.N., Gromov Ye.B., Shatova I.A. Eksperimentalnoye issledovaniye fazovogo sostava i povedeniya produktov korrozii stali v parovom trakte energobloka pri mikrodizirovaniii oktadetsilamina [Experimental study of the phase composition and behavior

Литература

1. Сухотин А.М., Богачев А.Ф., Пальмский В.Г. и др. Коррозионная стойкость оборудования химических производств. Коррозия под действием теплоносителей, хладогентов и рабочих тел. Л.: Химия, 1988, 360 с.
2. Гришкова А.В., Гаврилов В.Б. К вопросу о влиянии водно-химического режима систем централизованного теплоснабжения на работу систем отопления и горячего водоснабжения // Вестник ПНИПУ. Строительство и архитектура. 2014. № 1. С. 63–71.
3. Мезенова Д.В., Стародубцева О.С. Анализ причин несоответствия качества горячей воды требованиям санитарных правил // Медико-социальные и психологические аспекты безопасности промышленных агломераций: материалы международной научно-практической конференции. Екатеринбург: УрФУ, 2016. С. 42–47.
4. Кукушкин А.Н., Виноградов В.Н., Громов Е.Б., Шатова И.А. Экспериментальное исследование фазового состава и поведения продуктов коррозии стали в паровом тракте энергоблока при микродизировании октадециламина // Энергосбережение и водоподготовка. 2002. №3. С. 3–9.
5. Жилин В.Н., Ильин Д.Н. Очистка воды без водоподготовки и защита систем водотеплоснабжения от коррозии и отложений // Промышленная энергетика. 2010. №6. С. 14–19.
6. Рыженков А.В., Лукин М.В., Погорелов С.И. и др.

of the corrosion products of steel in the steam tract of the power unit during the microdisplacement of octadecylamine]. *Energosberezheniye i vodopodgotovka*. 2002. No. 3. Pp. 3–9. (rus)

5. Zhilin V.N., Ilin D.N. Ochistka vody bez vodopodgotovki i zashchita sistem vodoteplosnabzheniya ot korrozii i otlozheniy [Purification of water without water treatment and protection of water supply systems against corrosion and deposits]. *Promyshlennaya energetika.* 2010. No. 6. Pp. 14–19. (rus)
6. Ryzhenkov A.V., Lukin M.V., Pogorelov S.I. et al. Rezultaty raboty po povysheniyu effektivnosti sistem tsentralizovannogo teplosnabzheniya na osnove PAV-tekhnologiy za 2003-2013 g. [Results of work on increasing the efficiency of district heating systems based on SAW technologies for 2003-2013]. *Nadezhnost i bezopasnost energetiki.* 2014. No. 2(25). Pp. 18–22. (rus)
7. Zakhvatova M.A., Grishkova A.V. Neobkhodimost perevoda otkrytykh sistem teplosnabzheniya na zakrytyye [Necessity of transferring open heat supply systems to closed ones]. *Sovremennyye tekhnologii v stroitelstve. Teoriya i praktika.* 2016. Vol. 1. Pp. 414–418. (rus)
8. Makotrina L.V. Sravneniye nekotorykh razdelov sistemy goryachego vodosnabzheniya SNIP 2.04.01-85 «Vnutrenniy vodoprovod i kanalizatsiya zdaniy» s novymi normativnymi dokumentami [Comparison of some sections of the hot water supply system SNIP 2.04.01-85 "Internal water supply and sewerage of buildings" with new regulatory documents]. *Izvestiya vuzov. Investitsii. Stroitelstvo. Nedizhimost.* 2014. No. 5(10). Pp. 80–86. (rus)
9. Sharapov V.I. Preimushchestva i nedostatki otkrtykh i zakrytykh sistem teplosnabzheniya [Advantages and disadvantages of open and closed heat supply systems]. *Nadezhnost i bezopasnost energetiki.* 2012. No. 19. Pp. 65–68. (rus)
10. Sharapov V.I., Zamaleyev M.M. Puti predotvrashcheniya sulfidnogo zagryazneniya teplovykh setey [Ways to prevent sulphide contamination of heat networks]. *Energosberezheniya i vodopodgotovka.* 2014. No. 5(91). Pp. 13–17. (rus)
11. Zemskov A.N., Gaydin A.M., Sabirova L.B. Sposoby borby s serovodorodom v podzemykh vodakh [Methods to combat hydrogen sulphide in groundwater]. *Izvestiya vuzov. Gornyy zhurnal.* 2015. No. 4. Pp. 67–74. (rus)
12. Sharapov V.I., Zamaleyev M.M. Resheniye problem bakteriologicheskogo zagryazneniya sistem teplosnabzheniya [Solving the problems of bacteriological contamination of heat supply systems]. *Teploenergetika.* 2015. No. 9. Pp. 77. (rus)
13. Klyachko V.A., Apeltsin N.E. *Ochistka prirodnykh vod* [Purification of natural waters]. Moscow: Stroyizdat, 1971. 579 p. (rus)
14. Zolotareva Ye.F., Ass G.Yu. *Ochistka vod ot zheleza, margantsa, ftora i serovodoroda* [Purification of water from iron, manganese, fluorine and hydrogen sulphide]. Moscow: Stroryizdat, 1975. 176 p. (rus)
15. Zhurba M.G., Savelyev S.P., Urusov D.Yu. i dr. Usovershenstvovaniye tekhnologii obezzhelezivaniya i demanganatsii podzemnykh vod g. Ulyanovska [Improvement of technology of deironing and demanganization of underground waters in Ulyanovsk]. *Vodosnabzheniye i sanitarnaya tekhnika.* 2013. No. 2. Pp. 40–45. (rus)
16. Tarasenko S.Ya. Obezzhelezivaniye i demanganatsiya podzemnykh vod khozyaystvenno-pityevogo naznacheniya [Iron removal and demagnetization of groundwater for domestic and drinking purposes]. *Vestnik uchebno-metodicheskogo obyedineniya po obrazovaniyu v oblasti prirodoustroystva i vodopolzovaniy.* 2014. No. 6. Pp. 283–299. (rus)
17. Vatin N.I., Chechevichkin V.N., Chechevichkin A.V. Features of water purification from Vuoksa river during the

Результаты работы по повышению эффективности систем централизованного теплоснабжения на основе ПАВ-технологий за 2003-2013 г. // Надежность и безопасность энергетики. 2014. № 2(25). С. 18–22.

7. Захватова М.А., Гришкова А.В. Необходимость перевода открытых систем теплоснабжения на закрытые // Современные технологии в строительстве. Теория и практика. 2016. Т. 1. С. 414–418.
8. Макотрина Л.В. Сравнение некоторых разделов системы горячего водоснабжения СНИП 2.04.01-85 «Внутренний водопровод и канализация зданий» с новыми нормативными документами // Известия вузов. Инвестиции. Строительство. Недижимость. 2014. № 5(10). С. 80–86.
9. Шарапов В.И. Преимущества и недостатки откртых и закрытых систем теплоснабжения // Надежность и безопасность энергетики. 2012. № 19. С. 65–68.
10. Шарапов В.И., Замалеев М.М. Пути предотвращения сульфидного загрязнения тепловых сетей // Энергосбережения и водоподготовка. 2014. № 5(91). С. 13–17.
11. Земсков А.Н., Гайдин А.М., Сабирова Л.Б. Способы борьбы с сероводородом в подземых водах // Известия вузов. Горный журнал. 2015. № 4. С. 67–74.
12. Шарапов В.И., Замалеев М.М. Решение проблем бактериологического загрязнения систем теплоснабжения // Теплоэнергетика. 2015. № 9. С. 77.
13. Клячко В.А., Апельцин Н.Э. Очистка природных вод. М.: Стройиздат, 1971. 579 с.
14. Золотарева Е.Ф., Асс Г.Ю. Очистка вод от железа, марганца, фтора и сероводорода. М.: Сторйиздат, 1975, 176 с.
15. Журба М.Г., Савельев С.П., Урусов Д.Ю. и др. Усовершенствование технологии обезжелезивания и деманганации подземных вод г. Ульяновска // Водоснабжение и санитарная техника. 2013. № 2. С. 40–45.
16. Тарасенко С.Я. Обезжелезивание и деманганация подземных вод хозяйственно-питьевого назначения // Вестник учебно-методического объединения по образованию в области природоустройства и водопользования. 2014. № 6. С. 283–299.
17. Ватин Н.И., Чечевичкин В.Н., Чечевичкин А.В. Особенности очистки воды из р. Вуокса в летний период. // Инженерно-строительный журнал. 2010. № 2(12). С. 23–26.
18. Мельников В.И., Герасимчук Н.В., Полянская Е.Н. Совершенствование техники и технологии систем теплоснабжения высотных зданий // Вестник ТГАСУ. 2009. № 4. С. 113–119.
19. Батуев С.П., Аносов П.А. Применение инженерно-гравитационных фильтров-грязевиков в системах тепло- и водоснабжения // Энергобезопасность и энергоснабжение. 2016. № 1. С. 40–45.
20. Волков В.Н., Горбунов С.А. Новые материалы и технологии очистки вод в системах теплоснабжения // Энергосбережение и водоподготовка. 2011. № 2(70). С. 24–27.
21. Ватин Н.И., Чечевичкин В.Н., Чечевичкин А.В., Шилова Е.С. Применение цеолитов клиноптилолитового типа для очистки природных вод // Инженерно-строительный журнал. 2013. № 2. С. 81–88.
22. Самонин В.В., Чечевичкин А.В. Особенности поглощения иона двухвалентного марганца из водных растворов цеолитами // Журнал прикладной химии. 2013. Т. 86. № 11. С. 1724–1729.
23. Тарасевич Ю.И. Природные цеолиты в процессах очистки воды // Химия и технология воды. 1988. Т. 10. № 3. С. 210–218.
24. Вейсгейм А.С., Назаренко О.Б., Зарубина Р.Ф. Удаление железа из скважинной воды на фильтре с

summer period. *Magazine of Civil Engineering.* 2010. No. 2(12). Pp. 23–26. (rus)

18. Melnikov V.I., Gerasimchuk N.V., Polyanskaya Ye.N. Sovershenstvovaniye tekhniki i tekhnologii sistem teplosnabzheniya vysotnykh zdaniy [Perfection of engineering and technology of heat supply systems for high-rise buildings]. *Vestnik TGASU*. 2009. No. 4. Pp. 113–119. (rus)
19. Batuyev S.P., Anosov P.A. Primeneniye inzhenerno-gravitatsionnykh filtrov-gryazevikov v sistemakh teplo-i vodosnabzheniya [Application of engineering-gravity filters-muders in heat and water supply systems]. *Energobezopasnost i energosnabzheniye.* 2016. No. 1. Pp. 40–45. (rus)
20. Volkov V.N., Gorbunov S.A. Novyye materialy i tekhnologii ochistki vod v sistemakh teplosnabzheniya [New materials and technologies for water treatment in heat supply systems]. *Energosberezheniye i vodopodgotovka*. 2011. No. 2(70). Pp. 24–27.
21. Vatin N.I., Chechevichkin V.N., Chechevichkin A.V., Shilova Ye.S. Primeneniye tseolitov klinoptilolitovogo tipa dlya ochistki prirodnykh vod [Possible applications of clinoptilolites for natural water purification]. *Magazine of Civil Engineering.* 2013. No. 2(37). Pp. 81–88. (rus)
22. Samonin V.V., Chechevichkin A.V. Osobennosti pogloshcheniya iona dvukhvalentnogo margantsa iz vodnykh rastvorov tseolitami [Peculiarities of the absorption of a divalent manganese ion from aqueous solutions by zeolites]. *Zhurnal prikladnoy khimii.* 2013. Vol. 86. No. 11. Pp. 1724–1729. (rus)
23. Tarasevich Yu.I. Prirodnyye tseolity v protsessakh ochistki vody [Natural zeolites in water purification processes]. *Khimiya i tekhnologiya vody.* 1988. Vol. 10. No. 3. Pp. 210–218. (rus)
24. Veysgeym A.S., Nazarenko O.B., Zarubina R.F. Udaleniye zheleza iz skvazhinnoy vody na filtre s zagruzkoy iz Badinskogo tseolita [Removal of iron from borehole water on a filter loaded from Badinsky zeolite]. *Vestnik nauki Sibiri.* 2012. No. 4(5). Pp. 23–29. (rus)
25. Mahmoudi R., Falamaki C. Ni^{2+}-ion-exchanged dealuminated clinoptilolite: A superior adsorbent for deep desulfurization. *Fuel.* 2016. Vol. 173. No. 2. Pp. 277–284.
26. Karatayev O.R., Novikov V.F., Shamsutdinova Z.R. Ochistka stochnykh vod tseolito-soderzhashchimi porodami [Wastewater treatment with zeolite-containing rocks]. *Vestnik kazanskogo tekhnologicheskogo universiteta*. 2014. Vol. 17. No. 15. Pp. 169–174. (rus)
27. Gubonina Z.I., Tarchigina N.F., Kharichev O.Ye. Izucheniye vozmozhnosti ispolzovaniya modifitsirovannoy tseolitovoy porody v tekhnologii ochistki prirodnykh vod ot ftorid-ionov [Study of the possibility of using a modified zeolite rock in the technology of purifying natural waters from fluoride ions]. *Energosberezheniye i vodopodgotovka*. 2015. No. 1(93). Pp. 21–25. (rus)
28. Epova Ye.S., Yeremin O.V., Rusal O.S., Filenko R.A. Protsessy aktivatsii sorbtsionnykh svoystv tseolitovykh porod Shivyrtuyskogo mestorozhdeniya (Vostochnoye zabaykalye) [Processes of activation of sorption properties of zeolite rocks of the Shivirtui deposit (Eastern Transbaikalia)]. *Mineralogiya tekhnogineza.* 2015. No. 16. Pp. 148–154.
29. Gogina Ye.S., Yantsen O.V., Khodyrev V.M. i dr. Issledovaniya printsipialnoy vozmozhnosti ochistki stochnykh vod poligona TBO s primeneniyem tseolita [Research of the principle possibility of sewage treatment of the landfill with the use of zeolite]. *Yestestvennaya i tekhnicheskaya nauk.* 2014. No. 9-10. Pp. 404–406. (rus)
30. *EPA 635/R - 03/005/* Toxicological review of hydrogen sulphide. CAS№ 7783-06-4. Government printing office. Environmental Protection Agency, Washington, 2003. 62 p.
31. Dohnalek D.A., Fritzpatrick D.A. The chemistry of reduced

загрузкой из Бадинского цеолита // Вестник науки Сибири. 2012. № 4(5). С. 23–29.

25. Mahmoudi R., Falamaki C. Ni^{2+}-ion-exchanged dealuminated clinoptilolite: A superior adsorbent for deep desulfurization // Fuel. 2016. Vol. 173. № 2. Pp. 277–284.
26. Каратаев О.Р., Новиков В.Ф., Шамсутдинова З.Р. Очистка сточных вод цеолито-содержащими породами // Вестник казанского технологического университета. 2014. Т. 17. № 15. С. 169–174.
27. Губонина З.И., Тарчигина Н.Ф., Харичев О.Е. Изучение возможности использования модифицированной цеолитовой породы в технологии очистки природных вод от фторид-ионов // Энергосбережение и водоподготовка. 2015. № 1(93). С. 21–25.
28. Эпова Е.С., Еремин О.В., Русаль О.С., Филенко Р.А. Процессы активации сорбционных свойств цеолитовых пород Шивыртуйского месторождения (Восточное забайкалье) // Минералогия техногинеза. 2015. № 16. С. 148–154.
29. Гогина Е.С., Янцен О.В., Ходырев В.М. и др. Исследования принципиальной возможности очистки сточных вод полигона ТБО с применением цеолита // Естественная и техническая наука. 2014. № 9-10. С. 404–406.
30. EPA 635/R - 03/005/ Toxicological review of hydrogen sulphide. CAS№ 7783-06-4. Government printing office. Environmental Protection Agency Washington, 2003. 62 p.
31. Dohnalek D. A., Fritzpatrick D. A. The chemistry of reduced sulfur species and their removal from groundwater supplies // Journal of American water Works Association. 1983. Vol. 75. Pp. 298–308.
32. Kato S., Hirano V., Iwata M., et. al. Photo catalytic degradation of gaseous sulfus compounds by silver-deposited titanium dioxide // Applied Catalysis. 2005. Vol. 57. Pp. 109–115.
33. Thompson M.A., Kelkar U.G., Vickers J.C. The treatment of ground water containing hydrogen sulphide using microfiltration // Desalination. 1995. Vol. 102. Pp. 287–297.
34. Edwards S., Alharhi R., Ghaly A. E. Removal of hydrogen sulphide from water // American Journal of Environmental Sciences. 2011. Vol. 7. № 4. Pp. 295–305.
35. Бочкарев Г.Р., Скитер Н.А. Использование марганцевых руд для деманганации и обезжелезования подземных вод // Известия вузов. Строительство. 2005. № 11-12. С. 61–66.
36. Aguiar A.O., Duarte R.A., Ladeira A.C.Q. The application of MnO2 in the removal of manganese from acid mine water // WaterAirSoilPollut. 2013. Vol. 224. Pp. 1690.
37. Гончиков В.Ч., Губайдулина Т.А., Каминская О.В., Апкарьян А.С. Фильтрующий материал для очистки воды от железа, марганца и сереводорода // Известия Томского политехнического университета. 2012. Т. 320. № 3. С. 37–40.
38. Chen C., Wei L., Gno X. et. al. Investigation of heavy oil refinery wastewater treatment by integrated ozone and activated carbon-supported manganese oxides // Fuel Processing Technology. 2014. Vol. 124. № 2. Pp. 165–173.
39. Babaeivelni K., Khodadoust A. P., Bogdan D. Adsorption and removal of arsenic (V) using crystalline manganese (II, III) oxide: Kinetics, equilibrium effect of pH and ionic strength // Journal of Environmental Science and Health, Pat A. 2014. Vol. 49. Pp. 1462–1473.
40. Иванец. А.И., Кузнецова Т.Ф., Азарова Т.А. Варанец Е.А. Синтез и свойтва Mn – оксидных катализаторов нанесенных на доломитовую подложку // Физика и химия стекла. 2013. Т. 39. № 6. С. 920–926.
41. Апкарьян А.С., Губайдулина Т.А., Каминская О.В. Структура и свойства гранулированной пеностеклокерамики на основе боя стекла, модифицированный оксидами марганца //Экология

sulfur species and their removal from groundwater supplies. *Journal of American water Works Association*. 1983. Vol. 75. Pp. 298–308.

32. Kato S., Hirano V., Iwata M., et. al. Photo catalytic degradation of gaseous sulfus compounds by silver-deposited titanium dioxide. *Applied Catalysis*. 2005. Vol. 57. Pp. 109–115.
33. Thompson M.A., Kelkar U.G., Vickers J.C. The treatment of ground water containing hydrogen sulphide using microfiltration. *Desalination*. 1995. Vol. 102. Pp. 287–297.
34. Edwards S., Alharhi R., Ghaly A. E. Removal of hydrogen sulphide from water. *American Journal of Environmental Sciences*. 2011. Vol. 7. No. 4. Pp. 295–305.
35. Bochkarev G.R., Skiter N.A. Ispolzovaniye margantsevykh rud dlya demanganatsii i obezzhelezovaniya podzemnykh vod [Use of manganese ores for demanganization and deironization of groundwater]. *Izvestiya vuzov. Stroitelstvo.* 2005. No. 11-12. Pp. 61–66. (rus)
36. Aguiar A.O., Duarte R.A., Ladeira A.C.Q. The application of MnO2 in the removal of manganese from acid mine water. *Water Air Soil Pollut*. 2013. Vol. 224. Pp. 1690.
37. Gonchikov V.Ch., Gubaydulina T.A., Kaminskaya O.V., Apkaryan A.S. Filtruyushchiy material dya ochistki vody ot zheleza, margantsa i serevodoroda [Filter material for water purification from iron, manganese and hydrogen sulfide]. *Izvestiya Tomskogo politekhnicheskogo universiteta.* 2012. Vol. 320. No. 3. Pp. 37–40.
38. Chen C., Wei L., Gno X. et. al. Investigation of heavy oil refinery wastewater treatment by integrated ozone and activated carbon-supported manganese oxides. *Fuel Processing Technology.* 2014. Vol. 124. No. 2. Pp. 165–173.
39. Babaeivelni K., Khodadoust A. P., Bogdan D. Adsorption and removal of arsenic (V) using crystalline manganese (II, III) oxide: Kinetics, equilibrium effect of pH and ionic strength. *Journal of Environmental Science and Health, Pat A.* 2014. Vol. 49. Pp. 1462–1473.
40. Ivanets A.I., Kuznetsova T.F., Azarova T.A. Varanets Ye.A. Sintez i svoytva Mn – oksidnykh katalizatorov nanesennykh na dolomitovuyu podlozhku [Synthesis and properties of Mn-oxide catalysts deposited on a dolomite substrate]. *Fizika i khimiya stekla.* 2013. Vol. 39. No. 6. Pp. 920–926. (rus)
41. Apkaryan A.S., Gubaydulina T.A., Kaminskaya O.V. Struktura i svoystva granulirovannoy penosteklokeramiki na osnove boya stekla, modifitsirovannyy oksidami margantsa [Structure and properties of granular foam glass ceramics based on glass combat, modified with manganese oxides]. *Ekologiya promyshlennogo proizvodstva.* 2014. No. 4. Pp. 30–33.
42. Gohori R.J. , Halakoo E., Nazri N.A.M. et. al. Improving performance and antifouling capability of PES UF membranes via blending with highly hydrophilic hydrous manganese dioxide nanoparticles. *Desalination*. 2014. Vol. 335. No. 3. Pp. 87–95.
43. Maliye K.K. S.M., Lisha K.P., Pradeep T. A novel cellulose – manganese oxide hybrid material, by in citi soft chemical synthesis and its application for the removal of Pb (II) from water. *Journal of Hazardous Materials*. 2010. Vol. 131. No. 1-2. Pp. 986–995.
44. Comacho L.M., Parra R.R., Deng S. Arsenic removal from groundwater by MnO2 – modified natural clinoptilolite zeolite: Effects of pH and initial feed concentration. *Journal of Hazardous Material.* 2003. Vol. 163. No. 3. Pp. 286–293.
45. Jimenez-Cedillo M.J., Olguin M.T., Fall C. Adsorption kinetic of arsenates as water pollutant on iron, manganese – modified clinoptilolite-rich tuffs. *Journal of Hazardous Materials.* 2009. Vol. 163. No. 3. Pp. 939–945.
46. Chechevichkin A.V., Samonin V.V. Zhidkofaznaya MnO2–modifikatsiya klinoitilolita [Liquid-phase MnO2-modification of clinoitilolite]. *Zhurnal prikladnoy khimii*. 2017. Vol. 90.

промышленного производства. 2014. № 4. С. 30–33.

42. Gohori R.J. ,Halakoo E., Nazri N.A.M. et. al. Improving performance and antifouling capability of PES UF membranes via blending with highly hydrophilic hydrous manganese dioxide nanoparticles // Desalination. 2014. Vol. 335. № 3. Pp. 87–95.
43. Maliyekkal S.M., Lisha K.P., Pradeep T. A novel cellulose – manganese oxide hybrid material, by in citi soft chemical synthesis and its application for the removal of Pb (II) from water // Journal of Hazardous Materials. 2010. Vol. 131. № 1-2. Pp. 986–995.
44. Comacho L.M., Parra R.R., Deng S. Arsenic removal from groundwater by MnO2 – modified natural clinoptilolite zeolite: Effects of pH and initial feed concentration // Journal of Hazardous Material. 2003. Vol. 163. № 3. Pp. 286–293.
45. Jimenez-Cedillo M.J., Olguin M.T., Fall C. Adsorption kinetic of arsenates as water pollutant on iron, manganese – modified clinoptilolite-rich tuffs // Journal of Hazardous Materials. 2009. Vol. 163. № 3. Pp. 939–945.
46. Чечевичкин А.В., Самонин В.В. Жидкофазная MnO2–модификация клиноитилолита // Журнал прикладной химии. 2017. Т. 90. № 1. С. 18–24.
47. ГОСТ 16188-70 Сорбенты. Методы испытаний. М.: Издательство стандартов, 1970. 11 с.
48. Вода питьевая. Методы анализа. Сборник стандартов. М.: Издательство стандартов, 1984. 240 с.
49. Лурье Ю.Ю. Аналитическая химия сточных вод. М.: Химия, 1984. 448 с.
50. Yin H., Feng X., Qin G., et.al. Characterization of Co-doped birnessites and application for removal of lead and arsenite // Journal of Hazardous Material. 2011. Vol. 188. № 1-2. Pp. 341–349.

No. 1. Pp. 18–24. (rus)

47. *GOST 16188-70* Sorbenty. Metody ispytaniy [Russian State Standard GOST 16188-70 Sorbents. Test methods]. Moscow: Izdatelstvo standartov, 1970. 11 p. (rus)
48. Voda pityevaya. Metody analiza. Sbornik standartov [Drinking water. Methods of analysis. Collection of standards]. Moscow: Izdatelstvo standartov, 1984. 240 p. (rus)
49. Lurye Yu.Yu. *Analiticheskaya khimiya stochnykh vod* [Analytical chemistry of sewage]. Moscow: Khimiya, 1984. 448 p.
50. Yin H., Feng X., Qin G., et.al. Characterization of Co-doped birnessites and application for removal of lead and arsenite. *Journal of Hazardous Material.* 2011. Vol. 188. No. 1-2. Pp. 341–349.

Alexey Chechevichkin,
+7(921)971-84-47; 01@6400840.ru

Nikolai Vatin,
+7(921)964-37-62; vatin@mail.ru

Vyacheslav Samonin,
+7(812)903-84-65; samonin@mail.admiral.ru

Mikhail Grekov,
+7(812)297-20-45; disgpu@spbstu.ru

Алексей Викторович Чечевичкин,
+7(921)971-84-47; эл. почта: 01@6400840.ru

Николай Иванович Ватин,
+7(921)964-37-62; эл. почта: vatin@mail.ru

Вячеслав Викторович Самонин,
+7(812)903-84-65;
эл. почта: samonin@mail.admiral.ru

Михаил Александрович Греков,
+7(812)297-20-45; эл. почта: disgpu@spbstu.ru

Чечевичкин А.В., Ватин Н.И., Самонин В.В., Греков М.А. Очистка горячей сетевой воды цеолитом, модифицированным диоксидом марганца // Инженерно-строительный журнал. 2017. № 8(76). С. 201–213.

doi: 10.18720/MCE.76.19

Fluid filtration in the clogged pressure pipelines

Фильтрация жидкости в засоренных напорных трубопроводах

E.A. Loktionova,
D.R. Miftakhova,
Peter the Great St. Petersburg Polytechnic University, St. Petersburg, Russia

Канд. техн. наук, доцент Е.А. Локтионова,
аспирант Д.Р. Мифтахова,
Санкт-Петербургский политехнический университет Петра Великого, г. Санкт-Петербург, Россия

Key words: throughput of pipeline; discharge coefficient; resistance coefficient; clogged pipelines; degree of clogging; relative flow rate; filtration coefficient of pipeline

Ключевые слова: пропускная способность трубопровода; коэффициент расхода; коэффициент сопротивления; засоренные трубопроводы; степень засорения; относительный расход; коэффициент фильтрации трубопровода

Abstract. Reducing of the hydraulic characteristics of pressure pipelines in the course of their operation due to corrosion, clogging and other causes leads to an increasing of operating costs. The existing information on the change in the capacity of pipelines under the influence of certain factors is currently insufficient. The aim of the work is to determine the influence of the clogging degree of the pipeline on its throughput. This paper describes the results of hydraulic tests of a pressure pipeline with clogging of two types: expanded clay gravel and medium-grained sand. The discharge coefficient and resistance coefficient of the "clean" pipeline and the pipeline with clogging were determined during the experiments. The dependence of the relative flow rate of the pipeline on the clogging degree of the pipe was obtained. Influence of the type of filler on the throughput of the pipe was shown. An insignificant difference in the values of the relative flow rate for both fillers at low degrees of clogging of the pipeline was established. The transition from the discharge and resistance coefficients to filtration coefficients of pipeline was proposed. The values of the filtration coefficients of pipe from the experiments on the flow measurement were found. The ratio between the discharge coefficient and the filtration coefficient of pipeline was set. The values of filtration coefficients of pipe for emptying the pressure tank were found. The coincidence of the values of the filtration coefficients by the two methods was obtained.

Аннотация. Снижение гидравлических характеристик напорных трубопроводов в процессе их эксплуатации вследствие коррозии, засорения и других причин приводит к увеличению эксплуатационных затрат. Имеющиеся в литературе сведения об изменении пропускной способности трубопроводов под воздействием тех или иных факторов на настоящий момент недостаточны. Цель работы – установить влияние степени засорения трубопровода на его пропускную способность. Для достижения цели проведены гидравлические испытания напорного трубопровода с засорением двух типов: керамзит и среднезернистый песок. В ходе опытов определены коэффициенты расхода и сопротивления "чистого" трубопровода и трубопровода с засорением. Получена зависимость относительного расхода трубопровода от степени засорения трубы. Показано влияние вида наполнителя на пропускную способность трубы. Установлено несущественное различие в значениях относительных расходов для обоих наполнителей при малых степенях засорения трубопровода. Предложен переход от коэффициентов расхода и сопротивления к коэффициентам фильтрации трубопровода. Найдены численные значения коэффициентов фильтрации трубы из опытов по измерению расхода. Установлена связь между коэффициентом расхода и коэффициентом фильтрации трубы. Найдены значения коэффициентов фильтрации трубы по опорожнению напорного бака. Получено совпадение значений коэффициентов фильтрации по двум способам.

Introduction

Changes in the internal surface of the pipes occur during their operation. During design, the recording of these changes occurs, as a rule, within the reference range of the height variation of the roughness protrusions [1, 2], or there is no accounting at all. The forecast of the change in roughness is extremely difficult in view of the large number of factors determining the nature and intensity of this process. The change in the state of the internal surface of the pipes occurs both because of corrosion [3], and as a result of clogging, settling of suspended particles and other processes that increase the overall hydraulic resistance. In practice, this means an increase in pressure losses during fluid motion, which leads to a gradual decrease in the capacity of the pipelines and the average velocity of the fluid in comparison with the design values assumed. Reducing the throughput of pipes, for example, for water supply systems, can reach 50% or more, depending on the material, type of coating, pipe diameter, operating conditions, fluid properties, sediment profile, etc. [4].

The problem of clogging of pipes over time, and as a result, deterioration of their hydraulic characteristics (below the normative values) is an important practical task, because to provide consumers with the required amount of liquid, regular pipe cleaning or increasing pressure must be carried out, which leads to an increase in operational costs. However, these measures are not always sufficient, and there is a need to replace pipes or lay new pipelines, which, in turn, leads to an increase in capital costs.

A number of authors evaluated the pressure losses depending on the service life of the pipelines [4], and recommendations were given to increase design head losses at the design stage. However, as more recent research showed, the formation of deposits in pipelines is a complex multifactor process, the development of which is difficult to foresee. The currently available data about the influence of clogging on the pipeline throughput is mainly obtained experimentally [5–11]. There are also attempts to investigate clogged pipes on mathematical models [12–19].

For example, work [5] is devoted to a model, developed for the city's water supply system in St. Petersburg and includes more than 6.200 km of water networks with diameters up to 1.400 mm. The paper defines the actual hydraulic resistance of pipelines under different operating conditions. It was found that the resistance is 2-5 times higher than design engineers accepted for non-new pipes (lower values refer to pipes that are in operation for 5-10 years, larger ones to pipes with longer service lives).

The paper [12] presents the results of computer calculations of areas with an abruptly changing fluid motion, due to the presence of a sudden increase or decrease in the diameter of the pipeline and other devices.

The results of a study of the effect of operating parameters, diameter and weight of suspended particles on the rate of gas-abrasion wear of pipeline bends are presented in [13]. The main tasks solved by the authors were to analyze the statistics of the reasons for the failure of the gas pipeline offsets, and to verify the real objects and calculation models using the FLOWVISION PC. As a result, the zone location of the maximum concentration of particles on the wall of the tap was determined as a function of pressure, the mass of the abrasive at the inlet, and the diameter of the abrasive particles.

The results of numerical calculations are largely determined by the choice of the computational grid and the correct assignment of boundary conditions, so the reliability and veracity of these results should also be checked in the full-scale experiment.

Thus, the question of wearing and clogging of building services to the true hydraulic resistance of pipelines located in various operating conditions is an important practical problem.

The purpose is to study the influence of the degree of clogging of the pressure pipeline on its throughput.

To achieve the purpose, the following objectives were set and solved:

1. Develop a methodology for conducting the experiment;
2. Conduct a comparison of the results with the data of stationary resistances in pipelines;
3. Propose the approximate criteria for estimating the throughput capacity of a clogged pipeline.

Methods and Materials

To solve the problems, experimental studies were carried out on a model with a ratio of length to diameter equal to $\mathrm{l/D} = 20$.

Hydraulic measurements of the pipeline contained several series of experiments. Initially, the intensity of flow was determined by the volumetric method at the outlet from the pipeline with a free flow. Further, the numerical values of the discharge coefficients μ and the total resistance coefficient ζ_f of the "clean" pipe were determined from formulas

$$\mu = \frac{Q}{\omega_0 \cdot \sqrt{2gH}}, \tag{1}$$

$$\zeta_f = (1/\mu^2) - 1, \tag{2}$$

where Q – intensity of flow, ω_0 – sectional area of the "clean" pipe, H – pressure head above the gravity center of the outlet section of the pipe.

Then, the same characteristics were determined in a similar way for pipe with filler at different degrees of filling (degrees of clogging) of the pipe V_{fil}/V_0 (V_{fil} – volume of filler, V_0 – volume of "clean" pipe). In the experiments, there were used two types of filler: claydite gravel and medium-grained sand (Fig. 1).

a)

b)

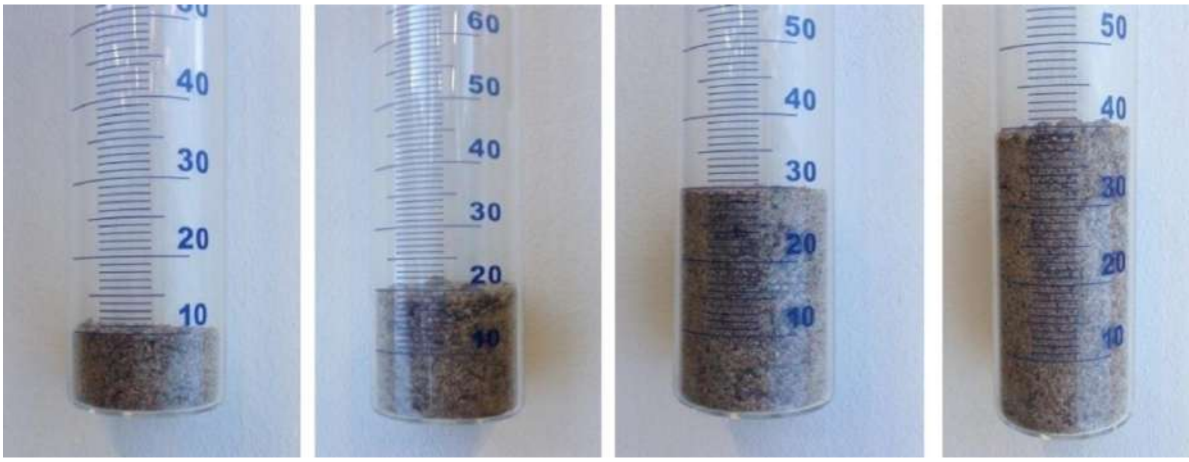

Figure 1. Samples of the test fillers: a) claydite gravel; b) medium-grained sand

To prevent the removal of the filler from the pipe, a sieve-containing grating was installed at the outlet, chosen in such a way so that the dimensions of its cells do not exceed the particle sizes of the test filler in both cases.

Results

The results of some series of experiments are shown on Figure 2 as a graph of the dependence $\mu = f(H/H_{max})$, where H_{max} – is the maximum possible pressure head in the current model. As can be seen from the graph, the values of discharge coefficients do not depend on the value of the pressure head (with an acceptable error), but are determined only by the type of filler and the degree of pipe clogging.

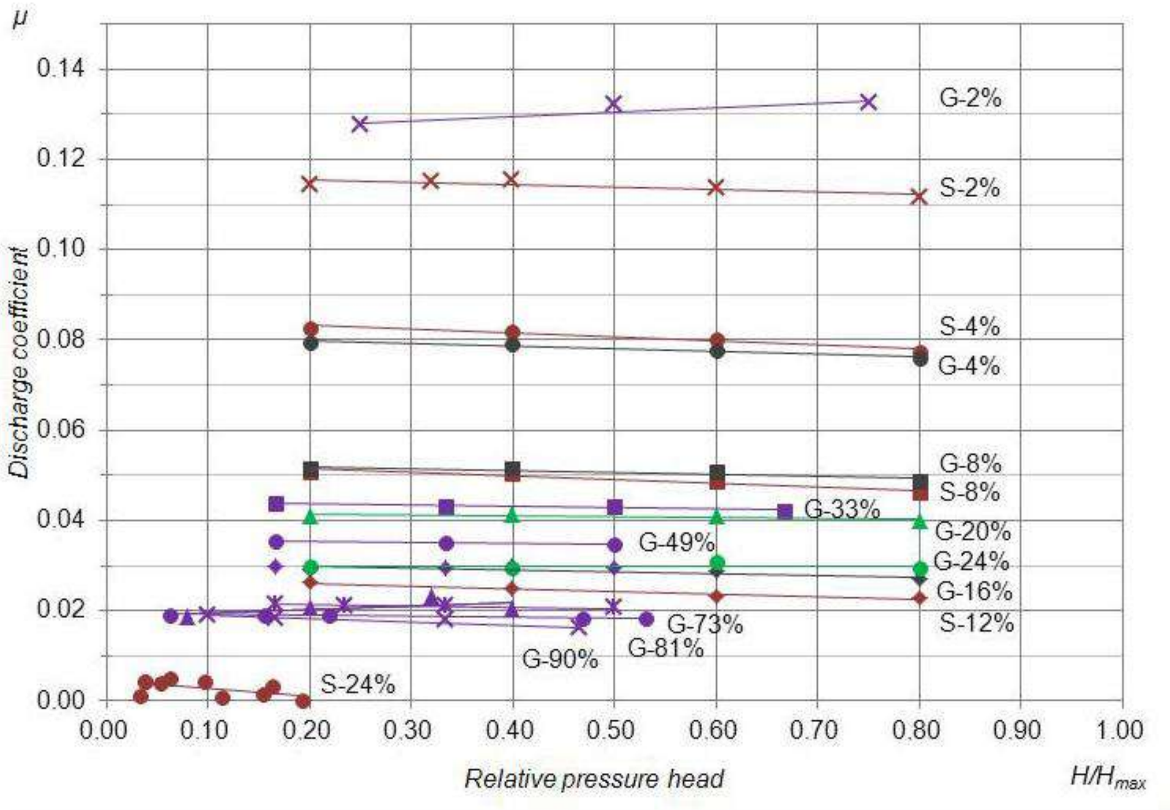

Figure 2. Dependence diagram μ=f(H/H_max)
(G – experimental data with claydite gravel, S –experimental data with sand)

Figure 3 shows the dependence of the total resistance coefficients of the pipeline ζ_f from the Reynolds number Re, calculated from the average velocity in the pipe. From Figure 3 it follows that for small degrees of clogging corresponding to Re > 2000, the values of ζ_f do not depend on the Reynolds number, but are determined only by the clogging degree of the pipe.

a)

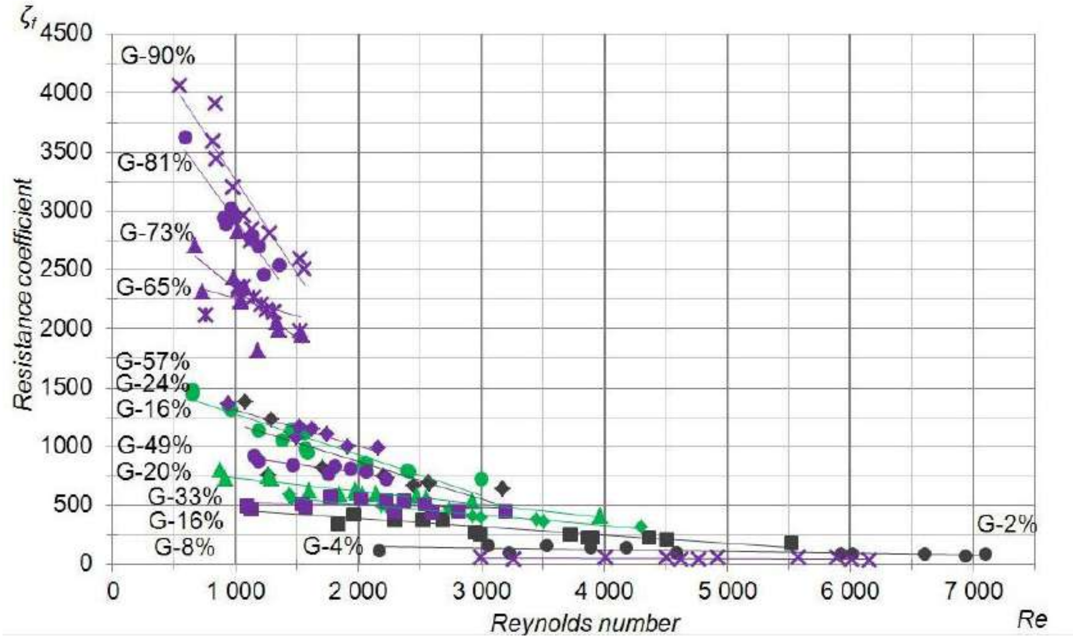

b)

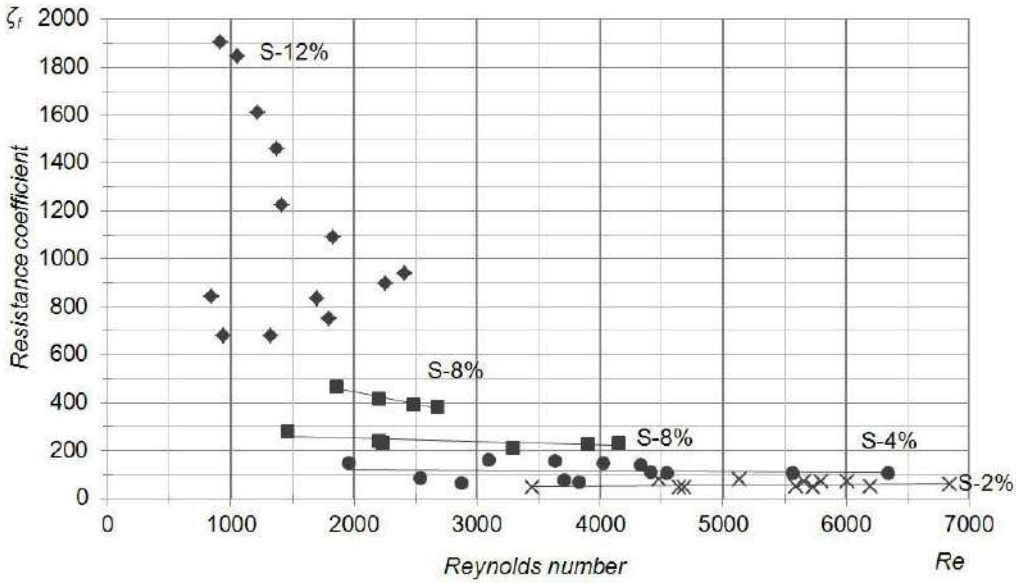

Figure 3. Dependence diagram $\zeta_f = f(Re)$
a) experiments with claydite gravel; b) experiments with sand

Figure 4 gives the dependence ζ_f as a function of the values V_0/V_{fil}. Experimental points on the diagram of figure 4 are approximated by power functions. It is evident from figures 3 and 4 that for large clogging, the spread of experimental data (corresponding to different pressure heads H) increases, because the size of the filler particles, their shape, the packing peculiarities within the flow section, and other factors exert an increasing influence as the Reynolds numbers decrease. In addition, it was found that for small clogging degrees ($V_{fil}/V_0 \leq 0{,}1(\leq 10\%)$) the influence of the filler type (the nature of the clogging) is insignificant, and with the increase of clogging degrees $V_{fil}/V_0 > 10\%$ the influence of the filler type is more noticeable.

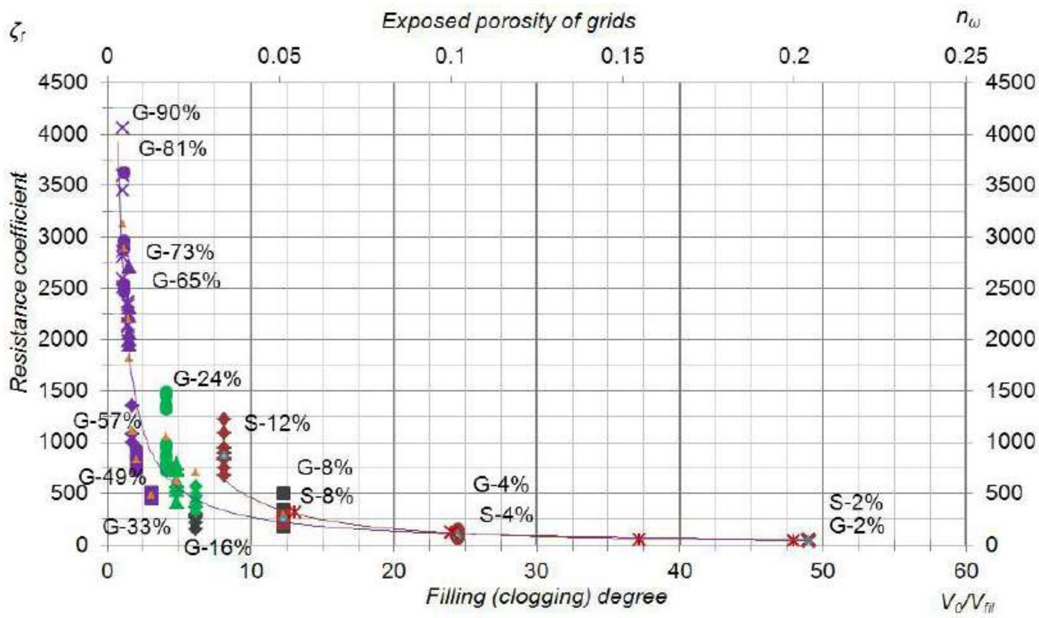

Figure 4. Dependence diagram $\zeta_f = f(V_0/V_{fil})$

For an approximate estimate of the change in throughput of pipeline with its clogging the dependence diagram $Q/Q_0 = f(V_0/V_{fil})$ was constructed, where Q – intensity of flow in the pipe with filler, Q_0 – intensity of flow in the clean pipe at the same pressure head H. The presented diagram makes it possible to determine the clogging degree of the pipeline with a known drop of intensity of flow in it during operation, and also to find the limiting clogging of the pipe with the containment grid, at which the flow of liquid in the pipe is practically absent. As can be seen from the Fig. 5, the ultimate clogging for sand occurs approximately when the content of the pipe is 20 % filler, and for claydite gravel – more than 90 %.

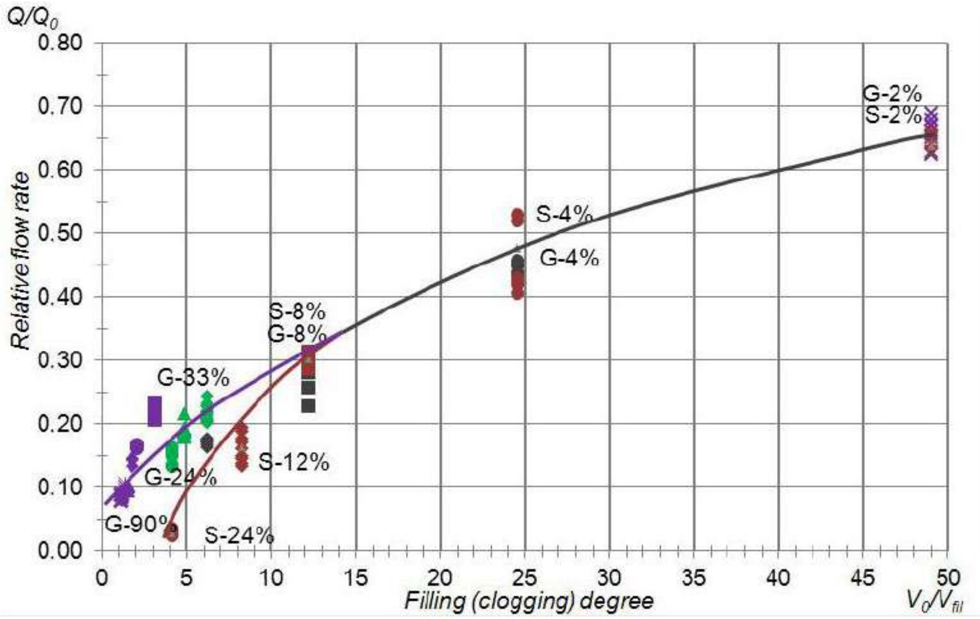

Figure 5. Dependence diagram $Q/Q_0 = f(V_0/V_{fil})$

Discussion

The research above is carried out under conditions where the filler in the pipe was in nonsteady state and had the ability to move, change its packaging, form compacted structures, settle, etc. The results of this research were compared with similar experiments in a pipeline without a filler with the same ratio $l/D = 20$, at the outlet of which perforated grids (Fig. 6) with different exposed porosity $n_\omega = \omega_h/\omega_0$ (ω_h– the total area of the grid holes (clearance area)) were set [20, 21].

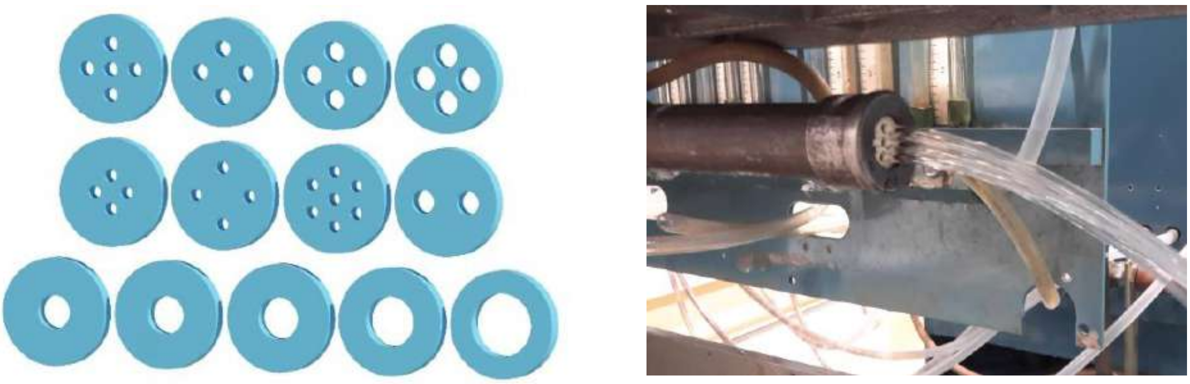

Figure 6. Types of perforated grids and imagine of the flow on the outlet of the pipe

Comparison of experimental data in pipelines with filler and with grids (Fig. 7) showed that in the general range of resistance coefficients ($\zeta \leq 500$) dependences $\zeta_f = f(V_0/V_{fil})$ and $\zeta_f = f(n_\omega)$ do not qualitatively differ. This means that there is a unique connection between the exposed porosity of the grids and the reciprocal of the clogging degree of the pipe. For clarity, the two horizontal axes on Fig. 7 are used: lower axis is for V_0/V_{fil}; the upper one is for n_ω.

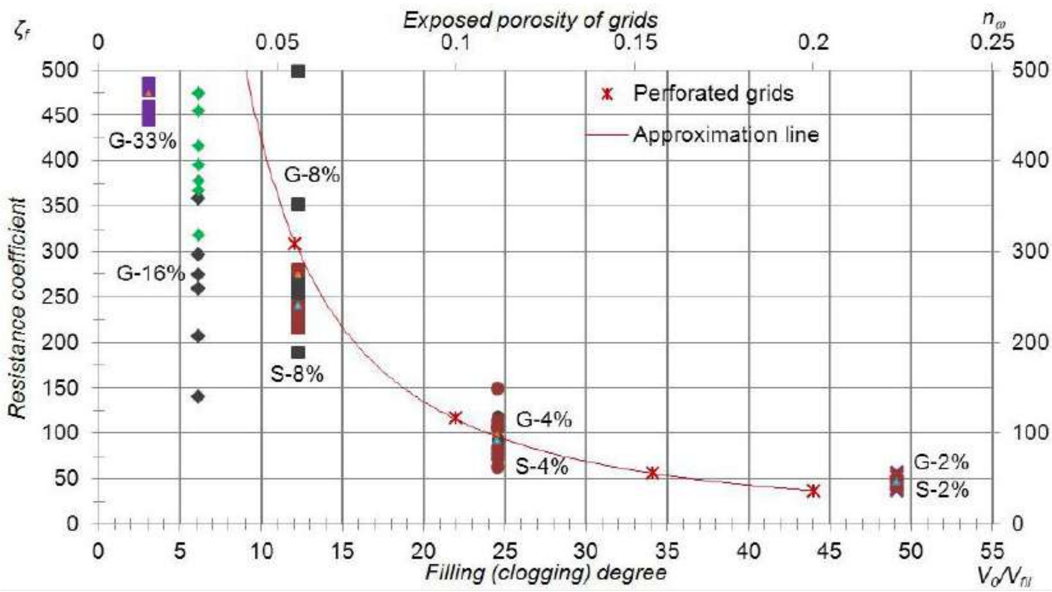

Figure 7. Combined dependency diagram $\zeta_f = f(V_0/V_{fil})$ and $\zeta_f = f(n_\omega)$ (markers – experimental points for the pipe with filler; solid line – approximation of data on grids without filler, proposed in [20])

The correspondence between the scales n_ω and V_0/V_{fil}, found by the averaged values of the experiments, is shown on Figure 8.

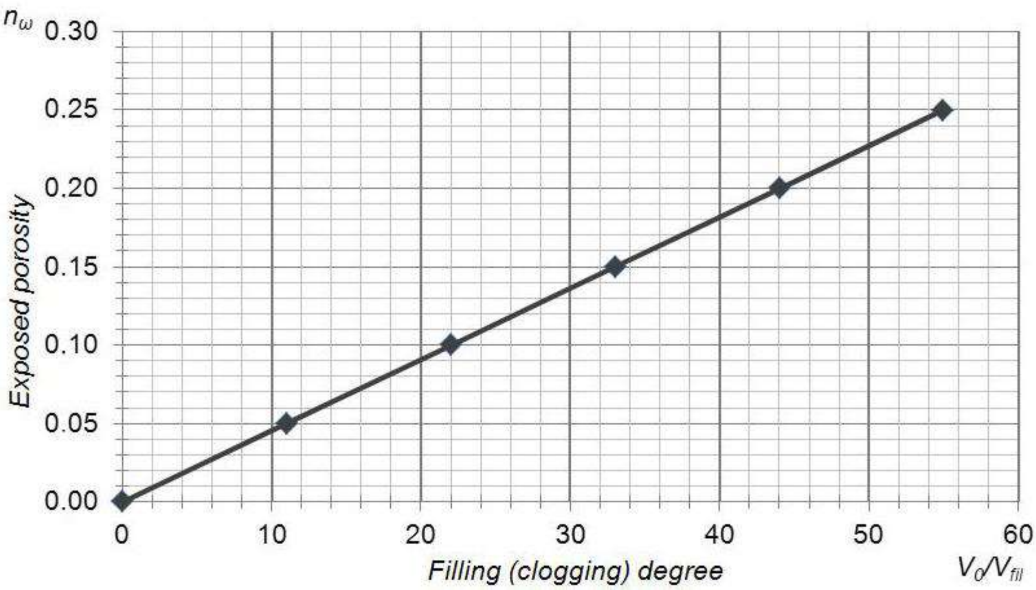

Figure 8. Relation between the clogging degree of the pipeline $\frac{V_0}{V_{fil}}$ with exposed porosity of grids n_ω

Thus, the dependence of Fig. 8 allows simulation of pipe clogging using any stationary devices, for example, grids.

As can be seen from Fig. 4, at large degrees of clogging of the pipe (>10% of the pipeline volume, $V_0/V_{fil} < 10$) the numerical values of the resistance coefficients ζ_f increase sharply, and their range of variation is several orders of magnitude. The obtained range significantly complicates the perception of the values, and also makes the amount of the resistance coefficient of the clogged pipeline absurd.

If instead of resistance we introduce the so-called permeability of the pipe (actually the value reciprocal of the resistance (some analog of the discharge coefficient)), then it is possible to imagine the flow of liquid in the pipeline with clogging as a filtration flow. Then the average velocity in the pipe v_0 will be interpreted as the filtration velocity, determined by the relation.

$$v_0 = k \cdot \sqrt{J}, \tag{3}$$

where k – filtration coefficient, J – hydraulic drop.

Equation (3) is the law of turbulent filtration in the theory of filtration [22-24].

Since for v_0 it is also true

$$v_0 = \mu \cdot \sqrt{2gH}, \tag{4}$$

where H – pressure head above the center of the outlet section of the pipeline. Equating (3) and (4), we obtain

$$\mu \cdot \sqrt{2gH} = k \cdot \sqrt{J} \text{ or}$$

$$k = \mu \cdot \frac{\sqrt{2gH}}{\sqrt{J}} \tag{5}$$

Substitution of the hydraulic drop in (5) $J = H/l$ (l – pipe length) leads to the expression for k

$$k = \mu \cdot \sqrt{2gl}. \tag{6}$$

According to the formula (6), k is a constant value for a pipe with a given geometry and fixed degree of clogging with a filler of a certain type. Filtration coefficient has unit of measurement of velocity and is a measure of the filtration conductivity of a clogged pipe in terms of its physical meaning. In this case, k should not be considered as a parameter expressing the filtration properties of the filler material, but as a characteristic of a particular pipe with specific filler.

The dependence of the pipeline filtration coefficients k on the value V_0/V_{fil} is shown in accordance with (6) on Figure 9.

The range of the values of the filtration coefficients on Fig. 9 for all degrees of clogging (from 2 % to 90 % of the volume of the pipe) is of the order of the average speed in the "clean" pipe.

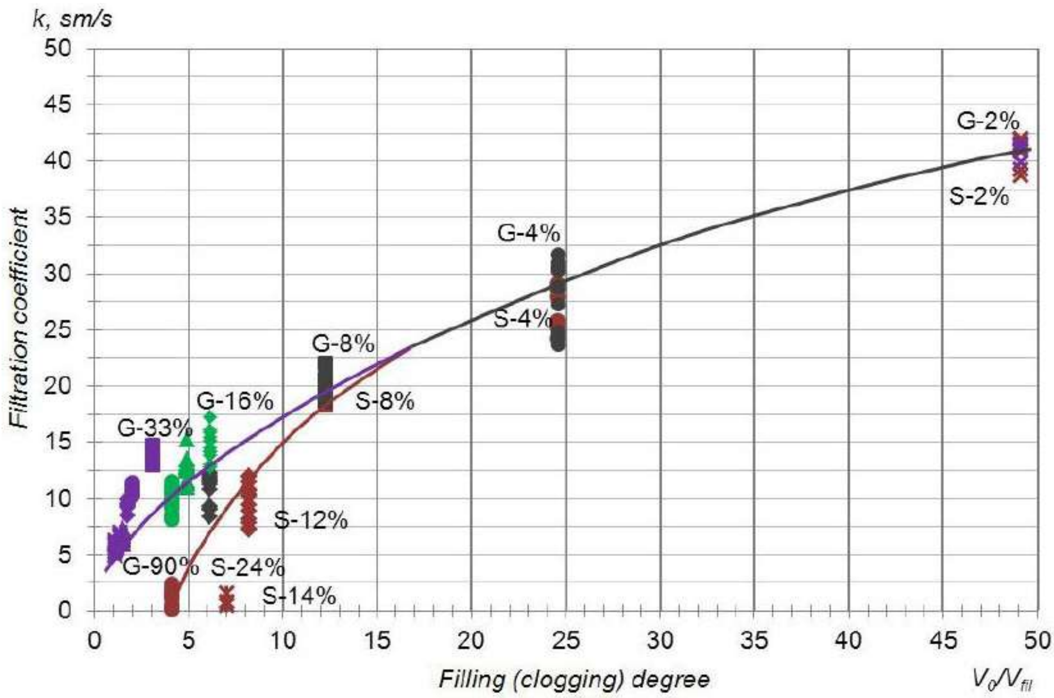

Figure 9. Dependence diagram $k = f(V_0/V_{fil})$

Equation (6) gives a directly proportional relation between the filtration coefficient and discharge coefficient of pipeline μ.

To determine the filtration coefficient in another way, experiments based on measuring the time of emptying the pressure tank between fixed heads at different degrees of clogging with claydite gravel and sand were used. From the continuity condition of fluid motion in the pipe and in the pressure tank, it follows that

$$\frac{dH}{dt} \cdot \Omega = k \cdot \sqrt{J} \cdot \omega_0$$

or

$$\frac{dH}{dt} \cdot \Omega = k \cdot \sqrt{\frac{H}{l}} \cdot \omega_0, \qquad (7)$$

where Ω – area of the horizontal section of the pressure tank.

Integration of (7) from the initial pressure head H_0 to the final H_t in time t leads to expression

$$k = \frac{2 \cdot \Omega \cdot \sqrt{l}}{\omega_0 \cdot t} \cdot \left(\sqrt{H_0} - \sqrt{H_t}\right). \qquad (8)$$

Experimental points, which were found from the time of emptying the pressure tank, are also plotted on Fig. 9. These data do not fall out of the range, which were found by the flow measurement.

Conclusions

1. The dependence of the relative flow rate of the pipeline from the degree of its clogging gives an approximate estimate of the reduction in the throughput of the clogged pipe.

2. At small degrees of clogging of the pipeline (<10% by volume of the pipe), the influence of the type of clogging on the flow rate is insignificant. With a further increase in the clogging degree, the curved lines of relative flow rate are qualitatively different.

3. An alternative to the discharge coefficient is filtration coefficient of pipeline. The filtration coefficient has the dimension and order of velocity in a clean pipe, so that it is more preferable in practical calculations of clogged pipes as a measure of the filtration conductivity of a pipe.

References

1. Idel'chik I. E. *Handbook of hydraulic resistance* 4th ed. rev. and augmented. United States: Begell House in Redding, CT, 2008. 881 p.
2. Buhalov A.A., Orehova E.E., Andreev V.V. Razrabotka metodiki prognozirovanija gidravlicheskogo soprotivlenija v gladkih trubah na osnove obobshhenija jeksperimental'nyh dannyh [Development of models and procedures for hydraulic resistance in smooth tubes prediction of the basis ot the experimental data generalization]. *Sovremennye problemy nauki i obrazovanija.* 2014. No. 6. Pp. 242–248. (rus)
3. Shabangu T.H., Ponnle A.A., Adedeji K.B., Abe B.T., Olubambi P.A., Jimoh A.A. Effects of soil properties on corrosion of buried steel pipeline: A case study of rand water pipeline, South Africa. *AFRICON 2015. IEEE Conference Publications*. 2015. Pp. 1–5.
4. Al'tshul' A.D. *Gidravlicheskie soprotivlenija* [Hydraulic resistances]. Moskow: Nedra, 1982. 224 p. (rus)
5. Hjamjaljajnen M.M., Judin M.Ju. Kompleksnye gidravlicheskie raschety sistemy podachi vody Sankt-Peterburga. [Complex hydraulic calculations of the water supply system of St. Petersburg]. *Vodosnabzhenie i sanitarnaja tehnika*. 2006. No. 9-1. Pp. 22–24. (rus)
6. Andreev V.V., Turchenko M.V., Abramov A.A. Preobrazovanie harakteristik gidravlicheskogo soprotivlenija s cel'ju obobshhenija jeksperimental'noj informacii o techenii zhidkosti v trubah. [Transformation of hydraulic resistance characteristics in order to generalize experimental information on fluid flow in pipes]. *Nauchno-tehnicheskij vestnik Povolzh'ja.* 2012. No. 4. Pp. 35-37. (rus)
7. Novoselov A.G., Chebotar' A.V., Guljaeva Ju.N., Meradzhi V.V. Jeksperimental'noe issledovanie gidravlicheskih soprotivlenij pri techenii vodno-zernovyh suspenzij v trubah. [Experimental study of hydraulic resistance during flow of water-grain suspensions in pipes]. *Nauchnyj zhurnal NIU ITMO, Serija "Processy i apparaty pishhevyh*

Литература

1. Idel'chik I. E. Handbook of hydraulic resistance 4th ed. rev. and augmented. United States: Begell House in Redding, CT, 2008. 881 p.
2. Бухалов А.А., Орехова Е.Е., Андреев В.В. Разработка методики прогнозирования гидравлического сопротивления в гладких трубах на основе обобщения экспериментальных данных // Современные проблемы науки и образования. 2014. № 6. С. 242–248.
3. Shabangu T.H., Ponnle A.A., Adedeji K.B., Abe B.T., Olubambi P.A., Jimoh A.A. Effects of soil properties on corrosion of buried steel pipeline: A case study of rand water pipeline, South Africa // AFRICON 2015. IEEE Conference Publications. 2015. Pp. 1–5.
4. Альтшуль А.Д. Гидравлические сопротивления. М.: Недра, 1982. 224 с.
5. Хямяляйнен М.М., Юдин М.Ю. Комплексные гидравлические расчеты системы подачи воды Санкт-Петербурга // Водоснабжение и санитарная техника. 2006. № 9-1. С. 22–24.
6. Андреев В.В., Турченко М.В., Абрамов А.А. Преобразование характеристик гидравлического сопротивления с целью обобщения экспериментальной информации о течении жидкости в трубах // Научно-технический вестник Поволжья. 2012. № 4. С. 35–37.
7. Новоселов А.Г., Чеботарь А.В., Гуляева Ю.Н., Мераджи В.В. Экспериментальное исследование гидравлических сопротивлений при течении водно-зерновых суспензий в трубах // Научный журнал НИУ ИТМО. Серия «Процессы и аппараты пищевых производств». 2014. № 3. С. 273–284.
8. Анциферов С.А., Филенков В.М. Апробация экспериментального стенда для определения гидравлического сопротивления шероховатой трубы // Вестник НГИЭИ. 2015. № 6(49). С. 10–15.
9. Duan H.F., Lee P.J., Tuck J. Experimental Investigation of Wave Scattering Effect of Pipe Blockages on Transient

proizvodstv". 2014. No. 3. Pp. 273–284. (rus)

8. Anciferov S.A., Filenkov V.M. Aprobacija jeksperimental'nogo stenda dlja opredelenija gidravlicheskogo soprotivlenija sherohovatoj truby. [Approbation of the experimental stand for the determination of the hydraulic resistance of a rough pipe]. *Vestnik NGIJeI*. 2015. No. 6(49). Pp. 10–15. (rus)
9. Duan H.F., Lee P.J., Tuck J. Experimental Investigation of Wave Scattering Effect of Pipe Blockages on Transient Analysis. *Procedia Engineering*. 2014. Vol. 89. Pp. 1314-1320.
10. Huang J., Chen G., Shu L., Chen Y., Yu Zhang. Impact of fouling on flow-induced vibration characteristics in fluid-conveying pipelines. *IEEE Journals & Magazines*. 2016. Vol. 4. Pp. 6631–6644.
11. Khan T.S., Al-Shehhi M.S. Review of black powder in gas pipelines – An industrial perspective. *Journal of Natural Gas Science and Engineering*. 2015. Vol. 25. Pp. 66–76.
12. Chemezov D. The character of the fluid flow in the pipelines with the local hydraulic resistances. *ISJ Theoretical & Applied Science.* No. 12(44). Pp. 62–68.
13. Zakirnichnaja M.M., Adeev I.Ju., Perederej T.I., Isanchurina G.F. Specifika modelirovanija gazodinamiki s abrazivnymi chasticami v truboprovode s ispol'zovaniem PK FlowVision. [Specificity of simulation of gas dynamics with abrasive particles in the pipeline using the software package FlowVision]. *Trudy mezhdunarodnogo foruma "Inzhenernye sistemy".* Moskow. 2016. Pp. 78-92. (rus)
14. Kaljakin A.M., Chesnokova E.V. Novaja zavisimost' dlja opredelenija kojefficienta gidravlicheskogo soprotivlenija v perehodnoj zon soprotivlenija (ot laminarnogo k turbulentnomu). [A new functional connectionfor determining the coefficient of hydraulic resistance in the transition resistance zone (from laminar to turbulent)]. *Magazine of Civil Engineering*. 2012. No. 2. Pp. 51-55. (rus)
15. Gomez-Martinez P., Cubillo F., Martin-Carrasco F.J., Garotte L. Statistical dependence of pipe breaks on explanatory variables. *Water (Switzerland).* 2017. No. 9.
16. Lecreps I., Orozovic O., Erden T., Jones M.G., Sommer K. Physical mechanisms involved in slug transport and pipe blockage during horizontal pneumatic conveying. *Powder Technology.* 2014. Vol. 262. Pp. 82–95.
17. Izmailova E.V., Politova T.O., Serov V.V. Development of methods of detection of pipelines corrosion defeat by computer modeling. 2016. *2nd International Conference on Industrial Engineering, Applications and Manufacturing (ICIEAM).* 2016. Pp. 1–4.
18. Aiyejina A., Chakrabarti D.P., Pilgrim A., Sastry M.K.S. Wax formation in oil pipelines: A critical review. *International Journal of Multiphase Flow.* 2011. Vol. 37. No. 7. Pp. 671–694.
19. Achebo Joseph I. Computational analysis of flow properties that could cause pipeline failure. *International Conference on Engineering Computation.* 2009. Pp. 257–260.
20. Latuhina A.I., Loktionova E.A., Polupanova Ju.R. Gidrodinamicheskoe soprotivlenie setok v napornyh vodovodah. [Hydraulic resistance of the grid in the pressure water conduit]. *St. Petersburg State Polytechnical University Journal*. 2016. No. 2(243). Pp. 174−180. (rus)
21. Latuhina A.I., Loktionova E.A., Miftakhova D.R., Polupanova Ju.R. Soprotivlenie i pronicaemost' napornyh gidrolinij s setkami [The resistance and permeability of the pressure hydroline with grids]. *St. Petersburg polytechnic university journal of engineering sciences and technology*. 2017. Vol. 23. No. 2. Pp. 205–214. (rus)
22. Polubarinova-Kochina P.Ja. *Teorija dvizhenija gruntovyh vod.* [Theory of ground water motion]. Moskow; Nauka.

Analysis // Procedia Engineering. 2014. Vol. 89. Pp. 1314-1320.

10. Huang J., Chen G., Shu L., Chen Y., Yu Zhang. Impact of fouling on flow-induced vibration characteristics in fluid-conveying pipelines // IEEE Journals & Magazines. 2016. Vol. 4. Pp. 6631–6644.
11. Khan T.S., Al-Shehhi M.S. Review of black powder in gas pipelines – An industrial perspective // Journal of Natural Gas Science and Engineering. 2015. Vol. 25. Pp. 66–76.
12. Chemezov D. The character of the fluid flow in the pipelines with the local hydraulic resistances // ISJ Theoretical & Applied Science. № 12(44). Pp. 62–68.
13. Закирничная М.М., Адеев И.Ю., Передерей Т.И., Исанчурина Г.Ф. Специфика моделирования газодинамики с абразивными частицами в трубопроводе с использованием ПК FlowVision // Труды международного форума «Инженерные системы». Москва. 2016. С. 78–92.
14. Калякин А.М., Чеснокова Е.В. Новая зависимость для определения коэффициента гидравлического сопротивления в переходной зон сопротивления (от ламинарного к турбулентному) // Инженерно-строительный журнал. 2012. № 2. С. 51–55.
15. Gomez-Martinez P., Cubillo F., Martin-Carrasco F.J., Garotte L. Statistical dependence of pipe breaks on explanatory variables // Water (Switzerland). 2017. № 9.
16. Lecreps I., Orozovic O., Erden T., Jones M.G., Sommer K. Physical mechanisms involved in slug transport and pipe blockage during horizontal pneumatic conveying // Powder Technology. 2014. Vol. 262. Pp. 82–95.
17. Izmailova E. V., Politova T. O., Serov V. V. Development of methods of detection of pipelines corrosion defeat by computer modeling // 2nd International Conference on Industrial Engineering, Applications and Manufacturing (ICIEAM). 2016. Pp.1–4
18. Aiyejina A., Chakrabarti D.P., Pilgrim A., Sastry M.K.S. Wax formation in oil pipelines: A critical review // International Journal of Multiphase Flow. 2011. Vol. 37. № 7. Pp. 671–694.
19. Achebo J.I. Computational analysis of flow properties that could cause pipeline failure // International Conference on Engineering Computation. 2009. Pp. 257-260.
20. Латухина А.И., Локтионова Е.А., Полупанова Ю.Р. Гидродинамическое сопротивление сеток в напорных гидролиниях // Научно-технические ведомости СПбГПУ. 2016. № 2(243). С. 174−180.
21. Латухина А.И, Локтионова Е.А., Мифтахова Д.Р., Полупанова Ю.Р. Сопротивление и проницаемость напорных гидролиний с сетками // Научно-технические ведомости СПбПУ. Естественные и инженерные науки. 2017. Т. 23. № 2. С. 205–214.
22. Полубаринова-Кочина П.Я. Теория движения грунтовых вод. М.: Наука. Главная редакция физико-математической литературы, 1977. 664 с.
23. Петриченко М.Р. Термодинамические тождества и уравнения неизотрмической фильтрации в изотропной пористой среде // Научно-технические ведомости СПбГПУ. 2013. № 2(171). С. 188–192.
24. Даценко Е.Н., Васильев Н.И., Авакимян Н.Н., Савенок О.В., Кошелев А.Т. Гидравлическое сопротивление течению жидкости через пористую среду // Строительство нефтяных и газовых скважин на суше и на море. 2014. № 12. С. 18–20.

Glavnaja redakcija fiziko-matematicheskoj literatury, 1977, 664 p. (rus)

23. Petrichenko M.R. Termodinamicheskie tozhdestva i uravnenija neizotermicheskoj fil'tracii v izotropnoj poristoj srede. [Thermodynamic identities and equations of non-isothermal filtration in an isotropic porous medium]. *St. Petersburg State Polytechnical University Journal.* 2013. No. 2 (171). Pp. 188–192. (rus)
24. Dacenko E.N., Vasil'ev N.I., Avakimjan N.N., Savenok O.V., Koshelev A.T. Gidravlicheskoe soprotivlenie techeniju zhidkosti cherez poristuju sredu. [Hydraulic resistance to flow of liquid through a porous medium]. *Stroitel'stvo neftjanyh i gazovyh skvazhin na sushe i na more*. 2014. No. 12. Pp. 18–20. (rus)

Elena Loktionova,
+7(921)423-93-02; elena.lokt@yandex.ru

Dinara Miftakhova,
+7(981)888-37-18; dinara.miftakhova@gmail.com

Елена Анатольевна Локтионова,
+7(921)4239302;
эл. почта: elena.lokt@yandex.ru,

Динара Робертовна Мифтахова,
+7(981)8883718;
эл. почта: dinara.miftakhova@gmail.com.

doi: 10.18720/MCE.76.20

Stress-strain state of clamped rectangular Reissner plates

Напряженно-деформированное состояние защемленной прямоугольной пластины Рейсснера

M.V. Sukhoterin,
S.O. Baryshnikov,
T.P. Knysh,
Admiral Makarov State University of Maritime and Inland Shipping, St. Petersburg, Russia

Д-р техн. наук, заведующий кафедрой М.В. Сухотерин,
д-р техн. наук, ректор С.О. Барышников,
канд. физ.-мат. наук, заместитель директора института водного транспорта Т.П. Кныш,
Государственный университет морского и речного флота имени адмирала С.О. Макарова, г. Санкт-Петербург, Россия

Key words: Plate Reissner; clamped contour; bending; Fourier series; computations

Ключевые слова: Пластина Рейсснера; защемленный контур; ряды Фурье; компьютерные вычисления

Abstract. The paper focuses on obtaining numerical results for a rectangular Reissner plate with clamped contour under the influence of a uniform load using the iteration superposition method of four types of trigonometric series (correcting functions). The initial function of bendings is selected as a quartic polynomial which turns into zero on the contour and is a specific solution to the main bending equation. Discrepancies in rotation angles from the initial polynomial are eliminated in turn on parallel edges by pairs of correcting functions of bendings and stresses which cause angular discrepancies themselves. During an infinite process of the superposition of these pairs, all discrepancies tend to zero, which gives a precise solution at the limit. The paper presents results of bending computations, bending moments, and shearing forces for square plates different thickness. The obtained results are compared with the results of other authors, as well as with Kirchhoff theory. It is shown that with the relative thicknesses less than 1/20, the results gained with both theories are almost the same.

Аннотация. В статье получены численные результаты для защемленной по контуру прямоугольной пластины Рейсснера под действием равномерной нагрузки итерационным методом суперпозиции четырех видов тригонометрических рядов (исправляющих функций). Начальная функция прогибов выбирается в виде многочлена четвертой степени, который обращается в нуль на контуре и является частным решением основного уравнения изгиба. Невязки по углам поворота от начального многочлена поочередно устраняются на параллельных краях парами исправляющих функций прогибов и напряжений, которые сами порождают угловые невязки. В ходе бесконечного процесса суперпозиции этих пар все невязки стремятся к нулю, что в пределе дает точное решение. Приведены результаты расчетов прогибов, изгибающих моментов и перерезывающих сил для квадратных пластин различной толщины. Дается сравнение с результатами других авторов, а также с теорией Кирхгофа. Показано, что при относительных толщинах, меньших 1/20 результаты по обеим теориям практически совпадают.

Introduction

Modern structures widely use metallic and non-metallic materials (composite, synthetic, etc.) which have increased pliability to an interlaminar shear. Such materials are often used for making plates (panels, slabs) which are main elements in ship, aero-, and other structures as well as in nanoengineering.

Solution to 3D problems of the elasticity theory, which include problems of the plates' elastic behavior, is connected with solving a complex system of differential equations and boundary conditions. It caused the necessity of shifting from 3D problems to more simple 2D ones. Historically, a simplified theory of thin plates, based on the hypotheses of Kirchhoff-Love, was the first to put forward; it is called the classical theory. Many engineering problems were successfully solved using this theory. However, it provides poor accuracy near the plate's contour, around the points of sharp change in boundary conditions and the points of applied concentrated forces, as well as when making computations for plates of average thickness. Therefore, there emerged a problem of shifting to more precise two-dimensional theories with using the altered hypotheses by Kirchhoff-Love. These theories were called refined theories (intermediate between the classical two-dimensional theory and the three-dimensional one).

Today, a variety of refined theories are developed and used, including theories that take into account the influence of transverse shear strain on the bending. Timoshenko [1] was the first to note the necessity of considering this influence when solving rod vibration problems. The number of refined theories today is quite large because there is no universal theory providing acceptable results for all types of problems.

The linear plate bending theory, which qualitatively refined the classical theory, was firstly put forward by Reissner [2]. Author rejected the hypothesis of the rectilinear element normality to the median surface and suggested replacing it with a hypothesis of rectilinearity of this element and introducing a law of stress variation based on thickness of the plate. Reissner, using a balance equation of the three-dimensional elasticity theory, compatibility conditions, and Castiglian's principle of minimum strain-energy, obtained new differential equations of the plate bending and the corresponding boundary conditions allowing for the transverse shear effect. The fundamental system consists of two equations. The first equation of the fourth order characterizes the plate bending. The second equation of the second order describes the stress state which is of local character and disappears quickly when moving away from the plate's edge. It increased the system's order to the sixth which allowed satisfying three boundary conditions (instead of two in the classical theory). The given and similar shear theories are often called Reissner - Mindlin [3] - Timoshenko [4] theories due to their similarity. Particularly, the difference between the theories by Reissner and Mindlin is basically values of the transverse shear coefficient: Reissner has it equal to 5/6 ($\approx$ 0.833) and Mindlin to $\pi^2/12$ ($\approx$ 0.822), which is very close.

Variant of shear theories presented in the work Ambartsumyan [5].

Applicability limits of the theories by Kirchhoff-Love, Poisson, and Reissner, as well as revision of refined theories are discussed in the works Goldenveizer et al. [6, 7], Vasiliev [8, 9], Zhilin [10, 11] an others.

Goldenveizer et al. [6, 7] in the refined theory divide the stress state into internal and edge. Researchers use the asymptotic method in combination with the variational principle. The authors state that the Reissner system of basic equations is incorrect because it does not result from the asymptotic method. Vasiliev [8, 9] notes that there are problems which cannot be solved with the Kirchhoff theory. The author reckons that the asymptotic method of the Goldenveizer refined theory is ambiguous and approximate. In the work Vasiliev [9], the author makes an attempt to show that with the help of certain transformations the sixth order refined theories can be presented as the modern form of the classical plate theory. Zhilin [10] points out that the Reissner theory is in line with the three-dimensional elasticity theory and the Kirchhoff theory should be considered as an asymptotic consequence of the Reissner theory. In the work Zhilin [11] author warns about possible negative consequences of the formal use of the classical plate theory in the Finite Difference Method (FDM), the Finite Element Method (FEM) and other computing systems if spatial structures have rectangular plates with free support on the framework. Actually, in the shear plate theory support reactions coincide with contour transverse forces Q_x and Q_y, which balance the pressure on the plate. It excludes any angular forces in the case of free contour support which takes place in the Kirchhoff theory.

Revision, refinement and generalization of the theory of Reissner-Mindlin-Timoshenko and dedicated work in recent years [12–19].

There is little information about numerical results of the bending problem of a rectangular plate with a clamped edge using shear theories due to the problem's complexity. Let us note the works [20–29].

A rigidly clamped uniformly-loaded plate was examined in the work of Rudiger [20]. The author used hyperbolic-trigonometric series. The series' ratios were found by the principle of virtual displacements. Numerical computations for two kinds of rectangular plates show that allowing for the transverse shear deformation significantly affects the plate bending (no computations were done for a square plate). The works [21, 22] is based on the Ambartsumyan [5] shear theory. To solve the problem, the author used trigonometric series with hyperbolic functions in a different coordinate. Indefinite coefficients are found from the problem's boundary conditions. The problem reduces to solving an infinite system of linear algebraic equations.

In the works [23–29] various modifications of FEM were used.

Xu [23, 24] used a triangular finite element. Values of bendings and bending moments in the center of a square plate with the relative thickness of 0.1 were obtained.

In the work by Zienkiewicz et al. [25], FEM with linear quadrilateral elements is used. Numerical results are obtained for a square plate with a clamped edge with under a uniform load for relative thicknesses 0.001, 0.01, and 0.1. The number of the elements increased from 4 to 1024.

In the work Weiming and Guangsong [26] "Rational FEM" is used for Reissner plates with various boundary conditions under a uniform load and a central force. The accuracy of computations with the number of elements up to 64 is studied.

Ayad et al. [27] used the hybrid-mixed variational FEM with triangular and quadrilateral elements which is based on the Hellinger-Reissner variational principle. There are numerical results, particularly the graphs of bendings in the center of a square plate for different relative plate thicknesses when dividing the plate into 144 elements.

The work Dhananjaya [28] presents a closed form solution for equilibrium and flexibility matrices of the Mindlin–Reissner plates using the Integrated Force Method (IFM) based on 4 node rectangular elements. The author obtained the numerical results for square clamped plates with the relative thicknesses of 0.01 and 0.2 as the graphs of bendings and moments in the center for different numbers of finite elements, but, unfortunately, the scale of images is small.

In the work Aghdam et al. [29], an approximate solution is obtained for the bending of a rectangular Reissner plate with clamped edges. Resolving equations are a system of three differential equations of the second order. The solution procedure is based on using the extended Kantorovich method (EKM) to transform resolving systems of equations into ordinary differential equations.

In [30] uses the method of Bergan-Wang for moderately thick plates (modified finite integral transform method – FIT method). The results of a clamped square plate are compared with the results of the classical plate theory, Reissner-Mindlin theory and the three dimensional theory of elasticity for different relative thickness of the plate.

The goal of this work is to obtain reliable numerical results on the stress-strain state of a rectangular plate with a clamped edge allowing for the transverse shear deformation within the Reissner theory, to compare with the classical theory and with works of other authors, to determine applicability limits of the classical theory.

Methods

The fundamental system of differential equations of the Reissner elastic plate (see [2, 4]) has the form:

$$\begin{aligned} &D\nabla^2\nabla^2 W = q - \frac{H^2}{10}\frac{2-\nu}{1-\nu}\nabla^2 q\ , \\ &\nabla^2\Psi - \frac{10}{H^2}\Psi = 0. \end{aligned} \tag{1}$$

where $D = EH^3/\ [12(1\text{-}\nu^2)]$ – cylindrical stiffness; E – Young's modulus; H – plate's thickness; ν – Poisson's ratio; ∇^2 – Laplace two-dimesional operator; $W(X, Y)$ – function of bending of the middle surface of the plate; X, Y – coordinates; $q(X, Y)$ – transverse load; $\Psi(X, Y)$ – stress function (edge potential).

For the uniform transverse load, directed at the negative side of oz axis, the system (1) in its dimensionless form will look as follows:

$$\begin{aligned} &\nabla^2\nabla^2 w(x,y) = -1, \\ &\psi(x,y) - \alpha\,\nabla^2\psi(x,y) = 0. \end{aligned} \tag{2}$$

where $w(x, y) = W/(qb^4/D)$ – dimensionless bending function; b – the width of the plate; $x = X/b$, $y = Y/b$- dimensionless coordinates; $\psi(x, y) = \Psi(X, Y)\ /qb^2$ – dimensionless stress function; $\alpha = h^2/10$ - shear factor; $h = H/b$ – dimensionless plate's thickness.

Boundary conditions of the rectangle plate with a clamped edge $x = \pm\gamma/2$, $y = \pm 1/2$ have the form:

$$w = 0\ , \qquad \varphi_x = 0\ , \qquad \varphi_y = 0 \tag{3}$$

where $\gamma = a/b$ – ratio of the plate's sides; a – length of the plate; φ_x, φ_y – the angles of rotation of sections:

$$\varphi_x = \frac{\partial}{\partial x}\left(w + \alpha_1 \nabla^2 w\right) - \alpha_1 \frac{\partial \psi}{\partial y}; \qquad \varphi_y = \frac{\partial}{\partial y}\left(w + \alpha_1 \nabla^2 w\right) + \alpha_1 \frac{\partial \psi}{\partial x}; \qquad \left(\alpha_1 = \frac{2\alpha}{1-\nu}\right).$$

The task is set to find bending functions w and stress functions ψ, satisfying fundamental Eq. (2) and the given conditions (3) on each edge.

To solve the problem, we use the system of functions:

$$w_0(x,y) = -\frac{1}{8}\left(x^2 - \frac{\gamma^2}{4}\right)\left(y^2 - \frac{1}{4}\right) \tag{4}$$

$$w_{1n}(x,y) = \sum_{k=1,3,...}^{\infty} (-1)^{k^*} \frac{A_{kn}}{\cosh \tilde{\lambda}_k}\left(x\sinh \lambda_k x - \frac{\gamma}{2}\tanh \tilde{\lambda}_k \cosh \lambda_k x\right)\cos \lambda_k y \tag{5}$$

$$w_{2n}(x,y) = \sum_{s=1,3,...}^{\infty} (-1)^{s^*} \frac{B_{sn}}{\cosh \tilde{\mu}_s}\left(y\sinh \mu_s y - \frac{1}{2}\tanh \tilde{\mu}_s \cosh \mu_s y\right)\cos \mu_s x \tag{6}$$

$$\psi_{1n}(x,y) = \sum_{k=1,3,...}^{\infty} (-1)^{k^*} C_{kn} \sinh \beta_k x \sin \lambda_k y \tag{7}$$

$$\psi_{2n}(x,y) = \sum_{s=1,3,...}^{\infty} (-1)^{s^*} D_{sn} \sinh \xi_s y \sin \mu_s x \tag{8}$$

where $w_0(x, y)$ is the initial bending function (null approximation); w_{1n}, w_{2n}, ψ_{1n}, ψ_{2n} are the correcting bending functions w and stress functions ψ; n is the number of the iteration; A_{kn}, B_{sn}, C_{kn}, D_{sn} are indefinite coefficients;

$$\lambda_k = k\pi, \quad \mu_s = \frac{s\pi}{\gamma}, \quad k^* = \frac{k+1}{2}, \quad s^* = \frac{s+1}{2}.$$

$$\tilde{\lambda}_k = \frac{\lambda_k \gamma}{2}, \quad \tilde{\mu}_s = \frac{\mu_s}{2}, \quad \beta_k = \sqrt{\lambda_k^2 + \frac{1}{\alpha}}, \quad \xi_s = \sqrt{\mu_s^2 + \frac{1}{\alpha}}.$$

The correcting bending functions are biharmonic and turn into zero on the plate's contour; the stress functions satisfy the second basic Eq. (2).

The initial function $w_0(x, y)$ is an isolated solution to the first Eq. (2). It equals to zero on the plate's contour but causes the contour to turn, i.e. creates the main discrepancies φ_x, φ_y in boundary conditions (4) which should be expanded into the Fourier series (on the edges $x = -\gamma/2$ *and* $y = -1/2$ they differ in signs):

$$\begin{gathered}
\varphi_{x0}\big|_{x=\frac{\gamma}{2}} = -\frac{\gamma}{8}\left(y^2 - \frac{1}{4} + 2\alpha_1\right) = \sum_{k=1,3....}^{\infty} (-1)^{k^*} a_{k0} \cos\lambda_k y, \\
\varphi_{y0}\big|_{x=\frac{\gamma}{2}} = -\frac{\alpha_1 y}{2} = \sum_{k=1,3,...}^{\infty} \left(-1\right)^{k^*} b_{k0} \sin\lambda_k y, \\
\varphi_{x0}\big|_{y=\frac{1}{2}} = -\frac{\alpha_1 x}{2} = \sum_{s=1,3...}^{\infty} \left(-1\right)^{s^*} u_{s0} \sin \mu_s x, \\
\varphi_{y0}\big|_{y=\frac{1}{2}} = -\frac{1}{8}\left(x^2 - \frac{\gamma^2}{4} + 2\alpha_1\right) = \sum_{s=1,3,...}^{\infty} \left(-1\right)^{s^*} g_{s0} \cos \mu_s x,
\end{gathered} \tag{9}$$

where a_{k0}, $bk0$, u_{s0}, g_{s0} – the coefficients of the decomposition.

The correcting functions during the infinite iteration process of their superposition must reduce these discrepancies to zero.

The idea of an infinite superposition of functions to elimination of the main deviations (residuals) from a private solution belongs to V.Z. Vasiliev [31].

The second discrepancy (9) (the first discrepancy will be allowed for in the next iteration to improve the series convergence) is eliminated by the first pair of correcting functions w_{11} and ψ_{11} with satisfying the conditions on the edges $x = \pm\gamma/2$ at the expense of coefficients A_{k1} and C_{k1}.

However, the functions themselves cause angular discrepancies on the edges $y = \pm 1/2$:

$$\varphi_{y11}\Big|_{y=\frac{1}{2}} = \sum_{k=1,3,...}^{\infty}\left[\frac{\lambda_k A_{k1}}{\cosh\tilde{\lambda}_k}\left(x\sinh\lambda_k x - \frac{\gamma}{2}\tanh\tilde{\lambda}_k\cosh\lambda_k x + 2\alpha_1\lambda_k\cosh\lambda_k x\right) - \alpha_1 C_{k1}\beta_k\cosh\beta_k x\right]. \quad (10)$$

They should be expanded into the Fourier series in $\cos\mu_s x$, we should invert the summation, plug expressions for the coefficients A_{k1}, C_{k1}, in them and put them together with the corresponding discrepancies $\varphi_{y0|y=1/2}$ from the initial polynomial (the fourth function (9)), i.e. transform into

$$\varphi^{*}_{y11}\Big|_{y=\frac{1}{2}} = \varphi_{y11}\Big|_{y=\frac{1}{2}} + \varphi_{y0}\Big|_{y=\frac{1}{2}} = \sum_{s=1,3,...}^{\infty}(-1)^{s^*}g^{*}_{s1}\cos\mu_s x. \quad (11)$$

where $g_{s1}{*} = g_{s0} + g_{s1}$ are the series' ratios.

Discrepancy (11) and the third discrepancy (9) are compensated by the second pair of correcting functions w_{21}, ψ_{21} at the expense of coefficients B_{s1} and D_{s1}.

Besides, functions w_{21} and ψ_{21} on the edges $x = \pm\gamma/2$ also create angular discrepancies:

$$\varphi_{x21}\Big|_{x=\frac{\gamma}{2}} = \sum_{s=1,3,...}^{\infty}\left[\frac{\mu_s B_{s1}}{\cosh\tilde{\mu}_s}\left(y\sinh\mu_s y - \frac{1}{2}\tanh\tilde{\mu}_s\cosh\mu_s y + 2\alpha_1\mu_s\cosh\mu_s y\right) + \alpha_1 D_{s1}\xi_s\cosh\xi_s y\right]. \quad (12)$$

which should be expanded into the Fourier series in $\cos\lambda_k y$ we should invert the summation, plug expressions for the coefficients B_{s1}, D_{s1} in them and put them together with the corresponding discrepancies $\varphi_{x0|x=\gamma/2}$ from the initial polynomial (the first function (9)), i.e. transform into

$$\left(\varphi_{x0} + \varphi_{x21}\right)_{x=\frac{\gamma}{2}} = -\sum_{k=1,3,...}^{\infty}(-1)^{k^*}a^{*}_{k1}\cos\lambda_k y;. \quad (13)$$

where $a^{*}_{k1} = a_{k0} + a_{k1}$.

Discrepancies (13) are compensated by the correcting pair of w12 and ψ 12 of the second iteration when satisfying the boundary conditions on the edges $x = \pm\gamma/2$. This gives the system of two equations to determine the coefficients A_{k2}, C_{k2}.

The discrepancies of this pair $\varphi_{y12|y=1/2}$ will have the form similar to (10, 11):

$$\varphi_{y12}\Big|_{y=\frac{1}{2}} = -\sum_{s=1,3,...}^{\infty}(-1)^{s^*}g_{s2}\cos\mu_s x. \quad (14)$$

Then series w_{22} and ψ_{22} are used to eliminate the discrepancies of this pair.

And then the process is repeated.

The convergence of the method

During the iteration process, discrepancies in boundary conditions should tend to zero, i.e. the iteration process should be convergent. Due to linearity of the problem, it is sufficient to prove, for example, that

$$\lim_{n\to\infty} A_{kn} = 0 \quad (k = 1,3,...;\ n = 1,2,...). \quad (15)$$

It is established that the coefficients A_k of two adjacent iterations are linked linearly. The dependence of A_{kn+1} on A_{kn} is a homogeneous infinite system of linear algebraic equations. This system should be regular [32]. Then, successive approximations will lead to a trivial solution from whatever initial values of the coefficients A_k, limited in total, we would start.

Since the discrepancy coefficients linearly depend on coefficients A_k, during the iteration process they will also tend to zero.

Analysis of the series convergence for bending moments and shearing forces

Moments M, and shearing forces Q according to [4] will have the following form:

$$M_x=-\left(\frac{\partial^2 w}{\partial x^2}+\nu\frac{\partial^2 w}{\partial y^2}+\alpha_2\frac{\partial^2}{\partial x^2}\nabla^2 w\right)+\alpha_2\frac{\partial^2\psi}{\partial x\partial y}+\alpha_3,$$

$$M_y=-\left(\frac{\partial^2 w}{\partial y^2}+\nu\frac{\partial^2 w}{\partial x^2}+\alpha_2\frac{\partial^2}{\partial y^2}\nabla^2 w\right)-\alpha_2\frac{\partial^2\psi}{\partial x\partial y}+\alpha_3,$$

$$M_{xy}=(1-\nu)\frac{\partial^2 w}{\partial x\partial y}+\alpha_2\frac{\partial^2}{\partial x\partial y}\nabla^2 w-\alpha\left(\frac{\partial^2\psi}{\partial y^2}-\frac{\partial^2\psi}{\partial x^2}\right).$$

$$Q_x=-\frac{\partial}{\partial x}\nabla^2 w+\frac{\partial\psi}{\partial y},\quad Q_y=-\frac{\partial}{\partial y}\nabla^2 w-\frac{\partial\psi}{\partial x}.$$

Here, the moments are referred to value qb2, shearing forces – to value qb; $\alpha_2 = 2\alpha$; $\alpha_3 = \nu\alpha/(1-\nu)$.

Let us show final expressions for bending moments M_x, torsion moments M_{xy} and shearing forces Q_x which were used for computing:

$$\begin{aligned}
M_x&=\frac{\alpha_1}{2}+\frac{1}{4}\left[y^2-\frac{1}{4}+\nu\left(x^2-\frac{\gamma^2}{4}\right)\right]\\
&-\sum_{k=1,3,...}^{\infty}(-1)^{k^*}\lambda_k\left\{[2\cosh\lambda_k x+4\alpha\lambda_k^2\left(\cosh\lambda_k x-\frac{\cosh\tilde{\lambda}_k}{\cosh\tilde{\beta}_k}\cosh\beta_k x\right)\right.\\
&\left.+(1-\nu)\left(\lambda_k x\sinh\lambda_k x-\tilde{\lambda}_k\tanh\tilde{\lambda}_k\cosh\lambda_k x\right)]\frac{A_{k\Sigma}}{\cosh\tilde{\lambda}_k}+\frac{4\alpha}{\lambda_k^2}\frac{\cosh\beta_k x}{\cosh\tilde{\beta}_k}\right\}\cos\lambda_k y\\
&+\sum_{s=1,3,...}^{\infty}(-1)^{s^*}\mu_s\left\{[-2\nu\cosh\mu_s y+4\alpha\mu_s^2\left(\cosh\mu_s y-\frac{\cosh\tilde{\mu}_s}{\cosh\tilde{\xi}_s}\cosh\xi_s y\right)\right.\\
&\left.+(1-\nu)\left(\mu_s y\sinh\mu_s y-\tilde{\mu}_s\tanh\tilde{\mu}_s\cosh\mu_s y\right)]\frac{B_{s\Sigma}}{\cosh\tilde{\mu}_s}+\frac{4\alpha}{\gamma\mu_s^2}\frac{\cosh\xi_s y}{\cosh\tilde{\xi}_s}\right\}\cos\mu_s x,
\end{aligned}\tag{16}$$

$$\begin{aligned}
M_{xy}&=-\frac{1-\nu}{2}xy-\sum_{k=1,3,...}^{\infty}(-1)^{k^*}\left\{\left(\left[(1-\nu)\left(1-\tilde{\lambda}_k\tanh\tilde{\lambda}_k\right)+4\alpha\lambda_k^2\right]\sinh\lambda_k x+(1-\nu)\lambda_k x\cosh\lambda_k x\right.\right.\\
&\left.\left.-2\alpha\frac{\lambda_k\cosh\tilde{\lambda}_k}{\beta_k\cosh\tilde{\beta}_k}\left(\lambda_k^2+\beta_k^2\right)\sinh\beta_k x\right)\frac{\lambda_k A_{k\Sigma}}{\cosh\tilde{\lambda}_k}+2\alpha\frac{\lambda_k^2+\beta_k^2}{\lambda_k^2\beta_k\cosh\tilde{\beta}_k}\sinh\beta_k x\right\}\sin\lambda_k y\\
&-\sum_{s=1,3,...}^{\infty}(-1)^{s^*}\left\{\left(\left[(1-\nu)(1-\tilde{\mu}_s\tanh\tilde{\mu}_s)+4\alpha\mu_s^2\right]\sinh\mu_s y+(1-\nu)\mu_s y\cosh\mu_s y\right.\right.\\
&\left.\left.-2\alpha\frac{\mu_s\cosh\tilde{\mu}_s}{\xi_s\cosh\tilde{\xi}_s}\left(\mu_s^2+\xi_s^2\right)\sinh\xi_s y\right)\frac{\mu_s B_{s\Sigma}}{\cosh\tilde{\mu}_s}+\frac{2\alpha}{\gamma}\frac{\mu_s^2+\xi_s^2}{\mu_s^2\xi_s\cosh\tilde{\xi}_s}\sinh\xi_s y\right\}\sin\mu_s x,
\end{aligned}\tag{17}$$

$$\begin{aligned}
Q_x&=\frac{x}{2}-2\sum_{k=1,3,...}^{\infty}(-1)^{k^*}\left[\lambda_k^2\left(\sinh\lambda_k x-\frac{\lambda_k}{\beta_k}\frac{\cosh\tilde{\lambda}_k}{\cosh\tilde{\beta}_k}\sinh\beta_k x\right)\frac{A_{k\Sigma}}{\cosh\tilde{\lambda}_k}+\frac{1}{\lambda_k\beta_k}\frac{\sinh\beta_k x}{\cosh\tilde{\beta}_k}\right]\cos\lambda_k y\\
&+2\sum_{s=1,3,...}^{\infty}(-1)^{s^*}\left[\mu_s^2\left(\cosh\mu_s y-\frac{\cosh\tilde{\mu}_s}{\cosh\tilde{\xi}_s}\cosh\xi_s y\right)\frac{B_{s\Sigma}}{\cosh\tilde{\mu}_s}+\frac{1}{\gamma}\frac{1}{\mu_s^2}\frac{\cosh\xi_s y}{\cosh\tilde{\xi}_s}\right]\sin\mu_s x,
\end{aligned}\tag{18}$$

where $A_{k\Sigma}=A_{k1}+A_{k2}+...+A_{kn}$; ...; $B_{s\Sigma}=B_{s1}+B_{s2}+...+B_{sn}$ are overall coefficients in all iterations; $\tilde{\beta}_k=\beta_k\gamma/2$, $\tilde{\xi}_s=\xi_s/2$.

Let us study the convergence of functional series that occur in formulae (16), (18).

The fastest to converge are the series of bending moments (16) in the center of the plate, where general terms have the order $O\left(1/\cosh\tilde{\lambda}_k\right)$ or $O\left(1/\cosh\tilde{\mu}_s\right)$, and the slowest – in the middle of clamped edges, where expressions for bending moments will take the form:

$$M_x\left(\frac{\gamma}{2};0\right)=\frac{2-\nu}{2}\alpha_1-\frac{1}{16}-2\sum_{k=1,3,...}^{\infty}(-1)^{k^*}\lambda_k A_{k\Sigma},$$
$$M_x\left(0;\pm\frac{1}{2}\right)=\nu\left(\frac{\alpha_1}{2}-\frac{\gamma^2}{16}\right)-2\nu\sum_{s=1,3,...}^{\infty}(-1)^{s^*}\mu_s B_{s\Sigma}. \tag{19}$$

The coefficients A_{kn} (5) and B_{sn} (6) have similar estimations $A_{kn}=O(1/k^2)$, $B_{sn}=O(1/s^2)$, and the corresponding series that occurs in (19), starting from some number, converges not worse than alternating series $\sum_{m=1,3,...}^{\infty}(-1)^{m^*}/m$. Although such a series converges slowly, it is good for computations because pursuing the Leibniz theory, it is possible to estimate the inaccuracy of computing its sum (from the moment when the series terms start to decay).

Let us note that in angular points of the plate

$$M_x\left(\pm\frac{\gamma}{2};\pm\frac{1}{2}\right)=\frac{\alpha_1}{2}=\frac{h^2}{10(1-\nu)}, \tag{20}$$

while for the Kirchhoff plate these moments equal to zero.

The most slowly the series of shearing forces converges on the side $x=\pm\gamma/2$:

$$Q_x\left(\frac{\gamma}{2};y\right)=\frac{\gamma}{4}-2\sum_{k=1,3,...}^{\infty}(-1)^{k^*}\left[\lambda_k^2\left(\tanh\tilde{\lambda}_k-\frac{\lambda_k}{\beta_k}\tanh\tilde{\beta}_k\right)A_{k\Sigma}+\frac{\tanh\tilde{\beta}_k}{\lambda_k\beta_k}\right]\cos\lambda_k y$$
$$-2\sum_{s=1,3,...}^{\infty}\left[\mu_s^2\left(\frac{\cosh\mu_s y}{\cosh\tilde{\mu}_s}-\frac{\cosh\xi_s y}{\cosh\tilde{\xi}_s}\right)B_{s\Sigma}+\frac{1}{\gamma\mu_s^2}\frac{\cosh\xi_s y}{\cosh\tilde{\xi}_s}\right], \tag{21}$$

It is proved that the series for the shear forces converge no worse than numerical series $\sum_{m=1,3,...}^{\infty}1/m^2$.

Similar conclusions are also valid for bending moments M_y, torsion moments M_{xy} and shearing forces Q_y.

Thus, a series of moments and shear forces are quite suitable for computer calculations.

Results and Discussion

Numerical results were obtained for square plates with relative thicknesses h = 0.05, 0.1, 0.2, 0.3 and Poisson's ratio ν = 0.3. Up to 150 terms were held in the series depending on the speed of convergence of a particular series. The process converged in a geometrical progression with the ratio ≤ 1/3 for all considered examples. The discrepancy coefficients were printed out in every iteration. The calculation stopped after ten iterations, when all discrepancies were nearly equal to zero; in the process, the overall coefficients $A_{k\Sigma}$ and $B_{s\Sigma}$ were calculated (due to linearity of the problem), using which the bendings, bending moments M_x, and shearing forces Q_x in different points of plates were obtained. Near the contour, computational points clustered in order to refine the influence of ends.

In Table 1 the first five coefficients $A_{k\Sigma}$ (= $B_{s\Sigma}$) are given, as well as their values with k = 299 (150 terms of the series) for different relative thicknesses of a square plate.

The table shows that the highest are the first coefficients; the second are lower in an absolute value approximately by two orders, then the coefficients decay, keeping the negative sign.

Tables 2–5 show values of relative bendings; Tables 6–9 show values of bending moments M_x; Tables 10–13 show values of shearing forces Q_x for square Reissner plates with the relative thicknesses of 0.05, 0.1, 0.2, 0.3.

Table 1. Values of coefficients $A_{k\Sigma}$ for the bending functions of a square plate (Reissner - CCCC, q = const)

h	k					
	1	3	5	7	9	299
0.05	1.774×10^{-2}	-1.063×10^{-4}	-3.966×10^{-5}	-1.173×10^{-5}	-3.971×10^{-6}	-1.013×10^{-9}
0.1	1.726×10^{-2}	-5.582×10^{-5}	-1.923×10^{-5}	-4.715×10^{-6}	-1.564×10^{-6}	-4.941×10^{-9}
0.2	1.543×10^{-2}	-5.191×10^{-5}	-3.400×10^{-5}	-2.000×10^{-5}	-1.356×10^{-5}	-2.229×10^{-8}
0.3	1.248×10^{-2}	-2.531×10^{-4}	-1.231×10^{-4}	-6.974×10^{-5}	-4.492×10^{-5}	-5.282×10^{-8}

Table 2. Values of bendings referred to value qb^4 / D $\times10^{-5}$ of a square plate h = 0.05 (Reissner - CCCC, q = const)

y	x									
	0	0.1	0.2	0.3	0.4	0.42	0.44	0.46	0.48	0.5
0	-132.70	-123.80	-98.33	-60.94	-21.70	-15.11	-9.40	-4.79	-1.56	0
0.1	-123.80	-115.50	-91.84	-57.01	-20.35	-14.19	-8.83	-4.51	-1.47	0
0.2	-98.33	-91.84	-73.23	-45.68	-16.43	-11.48	-7.17	-3.67	-1.21	0
0.3	-60.94	-57.01	-45.67	-28.70	-10.42	-7.30	-4.57	-2.35	-0.78	0
0.4	-21.70	-20.35	-16.43	-10.42	-3.77	-2.62	-1.62	-0.82	-0.26	0
0.42	-15.11	-14.19	-11.48	-7.30	-2.62	-1.82	-1.11	-0.55	-0.17	0
0.44	-9.40	-8.83	-7.17	-4.57	-1.62	-1.11	-0.67	-0.32	-0.09	0
0.46	-4.79	-4.51	-3.67	-2.35	-0.82	-0.55	-0.32	-0.14	-0.03	0
0.48	-1.56	-1.47	-1.21	-0.78	-0.26	-0.17	-0.09	-0.03	-0.001	0
0.5	0	0	0	0	0	0	0	0	0	0

Table 3. Values of bendings referred to value qb^4 / D $\times10^{-5}$ of a square plate h = 0.1 (Reissner - CCCC, q = const)

y	x									
	0	0.1	0.2	0.3	0.4	0.42	0.44	0.46	0.48	0.5
0	-150.50	-140.90	-113.60	-72.98	-28.88	-21.07	-14.04	-8.01	-3.23	0
0.1	-140.90	-132.00	-106.50	-68.56	-27.21	-19.88	-13.26	-7.57	-3.06	0
0.2	-113.60	-106.50	-86.19	-55.75	-22.32	-16.35	-10.94	-6.28	-2.55	0
0.3	-72.98	-68.56	-55.75	-36.36	-14.73	-10.83	-7.28	-4.20	-1.72	0
0.4	-28.88	-27.21	-22.32	-14.74	-6.03	-4.44	-2.98	-1.72	-0.70	0
0.42	-21.08	-19.88	-16.35	-10.83	-4.44	-3.26	-2.19	-1.26	-0.51	0
0.44	-14.04	-13.26	-10.94	-7.28	-2.98	-2.19	-1.46	-0.83	-0.34	0
0.46	-8.01	-7.57	-6.28	-4.20	-1.72	-1.26	-0.83	-0.47	-0.19	0
0.48	-3.23	-3.06	-2.55	-1.72	-0.70	-0.51	-0.34	-0.19	-0.07	0
0.5	0	0	0	0	0	0	0	0	0	0

Table 4. Values of bendings referred to value qb^4 / D ×10^{-5} of a square plate h = 0.2 (Reissner - CCCC, q = const)

y	*x*									
	0	0.1	0.2	0.3	0.4	0.42	0.44	0.46	0.48	0.5
0	-217.20	-205.40	-171.00	-118.20	-55.60	-43.20	-31.22	-19.87	-9.38	0
0.1	-205.40	-194.30	-161.90	-112.10	-52.91	-41.14	-29.77	-18.97	-8.96	0
0.2	-171.00	-161.90	-135.40	-94.29	-44.94	-35.04	-25.43	-16.26	-7.72	0
0.3	-118.20	-112.10	-94.29	-66.38	-32.24	-25.27	-18.45	-11.88	-5.68	0
0.4	-55.60	-52.91	-44.94	-32.24	-16.22	-12.85	-9.50	-6.21	-3.02	0
0.42	-43.20	-41.14	-35.04	-25.27	-12.85	-10.22	-7.59	-4.99	-2.45	0
0.44	-31.22	-29.77	-25.43	-18.45	-9.50	-7.59	-5.68	-3.76	-1.87	0
0.46	-19.87	-18.97	-16.26	-11.88	-6.21	-4.99	-3.76	-2.53	-1.28	0
0.48	-9.38	-8.96	-0.77	-5.68	-3.02	-2.45	-1.87	-1.28	-0.67	0
0.5	0	0	0	0	0	0	0	0	0	0

Table 5. Values of bendings referred to value qb^4 / D ×10^{-5} of a square plate h = 0.3 (Reissner - CCCC, q = const)

y	x									
	0	0.1	0.2	0.3	0.4	0.42	0.44	0.46	0.48	0.5
0	-324.60	-309.10	-263.40	-190.70	-98.19	-78.38	-58.47	-38.64	-19.07	0
0.1	-309.10	-294.40	-251.20	-182.20	-94.11	-75.19	-56.14	-37.13	-18.34	0
0.2	-263.40	-251.20	-215.00	-157.00	-81.92	-65.62	-49.13	-32.59	-16.16	0
0.3	-190.70	-182.20	-157.00	-116.00	-61.80	-49.78	-37.50	-25.04	-12.51	0
0.4	-98.19	-94.11	-81.92	-61.80	-34.29	-27.96	-21.36	-14.50	-7.38	0
0.42	-78.38	-75.19	-65.62	-49.78	-27.96	-22.90	-17.59	-12.02	-6.16	0
0.44	-58.47	-56.14	-49.13	-37.50	-21.36	-17.59	-13.60	-9.38	-4.87	0
0.46	-38.63	-37.13	-32.59	-25.04	-14.50	-12.02	-9.38	-6.55	-3.46	0
0.48	-19.07	-18.34	-16.16	-12.51	-7.38	-6.16	-4.87	-3.46	-1.90	0
0.5	0	0	0	0	0	0	0	0	0	0

Table 6. Values of bending moments M_x referred to value $qb^2 \times 10^{-6}$ of a square plate h = 0.05 (Reissner -CCCC, q = const)

y	x									
	0	0.1	0.2	0.3	0.4	0.42	0.44	0.46	0.48	0.5
0	-23110	-21450	-15860	-4413	16220	21860	28090	34980	42520	50670
0.1	-21460	-19950	-14830	-4244	15040	20340	26220	32720	39870	47610
0.2	-16570	-15480	-11690	-3555	11790	16090	20890	26230	32160	38640
0.3	-8553	-8087	-6281	-1850	7450	10150	13200	16630	20470	24730
0.4	2189	1948	1463	1554	3772	4614	5593	6693	7905	9298
0.42	4603	4222	3282	2498	3311	3802	4400	5080	5821	6691
0.44	7088	6570	5183	3542	2984	3142	3389	3696	4033	4465
0.46	9643	8991	7167	4688	2800	2645	2574	2563	2589	2717
0.48	12290	11510	9251	5945	2745	2290	1927	1646	1445	1466
0.5	15120	14210	11520	7342	2713	1944	1270	720	355	357

Table 7. Values of bending moments M_x referred to value $qb^2 \times 10^{-6}$ of a square plate h = 0.1 (Reissner -CCCC, q = const)

y	x									
	0	0.1	0.2	0.3	0.4	0.42	0.44	0.46	0.48	0.5
0	-23630	-21920	-16210	-4677	15810	21340	27420	34060	41260	48940
0.1	-22040	-20470	-15200	-4482	14730	19930	25670	31960	38790	46090
0.2	-17300	-16130	-12130	-3732	11760	16030	20760	25970	31670	37810
0.3	-9528	-8962	-6858	-1970	7824	10610	13740	17230	21100	25370
0.4	952	822	704	1454	4523	5566	6788	8212	9870	11830
0.42	3343	3072	2500	2400	4104	4800	5650	6681	7942	9514
0.44	5840	5428	4398	3444	3787	4140	4622	5274	6145	7307
0.46	8469	7913	6422	4600	3567	3573	3687	3956	4498	5432
0.48	11280	10580	8611	5876	3417	3067	2806	2635	2729	3348
0.5	14360	13540	11020	7338	3196	2620	1806	1456	472	1429

Table 8. Values of bending moments M_x referred to value $qb^2 \times 10^{-6}$ of a square plate h = 0.2 (Reissner -CCCC, q = const)

y	x									
	0	0.1	0.2	0.3	0.4	0.42	0.44	0.46	0.48	0.5
0	-25290	-23450	-17440	-5692	14220	19410	25050	31120	37630	44580
0.1	-23830	-22120	-16500	-5461	13380	18320	23680	29480	35700	42330
0.2	-19470	-18120	-13630	-4635	11080	15260	19840	24810	30190	35910
0.3	-12250	-11440	-8666	-2823	8012	11010	14330	18000	22030	26380
0.4	-2112	-1969	-1306	598	5157	6620	8348	10380	12750	15520
0.42	321	318	516	1554	4679	5780	7138	8809	10840	13400
0.44	2925	2770	2487	2627	4242	4946	5887	7155	8833	10880
0.46	5732	5418	4630	3834	3867	4127	4573	5333	6581	8066
0.48	8787	8305	6982	5196	3587	3366	3240	3296	3800	5341
0.5	12220	11510	9532	6654	3494	2992	2037	878	322	5714

Table 9. Values of bending moments M_x referred to value $qb^2 \times 10^{-6}$ of a square plate h = 0.3 (Reissner -CCCC, q = const)

y	x									
	0	0.1	0.2	0.3	0.4	0.42	0.44	0.46	0.48	0.5
0	-27650	-25710	-19460	-7598	11770	16720	22050	27780	33890	40490
0.1	-26300	-24480	-18580	-7348	11120	15860	20980	26490	32380	38680
0.2	-22230	-20750	-15890	-6489	9337	13460	17950	22800	28020	33500
0.3	-15340	-14370	-11160	-4692	6847	9979	13430	17230	21360	25720
0.4	-5251	-4951	-3860	-1340	4120	5845	7875	10250	12980	16170
0.42	-2763	-2613	-2000	-380	3566	4915	6572	8595	11040	14270
0.44	-82	-88	31	715	3028	3942	5148	6751	8832	11260
0.46	2818	2649	2252	1970	2552	2958	3594	4616	6205	7570
0.48	5965	5628	4696	3416	2215	2050	2007	2187	2871	4716
0.5	9552	8928	7253	4879	2245	1964	613	-1191	-1472	12860

Table 10. Values of shearing forces Q_x referred to value qb of a square plate h = 0.05 (Reissner -CCCC, q = const)

y	x									
	0	0.1	0.2	0.3	0.4	0.42	0.44	0.46	0.48	0.5
0	0	0.052	0.112	0.191	0.297	0.322	0.349	0.376	0.404	0.429
0.1	0	0.047	0.103	0.177	0.279	0.303	0.329	0.356	0.384	0.408
0.2	0	0.033	0.076	0.136	0.224	0.246	0.269	0.294	0.320	0.343
0.3	0	0.011	0.030	0.068	0.132	0.149	0.166	0.186	0.206	0.227
0.4	0	-0.021	-0.034	-0.027	0.010	0.020	0.031	0.041	0.052	0.067
0.42	0	-0.028	-0.048	-0.049	-0.016	-0.007	0.003	0.013	0.022	0.036
0.44	0	-0.035	-0.062	-0.070	-0.042	-0.032	-0.022	-0.012	-0.003	0.010
0.46	0	-0.039	-0.072	-0.087	-0.063	-0.053	-0.042	-0.031	-0.021	-0.008
0.48	0	-0.035	-0.066	-0.083	-0.066	-0.057	-0.047	-0.036	-0.027	-0.013
0.5	0	0	0	0	0	0	0	0	0	0

Table 11. Values of shearing forces Q_x referred to value qb of a square plate h = 0.1 (Reissner - CCCC, q = const)

y	x									
	0	0.1	0.2	0.3	0.4	0.42	0.44	0.46	0.48	0.5
0	0	0.051	0.112	0.189	0.292	0.316	0.340	0.366	0.390	0.412
0.1	0	0.047	0.103	0.176	0.274	0.298	0.322	0.346	0.370	0.392
0.2	0	0.034	0.077	0.137	0.222	0.243	0.265	0.287	0.309	0.331
0.3	0	0.013	0.034	0.072	0.136	0.152	0.169	0.187	0.207	0.226
0.4	0	-0.016	-0.023	-0.012	0.024	0.035	0.046	0.059	0.074	0.092
0.42	0	-0.021	-0.033	-0.028	0.002	0.012	0.022	0.035	0.049	0.066
0.44	0	-0.024	-0.041	-0.041	-0.016	-0.008	0.001	0.012	0.025	0.043
0.46	0	-0.024	-0.043	-0.047	-0.029	-0.022	-0.014	-0.005	0.006	0.023
0.48	0	-0.018	-0.033	-0.038	-0.027	-0.023	-0.018	-0.013	-0.005	0.009
0.5	0	0	0	0	0	0	0	0	0	0

Table 12. Values of shearing forces Q_x referred to value qb of a square plate h = 0.2 (Reissner - CCCC, q = const)

y	x									
	0	0.1	0.2	0.3	0.4	0.42	0.44	0.46	0.48	0.5
0	0	0.051	0.110	0.184	0.277	0.298	0.319	0.340	0.362	0.382
0.1	0	0.047	0.103	0.172	0.262	0.282	0.303	0.324	0.345	0.366
0.2	0	0.036	0.080	0.139	0.218	0.237	0.256	0.276	0.296	0.316
0.3	0	0.018	0.044	0.084	0.146	0.162	0.179	0.197	0.215	0.235
0.4	0	-0.002	0.003	0.019	0.055	0.065	0.078	0.092	0.109	0.128
0.42	0	-0.004	-0.004	0.008	0.037	0.046	0.057	0.070	0.086	0.105
0.44	0	-0.006	-0.008	-0.001	0.021	0.028	0.037	0.048	0.063	0.081
0.46	0	-0.007	-0.010	-0.007	0.008	0.013	0.019	0.028	0.040	0.057
0.48	0	-0.005	-0.008	-0.007	0.000	0.003	0.006	0.010	0.018	0.032
0.5	0	0	0	0	0	0	0	0	0	0

Table 13. Values of shearing forces Q_x referred to value qb of a square plate h = 0.3 (Reissner - CCCC, q = const)

y	x									
	0	0.1	0.2	0.3	0.4	0.42	0.44	0.46	0.48	0.5
0	0	0.051	0.109	0.179	0.266	0.285	0.304	0.324	0.344	0.365
0.1	0	0.048	0.102	0.169	0.253	0.272	0.291	0.311	0.331	0.351
0.2	0	0.038	0.082	0.140	0.216	0.234	0.252	0.271	0.290	0.310
0.3	0	0.023	0.052	0.093	0.154	0.170	0.186	0.204	0.222	0.242
0.4	0	0.006	0.017	0.036	0.073	0.083	0.096	0.110	0.127	0.146
0.42	0	0.004	0.011	0.026	0.055	0.064	0.075	0.089	0.104	0.123
0.44	0	0.002	0.006	0.016	0.038	0.046	0.055	0.066	0.080	0.099
0.46	0	0.000	0.002	0.008	0.023	0.028	0.034	0.043	0.055	0.072
0.48	0	0.000	0.000	0.003	0.010	0.012	0.015	0.020	0.027	0.042
0.5	0	0	0	0	0	0	0	0	0	0

Hereinafter CCCC -plate is clamped on all four edges.

Figure 1 illustrates bending lines of square Reissner plates under a uniform load at the section $y = 0$. Curve 1(the dotted line) represents the Kirchhoff plate, the following numbers are given to the Reissner plates with relative thickness h = 0.05, 0.1, 0.2, 0.3. Figures 2, 3 illustrate curves of bending moments M_x for these plates at the clamped section $x = \pm \gamma/2$, and Figures 4, 5 – on the adjacent side $y = \pm 1/2$. The curves numeration is similar to Figure 1.

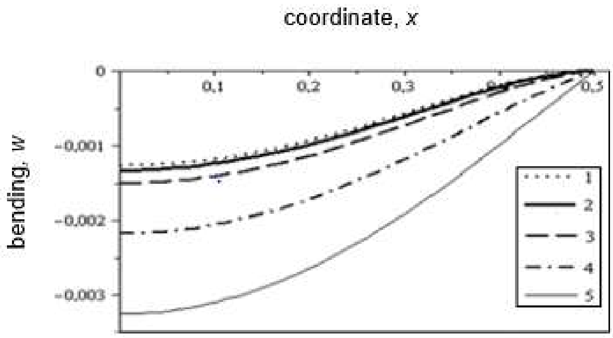

Figure 1. Lines of relative bendings of square plates (Reissner -CCCC, q = const) at the section y = 0

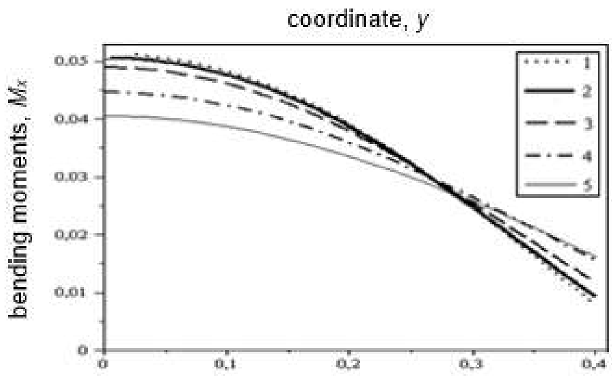

Figure 2. Curves of bending moments M_x of square plates (Reissner -CCCC, q = const) at the section $x = \pm\gamma/2$

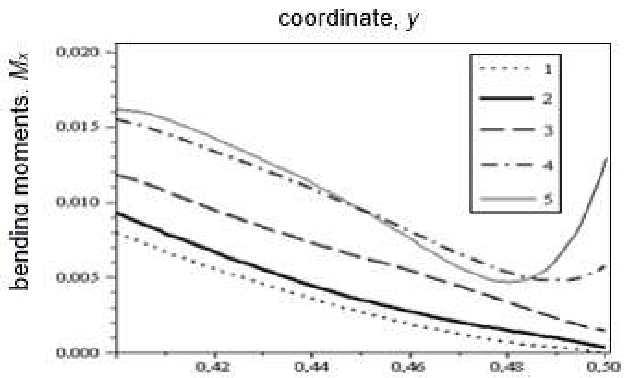

Figure 3. Magnified fragment of the curve of bending moments M_x of square plates (Reissner -CCCC, q = const) at the section $x = \pm\gamma/2$ near the plate's angle

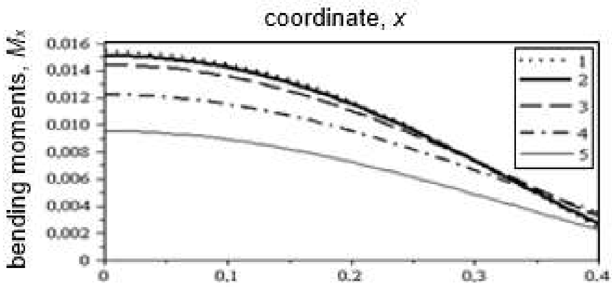

Figure 4. Curves of bending moments M_x of square plates (Reissner -CCCC, q = const) at the section $y = \pm 1/2$

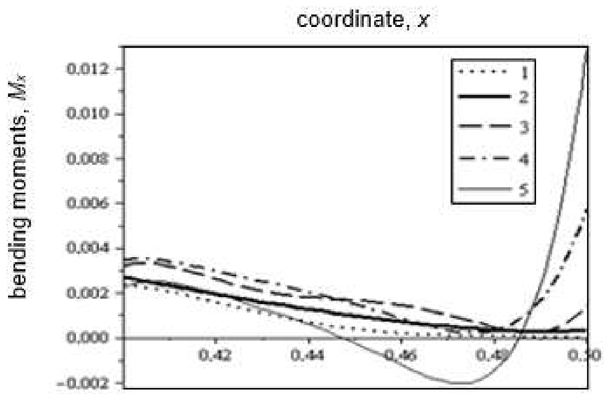

Figure 5. Magnified fragment of the curve of bending moments M_x of square plates (Reissner -CCCC, q = const) at the section $y = \pm 1/2$ near the plate's angle

The computations and graphs show that with small relative thicknesses $h \leq 1/20$, the results for the Kirchhoff and Reissner plates are almost equal. With the increase in the relative thickness, relative bendings also increase. Absolute bendings, of course, decrease, because they are obtained by multiplying relative bendings with the expression $qb^4/D = 12(1\text{-}\nu^2)\, qb/(Eh^3)$. If the bending in the center for the square Kirchhoff plate equals to 0.00126 [4], for the Reissner plates with thickness h = 0.05, 0.1, 0.2, 0.3 it amounts to 0.001327, 0.001505, 0.002172, 0.003246 respectively.

Thus, the Kirchhoff plate can be considered as a limit behavior of the Reissner plate, when $h \to 0$.

Bending moments in the middle of clamped edges decrease when h increases, but they rise when closer to angles of the plate. In angular points the bending moments different from zero and increase in a proportion to the square of relative thickness (see (17)). This is the fundamental difference from the Kirchhoff plate.

In the center of the plate, bending moments slightly increase in an absolute value when h increases; shearing forces change moderately.

The Shirakawa work [21] presents calculated correlations w/w_{cl} of the plate's bendings within the shear theory to the bendings within the classical theory for central points of the median z_0/h = 0 and top z_0/h = 0.5 surfaces. For a square plate with relative thicknesses h/a = 0.1, 0.2, 0.3 these values amounted to ≈ 1.25, 1.85, 2.95 and 1.2, 1.7, 2.6 respectively. In this paper, average values of thickness amounted to 1.2, 1.7, 2.6, i.e. were equal to the corresponding values [21] on the plate's surface.

In [22] shows diagrams of shear forces on the contour of the uniformly loaded clamped square plates with the relative thickness of 0.001, 0.04, 0.1 and 0.3. These results practically coincide with those obtained in the present work.

In the works of X_u [23, 24], for a square plate with the relative thickness of 0.1 the bending in the center amounted to 0.001499 and the bending moment amounted to 0.0231. In the work [25] of Zienkiewicz *et al*. 1993 with the grid of 1024 elements these values amounted 0.00150442 and 0.023195 respectively, opposing to 0.0015050 and 0.023630 in our work. It indicates a good agreement of the results.

In the work [26] by Weiming and Guangsong, the bending in the center of a square plate with the relative thickness h/a = 0.3 amounted to 0.0028997 and the bending moment amounted to 0.023538, while in this work – to 0.0032460 and 0.027650 respectively. The values in the aforementioned work were obtained using FEM with the grid of 8×8 elements; however, they poorly correlate with our results.

In the work of Ayad et al. [27], the maximum bending for a square clamped plate with the relative thickness of 0.1 amounted to ≈ 0.001575 (according to the graph).

The work of Dhananjaya [28] provides numerical results for square plates with the relative thicknesses of 0.01 and 0.2, represented as graphs of bendings and moments in the center depending on the number of finite elements. The scale of the images does not allow making a proper comparison, although the proximity of the results is obvious.

In the article [30] for a square plate with the relative thickness of 0.1 the bending in the center amounted to 0.0013636 (method FIT), 0.0015040 (FEM, theory of Reissner - Mindlin), 0.0014918 (FEM, 3D solution). The last two values are in good agreement with the value 0.0015050 obtained in the present work.

Conclusions

1. In the present work the iterative process of superposition of hyperbolic-trigonometric series to solve the problem of bending rectangular Reissner plate clamped along the contour as a result of the action of a uniform load is constructed and its convergence to the exact solution of the problem is proved.

2. Increasing the number of members in the ranks and the number of iterations, we can obtain the numerical solution with high accuracy having used a simple algorithm.

3. The convergence of the series and their suitability for computations of bending moments and shear forces an investigated.

4. Numerous examples of calculating deflections, bending moments and shear forces for square plates with different relative thickness are given.

5. It is shown that in case of small relative thicknesses theories of Reissner and Kirchhoff produced the same results.

6. We also analyzed the differences of the above theories when changing the relative thickness.

Acknowledgement

The authors express their gratitude to the government for financial support of this work.

The authors would like to gratefully acknowledge the unknown reviewers for their review and helpful comments.

References

1. Timoshenko S.P. On the Correction for Shear of the Differential Equation for Transverse Vibration of Prismatic Bars. *Philosophical Magazine*. 1921. No. 245(41). Series 6. Pp. 744–746.
2. Reissner E. The effect of transverse shear deformation on the bending of elastic plates. *Journal of Applied Mechanics*. 1945. No. 1(12). Pp. 69–77.
3. Mindlin R.D. Influence of rotatory inertia and shear on flexural motions of isotropic elastic plates. *Journal of Applied Mechanics.* 1951. No. 1(18). Pp. 31–38.
4. Timoshenko S., Woinowsky-Krieger S. *Theory of Plates and Shells.* McGraw-Hill Book Company. New York, Toronto, London.1959. 595 p.
5. Ambartsumyan S.A. *Theory of Anisotropic Plates.* Technomic Publishing Co. New York, 1970. 255 p.
6. Goldenveizer A.L., Kaplunov J.D., EV Nolde E.V. Asymptotic analysis and refinement of Timoshenko-Reisner-type theories of plates and shells. *Mechanics of Solids. (Izvestiya AN SSSR, Mekhanika Tverdogo Tela)* .1990. No. 6(25). Pp. 126–139.
7. Goldenveizer A.L, Kaplunov J.D. and Nolde E.V. On Timoshenko-Reissner type theories of plates and shells, *International Journal of Solids and Structures.* 1993. No. 5(30). Pp. 675–694.
8. Vasiliev V.V. An asymptotic method of justification of the plate theory. *Mechanics of Solids. (Izvestiya AN SSSR, Mekhanika Tverdogo Tela)*. 1997. No. 3. Pp. 150–155.
9. Vasiliev V.V. Modern conceptions of plate theory. *Composite Structures*. 2000. No. 1(48). Pp. 39–48.
10. Zhilin P.A. The view on Poisson`s and Kirchhoff`s theories of plates in terms of modern theory of plates. 1992. *Mechanics of Solids (Izvestia RAN, Mechanika Tverdogo Tela).* No. 3. Pp. 48–64.
11. Zhilin P.A. On the classical theory of plates and the Kelvin-Teit transformation. *Mechanics of Solids. (Izvestia RAN, Mechanika Tverdogo Tela).* 1995. No. 4. Pp. 133–140.
12. Shimpi R.P., Patel H.G., Arya H. New first order shear deformation plate theories. *Journal of Applied Mechanics.* 2007. No. 74. Pp. 523–533.
13. Vijayakumar K. A relook at Reissner's theory of plates in bending. *Archive of Applied Mechanics*. 2011. No. 11(81). Pp. 1717–1724.
14. Tovstik P.E., Tovstik T.P. A thin-plate bending equation of second-order accuracy. *Doklady Physics*. 2014. No. 8(59). Pp. 389–392.
15. Martínez Valle J.M., Martínez-Jiménez P. Modified Bolle - Reissner Theory of Plates Including Transverse Shear Deformations. *Latin American Journal of Solids and Structures*. 2015. No. 2(12). Pp. 295–316.
16. Nareen K., Shimpi R.P. Refined hyperbolic shear deformation plate theory. *Archive Proceedings of the Institution of Mechanical Engineers Part C Journal of Mechanical Engineering Science.* 2015. Vol. 203–210. Pp. 1989–1996
17. Senjanović I., Vladimir N., Tomić M. On new first-order shear deformation plate theories. *Mechanics Research Communications.* 2016. Vol. 73. Pp. 31–38.
18. Huu-Tai Thai, Trung-Kien Nguyen, Thuc P.Vo, Tuan Ngo. A new simple shear deformation plate theory. *Composite Structures.* 2017. Vol. 171. Pp. 277–285.

Литература

1. Timoshenko S.P. On the correction for shear of the differential equation for transverse vibration of prismatic bars // Philosophical Magazine. 1921. № 245(41). Series 6. Pp. 744–746.
2. Reissner E. The effect of transverse shear deformation on the bending of elastic plates // Journal of Applied Mechanics. 1945. № 1(12). Pp. 69–77.
3. Mindlin R.D. Influence of rotatory inertia and shear on flexural motions of isotropic elastic plates // Journal of Applied Mechanics. 1951. № 1(18). Pp. 31–38.
4. Timoshenko S., Woinowsky-Krieger S. Theory of Plates and Shells. McGraw-Hill Book Company. New York, Toronto, London. 1959. 595 p.
5. Ambartsumyan S.A. Theory of Anisotropic Plates, Technomic Publishing Co. New York, 1970. 255 p.
6. Goldenveizer A.L., Kaplunov J.D., EV Nolde E.V. Asymptotic analysis and refinement of Timoshenko-Reisner-type theories of plates and shells // Mechanics of Solids. (Izvestiya AN SSSR, Mekhanika Tverdogo Tela).1990. № 6(25). Pp. 126–139.
7. Goldenveizer A.L, Kaplunov J.D., Nolde E.V. On Timoshenko-Reissner type theories of plates and shells // International Journal of Solids and Structures. 1993. No. 5(30). Pp. 675–694.
8. Vasiliev V.V. An asymptotic method of justification of the plate theory // Mechanics of Solids. (Izvestiya AN SSSR, Mekhanika Tverdogo Tela). 1997. № 3. Pp. 150–155.
9. Vasiliev V.V. Modern conceptions of plate theory // Composite Structures. 2000. № 1(48). Pp. 39–48.
10. Zhilin P.A. The view on Poisson`s and Kirchhoff`s theories of plates in terms of modern theory of plates // Mechanics of Solids (Izvestia RAN, Mechanika Tverdogo Tela). 1992. № 3. Pp. 48–64.
11. Zhilin P.A. On the classical theory of plates and the Kelvin-Teit transformation // Mechanics of Solids. (Izvestia RAN, Mechanika Tverdogo Tela). 1995. № 4. Pp. 133–140.
12. Shimpi R.P., Patel H.G., Arya H. New first order shear deformation plate theories // Journal of Applied Mechanics. 2007. № 74. Pp. 523–533.
13. Vijayakumar K. A relook at Reissner's theory of plates in bending // Archive of Applied Mechanics. 2011. № 11(81). Pp. 1717–1724.
14. Tovstik P.E., Tovstik T.P. A thin-plate bending equation of second-order accuracy // Doklady Physics. 2014. № 8(59). Pp. 389–392.
15. Martínez Valle J.M., Martínez-Jiménez P. Modified Bolle - Reissner Theory of Plates Including Transverse Shear Deformations // Latin American Journal of Solids and Structures. 2015. № 2(12). Pp. 295–316.
16. Nareen K., Shimpi R.P. Refined hyperbolic shear deformation plate theory. Archive Proceedings of the Institution of Mechanical Engineers. Part C. // Journal of Mechanical Engineering Science. 2015. Vol. 203–210. Pp. 1989–1996
17. Senjanović I., Vladimir N., Tomić M. On new first-order shear deformation plate theories // Mechanics Research Communications. 2016. Vol. 73. Pp. 31–38.
18. Huu-Tai Thai, Trung-Kien Nguyen, Thuc P.Vo, Tuan Ngo. A new simple shear deformation plate theory // Composite Structures. 2017. Vol. 171. Pp. 277–285.

19. Morozov N.F., Tovstik P.E., Tovstik T.P. Generalized Timoshenko–Reissner model for a multilayer plate. *Mechanics of Solids*. 2016. No. 5(51). Pp. 527–537.
20. Rudiger D. Eingespannte Rechteckplatten mit Schubverzerrungen. *Zeitschrift für Angewandte Mathematik und Mechanik.* 1963. No. 1-2(43). Pp. 71-79.
21. Shirakawa K. Bending of plates based on improved theory. *Mechanics Research Communications*. 1983. No. 4(10). Pp. 205–211.
22. Belubekyan M.V., Sanoyan Yu.G. Raschet izgiba zhestko zakreplennoy plastiny pri ravnomernoy nagruzke po utochnennoy teorii [Calculation of the bending of a rigidly fixed plate with uniform load according to the refined theory]. *Trudy IV Vserossiyskoy nauchnoy konferentsii, ch. 1.* [Proceedings of All-Russian Scientific Conference]. Samara: Izd-vo SamGTU, 2007. Pp. 42–45. (rus)
23. Xu Z. A simple and efficient triangular finite element for plate bending. *Acta Mechanica Sinica*.1986. No. 2(2). Pp. 185–192.
24. Xu Z. A thick-thin triangular plate element. International *Journal for Numerical Methods in Engineering*.1992. No. 5(33). Pp. 963–973.
25. Zienkiewicz O.C., Xu Z., Zeng L.F., Samuelsson A. and Wiberg N-E. Linked interpolation for Reissner-Mindlin plate elements: Part I - A simple quadrilateral. International *Journal for Numerical Methods in Engineering.* 1993. No. 18(36). Pp. 3043–3056.
26. Weiming S., Guangsong Y. Rational finite method for elastic bending of Reissner plates. *Applied Mathematics and Mechanics (English Edition).* 1999. No. 2(20). Pp. 193–199.
27. Ayad R., Dhatt G. and Batoz J.L. A new hybrid-mixed variational approach for Reissner - Mindlin plates. The MiSP model*. International Journal for Numerical Methods in Engineering*. 1998. No. 7(42). Pp. 1149–1179.
28. Dhananjaya H.R.. Closed form solutions for element matrices of 4-node rectangular plate element using IFM. *Electronic Journal of Structural Engineering*. 2010. No. 10. Pp. 1–10.
29. Aghdam M.M., Shakeri M., Fariborz S.J. Solution to Reissner Plate with Clamped Edges. *Journal of Engineering Mechanics*. 1996. No. 7(122). Pp. 679–682.
30. Hassan K., Guirguis S., El-Hamouly H. Bending of an elastic rectangular clamped plate using Bergan-Wang approach. *African Journal of Engineering Research.* 2017. Vol. 5(1). Pp. 7–17.
31. Vasilyev V.Z. Primeneniye metoda nalozheniya nepolnykh resheniy v sluchaye pervoy osnovnoy zadachi dlya polubeskonechnogo tsilindra [The application of the method of imposing incomplete solutions in the case of the first fundamental problem for a semi-infinite cylinder]. *Sbornik "Mekhanika sterzhnevykh sistem i sploshnykh sred". Trudy Leningradskogo inzhenerno-stroitelnogo institute* [Collection "Mechanics of rod systems and continuous media". Proceedings of the Leningrad Civil Engineering Institute]. 1973. No. 73. Pp. 15–22.
32. Kantorovich L.V., Krylov V.I. *Approximate Methods of Higher Analysis*. Translated by C. D. Benster. Groningen, 1958. 695 p.

19. Morozov N.F., Tovstik P.E., Tovstik T.P. Generalized Timoshenko–Reissner model for a multilayer plate // Mechanics of Solids. 2016. № 5(51). Pp. 527–537.
20. Rudiger D. Eingespannte Rechteckplatten mit Schubverzerrungen // Zeitschrift für Angewandte Mathematik und Mechanik. 1963. No. 1-2(43). Pp. 71–79.
21. Shirakawa K. Bending of plates based on improved theory // Mechanics Research Communications. 1983. № 4(10). Pp. 205–211.
22. Белубекян М.В., Саноян Ю.Г. Расчет изгиба жестко закрепленной пластины при равномерной нагрузке по уточненной теории // Труды IV Всероссийской научной конференции, ч. 1. Самара: Изд-во СамГТУ. 2007. С. 42–45.
23. Xu Z. A simple and efficient triangular finite element for plate bending // Acta Mechanica Sinica.1986. № 2(2). Pp. 185–192.
24. Xu Z. A thick-thin triangular plate element // International Journal for Numerical Methods in Engineering. 1992. № 5(33). Pp. 963–973.
25. Zienkiewicz O.C., Xu Z., Zeng L.F., Samuelsson A. and Wiberg N-E. Linked interpolation for Reissner-Mindlin plate elements: Part I - A simple quadrilateral // International Journal for Numerical Methods in Engineering. 1993. № 18(36). Pp. 3043–3056.
26. Weiming S., Guangsong Y. Rational finite method for elastic bending of Reissner plates // Applied Mathematics and Mechanics (English Edition). 1999. № 2(20). Pp. 193-199.
27. Ayad R., Dhatt G. and Batoz J.L. A new hybrid-mixed variational approach for Reissner - Mindlin plates. The MiSP model // International Journal for Numerical Methods in Engineering. 1998. № 7(42). Pp. 1149–1179.
28. Dhananjaya H.R. Closed form solutions for element matrices of 4-node rectangular plate element using IFM // Electronic Journal of Structural Engineering. 2010. № 10. Pp. 1–10.
29. Aghdam M.M., Shakeri M., Fariborz S.J. Solution to Reissner Plate with Clamped Edges // Journal of Engineering Mechanics. 1996. № 7(122). Pp. 679–682.
30. Hassan K., Guirguis S., El-Hamouly H. Bending of an elastic rectangular clamped plate using Bergan-Wang approach // African Journal of Engineering Research. 2017. Vol. 5(1). Pp. 7–17.
31. Васильев В.З. Применение метода наложения неполных решений в случае первой основной задачи для полубесконечного цилиндра // Сборник "Механика стержневых систем и сплошных сред". Труды Ленинградского инженерно-строительного института. 1973. № 73. С. 15–22.
32. Kantorovich L.V., Krylov V.I. Approximate Methods of Higher Analysis. Translated by C. D. Benster. Groningen, 1958. 695 p.

Mikhail Sukhoterin,
+7(921)579-25-35; mv@sukhoterin.com

Sergey Baryshnikov,
+7(812)251-12-21; rector@gumrf.ru

Tatiana Knysh,
+7(812)748-96-73; KnyshTP@gumrf.ru

Михаил Васильевич Сухотерин,
+7(921)579-25-35;
эл. почта: mv@sukhoterin.com

Сергей Олегович Барышников,
+7(812)251-12-21; эл. почта: rector@gumrf.ru

Татьяна Петровна Кныш,
+7(812)748-96-73;
эл. почта: KnyshTP@gumrf.ru

Sukhoterin M.V., Baryshnikov S.O., Knysh T.P. Stress-strain state of clamped rectangular Reissner plates. *Magazine of Civil Engineering*. 2017. No. 8. Pp. 225–240. doi: 10.18720/MCE.76.20.

doi: 10.18720/MCE.76.21

Express-techniques in study of polluted suburban streams

Экспресс-методы в изучении загрязненных вод пригородных водотоков

Kh.V. Il'ina,
N.M. Gavrilova,
E.A. Bondarenko,
M.Ju. Andrianova,
A.N. Chusov,
Peter the Great St. Petersburg Polytechnic University, St. Petersburg, Russia

Студент Х.В. Ильина,
студент Н.М. Гаврилова,
ассистент Е.А. Бондаренко,
канд. техн. наук, доцент М.Ю. Андрианова,
канд. техн. наук, заведующий кафедрой А.Н. Чусов,
Санкт-Петербургский политехнический университет Петра Великого, г. Санкт-Петербург, Россия

Key words: environmental monitoring; water pollution; wastewater; surface water; fluorescence; conductivity

Ключевые слова: экологический мониторинг; контроль качества воды; бытовые сточные воды; поверхностные воды; флуоресценция; электропроводность

Abstract. Water samples from streams in suburban region of new builds were analyzed in order to suggest methods and parameters for pollution monitoring. Concentrations of total nitrogen (TN) varied from 0.6 to 9.0 mg/L, ammonium – from 0 to 6.8 mg/L, total organic carbon (TOC) from 8.3 to 21.1 mg/L. Electric conductivity (EC) varied from 80 to 640 mkSm/cm, optical density at 254 nm – from 0.41 to 1.07. Increased concentrations of TN and ammonium at several sampling sites confirmed wastewater discharge from dwelling area. Polluted waters also showed higher values of electric conductivity and molar fractions for sodium and chloride ions, lower values of optical density (in range 230 – 420 nm) and TOC. Fluorescence intensity (I) was measured at excitation wavelength 230 and 270 nm, emission wavelengths 300-350 nm (protein-like fluorescence, present in wastewaters), 420 nm (humic-like fluorescence, present in natural and waste waters). Character of correlation between fluorescence intensity and TN (marker of pollution) and TOC depended on wavelengths, fluorescence signal correction and dilution of sample. Only I at 230 nm excitation and 350 nm emission for 10-fold diluted sample of water could be recommended for water monitoring. EC can be used as additional parameter in studied streams.

Аннотация. Пробы воды из водотоков в районе новостроек исследовали с целью предложить методики для экспресс-мониторинга загрязнений. Концентрации общего азота (TN) изменялись от 0.6 до 9.0 мг/л, иона аммония – от 0 до 6.8 мг/л, общего органического углерода (TOC) - от 8.3 до 21.1 мг/л. Электропроводность воды (EC) изменялась от 80 до 640 мкСм/см, оптическая плотность воды при 254 нм – от 0.41 до 1.07. Повышение концентраций ионов аммония и TN в некоторых точках отбора подтверждает сброс сточных вод от жилых домов. Также в загрязненных водах отмечается: повышенные EC, мольные доли ионов натрия и хлоридов; пониженные TOC и оптическая плотность в диапазоне 230–420 нм. Интенсивность флуоресценции (I) измеряли при длинах волн возбуждения 230 и 270 нм, длинах волн регистрации 300–350 нм (флуоресценция белкового типа, характерная для сточных вод) и 420 нм (флуоресценция гуминового типа, регистрируемая в природных и сточных водах). Характер корреляции между I и TN (маркер загрязнения) и TOC зависел от длин волн, коррекции сигнала и разведения пробы. Только I при длинах волн возбуждения 230 нм и регистрации 350 нм для 10-кратно разведенной пробы можно рекомендовать для мониторинга загрязнений в изученных водотоках. EC может использоваться как дополнительный параметр.

Introduction

Surface water pollution is a great environmental problem all over the world. Pollutants from agricultural, industrial and municipal sources increase concentrations of harmful compounds in water

Ильина Х.В., Гаврилова Н.М., Бондаренко Е.А., Андрианова М.Ю., Чусов А.Н. Экспресс-методы изучения вод загрязненных пригородных водотоков // Инженерно-строительный журнал. 2017. № 8(76). С. 241–254.

bodies, causes degradation of natural ecosystems in lakes and rivers, insert microbiological contamination, complicate processes of drinking water treatment.

Conditions of water in natural water objects can be esteemed from results of regular water quality monitoring and from reports of water using organizations. Regular samples collection and full chemical analysis of water are usually done several days in a year [1]. Obviously these data do not provide complete information about situation in the water objects. In annual reports from organizations volumes of wastewater effluents and concentrations of pollutants could be less than in reality.

Application of express-methods (for example, in automatic water quality monitors or on-site measurements) could make water quality control more operative. Such methods could help to find illegal sources of pollution or register the beginning of pollution process. This is important for making rapid decisions about application of water protection measures [2–4]. Also it can help to prevent wastewater discharges in future. However, informativity of express-methods depends on properties of water, such as natural background parameters. That is why investigation of particular stream is needed before recommending exact express-method.

There are several parameters possible for express monitoring of water. One of them is optical density of water at 254 nm (D_{254}), usually used in water quality control to esteem amount of dissolved organic matter [5–8]. Electric conductivity of water (EC) allows esteeming concentration of total dissolved solids and detecting pollution in fresh waters [9–11].

Fluorescence of surface water samples also can be applied for this purpose [7, 11, 12]. River waters display two main types of peaks in fluorescence spectra (see Fig. 1). Protein-like peaks are observed at excitation wavelength 210–300 nm and emission wavelengths 300 nm (tyrosine-like peak) and 350 nm (tryptophan-like peak). Humic-like peak is wider and has maximal emission between 400 and 500 nm. In not polluted river waters, humic peak is prevailing. Spectra of organic pollutants, such as light oils, sewage, landfill leachate, have noticeable protein-like peaks that can be even higher than humic-like peak [11–14].

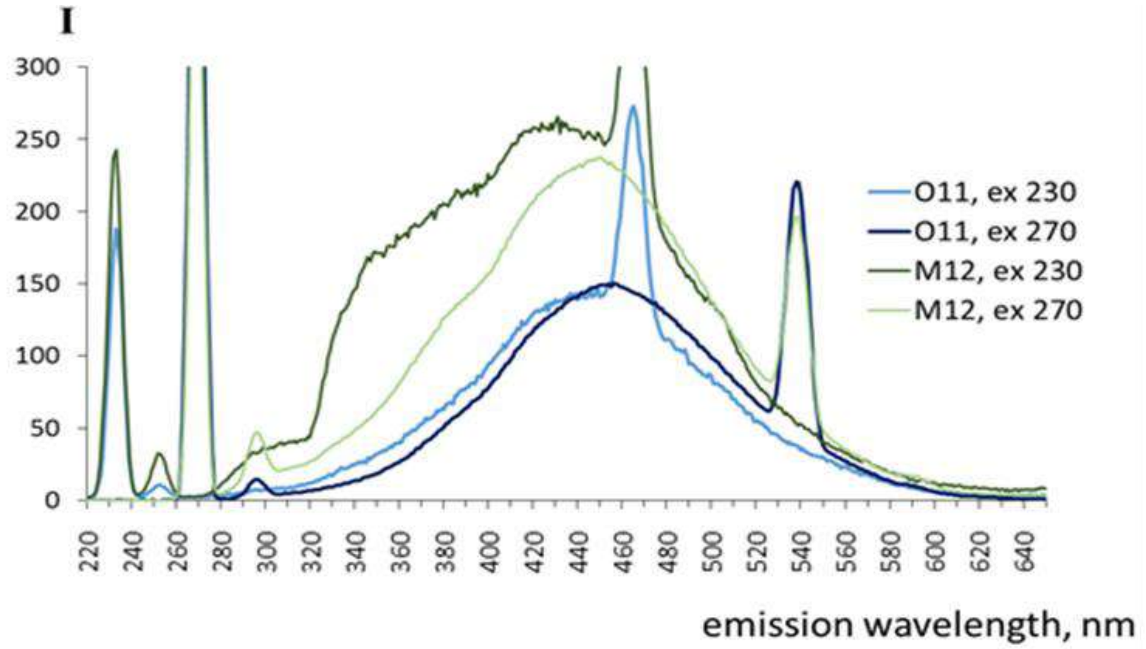

Figure 1. Examples of fluorescence spectra of studied water samples at excitation wavelengths 230 and 270 nm. I – fluorescence intensity

Correlations between fluorescence intensity ($I_{ex,\ em}$) at certain excitation (ex) and emission (em) wavelengths and chemical parameters of organic matter in natural, polluted waters and wastewaters were studied (reviewed in [12, 14]). Strong positive correlations were found between biochemical oxygen demand (BOD) and tryptophan-like peak (correlation coefficient r = 0.85 [15], r = 0.906 [16], r = 0.77 [17], r = 0.96 [18]), BOD and humic-like peak (r = 0.72 [17], total organic carbon (TOC) and humic-like peak or tryptophan-like peak (r = 0.876 [16], r = 0.96 [18]). Strong correlations were also shown between fluorescence parameters and concentrations of inorganic (not fluorescing) compounds typical for sewage pollution (phosphates, nitrates, ammonium) [14, 15].

However, in some studies strong relationship between TOC or COD and peaks intensities were not revealed (r = 0.1...0.51) [7, 12, 14, 19, 20]. These results show need in more detailed study of components forming organic matter in waters. Also they show that properties of real waters should be taken into account before applying fluorescence techniques for pollution monitoring.

The aim of the present study is to check if it is possible to use several express-methods for water quality monitoring in St.Petersburg. Previously we studied the Okhta and its tributary the Murinsky creek in the boundaries of St.Petersburg. It was shown that pollution with wastewaters increased electric conductivity, changed molar fractions of ions and fluorimetric parameters [21, 22]. The present study is focused on suburban region Murino. This region recently became an area of intensive housing construction with supposed direct discharges of domestic wastewater from new buildings to local streams and the Okhta.

Objects and Methods

Characteristic of water source

The Okhta is the most polluted river of St.Petersburg due to discharge of untreated wastewaters and surface runoff [23–26]. It starts in Leningrad region and flows into the Neva which is used as source of drinking water for the city. Length of the Okhta is 93 km; 17.5 km of the river flows through the territory of St.Petersburg [27, 28].

According to reports of water using organizations about 30% of river flow at its mouth is composed by wastewaters from the city. Wastewaters of Leningrad region form about 10% of the Okhta flow at monitoring station Novoye Devyatkino located at the boundary between St.Petersburg and Leningrad region [29]. Values higher than maximal allowable concentrations (MAC) were registered in the Okhta for such pollutants as ammonium, nitrites, iron, copper, manganese and some other metals [23, 24]. High concentrations of biodegradable organic matter were found as well; they caused decreasing of dissolved oxygen concentration [23, 24] and degradation of water plants communities [30].

Sampling sites

In the present study 11 water samples were collected in October 2016 from streams of the region Murino and near it. Murino is situated in Leningrad region near the city boundary. Sampling sites are located upstream the monitoring site Novoye Devyatkino. They are shown at Figure 2.

Order of samples` numbers was not sequential. Five samples (# 5, 8, 10, 11, 13) were taken from the Okhta. One sample (# 12) was collected from its heavily polluted tributary the Murinsky creek, located in St.Petersburg. Five samples (# 3, 4, 2, 7, 9) were taken from Kapraliev creek which inflows into the Okhta in Murino. Samples were collected at one day. At the same day they were taken to the laboratory and stored at +4 °C in vertical position. The upper part of water was analyzed. No filtration was done to prevent addition of fluorescing components from filters to water.

Water analysis

Concentrations of total carbon (TC), inorganic carbon (IC) and total nitrogen (TN) were determined by analyzers “TOC L vpn” and “TNM-L” (Shimadzu, Japan) with measurement error ± 15%. Concentration of total organic carbon (TOC) was calculated by subtraction of IC from TC.

Chemical oxygen demand (COD) was calculated from TOC according to the formula from [31]: COD (mgO/L) = TOC (mg/L)/0.375 .

Concentrations of inorganic cations (NH_4^+, K^+, Na^+, Mg^{2+}, Ca^{2+}) were determined at the next day after sampling. Method of capillary electrophoresis was used on device Capel 103P (Lumex, Russia). Concentrations of inorganic anions (sulfates and chlorides) were measured two days after sampling by the same device. Measurement errors were ± 15%.

Molar fraction of cation or anion among studied cations or anions were calculated according to the formula (1)

$$R(i) = (C_i \cdot 100\%) / (C_{sum}) \qquad (1)$$

where C_i – molar concentration of cation or anion (mol/L), C_{sum} – sum of molar concentrations for studied cations (K^+, Na^+, Mg^{2+}, Ca^{2+}) or anions (Cl^-, SO_4^{2-}, HCO_3^-), correspondingly.

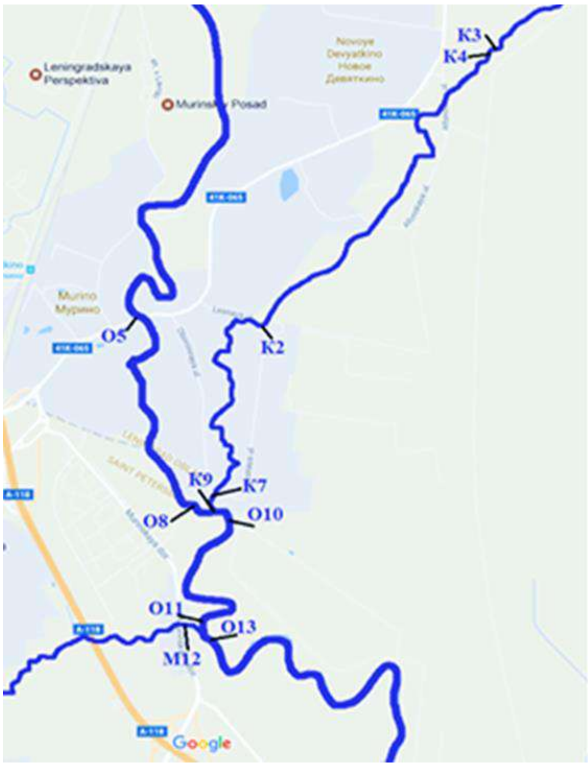

Figure 2. Scheme of sampling sites. Letter K denotes samples from Kapraliev creek, letter O – from the Okhta, letter M – from the Murinsky creek

Optical properties of samples were analyzed in collected samples of water without dilution and diluted 10-fold with distilled water. For diluted samples signal of distilled water was subtracted from signal of diluted sample.

Optic density (D) spectra were obtained by spectrophotometer “SF–56” (OKB Spectr, Russia) in 1 cm cuvette. Values at selected wavelengths were presented in this paper, for example optical density at 254 nm (D_{254}).

Fluorescence spectra were obtained by analyzer “RF 5301 PC” (Shimadzu, Japan) at two excitation wavelengths 230 nm and 270 nm near to maximums of excitation spectra for humic substances and proteins. Fluorescence was registered at emission wavelengths from 220 to 650 nm (step 1 nm, slit width 5 nm). Later basing on data from optic density spectra fluorescence intensity ($I_{ex,em}$) was corrected for the inner filters effect according to the formulas (2) [32]:

$$I_{1and2f} = I_{ex,em} \cdot k$$
$$k = 10^{0.5(D_{ex}+D_{em})} \qquad (2)$$

where I_{1and2f} – corrected data, $I_{ex,\,em}$ – measured fluorescence intensity, k – multiplying correcting factor, D_{ex} – optical density at excitation wavelength, D_{em} – optical density at emission wavelength.

Specific electric conductivity of water (EC) was measured on sampling site by “HI 8713” (HANNA Instruments) with measurement error ± 5%.

On site measurement of fluorescence intensity was done by portable fluorimeter Fluorat 02-3M (Lumex, Russia) with a set of light filters using recommendations of manufacturer.

Approximation of Fuoresence Spectra

In order to understand influence of the left part of humic peak on fluorescence intensity of protein-like peak data processing is needed. In the most detailed way it includes signal correction on inner filter effects, elimination of scattering peaks, and other actions, which require additional data and programs.

For rough estimation the following data processing was done. Humic-like peak on fluorescence spectra at excitation wavelengths 270 nm could be easily approximated by Gaussian curve without subtraction of scattering peaks.

Humic-like peak on fluorescence spectra at excitation wavelengths 270 nm was approximated by modified Gaussian curve described by the formula (3)

$$I = \frac{m}{\sigma\sqrt{2\pi}} exp\left[-\frac{(x-x_0)^2}{2\sigma^2}\right] \quad (3)$$

where I – fluorescence intensity (in arbitrary units)

m – maximal value of I for humic-like peak, multiplied by $\sigma \cdot 2\sqrt{2\pi}$,

σ – sigma, standard deviation (in nm), *x* – emission wavelength (in nm),

x_0 – mean value of emission wavelength for humic-like peak (in nm).

Mean value x_0 of humic-like peak was determined as wavelength at maximal *I* in the emission wavelength range 400-500 nm.

Sigma was found from the formula (4) connecting full width at half maximum (FWHM) for Gaussian curve [33]:

$$FWHM = \sigma \cdot 2\sqrt{2ln2} \approx 2.355\sigma \quad (4)$$

where *FWHM* – interval of wavelength (in nm) at half maximum of fluorescence intensity (in arbitrary units), σ - sigma in formula (3).

Spectra at excitation wavelength 230 nm are not suitable for such approximation because of scattering peak with maximum at emission wavelength 460 nm (it is produced by diffraction grid of excitation monochromator at doubled excitation wavelength). It does not allow to localize maximal *I* and determine mean value of emission wavelength for humic-like peak.

Program for calculation of approximated spectra was written in R programming language using IDE RStudio1.0.44 © 2009-2016 RStudio.

Results

Chemical Parameters of Water Samples

Results of chemical analysis and D_{254} of samples are given in Tables 1-3. Clean natural waters were collected from points #3 and 4 that were located close to each other, upstream from buildings, dump site and near swampy area with source of Kapraliev creek. Sample #3 was collected near the bank where water was still while #4 was taken several meters further from a place with small noticeable current. This explains higher concentrations of ions in sample # 3 due to longer interaction of water with ground and soil waters. In general waters from #3 and 4 had low content of TOC (about 10–14mgTOC/L), low concentrations of ions and EC (80–202 mkSm/cm). Values of TN (0.6 –0.8 mgTN/L) and concentrations of ammonium-ion (0–0.14 mgN_{NH4+}/L) were the lowest among studied samples.

Downstream that place sample #2 was taken. There Kapraliev creek became wider and deeper and passed through dwelled area from which wastewater discharge was supposed. In sample #2 concentration of ions, TOC, EC and D_{254} were near the ranges observed upstream (in #3 and 4). However, concentrations of TN (about 4 mgTN/L) and ammonium (2 mgN_{NH4+}/L) were increased, indicating discharge of fecal wastewaters.

Samples # 7 and 9 were collected at the end of the Kaprailev creek. Sample #9 was taken just before the inflow of the creek to the Okhta. Concentrations of ammonium and TN in samples # 7 and 9 became higher than in previous ones (5–4 mgN_{NH4+}/L and 8.5–9 mgTN/L), EC also significantly increased (to 290–480 mkSm/cm) while TOC remained approximately at the same level (15 mgTOC/L), and D_{254} decreased a little. The results show that the creek had received additional polluted waters on its way. Significant part of dissolved pollutants belonged to ions of sodium and chloride, concentrations of which seriously increased to the end of the creek (sample #9), rising molar ratio of these ions to the maximal values in the Kapraliev creek (see Table 3).

Samples #5, 8 and 10 were collected from the Okhta. Sample #8 was collected near inflow of the Kapraliev creek (#9) upstream it and sample # 10 – downstream it. Sample # 5 was taken far before the inflow of the creek. It can be seen from the data that waters of the Okhta changed most after addition of waters from the creek. They slightly increased TN (from 4 to 5 mgTN/L), noticeable increased EC (from 210 to 260 mkSm/cm) and concentration of chlorides, provided two-fold increase of ammonium (from approximately 1 to 2 mgN$_{NH4+}$/L). However, TOC remained the same and D_{254} showed decrease (from 1.07 to 0.86) downstream inflow of the creek.

Table 1. General parameters of water samples

#	TOC, [mg/L]	COD, [mgO/L]	TN, [mg/L]	IC, [mg/L]	EC, [mkSm/cm]	D_{254}
4	13.6	36	0.6	10.5	80	0.578
3	9.8	26	0.8	14.3	202	0.498
2	13.8	37	3.7	17.3	167	0.517
5	21.1	56	3.9	13.0	208	1.030
7	15.2	41	8.5	26.0	286	0.507
8	20.9	56	4.1	12.8	213	1.067
9	15.0	40	9.0	24.7	479	0.414
10	20.1	53	5.1	15.0	263	0.863
11	20.9	56	4.3	13.0	215	1.025
12	8.3	22	5.2	30.9	640	0.265
13	16.7	44	4.7	19.2	351	0.708

Table 2. Major ions concentrations (in mg/L)

#	NH_4^+	K^+	Na^+	Mg^{++}	Ca^{++}	Cl^-	SO_4^{--}	HCO_3^-
4	0.0	0.8	3.6	3.4	10.5	2.2	1.9	53.1
3	0.2	1.6	11.1	4.3	17.7	11.4	13.9	72.8
2	2.6	1.7	6.6	4.8	22.0	6.0	6.7	88.2
5	1.8	3.0	14.2	4.4	18.4	12.6	11.9	65.8
7	6.8	3.3	13.3	5.7	24.4	12.9	10.9	132.1
8	1.5	2.3	10.9	3.2	11.8	10.0	9.3	65,1
9	5.4	2.7	22.0	5.9	22.5	45.1	8.9	125.7
10	2.6	2.5	13.0	3.8	14.6	17.7	11.3	76.4
11	2.2	3.1	14.2	4.0	15.0	11.2	10.5	66.3
12	3.2	5.8	51.7	8.4	38.4	59.1	29.4	157.3
13	2.8	4.3	28.1	5.7	23.6	26.2	15.9	97.7

Table 3. Molar fractions for cations and anions

#	NH_4^+	K^+	Na^+	Mg^{++}	Ca^{++}	Cl^-	SO_4^{--}	HCO_3^-
4	0.00	0.04	0.27	0.24	0.45	0.07	0.02	0.91
3	0.01	0.03	0.42	0.15	0.38	0.19	0.09	0.72
2	0.12	0.03	0.24	0.16	0.45	0.10	0.04	0.86
5	0.07	0.05	0.43	0.13	0.32	0.23	0.08	0.69
7	0.20	0.05	0.31	0.12	0.32	0.14	0.04	0.82
8	0.08	0.06	0.45	0.13	0.28	0.19	0.07	0.74
9	0.14	0.03	0.45	0.11	0.26	0.37	0.03	0.60
10	0.11	0.05	0.44	0.12	0.28	0.27	0.06	0.67
11	0.09	0.06	0.45	0.12	0.28	0.21	0.07	0.72
12	0.05	0.04	0.58	0.09	0.25	0.37	0.07	0.57
13	0.07	0.05	0.53	0.10	0.25	0.30	0.07	0.64

The Murinsky creek (sample #12) is another polluted tributary of the Okhta which inflows downstream the Kapraliev creek. The Murinsky creek also added sodium chloride to waters of the Okhta, as it can be seen from the data for samples #11 (Okhta before inflow of the Murinsky creek) and #13 (Okhta after inflow of the Murinsky creek). Also it increased EC in the Okhta. TN and ammonium had close values in samples # 11, 12 and 13 (4-5 mgTN/L and 2-3 mg N$_{NH4+}$/L). TOC and D_{254} decreased after inflow of the creek.

In all studied samples correlation between EC and TN at p = 0.05 was moderate (r = 0.59), between EC and TN/TOC – high (r = 0.85). Also increasing of EC and molar fractions of sodium-ion and chloride-ion were observed as a result of pollution. EC had high positive correlation with concentrations of studied ions (except for NH_4^+); values of r were from 0.83 to 0.98. Molar fractions of sodium and chloride had high positive correlations with EC (r =0.70 for Na^+, 0.86 for Cl^-), while molar fractions for bivalent cations and hydrocarbonates had negative values of r: (-0.72) for Mg^{++} and EC; (-0.70) for Ca^{++} and EC, (-0.81) for HCO_3^- and EC. These values of r were significant at p<0.05. The same effect was detected during the study of other parts of the Okhta [22].

Fluorescence Parameters of Water Samples

In order to check applicability of fluorescent detectors in revealing pollution fluorescence spectra of waters were studied. We focused on fluorescence at selected emission wavelengths (see Figs. 3, 4): 300, 320 and 350 nm characteristic for protein-like fluorescence and 420 nm – for humic-like fluorescence. In order to take into account light absorption in cuvette at excitation and emission wavelength multiplying correcting factors were calculated. For undiluted samples multiplying correcting factor for fluorescence intensity $I_{ex,em}$ was in the range 2 – 18 for excitation at 230 nm and 1.1 – 4.5 for excitation at 270 nm. This values show great aberration of signal in cuvette. In this case using of undiluted sample in fluorimetric monitoring seems not informative. Also it can lead to misinterpretation of fluorimetric signal which can rise not only because of higher amount of fluorophores from pollutants but also as a result of increasing of water transparency.

For water samples diluted 10-fold multiplying correcting factor was 1.1–1.35 for excitation at 230 nm and 1.02–1.21 for excitation at 270 nm. Therefore we suppose that these uncorrected values could be suitable for water quality monitoring without data processing.

Some common patterns in spatial changing of $I_{ex,\ em}$ and chemical parameters (TOC, TN, EC) can be noted from Figures 3. In order to describe general trends correlation coefficients (r) were determined between pairs of optical and chemical parameters.

Optical density D at selected wavelengths (230, 254, 270, 320, 350, 420 nm) showed positive correlation with TOC with r = 0.92...0.82 (significant at p<0.05). However in correlations with TN values of r were negative and for the studied set of data they were not statistically significant. Resembling tendencies were observed in previous study of the Okhta and the Murinsky creek [32]: correlation of D_{254} with TOC was positive, with TN – negative.

Noticeable correlations were found with TN or TN/TOC and the intensity of protein-like fluorescence for undiluted water samples. In all cases r for TN was lower (and sometimes significantly) than for TN/TOC. For undiluted samples intensity of fluorescence (excitation at 230 or 270 nm, emission at 300, 320, 350 or 420 nm) without signal correction showed positive correlation with TN/TOC with r from 0.65 to 0.84. One exception was with $I_{230,420}$ and TN/TOC where r was +0.30 (insignificant for p<0.05). TOC and uncorrected $I_{ex,em}$ for undiluted samples showed negative correlation with TOC (r from -0.52 to -0.90).

Signal correction did not change much these tendencies for protein-like fluorescence in undiluted waters at excitation on 270 nm. Positive correlations were found between $I_{270,320}$ and TN/TOC or TN (r was 0.92 or 0.77 correspondingly), $I_{270,350}$ and TN/TOC or TN (r was 0.84 or 0.73 correspondingly). Weak negative correlation (r from -0.11 to -0.20, insignificant) was found between protein-like fluorescence and TOC. Humic-like fluorescence $I_{270,\ 420}$ showed positive correlation with TN/TOC (r = 0.14, insignificant) and TOC (r = 0.60).

However, corrected fluorescence signal at excitation 230 nm for undiluted sample showed quite another pattern: moderate or strong positive correlation with TOC (r from 0.54 to 0.77) and weak or moderate negative correlation with TN/TOC (r was from -0.08 to -0.57).

Fluorescence intensity of diluted samples without signal correction showed only one valuable example of correlation: it was strong between TN/TOC and $I_{230,\ 350}$ (r = 0.84).

Moderate or strong negative correlation was found between protein-like fluorescence (without signal correction) and TOC (r from -0.61 to -0.73). Humic-like fluorescence showed weak positive correlation with insignificant values of r.

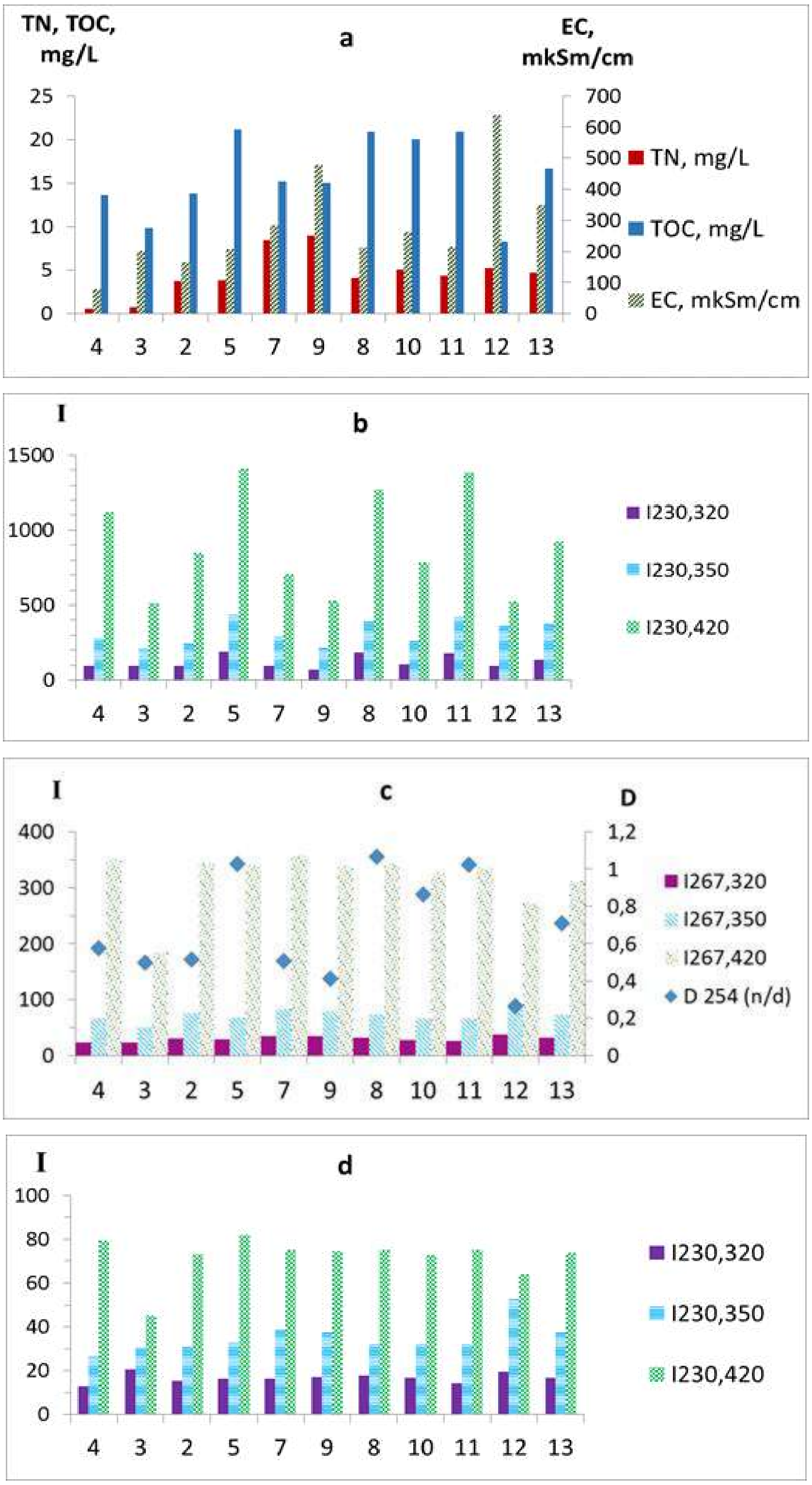

Figure 3. Chemical parameters of water samples (a). Examples of fluorescence intensities: b, c – undiluted samples without signal correction; d – diluted samples with signal correction

Fluorescence intensity of diluted samples with signal correction also showed only few examples of correlation. Positive correlation was found for the following pairs of parameters: $I_{230,350}$ and TN/TOC (r = 0.83), $I_{230,\ 350}$ and TN (r = 0.52, insignificant at p<0.05), $I_{230,\ 420}$ and TOC (r = 0.65).

Such strong influence of signal correction and sample dilution on dependences between pollution and protein-like fluorescence means that concentration of fluorophores in undiluted water samples are too high and do not belong to the part where linear dependence between $I_{ex,em}$ and their concentration is observed. Moreover, increasing of uncorrected signal of protein-like fluorescence might be interpreted as a sign of pollution while in fact it could be a result of decrease in D and not increase in concentration of fluorophores. However, wastewaters are able to decrease D of colored river waters as it was shown in [22] and in data of the present study. Thus increasing of uncorrected fluorescence signal in undiluted sample could be an indirect consequence of pollution.

These obtained results differ from tendencies found in previous study of the Oktha [22], where strong correlations were found in diluted samples between TN or TN/TOC and protein-like fluorescence (without signal correction) at all studied variants of excitation and emission wavelengths (excitation 230 or 270 nm, emission 300, 320 or 350 nm). In that study more samples were analyzed (n = 30), but ranges of TN, TOC and EC did not differ much from those of the present study. However $I_{ex,em}$ had varied in a wider range. For example in diluted samples (no correction) of $I_{230,350}$ had varied from 14 to 60 arbitrary units, $I_{230,\ 4200}$ – from 26 to 93 arbitrary units, $I_{270,350}$ – from 5 to 21 arbitrary units, $I_{270,\ 420}$ – from 13 to 48 arbitrary units [31]. In the present study the ranges are smaller: $I_{230,350}$ – from 24 to 48 arbitrary units, $I_{230,\ 420}$ – from 40 to 70 arbitrary units, $I_{270,350}$ – from 7 to 10 arbitrary units, $I_{270,\ 4200}$ – from 18 to 36 arbitrary units.

It can be seen from figures and tables that several values are very close to each other and the difference between them is explained by measurement error. However, tendencies of signal intensity changing with dose of pollutants are clearly observed.

Ratios of Fluorescence

On one hand wastewaters increase fluorescence intensity not only in protein wavelength range but also in the range of humic-like peak. On the other hand unpolluted waters can show high fluorescence intensity in protein-like range produced not by protein-like fluorophores (from wastewaters) but by the left part of humic-like peak of natural organic matter. In order to separate these two types of fluorescence rough estimation of humic-like fluorescence was done for uncorrected fluorescence spectra at excitation wavelengths 270 nm. Humic-like peak was approximated by Gaussian curve (see example in Fig. 4).

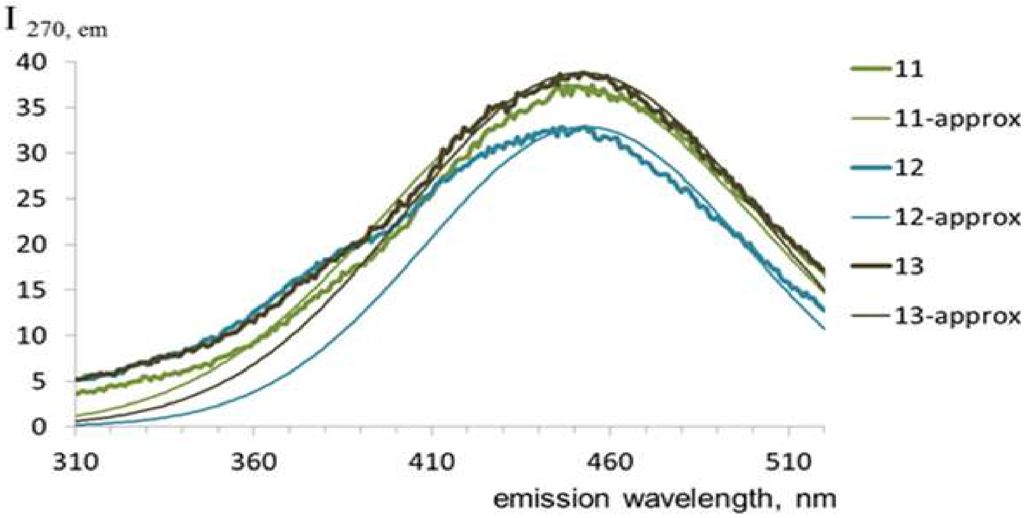

Figure 4. Example of humic-like peak approximation of by Gaussian curve for samples # 11–13. Fluorescence spectra are without correction

Results of approximation are summarized in Table 4. Differences between data from spectrum and approximated curve are shown for the studied emission wavelengths 320, 350 and 420 nm. In addition, data for 380 nm and 520 nm are shown. They are located almost symmetrical about maximums of humic-like peak (which is at 442-456 nm for undiluted spectra, 445-454 nm for diluted spectra). It is seen from the data that fluorescence of supposed left side of humic peak is rather significant.

Table 4. Results of approximation of humic peak on fluorescence spectra (uncorrected) at excitation wavelength 270 nm

emission wavelength, nm	difference, %	
	undiluted water	diluted water
320	39...80	57...93
350	10...59	11...76
380	-3...37	-10...52
420	-4...7	-10...12
520	9...17	12...19

In these circumstances ratio of protein-like to humic-like fluorescence could help to avoid misinterpretation of fluorimetric data. Fluorescence factor F showing this ratio was calculated by the formula

$$F_{ex,\,em1\,/em2} = \frac{I_{ex,em1}}{I_{ex,em2}} \quad (5)$$

where ex – 230 or 270 nm, em1 – 300, 320 or 350 nm, em2 – 420 nm.

Correlations of chemical parameters and fluorescence factors $F_{ex,\,em1/em2}$ were studied. Again, in contrast with the previous study of the Okhta [22], there were no significant correlations in diluted samples (with or without correction) with such markers of pollution as TN or TN/TOC.

In not diluted samples correlations between $F_{ex,\,em1/em2}$ (data with or without signal correction) and TN/TOC were observed with r from 0.34 (insignificant) to 0.75.

All types of $F_{ex,\,em1/em2}$ for undiluted and diluted samples with or without correction showed negative correlation with TOC with r from -0.19 to -0.85.

Discussion

Results in Tables 1–3 show that the Okhta and its tributaries (the Kapraliev creek and the Murinsky creek) were already polluted by wastewaters in Murino. The most significant signs of fresh pollution were increased concentrations of TN and ammonium in samples collected near buildings and houses. In these samples concentrations of ammonium were from 2.0 to 5.3 mgN_{NH4+}/L. This is higher than maximal allowable concentration (MAC) for water bodies in dwelled areas (1.5 mgN_{NH4+}/L) [34].

Typical concentrations of TN in unpolluted rivers of North-west of Russia are less than 1 mg/L, but in rare cases they could rise up to 6 mg/L [28]. Measured concentrations in samples of polluted waters were over these values and varied from 3.7 to 9.0 mgTN/L.

MAC for COD was also exceeded in most part of samples (30 mg/L in dwelled areas [35]). However COD and TOC did not increase significantly after pollution and in some places (after inflows of the Kapraliev creek and the Murinsky creek) they decreased. The same situation was with D_{254} that has high correlation with TOC. These results are in contrast to a number of studies where concentration of organic matter increased after wastewater discharge [36–37]. Lack of correlation between TN and optical density at 254 nm and other studied wavelengths (230–420 nm) demonstrate that these optical parameters could not be used to distinguish the fact of pollution.

Decrease of COD and optical density after pollution can be explained by high background concentrations of natural organic matter in the studied waters (COD can vary from 8 to 142 mgO/L in rivers of North-west of Russia [28]).

Concentrations of TN, ammonium and COD were lower than typical values for wastewaters. Average concentrations in St.Petersburg wastewaters were reported as about 30 mgTN/L, about 25 mgN_{NH4+}/L and about 300 mgO/L, correspondingly [40]. Lower values in polluted waters can be explained by partial treatment of wastewaters before discharge to rivers and surely by dilution of wastewaters in streams. Sedimentation of suspended organic matter in rivers also can significantly decrease COD because at least 50 % of COD in domestic wastewaters is present as suspended solids [38, 39].

It the present study values of EC, molar fractions of Na^+ and Cl^- were higher in polluted waters of the Kapraliev creek and the Murinsky creek. The same situation was observed in our previous studies at other sampling sites of the Okhta [22, 40]. These data correspond to investigations where EC was proved to be a useful tool for express-monitoring of pollution of surface waters (and increase of it was followed by increase of NaCl and other pollutants) [16, 18, 36]. However, applicability of EC in monitoring should be tested on real waters because there could be some interfering factors such as high water mineralization [39], hour variation in wastewater flow rate and pollutants concentrations, seasonal changes in natural and wastewater properties.

In the present study fluorimetric data were obtained and analyzed in several variants in order to compare their informativity for water quality monitoring. Dilution of water and correction for inner-filter effects can seriously influence spectral data. Inner filter effect caused by light absorption in the sample could be negligible in some waters as in [17] therefore making sample dilution or data correction unnecessary for fluorimetric analysis. There was even a supposition that inner filter effects should be negligible in natural waters because dissolved organic matter concentrations rarely exceed 20 mgC/L in them [41]. In other studies water dilution was recommended to 1–15 mgTOC/L [12] or from 1 to 10 fold for river waters and 100 and more fold for untreated sewage and leachates [14]. In the present study water had not high concentrations of TOC from 9.8 to 21.1 mg/L and no need for sample dilution could be expected. However correlations between fluorescence signal and TN, TOC and TN/TOC in diluted (10-fold) and undiluted samples were quite different. Also strong influence of signal correction on correlations was observed. These results show that concentrations of fluorophores in undiluted water samples from Murino are too high and do not belong to the part where linear dependence between $I_{ex,em}$ and their concentration is observed. Moreover, increasing of uncorrected signal of protein-like fluorescence (marker of pollution) might be interpreted as a sign of pollution while in fact it could be a result of decrease in light absorption (and optical density) and not increase in concentration of fluorophores. However, in some cases wastewaters are able to decrease optical density of colored river waters as it was shown in [22] and in data of the present study. Thus increasing of uncorrected fluorescence signal in undiluted sample could be an indirect consequence of pollution.

In general results of the present study represent a situation where ability of fluorimetric method to reveal pollution is limited due to closeness of values to the natural variation in fluorescence spectra. We tested several possible fluorimetric parameters that showed strong correlations with concentrations of sewage pollutants, such as BOD_5, phosphates, nitrates, ammonium [7, 11, 12, 14]. In our streams only $I_{230,350}$ for 10-fold diluted sample could be recommended for pollution monitoring.

Our research group was the first who suggested studying correlations between concentration of TN or TN/TOC and $F_{ex,\ em1/em2}$. The last one is relative parameter showing ratio of protein-like fluorescence to humic-like fluorescence. For diluted samples correlations were not found in contrast with the previous our study of the Okhta [22].

Conclusions

Waters of suburban streams were studied in order to suggest express methods for revealing of pollution. The studied streams were supposed to be polluted with wastewaters from dwelled area.

In waters from several sampling points increased concentrations of ammonium were registered (up to 3.5 of MAC), confirming the fact of wastewater discharge. Pollution also resulted in increasing of TN, EC, decreasing of D (in the range 230–420 nm). Increasing of EC correlated with increasing of molar fraction of sodium and chloride ions in water.

Increase or decrease of TOC was registered after pollution. It can be explained by high natural background and sedimentation of part of organics from wastewater as suspended matter.

Valuable positive correlation between protein-like fluorescence and TN or TN/TOC were found only for $I_{230,350}$ in diluted water samples. In this case ability of fluorimetric method to reveal pollution is limited due to closeness of values to the natural variation in fluorescence spectra.

For water quality monitoring combination of EC and fluorimetry at excitation on 230 nm and emission on 350 nm are recommended.

References

1. *RD 52.24.309-2011.* Rukovodaschij document. Organizatsiya i provedeniye rezhimnykh nablyudeniy za sostoyaniyem i zagryazneniyem poverkhnostnykh vod sushi [Guidance document. Organization and conduct of regime observations of the state and pollution of surface waters]. (rus)
2. *Skhema kompleksnogo ispolzovaniya i okhrany vodnykh obyektov basseyna reki Heva. Kniga 6. Perechen meropriyatiy po dostizheniyu tselevogo sostoyaniya*

Литература

1. РД 52.24.309-2011. Руководящий документ. Организация и проведение режимных наблюдений за состоянием и загрязнением поверхностных вод суши.
2. Схема комплексного использования и охраны водных объектов бассейна реки Нева. Книга 6. Перечень мероприятий по достижению целевого состояния речного бассейна. СПб, 2015, 72с. [Электронный ресурс]. URL: http://www.nord-west-water.ru/activities/ndv/scheme-of-complex-use-and-protection-of-water-

rechnogo basseyna [Scheme of complex use and protection of water bodies in the Neva River basin. Book 6. List of activities to achieve the target state of the river basin]. SPb: 2015. 72p. URL: http://www.nord-west-water.ru/activities/ndv/scheme-of-complex-use-and-protection-of-water-bodies-in-the-basin-of-the-river-neva/ (rus)

3. Romanov M.V., Tarakanov A.E. Elaboration of expert modelling geoinformation system for complex ecological normalization of technogenic load at small drainage areas. *Third Youth Environmental Conference "Ecobaltica-2000"*. SPb, 2000. Pp. 156–164. (rus).
4. Stenis J., Romanov M., Hogland W. Analysis and classification of modern methods of ecological normalization of anthropogenic load: Russia vs. the West. *The Open Environmental Engineering Journal*. 2011. Vol. 4. Pp. 181–189.
5. Szabo H.M., Tuhkanen T.T. UV/VIS Spectroscopy as a method to characterize well water quality. *VATTEN – Journal of Water Management and Research*. 2016. Vol. 72. Pp.169–175.
6. Potter B.B., Wimsatt J.C. *Method 415.3 – Measurement of total organic carbon, dissolved organic carbon and specific UV absorbance at 254 nm in source water and drinking water (EPA Document #: EPA/600/R-09/122).* U.S. Environmental Protection Agency, Cincinnati, Ohio, 2009. 56 p.
7. Comber S.D.W., Gardner M.J., Gunn A.M. Measurement of absorbance and fluorescence as potential alternatives to BOD. *Environmental Technology*. 1996. Vol. 17. Pp. 771–776.
8. Edzwald J., Kaminski G.S. A practical method for water plants to select coagulant dosing. *Journal of the New England Water Works Association*. 2009. Vol. 123. Pp. 15–31.
9. *Biogeochemistry of Small Catchments: A Tool for Environmental Research.* Edited by B. Moldan and J.Cerny. SCOPE Published by John Wiley & Sons Ltd, 1994. 420 p.
10. Vorobyev N.I. *Primeneniye izmereniya elektroprovodnosti dlya kharakteristiki khimicheskogo sostava prirodnykh vod* [Application of conductivity measurement to characterize chemical composition of natural waters]. Izd-vo AN SSSR, M. 1963. 141 p. (rus)
11. De Sousa D.N.R., Mozeto A.A., Carneiro R.L., Fadini P.S. Electrical Conductivity and Emerging Contaminant as Markers of Surface Freshwater Contamination by Wastewater. *Science of The Total Environment*. 2014. Vol. 484. Pp. 19–25.
12. Hudson N.J., Baker A., Reynolds D. Fluorescence analysis of dissolved organic matter in natural, waste and polluted waters – a review. *River Res. Appl.* 2007. Vol. 23(6). Pp. 631–649.
13. Coble P.G., Lead J., Baker A., Reynolds D.M., Spencer R.G.M. *Aquatic Organic Matter Fluorescence.* Cambridge University Press. 2014. 375p.
14. Molodkina L.M., Andrianova M.Ju., Chusov A.N. Specrtofluorimetry in study of bioorganic wastes degradation dynamics. *Nauchno-teknicheskie vedomosti SPbGPU*. 2012. Vol. 142. Pp. 243–250 (rus).
15. Henderson R.K., Baker A., Murphy K.R., Hambly A., Stuetz R.M., Khan S.J. Fluorescence as a potential monitoring tool for recycled water systems: A review. *Water Research*. 2009. Vol. 43. Pp. 863–881.
16. Baker A, Inverarity R. Protein-like fluorescence intensity as a possible tool for determining river water quality. *Hydrological Processes*. 2004. Vol. 18(15). Pp. 2927–2945.
17. Hudson N., Baker A., Ward D., Reynolds D.M., Brunsdon C., Carliell-Marquet C., Browning S. Can fluorescence spectrometry be used as a surrogate for the

bodies-in-the-basin-of-the-river-neva/ (дата обращения: 09.10.2017).

3. Romanov M.V., Tarakanov A.E. Elaboration of expert modelling geoinformation system for complex ecological normalization of technogenic load at small drainage areas // Third Youth Environmental Conference "Ecobaltica-2000". St.Petersburg, 2000. Pp. 156–164 (in Russian).
4. Stenis J., Romanov M., Hogland W. Analysis and Classification of Modern Methods of Ecological Normalization of Anthropogenic Load: Russia vs. the West // The Open Environmental Engineering Journal. 2011. Vol.4. Pp. 181–189.
5. Szabo H.M., Tuhkanen T.T. UV/VIS Spectroscopy as a method to characterize well water quality // VATTEN – Journal of Water Management and Research. 2016. Vol. 72. Pp. 169–175.
6. Potter B.B., Wimsatt J.C. Method 415.3 – Measurement of total organic carbon, dissolved organic carbon and specific UV absorbance at 254 nm in source water and drinking water (EPA Document #: EPA/600/R-09/122). U.S. Environmental Protection Agency, Cincinnati, Ohio, 2009. 56 p.
7. Comber S.D.W., Gardner M.J., Gunn A.M. Measurement of absorbance and fluorescence as potential alternatives to BOD // Environmental Technology. 1996. Vol. 17. Pp. 771–776.
8. Edzwald J., Kaminski G.S. A practical method for water plants to select coagulant dosing // Journal of the New England Water Works Association. 2009. Vol. 123. Pp. 15–31.
9. Biogeochemistry of Small Catchments: A Tool for Environmental Research. Edited by B. Moldan and J.Cerny. SCOPE Published by John Wiley & Sons Ltd, 1994, 420p.
10. Воробьев Н.И. Применение измерения электропроводности для характеристики химического состава природных вод. Изд-во АН СССР, М., 1963, 141 с.
11. De Sousa D.N.R., Mozeto A.A., Carneiro R.L., Fadini P.S. Electrical Conductivity and Emerging Contaminant as Markers of Surface Freshwater Contamination by Wastewater // Science of the Total Environment. 2014. Vol. 484. Pp. 19–25.
12. Hudson N.J., Baker A., Reynolds D. Fluorescence analysis of dissolved organic matter in natural, waste and polluted waters – a review // River Res. Appl. 2007. Vol. 23(6). Pp. 631–649.
13. Coble P.G., Lead J., Baker A., Reynolds D.M., Spencer R.G.M. Aquatic Organic Matter Fluorescence. Cambridge University Press. 2014, 375 p.
14. Молодкина Л.М., Андрианова М.Ю., Чусов А.Н. Спектрофлуориметрия в изучении динамики разложения биоорганических отходов // Научно-технические ведомости СПбГПУ. Естественные и инженерные науки. 2012. № 1(142). С. 243–250.
15. Henderson R.K., Baker A., Murphy K.R., Hambly A., Stuetz R.M., Khan S.J. Fluorescence as a potential monitoring tool for recycled water systems: A review // Water Research. 2009. Vol. 43. Pp. 863–881.
16. Baker A, Inverarity R. Protein-like fluorescence intensity as a possible tool for determining river water quality // Hydrological Processes. 2004. Vol. 18(15). Pp. 2927–2945.
17. Hudson N., Baker A., Ward D., Reynolds D.M., Brunsdon C., Carliell-Marquet C., Browning S. Can fluorescence spectrometry be used as a surrogate for the biochemical oxygen demand (BOD) test in water quality assessment? An example from South West England // Science of the Total Environment. 2008. Vol. 391(1). Pp. 149–158.
18. Baker A. Fluorescence excitation-emission matrix

biochemical oxygen demand (BOD) test in water quality assessment? An example from South West England. *Science of the Total Environment*. 2008. Vol. 391(1). Pp. 149–158.

18. Baker A. Fluorescence Excitation-Emission Matrix Characterization of Some Sewage-Impacted Rivers. *Environ. Sci. Technol.* 2001. Vol. 35. Pp. 948–953.
19. Reynolds D.M. The differentiation of biodegradable and non-biodegradable dissolved organic matter in wastewaters using fluorescence spectroscopy. *Journal of Chemical Technology and Biotechnology*. 2002. Vol. 77(8). Pp. 965–972.
20. Wu J., Pons M.N., Potier O. Wastewater fingerprinting by UV–visible and synchronous fluorescence spectroscopy. *Water Science and Technology.* 2006. Vol. 53(4–5). Pp. 449–456.
21. Cumberland S.A., Baker A.. The freshwater dissolved organic matter fluorescence-total organic carbon relationship. *Hydrological Processes*. 2007. Vol. 21(16). Pp. 2093–2099.
22. Andrianova M.J., Bondarenko E.A., Krotova E.O., Chusov A.N. Comparison of chemical and optical parameters in monitoring of urban river Okhta. *EESMS 2014 - 2014 IEEE Workshop on Environmental, Energy and Structural Monitoring Systems, Proceedings* . Naples, Italy, 2014. Pp. 198–202.
23. *Doklad ob ekologicheskoy situatsii v Sankt-Peterburge v 2015 godu* [Report on ecological situation in Saint-Petersburg in 2015]. SPb: OOO «Sezam-print», 2016, 168 c. Report on ecological situation in St.Petersburg in year 2015. 2016, 168p. (in Russian) URL: http://www.infoeco.ru/assets/files/Doklad/doklad_2015.pdf
24. *Doklad ob ekologicheskoy situatsii v Sankt-Peterburge v 2014 godu* [Report on ecological situation in Saint-Petersburg in 2014]. SPb.: OOO «Diton» 2015, 180 c.
25. Chechevichkin V.N., Vatin N.I. Specifics of surface runoff contents and treatment in large cities. *Magazine of Civil Engineering*. 2014. Vol. 50(6). Pp. 67–74.
26. Vatin N.I., Grekov M.A., Leonov L.V., Probirskiy M.D., Rublevskaya O.N., Chechevichkin A.V., Yakunin L.A.. Rezultaty testovoy ekspluatatsii filtra FOPS® dlya ochistki livnevogo stoka s selitebelnoy territorii Sankt-Peterburga [Results of test exploitation of filter FOPS for stormwater treatment from dwelled areas in St.Petersburg]. *Vodosnabzheniye i sanitarnaya tekhnika*. 2017. No. 1. Pp. 58–65.
27. Nezhikhovskiy R.A. *Reka Neva i Nevskaya guba* [River Neva and Neva Bay]. L., Gidrometeoizdat. 1981. 112 p.
28. *Resursy poverkhnostnykh vod SSSR. Tom 2. Kareliya i Severo-zapad. Chast 3. Gidrograficheskiye opisaniya rek i ozer* [Surface water resources of the USSR. Volume 2. Karelia and the North-West. Part 3 Hydrographical descriptions of rivers and lakes]. L.: Gidrometeoizdat, 1972. 959 p.
29. *Skhema kompleksnogo ispolzovaniya i okhrany vodnykh obyektov basseyna reki Heva. Kniga 2. Otsenka ekologicheskogo sostoyaniya i klyuchevyye problemy rechnogo basseyna*. [Scheme of integrated use and protection of water bodies in the Neva River basin. Book 2. Assessment of the ecological status and key problems of the river basin]. SPb, 2015, 141s. URL: http://www.nord-west-water.ru/activities/ndv/ scheme-of-complex-use-and-protection-of-water-bodies-in-the-basin-of-the-river-neva/
30. Zuyeva N.V., Galtsova V.V., Dmitriyev V.V., Stepanova A.B. Ispolzovaniye strukturnykh kharakteristik soobshchestv makrofitov kak indikatora ekologicheskogo sostoyaniya malykh rek zapada Leningradskoy oblasti. [Use of structural characteristics of macrophyte communities as an indicator of the ecological status of small rivers in the west of the Leningrad Region] *Vestnik Sankt-peterburgskogo universiteta. Seriya 7. Geologiya. Geografiya*. 2007. Vol. 4. Pp. 60–71.

characterization of some sewage-impacted rivers // Environ. Sci. Technol. 2001. Vol. 35. Pp. 948–953.

19. Reynolds D.M. The differentiation of biodegradable and non-biodegradable dissolved organic matter in wastewaters using fluorescence spectroscopy // Journal of Chemical Technology and Biotechnology. 2002. Vol. 77(8). Pp. 965–972.
20. Wu J., Pons M.N., Potier O. Wastewater fingerprinting by UV–visible and synchronous fluorescence spectroscopy // Water Science and Technology. 2006. Vol. 53(4–5). Pp. 449–456.
21. Cumberland S.A., Baker A. The freshwater dissolved organic matter fluorescence-total organic carbon relationship // Hydrological Processes. 2007. Vol. 21(16). Pp. 2093–2099.
22. Andrianova M.J., Bondarenko E.A., Krotova E.O., Chusov A.N. Comparison of chemical and optical parameters in monitoring of urban river Okhta // EESMS 2014 - 2014 IEEE Workshop on Environmental, Energy and Structural Monitoring Systems, Proceedings. 2014. Vol. 6. Pp. 198–202.
23. Доклад об экологической ситуации в Санкт-Петербурге в 2015 году. СПб: ООО «Сезам-принт», 2016, 168 с.
24. Доклад об экологической ситуации в Санкт-Петербурге в 2014 году. СПб.: ООО «Дитон» 2015, 180 с.
25. Чечевичкин В.Н., Ватин Н.И. Особенности состава и очистки поверхностного стока крупных городов // Инженерно-строительный журнал. 2014. № 6(50). С. 67–74.
26. Ватин Н.И., Греков М.А., Леонов Л.В., Пробирский М.Д., Рублевская О.Н., Чечевичкин А.В., Якунин Л.А.. Результаты тестовой эксплуатации фильтра ФОПС® для очистки ливневого стока с селитебельной территории Санкт-Петербурга // Водоснабжение и санитарная техника. 2017. № 1. С. 58–65.
27. Нежиховский Р.А. Река Нева и Невская губа. Л., Гидрометеоиздат, 1981. 112с.
28. Ресурсы поверхностных вод СССР. Том 2. Карелия и Северо-запад. Часть 3 Гидрографические описания рек и озер. Л.: Гидрометеоиздат, 1972, 959 с.
29. Схема комплексного использования и охраны водных объектов бассейна реки Нева. Книга 2. Оценка экологического состояния и ключевые проблемы речного бассейна. СПб, 2015, 141с. URL: http://www.nord-west-water.ru/activities/ndv/scheme-of-complex-use-and-protection-of-water-bodies-in-the-basin-of-the-river-neva/
30. Зуева Н.В., Гальцова В.В., Дмитриев В.В., Степанова А.Б. Использование структурных характеристик сообществ макрофитов как индикатора экологического состояния малых рек запада Ленинградской области // Вестник Санкт-Петербургского университета. Серия 7. Геология. География. 2007. № 4. С. 60–71.
31. Бондаренко Е.А., Ильина Х.В., Андрианова М.Ю., Чусов А.Н. Основные неорганические ионы и электропроводность загрязненных водотоков // Инженерно-строительный журнал. 2016. № 8(68). С. 37–44.
32. Sawyer C.N., McCarty P.L., Parkin G.F.. Chapter 24 - Chemical Oxygen demand // Chemistry for Environmental Engineering and Science. 2003. Pp. 625–629.
33. Mobed J.J., Hemmingsen S.L., Autry J.L., McGown L.B. Fluorescence characterization of IHSS humic substances: total luminescence spectra with absorbance correction // Env. Sci. Technol. 1996. Vol. 30. Pp. 3061–3065.
34. Tavernier S. Experimental Techniques in Nuclear and Particle Physics. Springer. 2010, 306 p.
35. ГН 2.1.5.1315-03 Предельно допустимые концентрации (ПДК) химических веществ в воде водных объектов хозяйственно-питьевого и культурно-бытового водопользования.

31. Bondarenko E.A., Il`ina Kh.V., Andrianova M. Ju., Chusov A. N.. Main inorganic ions and electric conductivity of polluted urban streams. *Magazine of Civil Engineering. 2016.* Vol. 8. Pp. 37–44.
32. Sawyer C.N., McCarty P.L., Parkin G.F.. Chapter 24 - Chemical Oxygen demand. *Chemistry for Environmental Engineering and Science.* 2003. Pp. 625–629.
33. Mobed J.J., Hemmingsen S.L., Autry J.L, McGown L.B. Fluorescence characterization of IHSS humic substances: total luminescence spectra with absorbance correction. *Env. Sci. Technol.* 1996. Vol. 30. Pp. 3061–3065.
34. Tavernier S. *Experimental Techniques in Nuclear and Particle Physics*. Springer. 2010, 306 p.
35. *GN 2.1.5.1315-03* Predelno dopustimyye kontsentratsii (PDK) khimicheskikh veshchestv v vode vodnykh obyektov khozyaystvenno-pityevogo i kulturno-bytovogo vodopolzovaniya [Maximal allowable concentrations of chemical substances in waters of water objects for economic-drinking and cultural-household use].(rus)
36. *SanPiN 2.1.5.980-00.* Gigiyenicheskiye trebovaniya k okhrane poverkhnostnykh vod. Sanitarnyye pravila i normy [Hygienic requirements for surface waters protection. Sanitary norms and rules]. (in Russian).
37. Daniel M., Monteneblo A., Bernardes M., et al. Effects of Urban Sewage on Dissolved Oxygen, Dissolved Inorganic and Organic Carbon, and Electrical Conductivity of Small Streams Along Graduate of Urbanization in the Piracicaba River basin. *Water, Air, and Soil Pollution.* 2002. Vol. 136. Pp. 189–206.
38. *Otvedeniye i ochistka stochnykh vod Sankt-Peterburga* [Wastewater disposal and treatment]. Eds. F.V. Karmazinov. St. Peterburg: Izdatelstvo «Novyy zhurnal», 2002. 668 p. (rus).
39. *Wastewater Engineering: Treatment and Reuse*. Metcalf and Eddy Inc. 2003. McGraw-Hill, 1780 p.
40. Sgroi M., Roccaro P., Korshin G.V., Vagliasindi F. Monitoring the Behavior of Emerging Contaminants in Wastewater-Impacted Rivers Based on the Use of Fluorescence Excitation Emission Matrixes (EEM). *Environmental Science & Technology*. 2017. Vol. 51(8). Pp. 4306–4316.
41. Vodacek A., Philpot W.D. Environmental effects on laser-induced fluorescence spectra of natural waters. *Remote Sensing of Environment*. 1987. Vol. 21(1). Pp. 83–95.

36. СанПиН 2.1.5.980-00. Гигиенические требования к охране поверхностных вод. Санитарные правила и нормы.
37. Daniel M., Monteneblo A., Bernardes M., et al. Effects of urban sewage on dissolved oxygen, dissolved inorganic and organic carbon, and electrical conductivity of small streams along graduate of urbanization in the Piracicaba river basin // Water, Air, and Soil Pollution. 2002. Vol. 136. Pp. 189–206.
38. Отведение и очистка сточных вод Санкт-Петербурга / Коллектив авторов. С.-Петербург: Издательство «Новый журнал», 2002 г. Под общей редакцией Ф.В. Кармазинова, 668с.
39. Wastewater Engineering: Treatment and Reuse. Metcalf and Eddy Inc. 2003. McGraw-Hill, 1780 p.
40. Sgroi M., Roccaro P., Korshin G.V., Vagliasindi F. Monitoring the behavior of emerging contaminants in wastewater-impacted rivers based on the use of fluorescence excitation emission matrixes (EEM) // Environmental Science & Technology. 2017. Vol. 51(8). Pp. 4306–4316.
41. Vodacek A., Philpot W.D. Environmental effects on laser-induced fluorescence spectra of natural waters // Remote Sensing of Environment. 1987. Vol. 21(1). Pp. 83–95.

Khristina Il'ina,
+7(812)297-59-28; Ilin220396@yandex.ru

Nadezhda Gavrilova,
+7(812)552-76-66; spbstung@yandex.ru

Ekaterina Bondarenko,
+7(812)297-59-28; katyushka-bond@mail.ru

Maria Andrianova,
+7(812)297-59-28; maandrianova@yandex.ru

Alexander Chusov,
+7(921)940-09-25; chusov17@mail.ru

Христина Владиславовна Ильина,
+7(812)297-59-28;
эл. почта: Ilin220396@yandex.ru

Надежда Михайловна Гаврилова,
+7(812)552-76-66;
эл. почта: spbstung@yandex.ru

Екатерина Анатольевна Бондаренко,
+7(812)297-59-28;
эл. почта: katyushka-bond@mail.ru

Мария Юрьевна Андрианова,
+7(812)297-59-28;
эл. почта: maandrianova@yandex.ru

Александр Николаевич Чусов,
+7(921)940-09-25; эл. почта: chusov17@mail.ru

Il'ina Kh.V., Gavrilova N.M., Bondarenko E.A., Andrianova M.Ju., Chusov A.N. Express-techniques of polluted suburban stream waters study. *Magazine of Civil Engineering*. 2017. No. 8. Pp. 241–254. doi: 10.18720/MCE.76.21.

doi: 10.18720/MCE.76.22

Creep behavior of geosynthetics by temperature accelerated testing

Ползучесть геосинтетических материалов при ускоренных температурных испытаниях

S.G. Srungeri,
N.N. Alekseev,
I.A. Kovalenko,
O.N. Stolyarov,
Peter the Great St. Petersburg Polytechnic University, St. Petersburg, Russia

Студент С. Срунгери,
студент Н.Н. Алексеев,
студент И.А. Коваленко,
канд. техн. наук, доцент О.Н. Столяров,
Санкт-Петербургский политехнический университет Петра Великого, г. Санкт-Петербург, Россия

Key words: geosynthetics; viscoelastic properties; creep; step isothermal method; prediction

Ключевые слова: геосинтетические материалы; вязкоупругие свойства; ползучесть; метод ступенчатых изотерм; прогнозирование

Abstract. Predicting the creep behaviour of geosynthetics is very important for determining the design life of geosynthetic based structures. In this paper, geogrids and geotextiles made of two major types of synthetic polymer namely, polyester and polypropylene were investigated for accelerated creep test. In short-term measurements, creep was accelerated by temperature in equal steps. As a result of the analysis, predicted creep curves for up to 30 years of design life were obtained by the stepped isothermal method. The predicted creep deformation for a period of 30 years has been analyzed. The geogrid samples made of polyester showed better creep resistance compared to polypropylene geogrids. Geosynthetic materials made of polyester are more suitable for various loaded applications as a reinforcement function.

Аннотация. Прогнозирование ползучести геосинтетических материалов является необходимым для определения расчетного срока службы конструкций с их применением. В данной работе были проведены испытания на ползучесть георешеток и геополотен, изготовленных из двух основных типов синтетических полимеров - полиэфира и полипропилена, используемых при производстве геосинтетических материалов. Прогнозируемые кривые были получены с помощью метода ступенчатых изотерм. При кратковременных измерениях деформация ползучести ускорялась при помощи увеличения температуры равными шагами. Проведено сравнение прогнозируемой деформации ползучести исследуемых образцов геосинтетических материалов на период до 30 лет. Образцы геосинтетических материалов из полиэфира показали лучшую устойчивость к деформации ползучести по сравнению с образцами, изготовленными из полипропилена. При практическом применении геосинтетические материалы из полиэфира являются предпочтительными при использовании в функции армирования.

Introduction

In world of innovation and rapid development, the changes occurring in the area of construction with respect to material properties of engineering structures is an important aspect of economical and efficient construction. Geosynthetics are polymeric products used to improve or resolve the problems in various civil engineering and geotechnical applications [1, 2]. They find there usage in almost all the applications of civil engineering [4, 14], such as geotechnical, hydraulic, transportation, environmental, and developmental applications such as roads [3, 6, 8, 10–12], airfields, embankments [9, 13, 16], retaining structures [5, 7, 15], reservoirs, canals, dams, erosion control, sediment control, landfill liners, mining, aquaculture and agriculture. In addition to the conventional structural materials like steel, concrete and other building material, geosynthetics find application in all fields of civil engineering due to their unprecedented high performance properties. With the recent development of geosynthetic reinforcement, the scope of usage has increased fourfold as it has both economical and eco-friendly benefits. Therefore, different forms of geosynthetic reinforcement such as geotextile, geogrid and geosynthetic strip reinforcement are developed.

Срунгери С., Алексеев Н.Н., Коваленко И.А., Столяров О.Н. Ползучесть геосинтетических материалов при ускоренных температурных испытаниях // Инженерно-строительный журнал. 2017. № 8(76). С. 255–265.

The viscoelastic properties of geosynthetics have been widely investigated by many researchers in the last three decades. Over the years, the accelerated test methods have gained popularity for predicting the long-term properties of geosynthetics materials along with conventional creep tests [18–24]. These methods include SIM – Stepped Isothermal Method [17, 25–27] and TTS - Time Temperature Superposition Method [28]. The viscoelastic properties mainly indicate the long-term strength of geosynthetic materials due to uneven forces resulting the deformation of the material over time. It is of utmost importance in evaluating the long-term structural durability of geosynthetic materials depicting the process of creep, as it is subjected to constant load in real working conditions. In some of the implementations, geosynthetics undergoes the process of reduction of internal forces due to fixation of their structure and dimensions.

Creep accelerated temperature test generally includes TTS and SIM tests. TTS is the concept; by increasing the temperature accelerates the creep rate. This acceleration reduces the time needed for a given amount of creep to occur. Thus, elevated temperature creep experiments can achieve the result in a short time, which can take many days, weeks or even years, to accomplish at laboratory-ambient temperature. On the other hand, SIM is a single specimen method in which the temperature is varied gradually for a given time at constant load, where the changes in deformation are measured as a function of time. Both the tests are used for characterization of viscoelastic properties of polymeric materials [28]. Lee et al [32] stated that the creep reduction of geosynthetics can be determined through conventional creep test and accelerated creep tests. They tested geotextiles made of coated PET yarns in TTS and SIM modes and the test results vary under different use of data from various methods. Zornberg et al [33] conducted a temperature-accelerated tensile testing program to characterize a woven polypropylene geotextile. Their test program was divided into three major steps and included: loading tensile tests at room and elevated temperatures; conventional and accelerated creep tests; and rapid loading tensile tests conducted after sustained creep loading. 8-hours long temperature accelerated test was used to predict the geotextile behavior for periods beyond 100 years at various load levels using SIM test. As a result, a new approach was developed to quantify the residual tensile strength of geosynthetics. Hsiesh et al [17] studied five different types (woven and warp-knitted) of polyester geogrids with tensile strengths ranging from 100 to 400 kN/m by conventional and SIM tests. They concluded that the results of SIM tests require a minimum of 6 to 8 steps to predict the creep behavior beyond 75-years. In addition, they showed that knitted geogrids showed higher creep strains than woven geogrids. Mok et al [34] presents the results of compressive creep deformations beyond 100,000 h of two types of geonets. S.R. Allen [35] used SIM of accelerated compression creep to measure the time dependent loss of thickness and porosity (and thus flow) of planar geosynthetic drains. He proposed some changes in testing approach of the existing product specification, design procedures and economy of cost. As a result, he concluded that there is opportunity to reach for real-time flow tests at pre-established time-dependent thicknesses and presents the test results with special emphasis on thickness. Zou et al [26] presents the creep behavior and stress relaxation of high-density polyethylene (HDPE) geogrid at four different load levels of 20%, 40%, 50% and 60% of ultimate tensile strength. Numerical modeling using finite element method has also been used to assess the impact of geogrids on the long-term performance of reinforced soil retaining wall on the deep soft soil foundation. The results shows the constitutive model to ensure the stability of the retaining wall and indicates that the working stress of geogrids should be less than 40% of ultimate tensile strength, and the high strength geogrids should be adopted in the middle of the wall or the spacing of geogrid reinforced layers should be reduced. The deep soft soil foundation, which is treated by piles, can ignore the creep behavior of soft soil. Hsuan et al [28] has studies and analyzed the creep behavior of HDPE geogrids using both TTS and SIM accelerated creep tests. They concluded stating that the application of the SIM test is well suited for PET geogrid whereas for HDPE georgids, the application of SIM has not been well established. The study confirmed that values for temperature steps of 7°C and a dwell time of 10,000 seconds are suitable for HDPE geogrids and the results of primary and secondary creep at 10%, 20%, 30% and 40% of ultimate tensile strength. Jin et al [29] presented the creep property of geogrids measured using three methods; conventional tests were carried out in comparison to TTS and SIM. All three methods showed similar behavior, but it turned out that there is more voltage to the SIM method at a higher temperature. Reducing coefficients for long-term strength and limited deformation were similar in each method. Tong et al [30] evaluated the creep tests were carried out for polymeric geogrids at various load levels and at an ambient temperature of 40 and 60 °C. Experimental results showed that the ambient temperature has a significant effect on the geogrid creep behavior, while the geogrid also shows a significant dependence of the load level. A certain creep strain during the first hour was greater than the total creep strain by about 80%. In the end, the specified parameters are proposed for predicting long-term creep behavior. Along with thermoplastic yarns and fabrics, in [31] the SIM test was applied to aramid fibers. However, the behavior of aramid fibers under the high temperature is differing to thermoplastic fibers. With increase of temperature, the shrink of fibers occur. Therefore, the correction in the form of vertical shift should be applied.

Creep accelerated test methods (SIM and TTS) are often used as it significantly reduces the test time by several order of magnitude and obtain satisfactory results and predicted curves. The use of this method is has many advantages in experimental analysis but it requires specialized equipment like computed controlled universal testing machines with thermochamber.

The aim of this work is to predict the creep deformation of the major types of geogrids and geotextiles using an accelerated test method. The objective of this work included:

1) study the creep of geosynthetic samples by the method of temperature acceleration using the stepped isothermal method;

2) comparative analysis of geosynthetic samples having different structure;

3) determination of characteristics in the temperature acceleration of creep deformation of geosynthetic samples made of PET and PP;

4) prediction of creep deformation and determination of the effectiveness of their practical application up to 30 years of the estimated service life, depending on the type of geosynthetics and the type of raw material.

Experimental materials and methods

Materials

This paper presents the work on two major types of geosynthetics, geotextile and geogrids. The geotextile fabrics include woven fabric made of PP slit yarn (indicated as 1-GTX), used majorly as reinforcement fabric and nonwoven thermobonded fabrics made of PP fibers (denoted as 2-GTX) used majorly as filter and separation of material layers. The geogrids studied in this work find application in various civil engineering structures, and are manufactured by textile and plastic processing technologies. The main purpose of the geogrid is the reinforcement of structures. The test sample 1-GGR is a geogrid with a cell size of 35 by 35 mm, made of high-strength polyester yarns. This sample further includes an additional nonwoven fabric. Test samples 2-GGR and 3-GGR are manufactured using plastic processing technology. The orientation of the samples reinforcing ribs is in bi-axial and uni-axial direction respectively. In case of biaxial stretched geogrid, the nodal joints of the geogrids form peculiar stress concentrators that can affect the properties of the geogrid. In unidirectional geogrid, longitudinal ribs are connected by additional non-load bearing ribs. The sample 4-GGR is a woven geogrid with 22 x 22 mm mesh cells, which is additionally coated with PVC to increase dimensional stability. The characteristic of the investigated samples are listed in Table 1. These two types of polymer are dominant in the market of geosynthetics.

Table 1. Characteristics of the geogrids

	Sample designation	Structure	Raw materials	Mass per unit area, g/m^2
1	1-GTX	Woven slit yarn geotextile fabric.	PP	400
2	2-GTX	Nonwoven thermobonded geotextile fabric.	PP	90
3	1-GGR	Warp-knitted geogrid with layer of nonwoven fabric, mesh size: 35×35	PET	285
4	2-GGR	Biaxial extruded geogrid, mesh size: 35×35	PP	530
5	3-GGR	Uniaxial extruded geogrid, mesh size: 42×42	PP	294
6	4-GGR	Woven PVC coated geogrid, mesh size: 22×22	PET	250

Methods

The testing machine used for conducting the SIM analysis for the materials mentioned in the above table is computer controlled high temperature electronic universal testing machine Instron 5965 with thermochamber, which enables us the mechanical testing of materials across a range of temperatures, humidity and caustic conditions which are ideal for conducting tension, compression testing of various materials. It also features a temperature-controlled chamber that is mounted to the back panel for convenient access in which hot and cold air is forced to circulate and re-circulate around the specimen to offer thermal stability (Figure 1). The front panel clearly displays the set time and loading points. Additionally, air circulates around the outer skin of the chamber to keep it neat and cool.

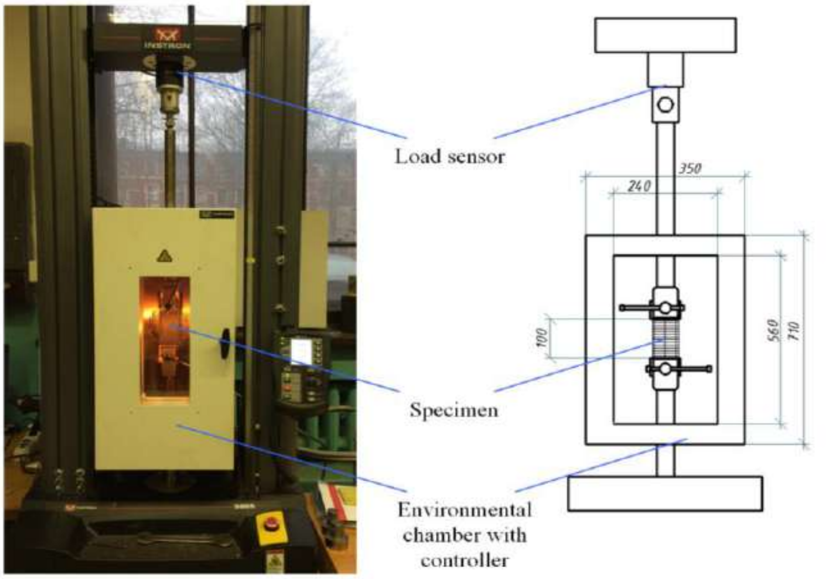

Figure 1. Experimental set-up

Considering the equipment is calibrated and ready for testing. The environment for testing is dry as the effect of elevated temperature is to reduce the humidity of ambient air without special control. The standard reference temperature is taken as 20±1 ^{0}C. Utmost importance has to be taken to ensure uniform thickness of the test specimen. The gauge length of the specimen was taken as 100 mm. Time, temperature, displacements and tensile load data were collected at a minimum rate and recorded using a automatic data acquisition system on the computer and were analyzed. Data were collected every second to adequately capture the strain response. The temperature steps for SIM are taken at 7^{0}C for PP samples and 14^{0}C for PET samples as it is recommended in [36]. In this case, the readings are taken for the temperature steps as per the specimen and creep curves were obtained at the level of 30% of ultimate tensile strength.

Figure 2 indicates the model of temperature steps taken in this analysis. In order to provide uniform testing results and comparison of sample results, the above temperature steps was adapted as mentioned in [36]. Here the black and red line in the graph indicates time vs. temperature steps for PET and PP samples respectively. At room temperature, i.e. 20^0, all the samples are under constant load for a span of 7200 seconds (two hours) and the next six hours the samples were exposed to higher temperatures. The creep strain behavior of the sample was noted during constant load portions of the test within the time.

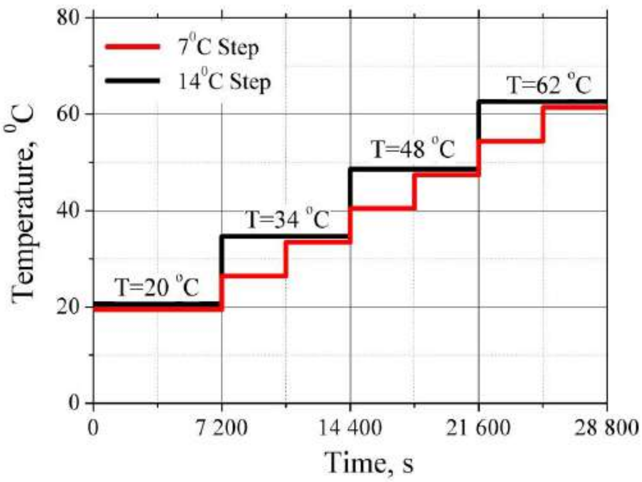

Figure 2. Experimental temperature steps

The computation procedure for SIM is indicated in Figure 3. This procedure includes four basic steps.

1) Stress and creep strain vs. linear time: This graph shows the raw data of the specimen tested under constant applied load. The creep strains are shown in the figure as a function of time at each temperature steps. The different color indicates the raw data at each temperature exposure scaled to its reference temperature of the specimen starting from room temperature 20 ^{0}C to 62^0 C.

2) Creep modulus vs. log time: The creep strains are shown in the figure as a function of time at each temperature steps. A shift time is selected and tabulated so that the final slope of strain time curve at a specific temperature step matches the initial slope of the strain time curve at the subsequent temperature step. The creep data at each temperature exposure is scaled so that stain rate corresponds to that of the reference temperature. The scaled data is plotted on a semi-logarithmic scale as presented.

3) Master creep modulus vs. log time after rescaling and applying horizontal shift factor. The scaled creep curve segments correspond to the reference temperature as shown in the figure. Appropriate horizontal shift factor was applied. The curve at 20^0 C was selected as a basis point and then the following curves were shifted along the x- (time) axis to obtain smooth master curve.

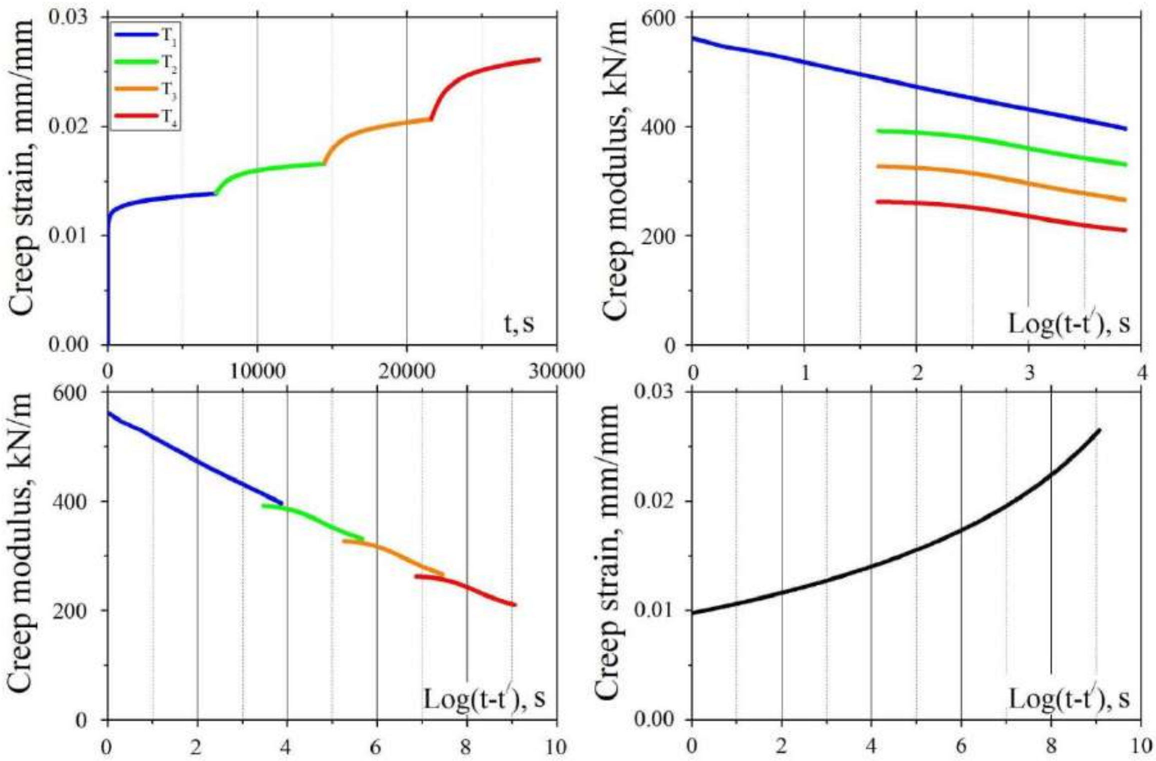

Figure 3. Stepped Isothermal method

Master creep strain vs. log time after rescaling and applying horizontal shift factor: Master curve can be defined by composing into a single curve of creep responses measured at different isothermal exposures during SIM testing. Master curve was obtained superimposing the creep strain responses measured at different temperatures by horizontal shifting. The rescaling for the shifting steps was done accordingly to achieve a smooth master curve.

In order to evaluate the long-term creep properties of various types of geosynthetics, the load level of 30% of T_{max} was chosen and temperature accelerated time was set at eight hours. As it was recommended in [33], these experiments parameters gave reliable results for comparative analysis.

Results and Discussions

Tensile properties

As noted above, geosynthetic materials have mechanical properties in a fairly wide range. In this work, the selected test samples also cover a wide range of mechanical behavior of geosynthetic materials. The tensile properties of the samples were determined using the Instron 5965 universal testing machine. Samples of geotextile fabrics were prepared in the form of strips with a width of 50 mm and a length of 200 mm. The gauge length was 100 mm. The samples of the geogrid were tested along the single rib. The crosshead speed was 50 mm/min.

Figure 4 shows the tensile curves of the samples investigated in the longitudinal (machine) direction. The curves obtained show the samples various tensile behavior. All samples tested, except 2-GTX, are intended for use in the reinforcement function. As a result, their tensile behavior is characterized by a high maximum breaking load and low elongation at maximum load. Sample 2-GTX demonstrates the cardinally opposite tensile behavior. The elongation of the specimen at maximum load is several times greater than that of the reinforcing samples. The tensile strength thus leaves the minimal values.

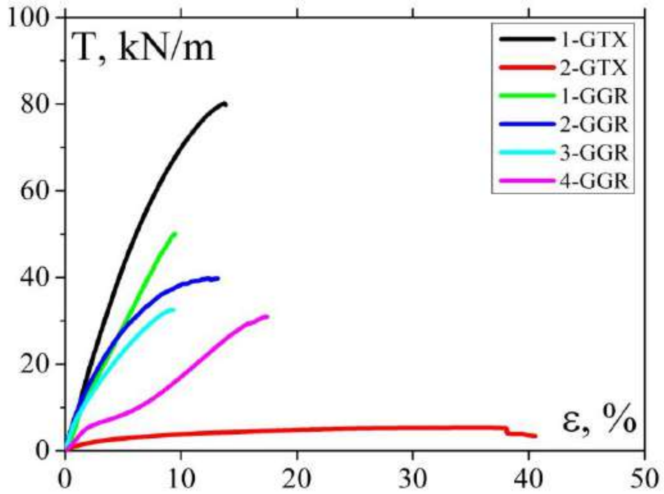

Figure 4. Tensile diagrams of investigated samples

The tensile strength of a geosynthetic is expressed in kilonewtons per meter (kN/m) directly from the data obtained from the tensile testing machine as follows:

$$T_{max} = F_{max} \cdot c, \tag{1}$$

where F_{max} is the recorded maximum load, in kilonewtons; c is the specimen width.

For geotextile fabrics c is determined as follow:

$$c = \frac{1}{B}, \tag{2}$$

where B is the specimen nominal width, in meters.

For geogrids c is determined as follow:

$$c = \frac{N_m}{N_s}, \tag{3}$$

where N_m is the minimum number of tensile ribs within a 1 m width of the geogrid; N_s is the number of tensile elements within the test specimen.

In addition to the tensile strength, the following characteristics were determined: strain (in percent) at maximum load and load at specified strain (at 2%). The latter characteristic is widely used for geosynthetic materials and expresses the tensile stiffness of the specimen. The application of this characteristic is due to the complexity of applying the tangent line to the initial part of the tensile curve due to its nonlinearity. The results for tensile strength, strain at maximum load and tensile load at specified strain of 2% are given in Figure 5a-5c respectively.

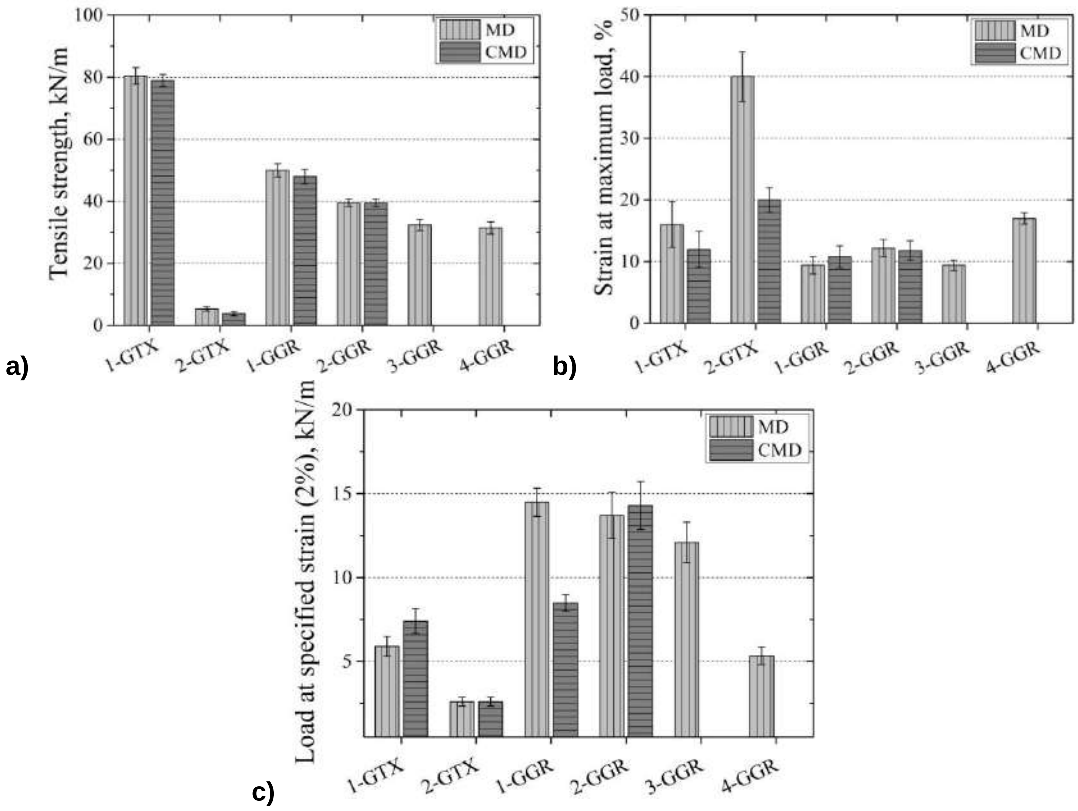

Figure 5. Results of tensile test: tensile strength (a), strain at maximum load (b) and tensile load at specified strain of 2% (c)

Analyzing the obtained data, it should be noted that the tensile strength of the investigated samples varies significantly. The maximum tensile strength is provided by the 1-GTX sample of the order of 80 kN/m, the minimum strength is the sample of 2-GTX of the order of 5 kN/m. The tensile strength of the investigated geogrid samples lies in the range of 30–40 kN/m that is typical for reinforcement function. The strain at the maximum load in the samples also varies significantly. The strain of reinforcing geogrids is in the range of 10–15 %, for the geotextile sample of 2-GGR it is dozens of percents. The tensile load at specified strain of 2 % also varies significantly for different samples. The difference between the minimum value for a 2-GTX sample and the maximum for a 1-GTX sample is one order of magnitude.

SIM analysis

SIM curves were obtained for all the samples in machine direction. The curves are shown in Figure 6. As can be seen from the data obtained, all curves have significantly different deformation behavior. Especially noticeable is the difference in the increase in elongation between the samples made of PP and PET. The first group is characterized by a noticeable increase in deformation when heated from the first temperature step (from 7200 s). The 2-GTX sample, made of PP fibers, experiences the greatest deformation. Unlike PP samples, the samples of the second group (1-GR and 4-GR) made of PET, although they show an increase in the creep rate, but not so significant. The obtained curves were analyzed by the stepped isothermal method described above. Each curve was divided into equal parts according to temperature steps, recalculated into a creep modulus. Then, a shift along the horizontal time axis was carried out, and the generalized master curve of the creep modulus obtained in this way was rearranged into a creep curve as shown in Figure 3.

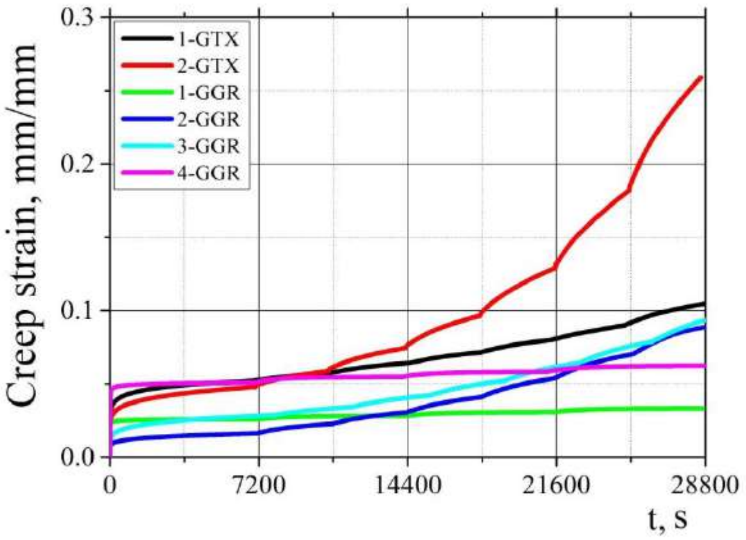

Figure 6. Results of SIM test

The results of analyzing the curves are shown in Figure 7. Along with the logarithmic time scale, an additional time grid is added, which allows estimating the predicted creep deformation of the geosynthetic material depending on the design life. Considering the dependence of the creep strain on time, it can be seen that the geosynthetic samples made of PET have a gradual linear slight increase in strain over the time. The predicted deformation of samples made of PP significantly increases already at relatively short times (for example, 1 day or 1 month). For longer times, the deformation increases even more, and, for example, for a 2-GTX sample, it becomes practically commensurable with a failure deformation. In order to assess the deformation achieved at a certain point in time, two time interval were taken, equal to 1 year and 30 years. The values of the predicted deformation for these time intervals are plotted in Figure 8. It can be seen from the histograms shown that samples made of PET fibers (1-GGR and 4-GGR) have the least increase in strain, as predicted earlier. In addition, they also have a minimal creep deformation among all the samples studied. Samples made of PP show a huge increase in deformation. Moreover, for a 2-GTX sample it is not possible to estimate the deformation after reaching 30 years, because during the test period, it practically reached a pre-failure deformation. On average, the predicted deformation of PP samples after 30 years is 8–12 %, which is quite a lot. The predicted deformation of PET samples is 2.6 % and 6.3 % for 1-GGR and 4-GGR samples, respectively, which is more acceptable for the reinforcement function.

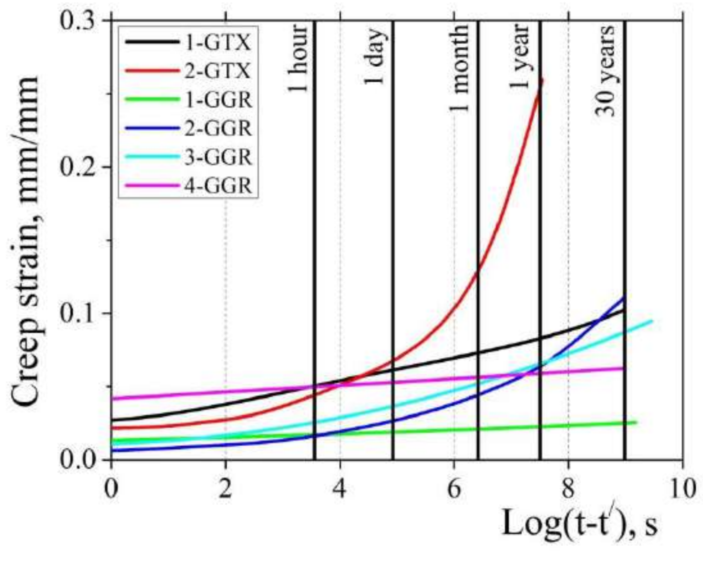

Figure 7. Predicted curves by SIM test

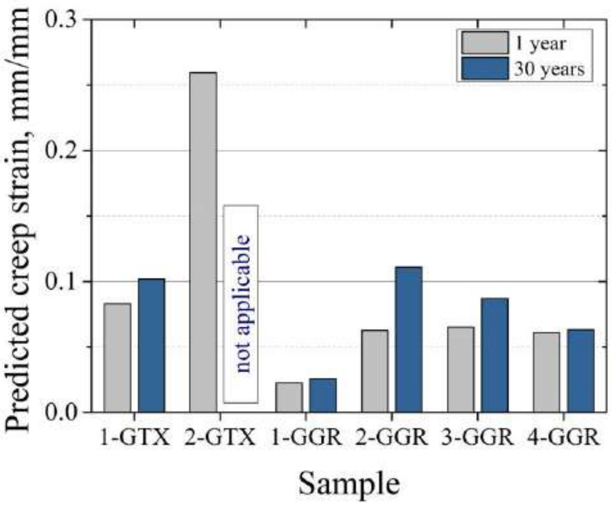

Figure 8. Predicted creep strain after 1 and 30 years

The results of this research provide useful information with regard to structural design applications of geotextiles and geogrids mainly concerning reinforcement function. The graphs presented show tensile, creep strain and creep deformation properties analyzed by SIM test at elevated temperature of the materials. Observing the graphs we can clearly conclude that woven split yarn and non-woven thermobonded geotextiles show maximum and minimum tensile behavior compared to all the other materials mentioned, whereas creep behavior of non-woven thermobonded geotextile shows highest deformation and wrap-knitted geogrid with a nonwoven fabric layer shows the least deformation comparatively. Therefore, this research can gives a better understanding of the results of temperature accelerated method of six different PP and PET samples of geosynthetics used primarily for reinforcement function.

Conclusions

In this work, the deformation behavior of various samples of geosynthetic materials was analyzed. Six samples, including two samples made of PET and four samples made of PP, were investigated for creep by SIM test. As a result of the analysis, predicted creep curves for up to 30 years of design life were obtained. The best resistance to creep is possessed by samples made of PET, which is mainly explained by their work below the glass transition temperature. Samples of PP have a much worse creep resistance, because the temperature range of operation lies above their glass transition temperature. As a result, it can be concluded that PET samples have better creep resistance and can be used in various loaded applications as a reinforcement function. The SIM test showed its applicability for predicting creep deformation for long periods based on short-term measurements.

Reference

1. Sarsby R.W. *Geosynthetics in Civil Engineering*. Woodhead Publishing Ltd. 2007. 295 p.
2. Koerner R.M. *Designing With Geosynthetics,* 6th Ed. Xlibris Publ. Co. 2012. 914 p.
3. Mounes S.M., Karim M.R., Khodaii A., Almasi M.H. Evaluation of permanent deformation of geogrid reinforced asphalt concrete using dynamic creep test. *Geotextiles and Geomembranes.* 2016. No. 44(1). Pp. 109–116.
4. Yang B.H., Lai J., Lin J.H., Tsai P.H. Simulating the loading behavior of reinforced strip footings with a double-yield soil model. *International Journal of Geomechanics*. 2016. No. 16(1).
5. Wang, H., Yang G.B., Liu H.C., Liu W.B., Wu L.D. Research on dynamic behavior of geogrid reinforced soil retaining wall with wrapped face. *Tiedao Xuebao/Journal of the China Railway Society.* 2016. No. 38(2). Pp. 131–140.
6. Ooi T.A., Tee C.H. Advance in geogrid reinforced slopes in Malaysia. *Geotechnical Engineering.* 2011. No. 42(1). Pp. 9–34.
7. Peng F.L., Li F.L., Hirakawa D., Tatsuoka F. Deformation and strength characteristics of geogrid-reinforced soil

Литература

1. Sarsby R.W. Geosynthetics in Civil Engineering. Woodhead Publishing Ltd. 2007. 295 p.
2. Koerner R.M. Designing With Geosynthetics, 6th Ed. Xlibris Publ. Co. 2012. 914 p.
3. Mounes S.M., Karim M.R., Khodaii A., Almasi M.H. Evaluation of permanent deformation of geogrid reinforced asphalt concrete using dynamic creep test // Geotextiles and Geomembranes. 2016. № 44(1). Pp. 109–116.
4. Yang B.H., Lai J., Lin J.H., Tsai P.H.Simulating the loading behavior of reinforced strip footings with a double-yield soil model // International Journal of Geomechanics. 2016. № 16(1).
5. Wang H., Yang G.B., Liu H.C., Liu W.B., Wu L.D. Research on dynamic behavior of geogrid reinforced soil retaining wall with wrapped face // Tiedao Xuebao/Journal of the China Railway Society. 2016. № 38(2). Pp. 131–140.
6. Ooi T.A., Tee C.H. Advance in geogrid reinforced slopes in Malaysia // Geotechnical Engineering. 2011. № 42(1). Pp. 9–34.
7. Peng F.L., Li F.L., Hirakawa D., Tatsuoka F. Deformation and strength characteristics of geogrid-reinforced soil

retaining wall under change of loading rate and its FEM simulation. *Yantu Gongcheng Xuebao/Chinese Journal of Geotechnical Engineering.* 2011. No. 33(2). Pp. 174–180.

8. Sannikov S., Kuyukov S., Kubasov D. Increase of a roadway covering durability by using the cement-concrete base fragmented with the geogrid. *MATEC Web of Conferences.* 2016. No. 73.
9. Christopher B.R., Holtz R.D., Berg R.R. Geosynthetic reinforced embankments on soft foundations. *Geotechnical Special Publication.* 2001. No. 122. Pp. 206-236.
10. Sannikov S., Kuyukov S., Kubasov D. Increase of a roadway covering durability by using the cement-concrete base fragmented with the geogrid. *MATEC Web of Conferences.* 2016. No. 73.
11. Tian Q.B. The application research of geogrids in road broadening engineering. *Resources, Environment and Engineering – 2nd Technical Congress on Resources, Environment and Engineering, CREE.2015*. 2016. Pp. 163–168.
12. Canestrari F., Ferrotti G., Abuaddous M., Pasquini E. Geocomposite-reinforcement of polymer-modified asphalt systems. *RILEM Bookseries.* No. 11. Pp. 383–395.
13. Leshchinsky B., Evans T.M., Vesper J. Microgrid inclusions to increase the strength and stiffness of sand. *Geotextiles and Geomembranes.* 2016. No. 44(2). Pp. 170–177.
14. Yang B.-H., Lai J., Lin J.-H., Tsai P.H. Simulating the loading behavior of reinforced strip footings with a double-yield soil model. *International Journal of Geomechanics.* 2016. No. 16(1).
15. Navarrete F., Reddy D.V., Lai P. Creep of geogrid reinforcement for retaining wall backfills. *Geosynthetics Conference.* 2001.
16. Singh A., Phanikumar B.R., Prasad R. Effect of geogrid reinforcement on load carrying capacity of a coarse sand bed. *International Journal of Civil Engineering and Technology.* 2016. No. 7(3). Pp. 1–6.
17. Hsiehl C.W., Lee K., Yoo H.K., Jeo, H. Tensile creep behavior of polyester geogrids by conventional and accelerated test methods. *Fibers and Polymers.* 2008. No. 9(4). Pp. 476–480.
18. Den Hoedt G. Creep and relaxation of geotextile fabrics. *Geotextiles and Geomembranes.* 1986. No. 4(2). Pp. 83–92.
19. Cho S.D., Lee K.W., Cazzuffi D.A., Jeon H.Y. Evaluation of combination effects of installation damage and creep behavior on long-term design strength of geogrids. *Polymer Testing.* 2006. No. 25(6). Pp. 819–828.
20. Alekseev N.N., Kovalenko I.A., Stolyarov O.N., Melnikov B.E. Viscoelastic properties of geosynthetic materials. *Construction of Unique Buildings and Structures*. 2017. No. 5(56). Pp. 17–32. (rus)
21. Suvorova Yu.V., Alekseyeva S.I, Kupriyanov D.Y. Modelirovaniye dlitelnoy polzuchesti georeshetok tipa Fortrac na osnove polietilentereftalata. [Modeling of the long creep of geogrids of the Fortrac type based on polyethylene terephthalate]. *High-molecular compounds.* 2005. No. 6. Pp. 1058–1061. (rus)
22. Suvorova Yu.V., Alekseyeva S.I. Eksperimentalnyye i analiticheskiye metody otsenki dolgovechnosti geosinteticheskikh materialov. Problemy mashinostroyeniya i nadezhnosti mashin. [Experimental and analytical methods for assessing the durability of geosynthetic materials]. *Problems of machine building and machine reliability.* 2010. No. 4. Pp. 105–110. (rus)
23. Loginova I.I., Artamonova D.A., Stolyarov O.N., Melnikov B.E. Vliyaniye struktury na vyazkouprugiye svoystva geosinteticheskikh materialov [Effects of structure type on viscoelastic properties of geosynthetics]. *Magazine of Civil Engineering.* 2015. No. 4(56). Pp. 11–18. (rus)
24. Koo H.-J., Kim Y.-K. Lifetime prediction of geogrids for

retaining wall under change of loading rate and its FEM simulation // Yantu Gongcheng Xuebao/Chinese Journal of Geotechnical Engineering. 2011. No. 33(2). Pp. 174–180.

8. Sannikov S., Kuyukov S., Kubasov D. Increase of a Roadway Covering Durability by Using the Cement-Concrete Base Fragmented with the Geogrid // MATEC Web of Conferences. 2016. № 73.
9. Christopher B.R., Holtz R.D., Berg R.R. Geosynthetic reinforced embankments on soft foundations // Geotechnical Special Publication. 2001. № 122. Pp. 206–236.
10. Sannikov S., Kuyukov S., Kubasov D. Increase of a roadway covering durability by using the cement-concrete base fragmented with the geogrid // MATEC Web of Conferences. 2016. № 73.
11. Tian Q.B. The application research of geogrids in road broadening engineering // Resources, Environment and Engineering – 2nd Technical Congress on Resources, Environment and Engineering, CREE.2015. 2016. Pp. 163-168
12. Canestrari F., Ferrotti G., Abuaddous M., Pasquini E. Geocomposite-reinforcement of polymer-modified asphalt systems // RILEM Bookseries. No. 11. Pp. 383–395.
13. Leshchinsky B., Evans T.M., Vesper J. Microgrid inclusions to increase the strength and stiffness of sand // Geotextiles and Geomembranes. 2016. № 44(2). Pp. 170–177.
14. Yang B.-H., Lai J., Lin J.-H., Tsai P.H. Simulating the loading behavior of reinforced strip footings with a double-yield soil model // International Journal of Geomechanics. 2016. № 16(1).
15. Navarrete F., Reddy D.V., Lai P. Creep of geogrid reinforcement for retaining wall backfills // Geosynthetics Conference. 2001.
16. Singh A., Phanikumar B.R., Prasad R. Effect of geogrid reinforcement on load carrying capacity of a coarse sand bed // International Journal of Civil Engineering and Technology. 2016. № 7(3). Pp. 1–6.
17. Hsiehl C.W., Lee K., Yoo H.K., Jeo, H. Tensile creep behavior of polyester geogrids by conventional and accelerated test methods // Fibers and Polymers. 2008. № 9(4). Pp. 476–480.
18. Den Hoedt G. Creep and relaxation of geotextile fabrics // Geotextiles and Geomembranes. 1986. № 4(2). Pp. 83–92.
19. Cho S.D., Lee K.W., Cazzuffi D.A., Jeon H.Y. Evaluation of combination effects of installation damage and creep behavior on long-term design strength of geogrids // Polymer Testing. 2006. № 25(6). Pp. 819–828.
20. Алексеев Н.Н., Коваленко И.А., Столяров О.Н., Мельников Б.Е. Вязкоупругие свойства геосинтетических материалов // Строительство уникальных зданий и сооружений. 2017. № 5(56). С. 17–32.
21. Суворова Ю.В., Алексеева С.И., Куприянов Д.Ю. Моделирование длительной ползучести георешеток типа Fortrac на основе полиэтилентерефталата // Высокомолекулярные соединения. Серия B. 2005. Т. 47. № 6. С. 1058–1061.
22. Суворова Ю.В., Алексеева С.И. Экспериментальные и аналитические методы оценки долговечности геосинтетических материалов // Проблемы машиностроения и надежности машин. 2010. № 4. С. 105–110. (rus)
23. Логинова И.И., Артамонова Д.А., Столяров О.Н., Мельников Б.Е. Влияние структуры на вязкоупругие свойства геосинтетических материалов // Инженерно-строительный журнал. 2015. № 4(56). С. 11–18.
24. Koo H.-J., Kim Y.-K. Lifetime prediction of geogrids for reinforcement of embankments and slopes // Polymer Testing. 2005. № 24(2). Pp. 181–188.
25. Cho S.D., Lee K.W., Cazzuffi D.A., Jeon H.Y. Evaluation of combination effects of installation damage and creep

reinforcement of embankments and slopes. *Polymer Testing.* 2005. No. 24(2). Pp. 181–188.

25. Cho S.D., Lee K.W., Cazzuffi D.A., Jeon H.Y. Evaluation of combination effects of installation damage and creep behavior on long-term design strength of geogrids. *Polymer Testing.* 2006. No. 25(6). Pp. 819–828.
26. Zou C., Wang Y., Lin J., Chen Y. Creep behaviors and constitutive model for high density polyethylene geogrid and its application to reinforced soil retaing wall on soft soil foundation. *Construction and Building Materials.* 2016. No. 114. Pp. 763–771.
27. Zhang Z., Zhu D.Y., Chen T.F., Wang T. Confined-accelerated creep tests to determine the creep reduction factor. *Applied Mechanics and Materials.* 2014. No. 539. Pp. 769–773.
28. Hsuan Y.G., Yeo S.S. Comparing the creep behavior of high density polyethylene geogrid using two accereration methods. *Geotechnical Special Publication.* 2005. No. 130(142). Pp. 2887–2901.
29. Jin Y.C., Jeon H.Y. Analysis of creep deformation behavior of geogrids by limited creep strain and rupture. *10th International Conference on Geosynthetics.* 2014.
30. Tong J., Gong B., Liu J. Experimental study and prediction on the long-term creep properties for geogrids at different temperatures. *9th International Conference on Geosynthetics - Geosynthetics: Advanced Solutions for a Challenging World.* 2010. Pp. 873–876.
31. Giannopoulos I.P., Burgoyne C.J. Accelerated and real-time creep and creep-rupture results for aramid fibers. *Journal of Applied Polymer Science.* 2012. No. 125(5). Pp. 3856–3870.
32. Lee K.W., Jung S.G., Koo H.J, Cho H.W., Lee J.S. The evaluation of creep reduction factor for geosynthetic strip by conventional creep test and stepped isothermal method. *10th International conference on geosynthetics.* Berlin. 2014.
33. Zornberg J.G, Byler B.R., Knudsen J.W. Creep of geotextiles using time–temperature superposition methods. *Journal of Geotechnical and Geoenvironmental Engineering.* 2004. Vol. 130(11). Pp. 1158–1168.
34. Mok M.S., Blond, E., Mylnarek J., Jeon H.Y. New approach to evaluate the long-term designing normal pressure of geonets using a short-term accelerated compressive creep test method. *Geotextiles and Geomembranes.* 2012. No. 30. Pp. 2–7.
35. Allen S.R. Geotextile durability. *Geotextiles.* Cambridge: Elsevier. 2016. Pp. 177–215.
36. *GRI Test Method GS10 Standard Test Method for Accelerated Tensile Creep and Creep-Rupture of Geosynthetic Materials Based on Time-Temperature Superposition Using the Stepped Isothermal Method*. 2000.

behavior on long-term design strength of geogrids // Polymer Testing. 2006. № 25(6). Pp. 819–828.

26. Zou C., Wang Y., Lin J., Chen Y. Creep behaviors and constitutive model for high density polyethylene geogrid and its application to reinforced soil retaing wall on soft soil foundation // Construction and Building Materials. 2016. № 114. Pp. 763–771.
27. Zhang Z., Zhu D.Y., Chen T.F., Wang T. Confined-accelerated creep tests to determine the creep reduction factor // Applied Mechanics and Materials. 2014. № 539. Pp. 769–773.
28. Hsuan Y.G., Yeo S.S. Comparing the creep behavior of high density polyethylene geogrid using two accereration methods // Geotechnical Special Publication. 2005. № 130(142). Pp. 2887–2901.
29. Jin Y.C., Jeon H.Y. Analysis of creep deformation behavior of geogrids by limited creep strain and rupture // 10th International Conference on Geosynthetics. 2014.
30. Tong J., Gong B., Liu J. Experimental study and prediction on the long-term creep properties for geogrids at different temperatures // 9th International Conference on Geosynthetics - Geosynthetics: Advanced Solutions for a Challenging World. 2010. Pp. 873–876.
31. Giannopoulos I.P., Burgoyne C.J. Accelerated and real-time creep and creep-rupture results for aramid fibers // Journal of Applied Polymer Science. 2012. № 125(5). Pp. 3856–3870.
32. Lee K.W., Jung S.G., Koo H.J, Cho H.W., Lee J.S. The evaluation of creep reduction factor for geosynthetic strip by conventional creep test and stepped isothermal method // 10th International conference on geosynthetics. Berlin. 2014.
33. Zornberg J.G, Byler B.R., Knudsen J.W. Creep of geotextiles using time–temperature superposition methods // Journal of Geotechnical and Geoenvironmental Engineering. 2004. Vol. 130(11). Pp. 1158–1168.
34. Mok M.S., Blond, E., Mylnarek J., Jeon H.Y. New approach to evaluate the long-term designing normal pressure of geonets using a short-term accelerated compressive creep test method // Geotextiles and Geomembranes. 2012. № 30. Pp. 2–7.
35. Allen S.R. Geotextile durability // Geotextiles. Cambridge: Elsevier. 2016. Pp. 177–215.
36. GRI Test Method GS10 Standard Test Method for Accelerated Tensile Creep and Creep-Rupture of Geosynthetic Materials Based on Time-Temperature Superposition Using the Stepped Isothermal Method. 2000.

Sanjeev Gautham Srungeri,
+7(931)270-59-65; sanjeevgautham18@gmail.com

Nikolai Alekseev,
+7(999)239-71-54; nikolas.alexeeff@yandex.ru

Ilya Kovalenko,
+7(906)262-52-47; ilyako27@mail.ru

Oleg Stolyarov,
+7(812)552-63-03; oleg.stolyarov@rambler.ru

Санджив Гаутам Срунгери,
+7(931)270-59-65;
эл. почта: sanjeevgautham18@gmail.com

Николай Николаевич Алексеев,
+7(999)239-71-54;
эл. почта: nikolas.alexeeff@yandex.ru

Илья Александрович Коваленко,
+7(906)262-52-47; эл. почта: ilyako27@mail.ru

Олег Николаевич Столяров,
+7(812)552-63-03;
эл. почта: oleg.stolyarov@rambler.ru

Срунгери С., Алексеев Н.Н., Коваленко И.А., Столяров О.Н. Ползучесть геосинтетических материалов при ускоренных температурных испытаниях // Инженерно-строительный журнал. 2017. № 8(76). С. 255–265.

doi: 10.18720/MCE.76.23

Dynamic stability of the lattice truss of the bridge taking into account local oscillations

Динамическая устойчивость решетчатой фермы моста с учетом местных колебаний

I.A. Indeykin ,
S.V. Chizhov,
E.B. Shestakova,
A.A. Antonyuk,
Petersburg State Transport University,
St. Petersburg, Russia
E.S. Evtukov,
Saint-Petersburg State University of Architecture and Civil Engineering, St. Petersburg, Russia
K.N. Kulagin,
Research and Design Institute "Lenmetrogiprotrans", St. Petersburg, Russia
V.V. Karpov,
Saint-Petersburg State University of Architecture and Civil Engineering, St. Petersburg, Russia
G.D. Golitsynsky,
Petersburg State Transport University,
St. Petersburg, Russia

Д-р техн. наук, заведующий кафедры А.В. Индейкин,
канд. техн. наук, доцент С.В. Чижов,
канд. техн. наук, Доцент Е.Б. Шестакова,
аспирант А.А. Антонюк,
Петербургский государственный университет путей сообщения Императора Александра I, г. Санкт-Петербург, Россия
д-р техн. наук, профессор С.А. Евтюков,
Санкт-Петербургский государственный архитектурно-строительный университет, г. Санкт-Петербург, Россия
д-р техн. наук, советник генерального директора Н.И. Кулагин,
ОАО Научно-исследовательский Проектно-изыскательский институт "Ленметрогипротранс", г. Санкт-Петербург, Россия
д-р техн. наук, профессор В. В. Карпов,
Санкт-Петербургский государственный архитектурно-строительный университет, г. Санкт-Петербург, Россия
д-р техн. наук, профессор Д.М. Голицынский,
Петербургский государственный университет путей сообщения Императора Александра I, г. Санкт-Петербург, Россия

Key words: bar element; building structure; kinematic perturbation; parametric resonance; decomposition model; excitation coefficient; influence line

Ключевые слова: стержневой элемент; строительная конструкция; кинематическое возмущение; параметрический резонанс; декомпозиционная модель; коэффициент возбуждения; линия влияния

Abstract. The carrying capacity of the railway and the service life of artificial structures primarily depend on the operational category of the structure and the dynamic state: dynamic stability, the condition that dangerous vibrations do not appear, and the dangerous resonance of the amplitude of the oscillations. Studies on the dynamics of railway bridges have gained relevance in connection with the new construction and reconstruction of bridges of high-speed and high-speed railroads. When choosing the restoration measures for the reconstruction of existing railway lines or when designing and building new structures, taking into account the current high operational requirements, a thorough evaluation of the efficiency and reliability of the span structures is necessary, taking into account the type of construction and analysis of the dynamic impact. In the article the analysis of factors is produced influencing on the possible loss of dynamic stability of bars of the latticed truss under act of kinematics indignations of ends of bar at the general vibrations of flight structure caused by dynamic factors accompanying moving of the temporal loading on a bridge. A novelty is made by the account of mutually influencing general and local vibrations of flight structure at the estimation of dynamic stability of the cored latticed truss. The spectrum of parametric vibrations of bars of the latticed truss is investigational in the conditions of remoteness from the areas of dynamic instability. The method of decomposition of

Индейкин А.В., Чижов С.В., Шестакова Е.Б., Антонюк А.А., Евтюков С.А., Кулагин Н.И., Карпов В.В., Голицынский Д.М. Динамическая устойчивость решетчатой фермы моста с учетом местных колебаний // Инженерно-строительный журнал. 2017. № 8(76). С. 266–278.

decision of differential equalizations of vibrations is applied on the Bessel function with a whole icon. Practical limitation of spectrum of frequencies is got near-by the value of bearing frequency to equal frequency of free vibrations taking into account influence of central forces and also relatively small influence of parametric vibrations in areas remote from living parametric resonance. Taking into account the dynamic stability presented by the authors, it is possible to expand the possibilities of using the existing norms and update them for dynamic calculations of railway metal bridges with lattice trusses, as well as to take into account the main factors that influence the occurrence of additional dynamic influences.

Аннотация. Пропускная способность железной дороги и срок службы искусственных сооружений прежде всего зависят от эксплуатационной категории сооружения и динамического состояния: динамической устойчивости, условию не появления опасных вибраций и опасного резонанса амплитуды колебаний. Исследования по динамике железнодорожных мостов приобрели актуальность в связи с новым строительством и реконструкцией мостов скоростных и высокоскоростных железнодорожных магистралей. При выборе восстановительных мероприятий по реконструкции существующих железнодорожных линий или при проектировании и строительстве новых конструкций с учетом актуальных повышенных требований по эксплуатации необходима тщательная оценка работоспособности и надежности пролетных строений с учетом типа конструкции и анализе динамического воздействия. В статье производится анализ факторов, влияющих на возможную потерю динамической устойчивости стержней решетчатых ферм под воздействием кинематических возмущений концов стержня при общих вибрациях пролетного строения, вызванных динамическими факторами, сопровождающими перемещение временной нагрузки по мосту. Новизну составляет учет взаимовлияющих общих и местных вибраций пролетного строения при оценке динамической устойчивости стержневых решетчатых ферм. Исследован спектр параметрических колебаний стержней решетчатых ферм в условиях удаленности от областей динамической неустойчивости. Применен метод разложения решения дифференциальных уравнений колебаний по функциям Бесселя с целым значком. Получено практическое ограничение спектра частот вблизи значения несущей частоты, равной частоте свободных колебаний с учетом влияния продольных сил, а также относительно малое влияние параметрических колебаний в областях, удаленных от живого параметрического резонанса. Учет динамической устойчивости, представленный авторами, позволяет расширить возможности использования действующих норм и актуализировать их для динамических расчетов железнодорожных металлических мостов с решётчатыми фермами, а также учитывать основные факторы, влияющих на возникновения дополнительных динамических воздействий.

Introduction

To ensure reliable and safe operation of the bridge structure throughout the life cycle, it is necessary to analyze and take into account many important factors, including dynamic stability.

In a historical aspect, it should be noted that the first work devoted to solving problems related to the dynamic stability of rods and rod systems subjected to longitudinal harmonic force is the work of N. Belyaev [9]. Since that time, the problem of studying the stability of elastic systems and related mathematical methods has attracted universal attention of scientists. Of the large number of scientists who worked and still work, it should be noted the work of A.V. Indeikin [1, 4], V.V. Bolotin [3], Ya.G. Panovko [2, 7], N.N. Moiseev [5], N.A. Alfutov [6], G. Ziegler [8], V.N. Chelomey [10] and many other authors.

In the literature, we mainly consider the power excitation of parametric oscillations of rods outside the connection with the general vibrations of the structure.

The interest in dynamic behaviour of railway different existing types including new ones bridges has increased in recent years, due to the introduction of high speed trains [11–17].

The main attention is paid to the complexes of measures to reduce the level of vibration of steel bridges, which subsequently ensures a reduction in costs for repair activities [18–22].

Under the loads of high speed, the bridges are subjected to large dynamic effects. Therefore, the demands on railway bridge structures are increased. The dynamic aspects have often shown to be the governing factor in the structural design. Generally, for all railway bridges induced by train speeds over 200 km/h, dynamic analysis is required. Correct understanding of Railway Bridge dynamic is essential, since a realistic prediction of the structural response contributes to an economic design of new bridges and to a rational exploitation of bridges in service. In railway bridge design, the dynamic effects are often considered by introducing dynamic amplification factors, specified in bridge design codes. Actually, the response of a railway bridge due to moving loads depends on span length, structure mass, stiffness and damping, train axle loads and speed. The dynamic factors are usually a function of the natural frequency or span length of the bridge, and states how many times the static effects have to be magnified in order to cover the additional dynamic loads. Another issue related to the dynamic of railway bridges, is the behaviour variations along the bridges, variations in the overall conditions, and in the materials. There exist a large number of studies, dealing with the dynamic moving load problem, by considering different bridge and vehicle models under different conditions. A more detailed list of previous investigations is given in works of professor Karoumi [23–28].

The dynamic effects for railway bridges are considered in Eurocode 1: Actions on structures – Part 2: Traffic loads on bridges, Dynamic effects (including resonance). For simple dynamic problems, only static analysis is required. The static analysis shall be carried out with the load models defined in Vertical loads – Characteristic values (static effects) and eccentricity and distribution of loading, and considered the load model LM71 and where required the load models SW/0 and SW/2. The results of the static analysis shall be multiplied by the dynamic factor Φ considered later on, and if required multiplied by a factor α in accordance with the load model LM71 [29, 30].

In this article kinematics excitation of vibrations of bars is examined as a result of the dynamic moving of nodes in composition the lattice truss. The method of decouplig is thus used at that the form of vibrations of the bar elements of the lattice truss is taken into account.

Methods

Research of dynamic stability of elements at influence of the wave parametric load

Structural design of the bar element a complementary model and conclusion of differential equalizations of vibration processes are presented on the Figure 1.

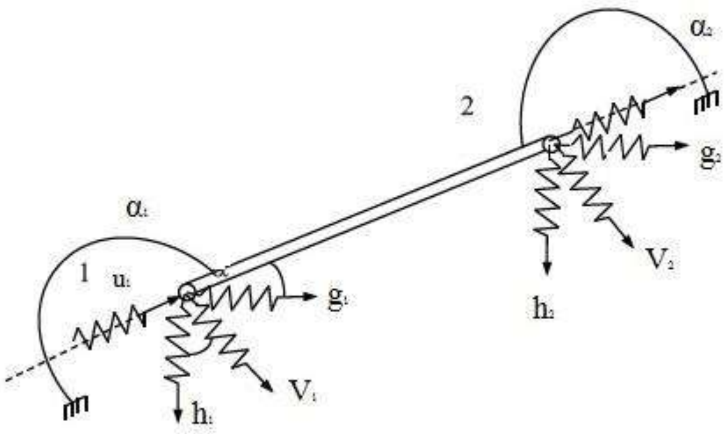

Figure 1. Structural design [1]: V_1; V_2 – transverse components of the displacement of nodes 1 and 2, g_1; g_2 – horizontal components of the displacement of nodes 1 and 2, u_1; u_2 – longitudinal components of the displacement of nodes 1 and 2; h_1; h_2 – vertical components of the displacement of nodes 1 and 2, α_1; α_2 – spring stiffness characteristic

In the case of a rod of a trellis truss loaded with a longitudinal force $S(t)$ consisting of the static component S_0 and the dynamic component St, whose nodes make the transverse motion $v_1(t)$ and $v_2(t)$ in the first approximation, a differential equation describing the dynamic processes is obtained:

$$\ddot{q} + \Omega^2 \left[1 \pm 2\mu(t)\right] q = -\frac{2}{\pi}\left(\ddot{v}_1 + \ddot{v}_2\right), \tag{1}$$

where $\Omega^2 = \dfrac{EI\,\pi^4}{m\ell^4}\left(1 \pm \dfrac{S_0}{S_{\text{кр}}}\right)$, $2\mu(t) = \dfrac{S_t}{S_{\text{cr}} \pm S_0}$, a sign "+" behaves to the case of the stretched bar, sign of "-" to the case of the compressed bar;

$S_{cr} = \frac{\pi^2 EI}{\ell^2}$ – Euler's critical force;

ℓ – bar length;

q – generalized coordinate;

m – linear mass of bar.

Homogeneous equalization corresponding to equalization (1) on condition of $\mu(t) = \mu \cos \omega \cdot t$ is Mathieu equation and describes the parametric vibrations of the bar element of construction:

$$\ddot{q} + \Omega^2 [1 - 2\mu \cos\omega t] q = 0. \tag{2}$$

It is known [2] that at the value of frequency of excitation:

$$\omega_* = 2\Omega \sqrt{1 \pm \mu}, \tag{3}$$

there can be main parametric resonance.

Taking into account this condition amplitude of parametrik vibrations increases in time on an exponential law:

$$A = A_0 e^{\nu t}. \tag{4}$$

In the absence of resistance, the maximum value of the exponent is: $\nu_{max} = \frac{\mu \Omega}{2}$.

Taking into account all the above equations, it follows that:

$$A = A_0 e^{\frac{\mu \Omega t}{2}}. \tag{5}$$

If to take into account influence of viscid resistance Mathieu differential equation assumes a next form:

$$\ddot{q} + 2n\dot{q} + \Omega^2 [1 - 2\mu \cos\omega t] q = 0. \tag{6}$$

The values of the critical frequencies corresponding to the boundaries of the first (main) region of dynamic instability at parametric resonance:

$$\omega_* = 2\Omega \sqrt{1 \pm \sqrt{\mu^2 - \left(\frac{\Delta}{\pi}\right)^2}}, \tag{7}$$

where Δ – logarithmic decrement of local free vibrations of bar.

Value of exponential index of growth of amplitude in this case:

$$\nu_{max} = \frac{\mu\Omega}{2} - n = \frac{\mu\Omega}{2} - \frac{\Delta}{T} = \frac{\mu\Omega}{2} - \frac{\Delta\Omega}{2\pi} = \frac{\Omega}{2}\left(\mu - \frac{\Delta}{\pi}\right) = \frac{\Omega}{2}(\mu - \mu_*), \tag{8}$$

where $\mu_* = \frac{\Delta}{\pi}$ – the critical value of the excitation coefficient, when it exceeds the phenomenon of dynamic instability.

In case of periodic character of coefficient $\mu(t)$ presented by Fourier's series $\mu(t)=\sum_{k=1}^{\infty}\mu_k\cos k\omega t$ the critical frequencies corresponding to parametric resonances are given by [3]:

$$\omega_* = \frac{2\Omega}{k}\sqrt{1\pm\mu_k}\ . \quad (9)$$

In case of polyharmonic excitation:

$$\mu(t)=\sum_{k=1}^{s}\mu_k\cos\omega_k t\ , \quad (10)$$

at that the values of ω_k are not multiple k.

$$\omega_{*k} = 2\Omega\sqrt{1\pm\mu_k}\ . \quad (11)$$

In last In the latter case, the influence of higher forms of oscillations and combination parametric resonances is neglected.

At the stationary applying of the harmonic loading in the nodes of truss bar stress of oscillation of that examined on a decouple drawing determined by expression:

$$S_j(t)=\sum_{k=1}^{n}\alpha_{jk}P_k(\omega t)\,, \quad (12)$$

where α_{jk} – coefficients of influence taking into account influences in k-node of truss;

S_j – force in the bar element;

P_k – force impact profile.

Taking into account character of form of vibrations of truss (Figure 2) of value α_{jk} quasistatic is determined.

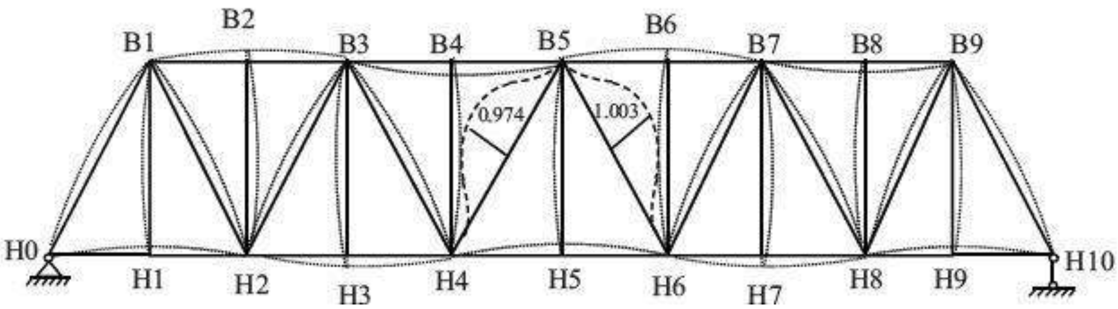

Figure 2. Higher form (mode) of vibrations of truss [1]

It is like possible to expect value $S_j(t)$ in case of the periodic key loading of general view presented through the Fourier series.

If node loads (forces) are applied at different nodes of the truss varying according to a harmonic law with different frequencies ω_k, then the force in the j-th bar of the truss is described by a polyharmonic process:

$$S_j(t) = \sum_{k=1}^{n} \alpha_{jk} \, P_k(\omega_k t). \tag{13}$$

At excitation of parametric vibrations stationary forces attached in the nodes of truss and operating during the indefinite interval of time the only method of protection against vibrations there is an exception of possibility of origin of parametric vibrations by the increase of parameters of damping (coefficient of fading of n) with that inequality was provided:

$$\mu_* < \mu_k. \tag{14}$$

From a vibration can such methods of protecting become, for example, application of paint coat for the bars materials possessing the high degree of absorption of energy of vibrations in a superficial layer and also perfection of constructions of nodes – connection of the truss bars in the nodes on high-strength bolts instead of riveted joints.

In the case of the action of the mobile load, the force at the nodes of the truss is determined by the expression:

$$S(t) = P\,\Psi(t)\,\eta(\upsilon t), \tag{15}$$

where $\eta(\upsilon t)$ – ordinate of the force influence line in the truss bar from the amplitude value of the moving variable force *P*(*t*).

We expand the equation of the line of influence $\eta(\upsilon t)$ in a Fourier series with respect to $\sin npt$ continuing the function in an odd manner:

$$\eta(\upsilon t) = \sum_{n=1}^{\infty} h_n \sin npt, \tag{16}$$

where, $p = \frac{\pi \upsilon}{\ell}$;

ℓ – truss span;

$\upsilon = const$ – load speed.

The values of the Fourier coefficients:

- for a single-valued influence line

$$h_n = \frac{2\eta}{n^2 \pi^2 \alpha_0 (1-\alpha_0)} \sin \alpha_0 \, n\pi; \tag{17}$$

- for a two-digit influence line

$$h_n = \frac{2}{n^2 \pi^2 (\beta_0 - \alpha_0)} \left[\left(\eta_1 \frac{\beta_0}{\alpha_0} + \eta_2 \right) \sin \alpha_0 \, n\pi - \left(\eta_1 + \eta_2 \frac{1-\alpha_0}{1-\beta_0} \right) \sin \beta_0 \, n\pi \right] \tag{18}$$

In equals (17) and (18): η, η_1, η_2 – absolute values of the ordinates of the vertices of the influence line, $\alpha_0 = \frac{\xi_1}{\ell}$, $\beta_0 = \frac{\xi_2}{\ell}$, ξ_1 and ξ_2 – abscissas of corresponding vertices.

When moving along the chord of force $P(t)=P(t)\cos\omega t$ the variable force in the truss bar is given by:

$$S(t)=P\cos\omega t\sum_{n=1}^{\infty}h_n\sin npt=\frac{P}{2}\sum_{n=1}^{\infty}h_n\left(\sin\omega_{1n}t-\sin\omega_{2n}t\right), \tag{19}$$

where $\omega_{1n}=\omega+np=\omega+\frac{n\pi v}{\ell}$;

$\omega_{2n}=\omega-np=\omega-\frac{n\pi v}{\ell}$.

In this case the value of the coefficient $\mu(t)$ in equation (6):

$$\mu(t)=\frac{P}{4\left(S_{\kappa p}\pm S_0\right)}\sum_{n=1}^{\infty}h_n\left(\sin\omega_{1n}t-\sin\omega_{2n}t\right)=\sum_{n=1}^{\infty}\mu_n\left(\sin\omega_{1n}t-\sin\omega_{2n}t\right), \tag{20}$$

where, $\mu_n=\frac{P}{4\left(S_{cr}\pm S_0\right)}$.

Frequencies ω_{1n} and ω_{2n} are modulated at carrier frequency ω.

In the first approximation, the critical frequencies corresponding to single-frequency parametric resonances are given by:

$$\omega_*=2\Omega\sqrt{1\pm\mu_n}\mp\frac{n\pi v}{\ell}. \tag{21}$$

The carrier frequencies are proportional to the speed of the load only if the source of the disturbance is the inertia forces of the unbalanced rotating masses associated with the object moving by the lattice truss (train).

I.e. $\omega=\frac{v}{R}$, where R – radius of wheels.

In this case:

$$\omega_{(1,2)n}=\omega\left(1\pm\frac{n\pi R}{\ell}\right), \tag{22}$$

and

$$\omega_*=\frac{2\Omega}{1\pm\frac{n\pi R}{\ell}}\sqrt{1\pm\mu_n}. \tag{23}$$

Usually $\frac{\pi R}{\ell}<<1$. For example, when the train is moving (R=0.525 m), the estimated span of the trusses ℓ =33…110 m value $\frac{\pi R}{\ell}$ is 0.005…0.015.

In this case, the regions of dynamic instability are concentrated around the region $\omega_* = 2\Omega\sqrt{1 \pm \mu_1}$, width of these regions decreases with increasing n as the value of $\omega_* = 2\Omega$ increases, since the Fourier coefficients h_n decrease substantially.

With the help of expression (23), it is possible to determine the critical speeds of load movement along the truss:

$$v_* = \omega_* R = \frac{2\Omega R\sqrt{1 \pm \mu_n}}{1 \pm \dfrac{n\pi R}{\ell}} . \tag{24}$$

Since the oscillations of the bar of the higher trusses are high-frequency, the critical speeds of the load motion along the railway bridge are realized only in the high-speed mode [4].

The increase in the time of the amplitudes of the resonance parametric vibrations occurs, without allowance for the resistance, according to the exponential law with the exponent $\nu = \dfrac{\mu\Omega}{2}$:

$$A = A_0 e^{\nu t} = A_0 e^{\frac{\mu_n \Omega t}{2}} . \tag{25}$$

Time of movement of load on the span of the truss is limited:

$$t = \frac{\ell}{v_{cr}} = \frac{\ell\left(1 \pm \dfrac{n\pi R}{\ell}\right)}{2\Omega R\sqrt{1 \pm \mu_n}} . \tag{26}$$

Consequently, the value of the exponent in this case:

$$\nu = \frac{\mu_n \ell}{4R} \frac{1 \pm \dfrac{n\pi R}{\ell}}{\sqrt{1 \pm \mu_n}} \approx \frac{\mu_n \ell}{4R} . \tag{27}$$

For a span structure with lattice trusses of a large railway bridge with parameter values μ_n =0.03, ℓ=110 m, R=0.525 m values of the parameters ν is 1.7 and $\dfrac{A}{A_0}$ =4.806.

In this case, there is a significant increase in the vibration amplitudes even with a relatively small excitation coefficient μ_n .

It should be noted that the parametric resonances of the bar elements of trusses can be realized only in higher forms of vibrations (oscillations), since they are high-frequency.

In this case, there is no significant superposition of parametric and forced oscillations of the bars, since the critical frequencies are twice the vibration frequencies of the bar at which ordinary resonance can take place $(\omega = \Omega)$. Forced oscillations in this case occur in the supercritical region where the dynamic coefficient is less than unity (in the considered case it is 0.33).

When studying forced oscillations, one can neglect the effect of the variable frequency of free oscillations and use equation (1) with the value μ=0. The values of the kinematic perturbations of the bar ends can be determined from an analysis of the general vibrations of the truss for the investigation of which it is necessary to apply known methods of structural dynamics or to use the corresponding computational complexes (for example, COSMOS/M).

In the domains of stable solutions we obtain the following asymptotic solution of the homogeneous equation (1) [5]:

$$q \approx \frac{1}{\sqrt[4]{1-2\mu(t)}}\left\{A\cos\Omega\int\limits_0^t\sqrt{1-2\mu(t)}\;dt + B\sin\Omega\int\limits_0^t\sqrt{1-2\mu(t)}\;dt\right\}, \tag{28}$$

Investigation of oscillations of bars in regions of dynamic stability

In the general case, the integrals in the right-hand side of equation (28) cannot be expressed in terms of elementary functions.

Taking this into account, we represent the equation $\sqrt{1-2\mu(t)}$ in the form of a uniformly convergent series:

$$\sqrt{1-2\mu(t)} = \sqrt{1-2\mu_0\,\Phi(t)} = 1-\mu_0\,\Phi(t) - \frac{\mu_0}{2}\,\Phi^2(t) - \ldots\;, \tag{29}$$

where, $\mu_0 = \dfrac{p}{2\left(S_{cr}-S_0\right)} << 1$ – small parameter.

Substituting equation (29) into (28), we obtain:

$$\begin{aligned} q \approx \frac{1}{\sqrt[4]{1-2\mu_0\,\Phi(t)}}\Bigg\{&A\cos\Omega\left[t-\mu_0\int\limits_0^t\Phi(t)\,dt - \frac{\mu_0^2}{2}\int\limits_0^t\Phi^2(t)\,dt - \ldots\right] + \\ &+ B\sin\Omega\left[t-\mu_0\int\limits_0^t\Phi(t)\,dt - \frac{\mu_0^2}{2}\int\limits_0^t\Phi^2(t)\,dt - \ldots\right]\Bigg\} \end{aligned} \tag{30}$$

Integrals of the form $\int\limits_0^t\Phi^n(t)\,dt$ in practically important cases are expressed in terms of elementary functions.

In the case where the function $\Phi(t)$ can be represented as a polyharmonic process $\Phi(t) = \sum\limits_{n=1}^{\infty} b_k\sin\omega_k t$, then the solution of equation (30) will be represented in the complex form of writing.

$$q \approx \frac{u}{\sqrt[4]{1-2\mu_0\,\Phi(t)}}\exp\left\{i\left[\Omega t + \sum_{k=1}^{n}\xi_k\cos\omega_k t + \gamma\right]\right\}, \tag{31}$$

where $\xi_k = \dfrac{\mu_0\,\Omega\,b_k}{\omega_k}$.

Using relation $e^{i\,z\sin\theta} = \sum\limits_{r=-\infty}^{\infty} J_r(z)\,e^{in\theta}$, where $J_r(z)$ Bessel functions with a whole icon we obtain the following equation:

$$q \approx \frac{u}{\sqrt[4]{1-2\mu_0\,\Phi(t)}} \sum_{r_1, r_2 \ldots = -\infty}^{\infty} J_{r_1}(\xi_1)\, J_{r_2}(\xi_2) \ldots J_{r_n}(\xi_n) \times \times \exp\{ i\, [(\Omega - r_1\omega_1 - r_2\omega_2 - \ldots - r_n\omega_n) t + \gamma] \} . \quad (32)$$

The analysis of expression (31) indicates the presence in the total vibration of harmonic components with frequencies of the $\Omega + r_1\omega_1 + r_2\omega_2 + \ldots + r_n\omega_n$ and amplitudes proportional to the product of Bessel functions $J_{r_1}(\xi_1)\, J_{r_2}(\xi_2) \ldots J_{r_n}(\xi_n)$.

The oscillation spectrum is practically limited due to the properties of Bessel functions and because of negligible values provided that their argument is much smaller than the index. For example, under the $|\xi| << 1$ condition for a fixed index *r*, we get:

$$J_r(\xi) \approx \frac{1}{\Gamma(r+1)} \left(\frac{\xi}{2}\right)^r \approx \frac{1}{r!} \left(\frac{\xi}{2}\right)^2 , \quad (33)$$

where $\Gamma(r+1)$ – gamma function of an integer argument with parameter values $\xi = 0.1$, $J_1(\xi) = 0.05$, $J_2(\xi) = 0.00125$.

At the same time, the value of the $J_0(\xi) = 1 - \left(\frac{\xi}{2}\right)^2$ function in this case is 0.9975, i.e. very close to unity.

Consequently, for small values of ξ_k the frequency spectrum of the oscillations essentially consists of the fundamental frequency Ω and the frequencies $\Omega \pm \omega_k$ (in the case of polyharmonic excitation) and $\Omega \pm k\omega$ (in the case of periodic excitation of vibrations of the Fourier series).

The increase in the amplitudes of free oscillations of bar in modes far from parametric resonance is estimated using equation:

$$\frac{A}{A_0} = \frac{1}{\sqrt[4]{1-2\mu(t)}} = \frac{1}{\sqrt[4]{1-2\mu_0\,\Phi(t)}} . \quad (34)$$

With the value $2\mu_0\,\Phi(t) = 0.1$ this ratio is $\frac{A}{A_0} = 1.026$.

Results and Discussion

Bridge structures for strength, stability and reliability must satisfy the conditions of uninterrupted and safe passage of trains with the maximum permissible axle loads and speeds depending on the class of tracks. The carrying capacity of the railway and the service life of artificial structures primarily depend on the operational category of the structure and the dynamic state (from dynamic stability, to the condition that dangerous vibrations do not appear and dangerous resonance of the amplitude of the oscillations).

The design of the span is made according to the conditions of strength, rigidity, dynamic stability with optimization of the design solution for the minimum cost of the entire life cycle. The tasks of optimizing the costs of maintaining the railway infrastructure require new approaches to managing reliability, risks, and the cost of the life cycle using the methodology for ensuring reliability, availability, maintainability and safety. The account of the dynamic stability of bridge structures is especially important at the initial stage of design development in the design, calculation and design, when the cost of making changes is minimal. This will make it possible to reduce the cost of the entire life cycle of bridge facilities, taking into account the repair work, while ensuring high reliability and the required level of safety for uninterrupted traffic.

There is a relationship between the degree of damage (wear, loss of bearing capacity) of structures and the dynamic state (deviation of the vibration indices from the normative values). Based on the application of the decomposition method for studying the vibrations of bar elements of latticed trusses of bridges, the possibility of a theoretical estimation of the growth indices of their amplitudes under the action of the dynamic load in the form of concentrated forces is investigated. These indices turn out to be high, even taking into account the small values of the excitation coefficients μ and the limited time for finding the force load on the structure $t = \frac{\ell}{v_{cr}}$. The nature of the interaction of forced and parametric oscillations of bar elements in resonance modes is also estimated. This factor has no significant effect on the system.

Conclusions

The authors of the article have taken into account the mutual influencing general and local vibrations of the span structure in assessing the dynamic stability of lattice trusses. The spectrum of parametric oscillations of lattice truss rods under conditions of remoteness from the regions of dynamic instability is investigated. Practical limitation of the frequency spectrum near the value of the carrier frequency equal to the frequency of free oscillations taking into account the effect of longitudinal forces is obtained, as well as the relatively small influence of parametric oscillations in regions remote from living parametric resonance.

Conclusions and further research prospects:

1. The author has clearly demonstrated the effectiveness of the application of the decomposition method for solving similar problems.

2. A methodology for the theoretical estimation of indicators characterizing the increase in the amplitudes of parametric oscillations and the rod elements of lattice trusses of bridges under the action of a dynamic load in the form of concentrated forces is developed.

3. It was proved that there is no explicit interaction of forced and parametric oscillations of the bar elements of lattice truss bridges in resonance modes with each other.

4. Taking into account the dynamic stability analysis presented by the authors, it is recommended to update the current standards for railway metal bridges with latticed trusses.

5. Development of recommendations and technical solutions to increase the dynamic stability and service life of the bridge structures of railway bridges at high speeds of railway transport.

Reference

1. Indejkin A.V. Parametricheskie kolebanija sterzhnevyh jelementov stroitel'nyh konstrukcij pri dejstvii stacionarnyh i podvizhnyh dinamicheskih nagruzok [Parametric oscillations of rod elements of building structures under the action of stationary and dynamic loads]. *Izvestija PGUPS.* 2014. No. 2. Pp. 84–92. (rus)
2. Solovyov S. Aerodinamicheskaya ustoichivost bolsheprolyotnyh stroeniy [Aerodynamic stability of the long-span bridges]. Transport of the Russian Federation. Journal of Science, Practice, Economics. 2016. No. 5(66). Pp. 47–50. (rus)
3. Bolotin V.V. *Dinamicheskaja ustojchivost' uprugih system* [Dynamic stability of elastic systems]. Moscow: Gosudarstvennoe izdatel'stvo tehniko-teoreticheskoj literatury, 1956. 595 p. (rus)
4. Indejkin A.V., Fedotova I.A. The rod elements oscillations of the railway truss bridge in the conditions of high-speed motion of the load. *Proceedings of the third european conference on structural dynamics: Eurodyn`96*. Florence, Italy, 1996. Pp. 783–789.
5. Moiseev N.N. *Asimptoticheskie metody nelinejnoj mehaniki* [Asymptotic methods of nonlinear mechanics]. Moscow: Nauka, 1969. 345 p.
6. Alfutov N.A. *Osnovy rascheta na ustojchivost' uprugih*

Литература

1. Индейкин А.В. Параметрические колебания стержневых элементов строительных конструкций при действии стационарных и подвижных динамирческих нагрузок **//** Известия ПГУПС. 2014. № 2. С. 84–92.
2. Соловьев С.Ю. Аэродинамическая устойчивость большепролетных мостов // Транспорт Российской Федерации. Журнал о науке, практике, экономике. 2016. № 5(66). С. 47–50.
3. Болотин В.В. Динамическая устойчивость упругих систем. М.: Гос. издательство технико-теоретической литературы, 1956. 595 с.
4. Indejkin A.V., Fedotova I.A. The rod elements oscillations of the railway truss bridge in the conditions of high-speed motion of the load // Proceedings of the third european conference on structural dynamics: Eurodyn`96. Florence, Italy, 1996. Pp. 783–789.
5. Моисеев Н.Н. Асимптотические методы нелинейной механики. М.: Наука, 1969. 345 с.
6. Алфутов Н.А. Основы расчета на устойчивость упругих систем. М.: Машиностроение, 1978. 312 с.
7. Пановко Я.Г., Губанова И.И. Устойчивость и колебания упругих систем. Современные концепции, парадоксы и ошибки. 4 изд. М.: Наука, 1987. 352 с.

system [Basics of calculating the stability of elastic systems]. Moscow: Mashinostroenie, 1978. 312 p. (rus)

7. Panovko Ja.G., Gubanova I.I. *Ustojchivost' i kolebanija uprugih sistem. Sovremennye koncepcii, paradoksy i oshibki, 4th ed.* [Stability and oscillations of elastic systems. Modern concepts, paradoxes and mistakes, 4th ed.]. Moscow: Nauka, 1987. 352 p. (rus)
8. Cigler G. *Osnovy teorii ustojchivosti konstrukcij* [Fundamentals of the theory of structural stability]. Moscow: Mir, 1971. 192 p.
9. Beljaev N.M. Ustojchivost' prizmaticheskih sterzhnej pod dejstviem peremennyh prodol'nyh sil [Stability of prismatic rods under the influence of variable longitudinal forces]. *Inzhenernye sooruzhenija i stroitel'naja mehanika.* Leningrad, 1924. Pp. 149–167. (rus)
10. Chelomej V.N. *Dinamicheskaja ustojchivost' aviacionnyh konstrukcij* [Dynamic Stability of Aviation Structures]. Moscow: Aeroflot, 1939. (rus)
11. Brucknall I. New Eurocode requirements for design in high speed railway bridges. *Structures for High-Speed Railway Transportation, IABSE Symposium.* Antwerp, 2003. Vol. 87.
12. Guo W.-W., Xia H., Li H.-L., Zhang T. Dynamic analysis of a new type of railway steel-concrete composite trussed bridge under running trains excitation. *Zhendong yu Chongji/Journal of Vibration and Shock*. 2012. Vol. 31(4). Pp. 128–133.
13. Ding Y., An Y., Wang C. Field monitoring of the train-induced hanger vibration in a high-speed railway steel arch bridge. *Smart Structures and Systems*. 2003. Vol. 17(6). Pp. 1107–1127.
14. Ding Y.-L., Zhao H.-W., Deng L., Li A.-Q., Wang M.-Y. Early warning of abnormal train-induced vibrations for a steel-truss arch railway bridge: case study // Journal of Bridge Engineering. 2017. Vol. 22(11). Article no. 05017011.
15. Sheng X.-W., Zheng W.-Q., He T., Shen Q.-C. Analysis of train-bridge coupling vibration of main bridge of Rongjiang river bridge on Xiamen-Shenzhen Railway. *Bridge Construction*. 2017. Vol. 47(2). Pp. 66–71.
16. Xia H., De Roeck G., Zhang N., Maeck J., Experiment analysis of a high-speed railway bridge under Thalys trains. *Journal of Sound and Vibration*. 2003. No. 268. Pp. 103–113.
17. Xia H., Zhang N., De Roeck G. Dynamic analysis of high speed railway bridge under articulated trains. *Computer and Structures*. 2002. No. 81. Pp. 2467–2478.
18. Martínez-Rodrigo M.D., Lavado J., Museros P. Dynamic performance of existing high-speed railway bridges under resonant conditions retrofitted with fluid viscous dampers. *Engineering Structures*. 2010. Vol. 32(3). Pp. 808–828.
19. Shin J.-R., An Y.-K., Sohn H., Yun C.-B. Vibration reduction of high-speed railway bridges by adding size-adjusted vehicles. *Engineering Structures*. 2010. Vol. 32(9). Pp. 2839–2849.
20. Rocha J.M., Henriques A.A., Calçada R., Rönnquist A. Efficient methodology for the probabilistic safety assessment of high-speed railway bridges. *Engineering Structures*. 2015. Vol. 101. Pp. 138–149.
21. Nan Hu, Gong-Lian Dai, Bin Yan, Ke Liu Recent development of design and construction of medium and long span high-speed railway bridges in China. *Engineering Structures*. 2014. Vol. 74. Pp. 233–241.
22. Mellat P., Andersson A., Pettersson L., Karoumi R. Dynamic behaviour of a short span soil–steel composite bridge for high-speed railways – Field measurements and FE-analysis. *Engineering Structures.* 2014. Vol. 69. Pp. 49–61.
23. Radeström S., Ülker-Kaustell M., Andersson A., Tell V., Karoumi R. Application of fluid viscous dampers to mitigate

8. Циглер Г. Основы теории устойчивости конструкции. М.: Мир, 1971. 192 с.
9. Беляев Н.М. Устойчивость призматических стержней под действием переменных продольных сил // Инженерные сооружения и строительная механика. Л., 1924. С. 149–167.
10. Челомей В.Н. Динамическая устойчивость авиационных конструкций. М.: Аэрофлот, 1939.
11. Brucknall I. New Eurocode requirements for design in high speed railway bridges // Structures for High-Speed Railway Transportation, IABSE Symposium. Antwerp, 2003. Vol. 87.
12. Guo W.-W., Xia H., Li H.-L., Zhang T. Dynamic analysis of a new type of railway steel-concrete composite trussed bridge under running trains excitation // Zhendong yu Chongji/Journal of Vibration and Shock. 2012. Vol. 31(4). Pp. 128–133.
13. Ding Y., An Y., Wang C. Field monitoring of the train-induced hanger vibration in a high-speed railway steel arch bridge // Smart Structures and Systems. 2003. Vol. 17(6). Pp. 1107–1127.
14. Ding Y.-L., Zhao H.-W., Deng L., Li A.-Q., Wang M.-Y. Early warning of abnormal train-induced vibrations for a steel-truss arch railway bridge: case study // Journal of Bridge Engineering. 2017. Vol. 22(11). Article no. 05017011.
15. Sheng X.-W., Zheng W.-Q., He T., Shen Q.-C. Analysis of train-bridge coupling vibration of main bridge of Rongjiang River Bridge on Xiamen-Shenzhen Railway // Bridge Construction. 2017. Vol. 47(2). Pp. 66–71.
16. Xia H., De Roeck G., Zhang N., Maeck J., Experiment analysis of a high-speed railway bridge under Thalys trains // Journal of Sound and Vibration. 2003. № 268. Pp. 103–113.
17. Xia H., Zhang N., De Roeck G. Dynamic analysis of high speed railway bridge under articulated trains // Computer and Structures. 2002. № 81. Pp. 2467–2478.
18. Martínez-Rodrigo M.D., Lavado J., Museros P. Dynamic performance of existing high-speed railway bridges under resonant conditions retrofitted with fluid viscous dampers // Engineering Structures. 2010. Vol. 32(3). Pp. 808–828.
19. Shin J.-R., An Y.-K., Sohn H., Yun C.-B. Vibration reduction of high-speed railway bridges by adding size-adjusted vehicles // Engineering Structures. 2010. Vol. 32(9), Pp. 2839–2849.
20. Rocha J.M., Henriques A.A., Calçada R., Rönnquist A. Efficient methodology for the probabilistic safety assessment of high-speed railway bridges // Engineering Structures. 2015. Vol. 101. Pp. 138–149.
21. Hu N., Dai G.-L., Yan B., Liu K. Recent development of design and construction of medium and long span high-speed railway bridges in China // Engineering Structures. 2014. Vol. 74. Pp. 233–241.
22. Mellat P., Andersson A., Pettersson L., Karoumi R. Dynamic behaviour of a short span soil–steel composite bridge for high-speed railways – Field measurements and FE-analysis // Engineering Structures. 2014. Vol. 69. Pp. 49–61.
23. Radeström S., Ülker-Kaustell M., Andersson A., Tell V., Karoumi R. Application of fluid viscous dampers to mitigate vibrations of high-speed railway bridges // International Journal of Rail Transportation. 2017. Vol. 5. № 1. Pp. 47–62.
24. Cantero D., Arvidsson T., Obrien E., Karoumi R. Train–track–bridge modelling and review of parameters // Structure and Infrastructure Engineering. 2016. Vol. 12. № 9. Pp. 1051–1064.
25. Svedholm C., Zangeneh A., Pacoste C., François S., Karoumi R. Vibration of damped uniform beams with general end conditions under moving loads // Engineering

Indeykin I.A., Chizhov S.V., Shestakova E.B., Antonyuk A.A., Evtukov E.S., Kulagin K.N., Karpov V.V., Golitsynsky G.D. Dynamic stability of the lattice truss of the bridge taking into account local oscillations. *Magazine of Civil Engineering*. 2017. No. 8. Pp. 266–278. doi: 10.18720/MCE.76.23.

vibrations of high-speed railway bridges. *International Journal of Rail Transportation*. 2017. Vol. 5. No. 1. Pp. 47–62.

24. Cantero D., Arvidsson T., Obrien E., Karoumi R. Train–track–bridge modelling and review of parameters. *Structure and Infrastructure Engineering.* 2016. Vol. 12. No. 9. Pp. 1051–1064.
25. Svedholm C., Zangeneh A., Pacoste C., François S., Karoumi R. Vibration of damped uniform beams with general end conditions under moving loads. *Engineering Structures*. 2016. Vol. 126. Pp. 40–52.
26. Cantero D., Ülker-Kaustell M., Karoumi R. Time-frequency analysis of railway bridge response in forced vibration. *Mechanical Systems and Signal Processing*. 2016. Vol. 76-77. Pp. 518–530.
27. Cantero D., Karoumi R. Numerical evaluation of the mid-span assumption in the calculation of total load effects in railway bridges. *Engineering Structures*. 2016. Vol. 107. Pp. 1–8.
28. Andersson A., Karoumi R. Dynamics of railway bridges, analysis and verification by field tests. *EVACES'15, 6th International Conference on Experimental Vibration Analysis for Civil Engineering Structures*. 2015. Vol. 24. Pp. 12.
29. *EN 1991-2 (2003)* (English): Eurocode 1: Actions on structures - Part 2: Traffic loads on bridges [Authority: The European Union Per Regulation 305/2011, Directive 98/34/EC, Directive 2004/18/EC]
30. *EN 1991-1-1 (2002)* (English): Eurocode 1: Actions on structures - Part 1-1: General actions - Densities, self-weight, imposed loads for buildings [Authority: The European Union Per Regulation 305/2011, Directive 98/34/EC, Directive 2004/18/EC]

Structures. 2016. Vol. 126. Pp. 40–52.

26. Cantero D., Ülker-Kaustell M., Karoumi R. Time-frequency analysis of railway bridge response in forced vibration // Mechanical Systems and Signal Processing. 2016. Vol. 76–77. Pp. 518–530.
27. Cantero D., Karoumi R. Numerical evaluation of the mid-span assumption in the calculation of total load effects in railway bridges // Engineering Structures. 2016. Vol. 107. Pp. 1–8.
28. Andersson A., Karoumi R. Dynamics of railway bridges, analysis and verification by field tests // EVACES'15, 6th International Conference on Experimental Vibration Analysis for Civil Engineering Structures. 2015. Vol. 24. Pp. 12.
29. EN 1991-2 (2003) (English): Eurocode 1: Actions on structures - Part 2: Traffic loads on bridges [Authority: The European Union Per Regulation 305/2011, Directive 98/34/EC, Directive 2004/18/EC]
30. EN 1991-1-1 (2002) (English): Eurocode 1: Actions on structures - Part 1-1: General actions - Densities, self-weight, imposed loads for buildings [Authority: The European Union Per Regulation 305/2011, Directive 98/34/EC, Directive 2004/18/EC]

Andrey Indeykin,
+7(812)457-82-49; andrey.indeykin@mail.ru

Sergei Chizhov,
+7(921)793-53-21; sergchizh@yandex.ru

Ekaterina Shestakova,
+7(921)094-51-06; ekaterinamost6@gmail.com

Anatoly Antonyuk,
+7(999)025-18-33; aaa.12.03.1992@mail.ru

Sergey Evtukov,
+7(911)258-85-55; s.a.evt@mail.ru

Nikolay Kulagin,
+7(812)316-20-22; lmgt@lenmetro.ru

Vladimir Karpov,
+7(911)710-59-38; vvkarpov@lan.spbgasu.ru

Dmitriy Golitsynsky,
+7(812)457-82-69; pgupstm@yandex.ru

Андрей Викторович Индейкин,
+7(812)457-82-49;
эл. почта: andrey.indeykin@mail.ru

Сергей Владимирович Чижов,
+7(921)793-53-21;
эл. почта: sergchizh@yandex.ru

Екатерина Борисовна Шестакова,
+7(921)094-51-06;
эл. почта: ekaterinamost6@gmail.com

Анатолий Анатольевич Антонюк,
+7(999)025-18-33;
эл. почта: aaa.12.03.1992@mail.ru

Сергей Аркадьевич Евтюков,
+7(911)258-85-55; эл. почта: s.a.evt@mail.ru

Николай Иванович Кулагин,
+7(812)316-20-22; эл. почта: lmgt@lenmetro.ru

Владимир Васильевич Карпов,
+7(911)710-59-38;
эл. почта: vvkarpov@lan.spbgasu.ru

Дмитрий Михайлович Голицынский,
+7(8124578269; эл. почта: pgupstm@yandex.ru

Индейкин А.В., Чижов С.В., Шестакова Е.Б., Антонюк А.А., Евтюков С.А., Кулагин Н.И., Карпов В.В., Голицынский Д.М. Динамическая устойчивость решетчатой фермы моста с учетом местных колебаний // Инженерно-строительный журнал. 2017. № 8(76). С. 266–278.

doi: 10.18720/MCE.76.24

Methods of identification of concrete elastic-plastic-damage models

Методы идентификации упруго-пластических моделей бетона с учетом накопления повреждений

A.V. Benin,
Petersburg State Transport University, St. Petersburg, Russia
A.S. Semenov,
S.G. Semenov,
M.O. Beliaev,
V.S. Modestov,
Peter the Great St. Petersburg Polytechnic University, St. Petersburg, Russia

Канд. техн. наук, заведующий ИЛ "Механическая лаборатория им. проф. Н.А. Белелюбского" А.В. Бенин,
Петербургский государственный университет путей сообщения Императора Александра I, г. Санкт-Петербург, Россия
канд. физ.-мат. наук, доцент А.С. Семенов,
инженер С.Г. Семенов,
студент М.О. Беляев,
ведущий инженер В.С. Модестов,
Санкт-Петербургский политехнический университет Петра Великого, г. Санкт-Петербург, Россия

Key words: concrete; parameter identification; elasticity; plasticity; damage; experiment; finite-element simulation

Ключевые слова: бетон; идентификация параметров материала; упругость; пластичность; повреждение; эксперимент; конечно-элементное моделирование

Abstract. The methodology for identification of mechanical characteristics of the nonlinear material model for concrete, taking into account the elastic-plastic deformation and the damage accumulation under monotonous and cyclic loading, is proposed. The using such improved models of concrete deformation is actual for carrying out finite-element computations of the most important elements of unique and responsible buildings and structures. The proposed methodology is verified for three different types of concrete (B45, B25, B5), including also their preliminary heat treatment at 200 °C, 300 °C, 400 °C and 600 °C. The experiments were carried out on standard specimens of cubic and prismatic form under compression, as well as on dog-bone-shaped specimens under tension. Elasticity and plasticity moduli, ultimate strengths in compression and tension, damage evolutions during deformation process were obtained in tests. Particular attention has been paid to the search for reliable and effective methods for determining damage based on cyclic deformation curves in the pre-peak and after-peak loading regimes. Comparison of simulation results with experimental data under monotonic and cyclic compression demonstrates a good agreement for regular and for overheated concrete.

Аннотация. Предложена методика идентификации механических характеристик модели неупругого деформирования бетона, учитывающая упруго-пластическое деформирование и накопление повреждений при монотонном и циклическом нагружении. Использование подобных уточненных моделей деформирования бетона актуально при проведении конечно-элементных расчетов наиболее ответственных узлов уникальных зданий и сооружений. Методика верифицирована для трех различных сортов бетона (B45, B25, B5), включающих также их предварительную термическую обработку при 200 °C, 300 °C, 400 °C и 600 °C. Эксперименты выполнялись на стандартных кубических и призматических образцах при сжатии, а также на образцах-восьмерках при растяжении. В процессе идентификации определялись упругие и пластические модули, характеристики прочности при сжатии и растяжении, а также зависимости характеризующие процесс накопления повреждений с ростом пластических деформаций. Особое внимание уделялось поиску надежных и эффективных методов определения поврежденности на основе кривых циклического деформирования в допиковой и запиковой областях нагружения. Сравнение полученных результатов конечно-элементных расчетов с использованием предложенной модели материала с экспериментальными данными продемонстрировало хорошее соответствие для стандартных и термообработанных бетонов.

Бенин А.В., Семенов А.С., Семенов С.Г., Беляев М.О., Модестов В.С. Методы идентификации упруго-пластических моделей бетона с учетом накопления повреждений // Инженерно-строительный журнал. 2017. № 8(76). С. 279–297.

Introduction

The elastic-plastic models with account of damage accumulation [1–6] provide effective tools for the modeling nonlinear concrete behavior [7, 8] with taking into account irreversible deformation after unloading, softening effect after strength peak, inelastic volumetric expansion and stiffness degradation. The considered class of concrete models is able also to describe different damage nature under tension (due to progressive microcracking) and under compression (because of crushing); permanent degradation of material stiffness under cyclic loading conditions; stiffness recovery while transiting from tension to compression; anisotropy of mechanical characteristics (concerning strength, hardening, damage) under tension and compression.

There are many numerical implementations of such type of material models, for example, in commercial software ABAQUS [9]. One of the main difficulties in use of such models in practice is an identification of the material parameters for the computation of real concrete and reinforced concrete structures [10–13]. There are few resent researches aimed to obtain all parameters for elastic-plastic-damage model [14, 15]. A calibration of concrete parameters based on digital image correlation was proposed in [16]. Analytical methods of concrete stress-strain analysis under cyclic loading with taking into account of creep are used in [17, 18]. Features of the concrete behavior at elevated temperatures are considered in [15, 19].

The main aim of the study is development of the methodology for the elastic-plastic-damage concrete model parameter identification. To achieve the goal, the following tasks were accomplished:

- design of test setup for the correct control test and obtaining stress-strain curves;
- carrying out experiments using recommended Russian State Standard specimens [20] and identifying model parameter;
- search for reliable and effective methods for damage evaluation based on cyclic deformation curves in the pre-peak and after-peak loading regimes;
- validation of identified parameters using finite-element computations of stress-strain state and fracture of experimental specimens and structural elements.

To use the concrete damage plasticity model in ABAQUS [9] the following concrete parameters must be experimentally defined and set:

- initial (undamaged) elastic moduli (E_0, v_0);
- plasticity characteristics (stress-strain curves under compression σ_c (ε_{in}) and under tension σ_t (ε_{cr}), dilation angle β; flow potential eccentricity m;. the ratio of initial equibiaxial compressive yield stress to initial uniaxial compressive yield stress f_{b0} / f_c; the ratio K_c of the second stress invariant on the tensile meridian to that on the compressive meridian);
- viscosity parameter μ, used for the visco-plastic regularization of the concrete constitutive equations;
- damage evolution diagrams under compression D_c (ε_{in}) and under tension D_t (ε_{cr}).

The procedure of plasticity parameters identification is considered in detail in [14].

To determine material parameters the following types of experiments are necessary in general case:

- monotonic uniaxial compression test;
- monotonic uniaxial tension test;
- biaxial loading test;
- cyclic loading test.

The main focus of this paper is on the definition of the concrete damage based on cyclic stress-strain curves. The curves of monotonous loading are not sufficient to determine the plastic deformation and damage of concrete therefore an analysis of the cyclic deformation curves is necessary for our aims. The results of previous basic experimental investigations of concrete under cyclic loading are presented in [21–25] for compression and in [26–28] for tension. In dimensionless coordinates the cyclic stress-strain curves under tension (Fig. 1b) demonstrate a larger scattering than the curves under compression (Fig. 1a). However, in both cases, nonlinearities of the unloading and reloading branches are observed for each cycle. This presents the main difficulty in identifying the damage. To eliminate this uncertainty a comparison of 30 different (known and original) methods for determining the degraded stiffness is performed in this paper with taking into account the conditions of admissible values of the damage, the monotonic damage growth, and the localization conditions. The validation of the considered methods is carried out on the basis of comparison with the results of the performed tests and verification in the finite element simulations of characteristic structural elements.

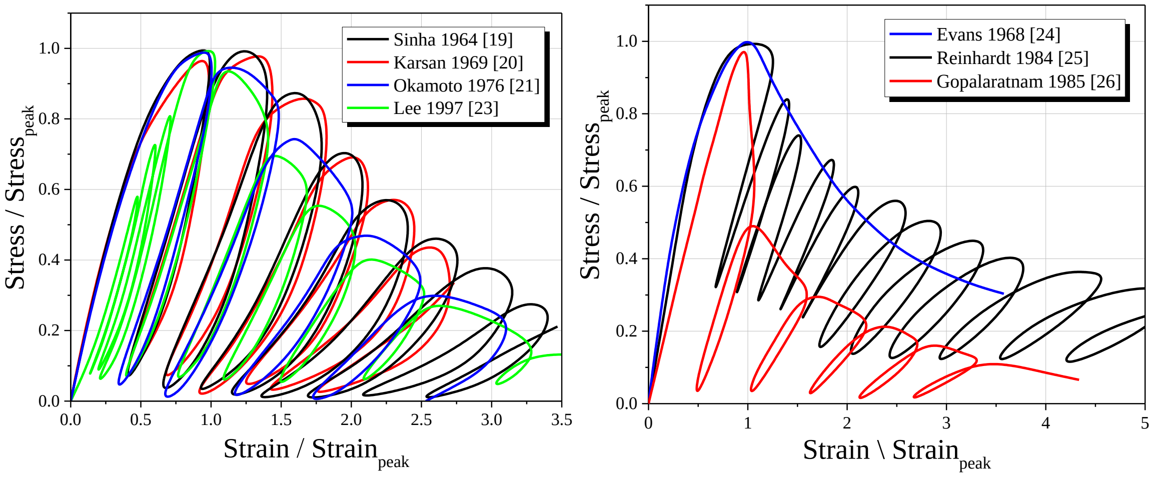

a) b)

Figure 1. Cyclic stress-strain curves: a) compression and b) tension for various concretes [21–28]

Methods

Test setup

The test setup (Fig. 2a) is based on Shimadzu AGX300 electromechanical test machine. The fixtures (Fig. 2b) for tensile tests and deformation sensor frame (Fig. 2c) were designed and produced.

a) b) c)

Figure 2. Test machine (a), tensile test fixtures (b) and strain sensor frame (c)

There are two Heidenhain ST1278 length gauge sensors used for strain measurement. The sensors were interfaced with test machine controller and result strain was calculated as average of two sensors measurements for neglecting influence of bending effect. The strain sensor frame was installed directly on the specimen. This approach allows obtaining the direct strain measurement during testing and as result to measure correctly elastic modulus (see, for example, comparison of modules measured by different methods in table 2 from [15]). Such design allows to perform experiments in the temperature chamber and using quartz glass tubes for precisely strain measurement.

Бенин А.В., Семенов А.С., Семенов С.Г., Беляев М.О., Модестов В.С. Методы идентификации упруго-пластических моделей бетона с учетом накопления повреждений // Инженерно-строительный журнал. 2017. № 8(76). С. 279–297.

Specimens

Specimens were prepared according to the recommendation of Russian State Standard [22]. There are three types of specimens:

- cubes 100×100×100 mm for concrete class (cube strength) definition,
- prisms 100×100×400 mm for compression experiments,
- dog-bone specimens for tension experiments.

The samples were made from three different types of concrete with standard cube strength class of:

- B45 (Concrete 1),
- B25 (Concrete 2),
- B5 (Concrete 3).

Concrete mixture recipe for Concrete 1 is 400 kg/m^3 of CEM I 42.5R, 700 kg/m^3 of 0/4 gabbro sand, 1125 kg/m^3 of 5/10 gabbro coarse aggregate, 120 kg/m3 of fly-ash, 230 kg/m^3 of water and 35 kg/m^3 of plasticizers and modifiers; for Concrete 2 is 410 kg/m^3 of CEM I 42.5R, 340 kg/m^3 of 0/5 haydite sand, 400 kg/m^3 of 5/10 claydite gravel, 95 kg/m3 of fly-ash, 216 kg/m^3 of water and 40 kg/m^3 of modifiers; for Concrete 3 is 180 kg/m^3 of CEM I 42.5R, 185 kg/m^3 of 0/5 haydite sand, 150 kg/m^3 of 5/10 claydite gravel, 120 kg/m3 of fly-ash, 130 kg/m^3 of water and 25 kg/m^3 of plasticizers and modifiers. Specimens were casted in standard steel forms, extracted from forms after 3 days and cured in the 95% humidity and 20°C temperature environment during 28 days.

A part of specimens have a preliminary heating treatment at temperatures at 200 °C, 300 °C, 400 °C and 600 °C. The heating rate was 10 °C/h. It should be noted that when overheating concrete at temperature higher than 400 °C a network of cracks appears (Fig. 3). While overheating at temperature of up to 600 °C with increased heating rate of 100 °C/h, which simulated the emergency mode, a specimen of Concrete 2 exploded in the furnace.

Some microstructural stresses appear in the process of heating, being caused by different coefficients of linear expansion of aggregate and matrix or by other processes, which requires a special individual study.

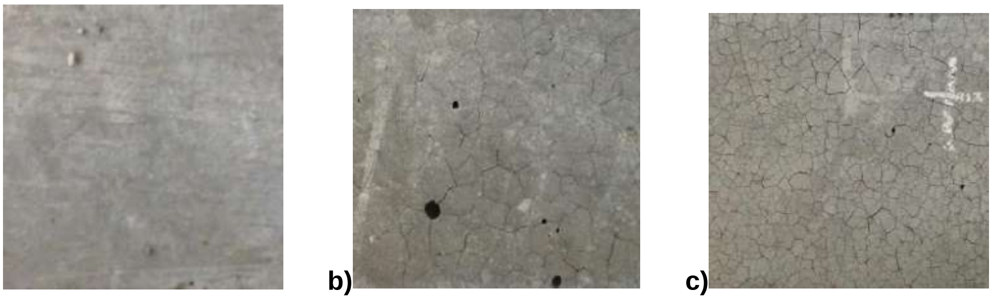

a) b) c)

Figure 3. Surfaces of Concrete 2 specimens with different overheating temperatures: a) 300°C, b) 400°C, c) 600°C

Results and Discussion

Experimental results

As a result of numerous experiments, the following data were obtained:

- cube strength for Concrete 1,2,3 at 20°C;
- concrete-to-steel bond strength at different test temperatures (Concrete 1);
- monotonic compression stress-strain curves for Concrete 1,2,3 for different overheating temperatures;
- monotonic tension stress-strain curves for Concrete 1,2,3 for different overheating temperatures;
- cyclic compression stress-strain curves for Concrete 1,2,3 for different overheating temperatures;
- cyclic tension stress-strain curves for Concrete 1,2,3 for different overheating temperatures.

Typical cyclic stress-strain curves containing the post-peak behavior under compression and tension for the specimens from the overheated concrete are given in Figs. 4a and b. These curves are basis for the parameter determination of the evolution law for the plastic strain and damage.

Specimens from non-overheated concrete show in experiments a sudden failure, displacement instability and snap-back phenomena usually in the softening branch. It is especially difficult to obtain the tensile curves (see Fig. 4b). Therefore pure load or displacement control test techniques are not enough to control the whole test including softening branch. The optimal test technique is a mixed control system [29, 30]. Specimens from the overheated concrete allow for more easily to measure the after-peak behavior (compare Figs. 4c,d with Figs. 4a,b). Carrying out experiments on such concretes opens the possibility of investigating in more detail the post-peak behavior on test machines with standard control.

Failure modes of specimens under compression and tension are shown in Figure 5 for Concrete 1,2,3. Overheating and concrete type have no significant effect of failure mode. The greatest differences are observed when comparing tension and compression.

The overheating has a significant effect on the elastic modulus and strength (Fig. 6). A noticeable drop in properties is observed after 300 °C. This correlates well with the appearance of cracks network (Fig. 3).

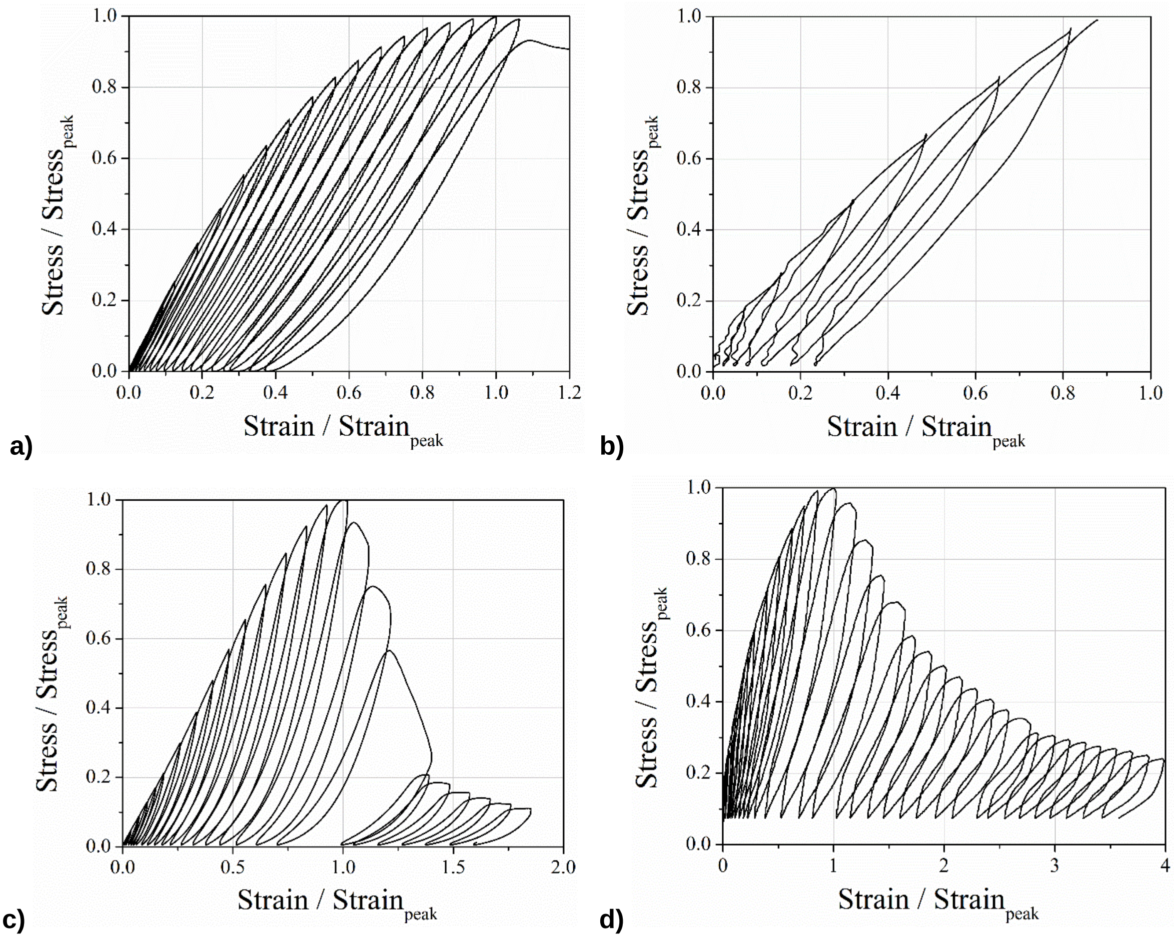

Fig. 4. Typical cyclic stress-strain curves for Concrete 1:
a) compression (non-overheated), b) tension (non-overheated),
c) compression (overheated at 600°C), d) tension (overheated at 600°C)

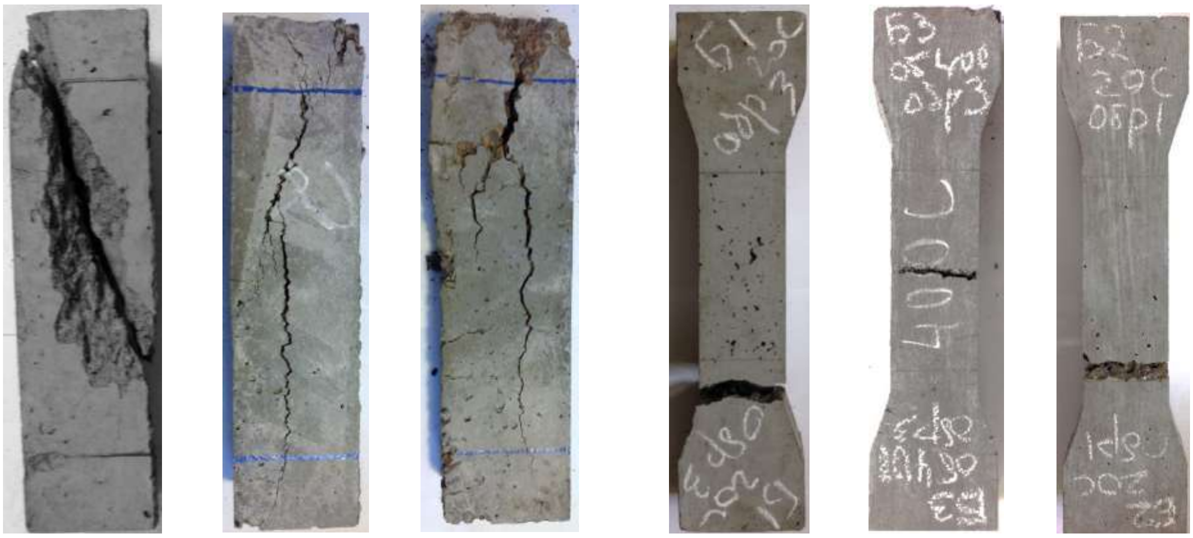

a) b) c) d) e) f)

Figure 5 Failure modes: a) compression of non-overheated Concrete 1, b) compression overheated at 400°C Concrete 2, c) compression of non-overheated Concrete 3, d) tension of non-overheated Concrete 1, e) tension of overheated at 400°C Concrete 2, f) tension of non-overheated Concrete 3

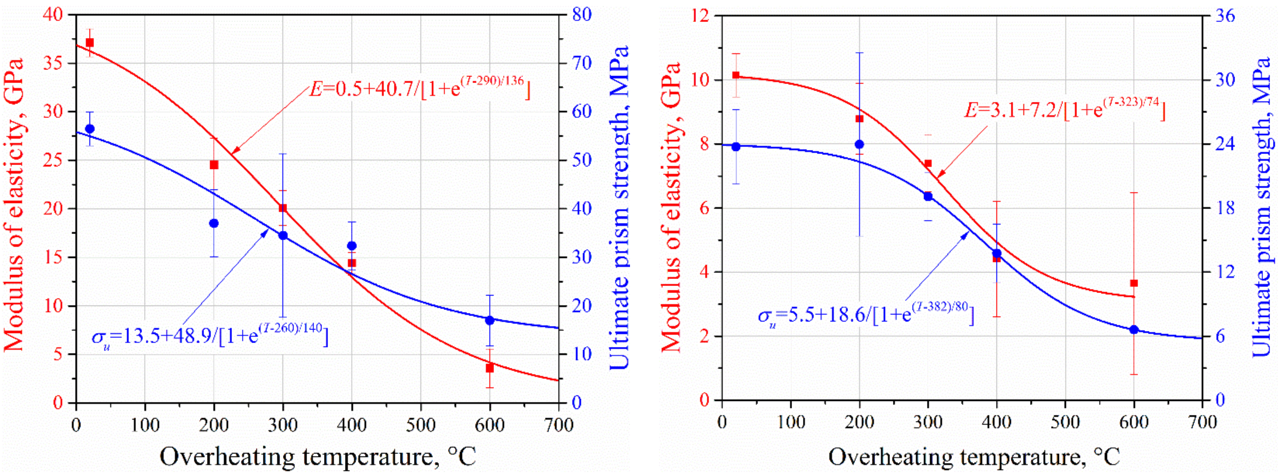

a) b)

Figure 6 Overheating temperature dependence of the elastic modulus and compressive strength for: a) Concrete 1 and b) Concrete 2

Constitutive equations

The three dimensional rate-independent elastic-plastic material model of concrete deformation with taking into account damage accumulation is considered. In order to capture the phenomenon of elastic stiffness degradation of the concrete as well as its irreversible deformations upon monotonic and cyclic loading, the combined use of elastic-plastic constitutive equations along with methods of continuum damage mechanics became vital to better describe the mechanical behavior of concrete. The damage growth is considered as a function of accumulated plastic strains in the coupled elastic-plastic-damage model [1–3].

The difference of the presented model from the elastic-damage and elastic-plastic models consists in the possibility of simultaneously taking into account the accumulation effect of residual strains and elastic stiffness degradation (see Fig. 7).

Benin A.V., Semenov A.S., Semenov S.G., Beliaev M.O., Modestov V.S. Methods of identification of concrete elastic-plastic-damage models. *Magazine of Civil Engineering*. 2017. No. 8. Pp. 279–297. doi: 10.18720/MCE.76.24.

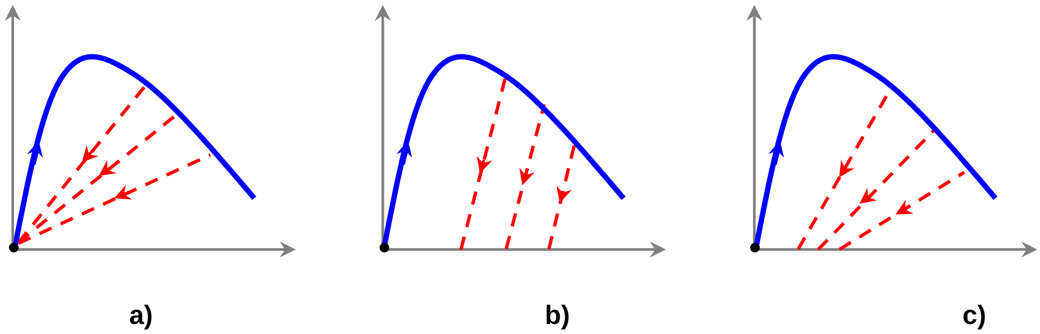

Figure 7. Schematic representation of stress-strain curves with intermediate unloadings for: a) elastic-damage, b) elastic-plastic and c) elastic-plastic-damage models

The progressive propagation of microcracks plays a decisive role in the irreversible deformation of concrete, as it results in the elastic stiffness degradation. This effect is captured in the models by introducing of damage variables. In the simples case the influence of microcracking is introduced via a single scalar damage variable *D* ranging from 0 for the undamaged material to 1 for completely damaged material. The constitutive equations of material with scalar isotropic damage have been introduced by Kachanov [31] and further developed by Rabotnov [32] and others.

The constitutive equation of elastic-plastic material with scalar isotropic damage for three dimensional general multiaxial case takes the following form:

$$\boldsymbol{\sigma} = (1-D)\ {}^4\mathbf{C}_0^e \cdot\cdot (\boldsymbol{\varepsilon}-\boldsymbol{\varepsilon}^p) = {}^4\mathbf{C}^e \cdot\cdot (\boldsymbol{\varepsilon}-\boldsymbol{\varepsilon}^p)\,, \tag{1}$$

where $\boldsymbol{\sigma}$ is Cauchy stress tensor, $\boldsymbol{\varepsilon}$ is the strain tensor, $\boldsymbol{\varepsilon}^p$ is the plastic strain tensor, ${}^4\mathbf{C}_0^e$ the initial (undamaged) elastic stiffness of the material, while ${}^4\mathbf{C}^e = (1-D)\ {}^4\mathbf{C}_0^e$ is the degraded elastic stiffness tensor. The effective stress tensor is defined by the relation:

$$\overline{\boldsymbol{\sigma}} = {}^4\mathbf{C}_0^{el} \cdot\cdot (\boldsymbol{\varepsilon}-\boldsymbol{\varepsilon}^p) = \frac{\boldsymbol{\sigma}}{1-D}\,, \tag{2}$$

Microcracking (under tension) and crushing (under compression) in concrete are represented by increasing values of the hardening (softening) variables. These variables control the evolution of the yield surface and the degradation of the elastic stiffness. The yield function represents a surface in effective stress space $F(\overline{\boldsymbol{\sigma}},\tilde{\varepsilon}^p) \le 0$ which determines the states of failure or damage.

The evolution of the scalar degradation variable is defined by the function

$$D = D\left(\overline{\boldsymbol{\sigma}},\tilde{\varepsilon}^p\right), \tag{3}$$

governed by a set of the effective stress tensor $\overline{\boldsymbol{\sigma}}$ and hardening (softening) variables $\tilde{\varepsilon}^p$. In the used in further Lubliner model [1], the stiffness degradation is initially isotropic and defined by degradation variable D_c in a compression zone and variable D_t in a tension zone. Total damage is defined as $D = 1-(1-D_c)(1-D_t)$. Damage states in tension and compression are characterized independently by two hardening variables $\tilde{\varepsilon}_t^p$ and $\tilde{\varepsilon}_c^p$, which are referred to equivalent plastic strains in tension and compression, respectively. The evolution of the hardening variables is given by the following expressions $\dot{\tilde{\varepsilon}}_t^p = r(\overline{\boldsymbol{\sigma}})\dot{\varepsilon}_1^{pl}$ and $\dot{\tilde{\varepsilon}}_c^p = -[1-r(\overline{\boldsymbol{\sigma}})]\dot{\varepsilon}_3^{pl}$, where $r(\overline{\boldsymbol{\sigma}}) = \sum_{\mathrm{i}=1}^{3}\langle\overline{\sigma}_i\rangle / \sum_{\mathrm{i}=1}^{3}|\overline{\sigma}_i|$, ε_1^{pl} and ε_3^{pl} are the maximum and minimum eigenvalues of the plastic strain tensor $\boldsymbol{\varepsilon}^p$; $\overline{\sigma}_1 \ge \overline{\sigma}_2 \ge \overline{\sigma}_3$ are the eigenvalues of the effective stress tensor $\overline{\boldsymbol{\sigma}}$ (2). The Macaulay brackets are defined as $\langle \mathrm{x}\rangle = \frac{1}{2}\left(|\mathrm{x}| + \mathrm{x}\right)$.

The plastic flow is governed by a flow potential function $G(\overline{\boldsymbol{\sigma}})$ according to non-associative flow rule:

$$\dot{\boldsymbol{\varepsilon}}^p = \begin{cases} \mathbf{0}, & F < 0 \text{ or } F = 0, \dot{F} < 0; \\ \dot{\lambda}\dfrac{\partial G(\bar{\boldsymbol{\sigma}})}{\partial \bar{\boldsymbol{\sigma}}}, & F = 0, \dot{F} = 0; \end{cases} \quad . \tag{4}$$

where the loading function $F\left(\bar{\sigma},\tilde{\varepsilon}^p\right) \le 0$ is introduced for the description of the plastic flow onset and is defined by the expression generalized the Drucker-Prager yield condition [1]:

$$F = \frac{1}{1-\alpha}\left(\sqrt{3\bar{J}_2} + \alpha \bar{I}_1 + \theta(\tilde{\varepsilon}^p)\langle \bar{\sigma}_1 \rangle - \gamma \langle -\bar{\sigma}_1 \rangle\right) - \bar{\sigma}_c(\tilde{\varepsilon}_c^p) = 0, \tag{5}$$

where α and γ are material parameters; $-\bar{I}_1/3$ is the effective hydrostatic stress ($\bar{I}_1 = \mathbf{1}\cdot\cdot\bar{\boldsymbol{\sigma}}$, where **1** is the unit tensor); $\sqrt{3\bar{J}_2}$ is the equivalent von Mises stress ($\bar{J}_2 = \frac{1}{2} dev\bar{\boldsymbol{\sigma}}\cdot\cdot dev\bar{\boldsymbol{\sigma}}$), $dev\bar{\boldsymbol{\sigma}} = \bar{\boldsymbol{\sigma}} - \frac{1}{3}\mathbf{1}\bar{I}_1$ is the effective stress deviator. The shape of the loading surface on the deviator plane is determined by the parameter γ. The parameter $\alpha = \dfrac{f_{b0}/f_c - 1}{2f_{b0}/f_c - 1}$ is calculated from the Kupfer curve [33], where f_{b0}, f_c are the initial equibiaxial and uniaxial compressive yield stresses. The function $\theta(\tilde{\boldsymbol{\varepsilon}}^p)$ is defined by the expression $\theta(\tilde{\varepsilon}^p) = \dfrac{\bar{\sigma}_c(\tilde{\varepsilon}_c^p)}{\bar{\sigma}_t(\tilde{\varepsilon}_t^p)}(1-\alpha) - (1+\alpha)$ with $\bar{\sigma}_c, \bar{\sigma}_t$ being effective yield strength values at compression and tension. If a biaxial compression is applied with $\bar{\sigma}_1 = 0$, the Eq. (5) is reduced to the well-known Drucker-Prager yield condition. The shape of loading surface in the deviatoric plane is determined by the parameter $\gamma = \dfrac{3\left[1 - \left(\sqrt{3\bar{J}_2}\right)_{TM} / \left(\sqrt{3\bar{J}_2}\right)_{CM}\right]}{2\left(\sqrt{3\bar{J}_2}\right)_{TM} / \left(\sqrt{3\bar{J}_2}\right)_{CM} + 3}$, where indices TM and CM mean, respectively, the „Tensile Meridian” ($\sigma_1 > \sigma_2 = \sigma_3$) and the „Compressive Meridian” ($\sigma_1 = \sigma_2 > \sigma_3$) in the yield surface.

The plastic potential *G*, which is in general case different from *F*, sets the direction of the plastic flow in (4) and is defined by the expression generalizing the Drucker and Prager yield criterion [1]:

$$G = \sqrt{\left(f_c - m\cdot f_t \cdot \tan\beta\right)^2 + 3\bar{J}_2} + \tfrac{1}{3}\bar{I}_1 \cdot \tan\beta, \tag{6}$$

where f_t and f_c are the uniaxial tensile and compressive strengths of concrete, respectively; β is the dilatation angle, measured in the plane $\frac{1}{3}\bar{I}_1 - \sqrt{3\bar{J}_2}$ at high confining pressure; *m* is flow potential eccentricity, defining the slope of the potential asymptotic behavior.

Further improvements in the accuracy of model predictions can be achieved by using three-invariant loading function in form of the CAP model [34], ensuring the closed yield surfaces, and consideration of anisotropic damage tensor variables [35, 36].

Features of numerical implementation and optimal strategies for obtaining results of finite element modeling for this class of problems are considered in [5, 9, 19, 37].

Material parameter identification

The progressive elastic stiffness degradation from cycle to cycle provides information for the damage calculation. The damage (in compression) is considered as a scalar variable *D*, which is equal to 0 for virgin material and equal to 1 at the failure. As consequence of the equation $E = (1-D)E_0$ (valid under the hypothesis of strain equivalence) the damage variable at *k*-th cycle can be evaluated as:

$$D_k = 1 - E_k / E_0, \tag{7}$$

where E_0 is the value of the initial (undamaged) modulus and E_k is the values of the damaged moduli at the at *k*-th cycle. A typical example of calculation of the current elastic moduli based on a cyclic stress-strain curve for Concrete 2 at 20 ºC (preliminarily overheated at 600 ºC) is shown in Figure 8.

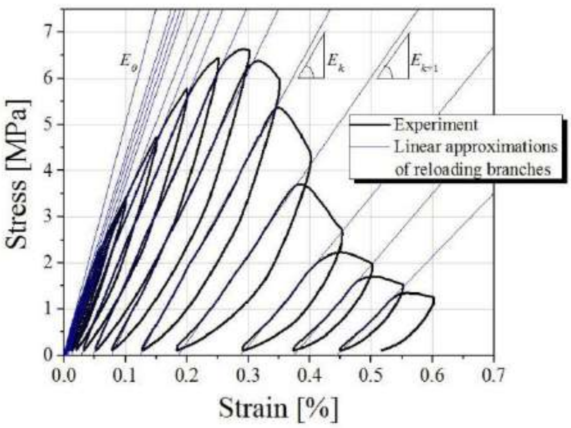

Figure 8. Illustration of the determination of the elastic reloading moduli of the damaged material (cyclic compression of Concrete 2 overheated at 600 °C)

Due to non-linear shape of both unloading and reloading branches of cyclic stress-strain curve it is a non-trivial problem to calculate appropriate elastic moduli of the damaged material. In the plasticity of metals, the current elastic modulus is determined by the tangential modulus at the beginning of the unloading or reloading curves (both are parallel). For the concrete this approach is not acceptable, the unloading and reloading curves are noticeably nonlinear and nonparallel. Therefore, we considered various (three-parametric family) methods for determining elastic modulus degradation based on using:

- different slope definition (tangent, secant, averaging);
- different branches of the cycle (unloading, reloading);
- different locations on the branch (tangent point or averaging range).

The secant slope is defined as an arc chord, connecting the beginning and the end of the branch. The averaging is performed within the branch (reloading (ascending) or unloading (descending)) or part of it. In this case the slope is identified for the selected group of points by the method of least squares.

In a comparative analysis 30 different methods are examined among them:

- 11 variants of tangent to reloading branch at 0%, 10%, 20%, ... , 90%, 100% of load;
- 11 variants of tangent to unloading branch at 0%, 10%, 20%, ... , 90%, 100% of load;
- 3 variants of averaging slope to reloading branch in ranges 0÷100%, 0÷10%, 90÷100% of load;
- 3 variants of averaging slope to unloading branch in ranges 0÷100%, 0÷10%, 90÷100% of load;
- secant slope (chord) of reloading branch in range 0÷100% of total load;
- secant slope (chord) of unloading branch in range 0÷100% of total load.

The following conditions are considered as criteria for the admissibility of the methods:

- $D>0$ (the slope of E_k should be less than E_0);
- $D<1$ (the slope of E_k should be greater than 0);
- monotonic decreasing elastic modulus with plastic deformation, or that is equivalent, monotonic increasing damage from cycle to cycle;
- condition of the possibility of strain localization [38];
- visually, the change in slope should correspond to the observed evolution of hysteresis loops.

For validation of the slope determination methods the obtained experimental cyclic stress-strain curves for Concrete 1, 2, 3 under various heat treatment conditions were used.

The results comparison of the tangents slopes for a representative cycle for Concrete 2 overheated at the temperature of 600 °C are shown in Figure 9. The tangents to the unloading branch shows a significantly larger scatter than the tangents to the reloading curve. The tangential modulus at the beginning of the unloading or reloading curves can't be considered as an adequate approximation of the slope. Appropriate slope approximations are obtained for tangents to reloading branch in the range 20÷60 % of total load for the considered cycle (see also Fig. 10).

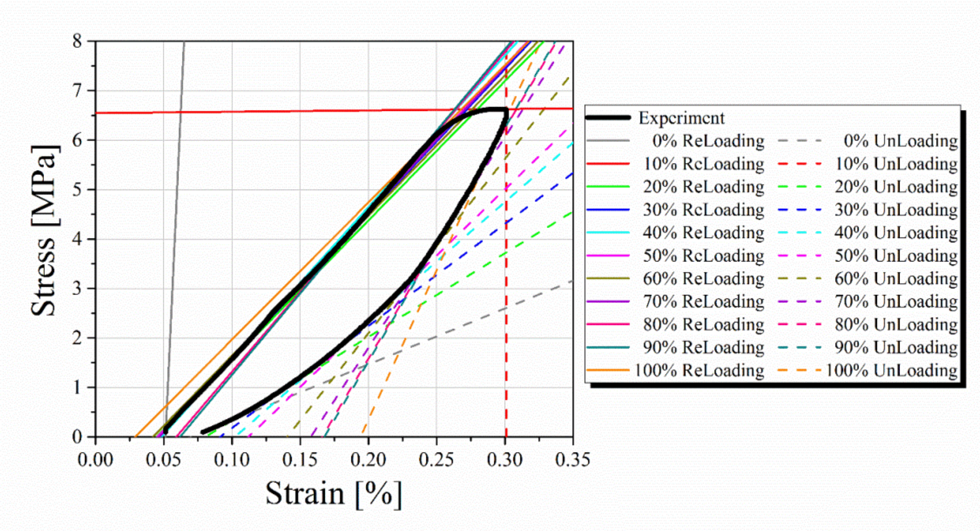

Figure 9. Comparison of tangents slopes for a representative compressive cycle for Concrete 2 overheated at 600 °C

A comparison of all 30 methods for the considering cycle is shown in Figure 10. The results of multivariant computations for the considering cycle and also for others cycles and for others considered concretes show that the averaging slopes in the ranges 0÷100 % and 0÷10 % to reloading branch as well as tangents in the range 20÷60 % to reloading branch provide the best variant of approximation. The range of unallowable damage values is indicated by red shading. The curves, visually corresponding to the slope of the hysteresis loop, are marked with a shaded green area. As a rule, outside this region, there is a lack of monotony (oscillations) in the dependence of the elasticity modulus and damage with the growth of plastic strain.

For the convenience of visual comparison, the most characteristic variants are presented on one graph in Figure 11 for the same hysteresis loop as in Fig. 9 in the form of lines emanating from one point.

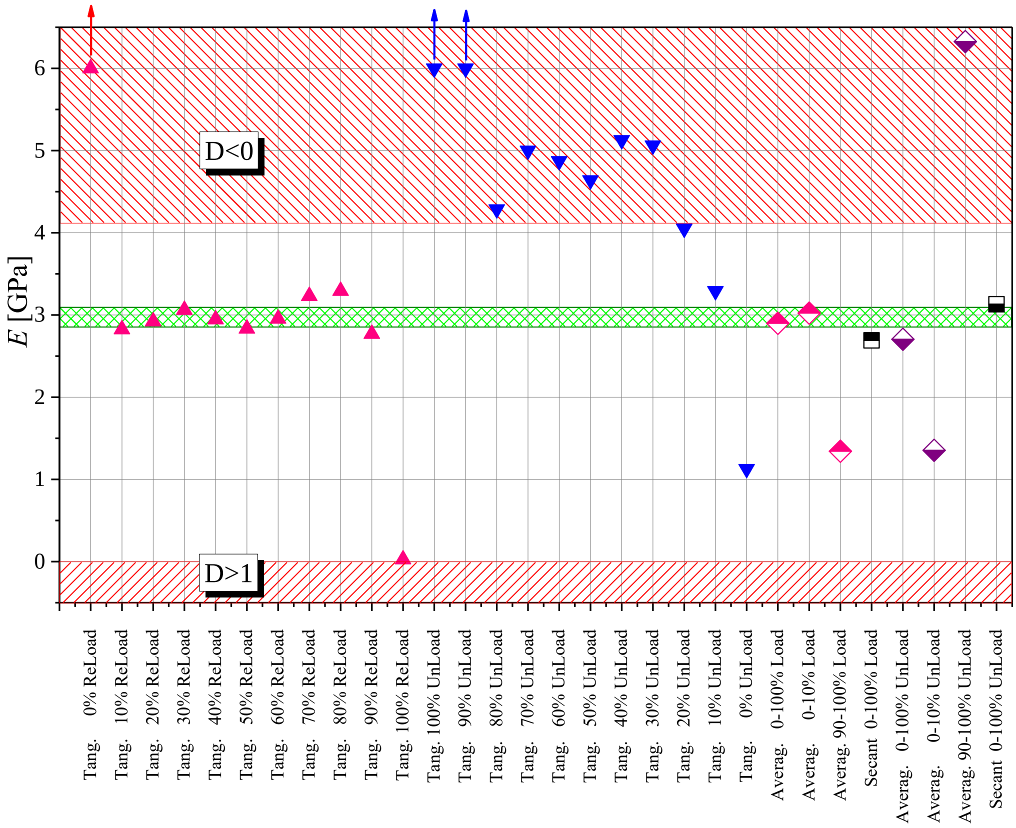

Figure 10. Comparison of slope predictions for a representative compressive cycle for Concrete 2 overheated at 600 °C

Benin A.V., Semenov A.S., Semenov S.G., Beliaev M.O., Modestov V.S. Methods of identification of concrete elastic-plastic-damage models. *Magazine of Civil Engineering*. 2017. No. 8. Pp. 279–297. doi: 10.18720/MCE.76.24.

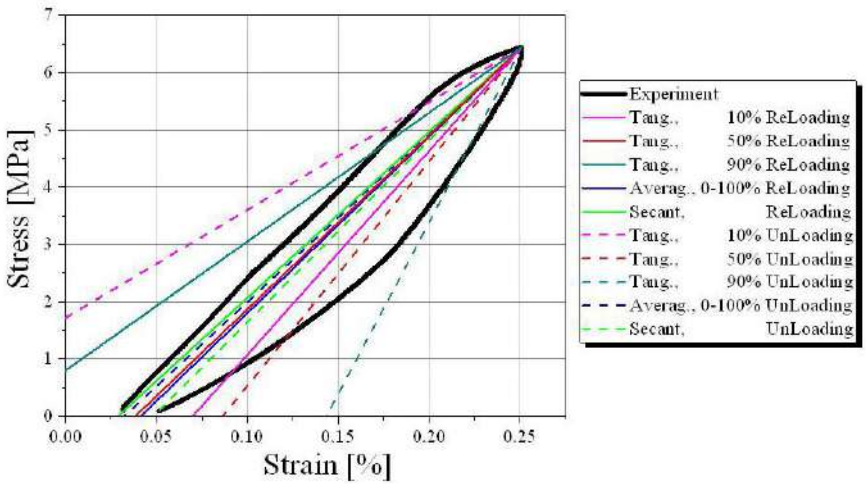

Figure 11. Comparison of tangents slopes for a representative compressive cycle for Concrete 2 overheated at 600 °C

The accuracy of the calculation of the damage affects the accuracy of the definition of plastic strain, which is determined in uniaxial case by the equation:

$$\varepsilon^{p} = \varepsilon - \frac{\sigma}{E} = \varepsilon - \frac{\sigma}{(1-D)E_0}. \tag{8}$$

When specifying the input data in ABACUS, inelastic strain is also used, which is determined as

$$\varepsilon^{in} = \varepsilon - \frac{\sigma}{E_0} = \varepsilon - \frac{(1-D)\sigma}{E}. \tag{9}$$

The relationship between plastic and inelastic deformations can be obtained by the total strain decomposition $\boldsymbol{\varepsilon} = \boldsymbol{\varepsilon}^{e} + \boldsymbol{\varepsilon}^{p} = \boldsymbol{\varepsilon}^{e0} + \boldsymbol{\varepsilon}^{D} + \boldsymbol{\varepsilon}^{p} = \boldsymbol{\varepsilon}^{e0} + \boldsymbol{\varepsilon}^{in}$ and written in the form:

$$\varepsilon^{p} = \varepsilon^{in} + \frac{\sigma}{E_0} - \frac{\sigma}{(1-D)E_0} = \varepsilon^{in} - \frac{D\sigma}{(1-D)E_0}. \tag{10}$$

The results of elastic moduli degradation and damage calculation as function of plastic strain under compression are given in Fig. 12 for Concrete 1 (non-overheated) and Concrete 2 (overheated at 600º).

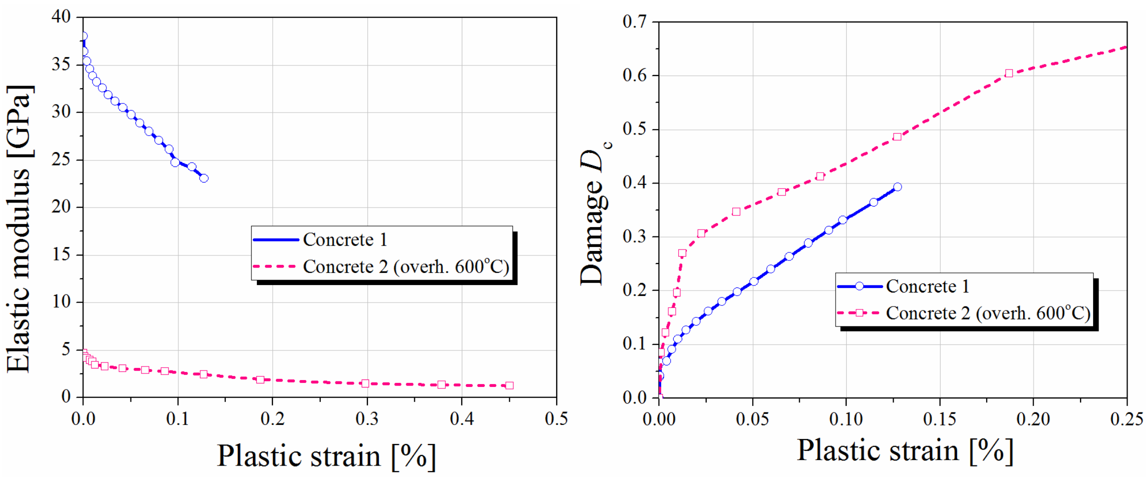

a) **b)**

Figure 12. Elastic modulus degradation (a) and damage evolution (b) with increasing of plastic strain for regular and overheated at 600o Concrete 2 under compression

Comparison of obtained results of damage evolution with experimental data from literature [21-28] are given in Fig. 13. Damage evolution curves are obtained on the base stress-strain curves, which are shown in Figs. 1a, 1b, 4a, 4d, 8. Dependences of the damage on the dimensionless (by the peak value) strain show close monotonic increasing results both in tension and compression. Inflection point in the damage curve for overheated at 600° Concrete 2 is observed at strain peak that corresponds also to the experimental data for overheated concretes considered in [15].

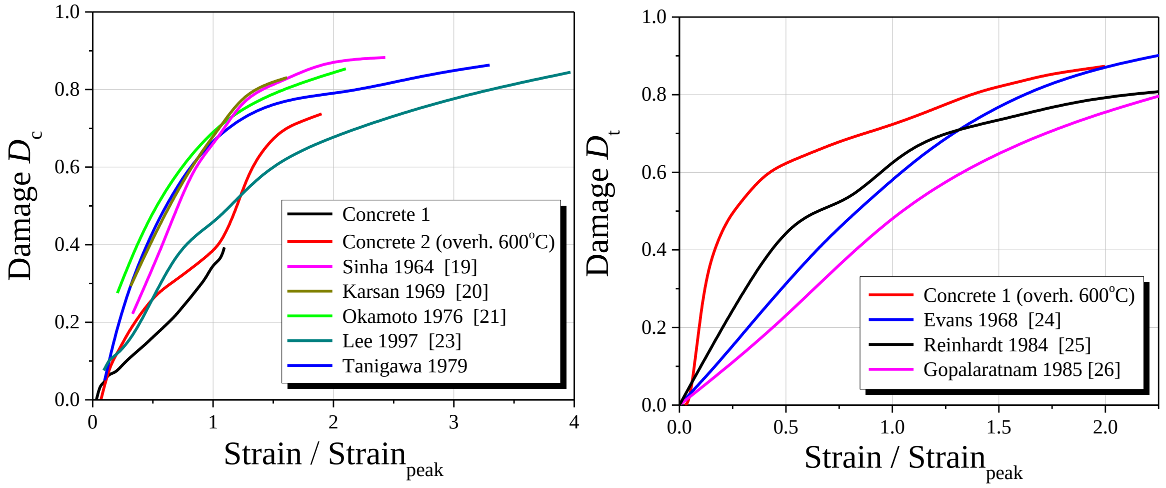

a) b)

Figure 13. Damage evolution under: a) compression and b) tension for various concretes

The exponential approximation [3,6,19,37] can be considered as the simplest approximation of the damage curve:

$$D = 1 - e^{-b\varepsilon}, \tag{11}$$

where *b* is a material constant. An example of a more complex approximation, which allows to more accurately take into account the shape of the curve, is the following expression [39]:

$$D = \begin{cases} 0, & \varepsilon < \varepsilon_0, \\ 1 - e^{-b(\varepsilon - \varepsilon_0)^g}, & \varepsilon \geq \varepsilon_0, \end{cases} \tag{12}$$

where material constant *b* rules how fast *D* approaches 1, *g* is a shape parameter, ε_0 introduces a threshold value.

It is obvious that the compressive and tensile constants must be different.

Note that the experimental data shown in Figure 13 do not allow us to identify the appearance of a clearly expressed threshold greater than 0.2 ε_{peak}.

Validation and verification

Comparison of simulation results with experimental data for samples

The comparison of simulation results with experimental data under monotonic compression for regular Concrete 1 and for overheated at 600 °C Concrete 2 are given in Figure 14. A good agreement is observed in both cases. The model parameters are identified with help of the relations (7) and (10). The constitutive equations (1)-(6) are used in simulations. Note that the considered approach allows to describe strain hardening, softening and post-peak behavior under compression and tension. An example of material constants used in simulations for regular Concrete 1 at 20 °C is given in Table 1.

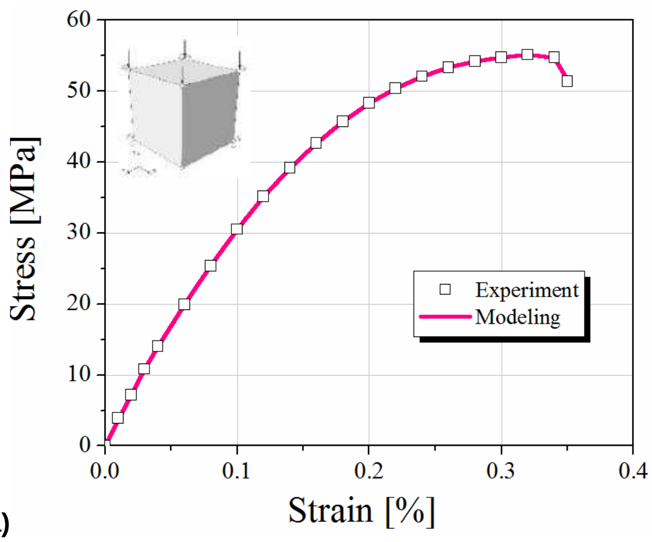

a)

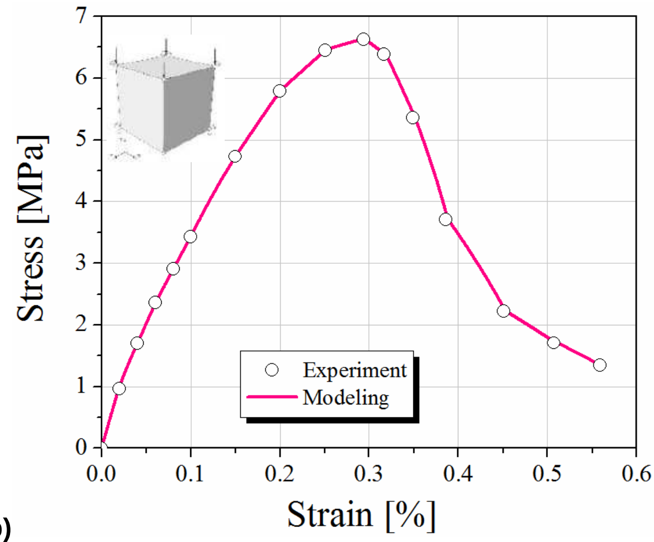

b)

Figure 14. Comparison of simulation results with experimental data under compression for regular Concrete 1 (a) and for overheated at 600 oC Concrete 2 (b)

The validation results of proposed identification procedure under cyclic loading for regular and for overheated concrete are given in Figure 15. Prediction accuracy is lower in comparison with monotonic case, but a satisfactory agreement of experiment and simulation results is observed in this case too.

The considered model is limited by the possibility to predict only the linear unloading. This reduces the accuracy of the computations. One of the possible ways to further improve the material model is to consider structural or multisurface models.

Table 1. Material constants for regular Concrete 1 used in simulations of monotonic and cyclic loading of samples

E [GPa]	ν [-]	β [º]	$\frac{f_{b0}}{f_{c0}}$	σ_c^{peak} [MPa]	ε_c^{peak} [%]	σ_t^{peak} [MPa]	ε_t^{peak} [%]
38	0.2	38	1.12	-55.1	-0.32	2.77	0.035

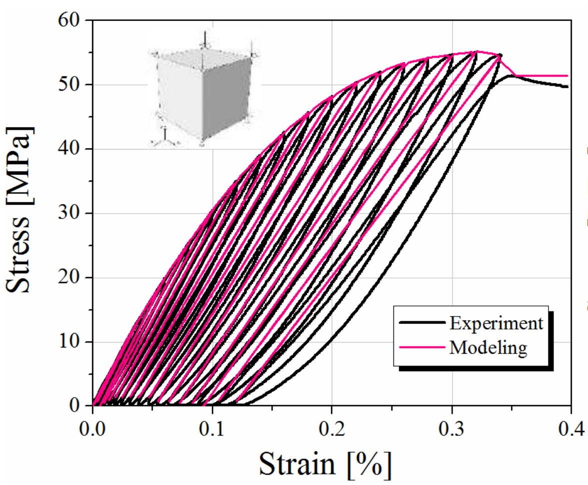

a)

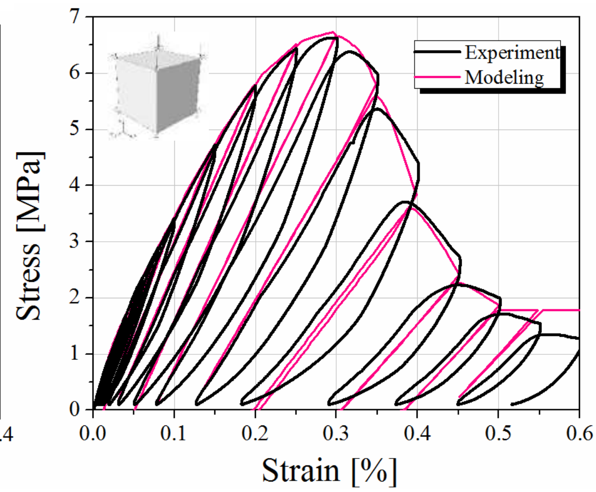

b)

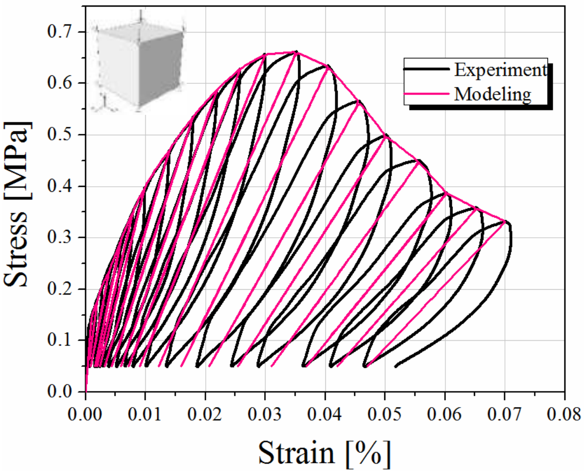

c)

Figure 15. Comparison of simulation results with experimental data for cyclic loading:
a) compression for regular Concrete 1;
b) compression for overheated at 600 °C Concrete 2;
c) tension for overheated at 600 °C Concrete 1

Pulling the reinforcing bar from the concrete block

A direct finite element modeling of the pulling process of the steel reinforcing bar out from the concrete block (in accordance with RILEM/CEB/FIB [40] requirements) with using the elastic-plastic-damage constitutive equations (1)–(6) for the concrete and with taking into account the cohesive behavior of steel-concrete bond is considered.

Geometric parameters, pull-out test experiment (used tensile tester Shimadzu AG-300kN) and axisymmetrical finite-element model are shown in Figures 16 a-c. Material constants used in finite-element simulations are listed in Table 2. A detailed description of the problem and an analysis of the results are given in [41, 11, 12]. Damage field distributions are shown in Figures 16d and e. The damage localization is observed in the vicinity of the reinforcing rod-to-concrete contact.

The comparison of obtained results of finite element simulations with experimental data for the problem of pulling the reinforcing bar from the concrete block demonstrates a good agreement (see Fig. 16f). The proposed approach, which is based on direct FE modeling of reinforced concrete elements with account of elastic-plastic-damage material model of concrete in combination with taking into account cohesive behavior for interface between reinforcement and concrete, allows to describe correctly reinforced-concrete bond at pulling the rod out of the concrete body.

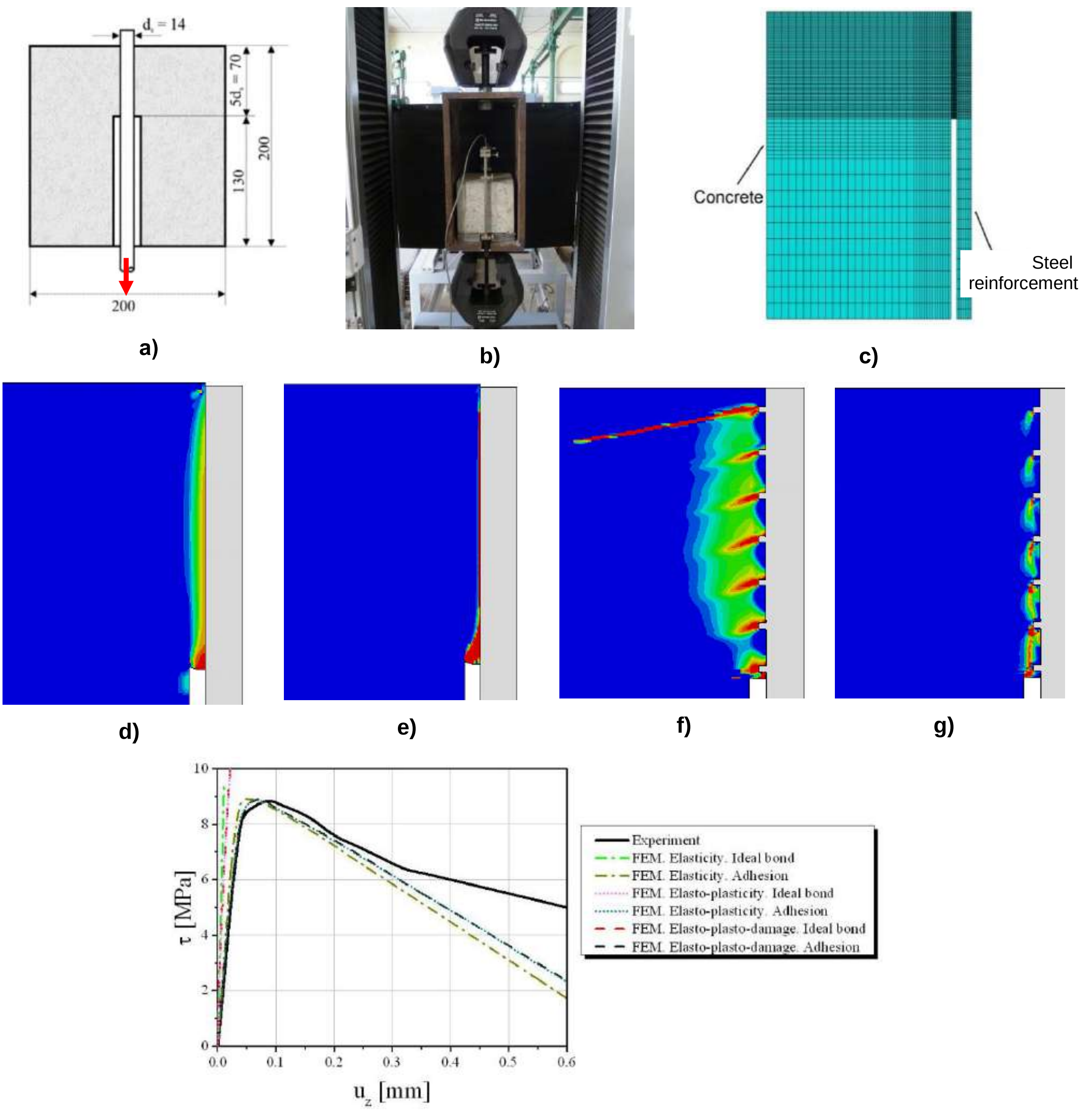

Figure 16. Pull-out test: a) specimen geometry; b) test setup; c) finite-element model; d) damage at tension D_t (model with account of reinforcement ribs); e) damage at compression D_c (model with account of ribs); f) damage at tension D_t (model without account of ribs); g) damage at compression D_c (model without account of ribs); h) shear stress in bond τ vs displacement of reinforcement u_z for various models

Table 2. Concrete material constants used in simulation of pulling the reinforcing bar from the concrete block

E [GPa]	ν [-]	β [º]	$\dfrac{f_{b0}}{f_{c0}}$	σ_c^{peak} [MPa]	ε_c^{peak} [%]	σ_t^{peak} [MPa]	ε_t^{peak} [%]
30	0.2	38	1.12	-18.5	-0.136	1.55	0.0403

Three-point bending of reinforced concrete beam

Finite-element simulation of the fracture process of the reinforced concrete straight beam (Fig. 17) of rectangular cross-section with longitudinal reinforcement under a three-point bending with using of the elastic-plastic-damage constitutive equations (1)–(6) for the concrete is considered.

Geometric parameters, three-point bending experiment (used Instron 1200 KN series SATEC™) and finite-element model (one-fourth of the specimen due to symmetry) are shown in Figure 17a-c. Material properties are listed in Table 3. Maximum principal strain and damage field distributions are shown in Figures 17e and f. The zones of strain and damage localizations are in an agreement with the macrocracks locations and orientations observed in the experiments (Fig. 17d).

The comparison of obtained results of finite element simulations for displacements with experimental data demonstrates a good agreement (see Fig. 17g).

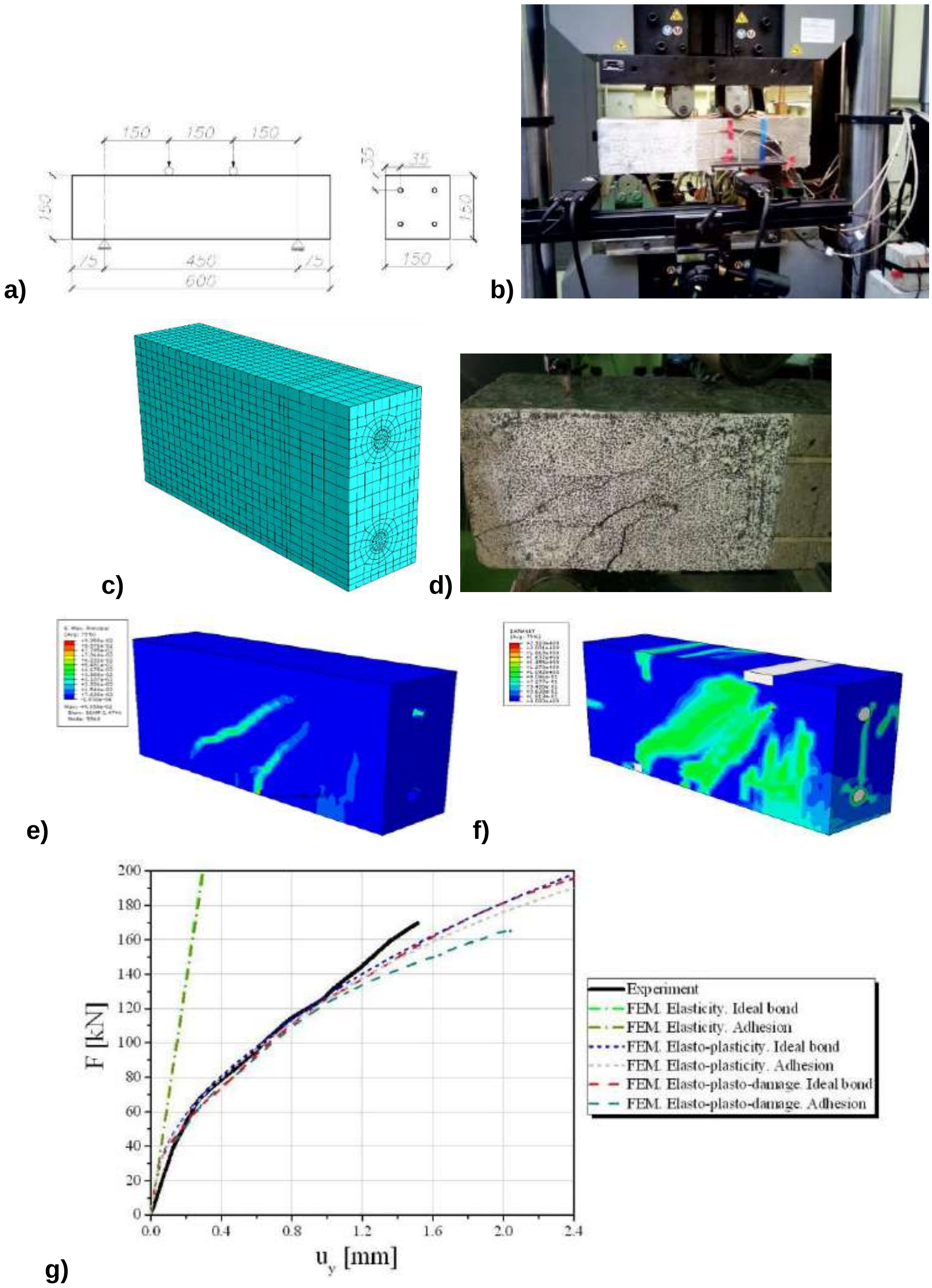

Figure 17. Three-point bending of reinforced concrete beam: a) specimen geometry; b) test setup; c) finite-element model; d) specimen after fracture, e) maximum principal strain; f) damage at tension Dt; g) load vs displacement of the bottom point of the central section of the concrete beam for various models

Benin A.V., Semenov A.S., Semenov S.G., Beliaev M.O., Modestov V.S. Methods of identification of concrete elastic-plastic-damage models. *Magazine of Civil Engineering*. 2017. No. 8. Pp. 279–297. doi: 10.18720/MCE.76.24.

Table 3. Concrete material constants used in simulation of three-point bending of reinforced concrete beam

E [GPa]	ν [-]	β [º]	$\frac{f_{b0}}{f_{c0}}$	σ_c^{peak} [MPa]	ε_c^{peak} [%]	σ_t^{peak} [MPa]	ε_t^{peak} [%]
34.5	0.2	38	1.12	-25.5	-0.163	1.95	0.0441

Examples of other applications of the considered elastic-plastic-damage model in solving real problems of practice, such as corrosion driven spalling of concrete cover at automobile bridge [42] and simulation of fracture process of ballastless deck at railway bridge [13] have been also demonstrated the possibility of applying the considered approach.

Conclusion

The material parameter identification procedure of elastic-plastic-damage concrete model is proposed and validated. The results of multivariant calculations of damage on the base of experimental cyclic stress-strain curves under tension and compression show that the averaging slopes of reloading branch as well as tangents in the middle of reloading branch provide the best variant of approximation. Comparison of simulation results with experimental data under monotonic and cyclic compression demonstrates a good agreement for regular and for overheated concrete. Additional indirect verification of the considered material model and the proposed methods for identifying its parameters is the good accuracy of the simulation results in comparison with the results of the experiments when solving real practical problems, such as the pulling the reinforcing bar from the concrete block and three-point bending of reinforced concrete beam. The offered approach, which is based on direct three-dimensional modeling of reinforced concrete structures with account of continuum damage evolution, allows to describe inelastic deformation, define cracking mechanisms and to evaluate a residual resource of partially destroyed structures. However, practical realization of this approach requires considerable computational effort and additional experimental data concerning concrete mechanical properties.

Reference

1. Lubliner J., Oliver J., Oller S., Oñate E. A Plastic-Damage Model for Concrete. *Int. Journal of Solids and Structures*. 1989. No. 3(25). Pp. 229–326.
2. Voyiadjis G.Z., Abu Lebdeh T.M. Plasticity model for concrete using the bounding surface concept. *Int. J. Plast.* 1994. No. 10(1). Pp. 1–21.
3. Lee J., Fenves G.L. Plastic-damage model for cyclic loading of concrete structures. *Journal of Engineering Mechanics.* 1998. No. 124(8). Pp. 892–900.
4. Kratzig W.B., Pölling R. An elasto-plastic damage model for reinforced concrete with minimum number of material parameters. *Computers and Structures.* 2004. No. 82(15–16). Pp. 1201–1215.
5. Jason L., Huerta A., Pijaudier-Cabot G., Ghavamian, S. An elastic plastic damage formulation for concrete: Application to elementary tests and comparison with an isotropic damage model. *Computer Methods in Applied Mechanics and Engineering.* 2006. No. 195(52). Pp. 7077–7092.
6. Grassl P., Jirasek M. Damage-plastic model for concrete failure. *International Journal of Solids and Structures.* 2006. No. 43. Pp. 7166–7196.
7. Mazars J., Pijaudier-Cabot G. Continuum damage theory- Application to concrete. *Journal of Engineering Mechanics.* 1989. No. 115(2). Pp. 345–365.
8. Voyiadjis G.Z., Taqieddin Z.N. Elastic plastic and damage model for concrete materials: part i - theoretical formulation. *International Journal of Structural Changes in Solids – Mechanics and Appl.* 2009. No. 1(1). Pp. 31–59.
9. ABAQUS User's manual, ver. 6.12 Abaqus Inc.; 2012.
10. Benin A.V., Semenov A.S., Semenov S.G. Fracture simulation of reinforced concrete structure with account of bond degradation and concrete cracking under steel corrosion. *Advances in Civil Engineering and Building Materials. Proc. 2nd Int. Conf. on Civil Eng. and Building Materials.* 2012. Taylor & Francis Group, London.

Литература

1. Lubliner J., Oliver J., Oller S., Oñate E. A plastic-damage model for concrete // Int. Journal of Solids and Structures. 1989. № 3(25). Pp. 229–326.
2. Voyiadjis G.Z., Abu Lebdeh T.M. Plasticity model for concrete using the bounding surface concept // Int. J. Plast. 1994. № 10(1). Pp. 1–21.
3. Lee J., Fenves G.L. Plastic-damage model for cyclic loading of concrete structures // Journal of Engineering Mechanics. 1998. № 124(8). Pp. 892–900.
4. Kratzig W.B., Pölling R. An elasto-plastic damage model for reinforced concrete with minimum number of material parameters // Computers and Structures. 2004. № 82(15–16). Pp. 1201–1215.
5. Jason L., Huerta A., Pijaudier-Cabot G., Ghavamian, S. An elastic plastic damage formulation for concrete: Application to elementary tests and comparison with an isotropic damage model // Computer Methods in Applied Mechanics and Engineering. 2006. № 195(52). Pp. 7077–7092.
6. Grassl P., Jirasek M. Damage-plastic model for concrete failure // International Journal of Solids and Structures. 2006. № 43. Pp. 7166–7196.
7. Mazars J., Pijaudier-Cabot G. Continuum damage theory- Application to concrete // Journal of Engineering Mechanics. 1989. № 115(2). Pp. 345–365.
8. Voyiadjis G.Z., Taqieddin Z.N. Elastic plastic and damage model for concrete materials: Part I - Theoretical Formulation // International Journal of Structural Changes in Solids – Mechanics and Appl. 2009. № 1(1). Pp. 31–59.
9. ABAQUS User's manual, ver. 6.12 Abaqus Inc.; 2012.
10. Benin A.V., Semenov A.S., Semenov S.G. Fracture simulation of reinforced concrete structure with account of bond degradation and concrete cracking under steel corrosion // Advances in Civil Engineering and Building Materials. Proc. 2nd Int. Conf. on Civil Eng. and Building Materials. 2012. Taylor & Francis Group, London.

Pp. 233–237.
11. Benin A.V., Semenov A.S., Semenov S.G., Melnikov B.E. Simulation of degradation of bond between reinforcing bar and concrete. Part 1. Models with account of the discontinuity. *Magazine of Civil Engineering.* 2013. No. 5(40). Pp. 86-99. (rus)
12. Benin A.V., Semenov A.S., Semenov S.G., Melnikov B.E. The simulation of bond fracture between reinforcing bars and concrete. Part 2. Models without taking the bond discontinuity into account. *Magazine of Civil Engineering.* 2014. No. 1 (45). Pp. 23–40. (rus)
13. Benin A.V., Semenov A.S., Semenov S.G. Fracture analysis of reinforced concrete bridge structures with account of concrete cracking under steel corrosion. *Advanced Materials Research.* 2014. No. 831. Pp. 364–369.
14. Jankowiak T., Lodygowski T. Identification of parameters of concrete damage plasticity constitutive model. *Found. Civ. Environ. Eng.* 2005. No 6. Pp. 53–69.
15. Neuenschwander M., Knobloch M., Fontana M. Suitability of the damage-plasticity modelling concept for concrete at elevated temperatures: Experimental validation with uniaxial cyclic compression tests. *Cem. Concr. Res.* 2016. No. 79. Pp. 57–75.
16. Gajewski T., Garbowski T. Calibration of concrete parameters based on digital image correlation and inverse analysis. *Archives of Civil and Mechanical Engineering*. 2014. No. 1(14). Pp. 170–180.
17. Barashikov A.Ia. *Raschet zhelezobetonny`kh konstruktcii` na dei`stvie dlitel`ny`kh peremenny`kh nagruzok* [Structural analysis of reinforced concrete structures under permanently acting loads]. Kiev: Budivel`nik, 1977. 156 p. (rus)
18. Barashikov A.Ia., Shevchenko B.A., Valovoi` A.I. Malotciclovaia vy`noslivost` betona pri szhatii [Low-cycle fatigue of concrete under pressure]. *Beton i zhelezobeton.* 1985. No. 4. Pp. 27–28. (rus)
19. Nechnech W., Meftah F., Reynouard J.M. An elasto-plastic damage model for plain concrete subjected to high temperatures. *Engineering Structures*. 2002. No. 24. Pp. 597–611.
20. *Russian State Standard GOST 10180-12* Concretes. Methods for strength determination using reference specimens. 2013. 30 p. (rus)
21. Sinha B.P., Gerstle. K.H., Tulin.L.G. Stress-strain relations for concrete under cyclic loading. *ACI J Proc.* 1964. No. 61(2). Pp. 195–211.
22. Karsan I.D., Jirsa J.O. Behavior of concrete under compressive loading. *Journal of the Structural Division*. 1969. No. 95(ST12). Pp. 2543–2563.
23. Okamoto S., Shiomi S., Yamabe K. Earthquake resistance of prestressed concrete structures. *Proceedings of Annual Architectural Instititute of Japan*. 1976. Pp. 1251–1252.
24. Mazars J., Berthaud Y., Ramtani S. The unilateral behavior of damaged concrete. *Engineering Fracture mechanics.* 1990. No. 35(4). Pp. 629–635.
25. Lee Y.-H., Willam K. Mechanical properties of concrete in uniaxial compression. *ACI Materials Journal.* 1997. No. 94(6). Pp. 457–471.
26. Evans R.H., Marathe M.S. Microcracking and stress-strain curves for concrete in tension. *Materials and Structures*. 1968. No. 1(1). Pp. 61–64.
27. Reinhardt H.W. Fracture mechanics of an elastic softening material like concrete. *HERON.* 1984. No. 29(2). Pp. 3–41.
28. Gopalaratnam V.S., Shah S.P. Softening response of plain concrete in direct tension. *ACI Journal proceedings.* 1985. No. 82(3). Pp. 310–323.
29. Taerwe L.R. Influence of steel fibers on strain-softening of high-strength concrete. *ACI Mater J.* 1993.No. 89(1). Pp. 54–60.
30. Osorio E., Bairan J.M., Marı A.R. Lateral behavior of concrete under uniaxial compressive cyclic loading. *Materials and Structures.* 2013. No. 46. Pp. 709–724.

Pp. 233–237.
11. Бенин А.В., Семенов А.С., Семенов С.Г., Мельников Б.Е. Математическое моделирование процесса разрушения сцепления арматуры с бетоном. Часть 1. Модели с учетом несплошности соединения // Инженерно-строительный журнал. 2013. № 5(40). С. 86–99.
12. Бенин А.В., Семенов А.С., Семенов С.Г., Мельников Б.Е. Математическое моделирование процесса разрушения сцепления арматуры с бетоном. Часть 2. Модели без учета несплошности соединения // Инженерно-строительный журнал. 2014. № 1(45). С. 23–40
13. Benin A.V., Semenov A.S., Semenov S.G. Fracture analysis of reinforced concrete bridge structures with account of concrete cracking under steel corrosion // Advanced Materials Research. 2014. № 831. Pp. 364–369.
14. Jankowiak T., Lodygowski T. Identification of parameters of concrete damage plasticity constitutive model // Found. Civ. Environ. Eng. 2005. Vol. 6(1). Pp. 53–69.
15. Neuenschwander M., Knobloch M., Fontana M. Suitability of the damage-plasticity modelling concept for concrete at elevated temperatures: Experimental validation with uniaxial cyclic compression tests // Cem. Concr. Res. 2016. № 79. Pp. 57–75.
16. Gajewski T., Garbowski T. Calibration of concrete parameters based on digital image correlation and inverse analysis // Archives of Civil and Mechanical Engineering. 2014. № 1(14). Pp. 170–180.
17. Барашиков А.Я. Расчет железобетонных конструкций на действие длительных переменных нагрузок. Киев: Будивельник, 1977. 156 с.
18. Барашиков А.Я., Шевченко Б.А., Валовой А.И. Малоцикловая выносливость бетона при сжатии // Бетон и железобетон. 1985. № 4. С. 27–28.
19. Nechnech W., Meftah F., Reynouard J.M. An elasto-plastic damage model for plain concrete subjected to high temperatures // Engineering Structures. 2002. № 24. Pp. 597–611.
20. ГОСТ 10180-12 Бетоны. Методы определения прочности по контрольным образцам. 2013. 30 с.
21. Sinha B.P., Gerstle. K.H., Tulin.L.G. Stress-strain relations for concrete under cyclic loading // ACI J Proc. 1964. № 61(2). Pp. 195–211.
22. Karsan I.D., Jirsa, J.O. Behavior of concrete under compressive loading // Journal of the Structural Division. 1969. № 95(ST12). Pp. 2543–2563.
23. Okamoto S., Shiomi S., Yamabe K. Earthquake resistance of prestressed concrete structures // Proceedings of Annual Architectural Instititute of Japan. 1976. Pp. 1251–1252.
24. Mazars J., Berthaud Y., Ramtani S. The unilateral behavior of damaged concrete // Engineering Fracture mechanics. 1990. № 35(4). Pp. 629–635.
25. Lee Y.-H., Willam, K. Mechanical properties of concrete in uniaxial compression // ACI Materials Journal. 1997. № 94(6). Pp. 457–471.
26. Evans R.H., Marathe M.S. Microcracking and stress-strain curves for concrete in tension // Materials and Structures. 1968. № 1(1). Pp. 61–64.
27. Reinhardt H.W. Fracture mechanics of an elastic softening material like concrete // HERON. 1984. № 29(2). Pp. 3–41.
28. Gopalaratnam V.S., Shah S.P. Softening response of plain concrete in direct tension // ACI Journal proceedings. 1985. № 82(3). Pp. 310–323.
29. Taerwe L.R. Influence of steel fibers on strain-softening of high-strength concrete // ACI Mater J. 1993. № 89(1). Pp. 54–60.
30. Osorio E., Bairan J.M., Marı A.R. Lateral behavior of concrete under uniaxial compressive cyclic loading // Materials and Structures. 2013. № 46. Pp. 709–724.
31. Качанов Л.М. О времени разрушения в условиях ползучести // Известия АН СССР. Отд-ние техн. наук. 1958. № 8. С. 26–31.

Benin A.V., Semenov A.S., Semenov S.G., Beliaev M.O., Modestov V.S. Methods of identification of concrete elastic-plastic-damage models. *Magazine of Civil Engineering*. 2017. No. 8. Pp. 279–297. doi: 10.18720/MCE.76.24.

31. Kachanov L.M. O vremeni razrusheniya v usloviyakh polzuchesti [On the creep-rapture life]. *Izv. AN SSSR. Ser. Techn. Sci.* 1958. No. 8. Pp. 26–31. (rus)
32. Rabotnov Yu.N. O mekhanizme dlitelnogo razrusheniya [On the delayed fracture mechanics]. *Voprosy prochnosti materialov i konstruktsiy*. Moscow, AN SSSR. 1959. Pp. 5–7. (rus)
33. Kupfer H., Hilsdorf H.K., Rusch H. Behavior of concrete under biaxial stress. *Journal of the American Concrete Institute.* 1969. No. 66. Pp. 656–666.
34. Schwer L.E., Murry Y.D. A three-invariant smooth cap model with mixed hardening. *Int. J. for Num. Anal. Mech. In Geomech.* 1994. No. 18. Pp. 657–688.
35. Voyiadjis G.Z., Taqieddin Z.N., Kattan P.I. Anisotropic damage–plasticity model for concrete. *Int. Journal of Plasticity.* 2008. No. 10(24). Pp. 1946–1965.
36. Semenov A.S. Symmetrization of the effective stress tensor for anisotropic damaged continua. *St. Petersburg State Polytechnical University Journal. Physics and Mathematics.* 2017. No. 2(10). (rus)
37. Abu Al-Rub R.K., Kim S.-M. Computational applications of a coupled plasticity-damage constitutive model for simulating plain concrete fracture. *Engineering Fracture Mechanics.* 2010 No. 10(77). Pp. 1577–1603.
38. Beliaev M.O., Semenov A.S. Lokalizatsiia deformatsii pri chetyrekhtochechnom izgibe armirovannoi betonnoi balki [Strain localization under four-point bending of a reinforced concrete beam]. *Materialy Nauchnogo foruma s mezhdunarodnym uchastiem. Nedelia nauki SPbPU* [Proceedings of Scientific forum with international participation: Science Week SPbPU]. *2*015. Pp. 60–62. (rus)
39. Häussler-Combe U., Hartig J. Formulation and numerical implementation of a constitutive law for concrete with strain-based damage and plasticity. *International Journal of Non-Linear Mechanics.* 2008. No. 43. Pp. 399–415.
40. *RILEM/CEB/FIB.* Recommendation on reinforcement steel for reinforced concrete. RC6. Bond test for reinforcement steel. 2. Pull-out tests. 1983.
41. Beliaev M., Semenov A., Semenov S., Benin A. Simulation of pulling the reinforcing bar from concrete block with account of friction and concrete damage. *MATEC Web of Conferences.* 2016. Vol. 73. No. 04010.
42. Benin A.V., Semenov A.S., Semenov S.G., Melnikov B.E. Finite element modeling of fracture processes and estimation of durability of the road bridge with account of corrosion cracking. *Magazine of Civil Engineering.* 2012. No. 7(33). Pp. 32–42. (rus)

32. Работнов Ю.Н. О механизме длительного разрушения // Вопросы прочности материалов и конструкций. М.: Изд-во АН СССР, 1959. С. 5–7.
33. Kupfer H., Hilsdorf H.K., Rusch H. Behavior of concrete under biaxial stress // Journal of the American Concrete Institute. 1969. № 66. Pp. 656–666.
34. Schwer L.E., Murry Y.D. A three-invariant smooth cap model with mixed hardening // Int. J. for Num. Anal. Mech. In Geomech. 1994. № 18. Pp. 657–688.
35. Voyiadjis G.Z., Taqieddin Z.N., Kattan P.I. Anisotropic damage–plasticity model for concrete // Int. Journal of Plasticity. 2008. № 10(24). Pp. 1946–1965.
36. Семенов А.С. Симметризация тензора эффективных напряжений для сред с анизотропной поврежденностью // Научно-технические ведомости СПБГПУ. Физико-математические науки. 2017. Т. 10. № 2.
37. Abu Al-Rub R.K., Kim S.-M. Computational applications of a coupled plasticity-damage constitutive model for simulating plain concrete fracture // Engineering Fracture Mechanics. 2010. № 10(77). Pp. 1577–1603.
38. Беляев М.О., Семёнов А.С. Локализация деформаций при четырехточечном изгибе армированной бетонной балки // Материалы Научного форума с международным участием. Неделя науки СПбПУ. 2015. С. 60–62.
39. Häussler-Combe U., Hartig J. Formulation and numerical implementation of a constitutive law for concrete with strain-based damage and plasticity // International Journal of Non-Linear Mechanics. 2008. № 43. Pp. 399–415.
40. RILEM/CEB/FIB. Recommendation on reinforcement steel for reinforced concrete. RC6. Bond test for reinforcement steel. 2. Pull-out tests. 1983.
41. Beliaev M., Semenov A., Semenov S., Benin A. Simulation of pulling the reinforcing bar from concrete block with account of friction and concrete damage // MATEC Web of Conferences. 2016. № 73. № 04010.
42. Бенин А.В., Семёнов А.С., Семёнов С.Г., Мельников Б.Е. Конечно-элементное моделирование процессов разрушения и оценка ресурса элементов автодорожного моста с учётом коррозионных повреждений // Инженерно-строительный журнал. 2012. № 7(33). С. 32–42.

Andrey Benin,
+7(921)911-50-80; benin.andrey@mail.ru

Artem Semenov,
+7(905)272-11-88;
Semenov.Artem@googlemail.com

Sergey Semenov,
+7(921)983-44-56; ssgrus@gmail.com

Mikhail Beliaev,
+7(911)733-87-09; belyaev-m-o@yandex.ru

Victor Modestov,
+7(904)335-22-22; modestov@compmechlab.com

Андрей Владимирович Бенин,
+7(921)911-50-80;
эл. почта: benin.andrey@mail.ru

Артем Семенович Семенов,
+7(905)272-11-88;
эл. почта: Semenov.Artem@googlemail.com

Сергей Георгиевич Семенов,
+7(921)983-44-56; эл. почта: ssgrus@gmail.com

Михаил Олегович Беляев,
+7(911)733-87-09;
эл. почта: belyaev-m-o@yandex.ru

Виктор Сергеевич Модестов,
+7(904)335-22-22;
эл. почта: modestov@compmechlab.com

Бенин А.В., Семенов А.С., Семенов С.Г., Беляев М.О., Модестов В.С. Методы идентификации упруго-пластических моделей бетона с учетом накопления повреждений // Инженерно-строительный журнал. 2017. № 8(76). С. 279–297.

Федеральное государственное автономное образовательное учреждение
высшего образования
Санкт-Петербургский политехнический университет Петра Великого

Инженерно-строительный институт
Центр дополнительных профессиональных программ

ПОЛИТЕХ
Санкт-Петербургский политехнический университет Петра Великого

195251, г. Санкт-Петербург, Политехническая ул., 29,
тел/факс: 552-94-60, www.stroikursi.spbstu.ru,
stroikursi@mail.ru

Приглашает специалистов проектных и строительных организаций,
не имеющих базового профильного высшего образования
на курсы профессиональной переподготовки (от 500 часов)
по направлению «Строительство» по программам:

П-01 «Промышленное и гражданское строительство»

Программа включает учебные разделы:

- ***Основы строительного дела***
- ***Инженерное оборудование зданий и сооружений***
- ***Технология и контроль качества строительства***
- ***Основы проектирования зданий и сооружений***
- ***Автоматизация проектных работ с использованием AutoCAD***
- ***Автоматизация сметного дела в строительстве***
- ***Управление строительной организацией***
- ***Управление инвестиционно-строительными проектами. Выполнение функций технического заказчика***

П-02 «Экономика и управление в строительстве»

Программа включает учебные разделы:

- ***Основы строительного дела***
- ***Инженерное оборудование зданий и сооружений***
- ***Технология и контроль качества строительства***
- ***Управление инвестиционно-строительными проектами. Выполнение функций технического заказчика и генерального подрядчика***
- ***Управление строительной организацией***
- ***Экономика и ценообразование в строительстве***
- ***Управление строительной организацией***
- ***Организация, управление и планирование в строительстве***
- ***Автоматизация сметного дела в строительстве***

П-03 «Инженерные системы зданий и сооружений»

Программа включает учебные разделы:

- ***Основы механики жидкости и газа***
- ***Инженерное оборудование зданий и сооружений***
- ***Проектирование, монтаж и эксплуатация систем вентиляции и кондиционирования***
- ***Проектирование, монтаж и эксплуатация систем отопления и теплоснабжения***
- ***Проектирование, монтаж и эксплуатация систем водоснабжения и водоотведения***
- ***Автоматизация проектных работ с использованием AutoCAD***
- ***Электроснабжение и электрооборудование объектов***

П-04 «Проектирование и конструирование зданий и сооружений»

Программа включает учебные разделы:

- ***Основы сопротивления материалов и механики стержневых систем***
- ***Проектирование и расчет оснований и фундаментов зданий и сооружений***
- ***Проектирование и расчет железобетонных конструкций***
- ***Проектирование и расчет металлических конструкций***
- ***Проектирование зданий и сооружений с использованием AutoCAD***
- ***Расчет строительных конструкций с использованием SCAD Office***

П-05 «Контроль качества строительства»

Программа включает учебные разделы:

- ***Основы строительного дела***
- ***Инженерное оборудование зданий и сооружений***
- ***Технология и контроль качества строительства***
- ***Проектирование и расчет железобетонных конструкций***
- ***Проектирование и расчет металлических конструкций***
- ***Обследование строительных конструкций зданий и сооружений***
- ***Выполнение функций технического заказчика и генерального подрядчика***

По окончании курса слушателю выдается диплом о профессиональной переподготовке установленного образца, дающий право на ведение профессиональной деятельности